Jan Lunze

Networked Control of Multi-Agent Systems

Consensus and synchronisation,
Communication structure design,
Self-organisation in networked systems,
Event-triggered control

Figures

Edition MoRa

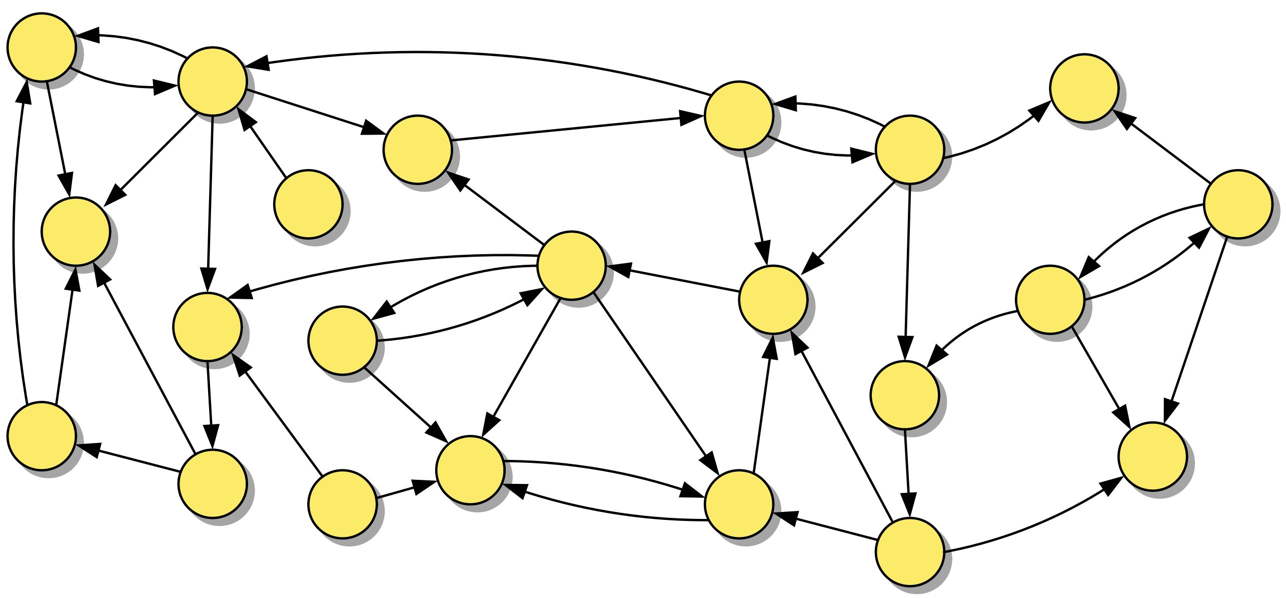

Fig. 1.1: Graph-theoretical representation of a networked system

J. Lunze: *Networked Control of Multi-Agent Systems*, Edition **MoRa** 2022

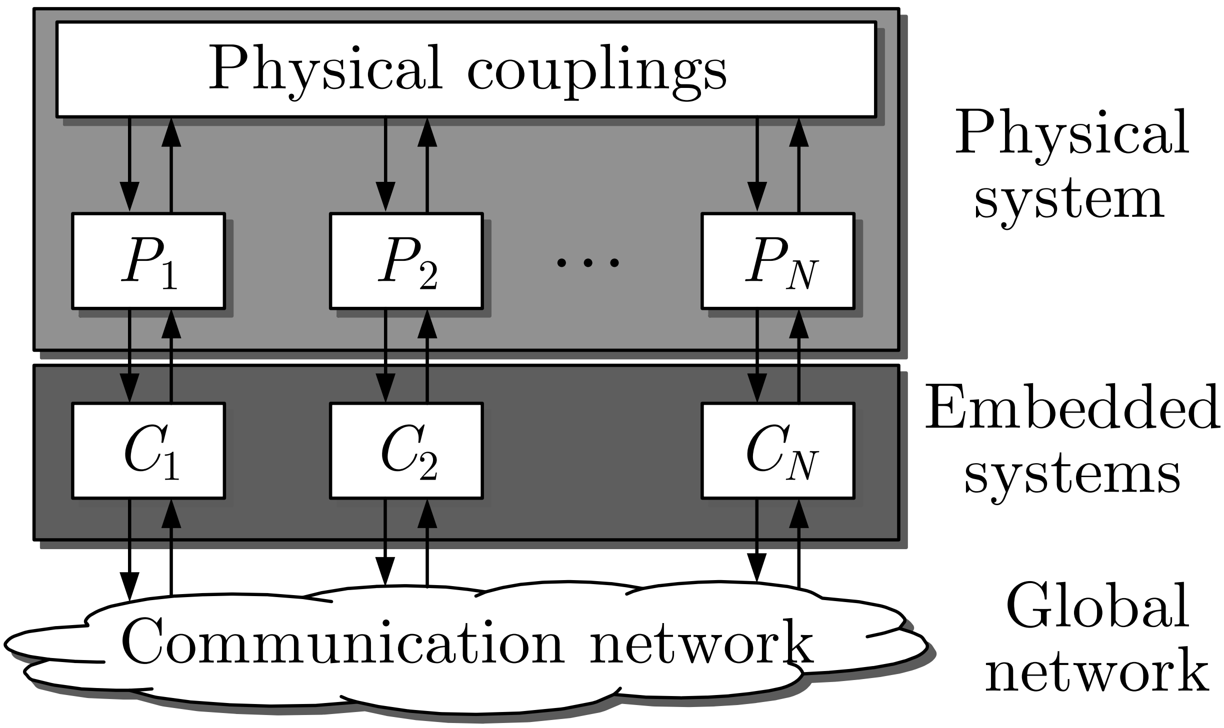

Fig. 1.2: Structure of a cyber-physical system

J. LUNZE: *Networked Control of Multi-Agent Systems,* Edition MoRa 2022

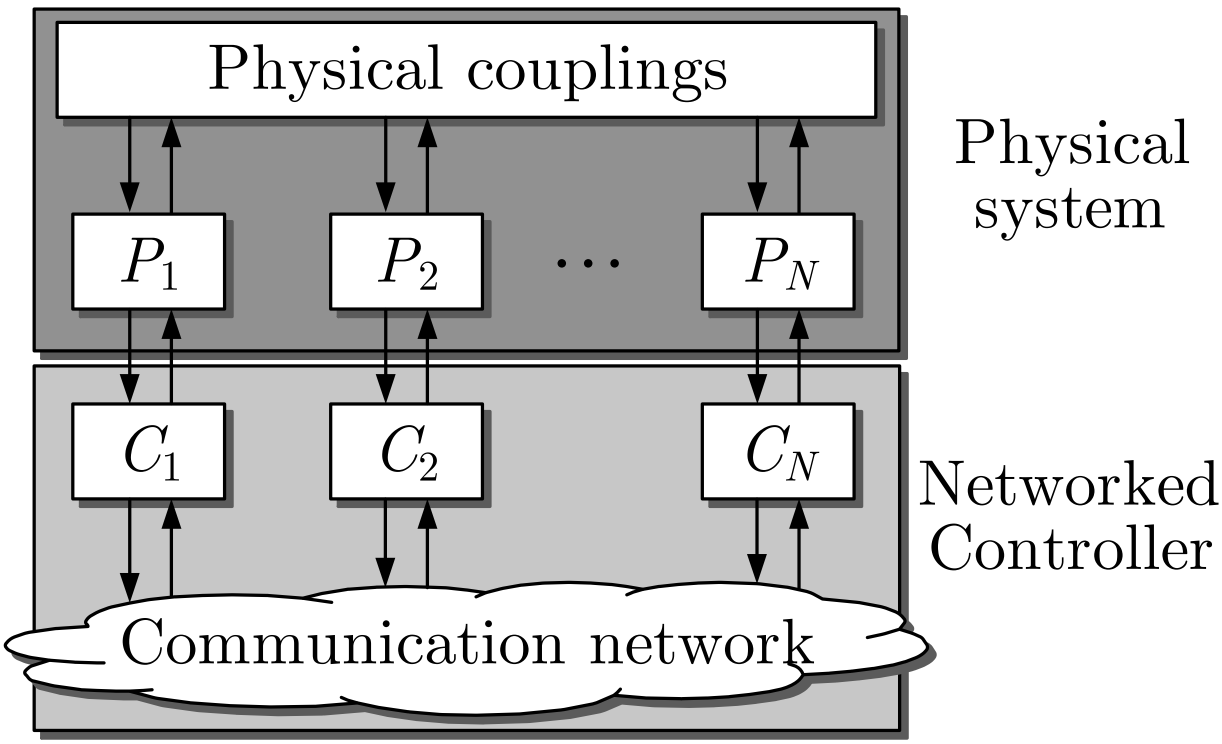

Fig. 1.2: Control-theoretical interpretation of cyber-physical systems

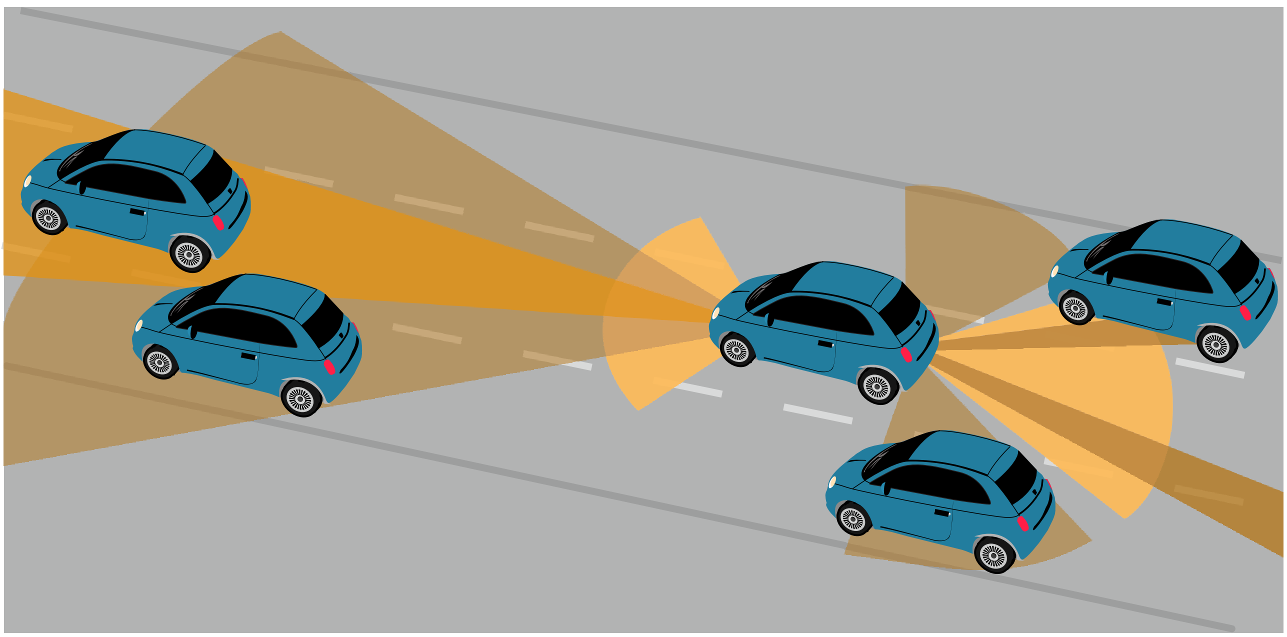

Fig. 1.3: Cognitive vehicles

J. Lunze: *Networked Control of Multi-Agent Systems,* Edition **MoRa** 2022

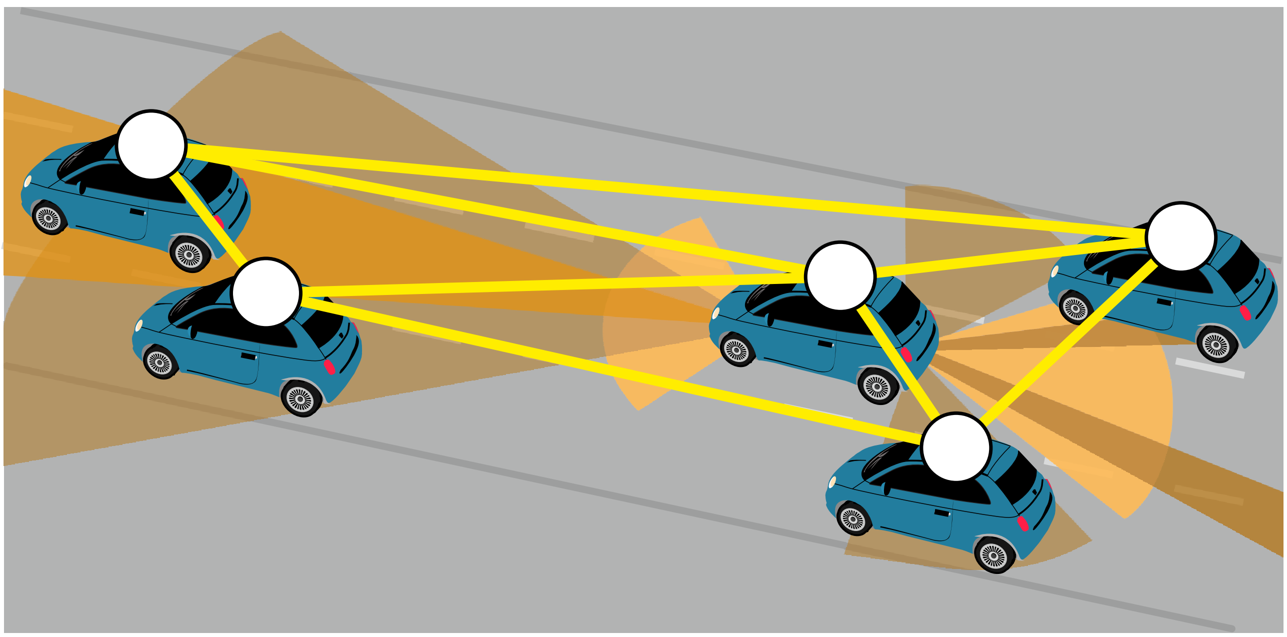

Fig. 1.3: Cooperative vehicles

J. Lunze: *Networked Control of Multi-Agent Systems*, Edition **M**o**R**a 2022

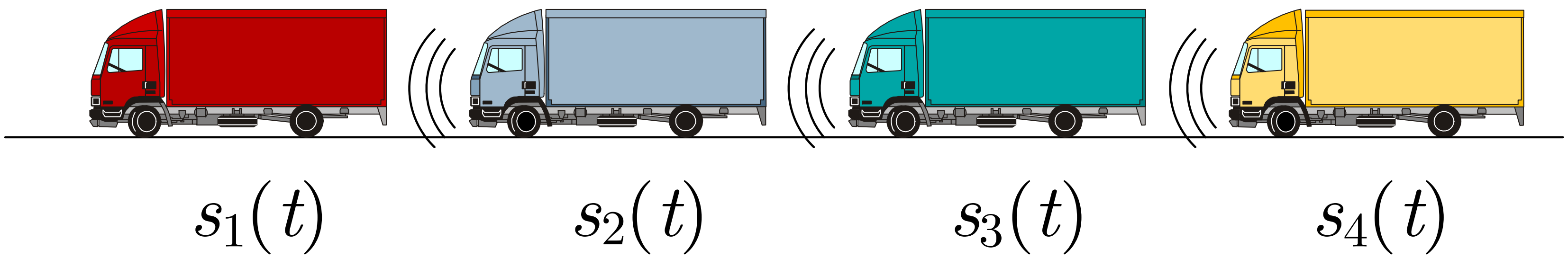

Fig. 1.4. Vehicle platoon with ACC

J. Lunze: *Networked Control of Multi-Agent Systems*, Edition MoRa 2022

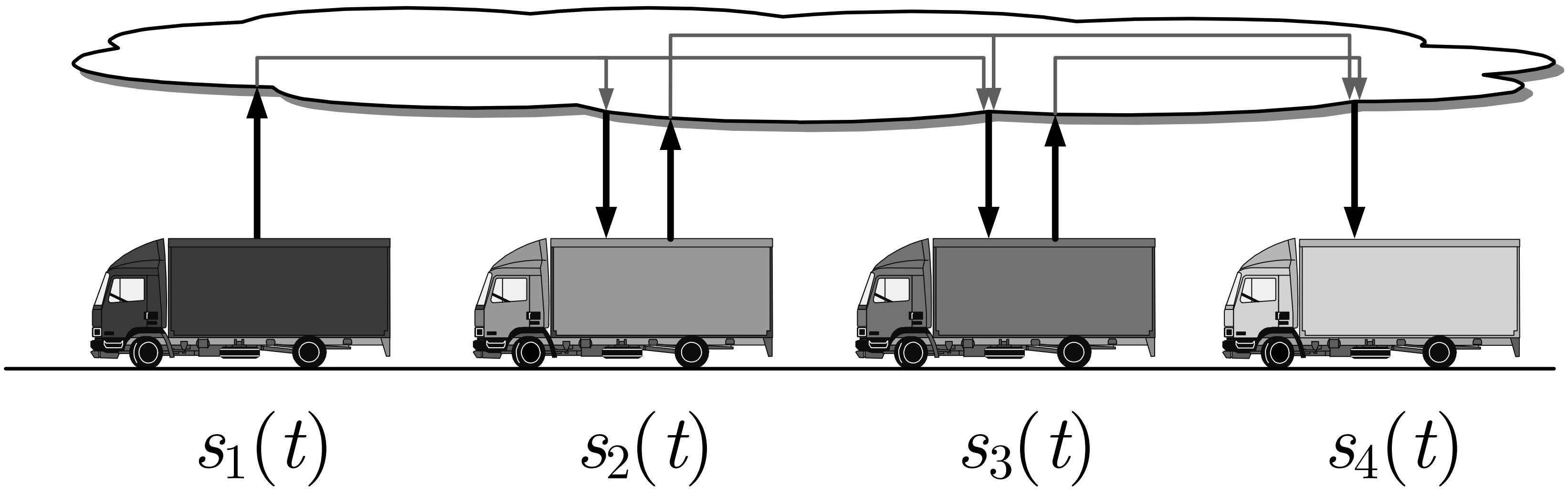

Fig. 1.4. Vehicle platoon with CACC

J. LUNZE: *Networked Control of Multi-Agent Systems*, Edition MoRa 2022

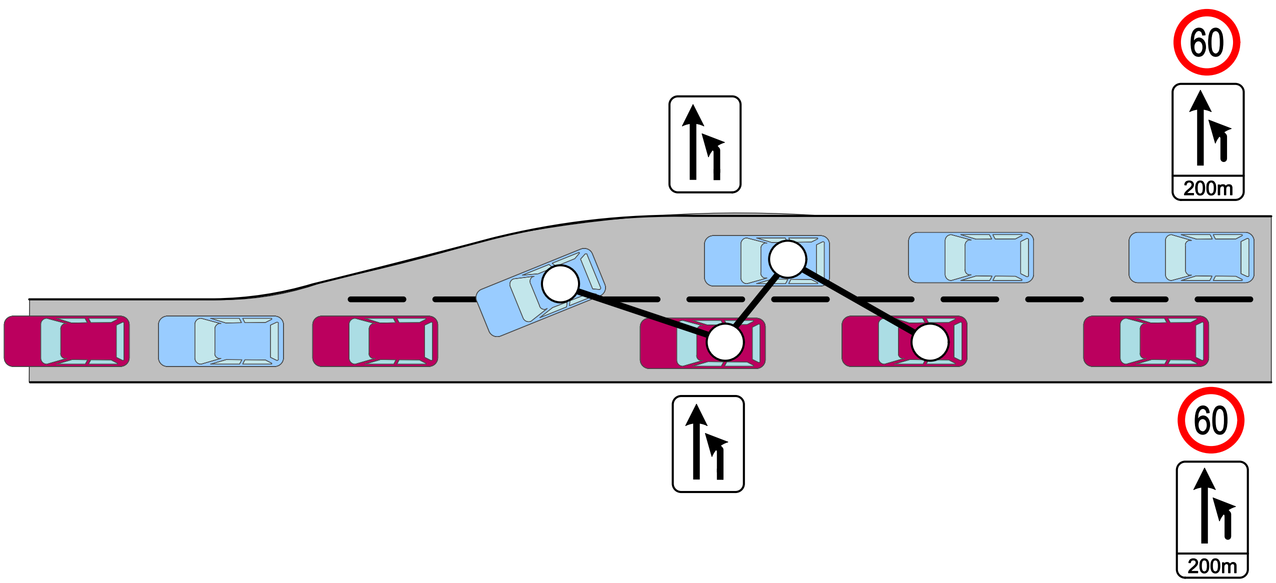

Fig. 1.5: Vehicle merging at a lane end

J. LUNZE: *Networked Control of Multi-Agent Systems,* Edition **MoRa** 2022

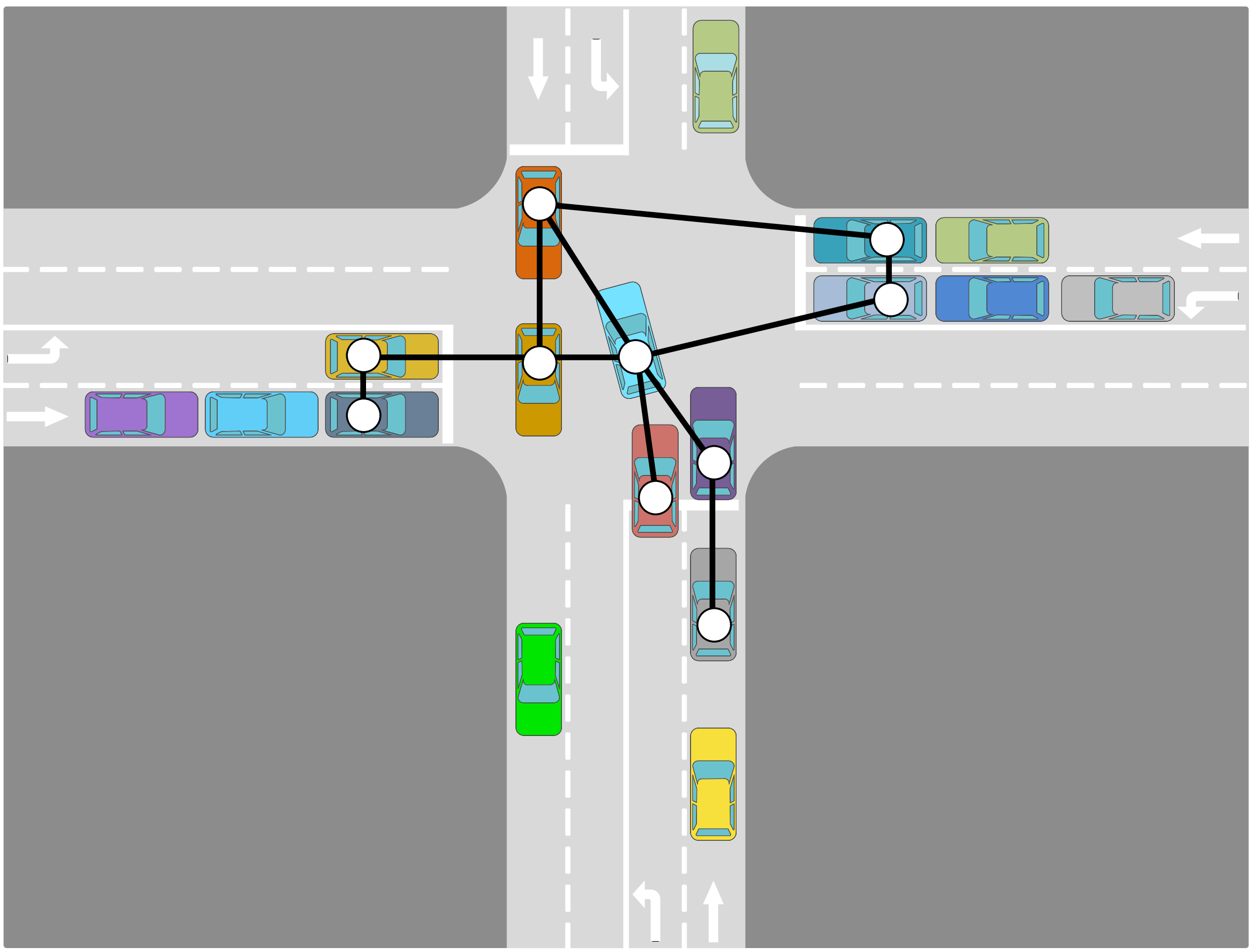

Fig. 1.5: Crossroads management without traffic lights

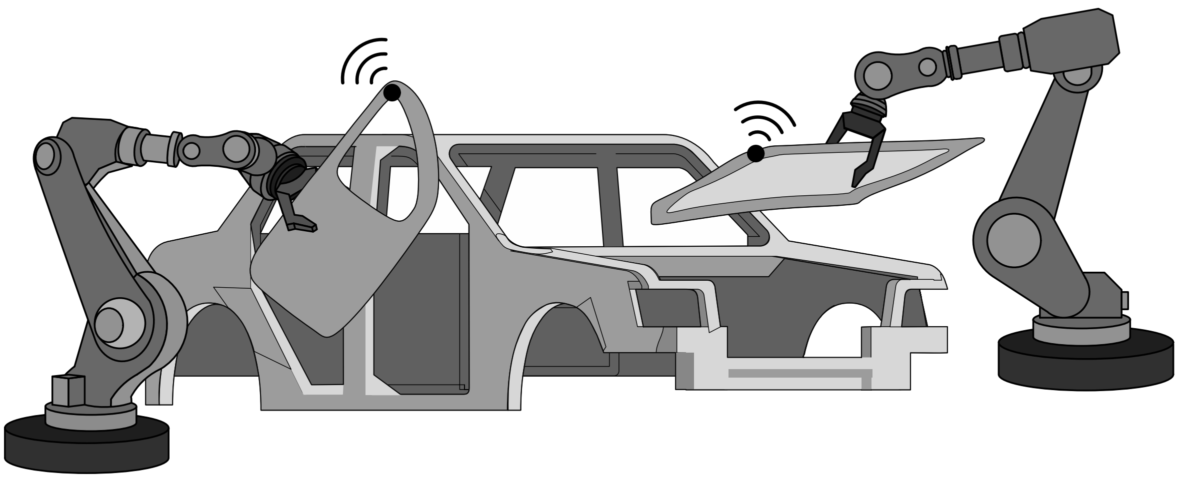

Fig. 1.6: Autonomous assemblage

J. Lunze: *Networked Control of Multi-Agent Systems,* Edition **MoRa** 2022

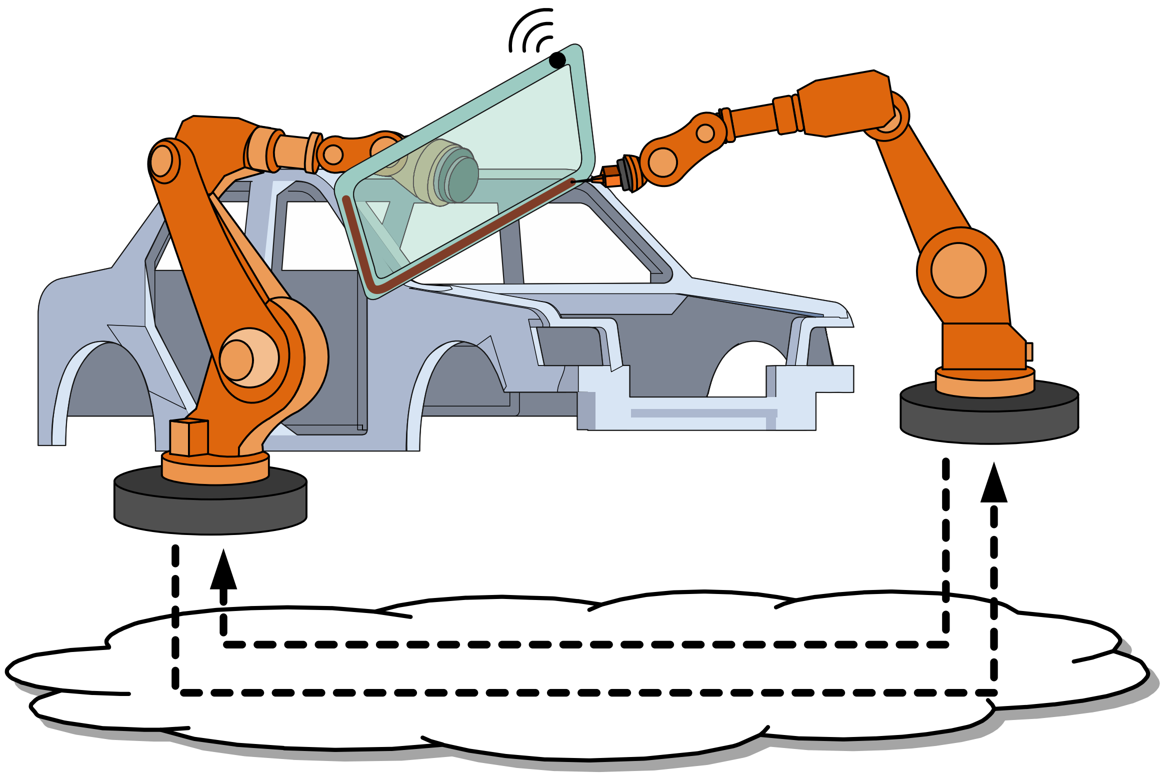

Fig. 1.6: Cooperative assemblage

J. Lunze: *Networked Control of Multi-Agent Systems*, Edition **MoRa** 2022

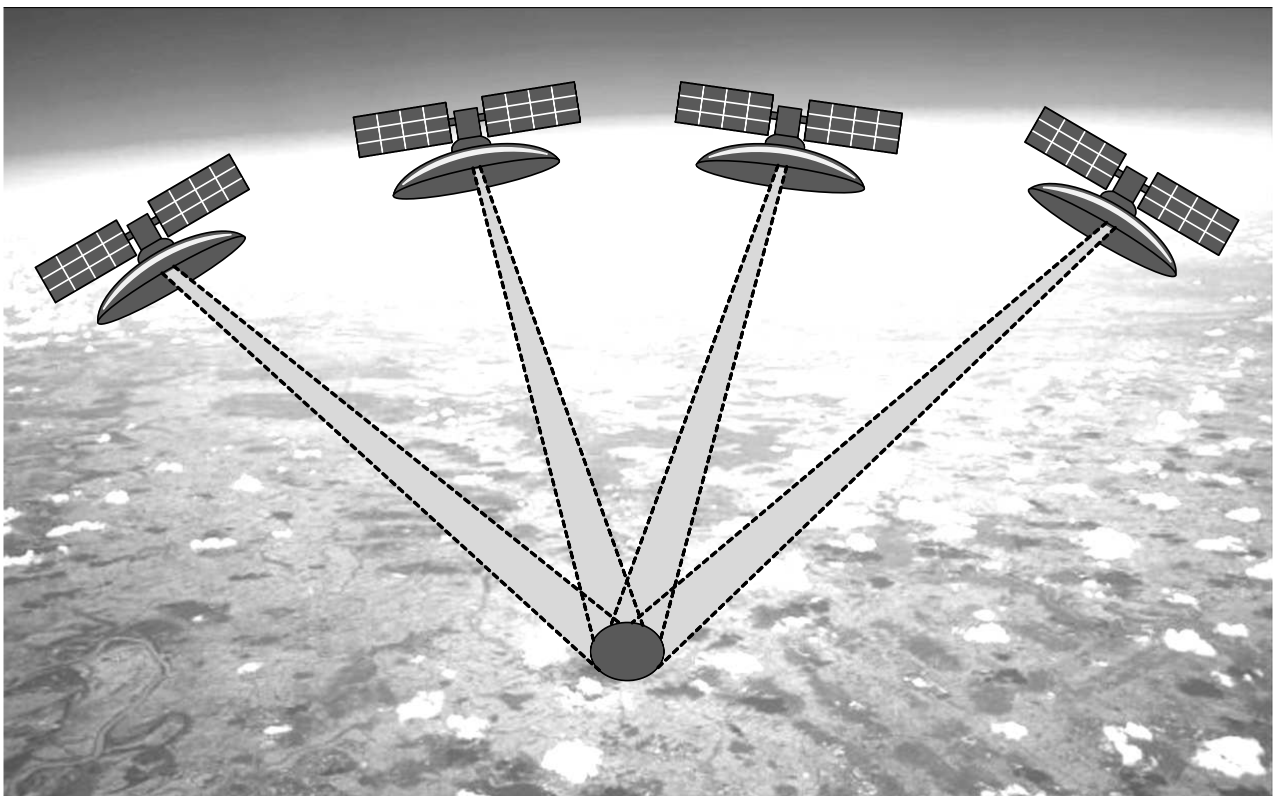

Fig. 1.7: Formation flight of micro satellites for cooperative surveillance of the earth

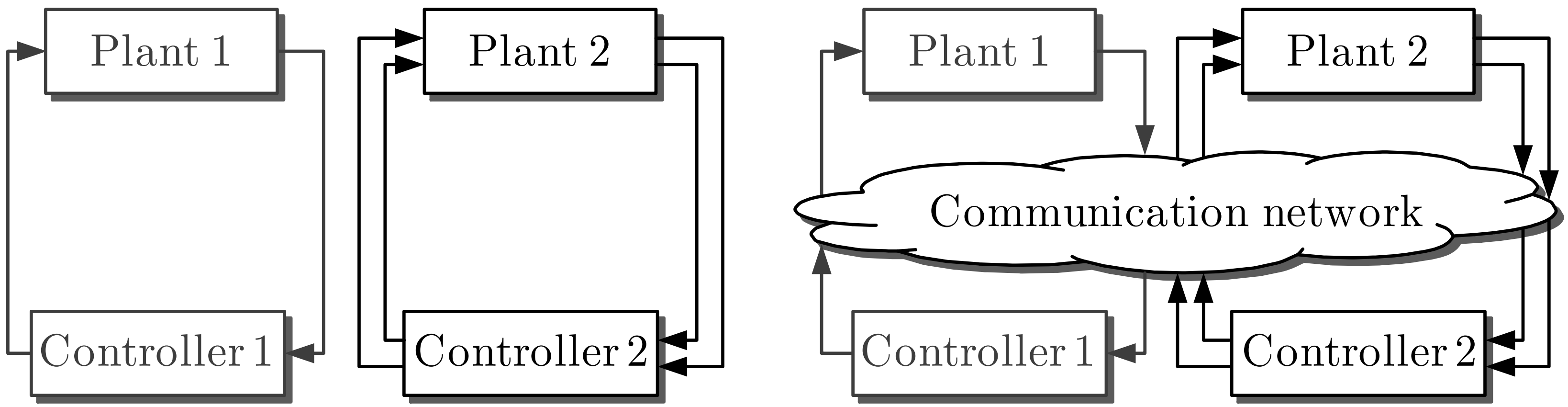

Fig. 1.8. Subject of classical control theory (left) and of the theory of digitally networked control systems (right)

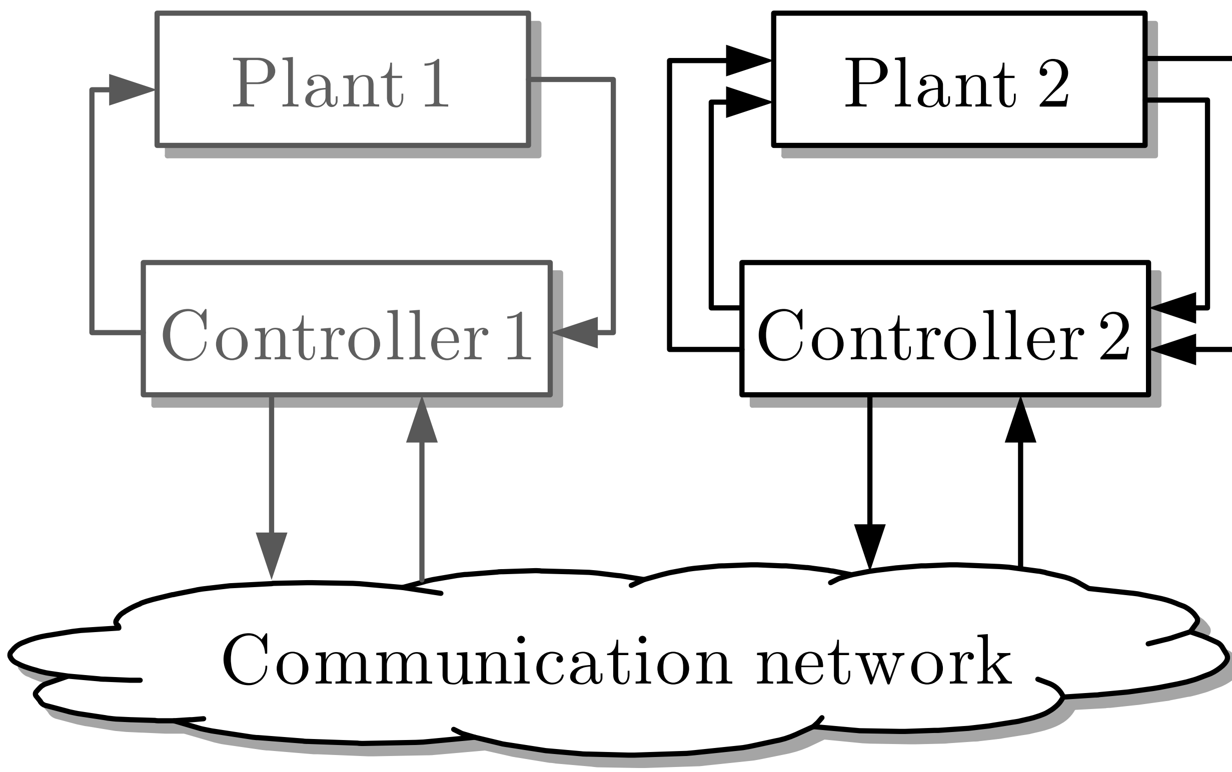

Fig. 1.9: Networking of control loops

J. Lunze: *Networked Control of Multi-Agent Systems*, Edition MoRa 2022

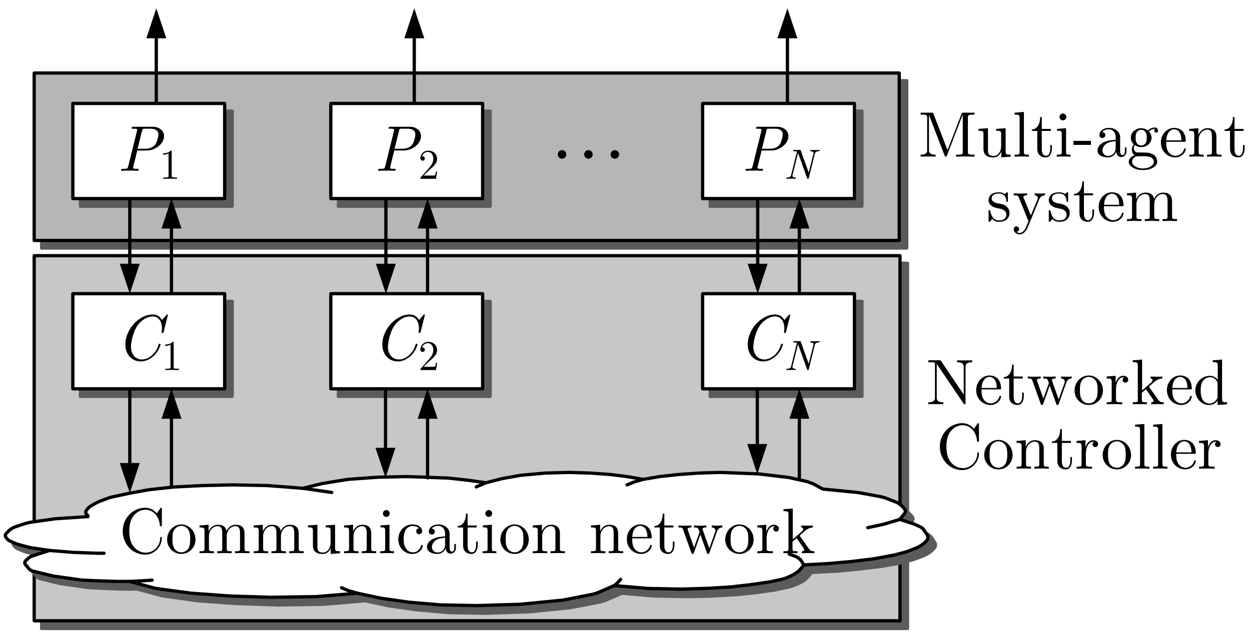

Fig. 1.10: Networked systems as an interconnection of a group of agents and a networked controller

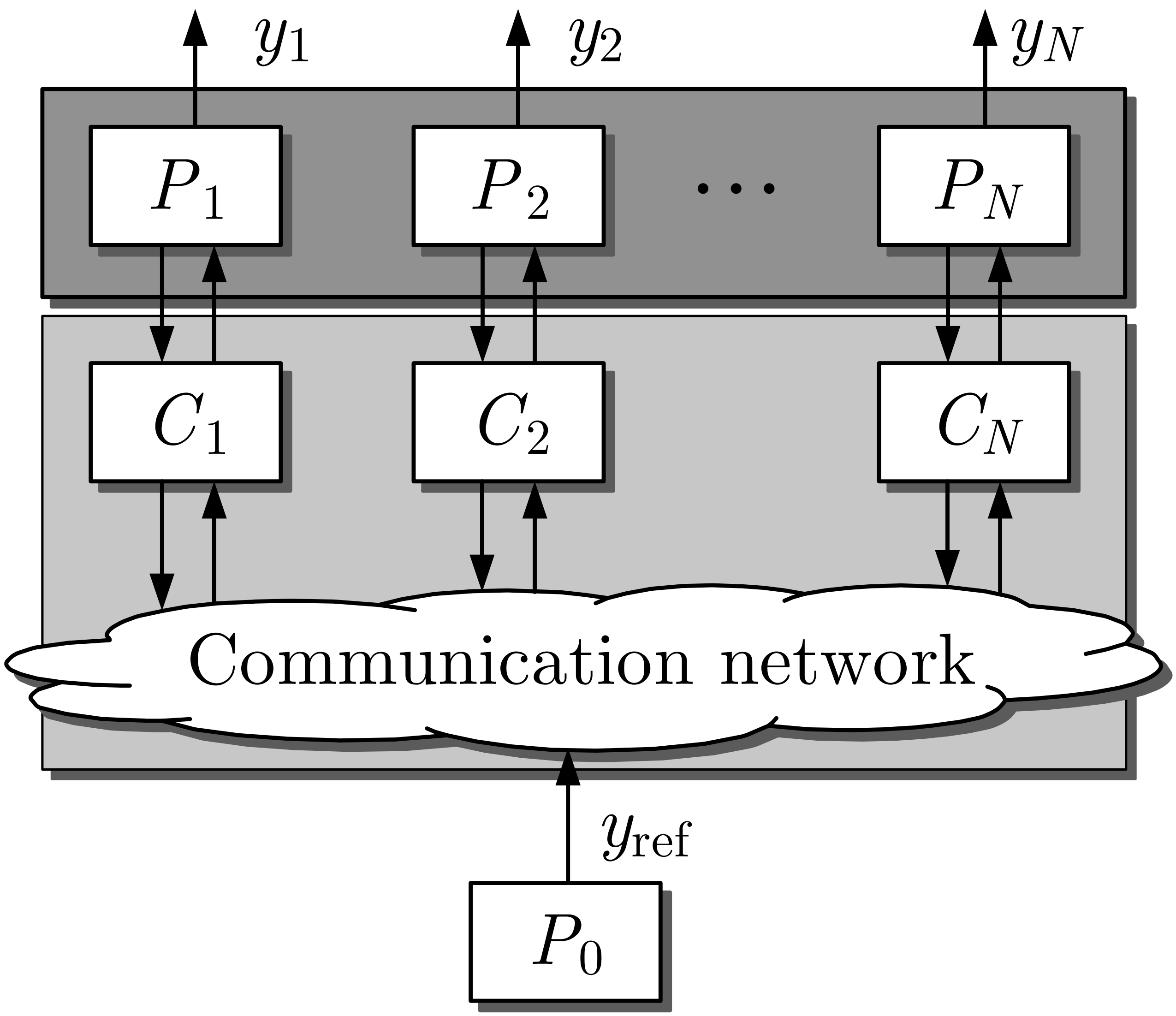

Fig. 1.11: Leader-follower system

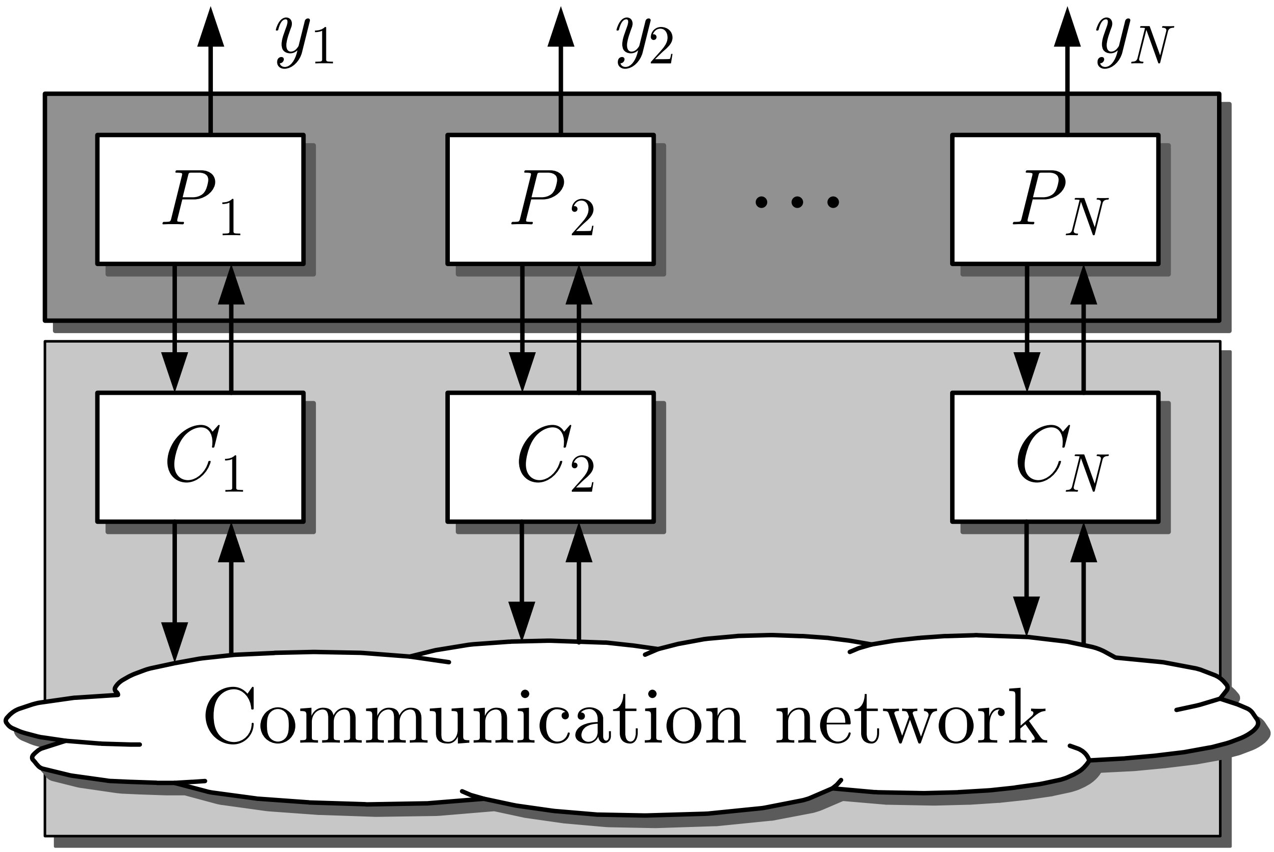

Fig. 1.11: Leaderless multi-agent system

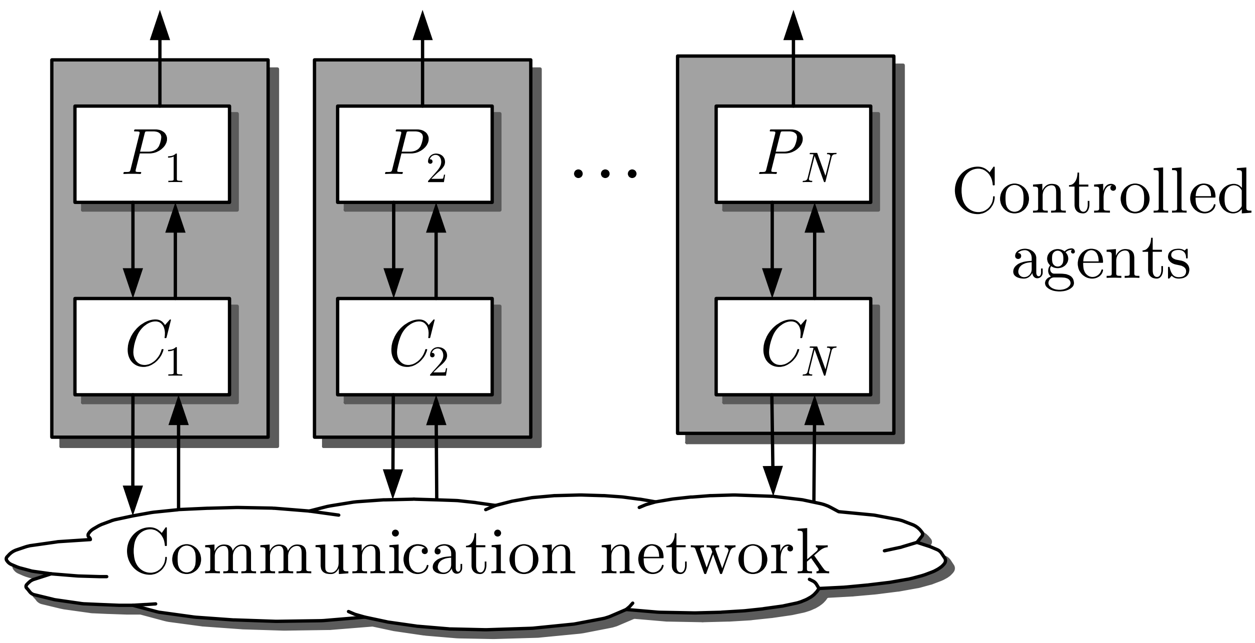

Fig. 1.12: Networked system as an interconnection of controlled agents

J. LUNZE: *Networked Control of Multi-Agent Systems,* Edition **MoRa** 2022

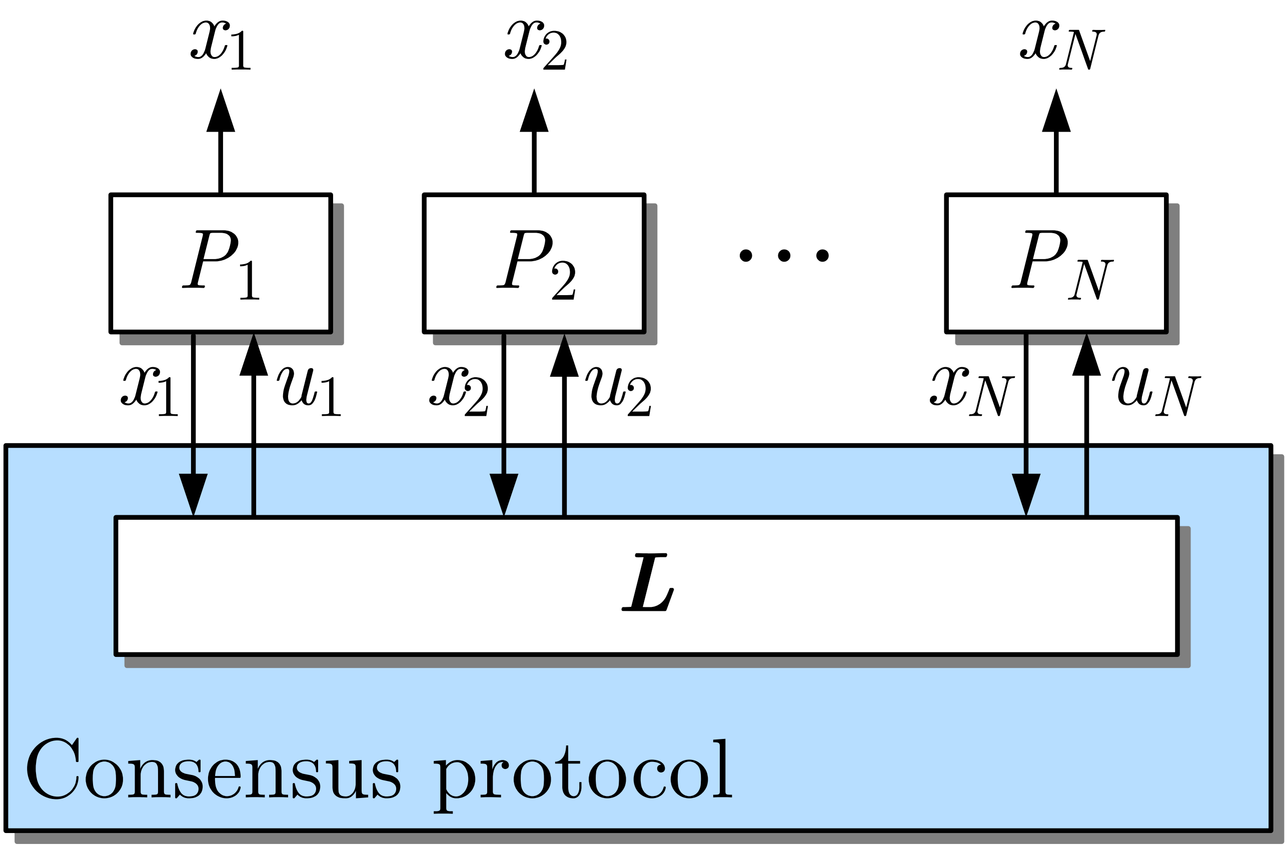

Fig. 1.13: Consensus system

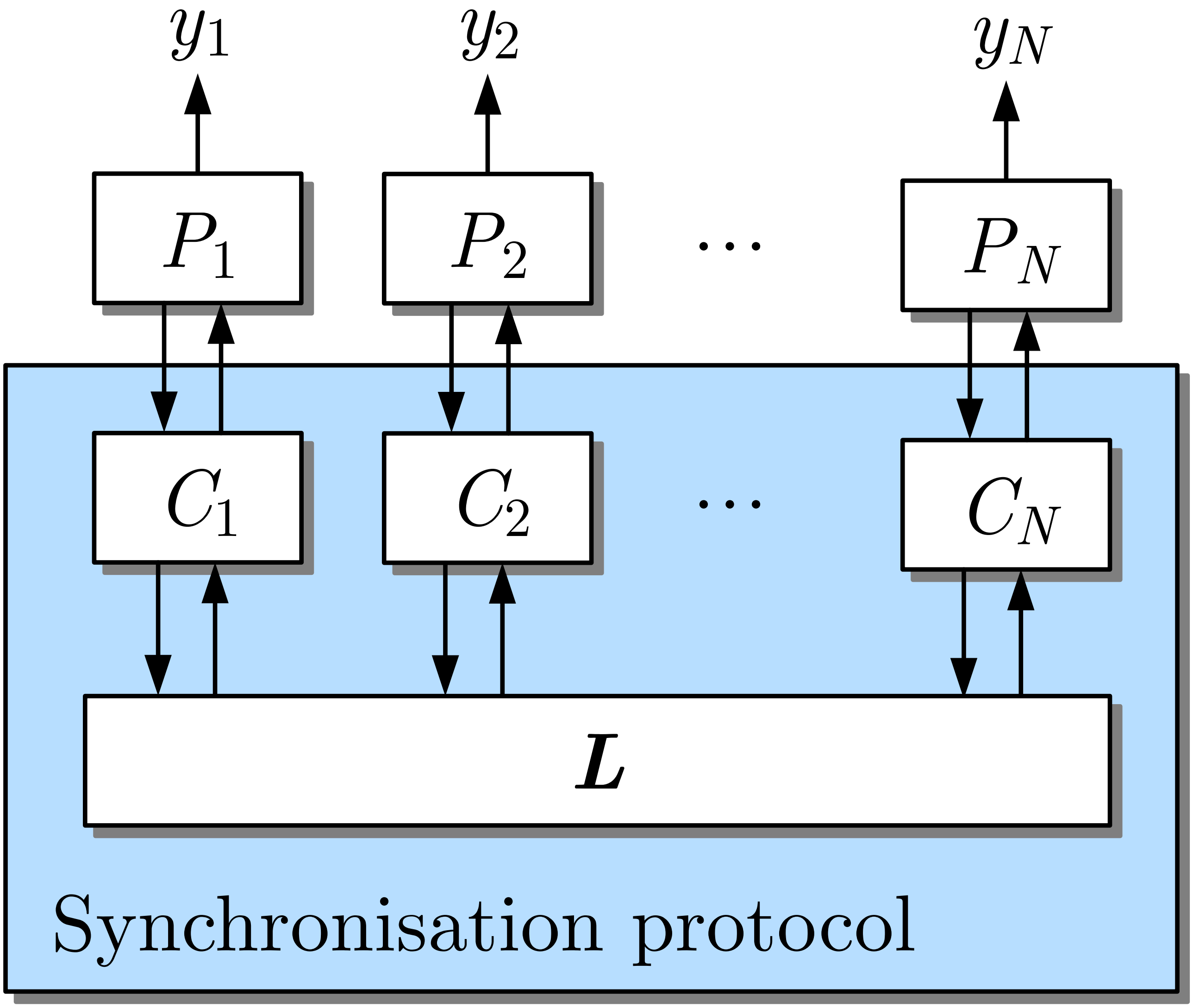

Fig. 1.14: Synchronisation of multi-agent systems

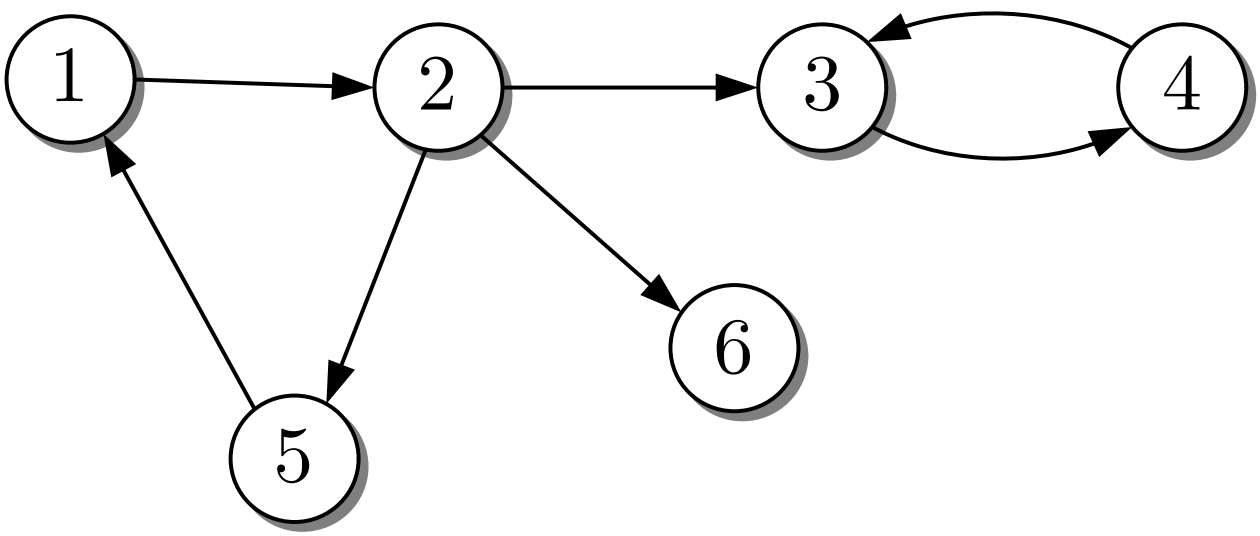

Fig. 2.1: Directed graph

J. Lunze: *Networked Control of Multi-Agent Systems*, Edition MoRa 2022

page 32

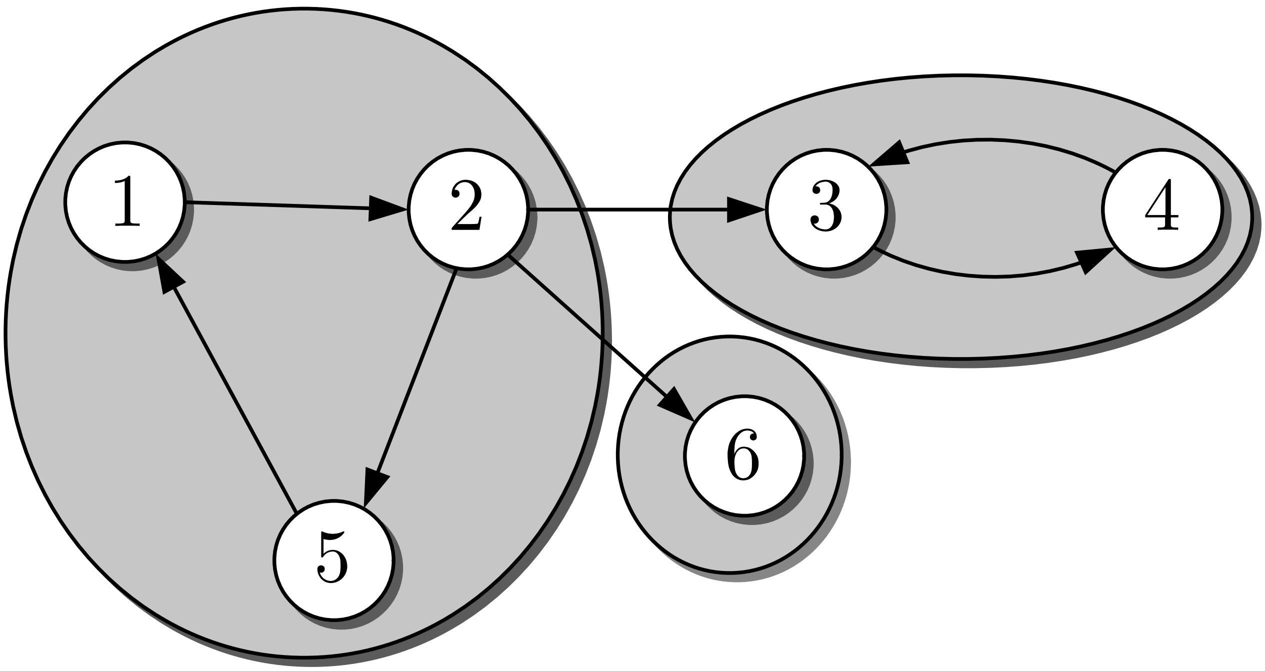

Fig. 2.2: Strongly connected components of the directed graph of Fig. 2.1

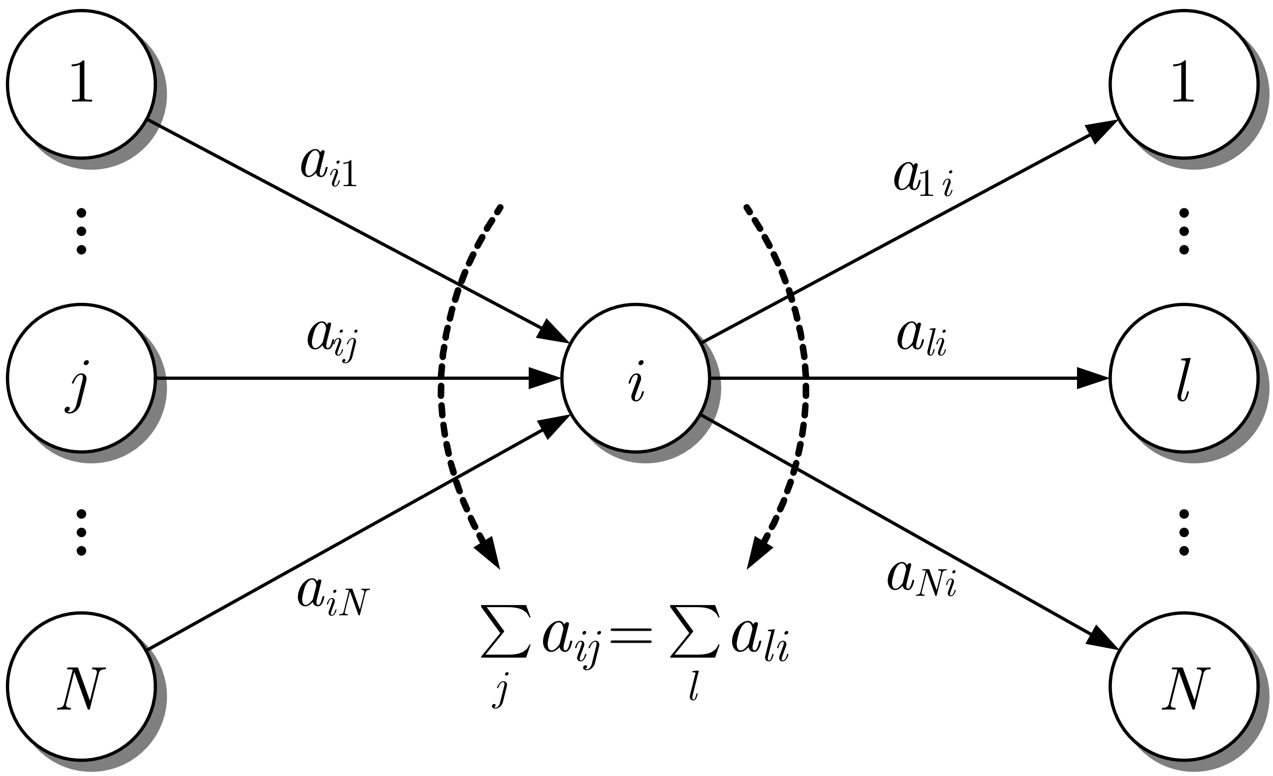

Fig. 2.3: Interpretation of the condition (2.9) for weight-balanced graphs

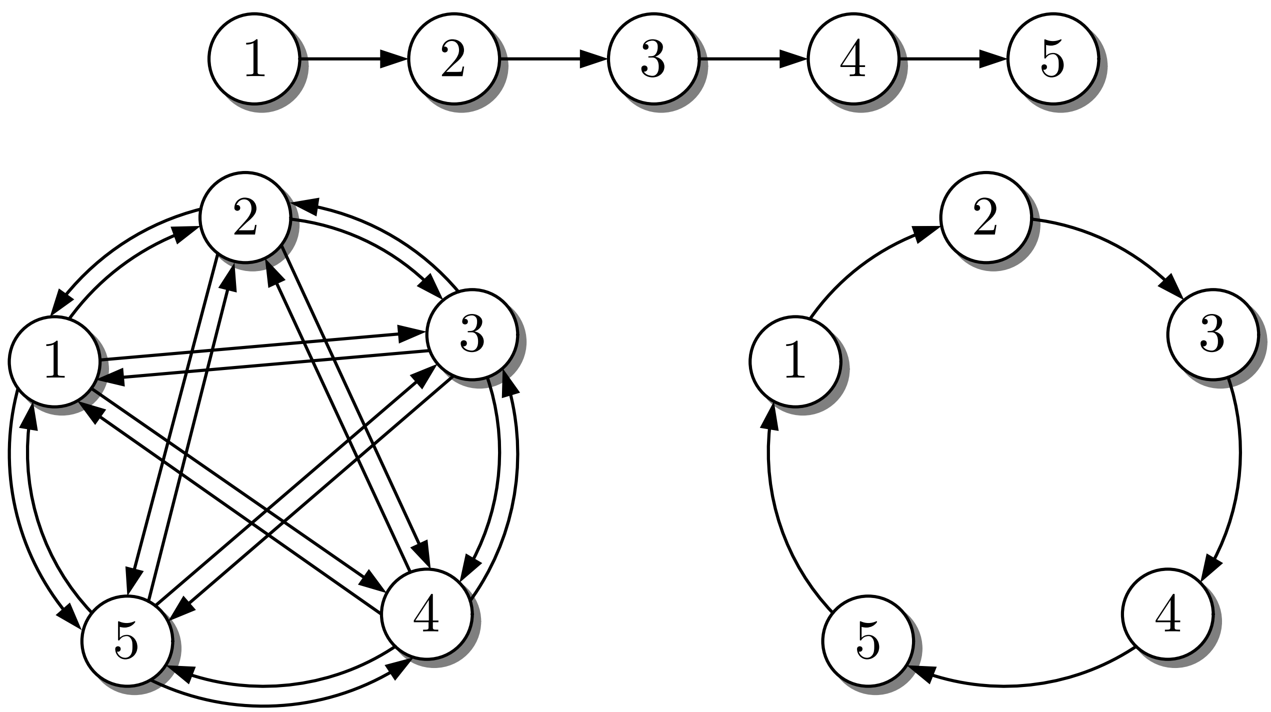

Fig. 2.4: Specific graphs: path graph, complete graph, ring graph

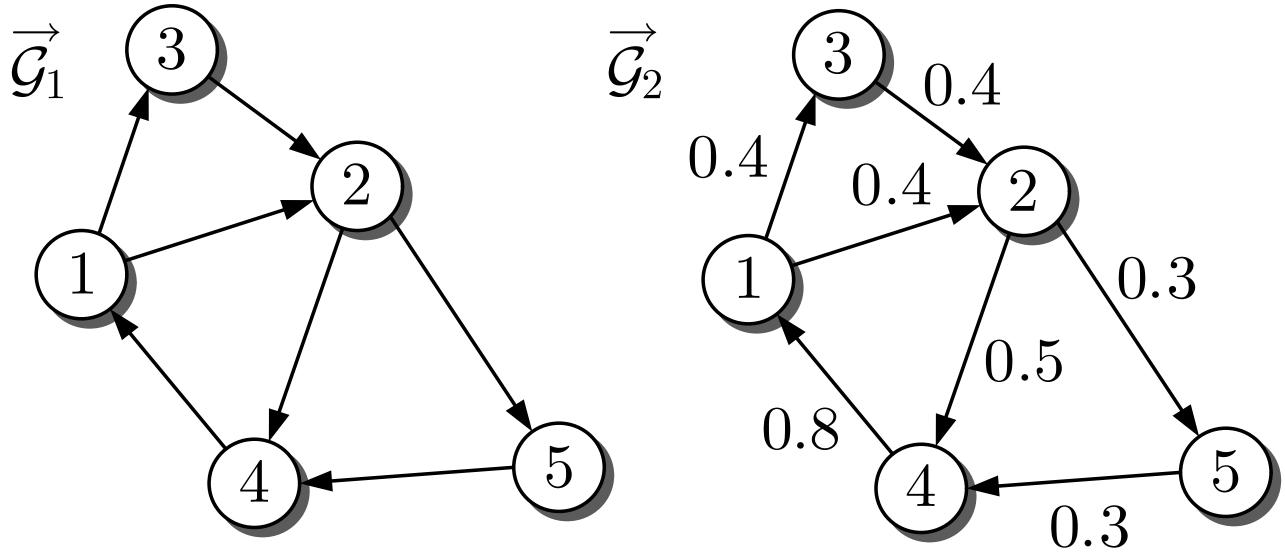

Fig. 2.5: Two example graphs

J. Lunze: *Networked Control of Multi-Agent Systems*, Edition **MoRa** 2022

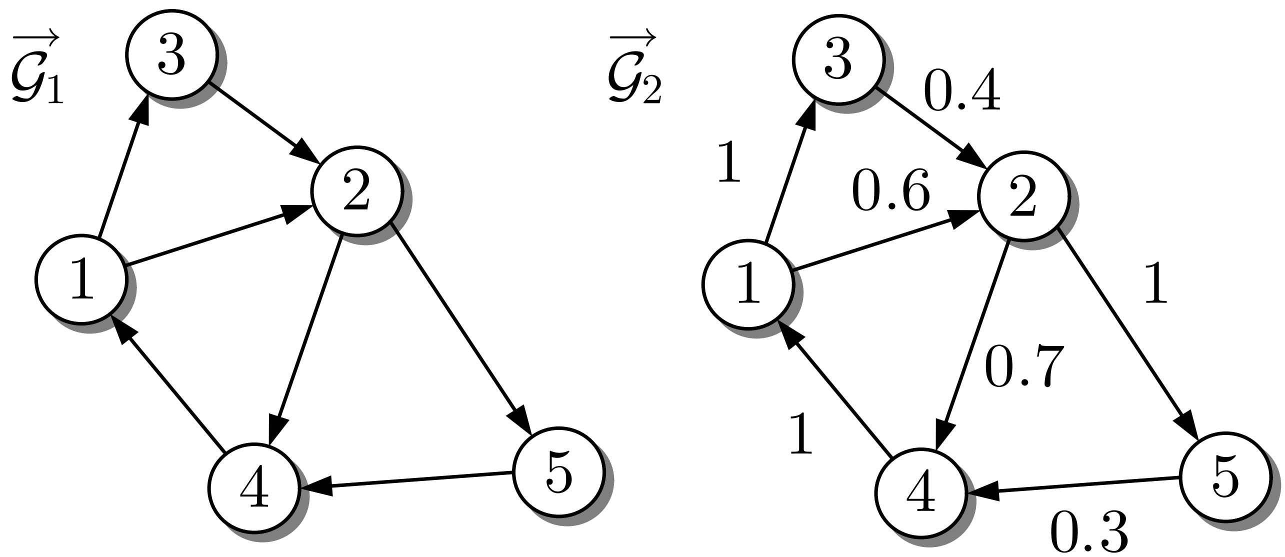

Fig. 2.6: Two weighted graphs

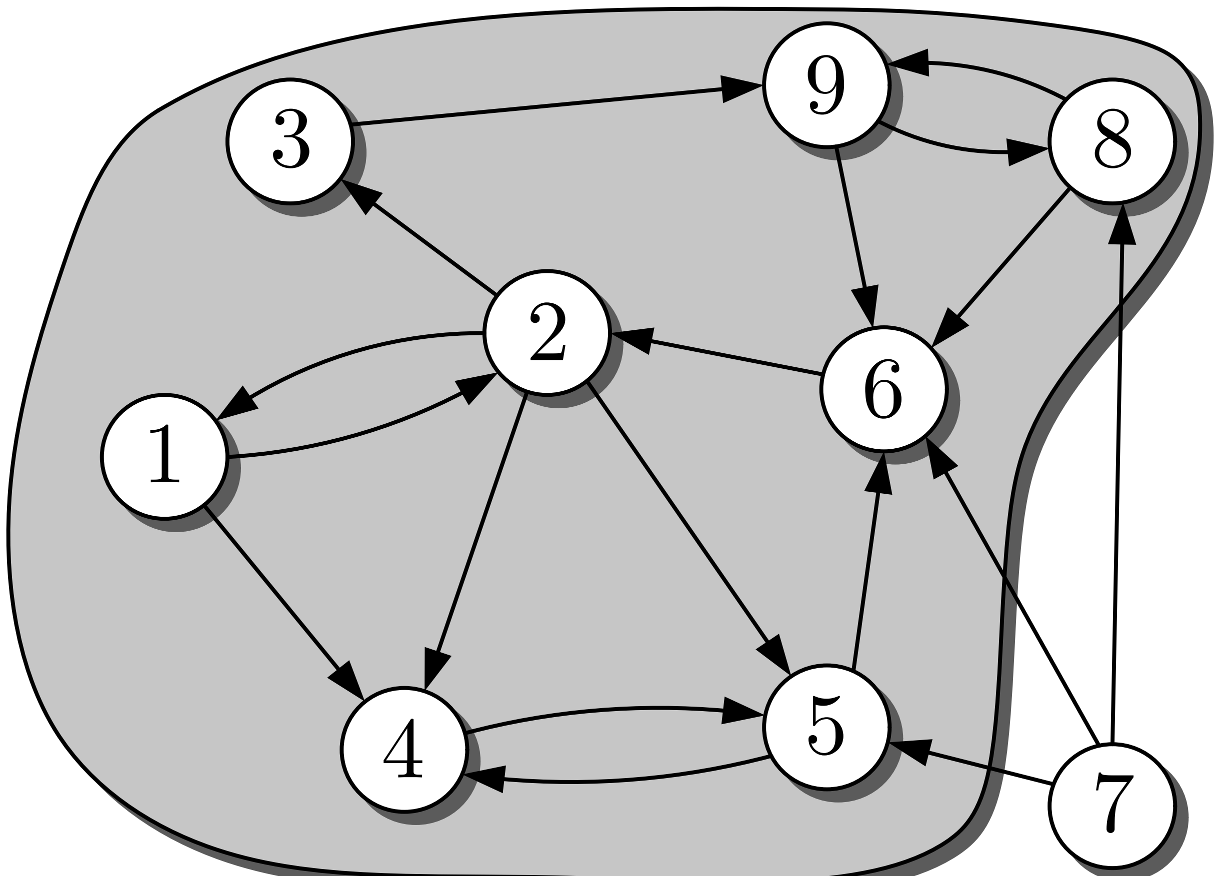

Fig. 2.7: The directed graph to be investigated in Exercise 2.2

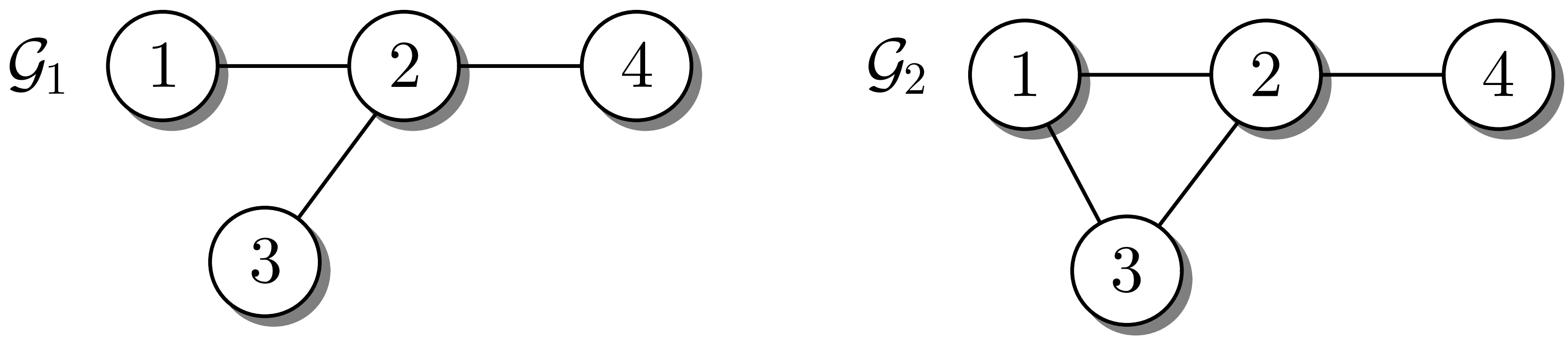

Fig. 2.8. A tree and a general graph

J. Lunze: *Networked Control of Multi-Agent Systems*, Edition MoRa 2022

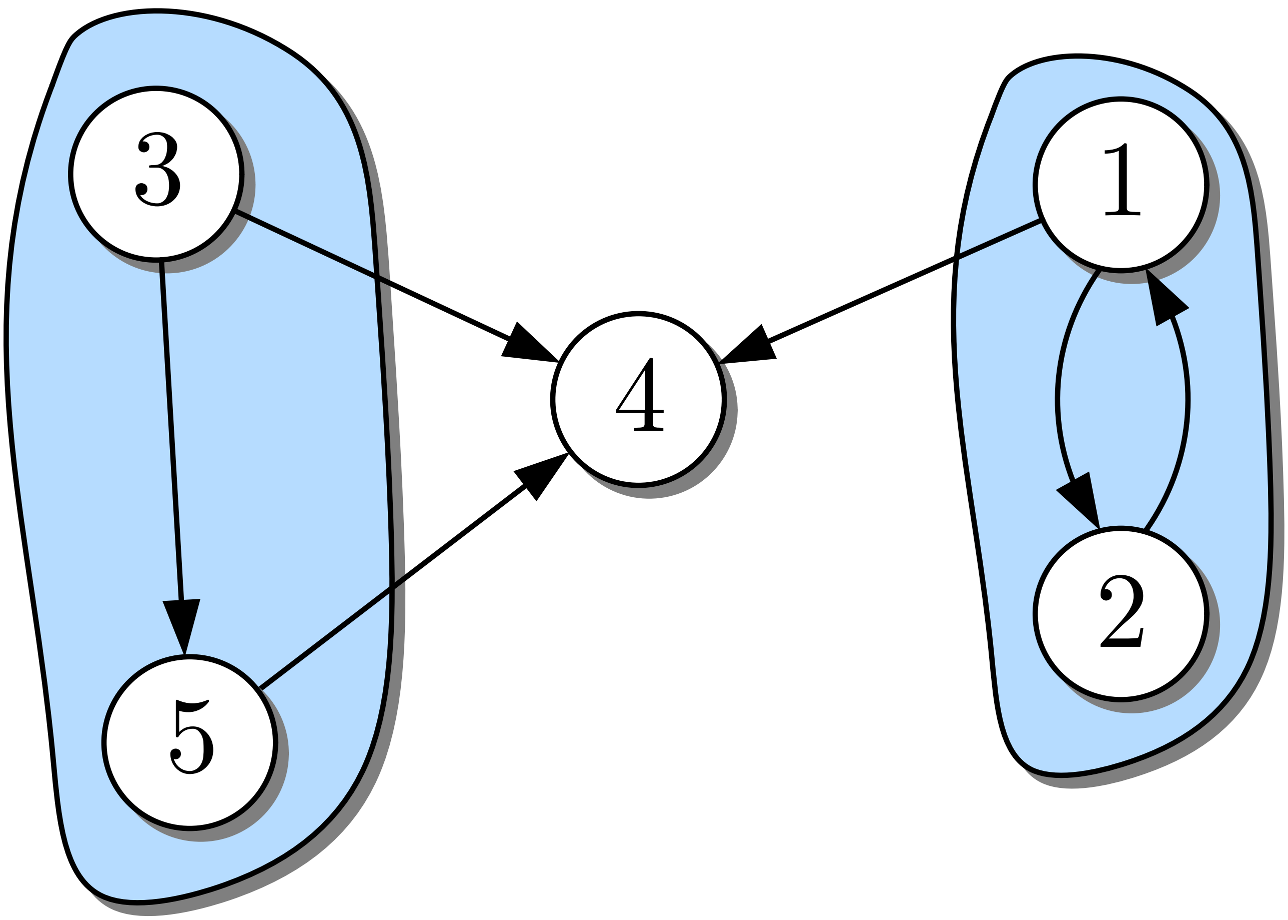

Fig. 2.9: Graph with no spanning tree

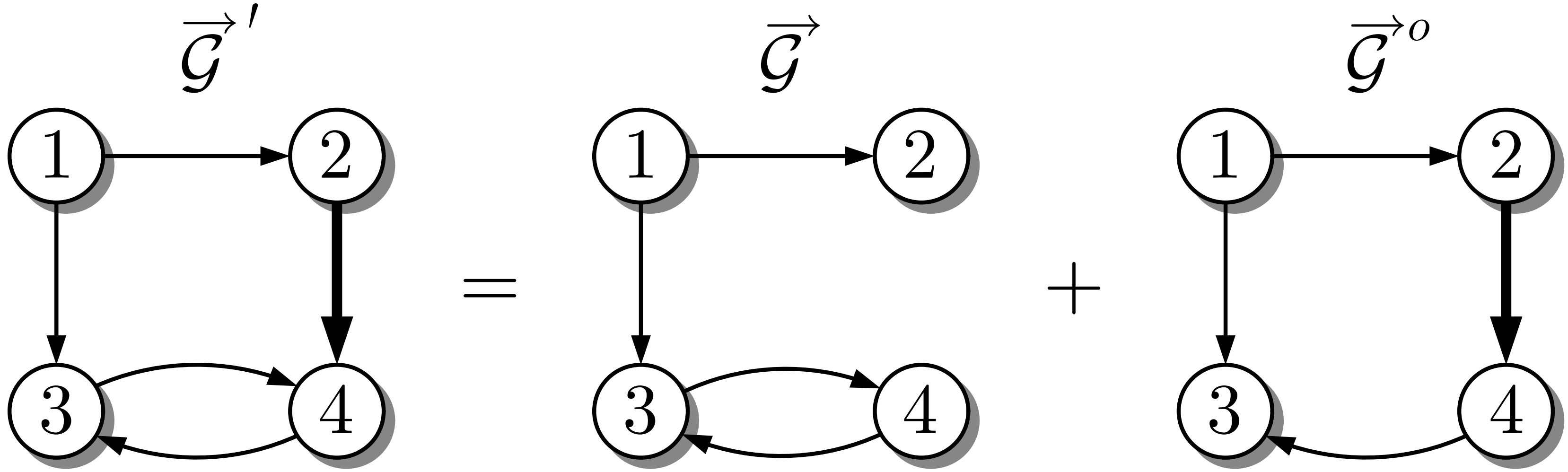

Fig. 2.10. Graph with an additional edge (thick arrow)

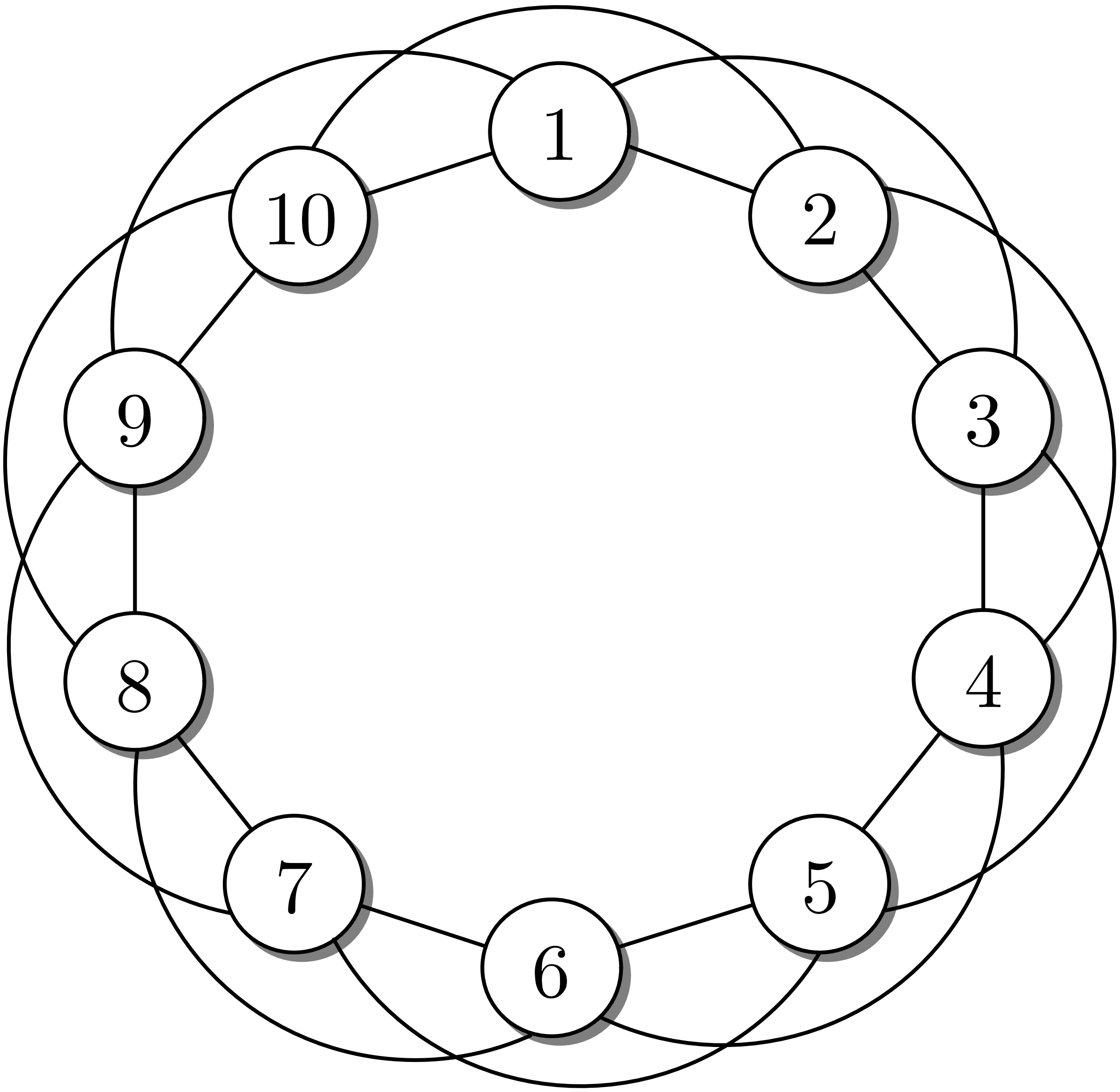

Fig. 2.11: Regular graph for $k = 4$

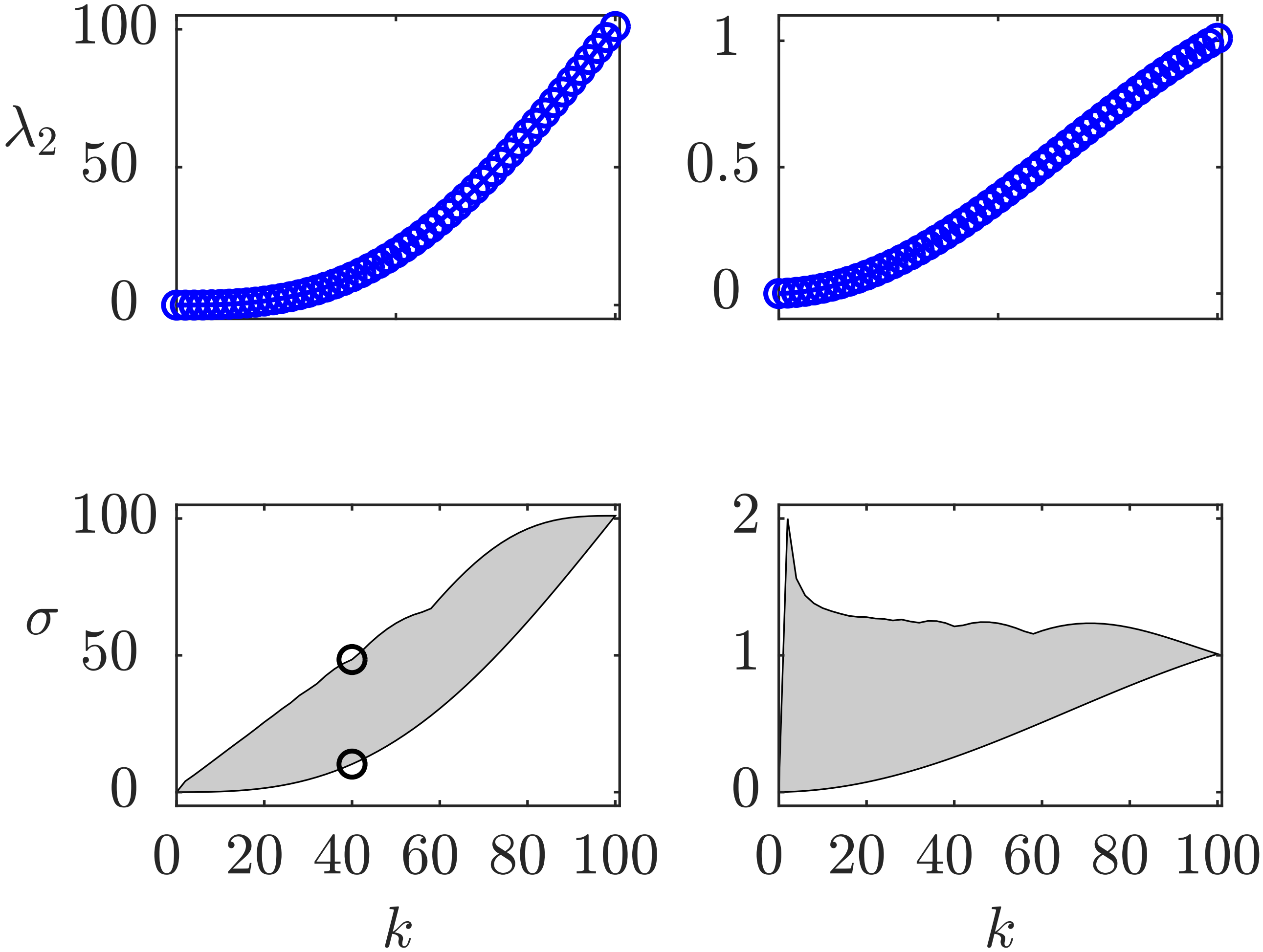

Fig. 2.11: Eigenvalue λ_2 and spectrum σ of the Laplacian matrix and of the normalised Laplacian matrix for $N = 101$

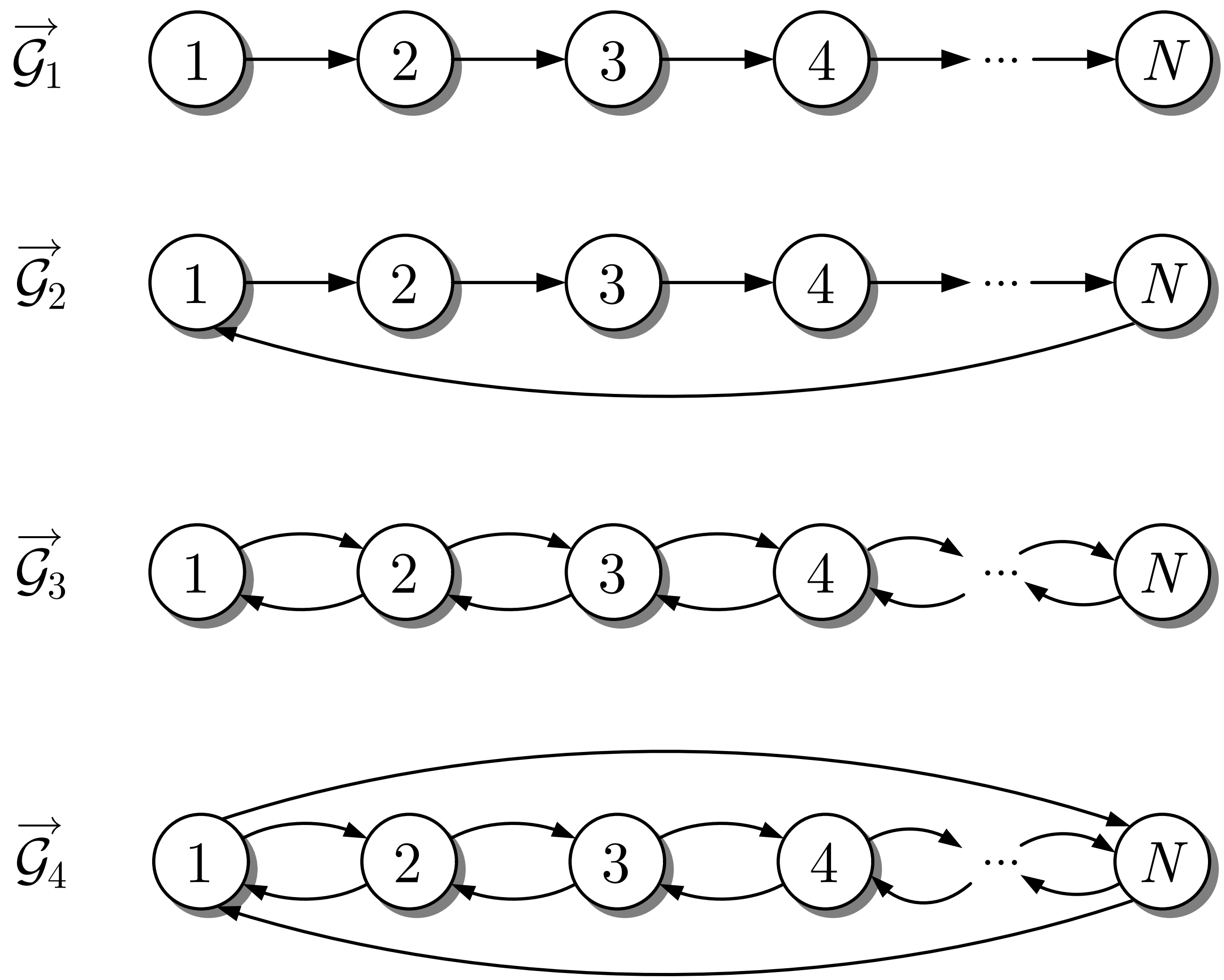

Fig. 2.12: Directed graphs to be analysed in Exercises 2.7 and 2.9

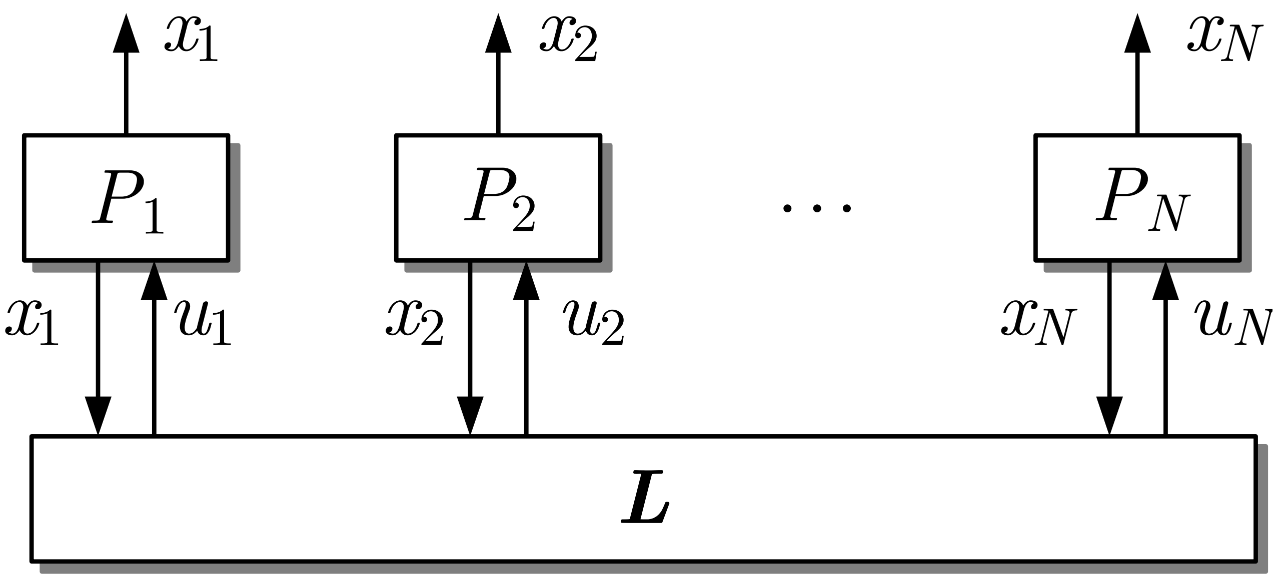

Fig. 3.1: System $\overline{\Sigma}$ considered in the consensus problem

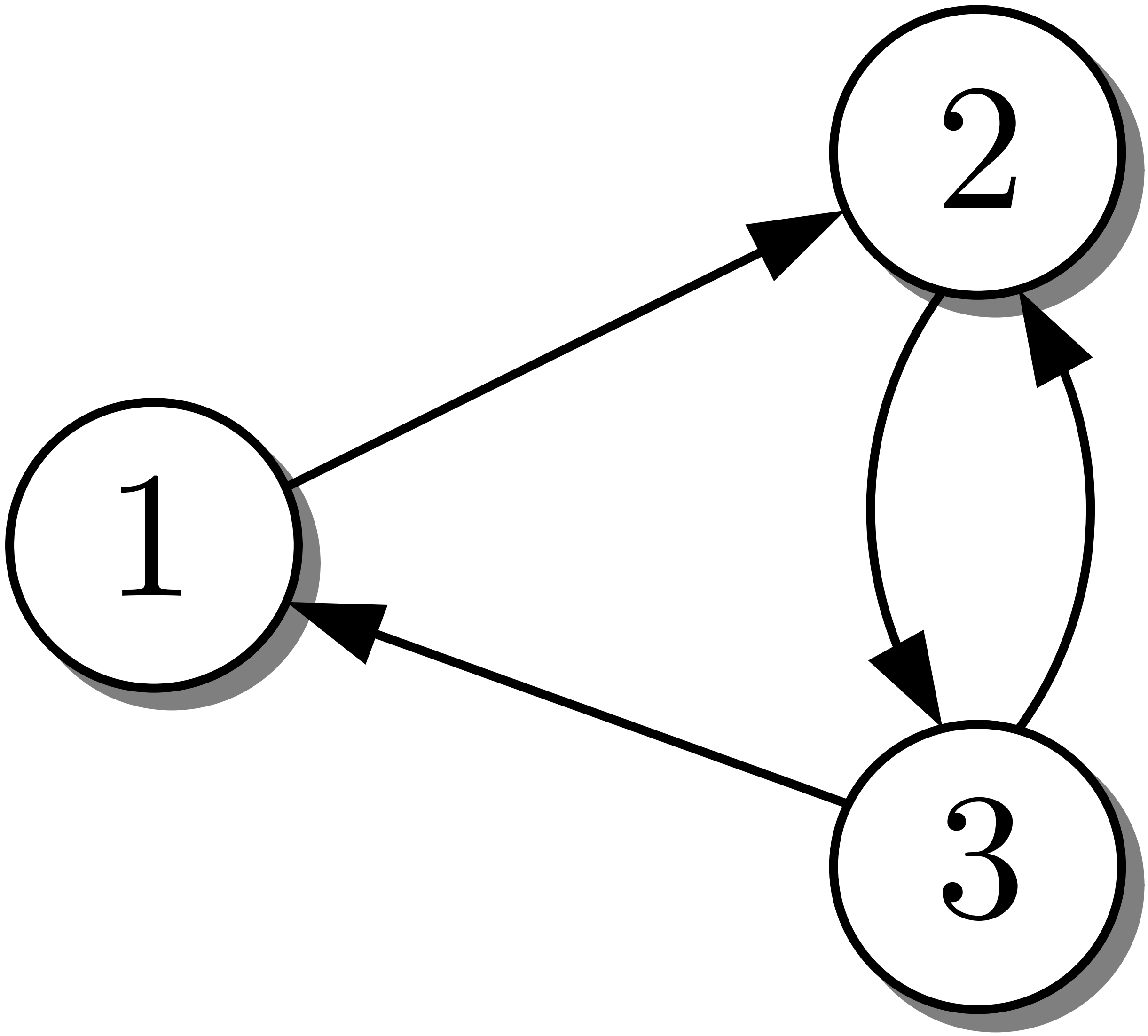

Fig. 3.2: Communication graph considered in Example 3.1

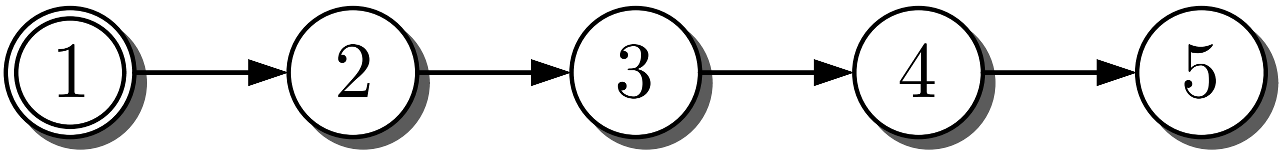

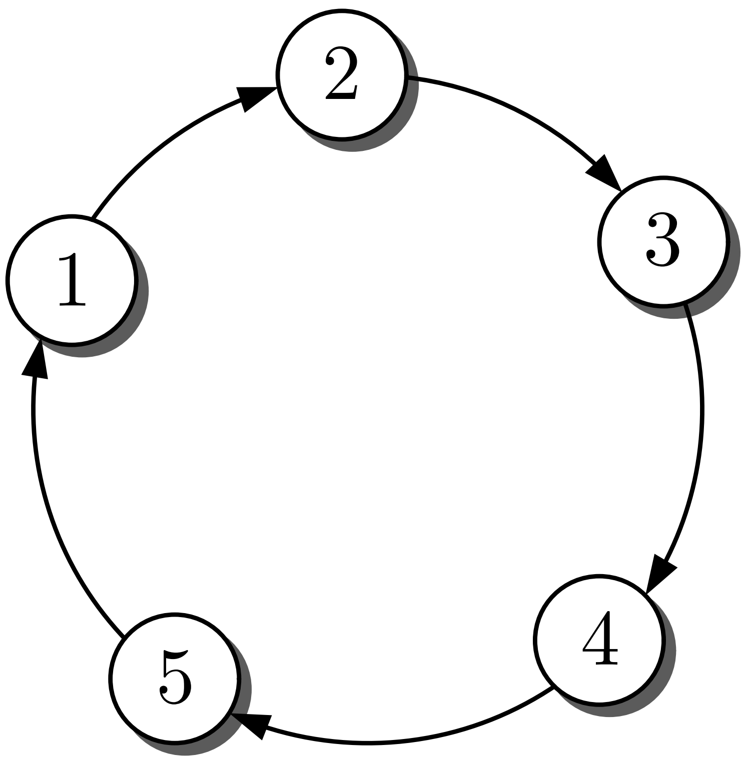

Fig. 3.3: Structure and consensus behaviour of the systems considered in Example 3.2

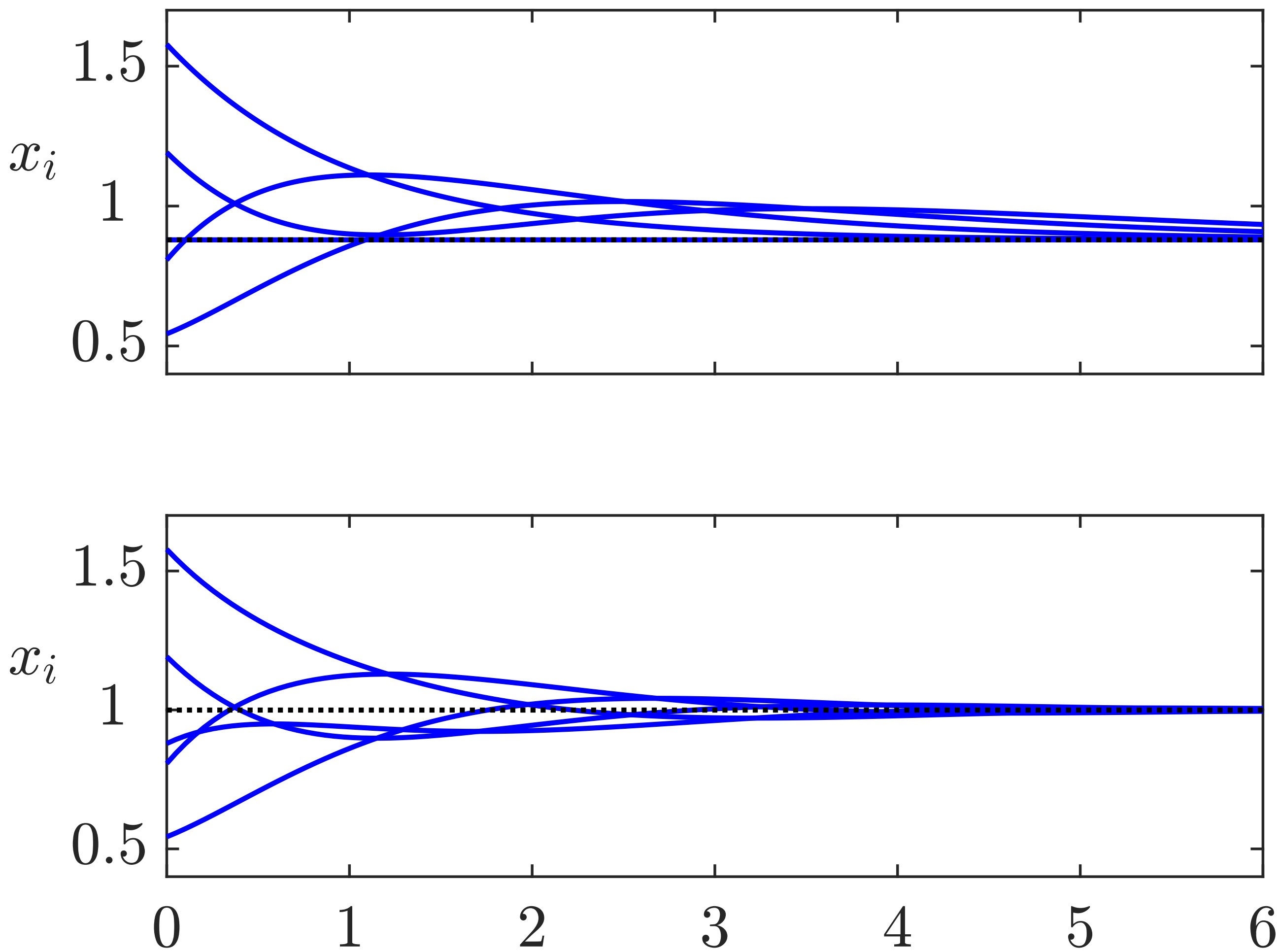

Fig. 3.3: Structure and consensus behaviour of the systems considered in Example 3.2

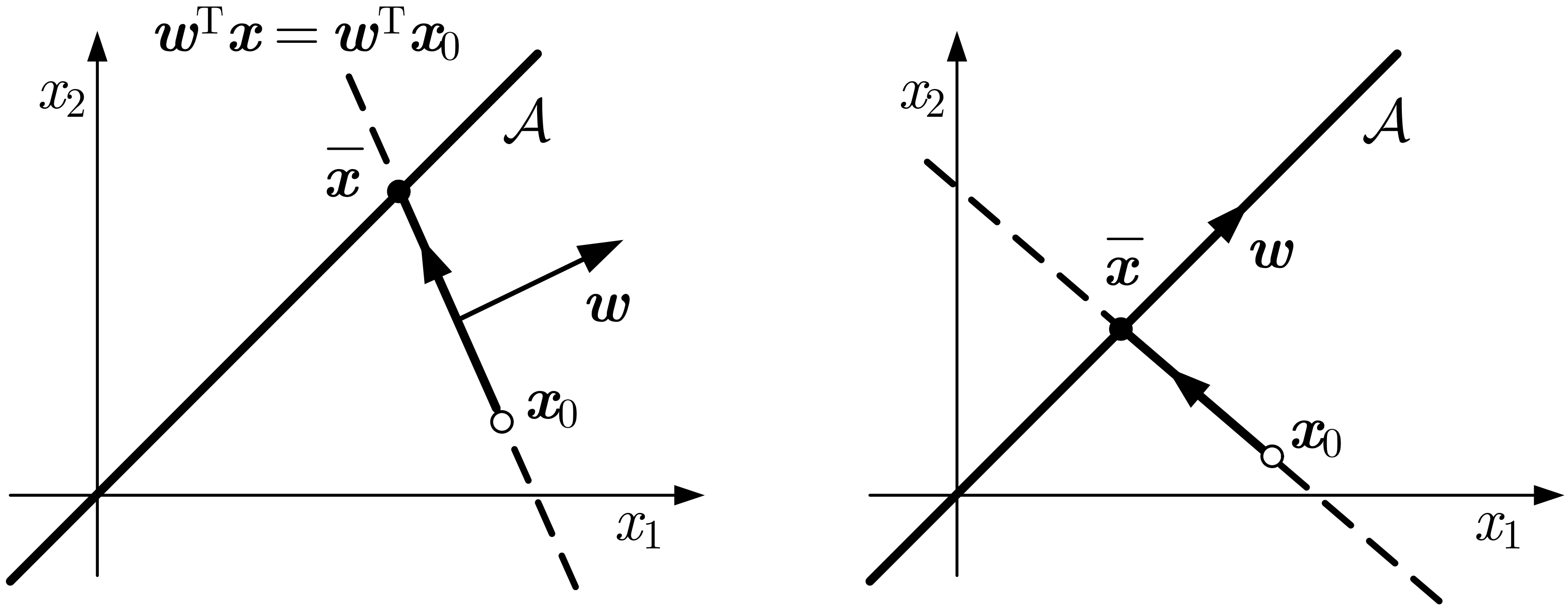

Fig. 3.4. Dynamics towards the consensus value

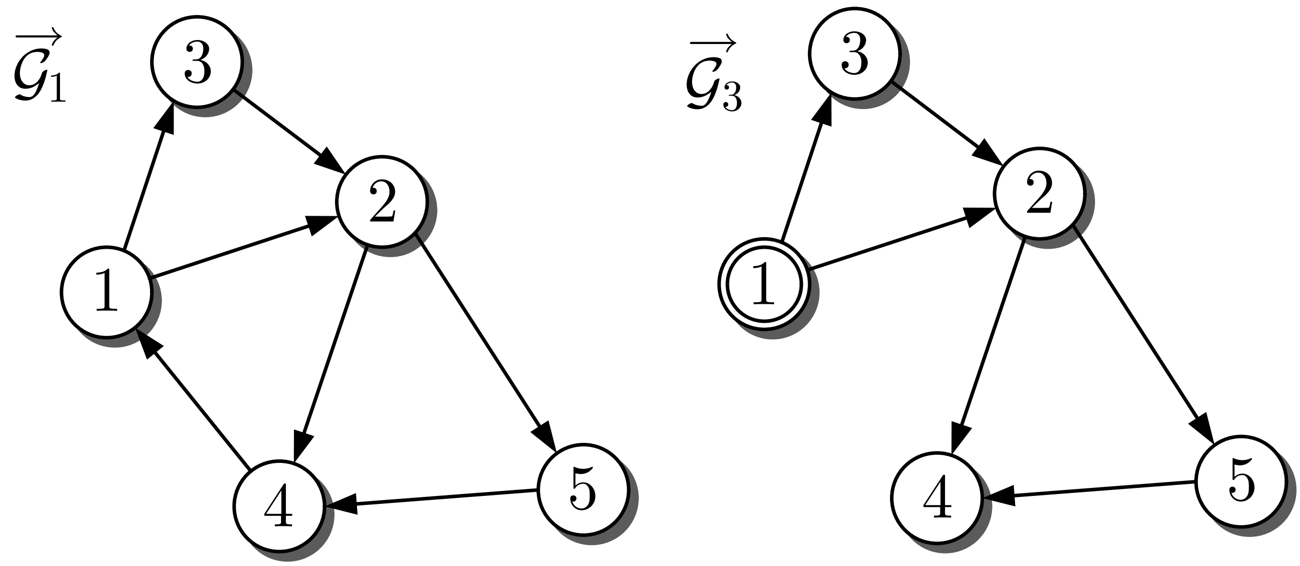

Fig. 3.5: Graphs considered in Example 3.3

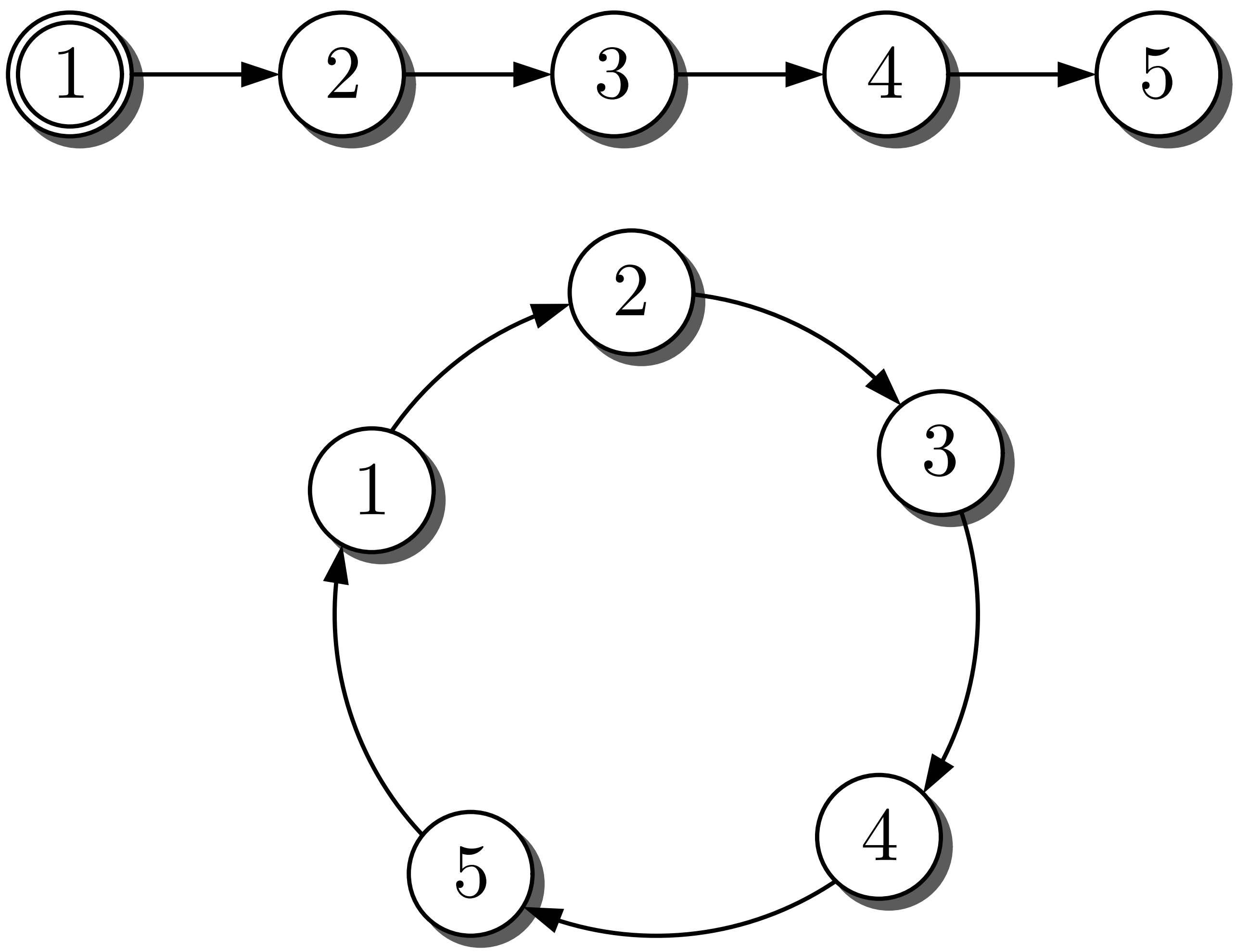

Fig. 3.6: Bounds for the trajectories of the systems with the same structure as in Fig. 3.3 (I)

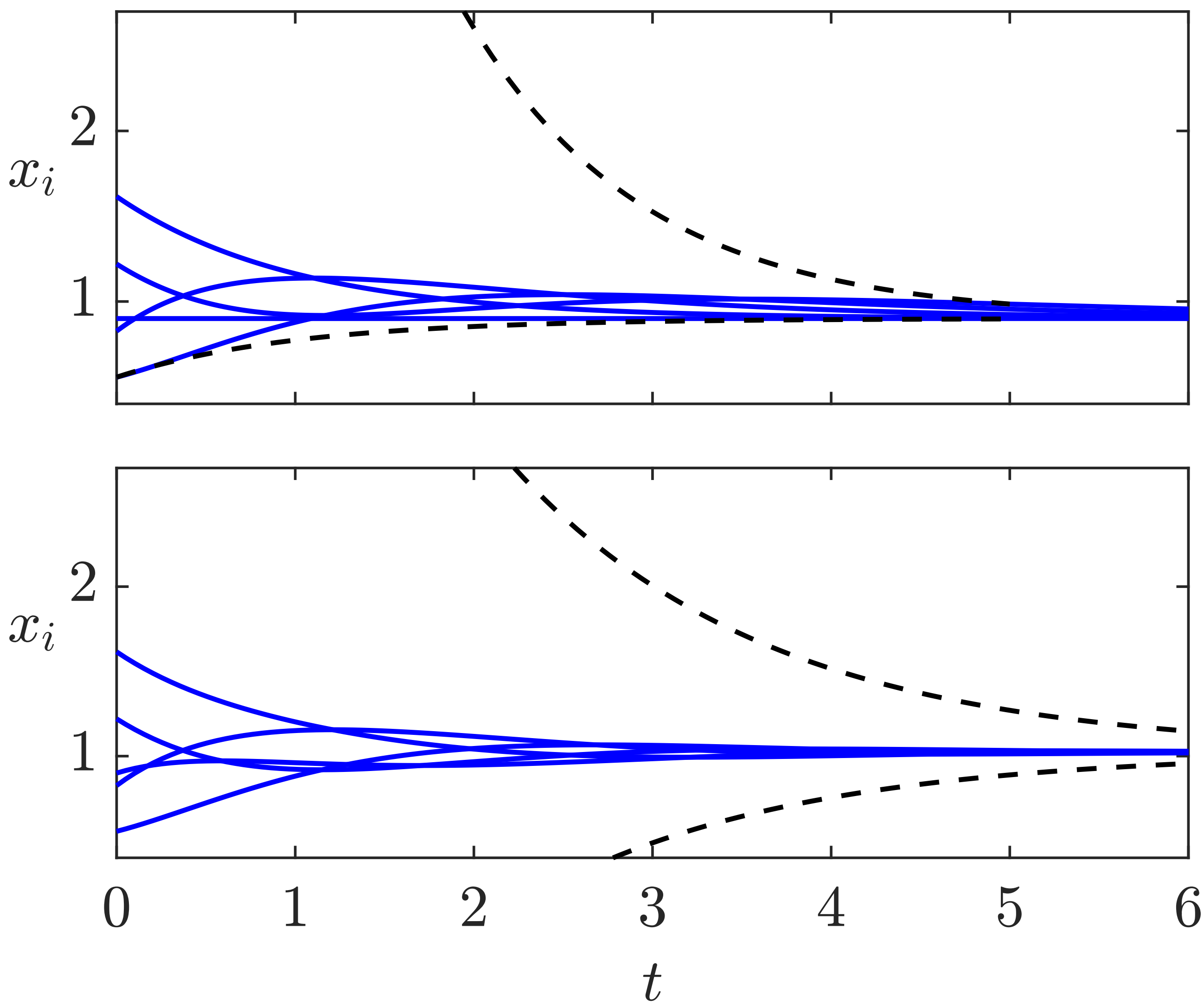

Fig. 3.6: Bounds for the trajectories of the systems with the same structure as in Fig. 3.3 (II)

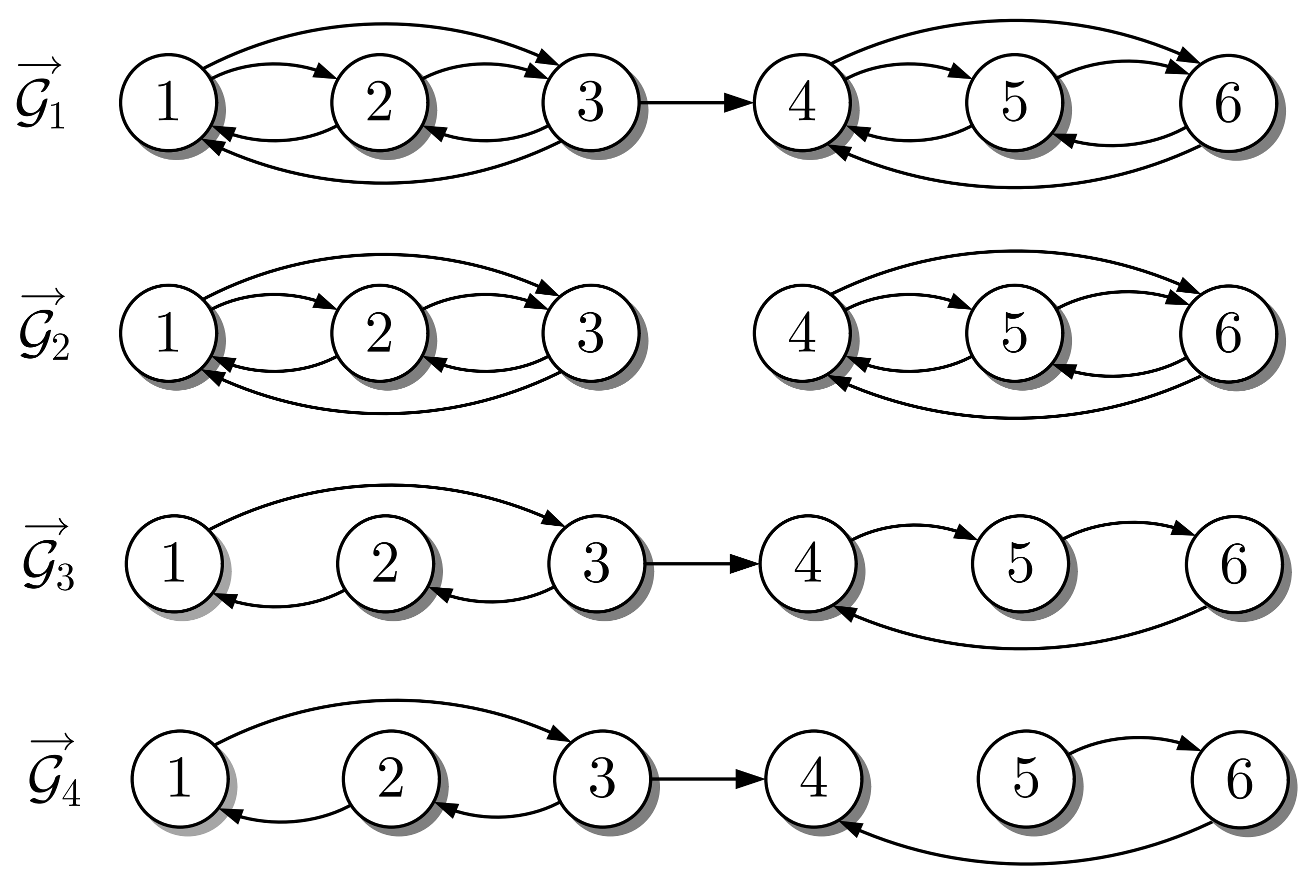

Fig. 3.7: Four directed graphs that are not strongly connected

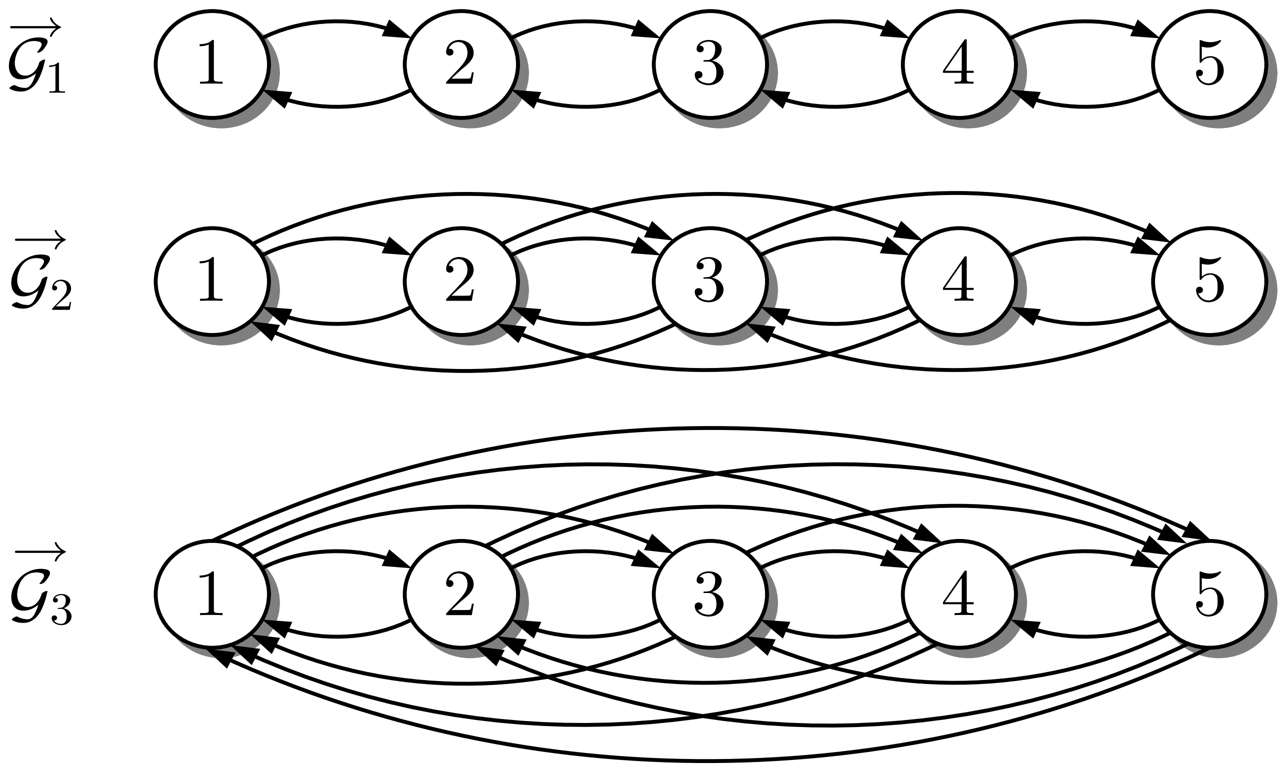

Fig. 3.8: Three directed graphs

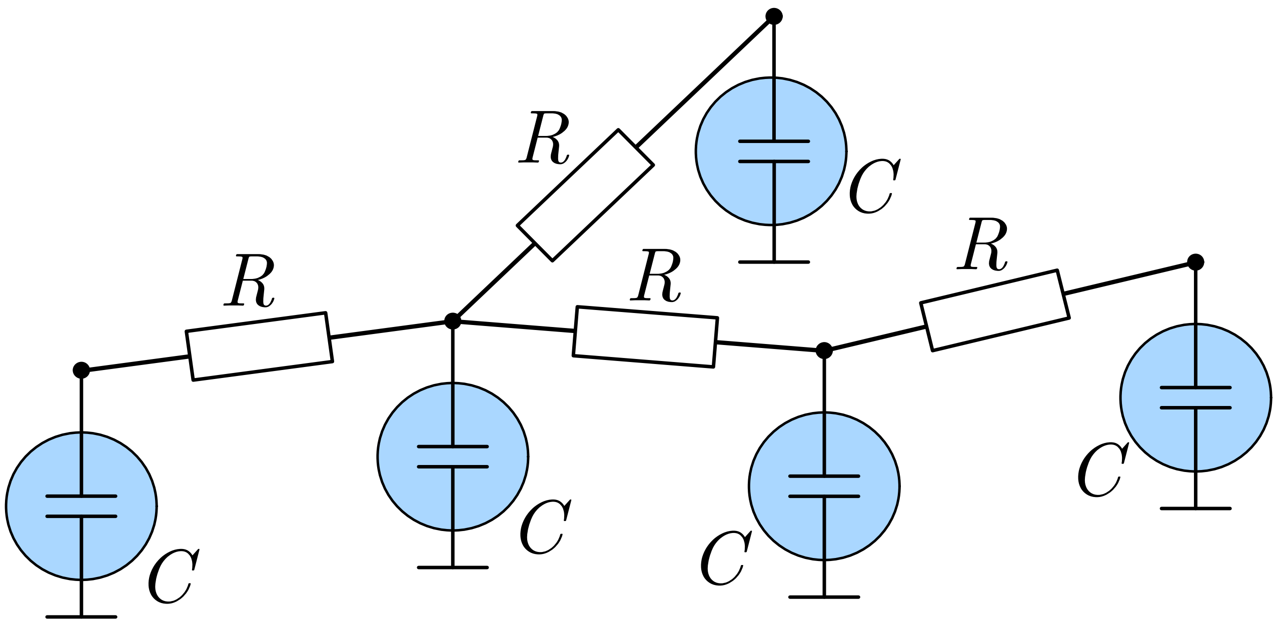

Fig. 3.9: Capacitor network (circuit diagram)

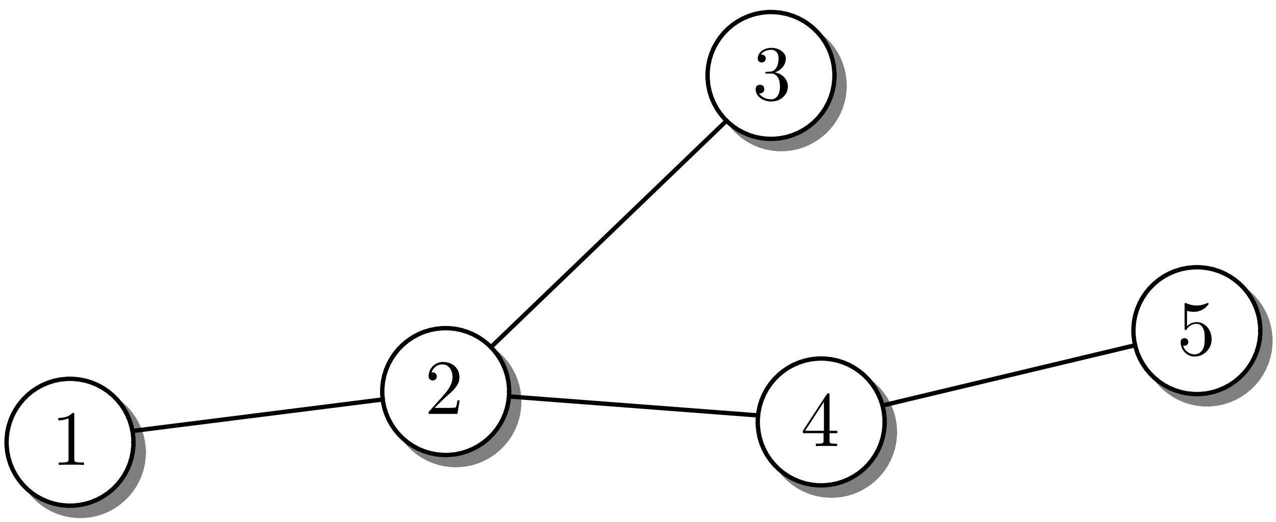

Fig. 3.9: Capacitor network (structure)

J. Lunze: *Networked Control of Multi-Agent Systems*, Edition MoRa 2022

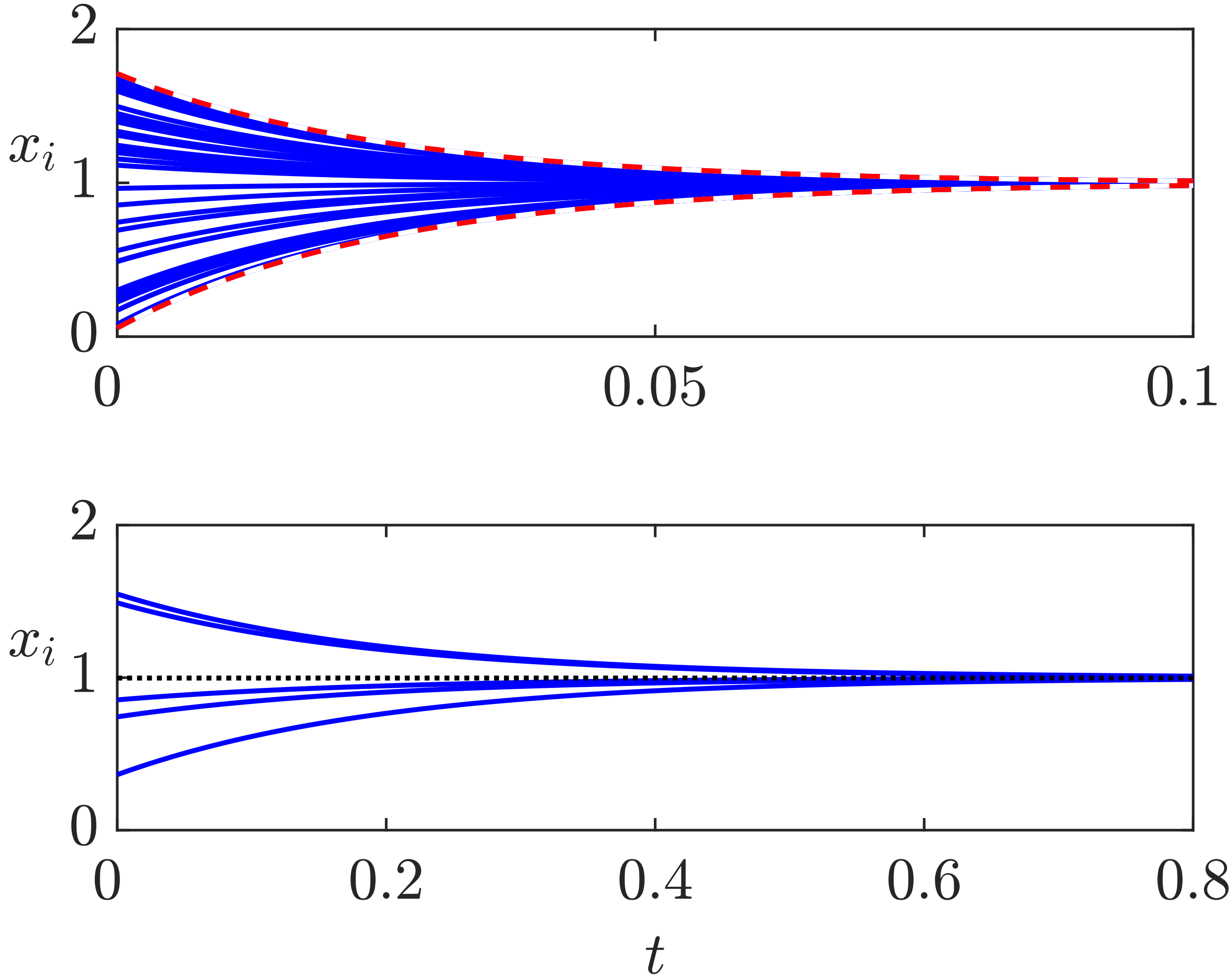

Fig. 3.10: Consensus dynamics of the system $\overline{\Sigma}$ with complete couplings for $N = 40$ (top) and $N = 5$ (bottom)

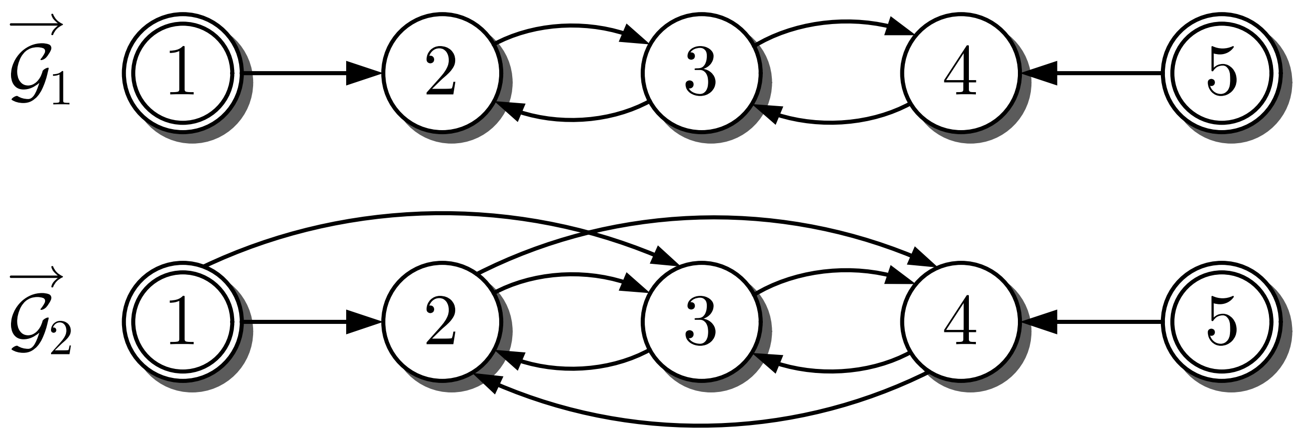

Fig. 3.11: Communication graph of systems with two leaders

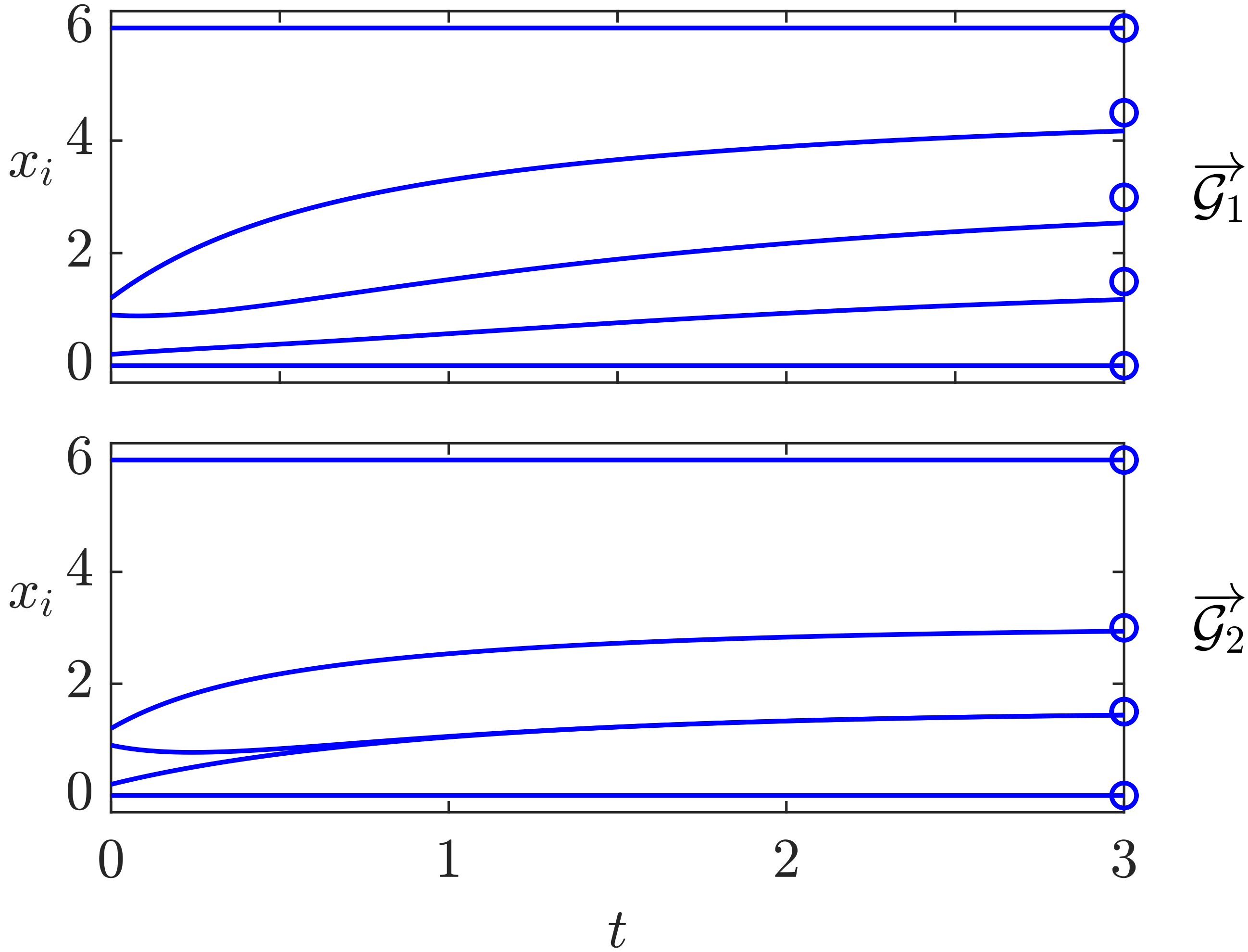

Fig. 3.12: Behaviour of the systems with two leaders

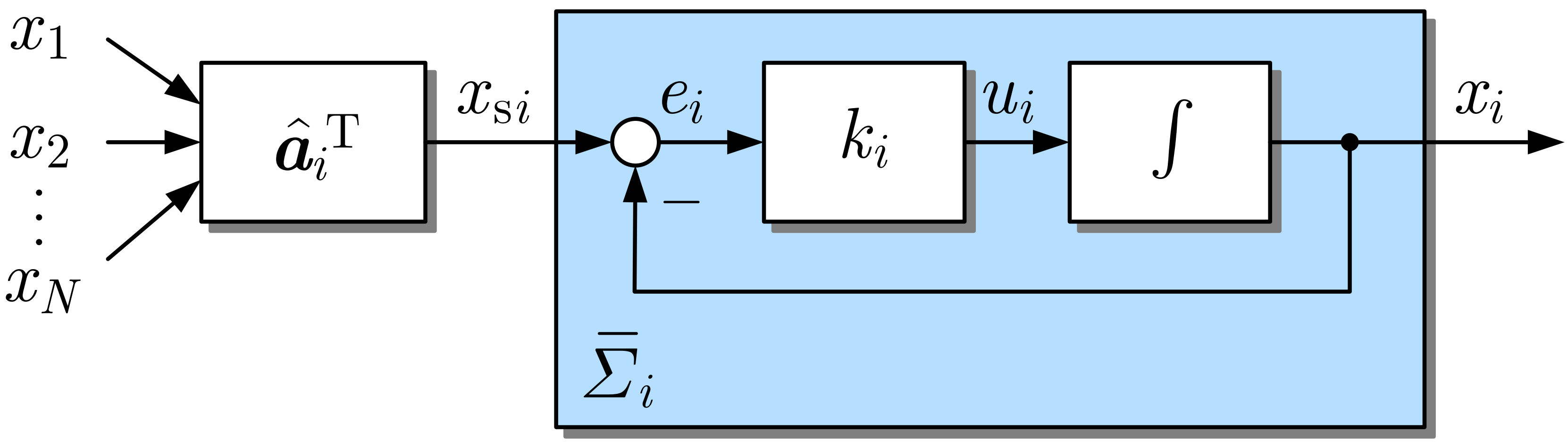

Fig. 3.13. Controlled agent

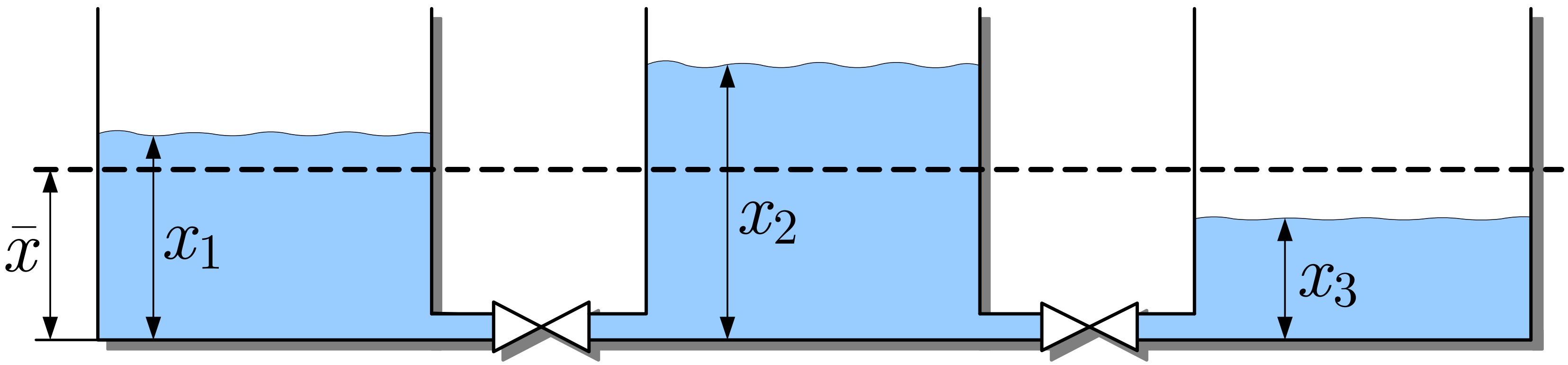

Fig. 3.14. Three coupled vessels

J. Lunze: *Networked Control of Multi-Agent Systems*, Edition **M**o**R**a 2022

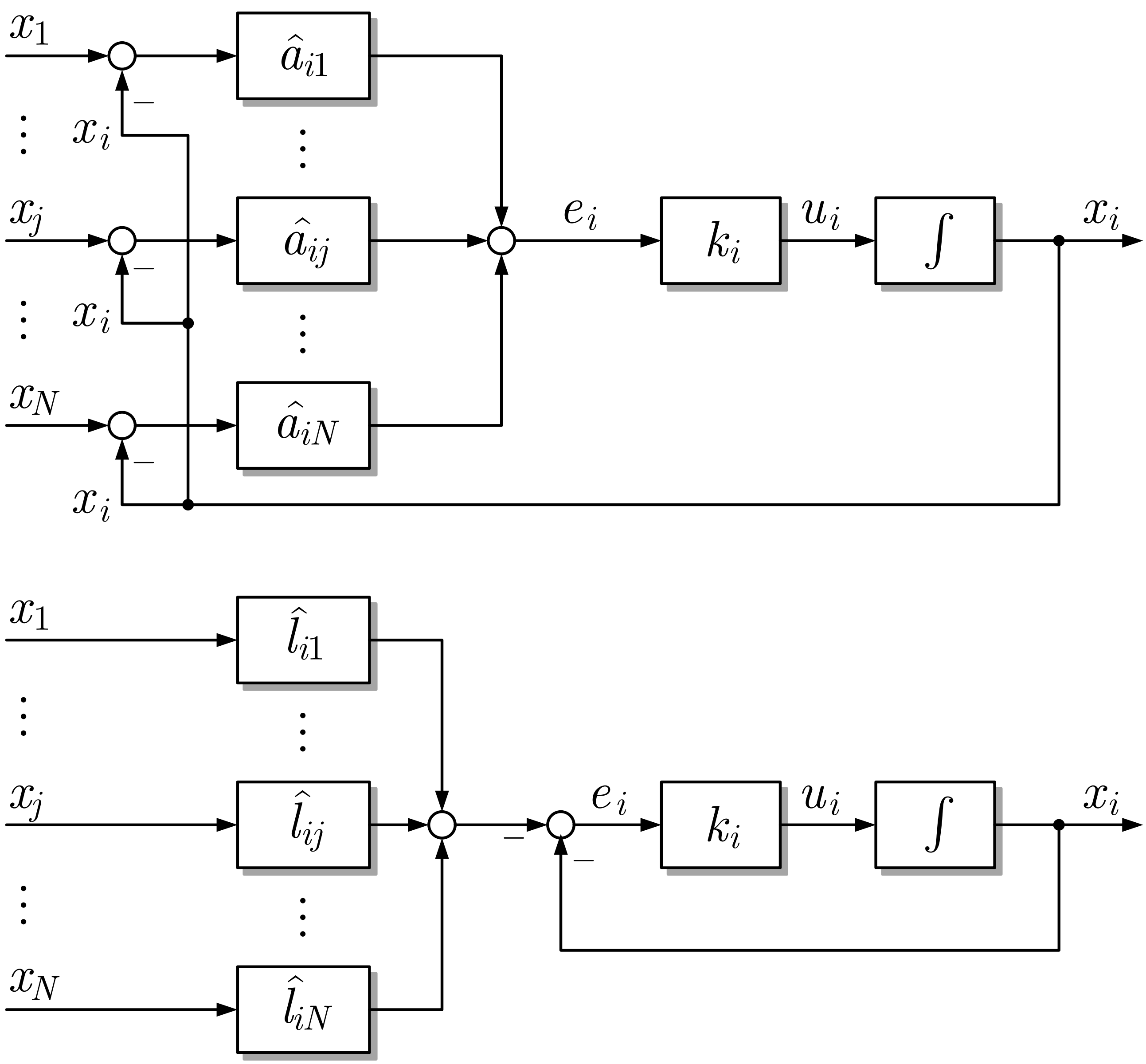

Fig. 3.15: Two implementation schemes of a consensus protocol

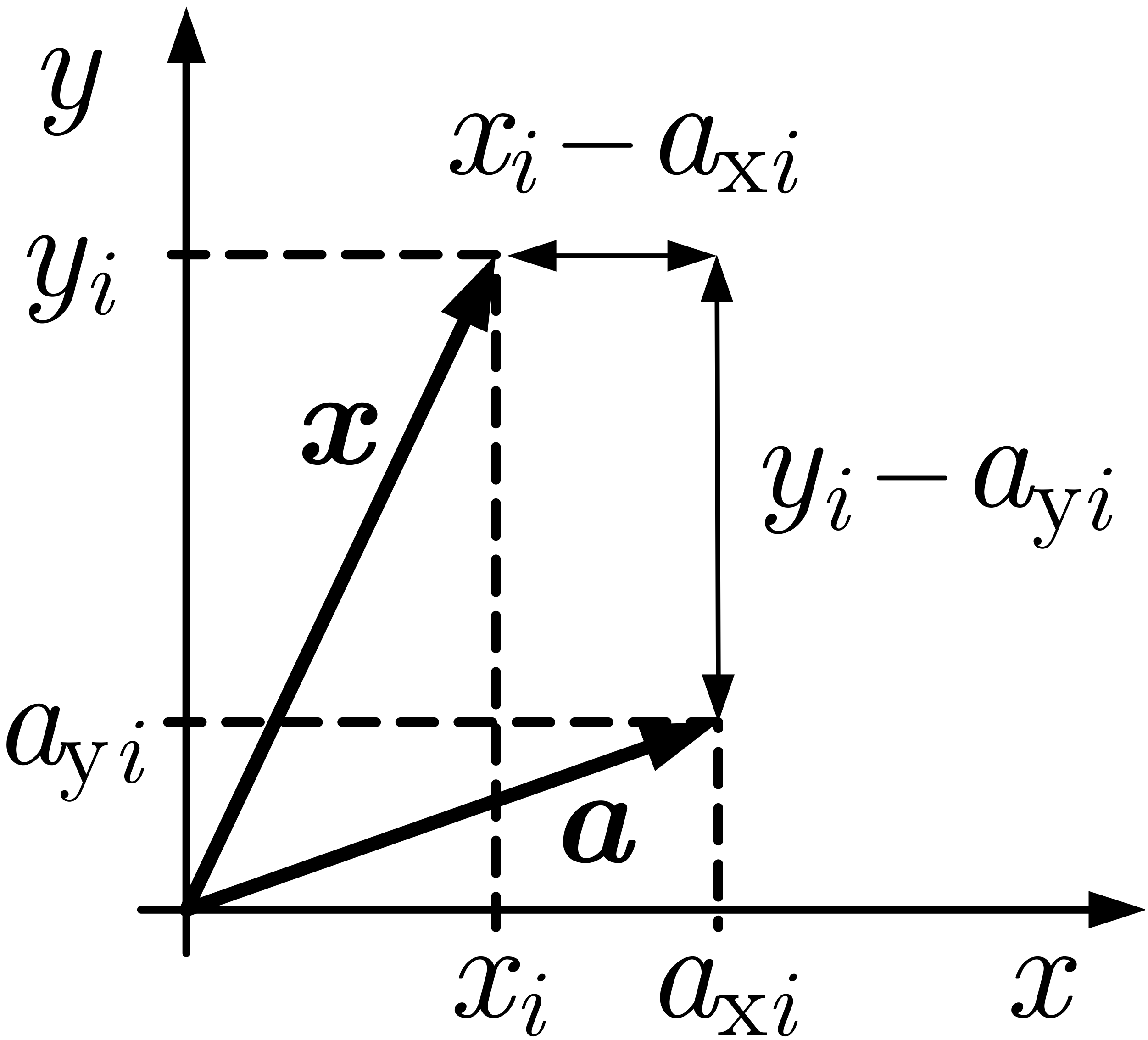

Fig. 3.16: Definition of a formation

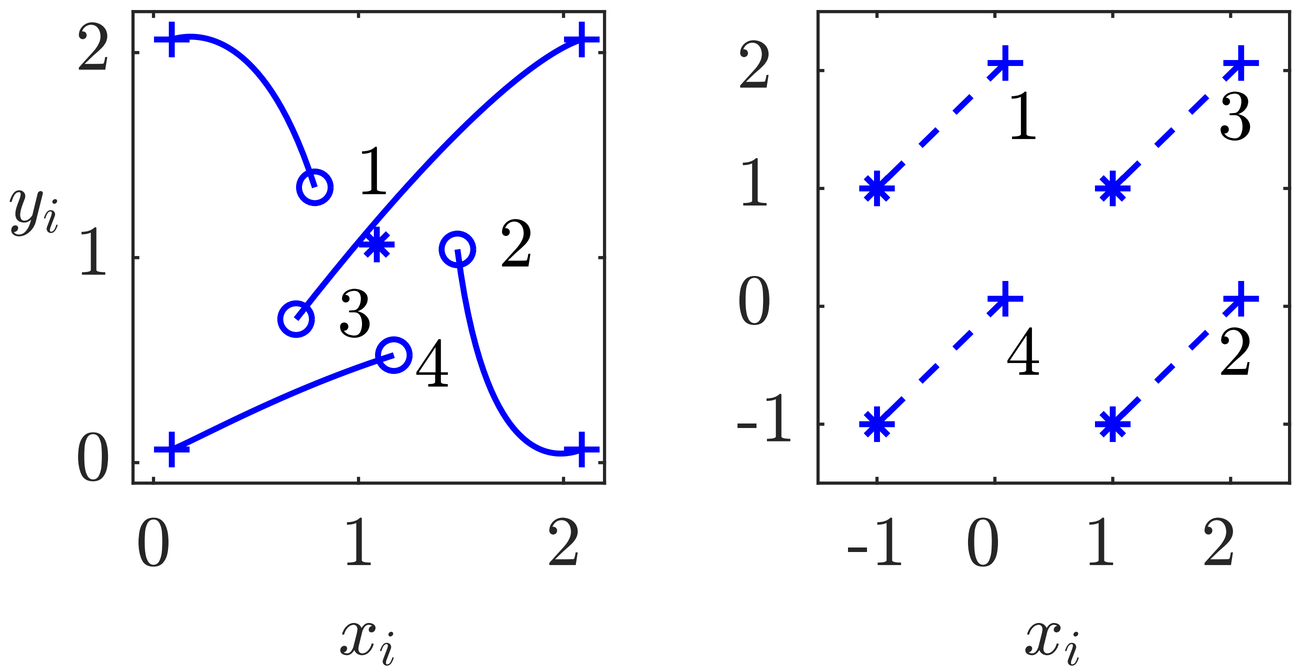

Fig. 3.17: Formation control

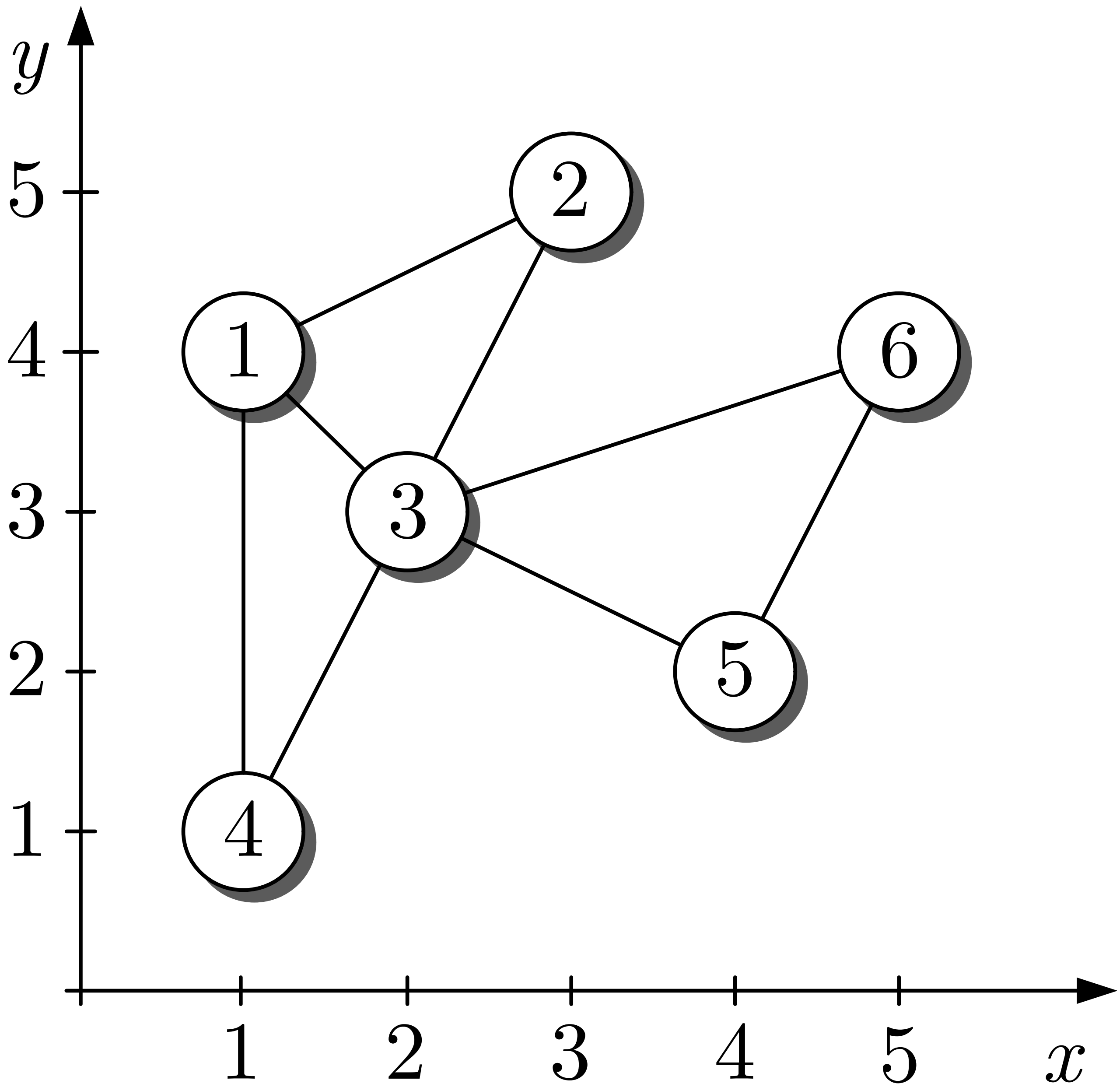

Fig. 3.18: Six robots distributed in the x/y-space

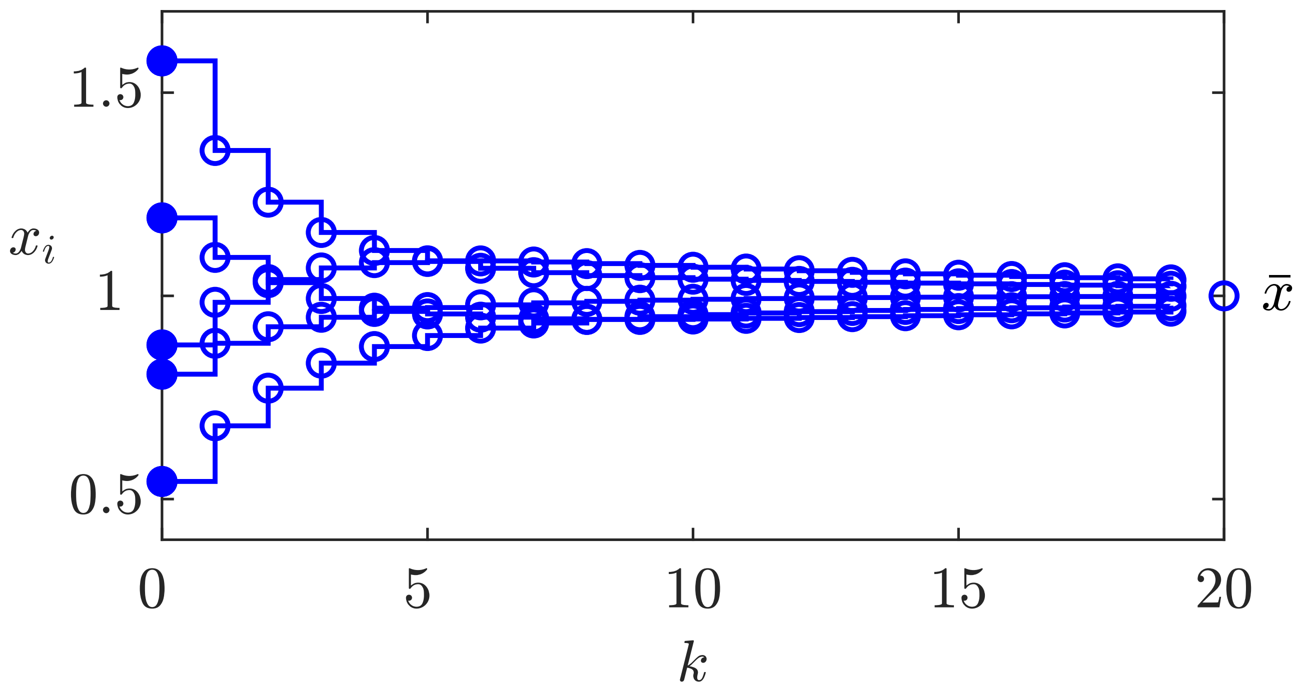

Fig. 3.19: Results of the distributed estimation algorithm

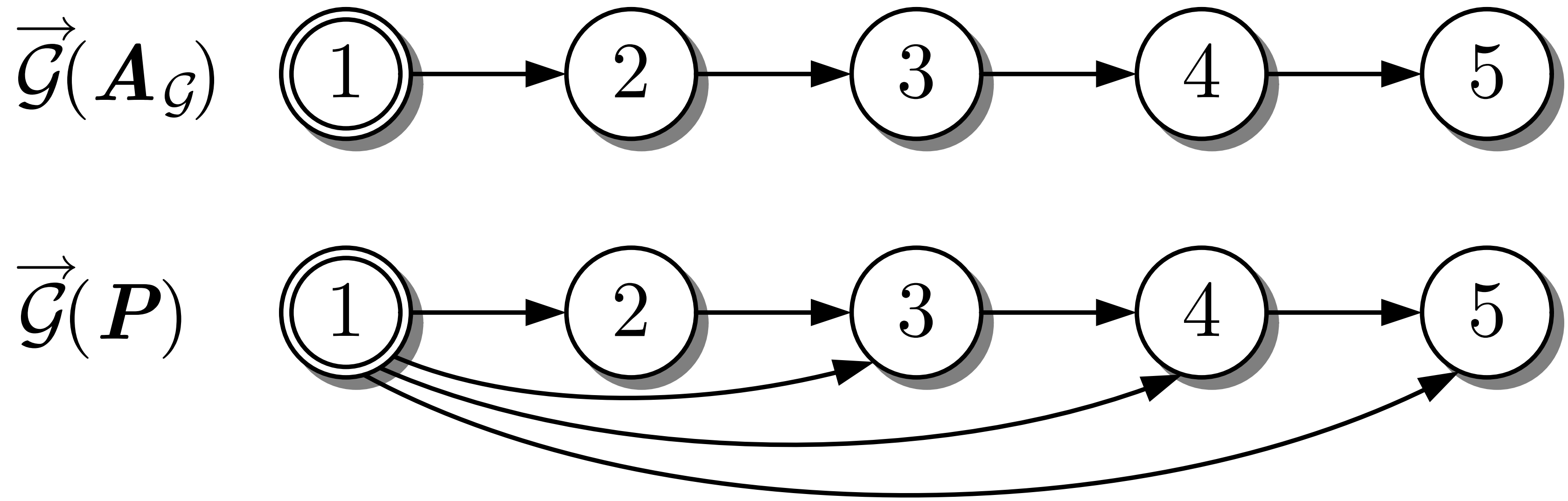

Fig. 3.20. Communication graph of a continuous-time consensus system and the graph induced by the matrix of the discrete-time counterpart

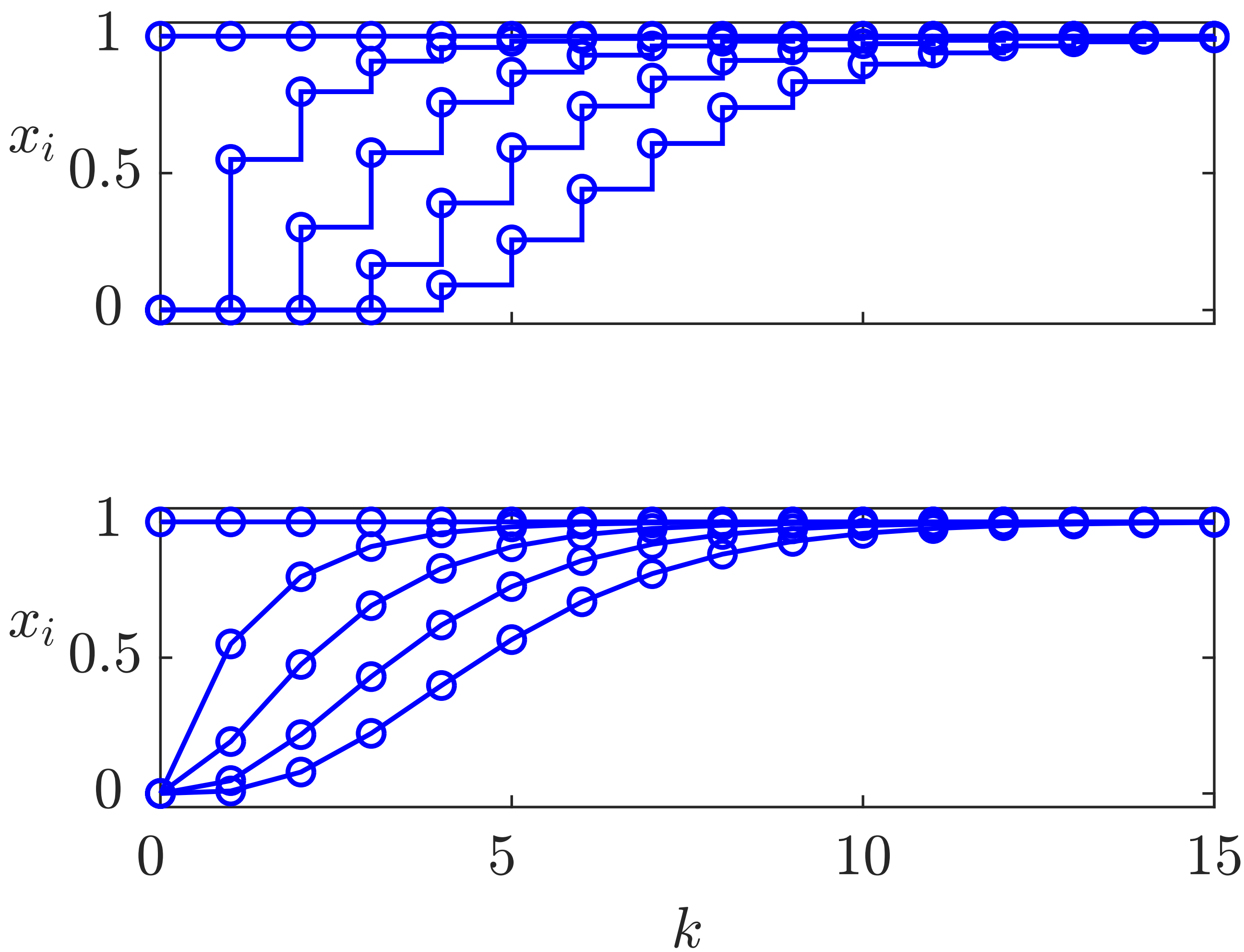

Fig. 3.21: Discrete-time consensus

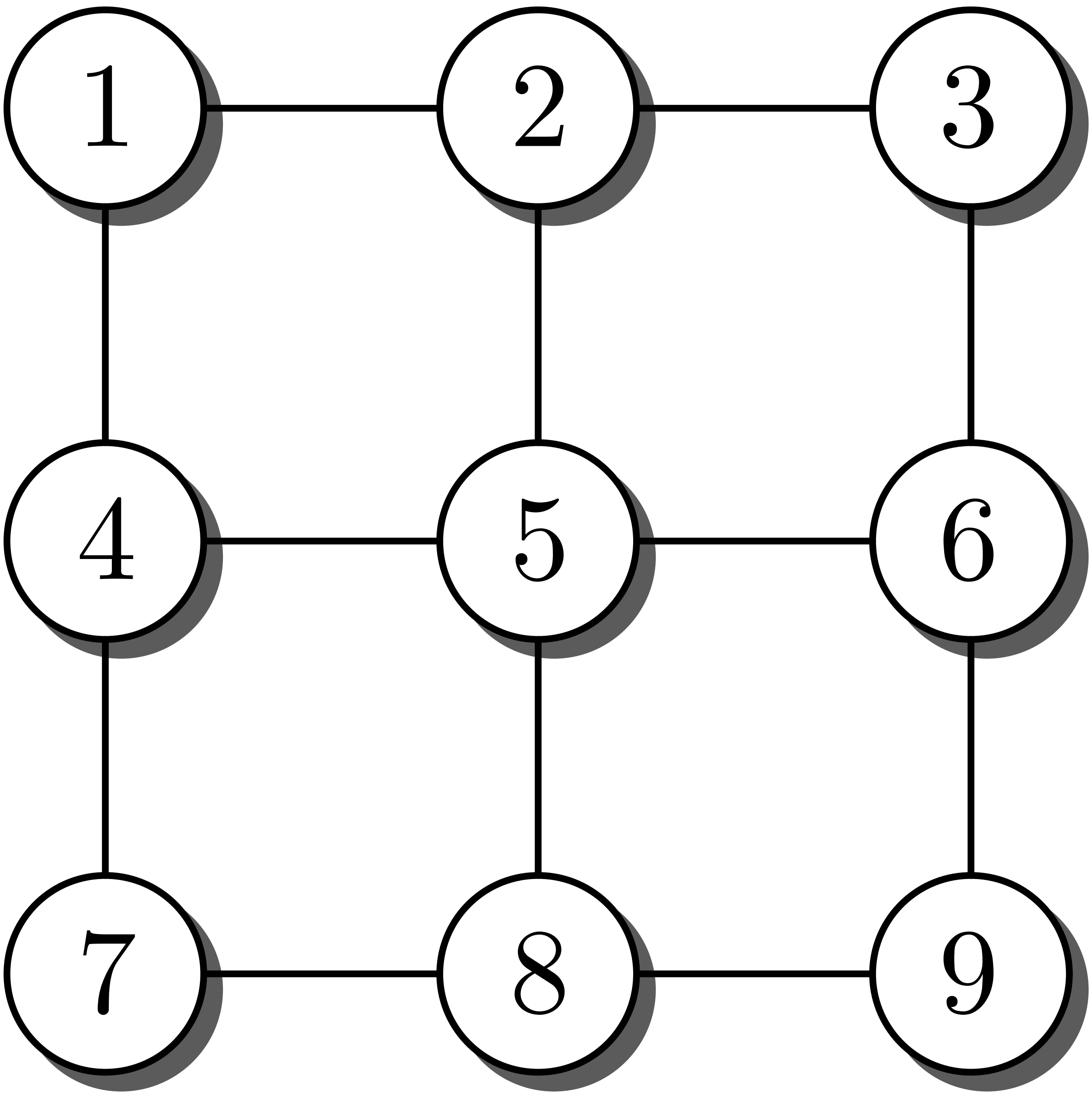

Fig. 3.22: Grid structure of the multiprocessor system

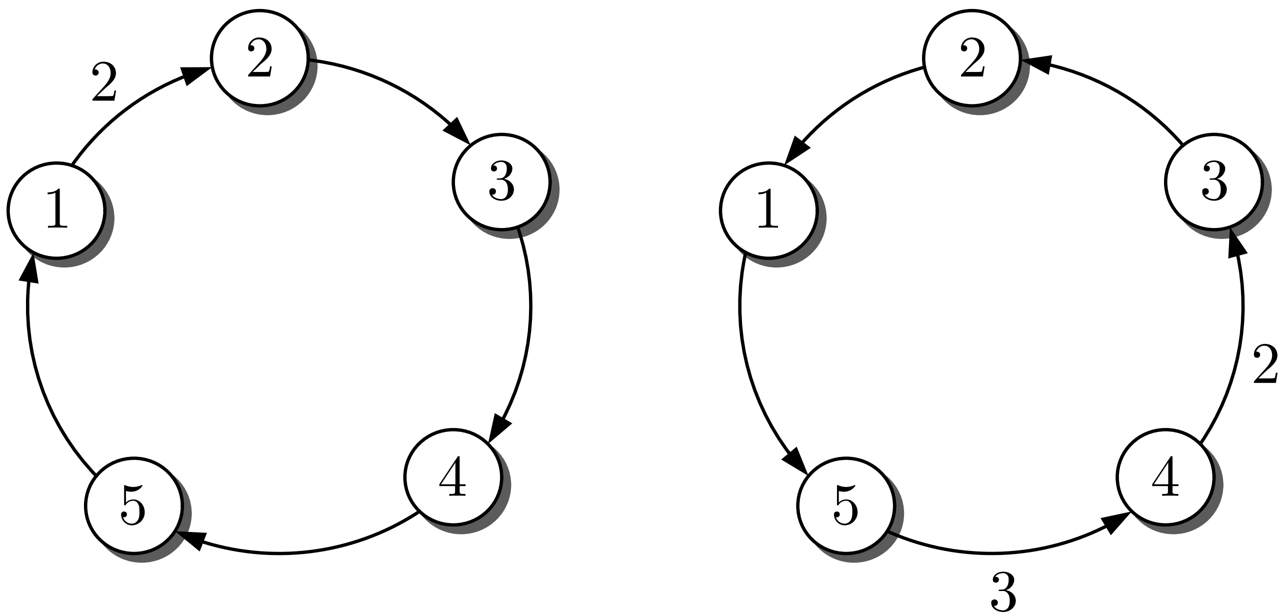

Fig. 3.23: Two graphs considered in Example 3.10

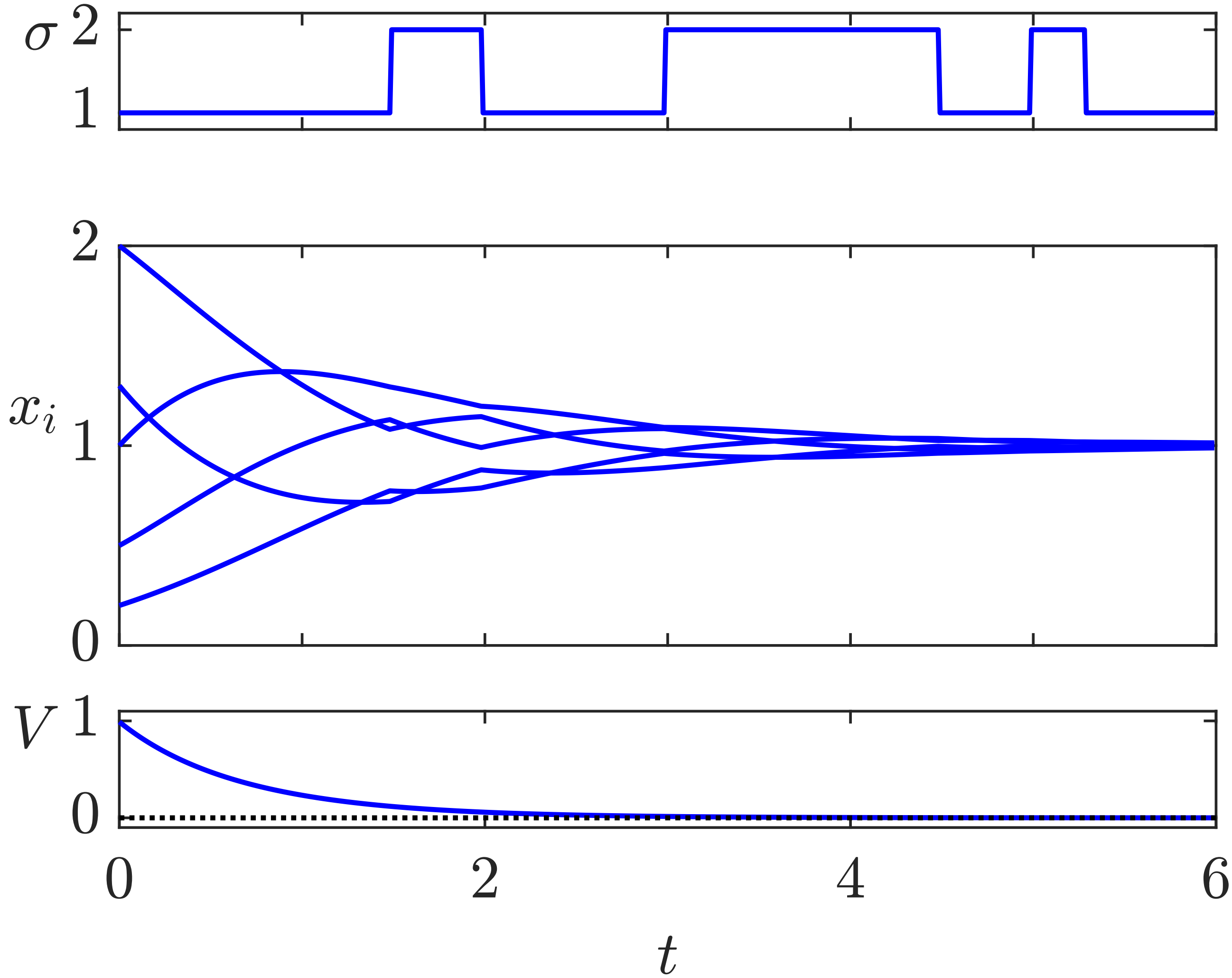

Fig. 3.24: Behaviour of the switching system with strongly connected, weight-balanced graphs

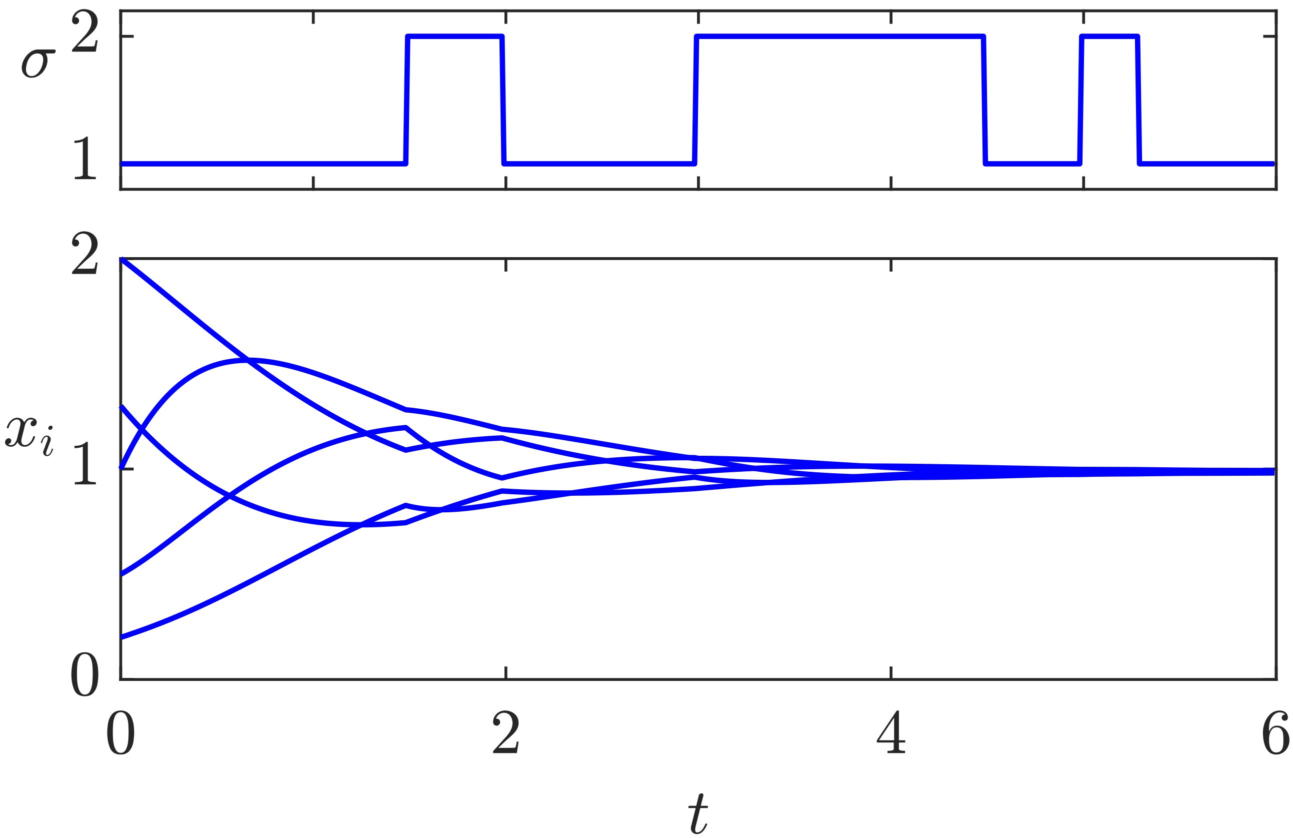

Fig. 3.25: Consensus behaviour of the same system with the same initial state but different switching functions (I)

J. Lunze: *Networked Control of Multi-Agent Systems,* Edition MoRa 2022

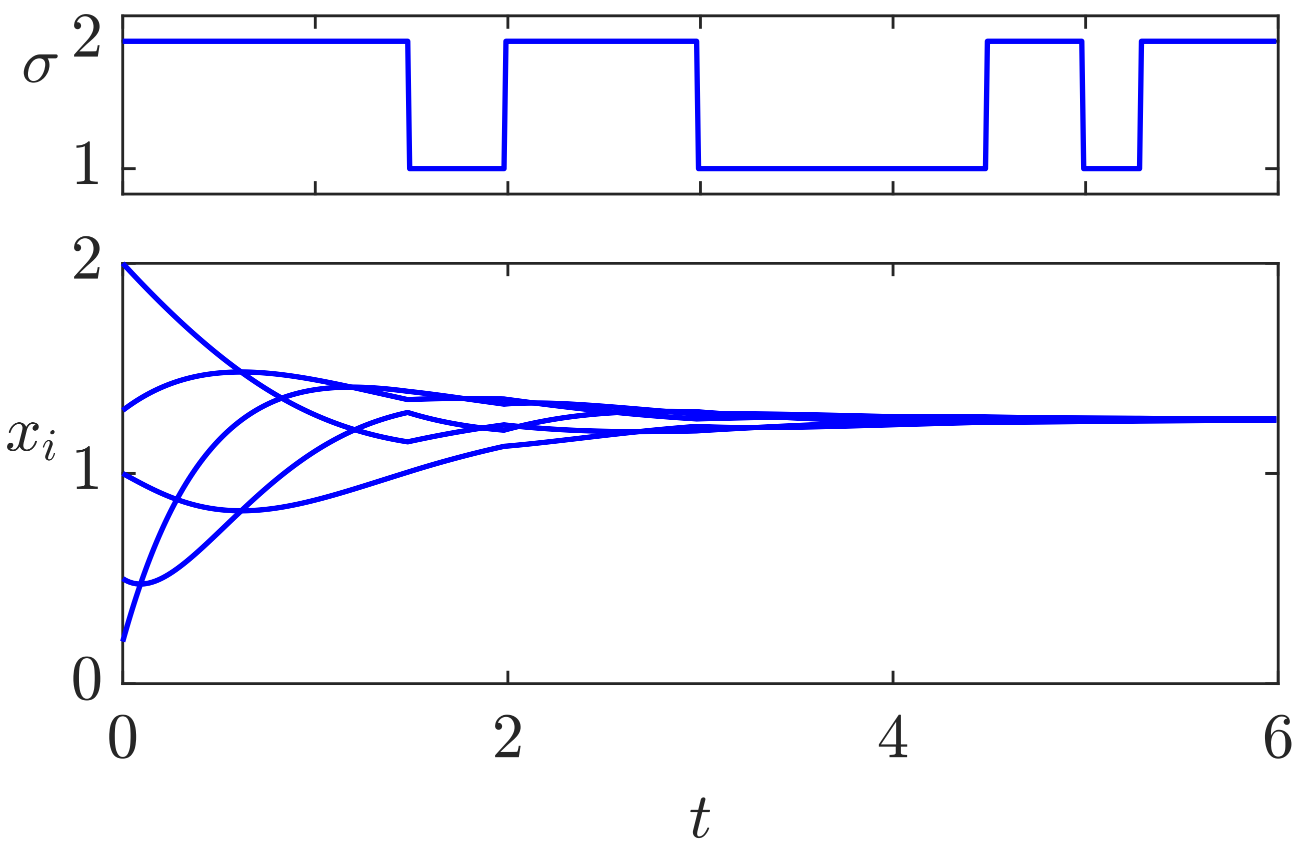

Fig. 3.25: Consensus behaviour of the same system with the same initial state but different switching functions (II)

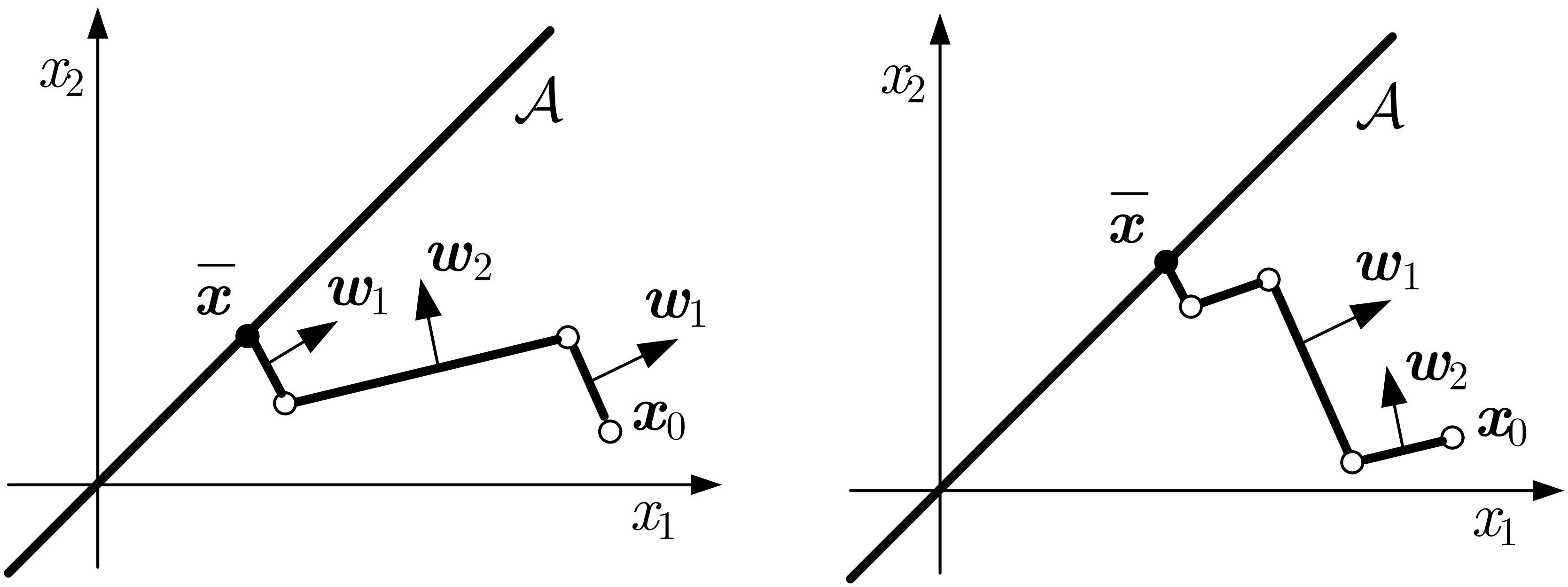

Fig. 3.26. Two state trajectories of a switching consensus system

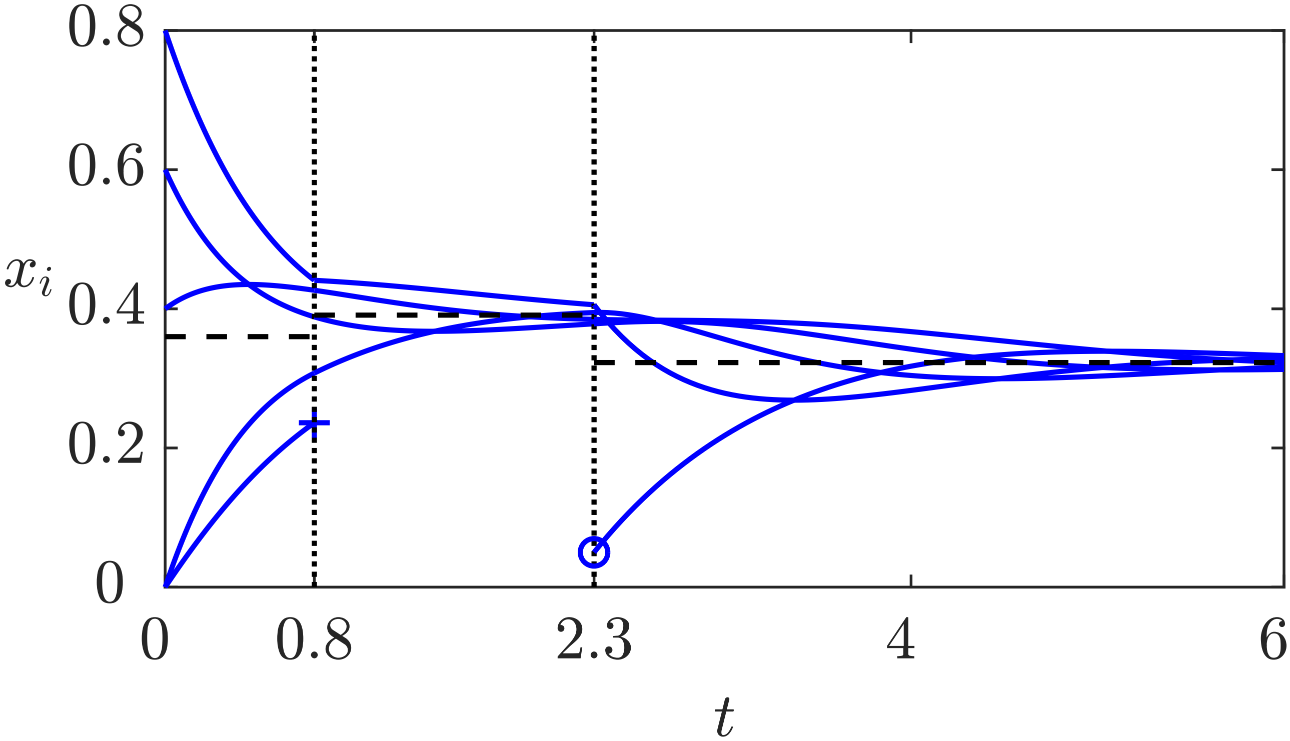

Fig. 3.27: Behaviour of the network with changing number of agents

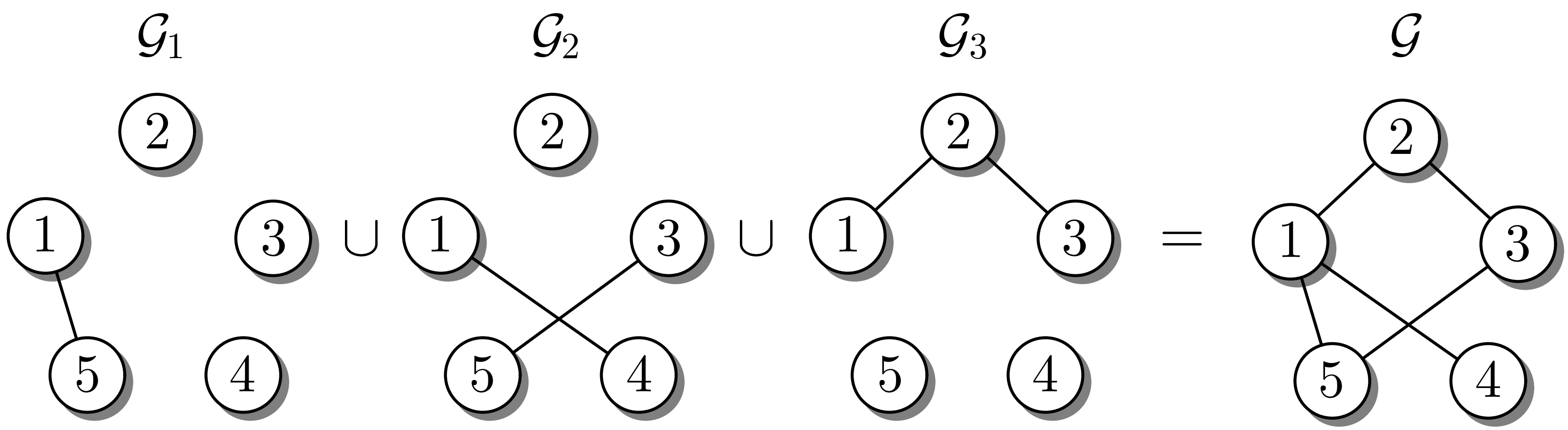

Fig. 3.28. Sequence of graphs

J. LUNZE: *Networked Control of Multi-Agent Systems*, Edition **M**o**R**a 2022

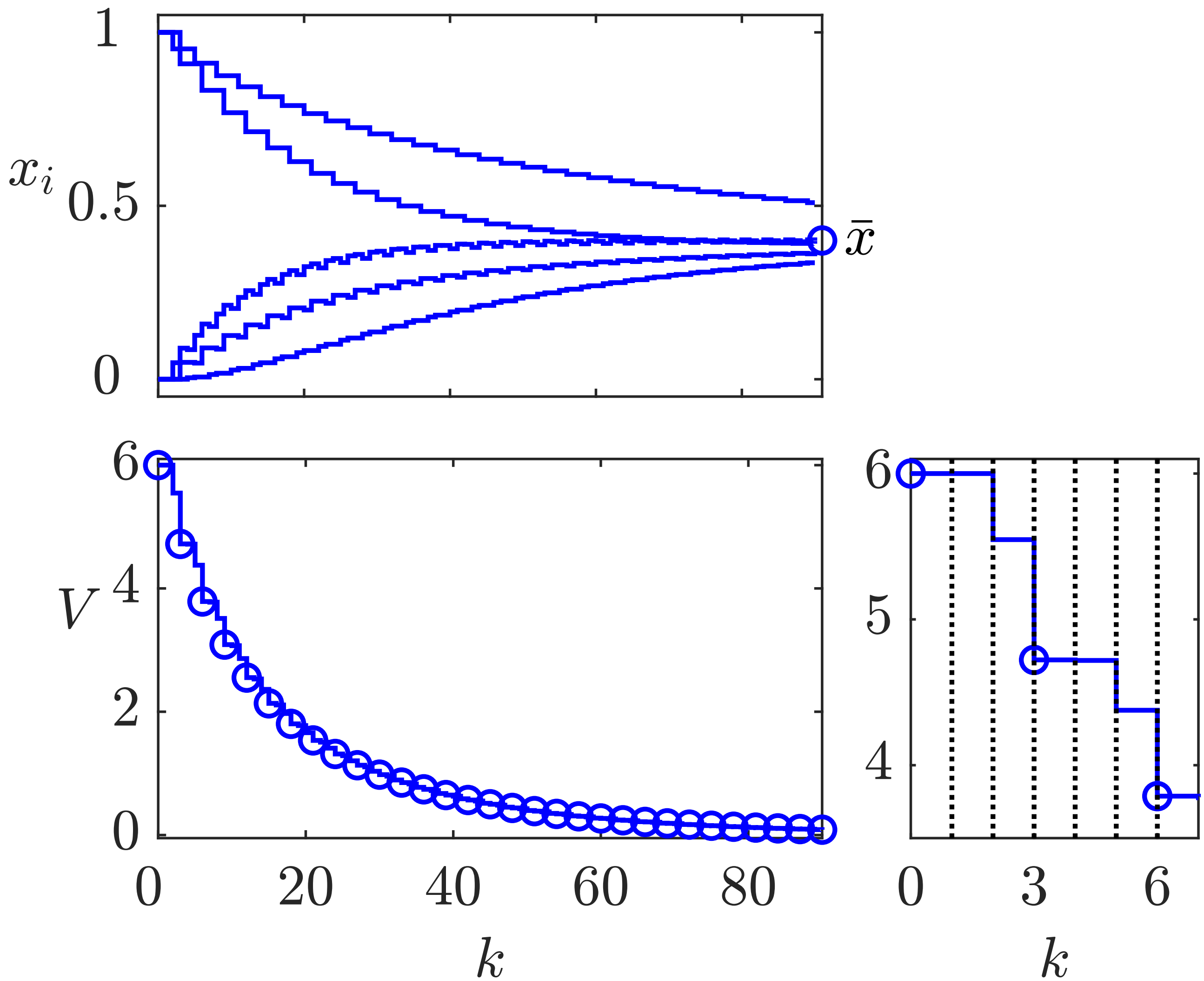

Fig. 3.29: Consensus behaviour of the switching system

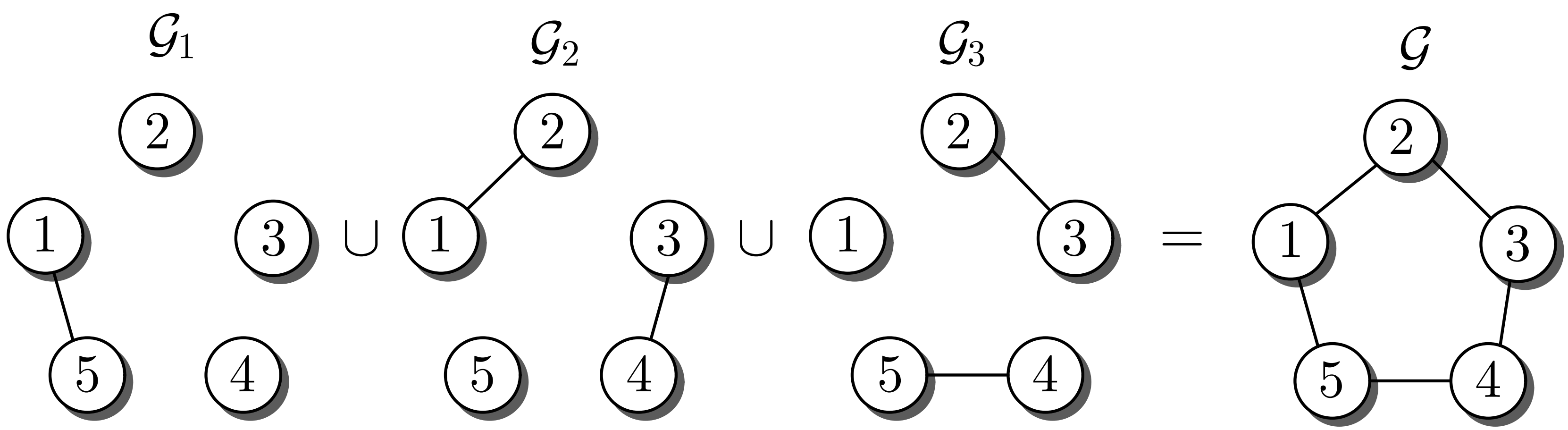

Fig. 3.30. Communication structure of a gossiping algorithm

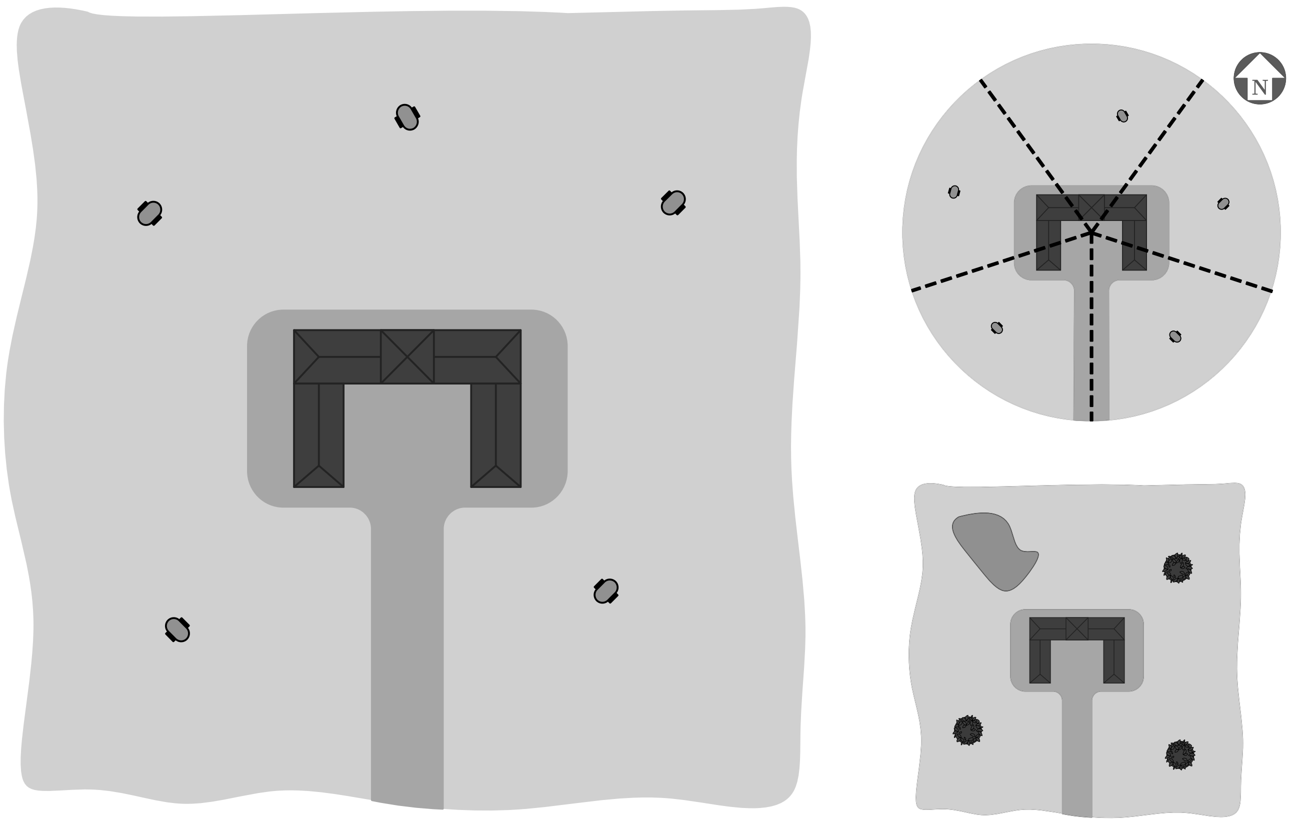

Fig. 3.31: Site plan of a real estate (left) and detailed plans (right)

J. Lunze: *Networked Control of Multi-Agent Systems*, Edition **MoRa** 2022

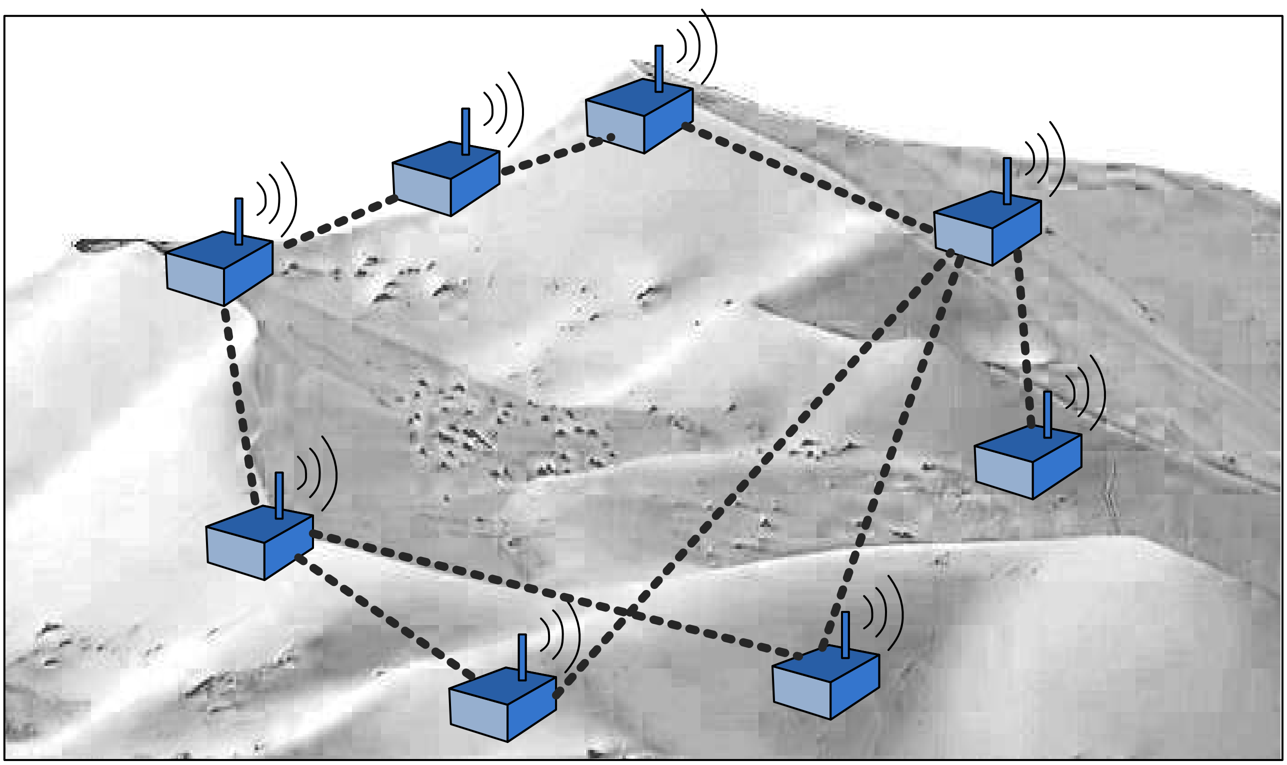

Fig. 3.32: Sensor network

J. Lunze: *Networked Control of Multi-Agent Systems,* Edition **MoRa** 2022

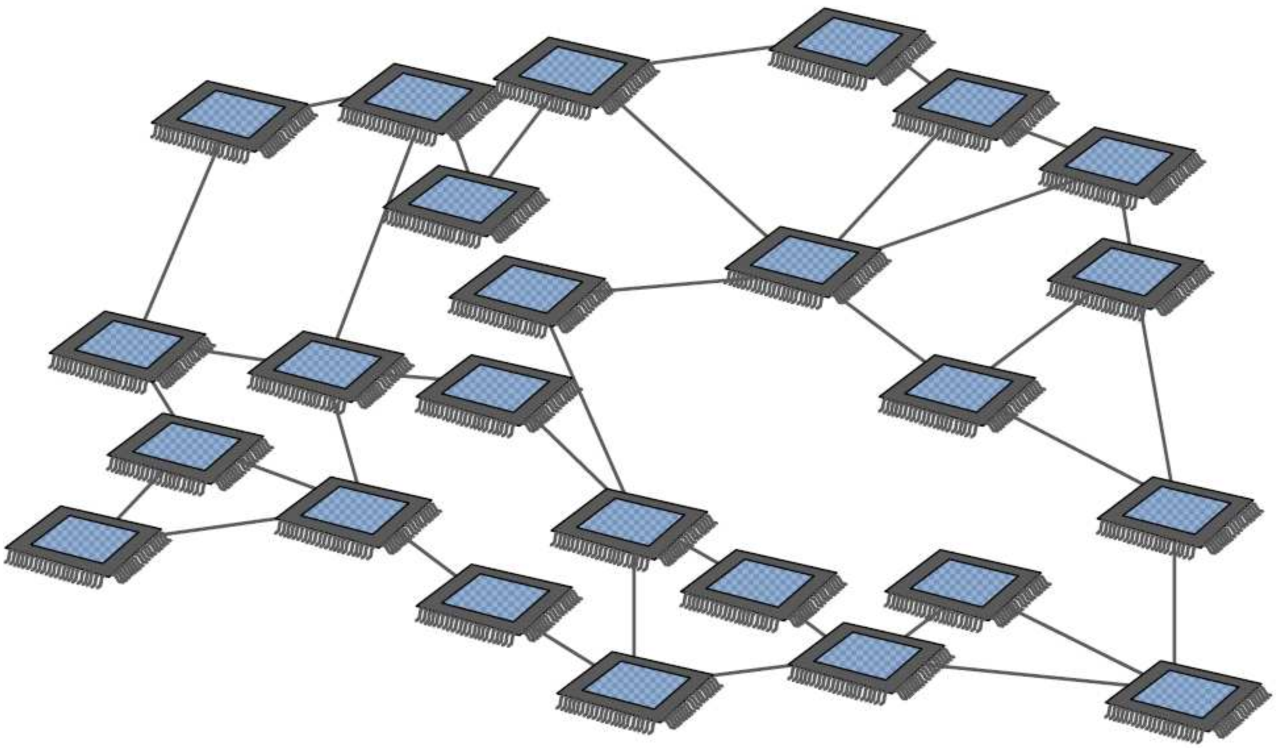

Fig. 3.33: Networked processors cooperate to solve a linear equation

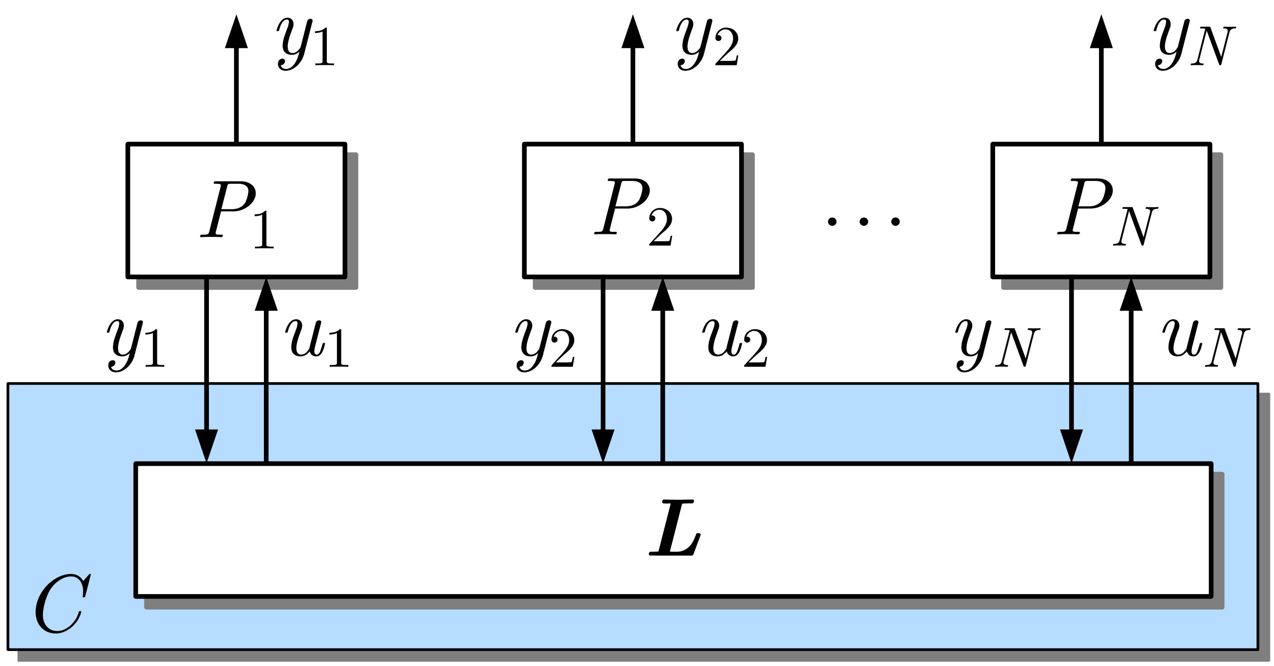

Fig. 4.1: Networked control of multi-agent systems with static couplings

J. Lunze: *Networked Control of Multi-Agent Systems*, Edition MoRa 2022

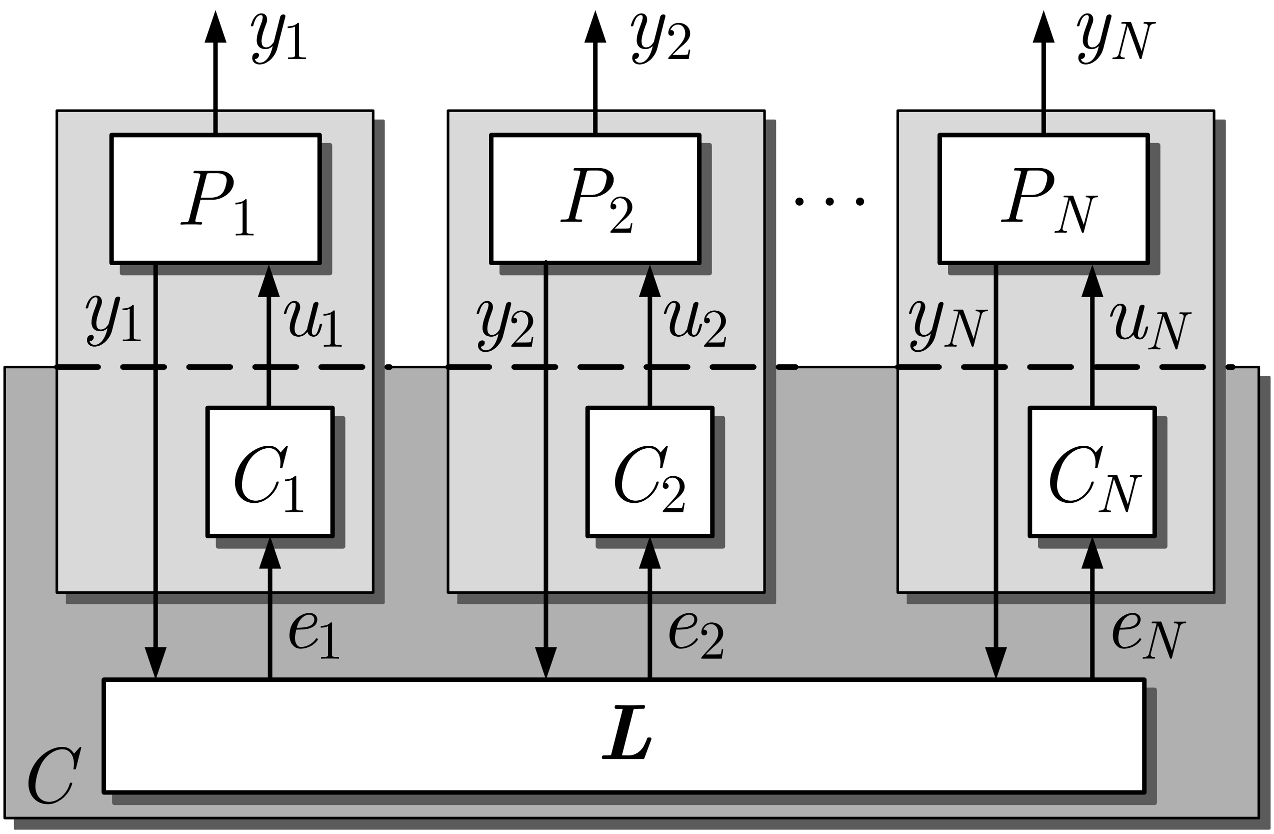

Fig. 4.1: Networked control of multi-agent systems with dynamical couplings

J. Lunze: *Networked Control of Multi-Agent Systems*, Edition MoRa 2022

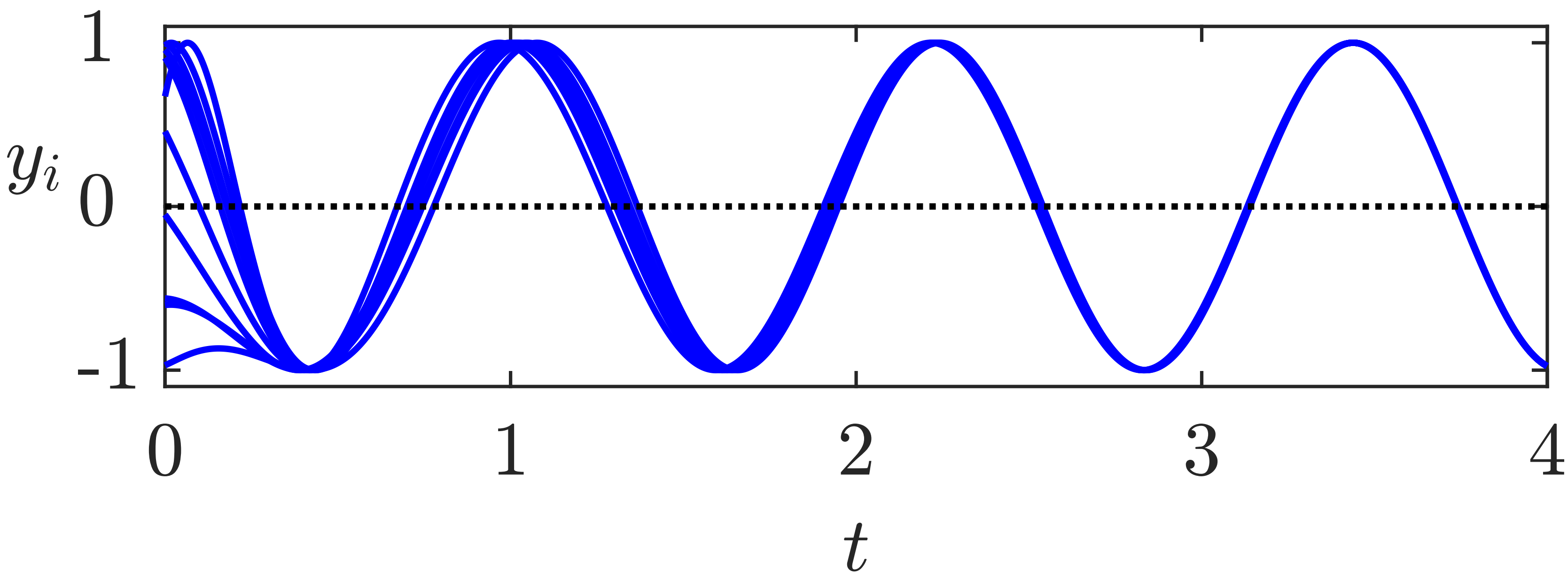

Fig. 4.2. Trajectories of synchronised oscillators

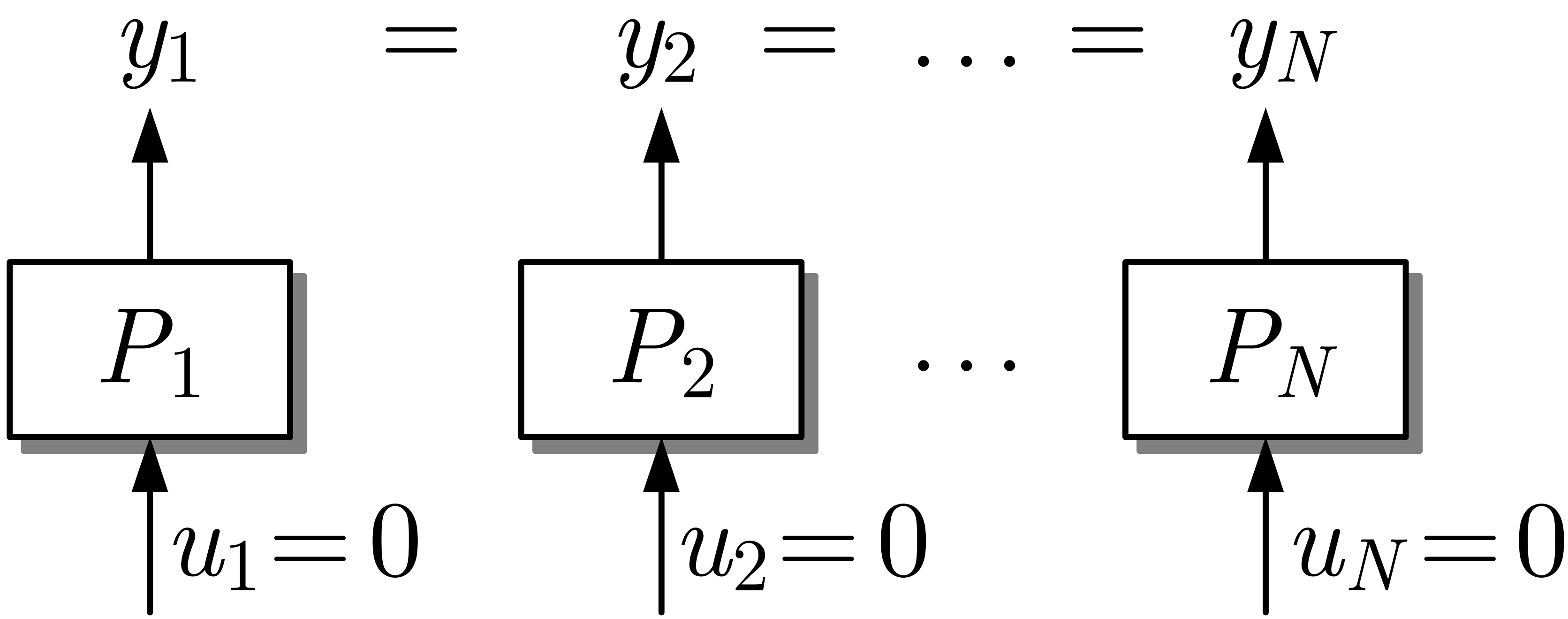

Fig. 4.3. Synchronised agents

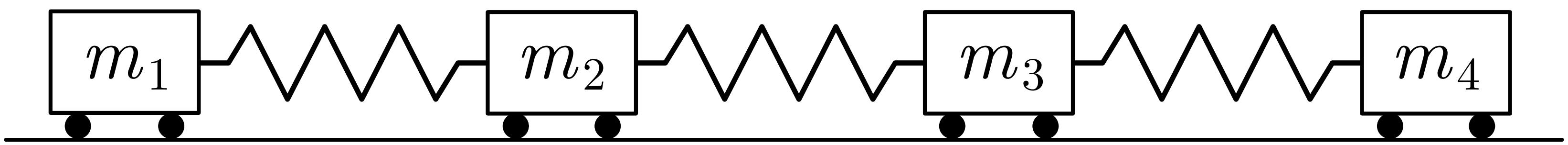

Fig. 4.4. Spring-mass system

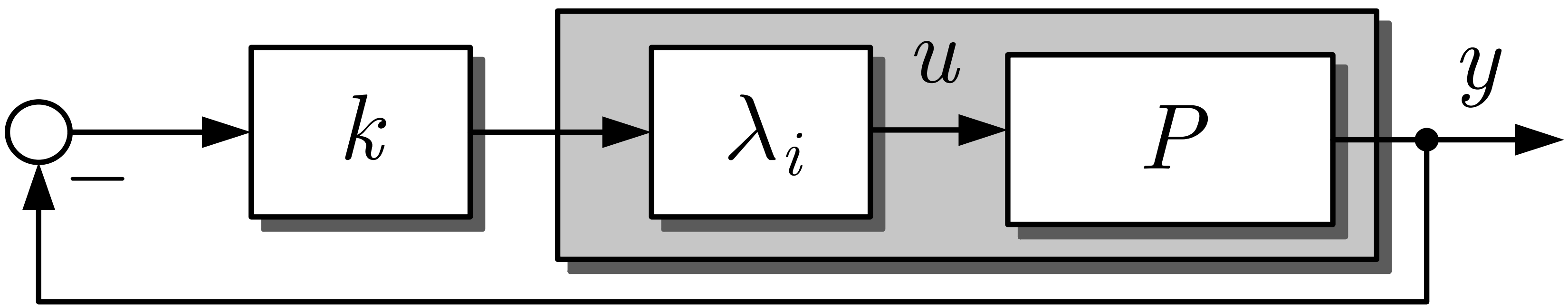

Fig. 4.5. Interpretation of the synchronisation condition as a condition of robust control

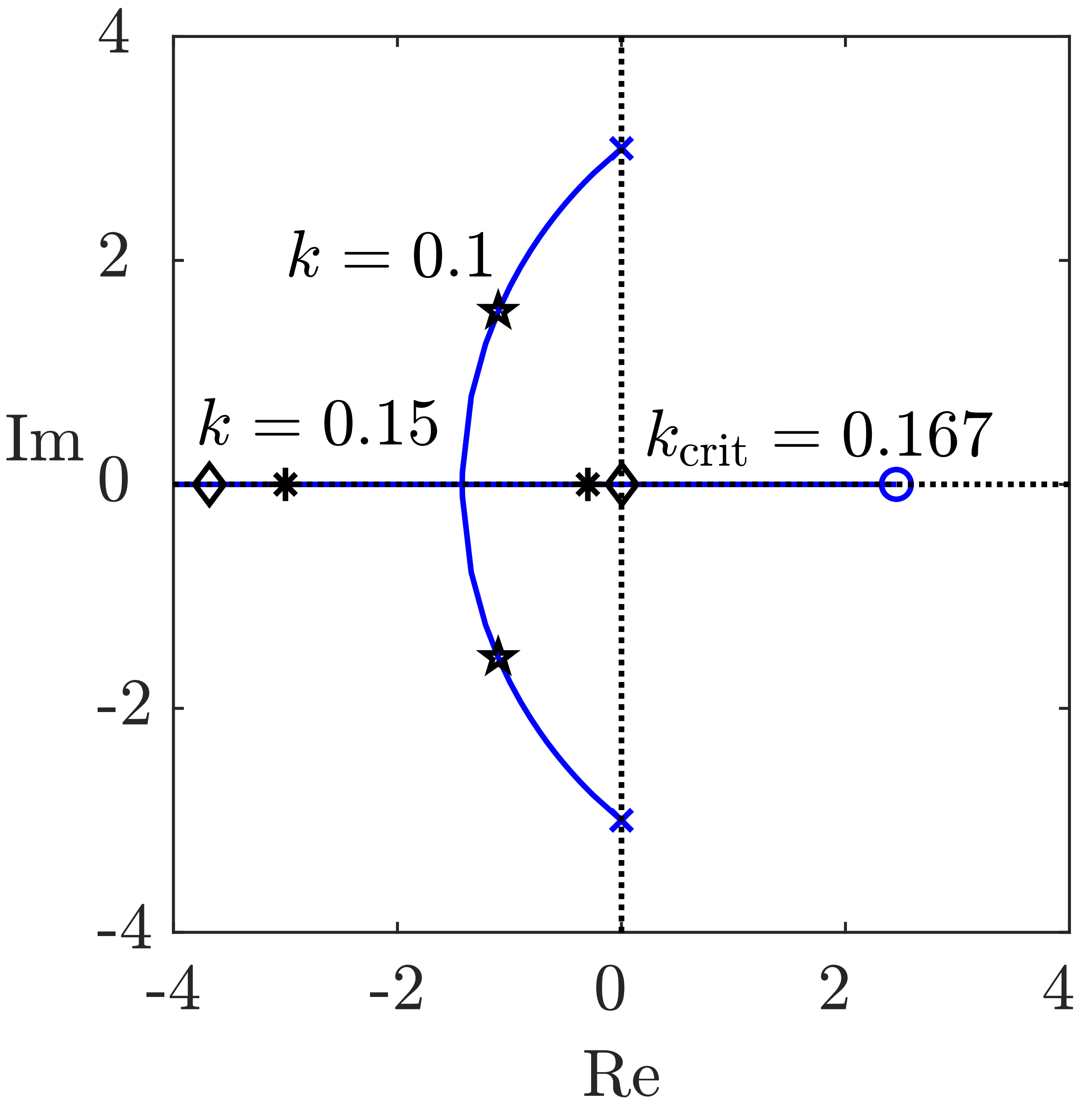

Fig. 4.6: Root locus of the agent

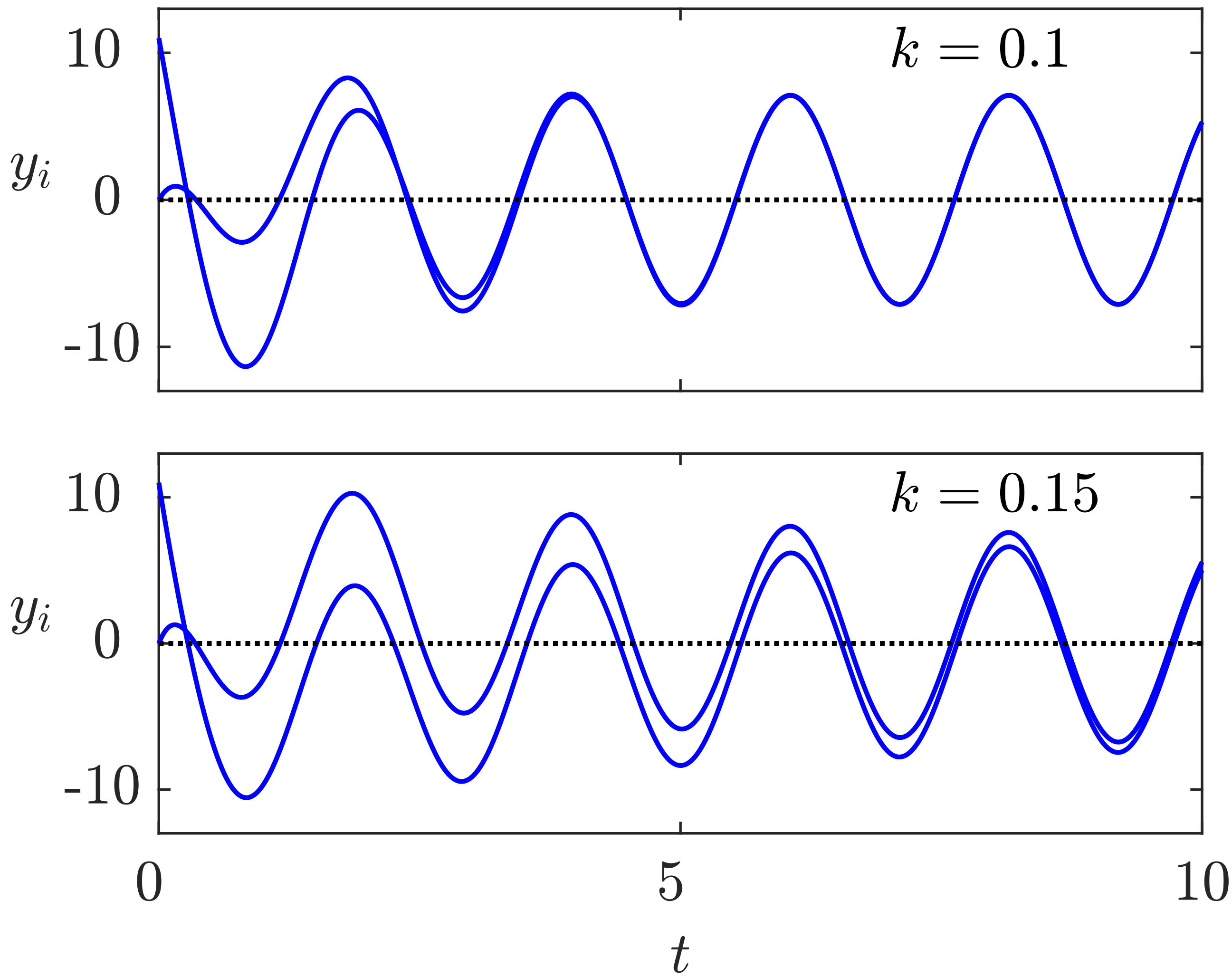

Fig. 4.7: Synchronisation behaviour of the harmonic oscillators

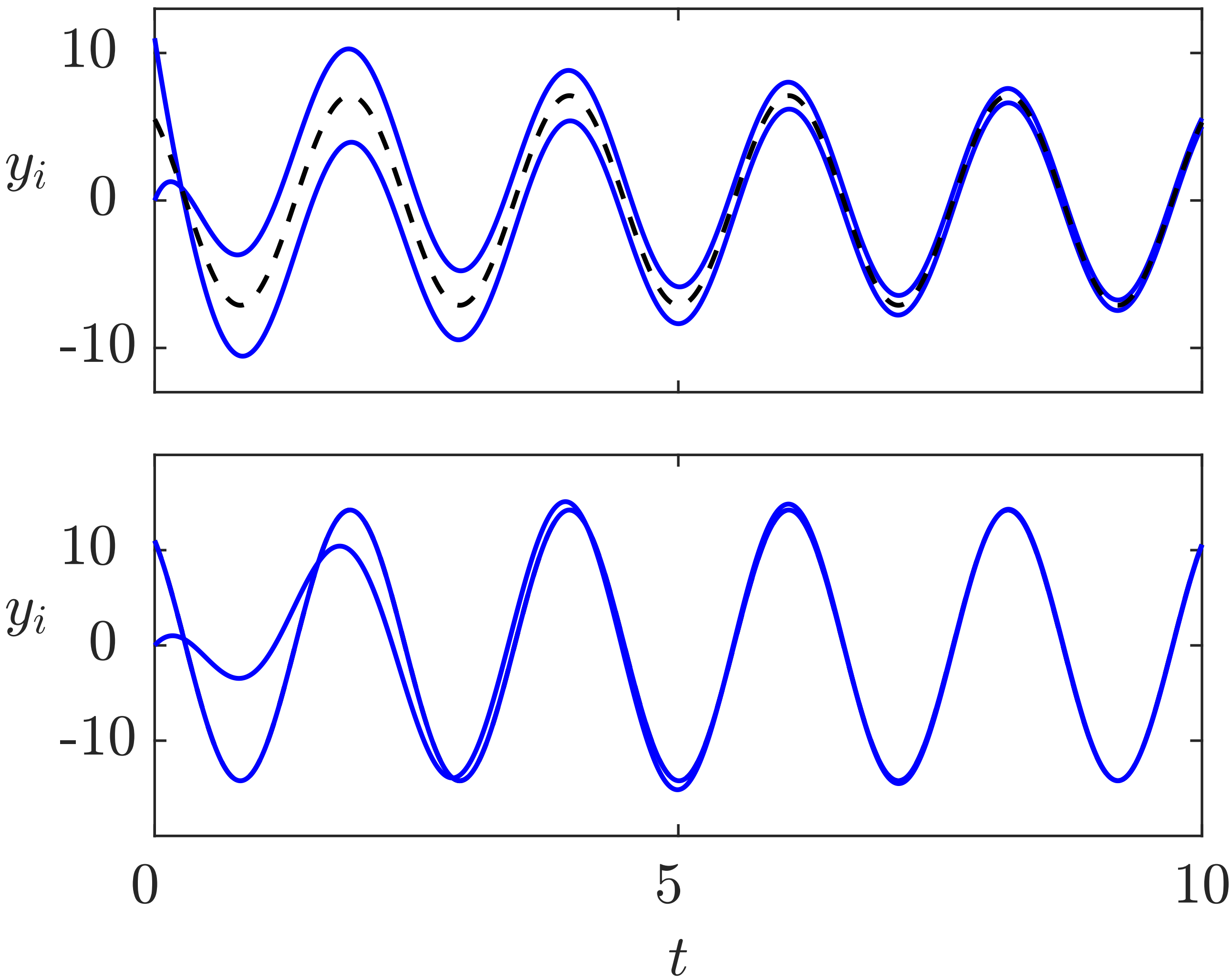

Fig. 4.8: Trajectories of two oscillators with different coupling structure

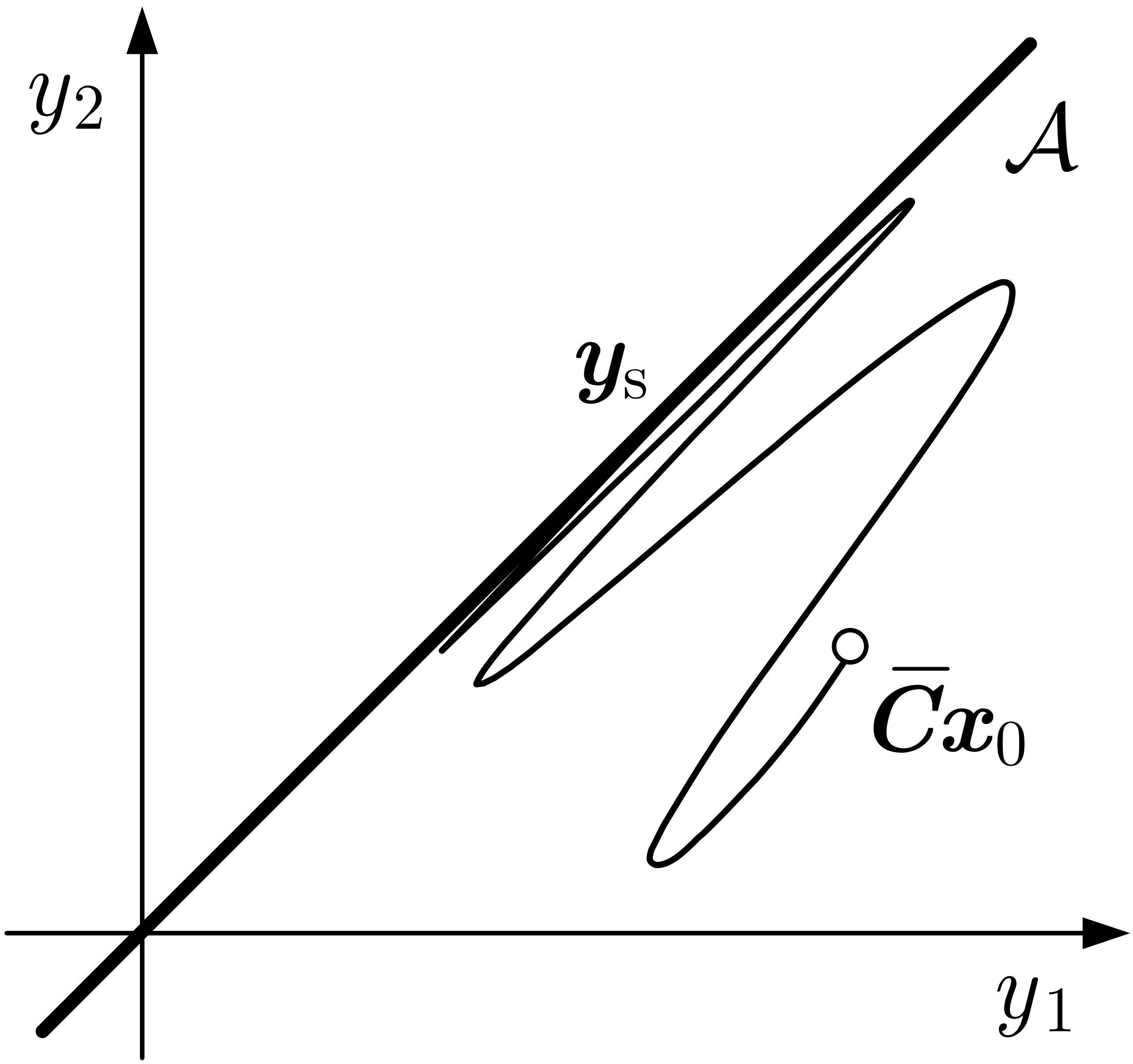

Fig. 4.9: Dynamics of two oscillators towards the synchronisation manifold

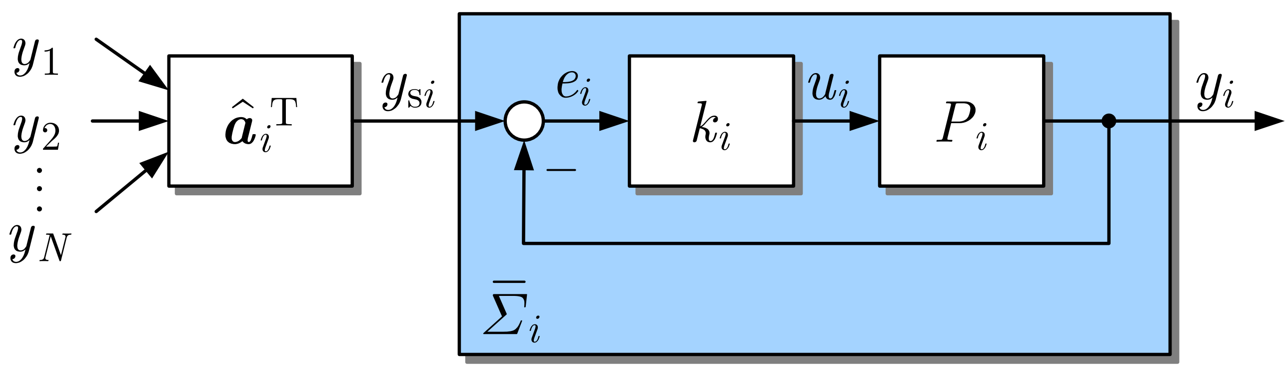

Fig. 4.10: Structure of the controlled agent

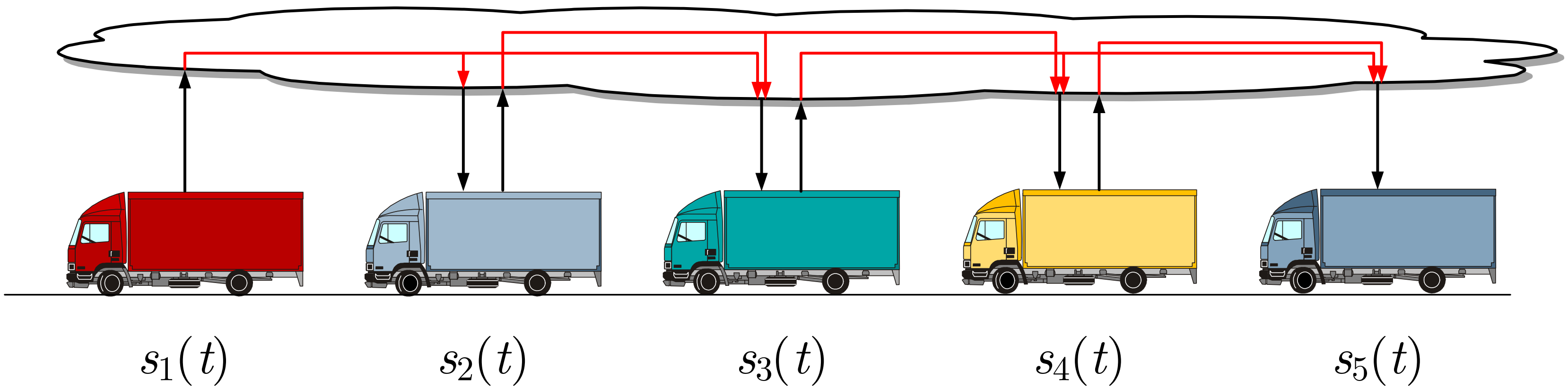

Fig. 4.11. Vehicle platoon

J. Lunze: *Networked Control of Multi-Agent Systems*, Edition **M**o**R**a 2022

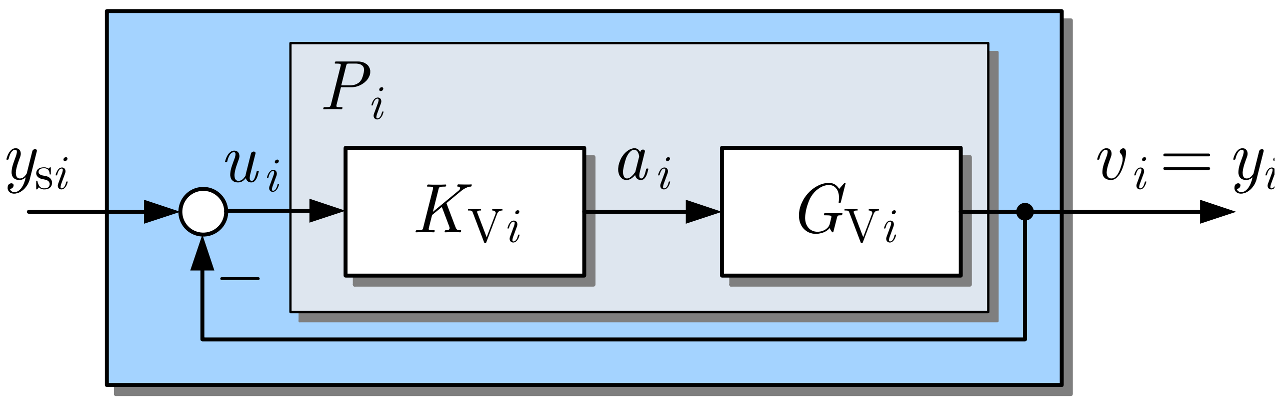

Fig. 4.12: Vehicle model

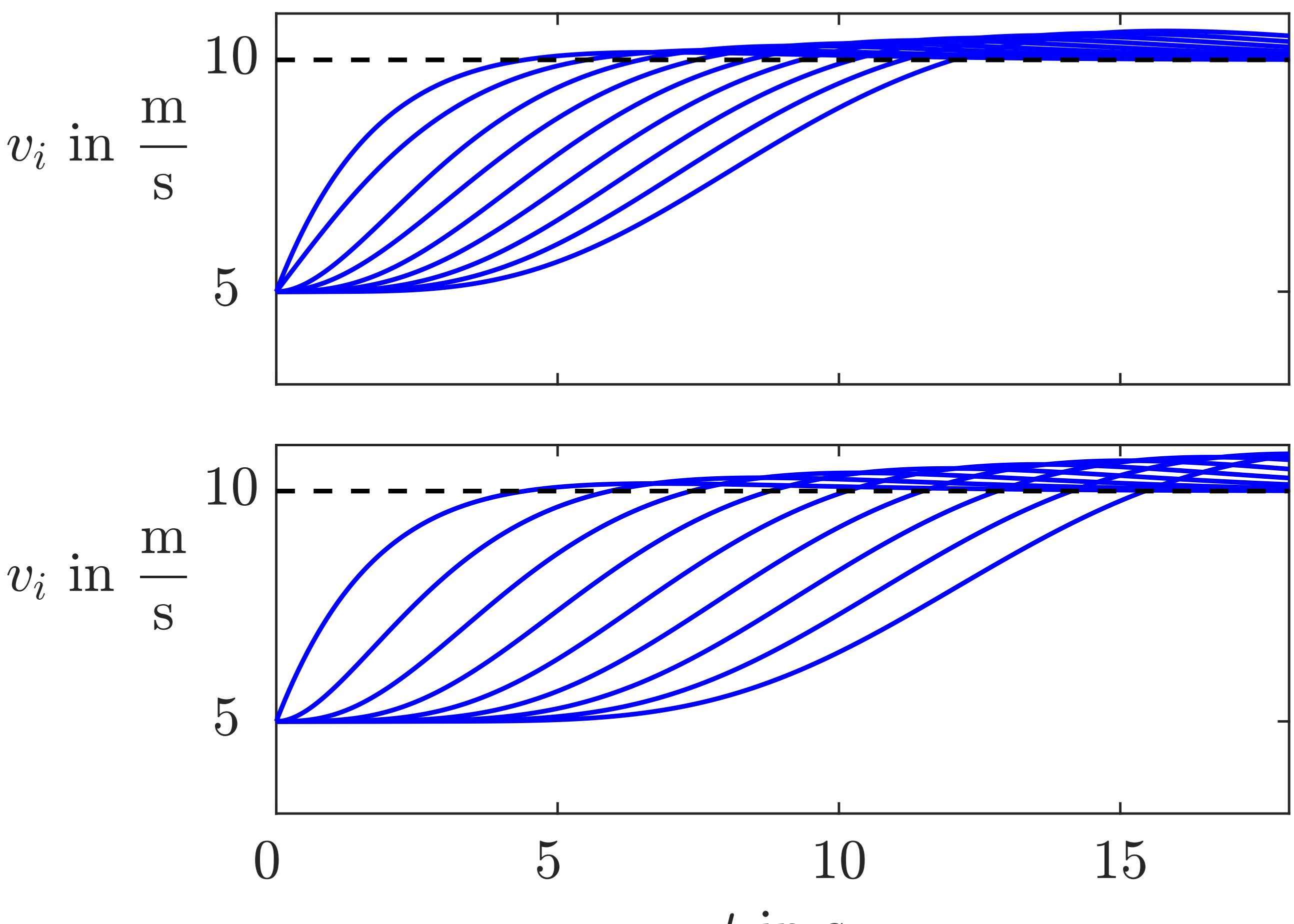

Fig. 4.13: Behaviour of the vehicle platoon

$(N = 10)$

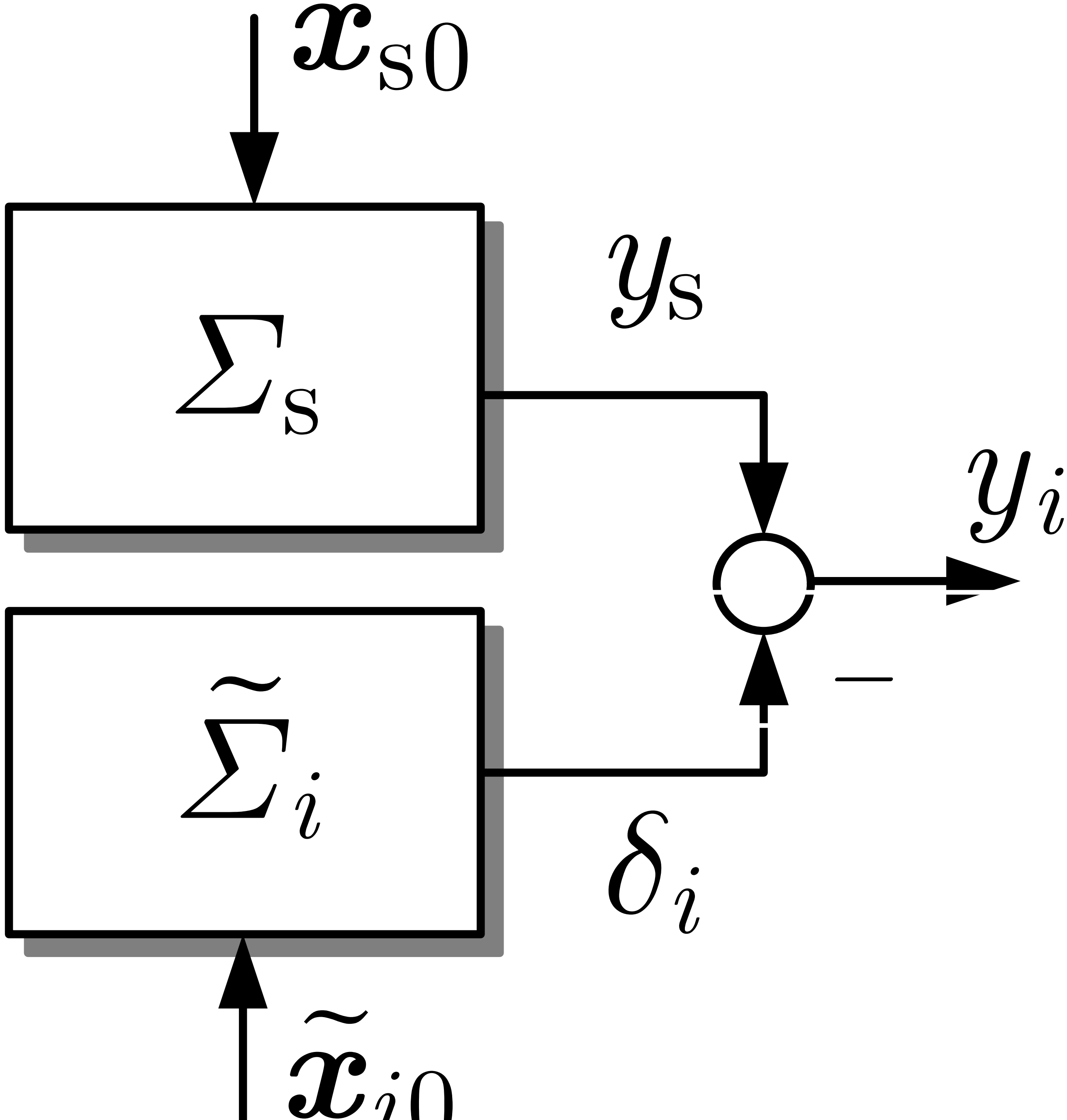

Fig. 4.14: Simplified model of the i-th agent in a completely coupled network

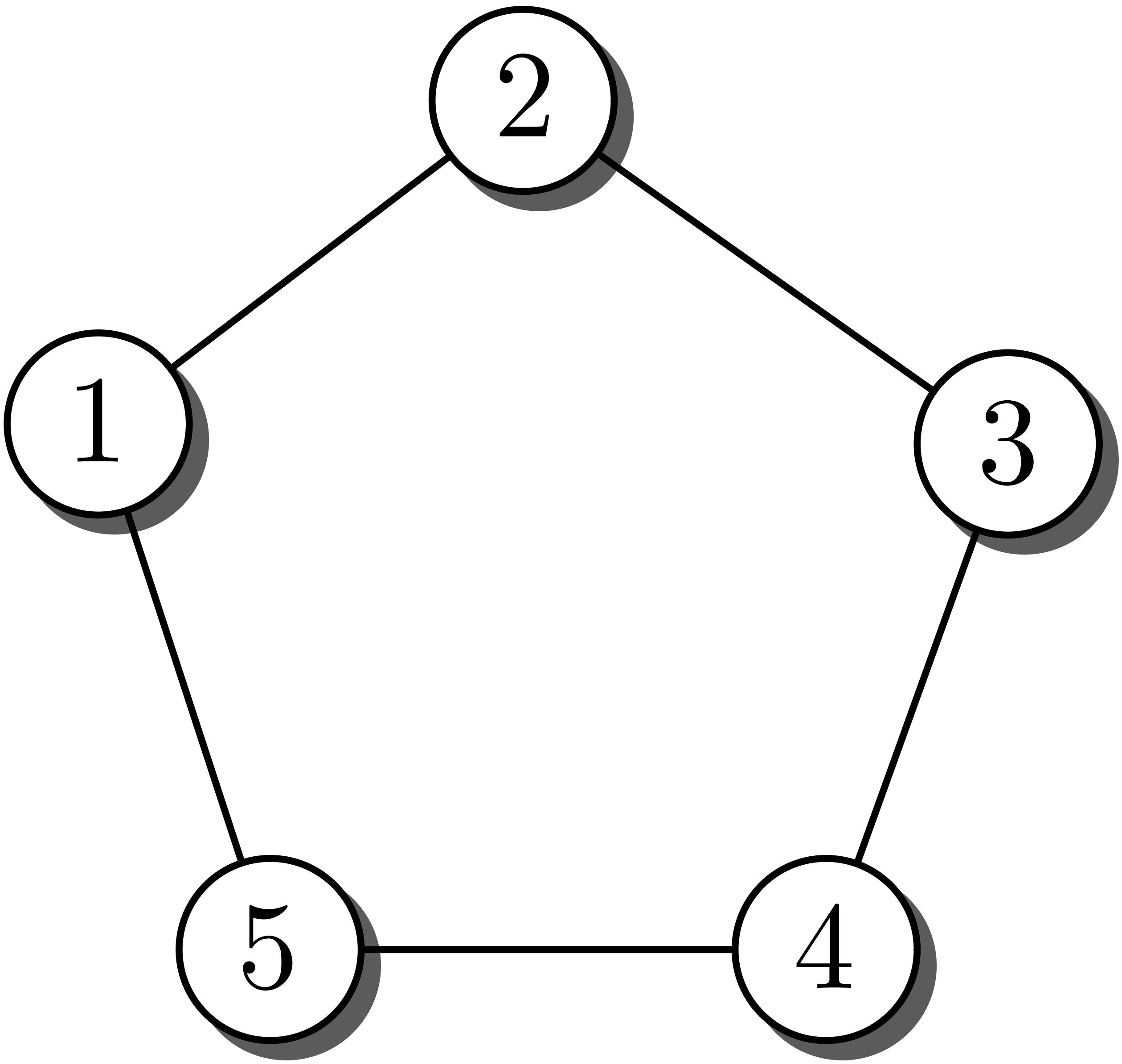

Fig. 4.15: Communication structure considered in Exercise 4.3

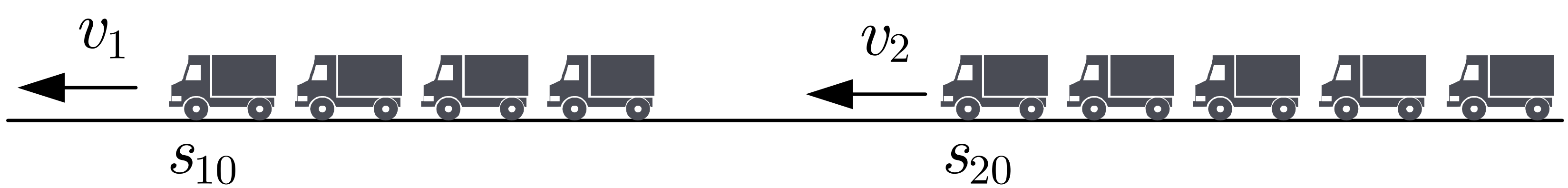

Fig. 4.16. Two vehicle platoons on a highway

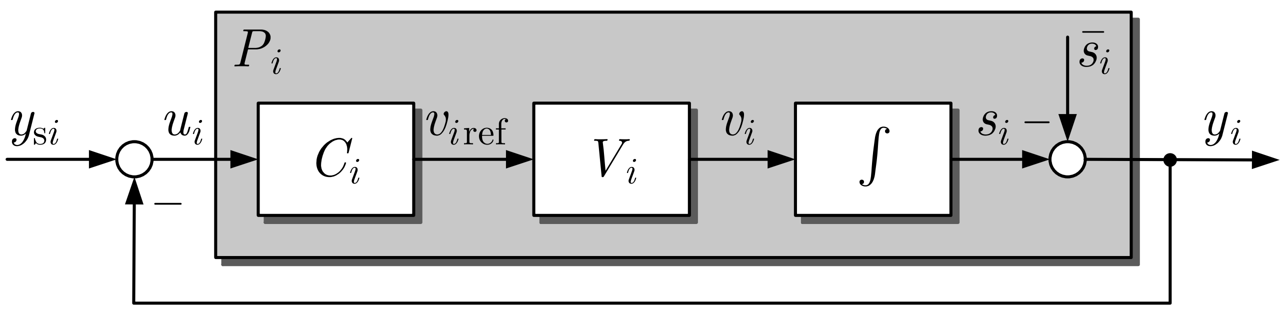

Fig. 4.17: Structure of the position control loop of a vehicle

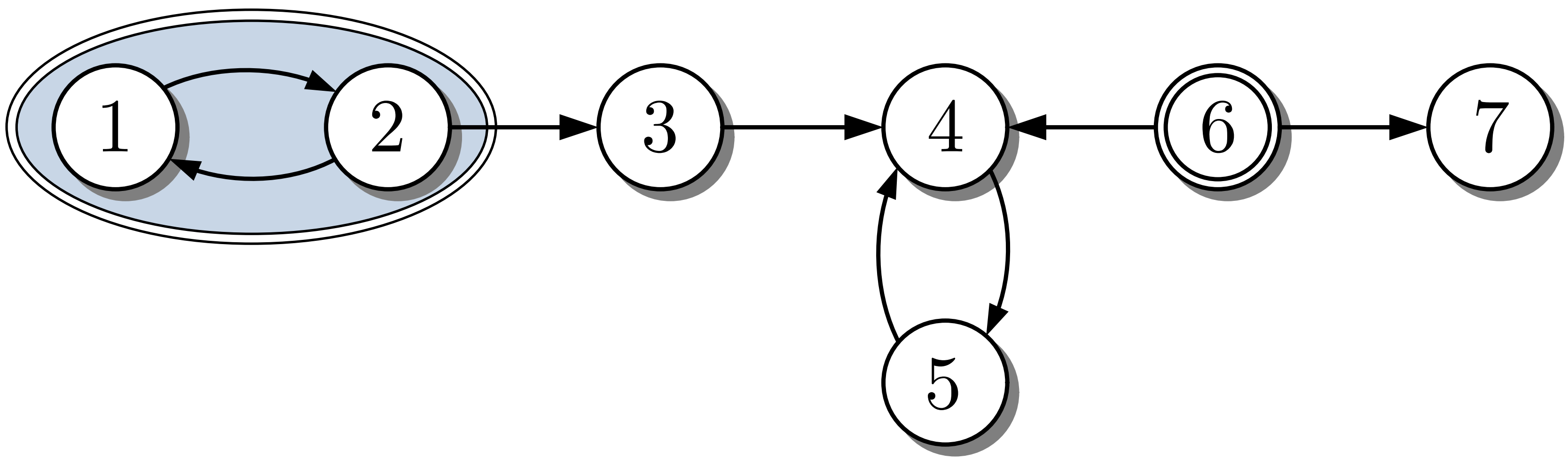

Fig. 4.18. Graph with five strongly connected vertex sets

J. Lunze: *Networked Control of Multi-Agent Systems,* Edition MoRa 2022

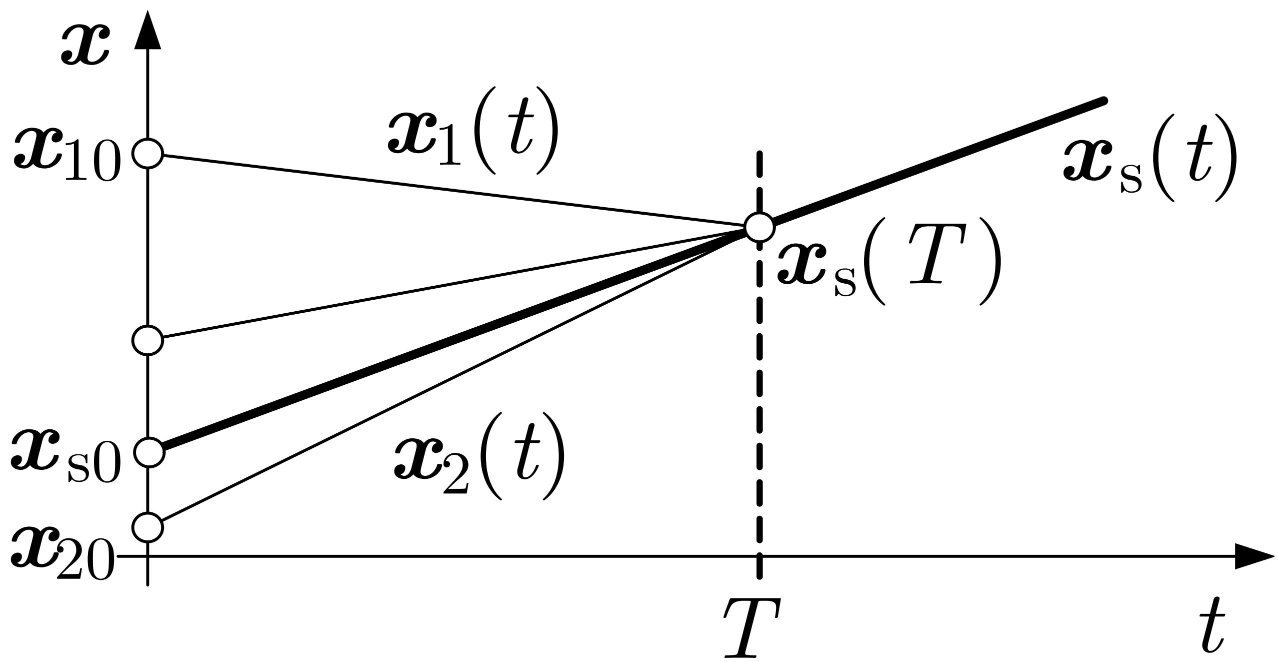

Fig. 4.19: Interpretation of synchronisation as an agreement problem

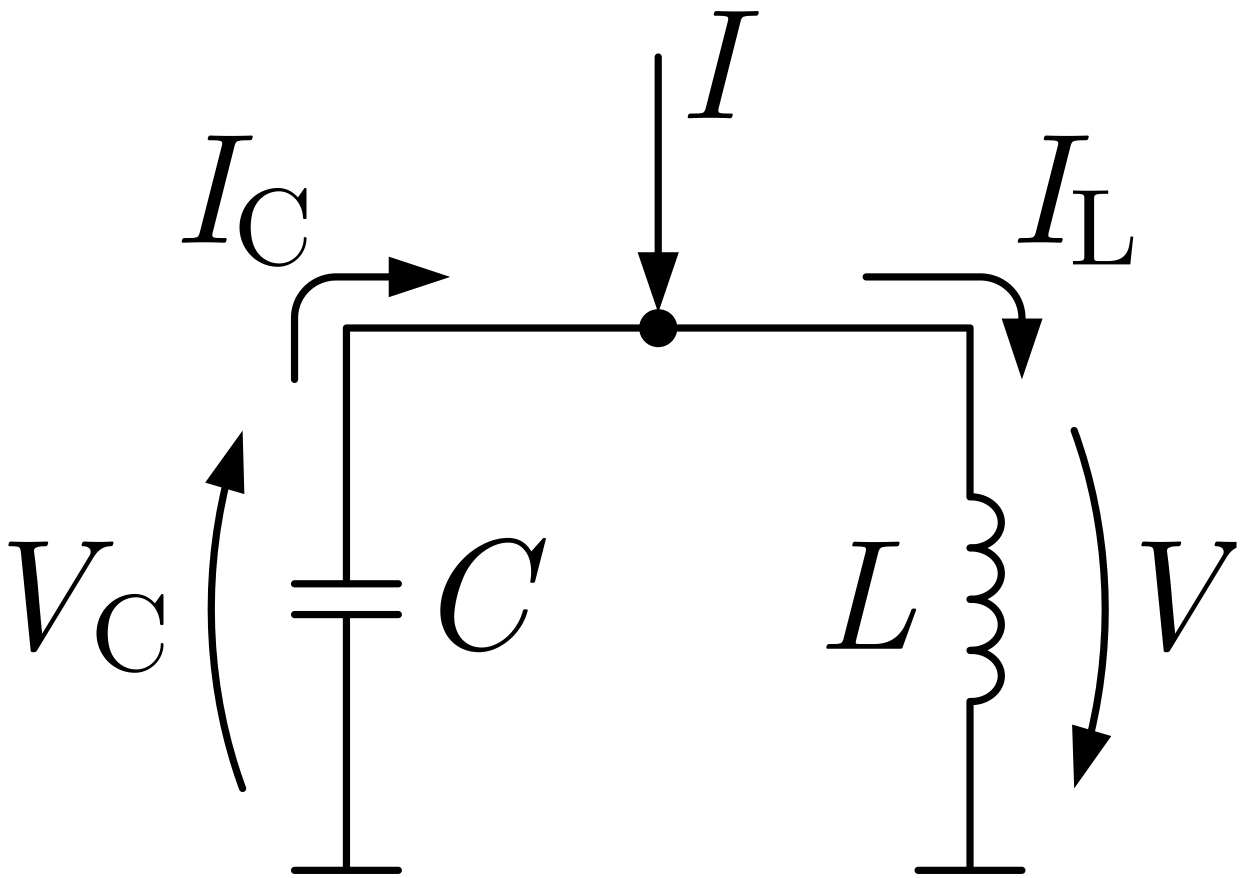

Fig. 4.20: Circuit diagram of an oscillator

J. Lunze: *Networked Control of Multi-Agent Systems*, Edition **MoR**a 2022

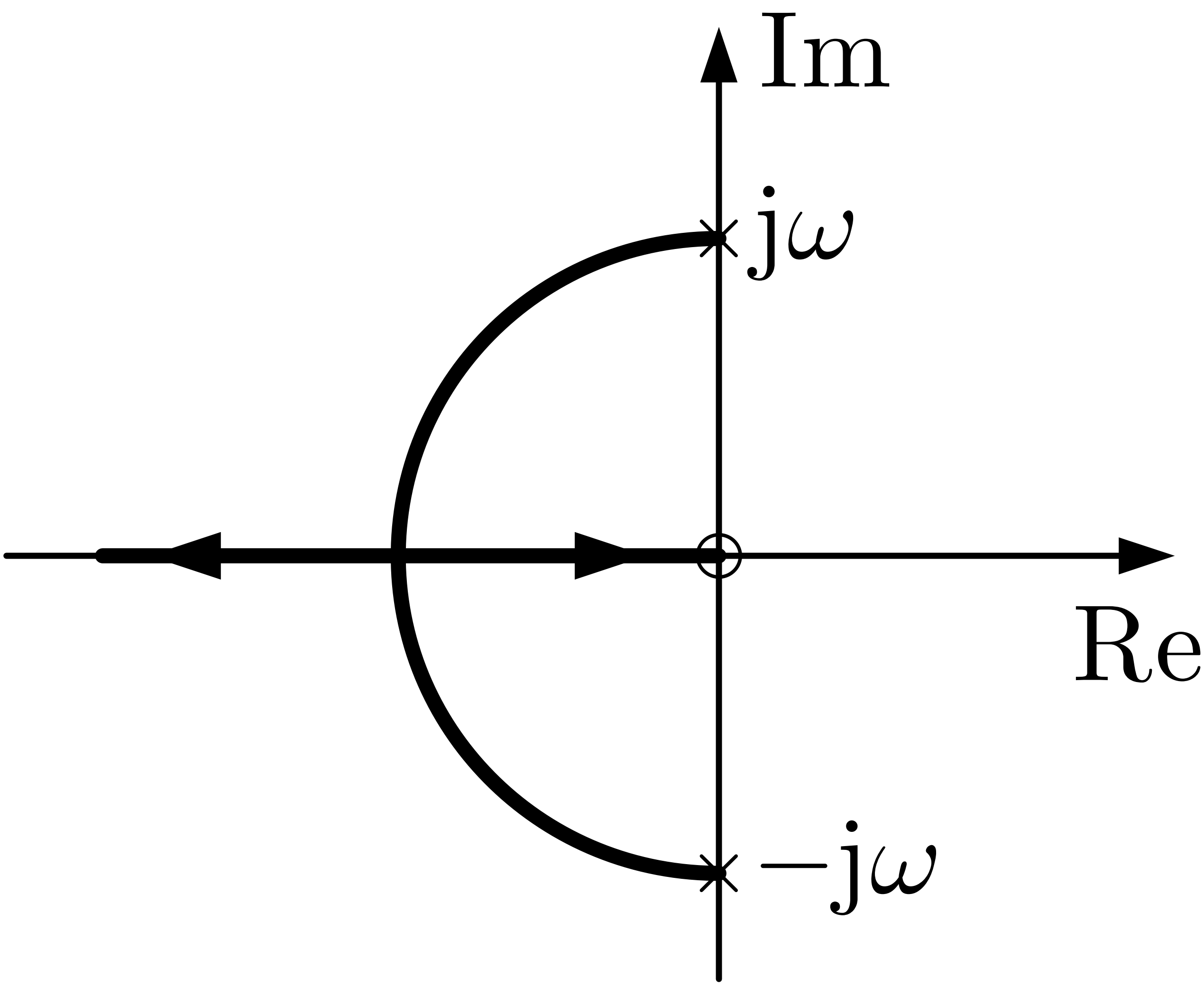

Fig. 4.21: Root locus of an oscillator subject to the output feedback $u(t) = -ky(t)$

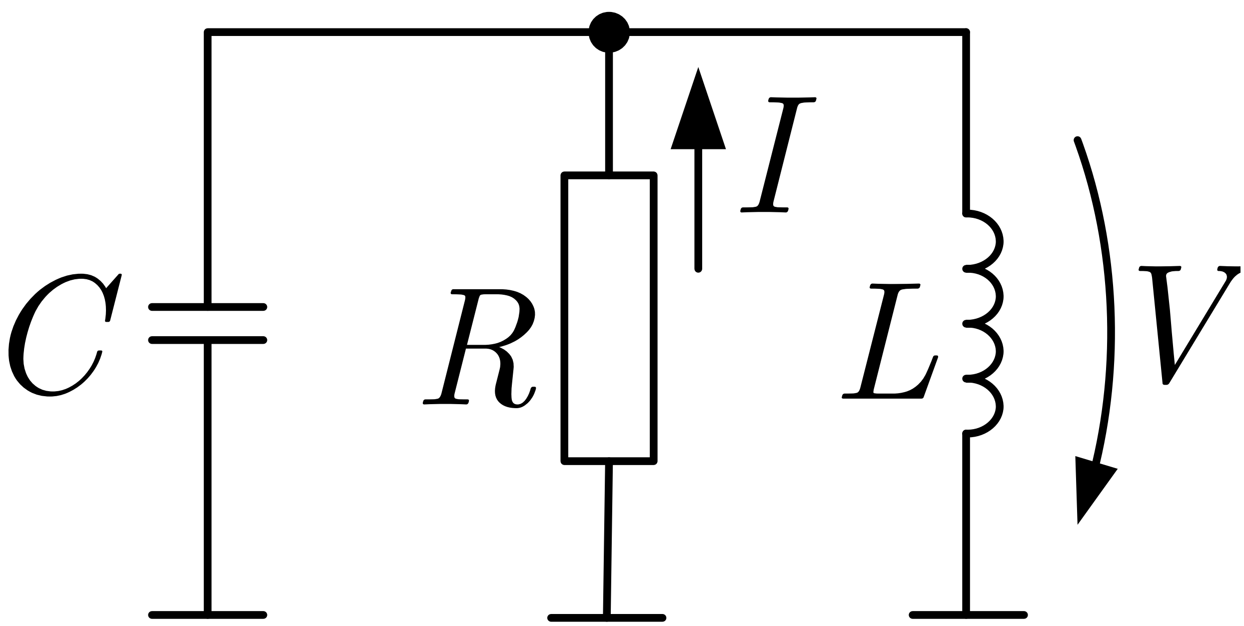

Fig. 4.22: Oscillator with output feedback implemented by the resistor R

J. Lunze: *Networked Control of Multi-Agent Systems*, Edition **M**o**R**a 2022

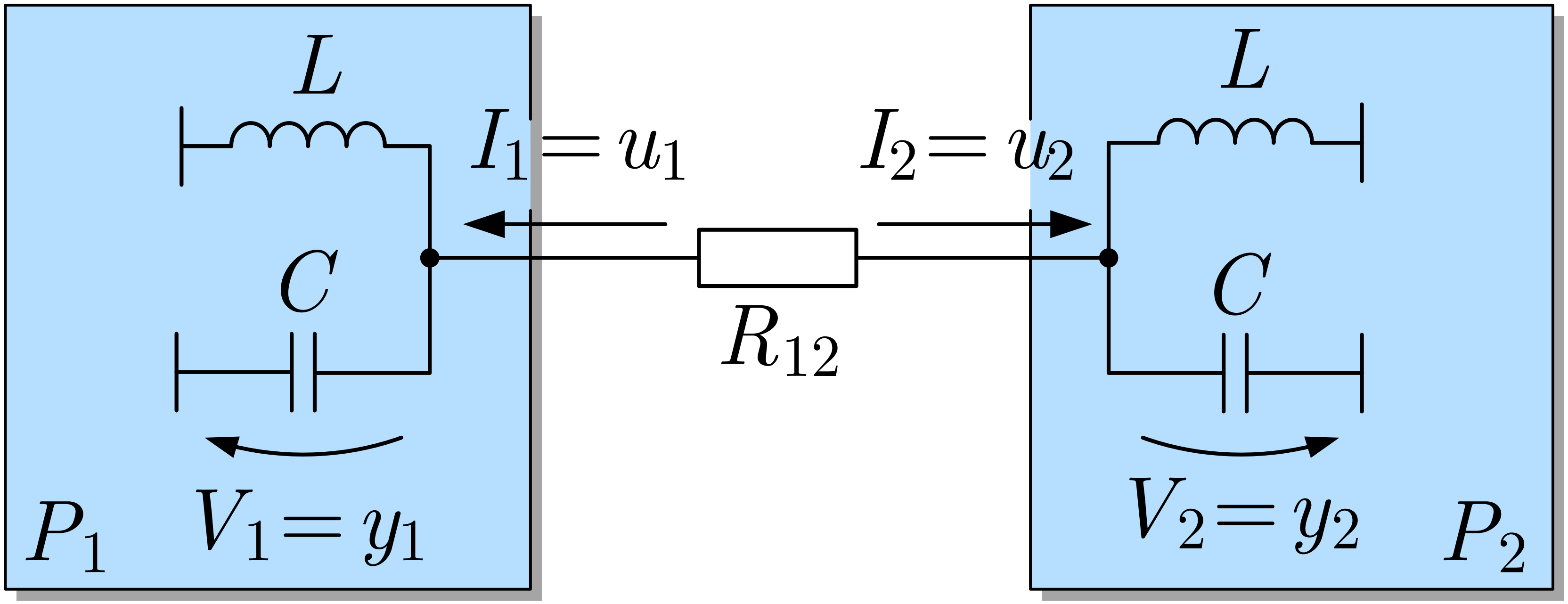

Fig. 4.23. Two coupled oscillators

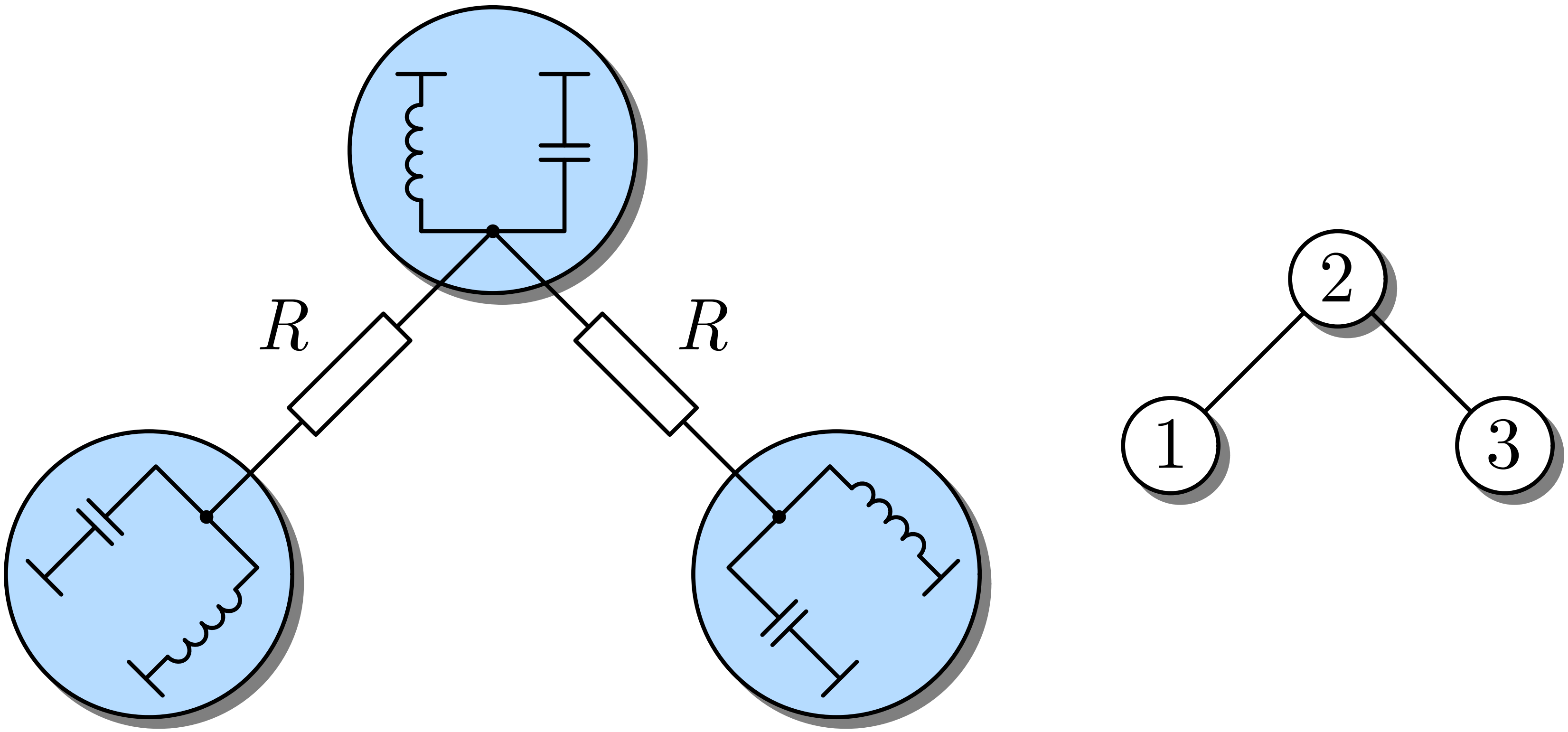

Fig. 4.24. Oscillator network with three subsystems: circuit (left) and coupling graph (right)

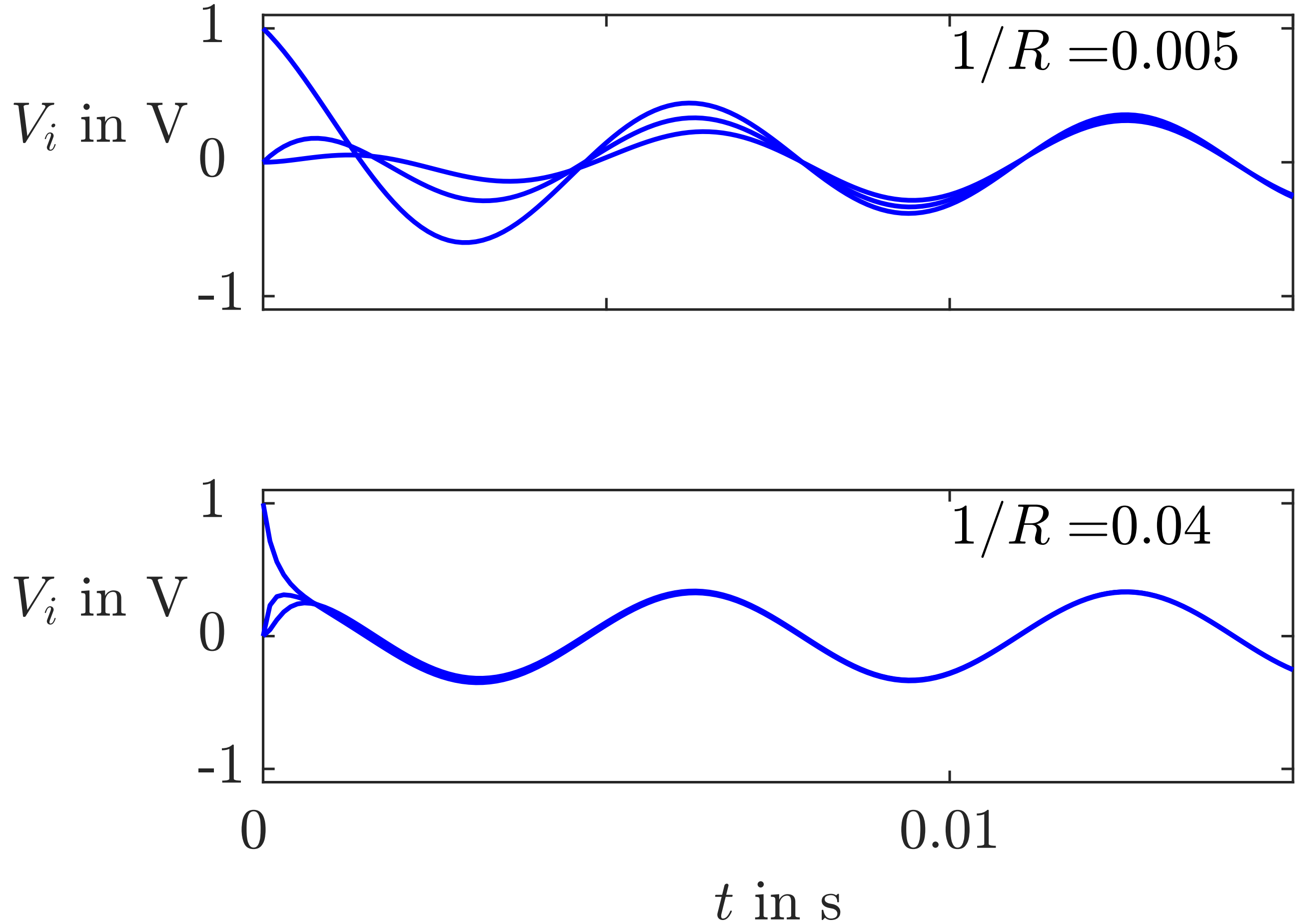

Fig. 4.25: Behaviour of three coupled oscillators with different coupling strength

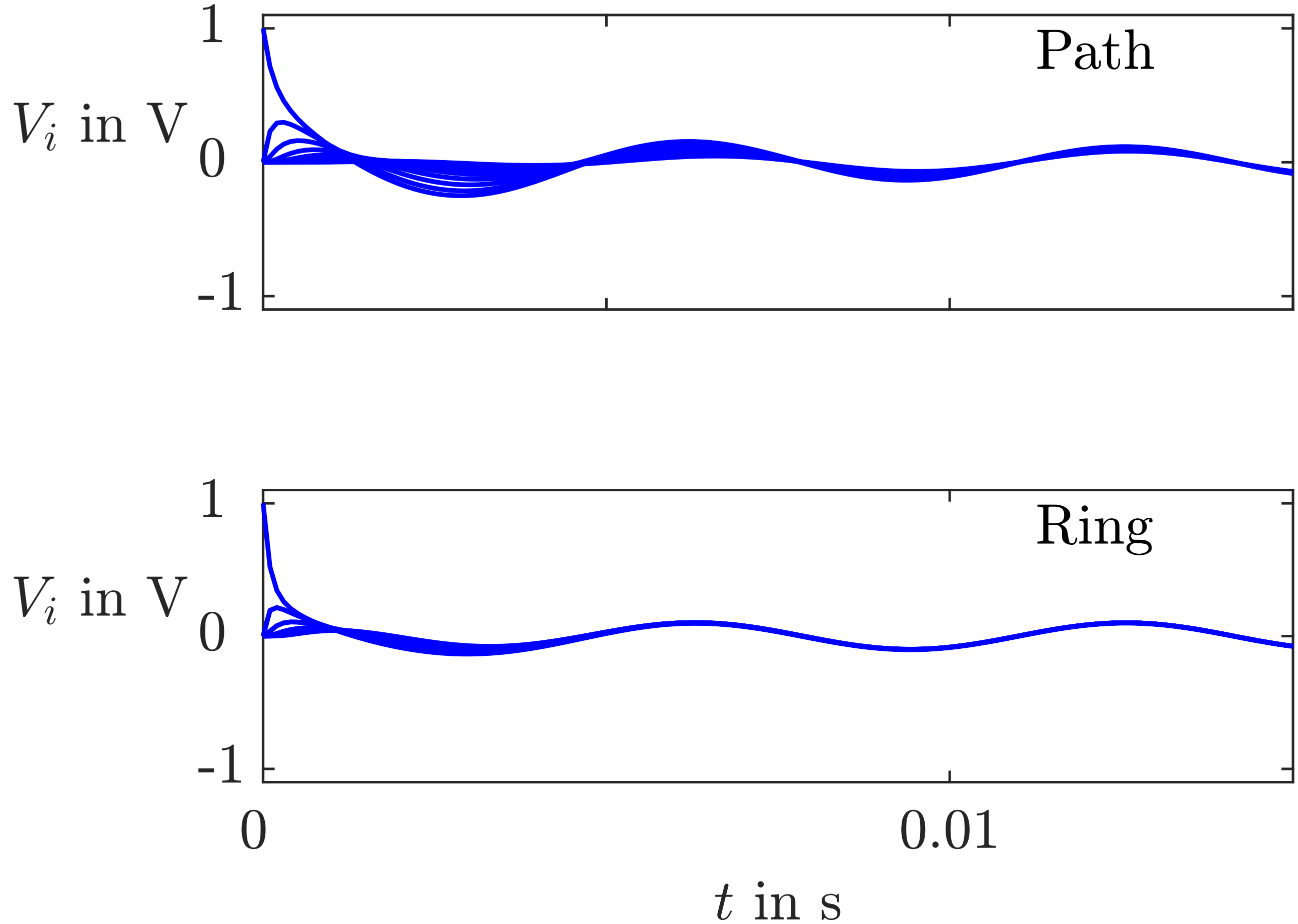

Fig. 4.26: Behaviour of an oscillator network with ten nodes

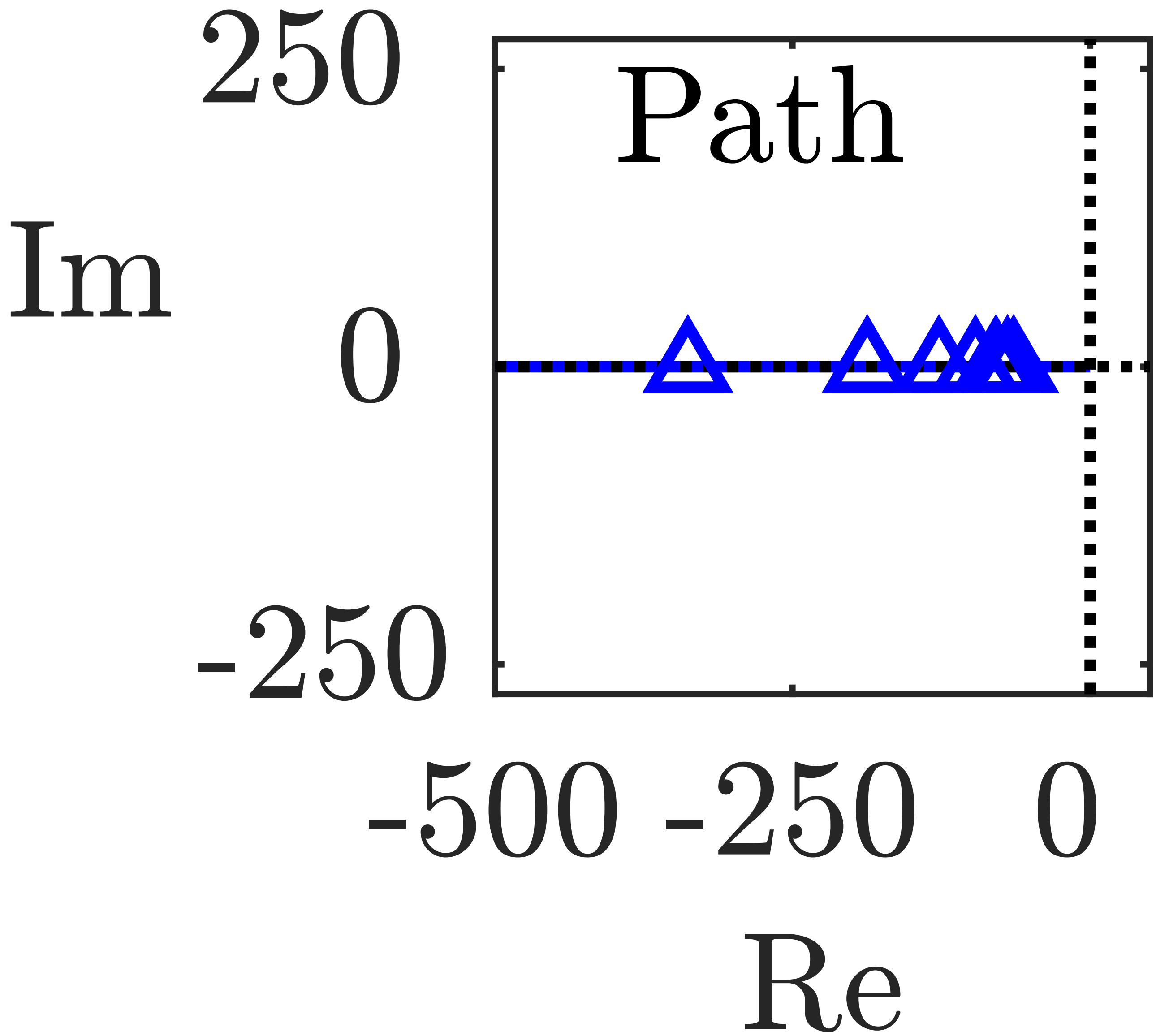

Fig. 4.27: Eigenvalues of the oscillator networks with path structure

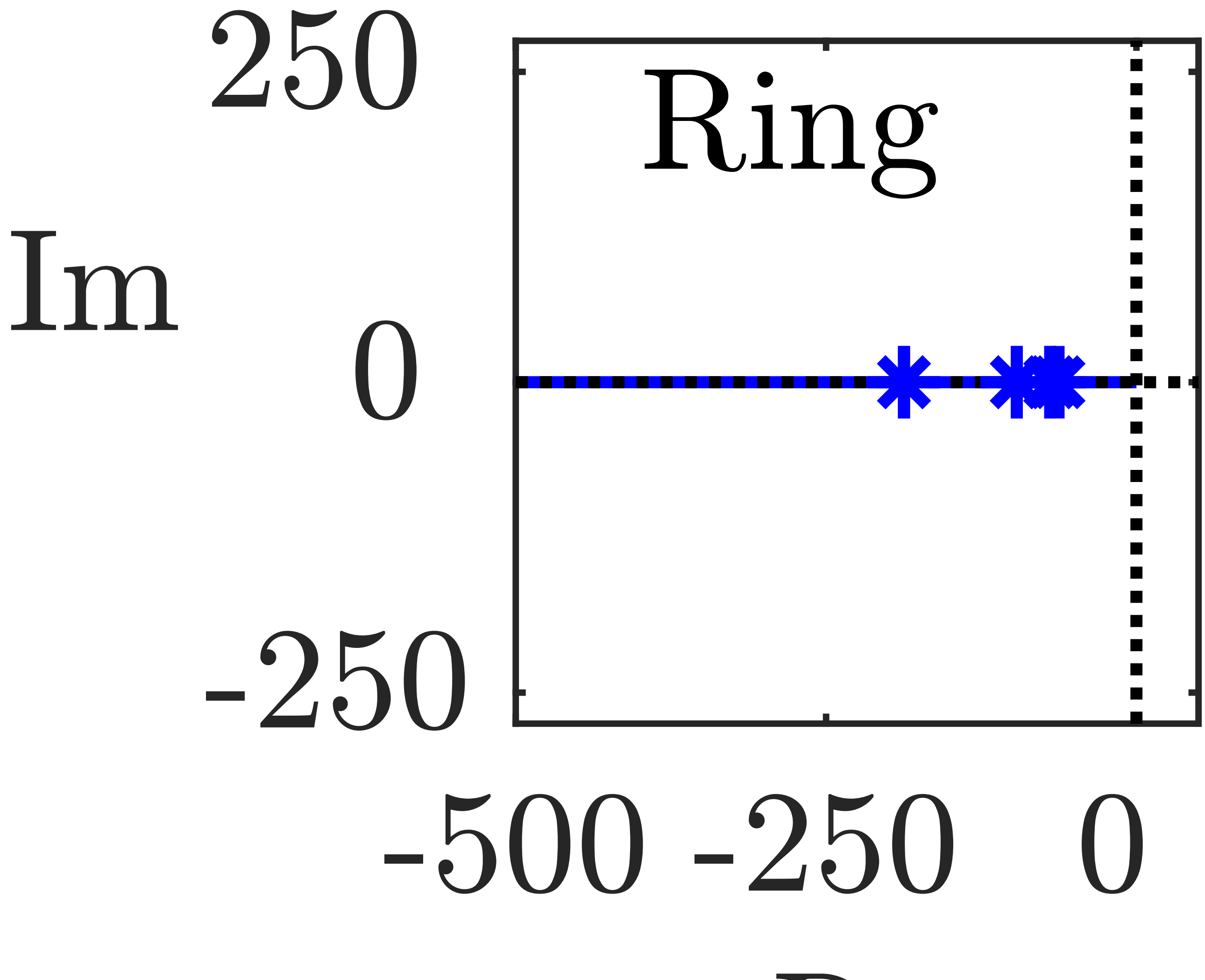

Fig. 4.27: Eigenvalues of the oscillator networks with ring structure

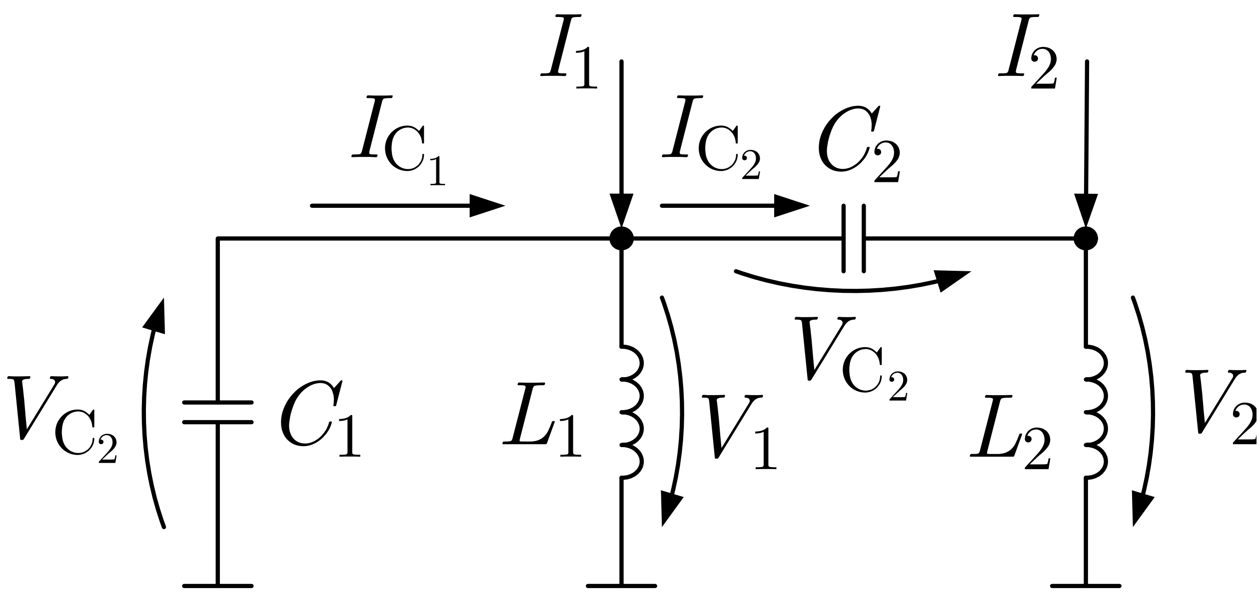

Fig. 4.28: Circuit diagram of an extended oscillator

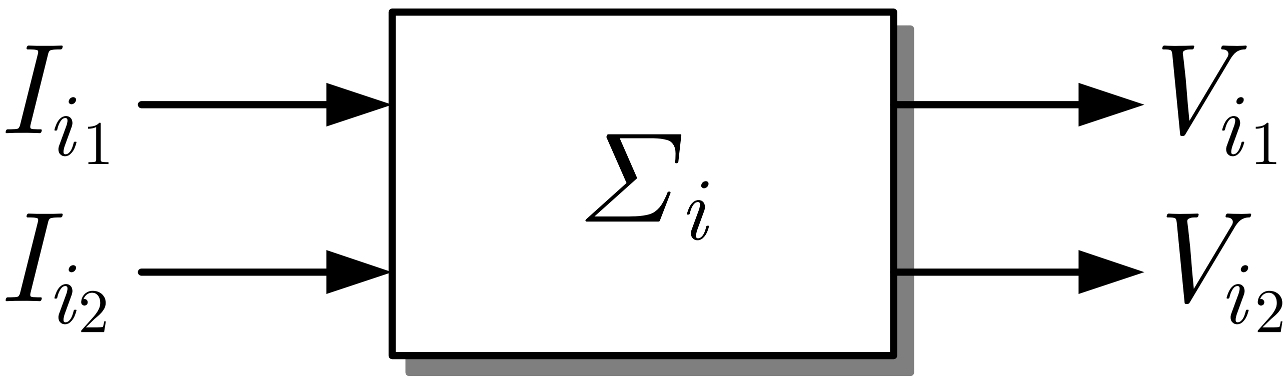

Fig. 4.28: Interpretation of the oscillator as vertex in a networked system

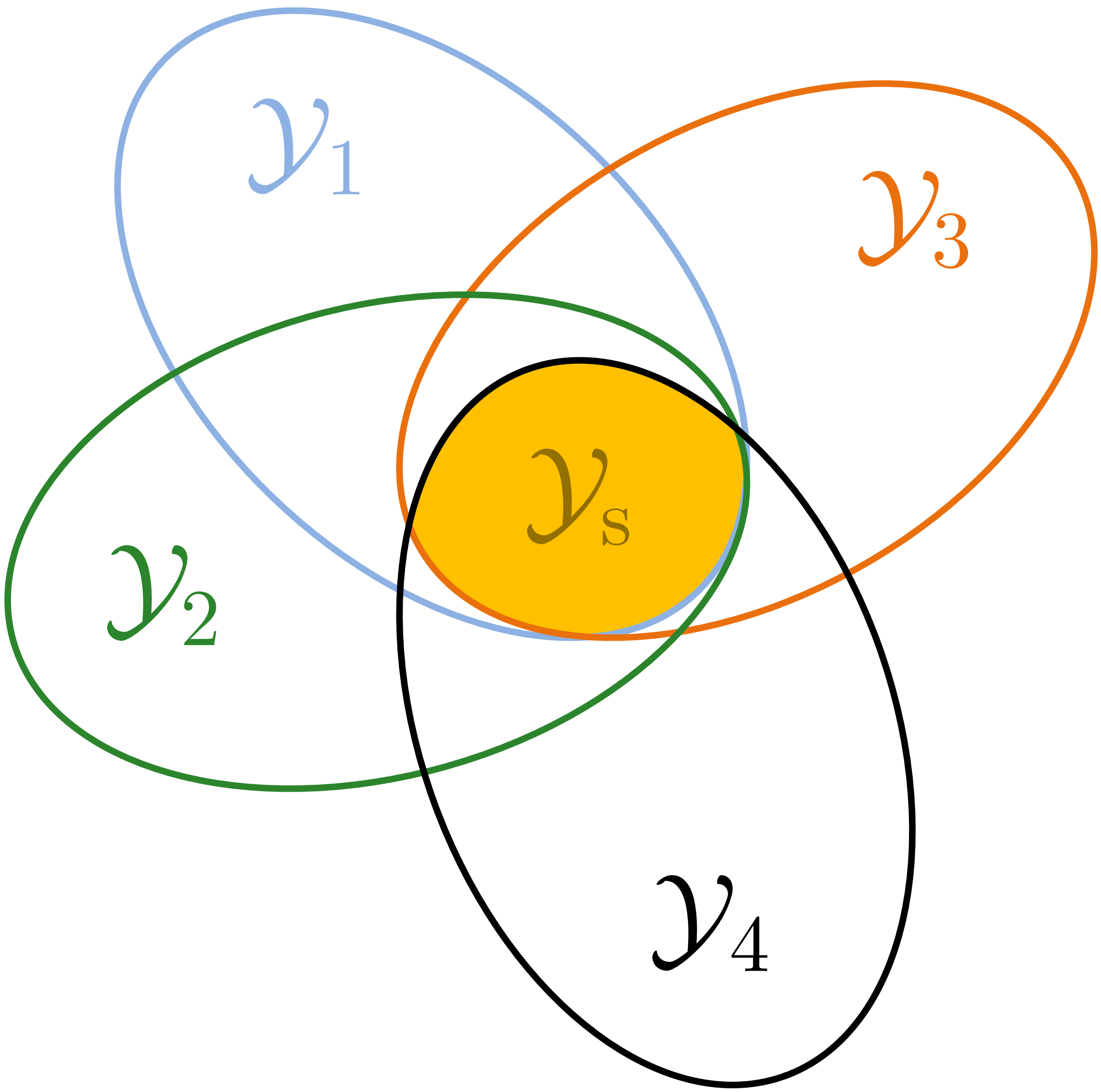

Fig. 4.29: Intersection of the output sets

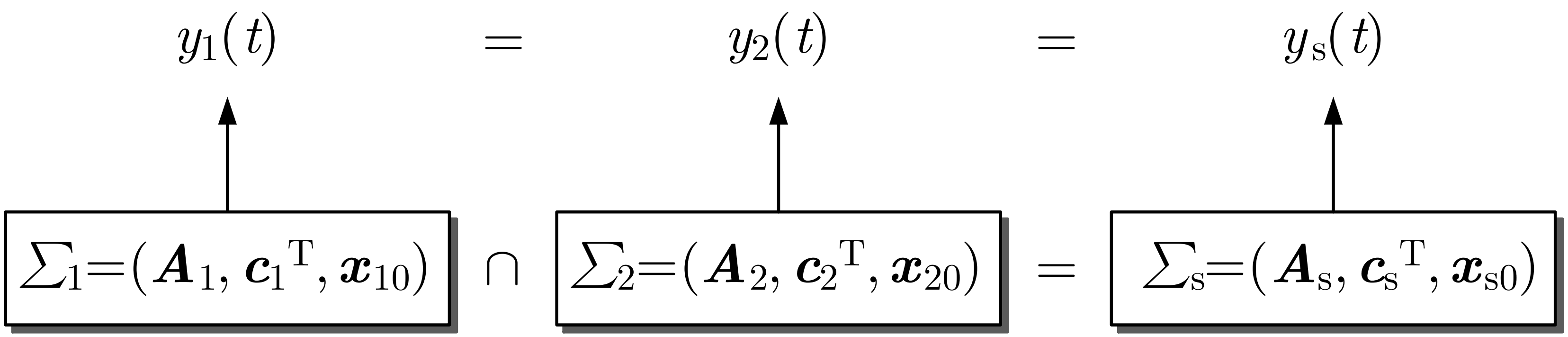

Fig. 4.30. System intersection

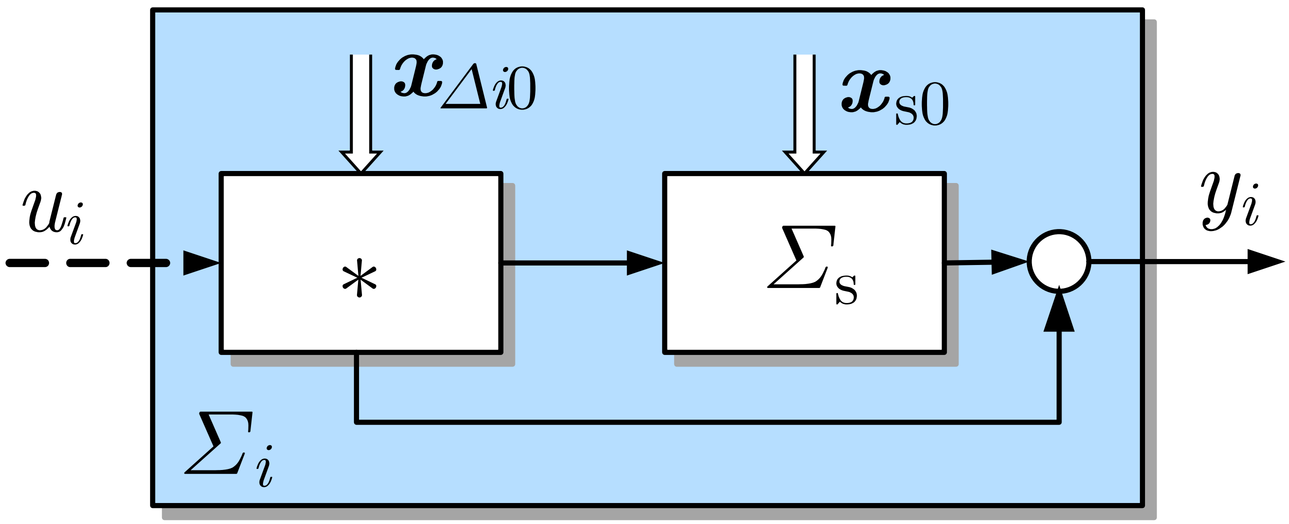

Fig. 4.31: Structure of agents that have the common dynamics represented by Σ_s

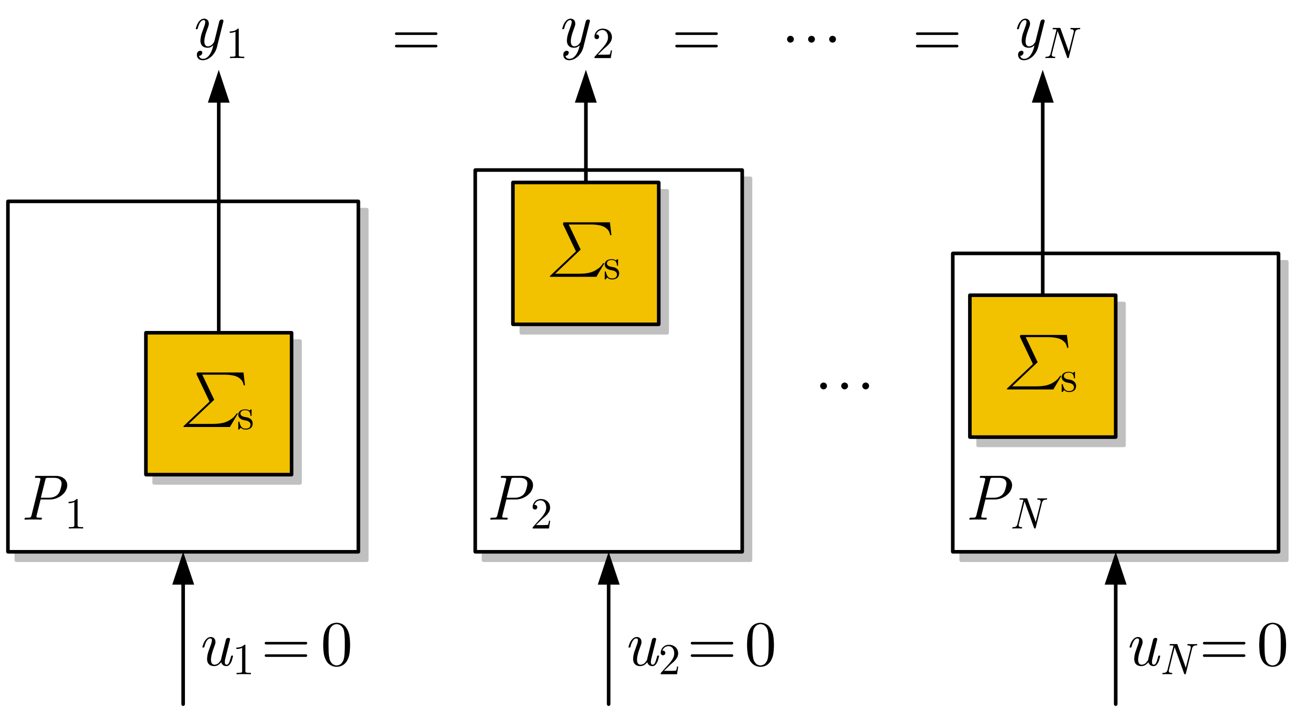

Fig. 4.32: Agents with common dynamics

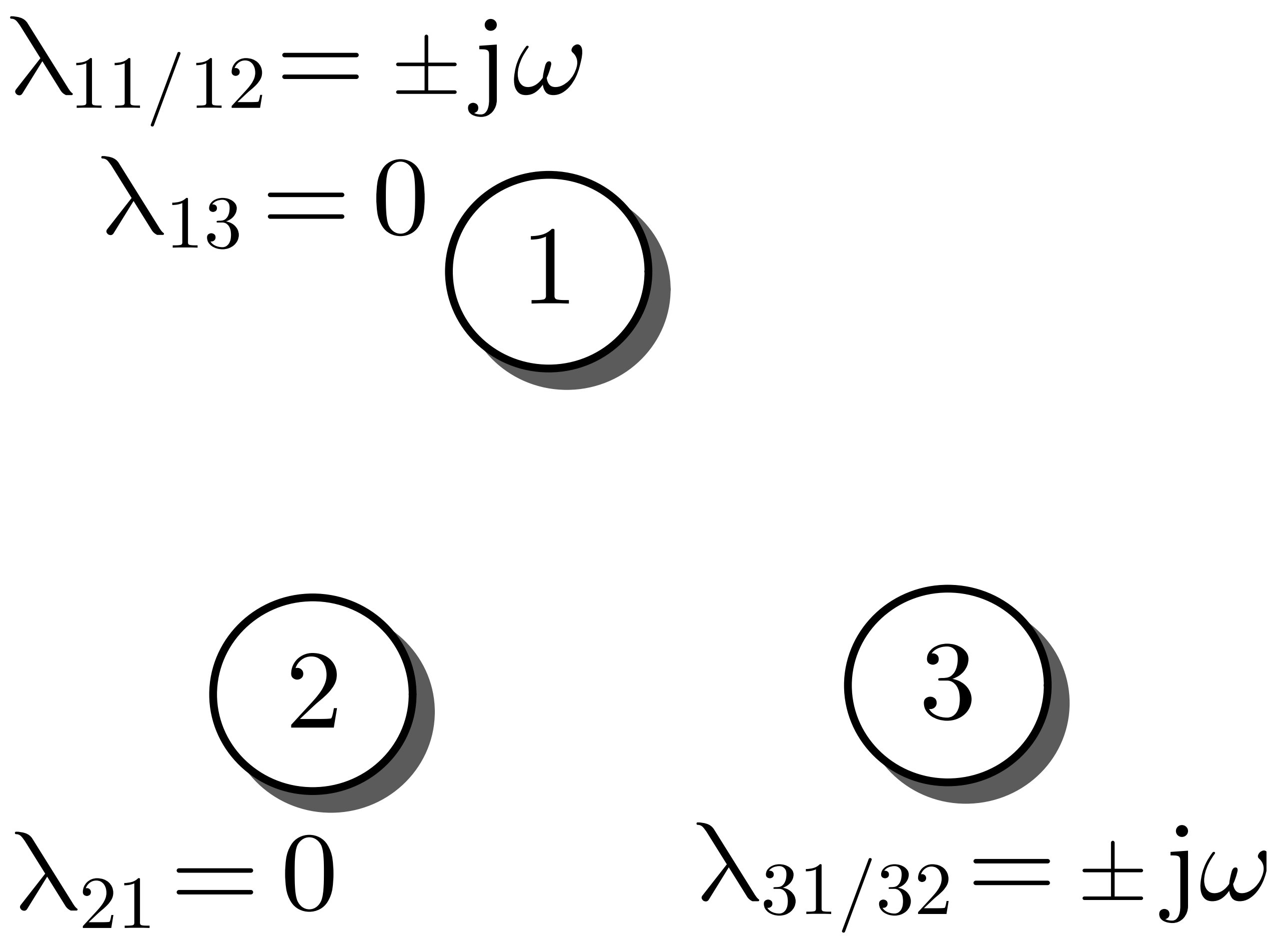

Fig. 4.33: Three agents with individual properties

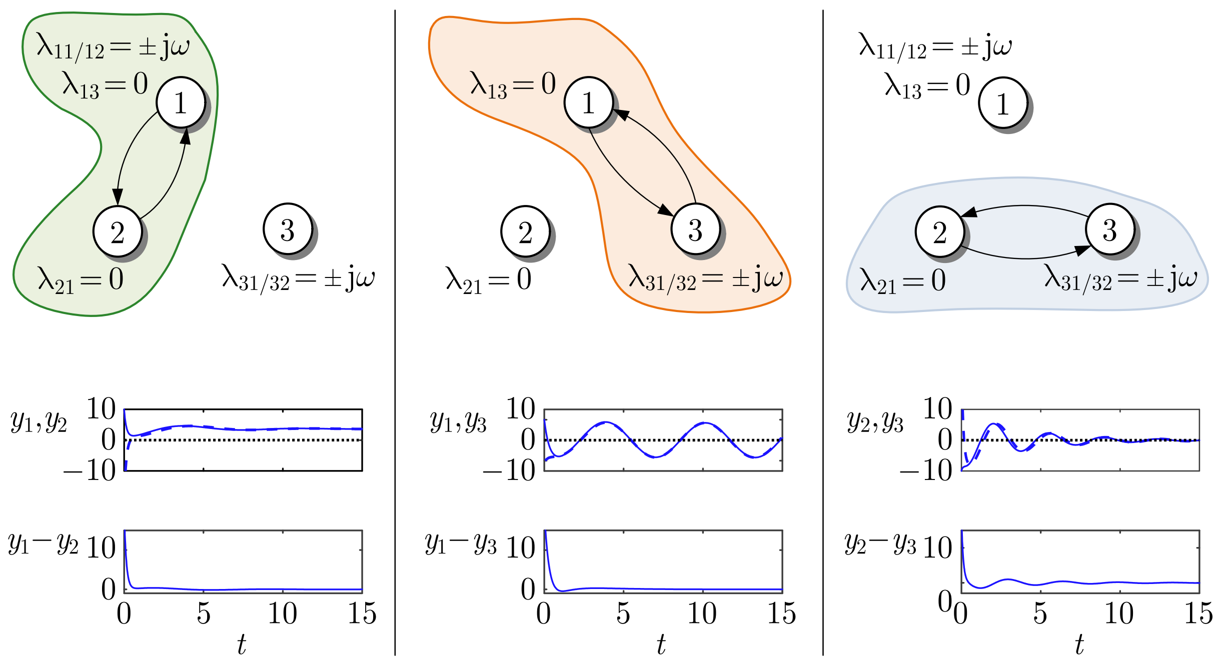

Fig. 4.34: Synchronisation behaviour of three pairs of agents

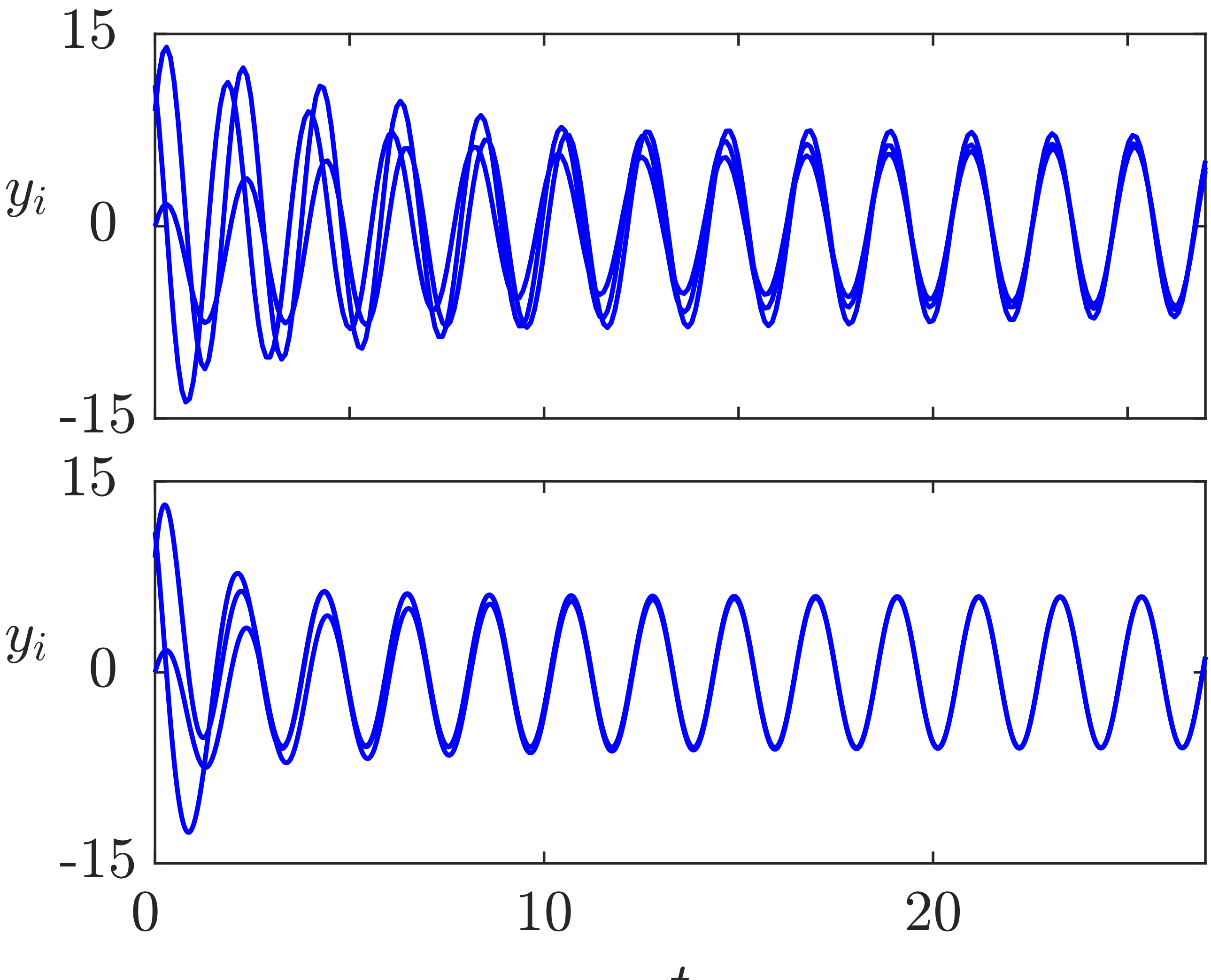

Fig. 4.35: Synchronisation of three oscillators with different additional first-order dynamics

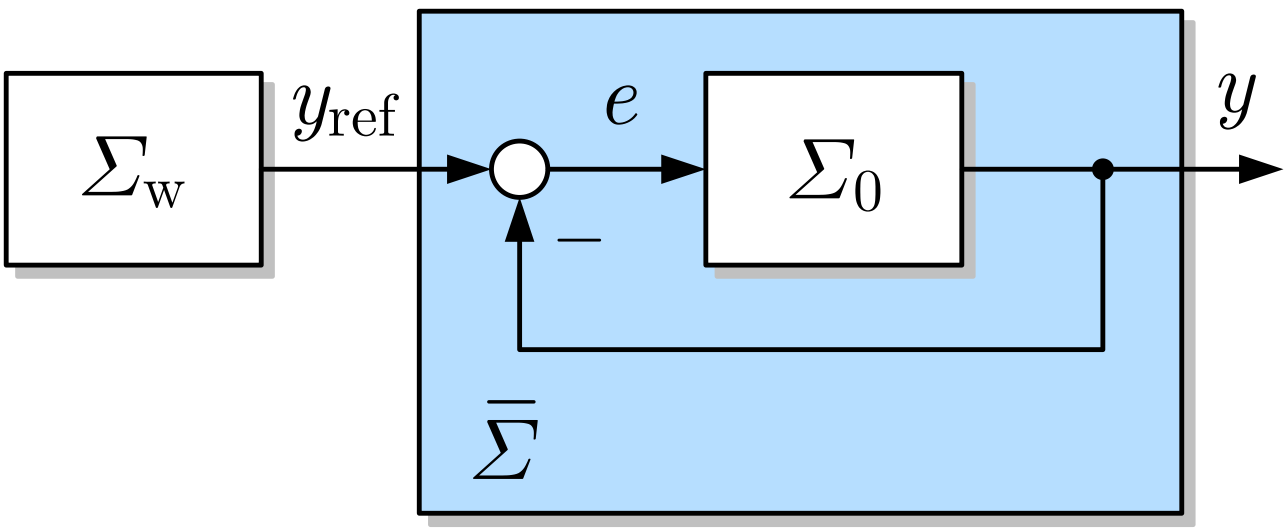

Fig. 4.36: Servomechanism problem

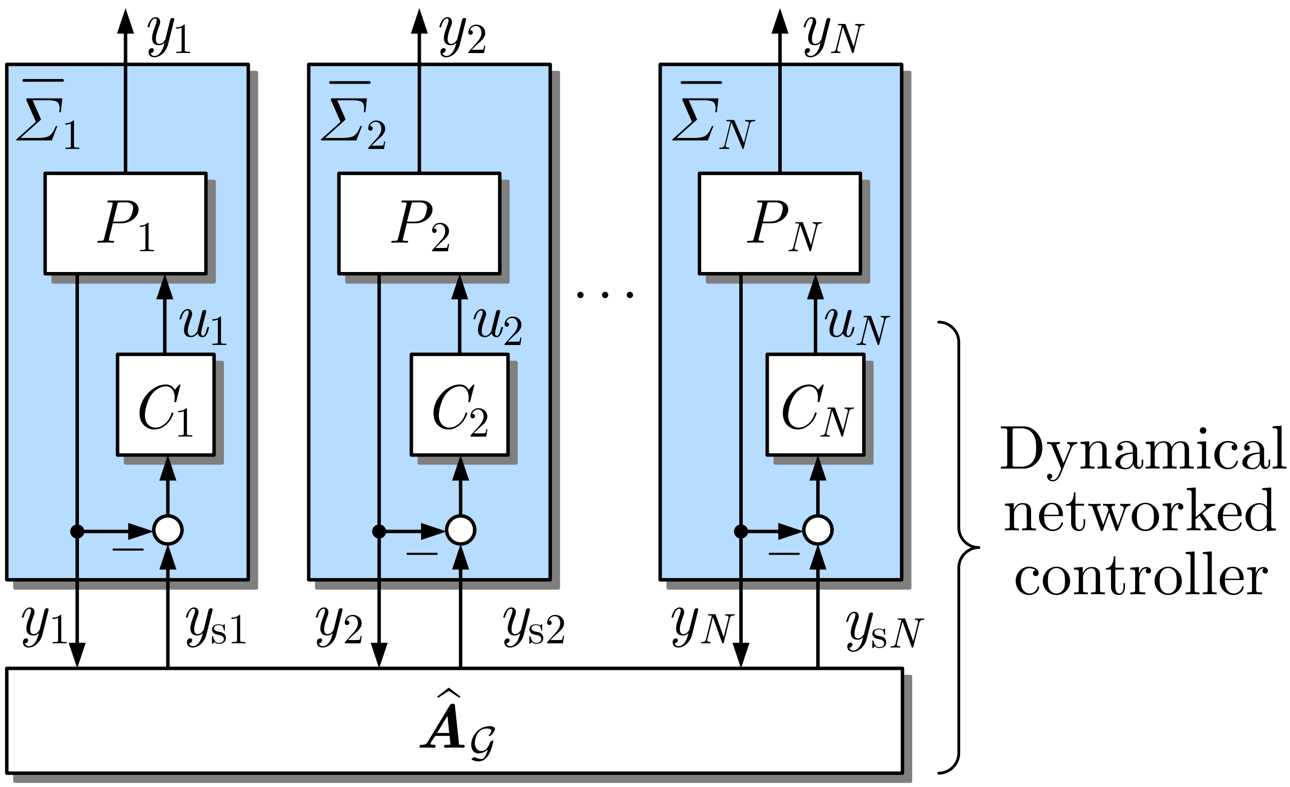

Fig. 4.37: Multi-agent system with dynamical networked controller

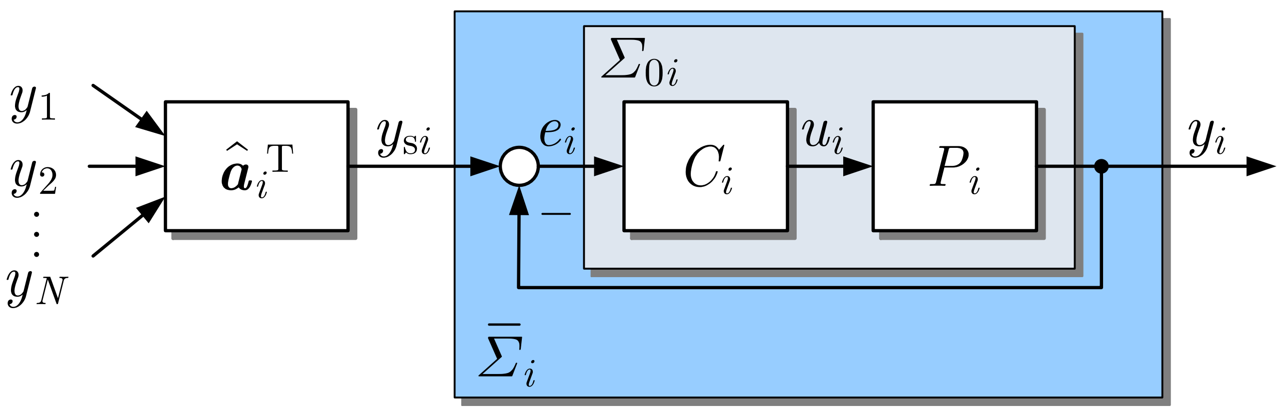

Fig. 4.38: Control-theoretical interpretation of the controlled agent

J. Lunze: *Networked Control of Multi-Agent Systems*, Edition MoRa 2022

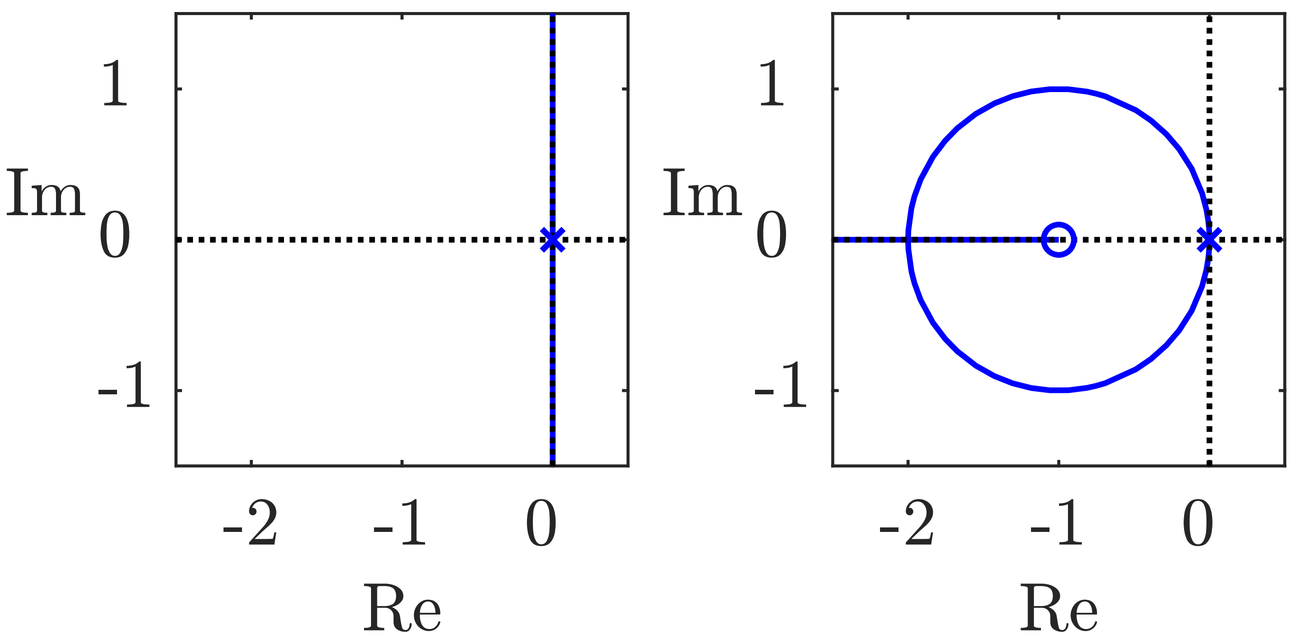

Fig. 4.39: Root loci of the closed-loop agent and the extended closed-loop agent

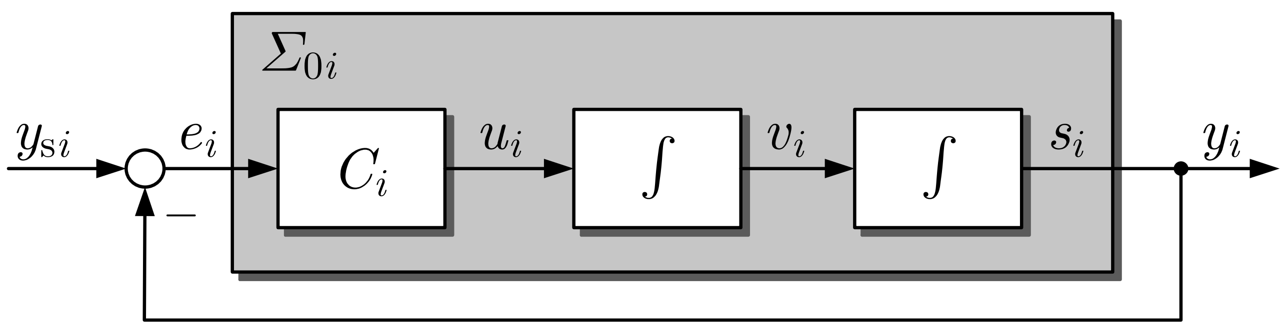

Fig. 4.40: Position control loop of a double-integrator vehicle

J. Lunze: *Networked Control of Multi-Agent Systems*, Edition MoRa 2022

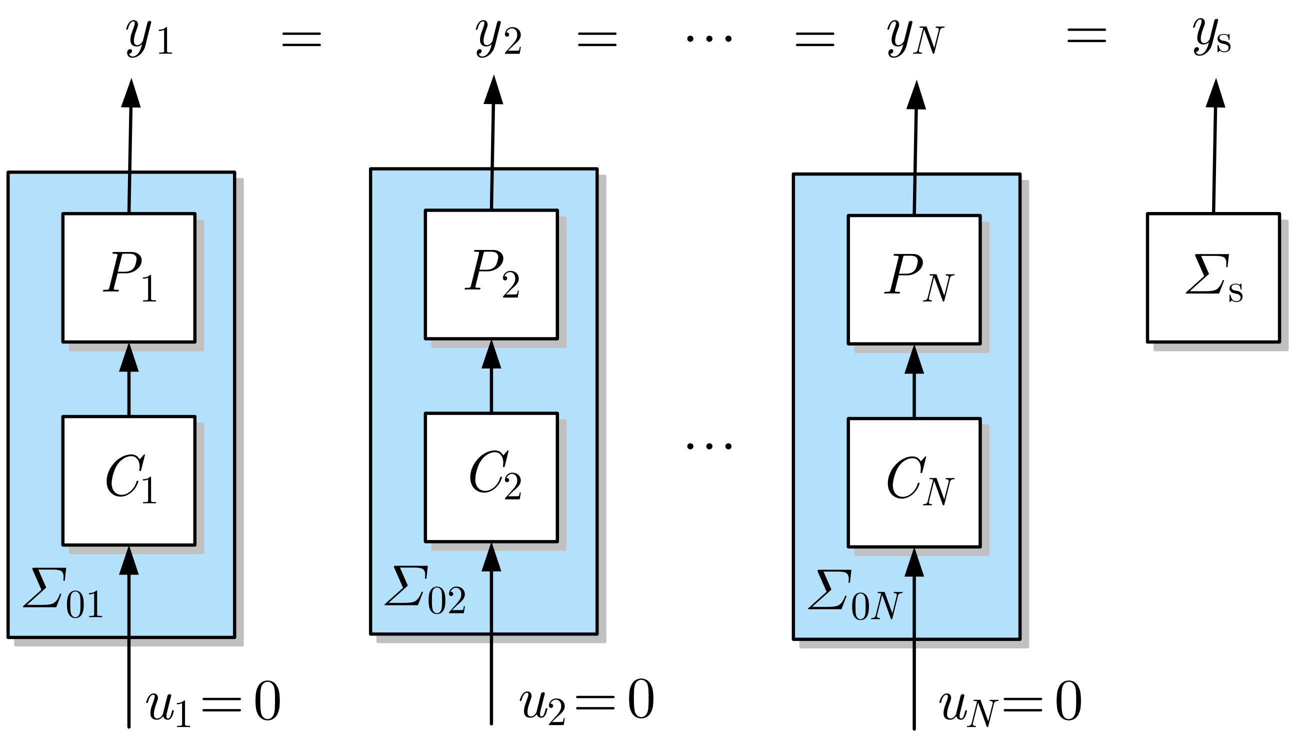

Fig. 4.41: Introduction of the common dynamics into the extended agents by local controllers

J. Lunze: *Networked Control of Multi-Agent Systems*, Edition MoRa 2022

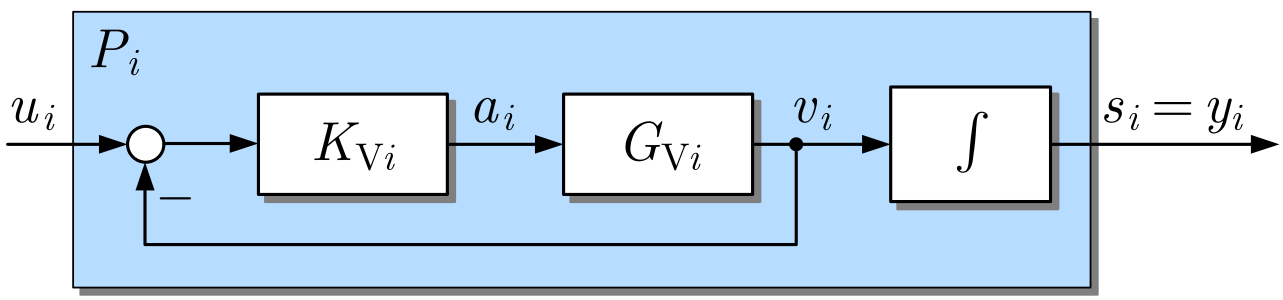

Fig. 4.42: Vehicle model

J. Lunze: *Networked Control of Multi-Agent Systems,* Edition MoRa 2022

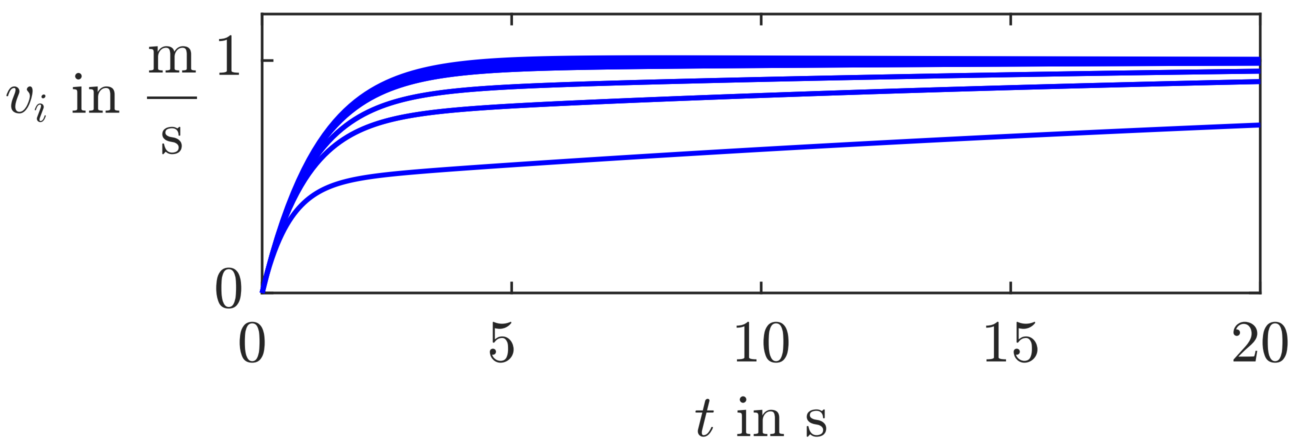

Fig. 4.43: Command step response of the vehicle P_i with the velocity control loop with different masses

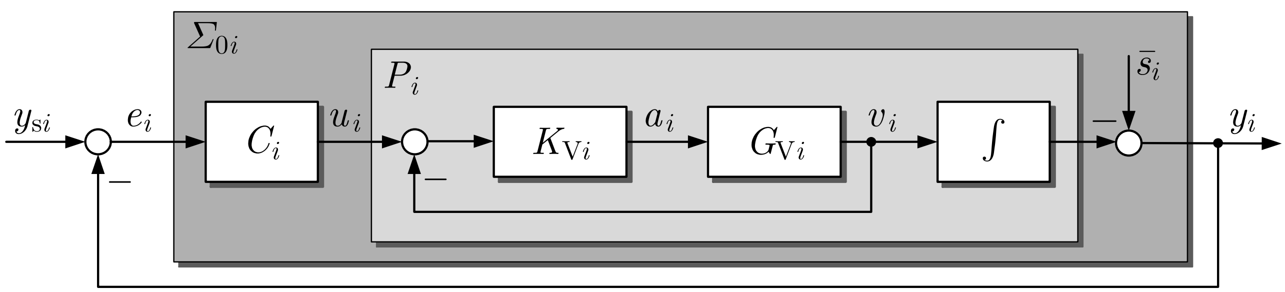

Fig. 4.44: Controlled vehicle

J. LUNZE: *Networked Control of Multi-Agent Systems*, Edition **MoRa** 2022

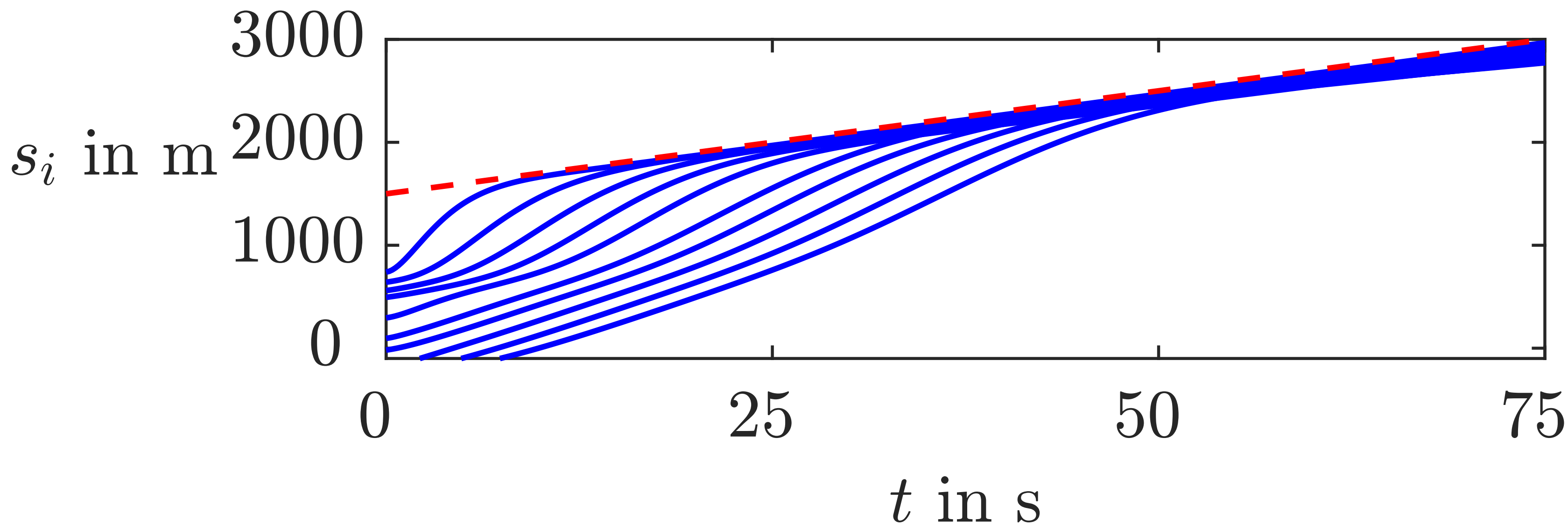

Fig. 4.45. Behaviour of the platoon with neighbouring couplings

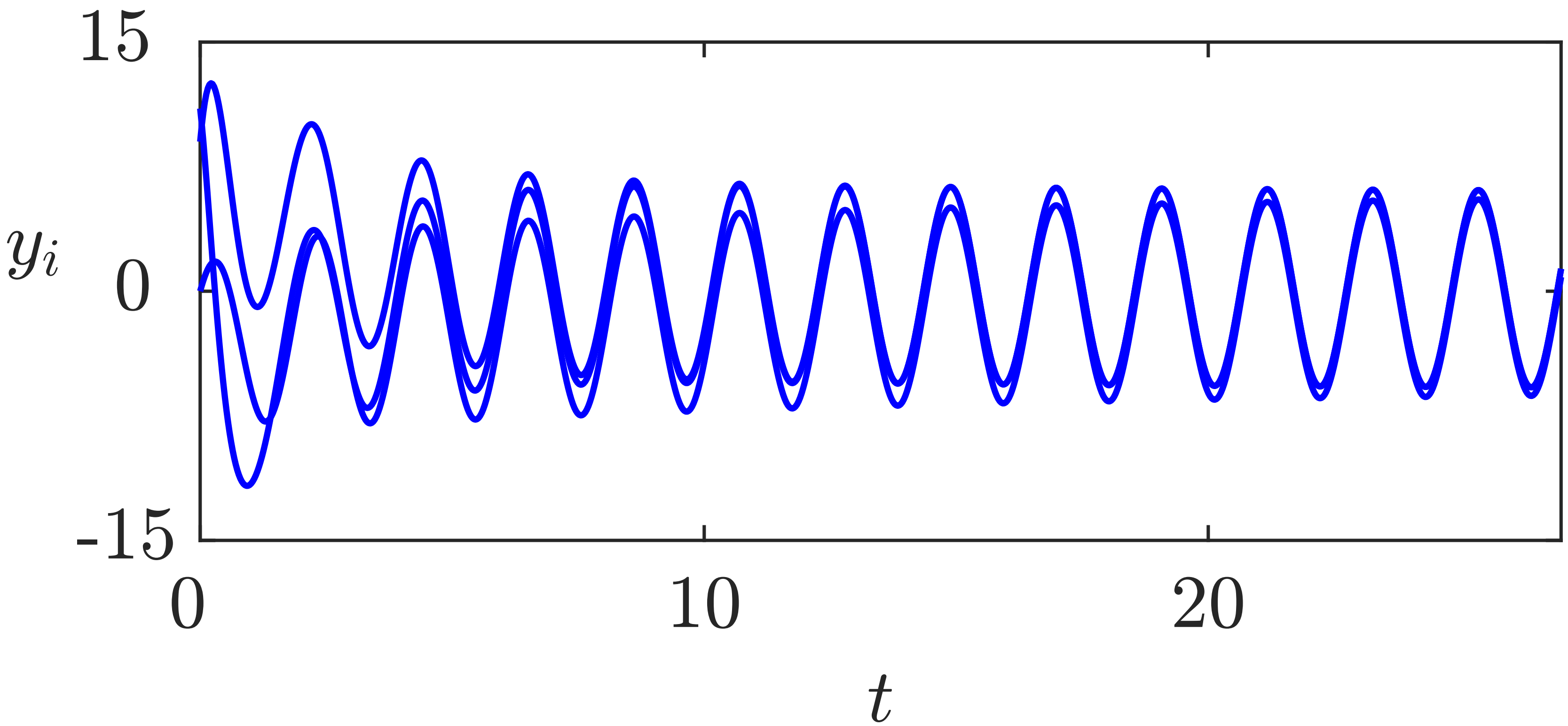

Fig. 4.46. Robust synchronisation of three oscillators with increased coupling gain

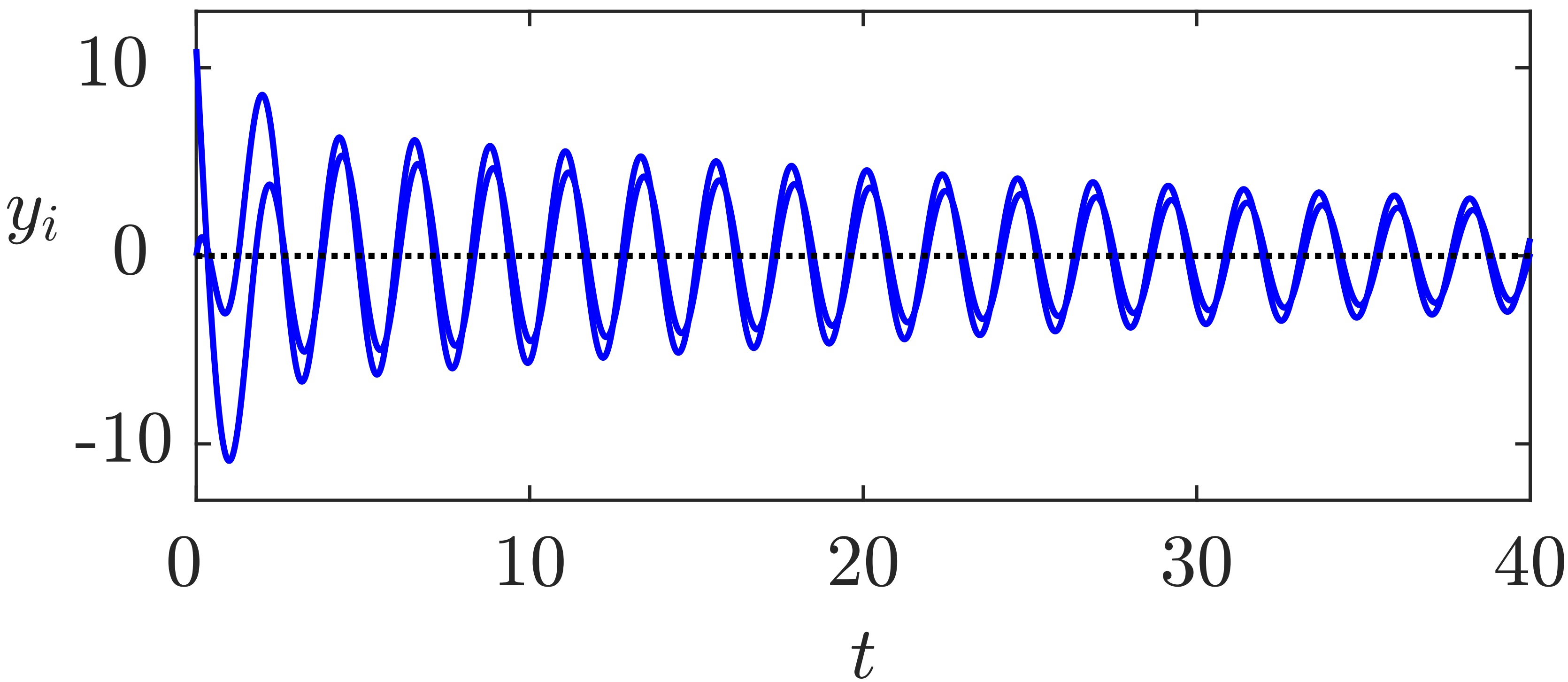

Fig. 4.47. Two oscillators with different eigenfrequencies $\omega_1 = 3$ and $\omega_2 = 2.5$ do not synchronise but constitute an asymptotically stable system

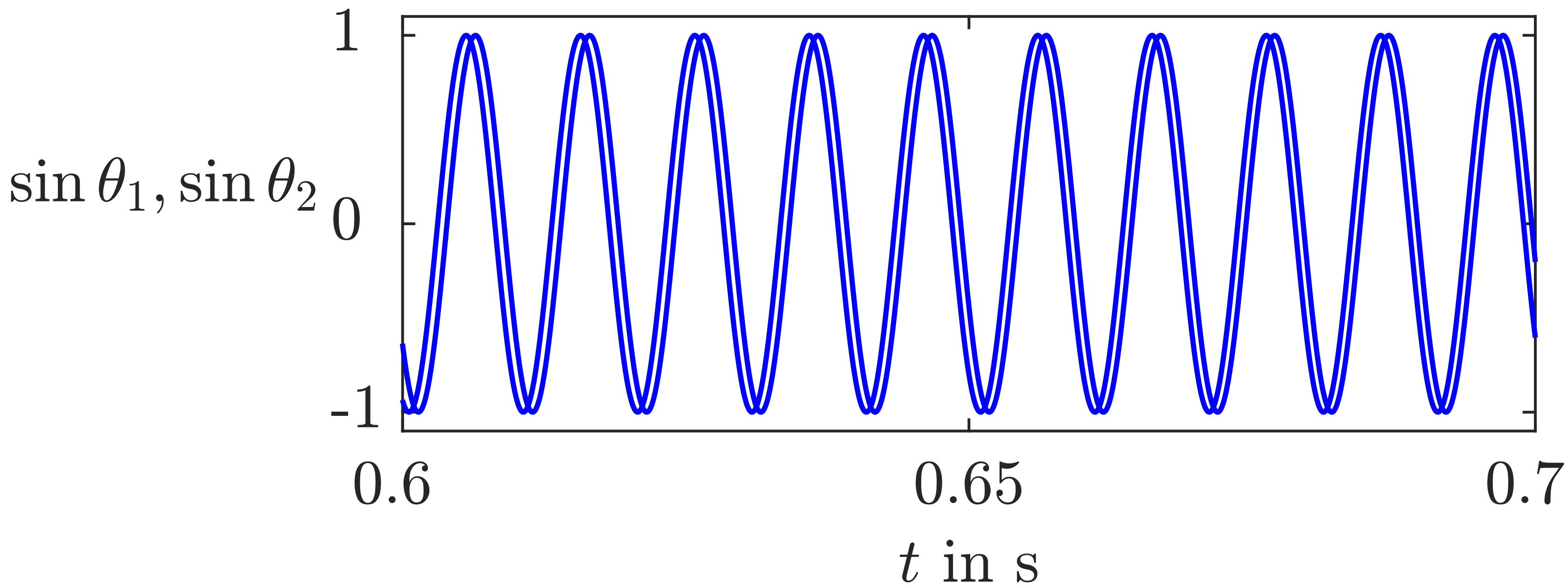

Fig. 4.48. Practical synchronisation of two coupled motors: The outputs follow the same sinusoidal trajectory with a small phase shift

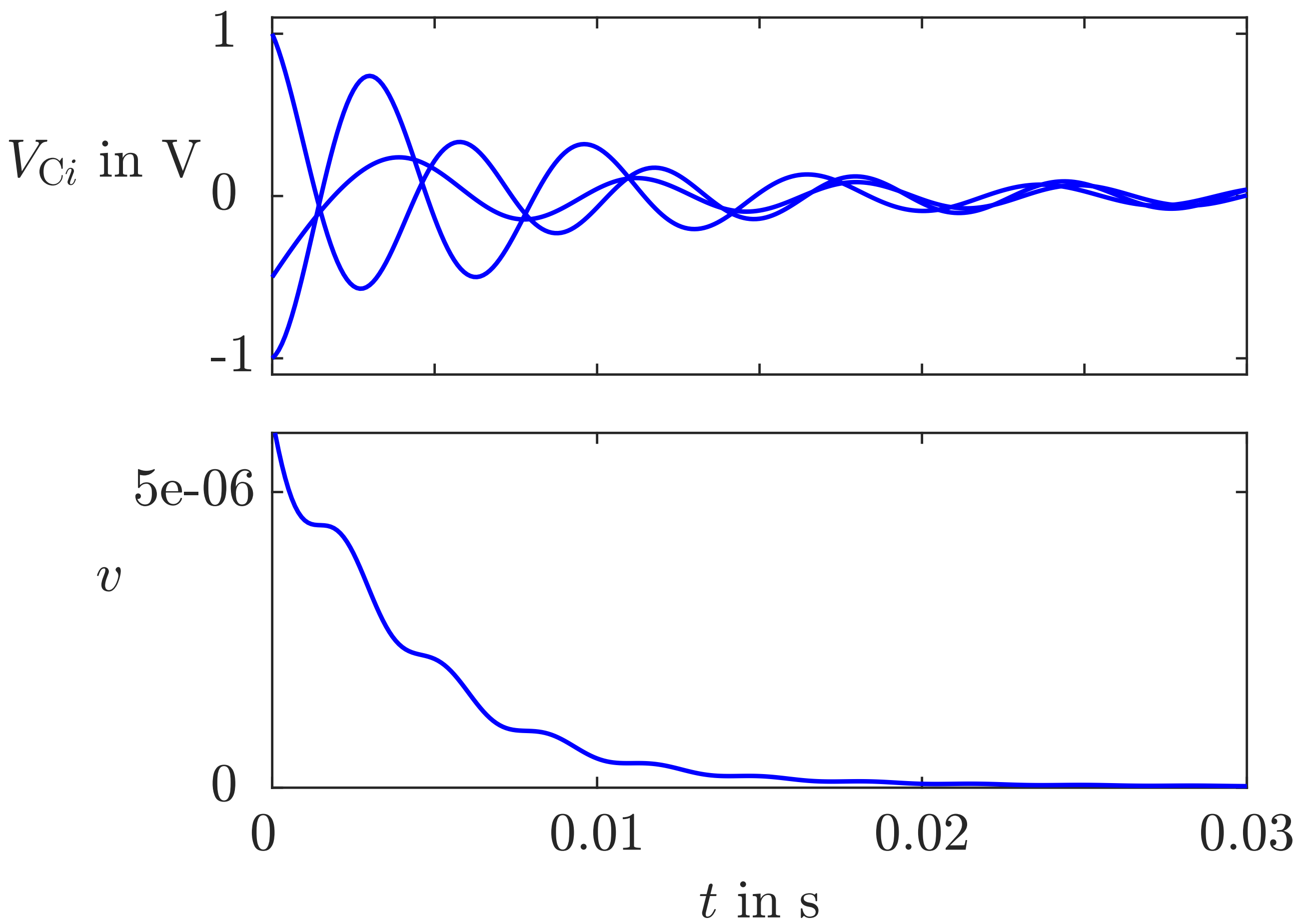

Fig. 4.49: Trajectories of the three non-uniform oscillators and Lyapunov function

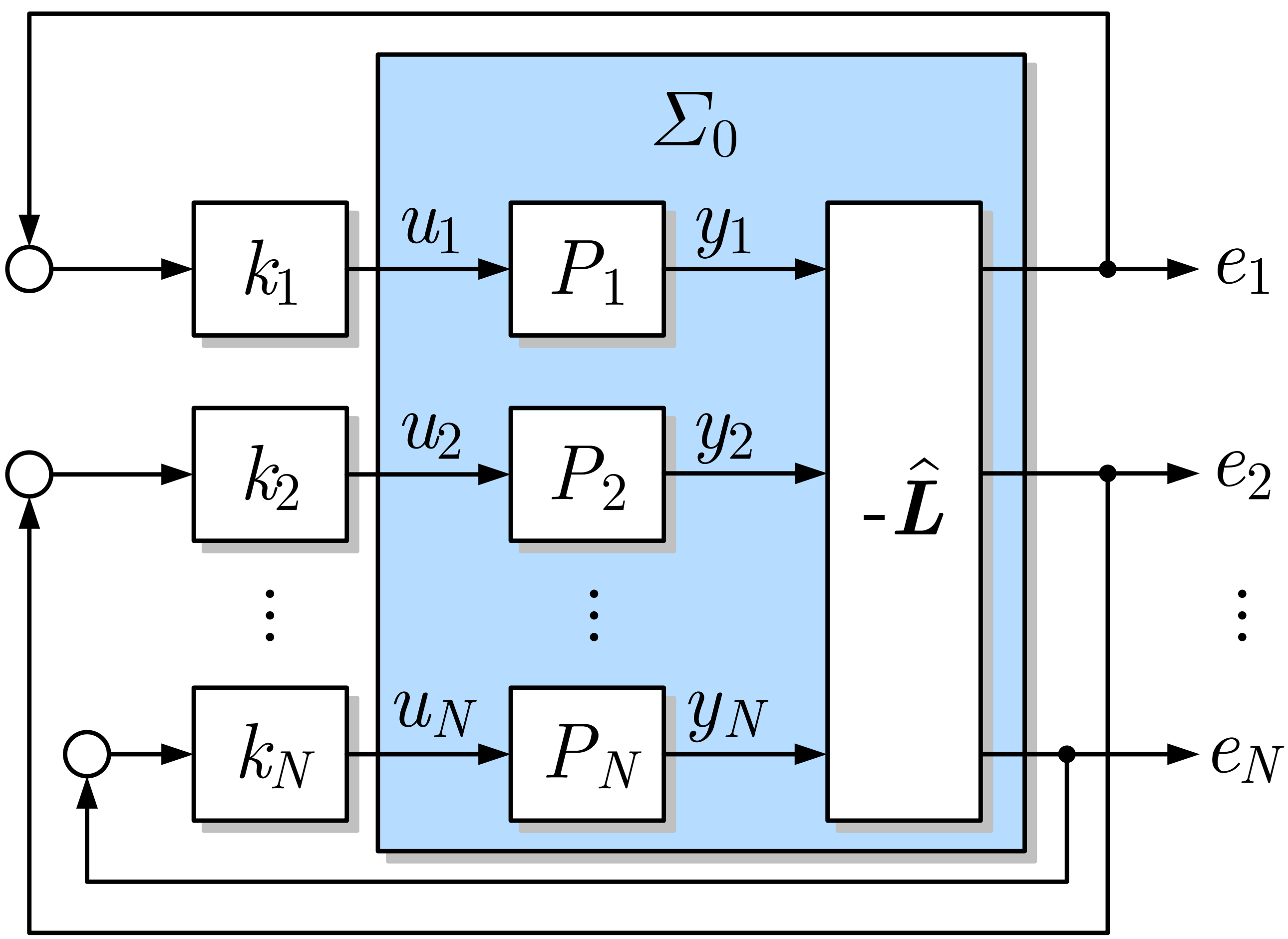

Fig. 4.50: Structure of the overall system $\overline{\Sigma}$

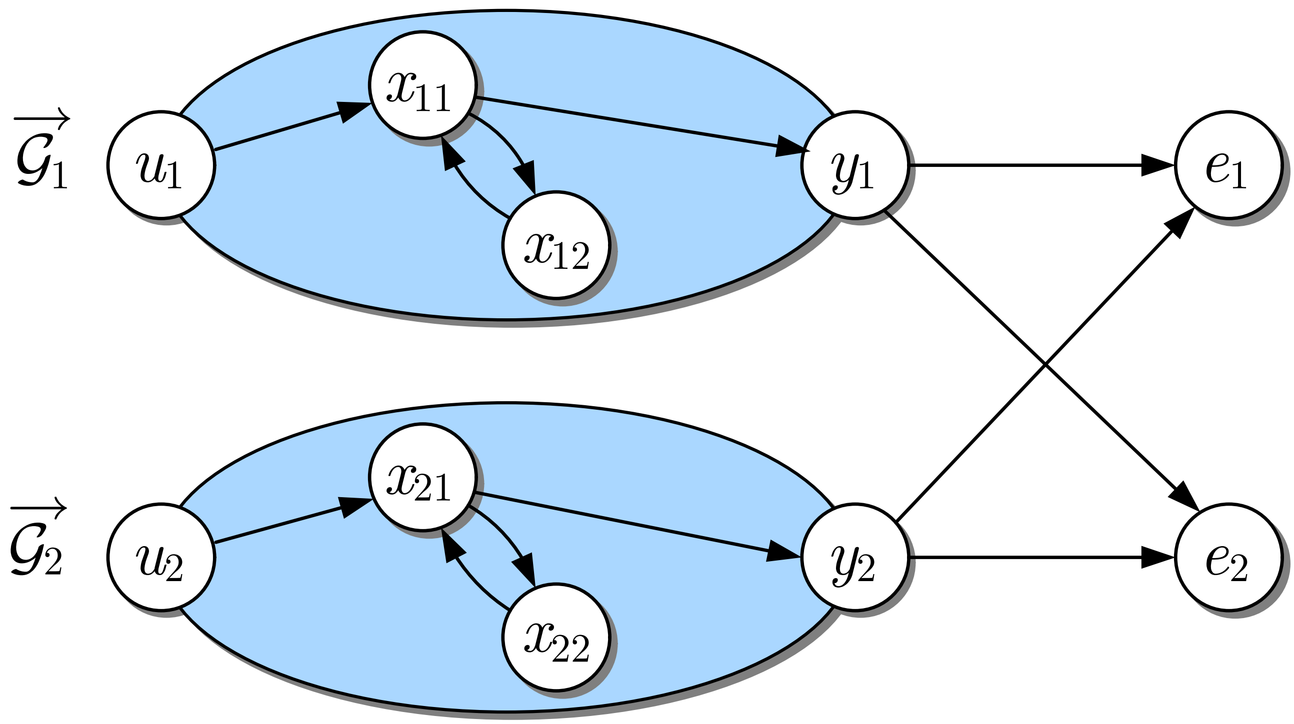

Fig. 4.51: Structure graph of the two coupled oscillators

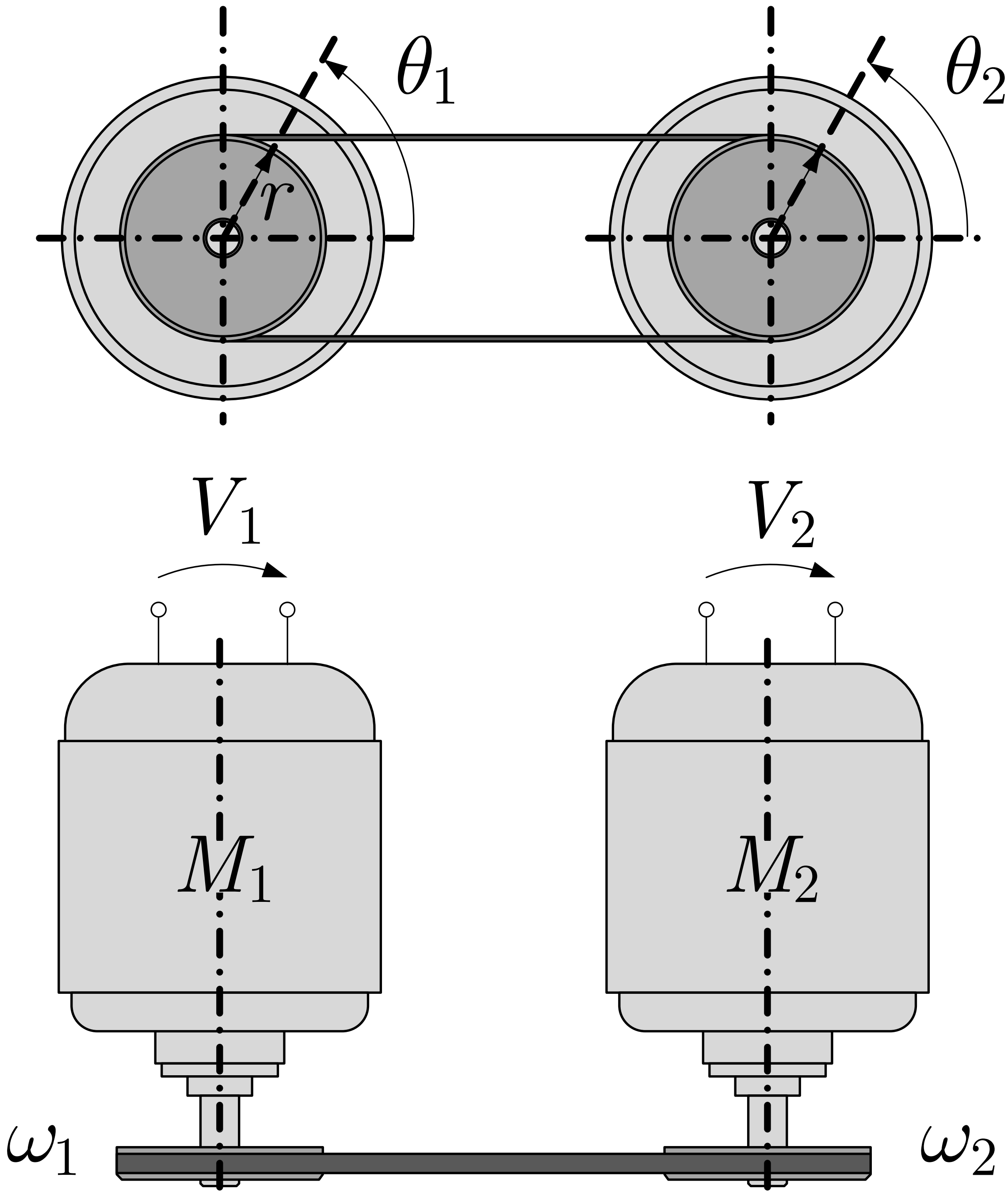

Fig. 4.52. Two coupled DC motors

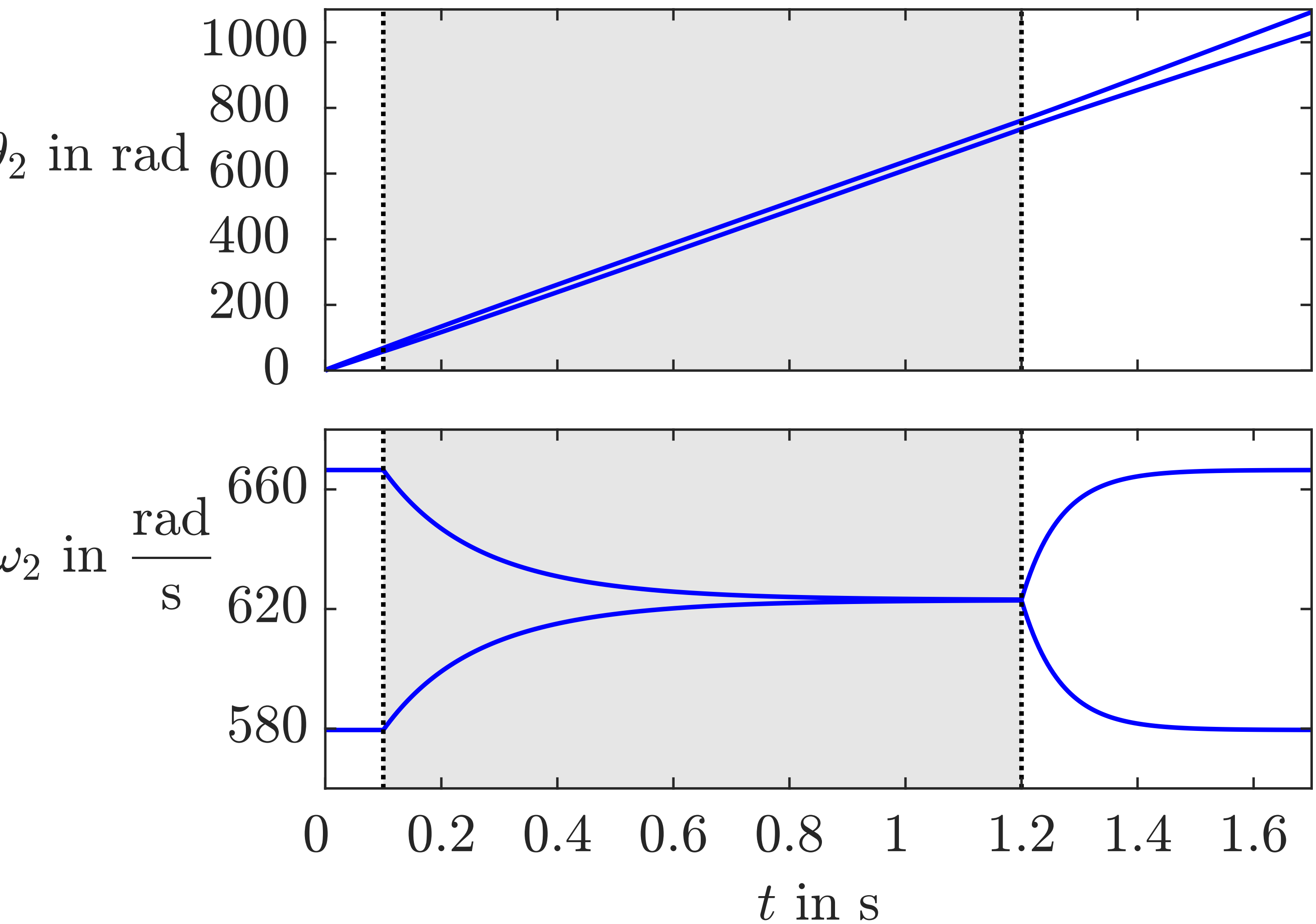

Fig. 4.53: Synchronising behaviour of the two motors

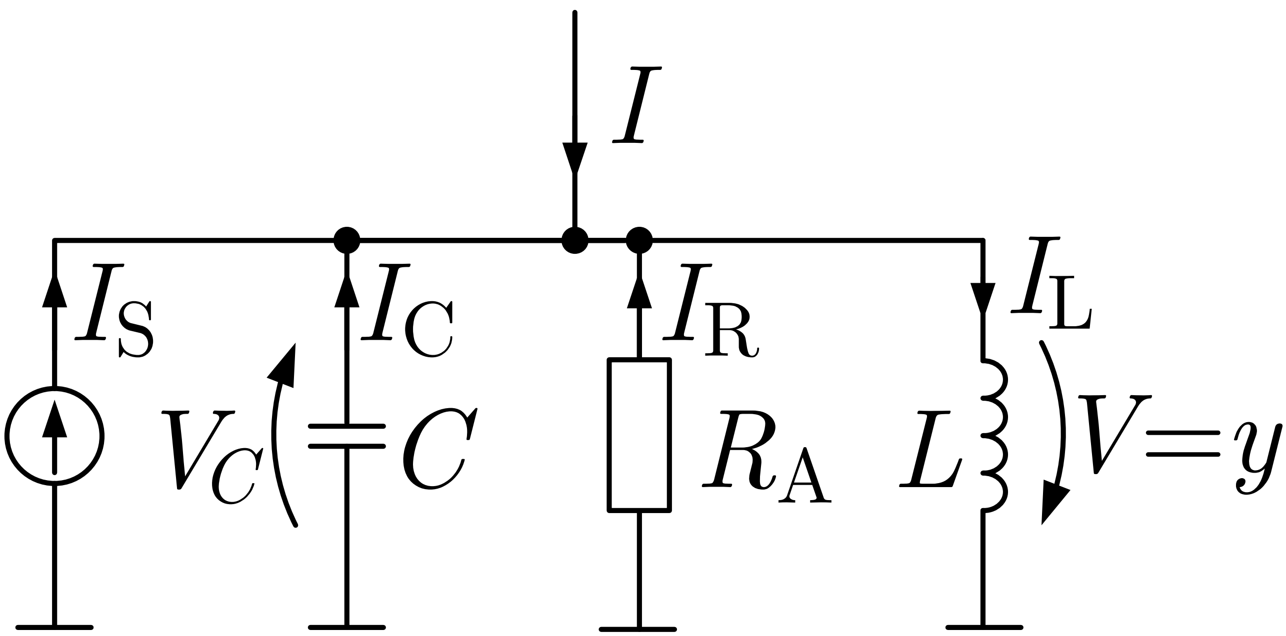

Fig. 4.54: Oscillator with voltage-controlled current source

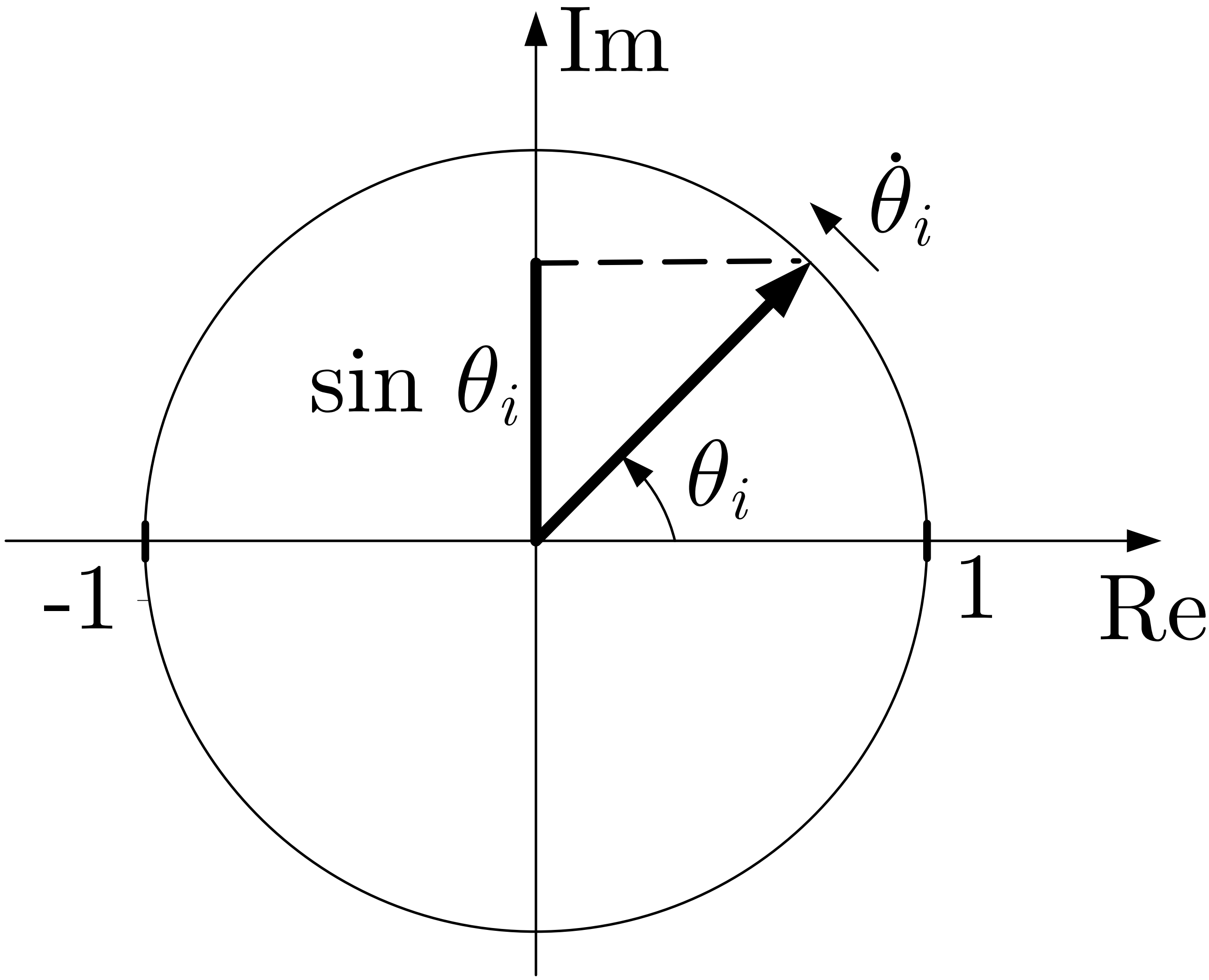

Fig. 4.55: Arrow representation of the i-th oscillator

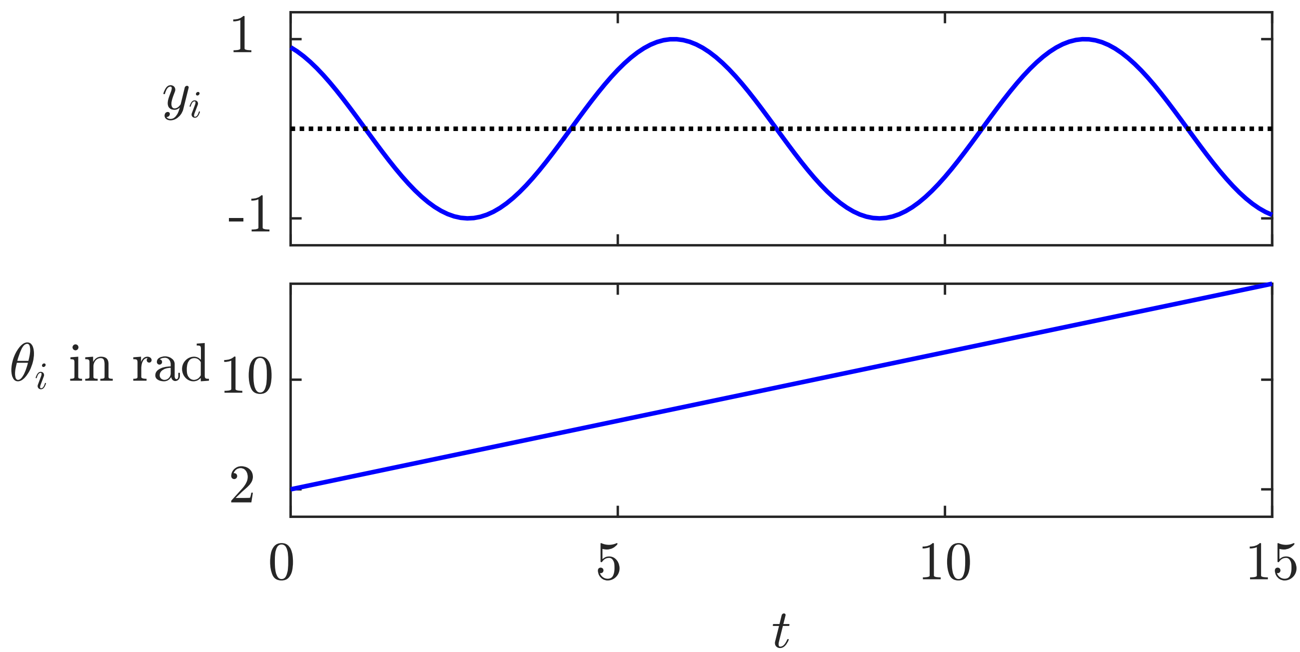

Fig. 4.56: Behaviour of a single Kuramoto oscillator with $\omega_i = 1\,\frac{\text{rad}}{\text{s}}$, $\theta_{i0} = 2\,\text{rad}$ and $u_i(t) = 0$

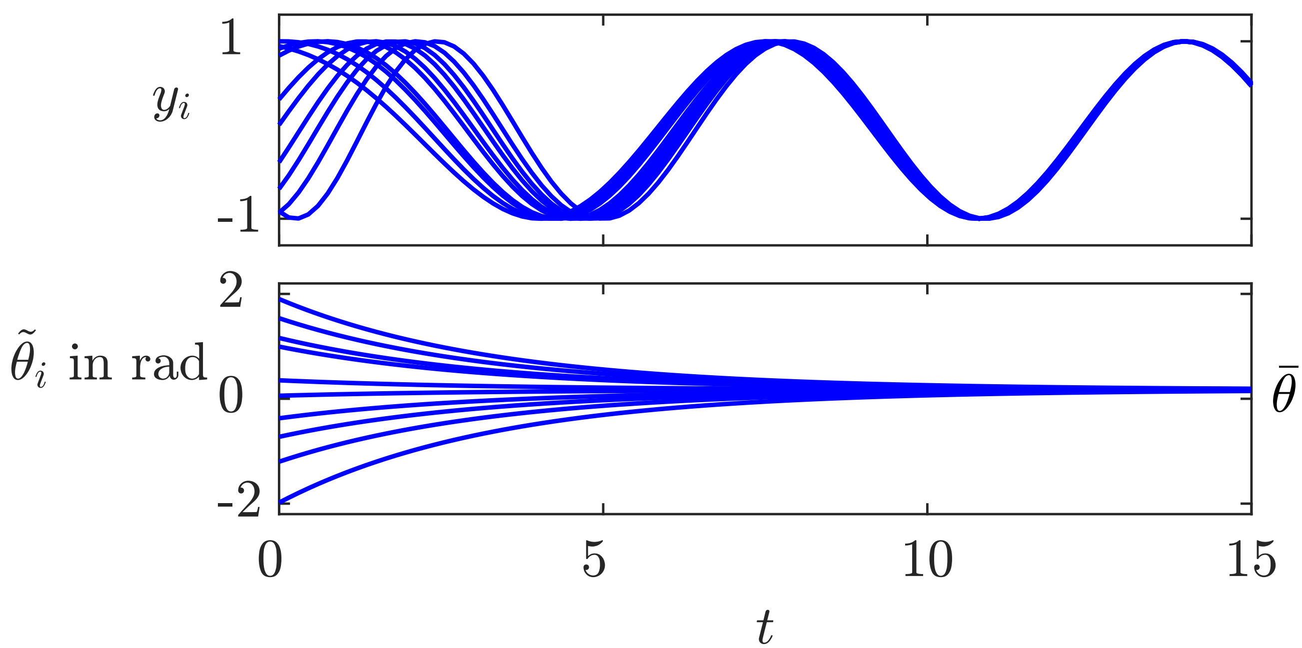

Fig. 4.57: Synchronisation of ten uniform Kuramoto oscillators with complete linear couplings ($\omega_i = 1\,\frac{\text{rad}}{\text{s}}$**,** $k = 0.03$)

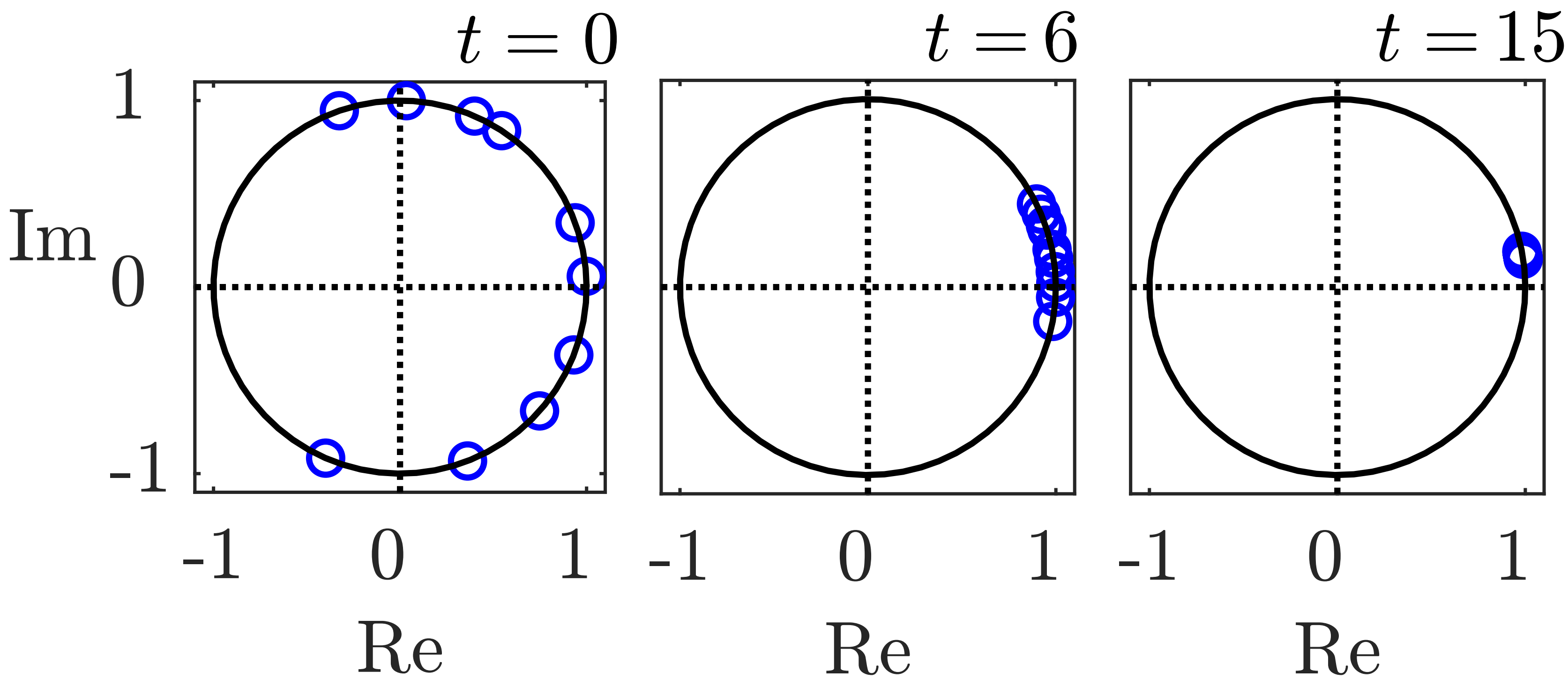

Fig. 4.58. Arrow representation of the synchronisation behaviour of Fig. 4.57

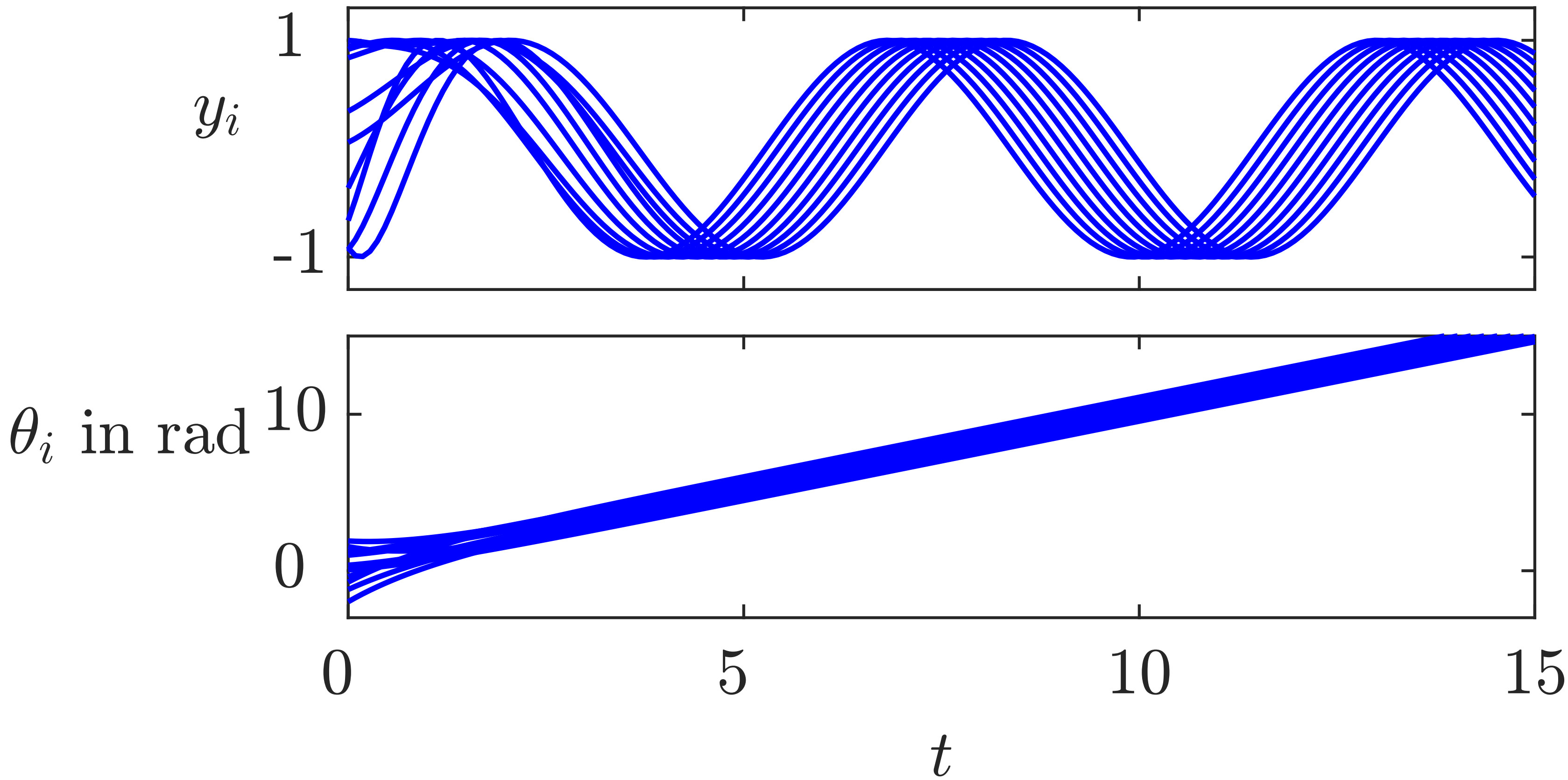

Fig. 4.59. Phase-locking behaviour of ten non-uniform Kuramoto oscillators with complete linear couplings $(k = 0.1)$

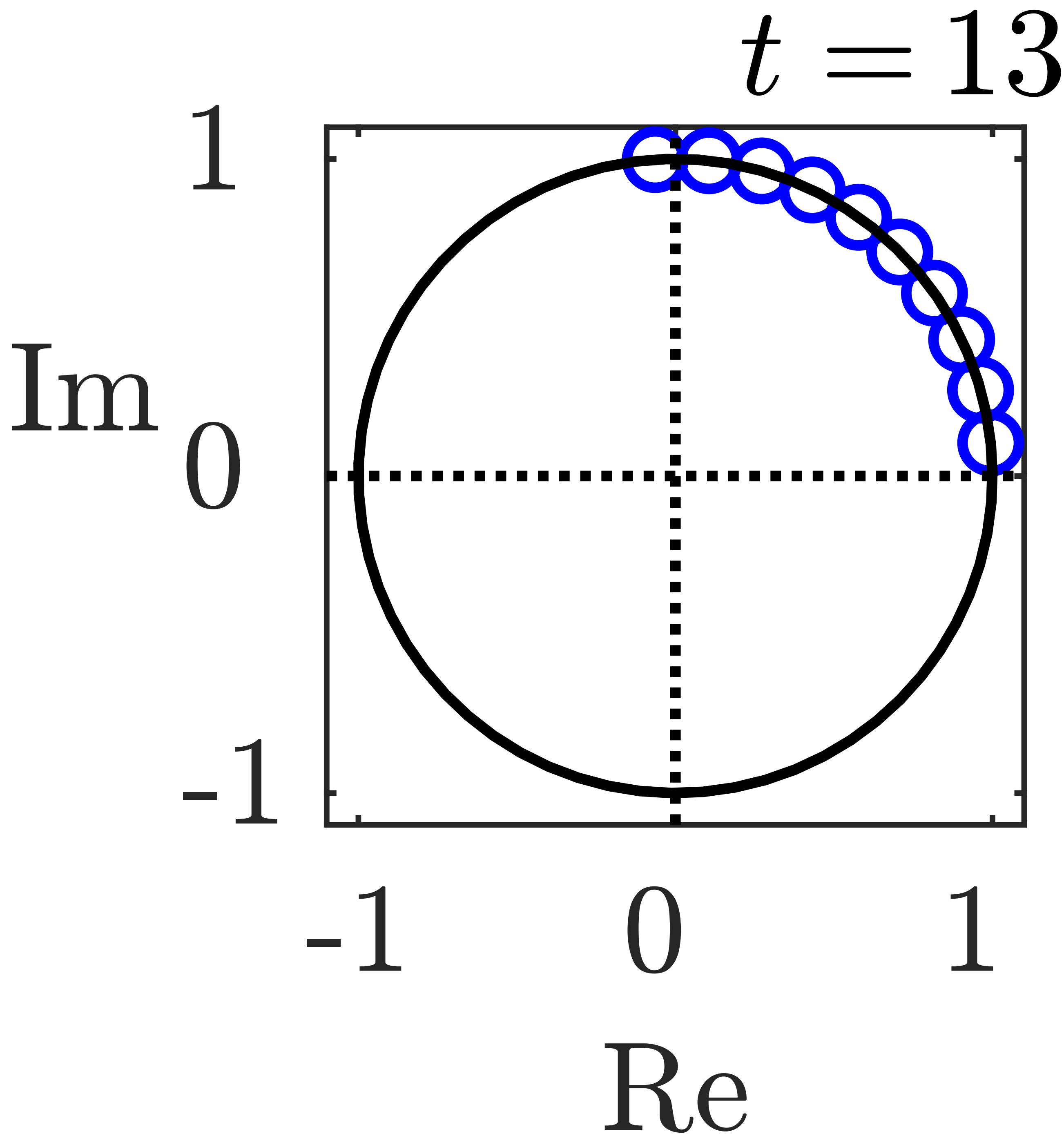

Fig. 4.59: Phase-locking behaviour of ten non-uniform Kuramoto oscillators with complete linear couplings $(k = 0.1)$

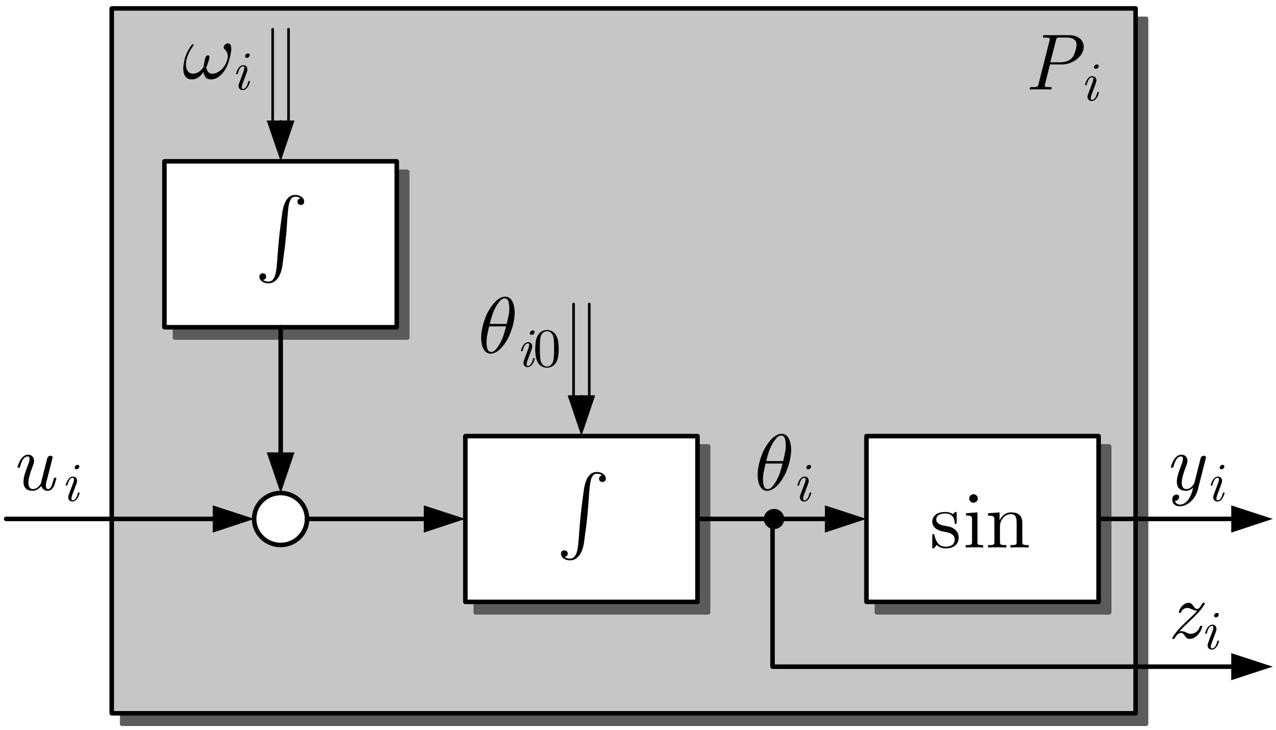

Fig. 4.60: Structure of the state-space model of a Kuramoto oscillator

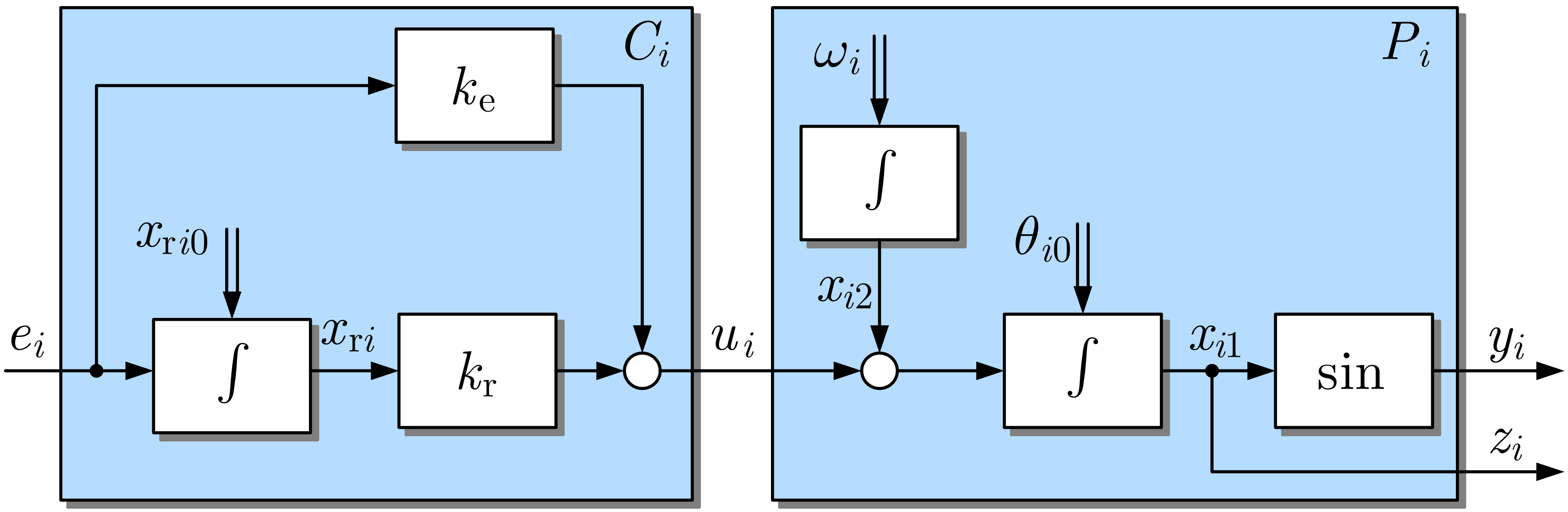

Fig. 4.61. Extended Kuramoto oscillator Σ_{0i}

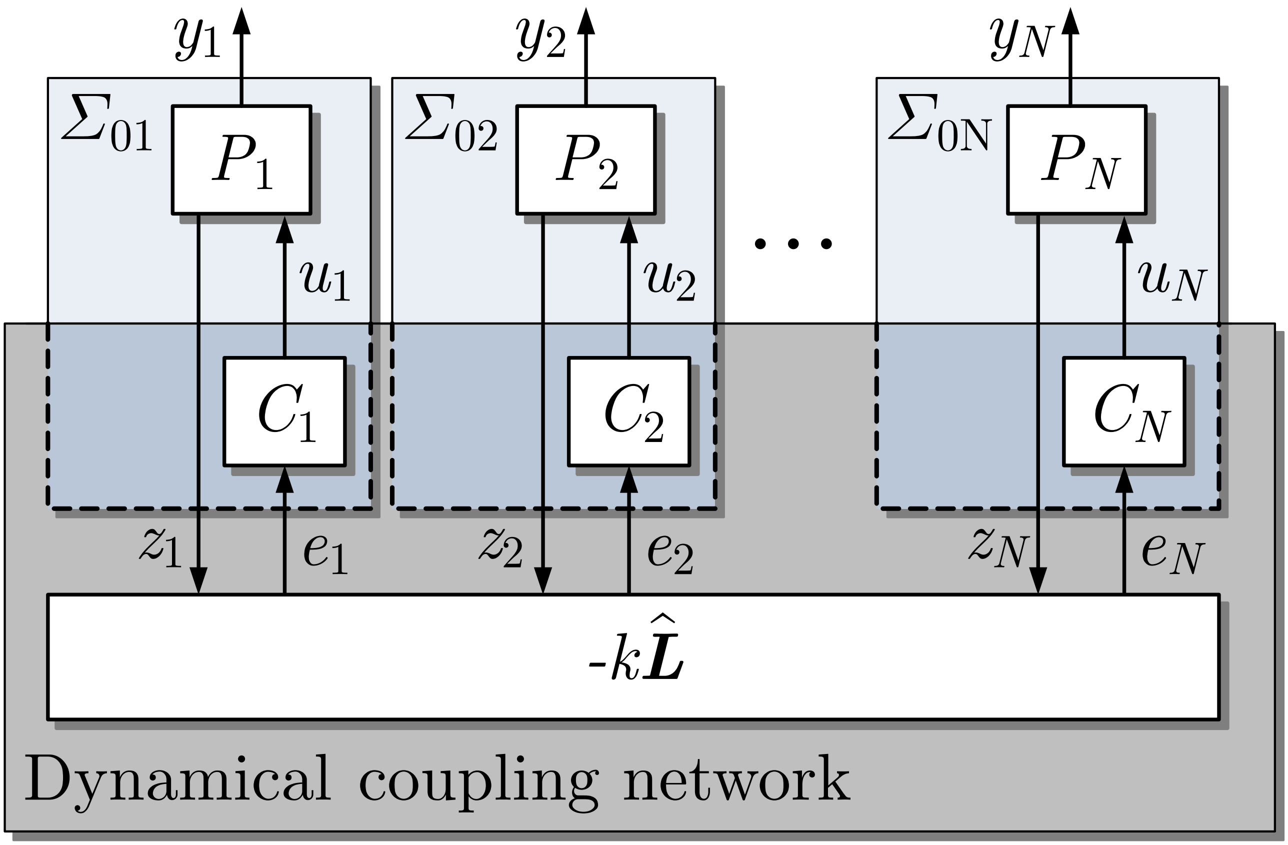

Fig. 4.62: Extended Kuramoto oscillators with linear coupling network

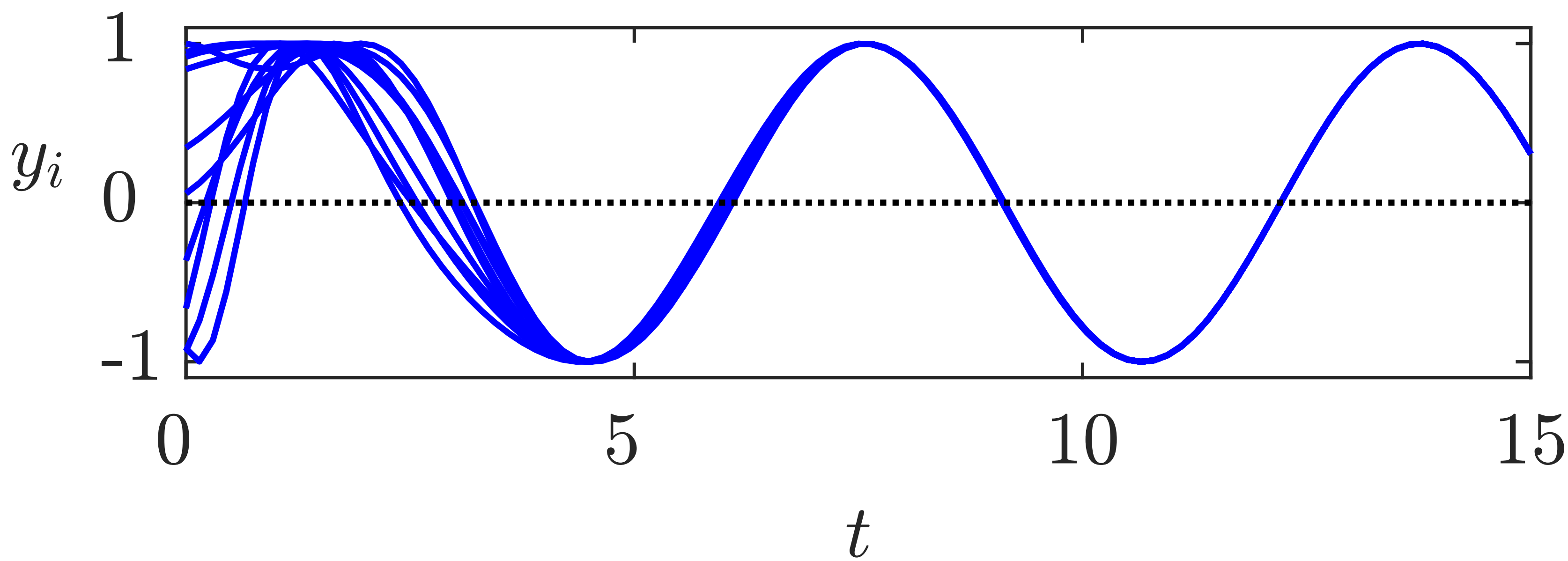

Fig. 4.63. Asymptotic synchronisation of non-uniform Kuramoto oscillators

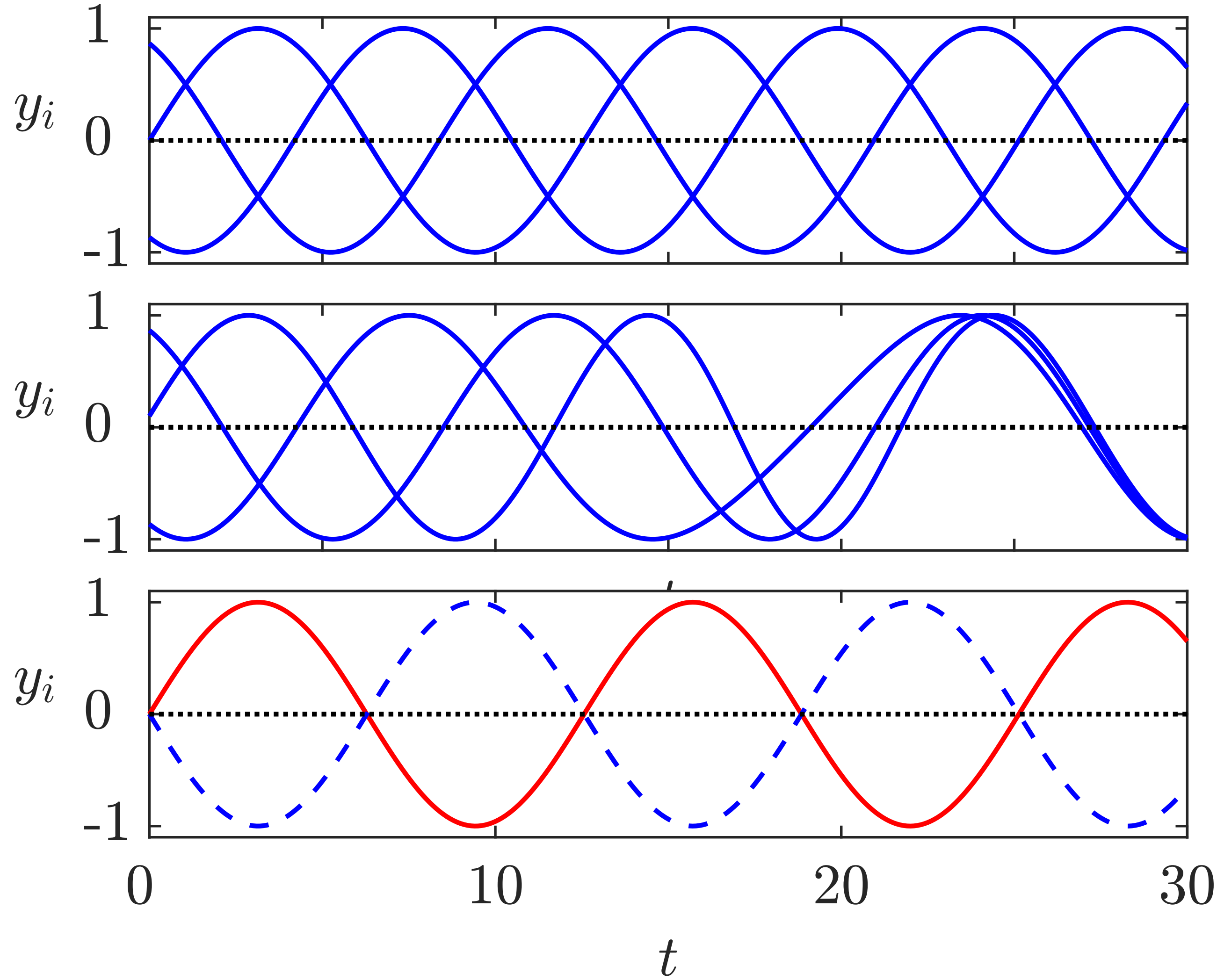

Fig. 4.64: Behaviour of uniform Kuramoto oscillators with non-synchronisable phases

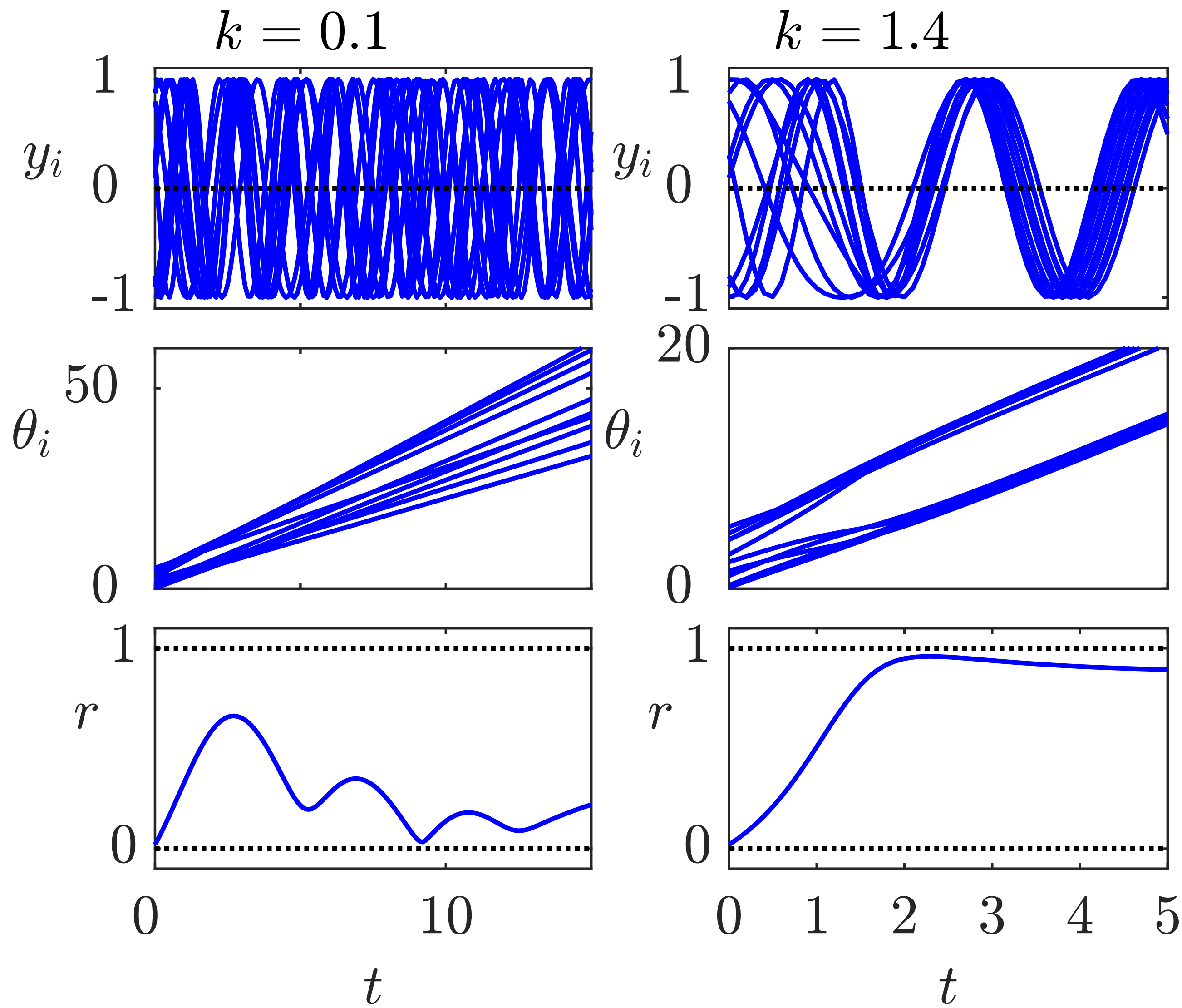

Fig. 4.65: Behaviour of ten nonlinearly coupled non-uniform Kuramoto oscillators for two coupling strengths

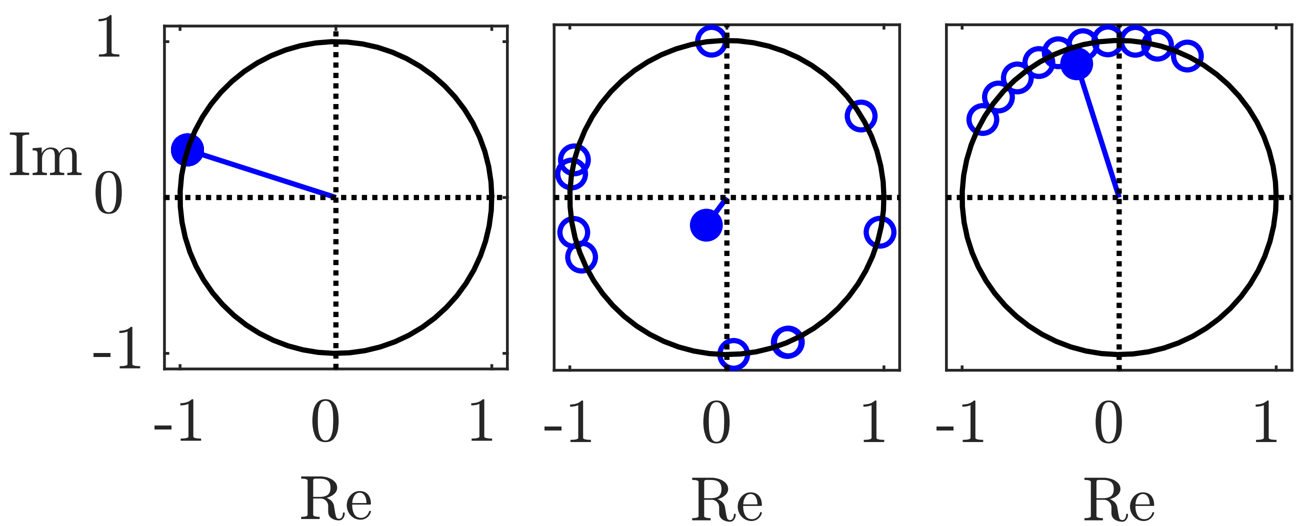

Fig. 4.66: Evaluation of the synchrony of the network behaviours shown in Figs. 4.63 and 4.65

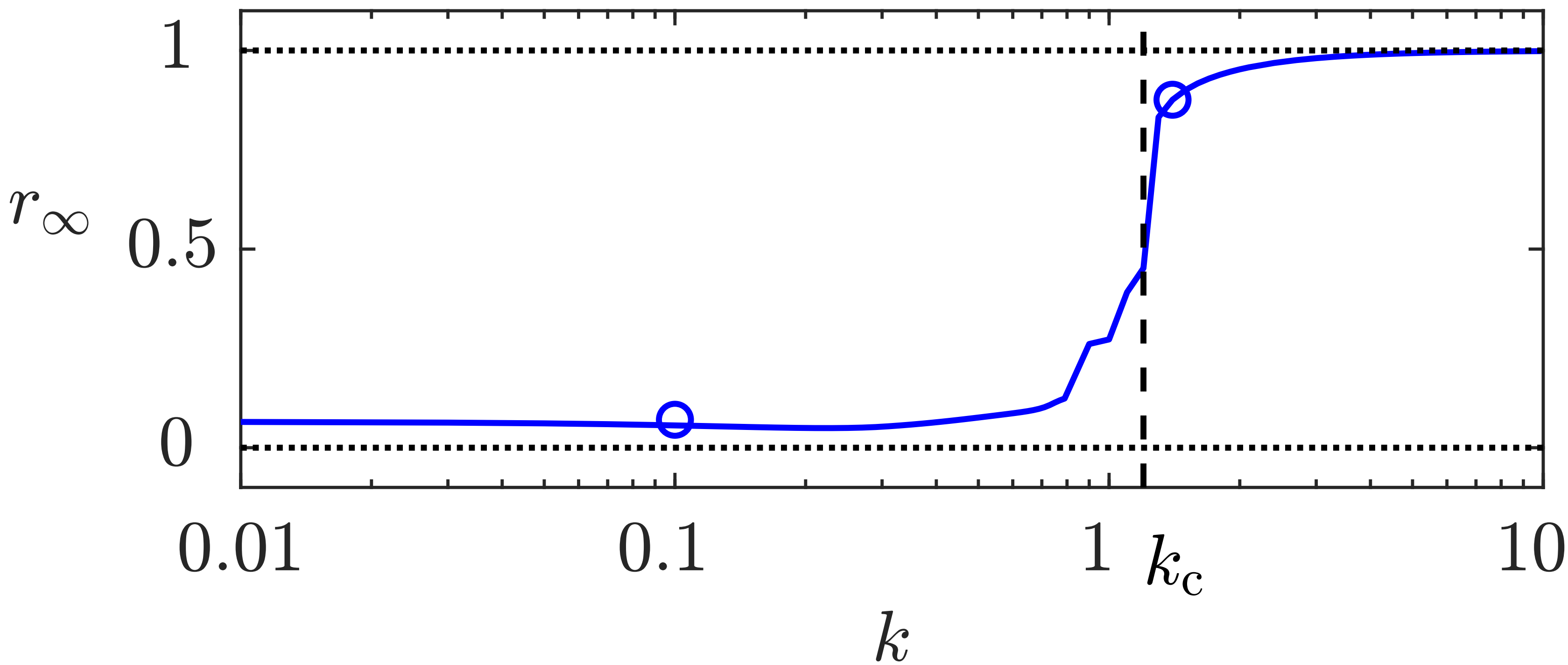

Fig. 4.67. Relation between the coupling strength k and the order parameter r_∞, which has been numerically determined for non-uniform oscillators with natural frequencies $\omega_i \in [2, 4]\,\frac{\mathrm{rad}}{\mathrm{s}}$ and all-to-all couplings

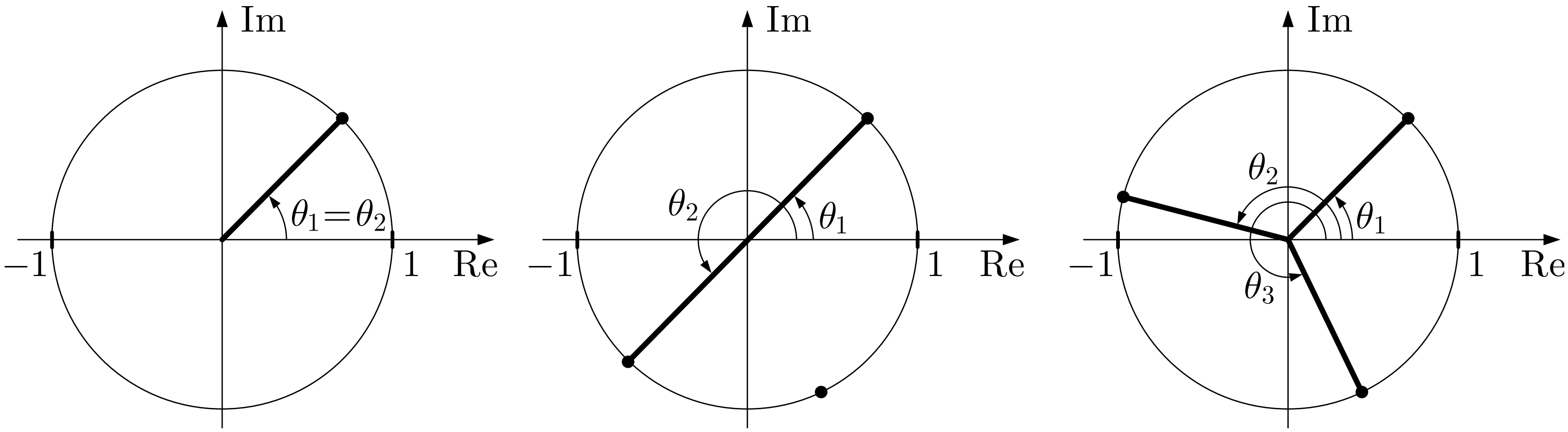

Fig. 4.68. Examples for non-synchronisable phases

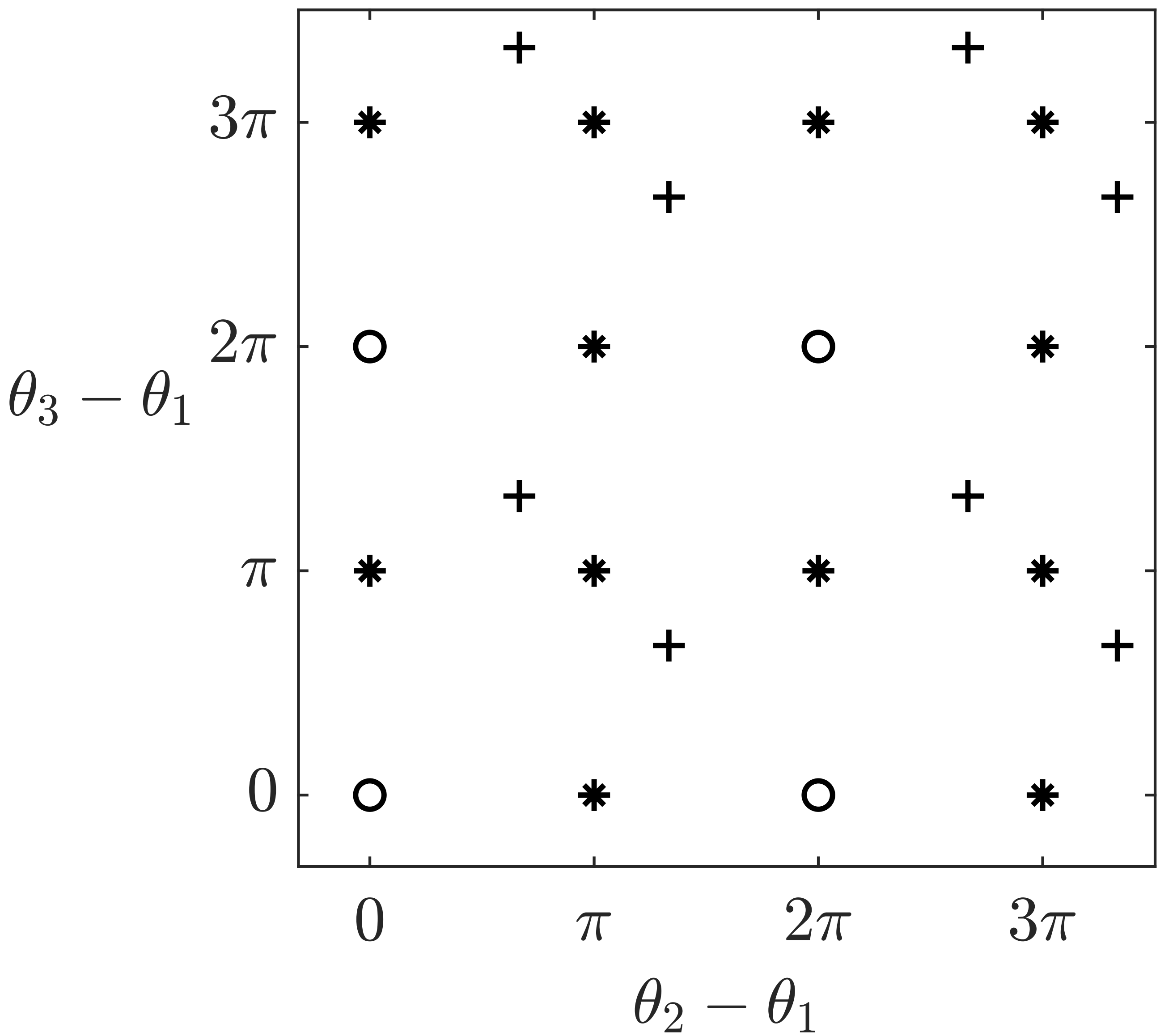

Fig. 4.69: Equilibrium states

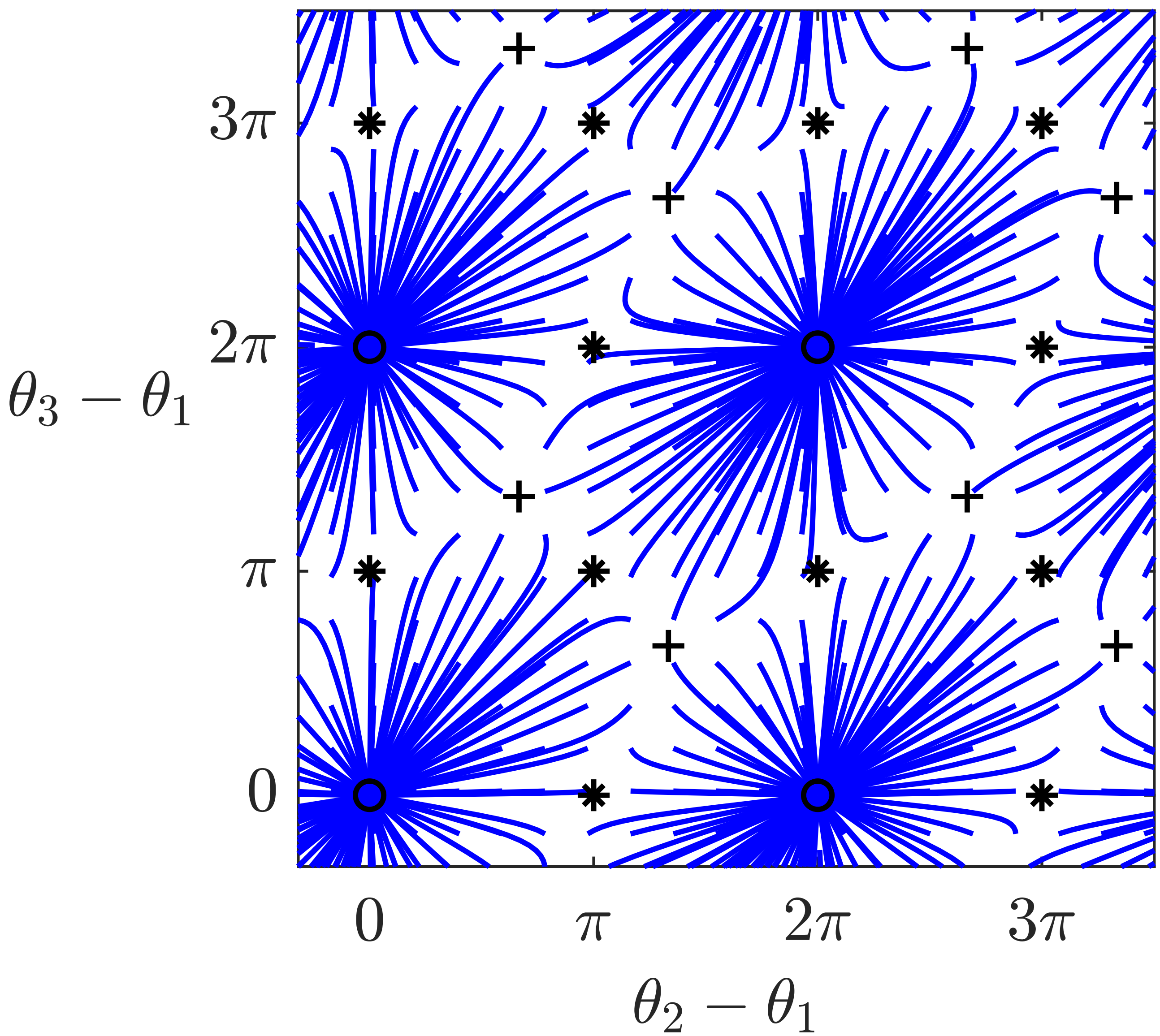

Fig. 4.69: Synchronisation behaviour of the uniform oscillators with $\theta_{10} = 0$

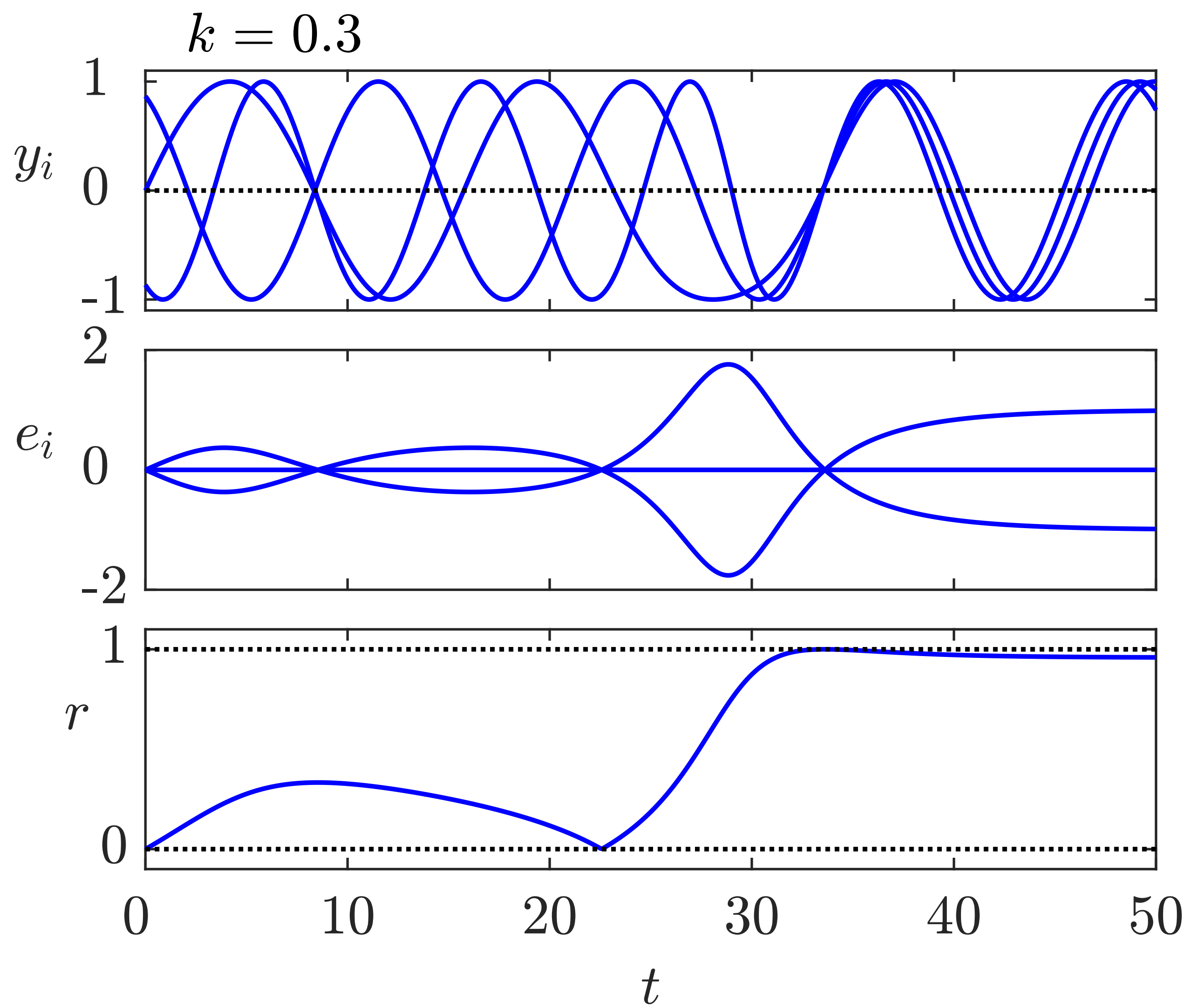

Fig. 4.70: Phase-locking of three non-uniform Kuramoto oscillators with initial phases (4.232)

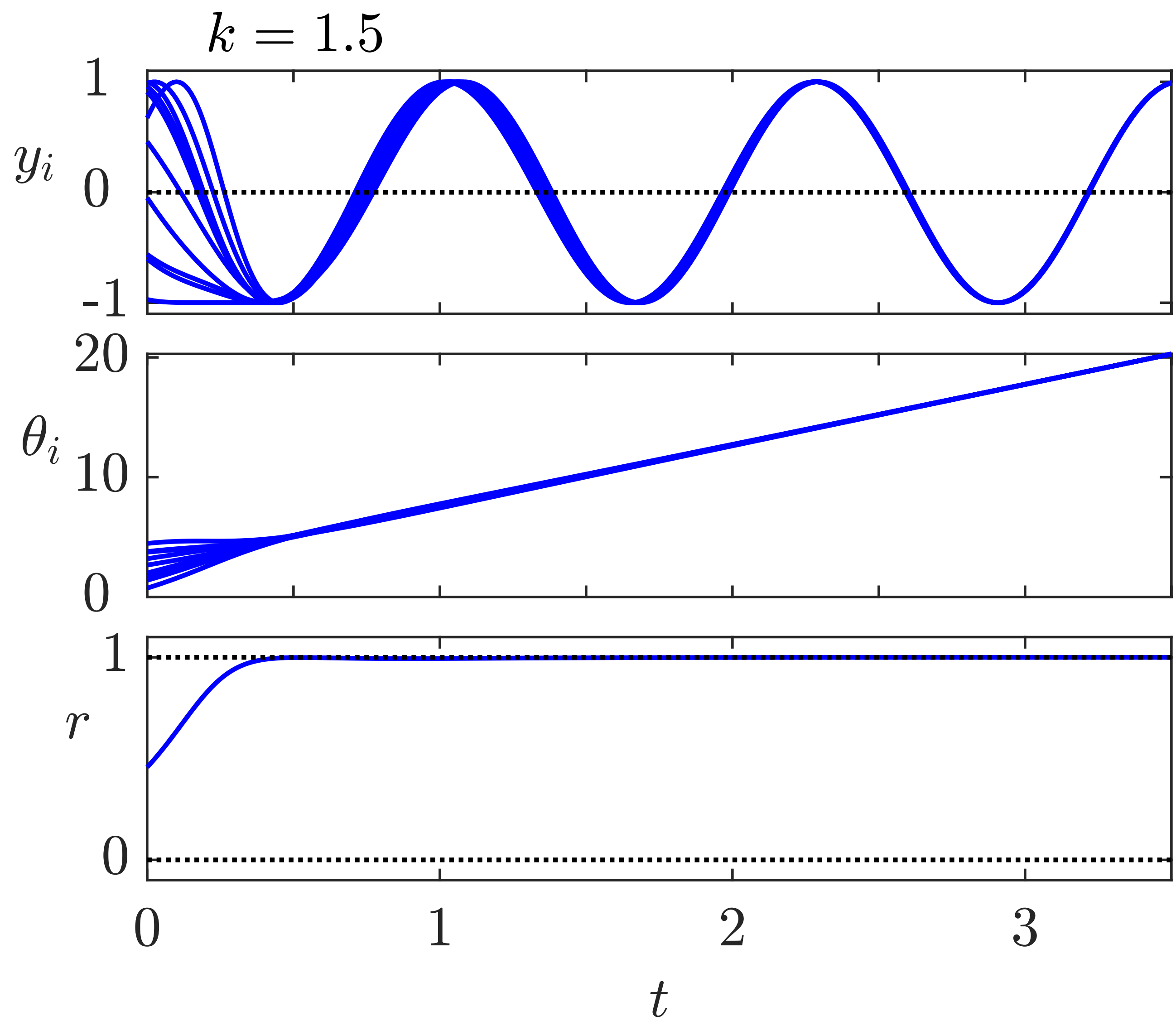

Fig. 4.71: Synchronisation of ten extended oscillators with nonlinear all-to-all couplings and coupling strength $k = 1.5$

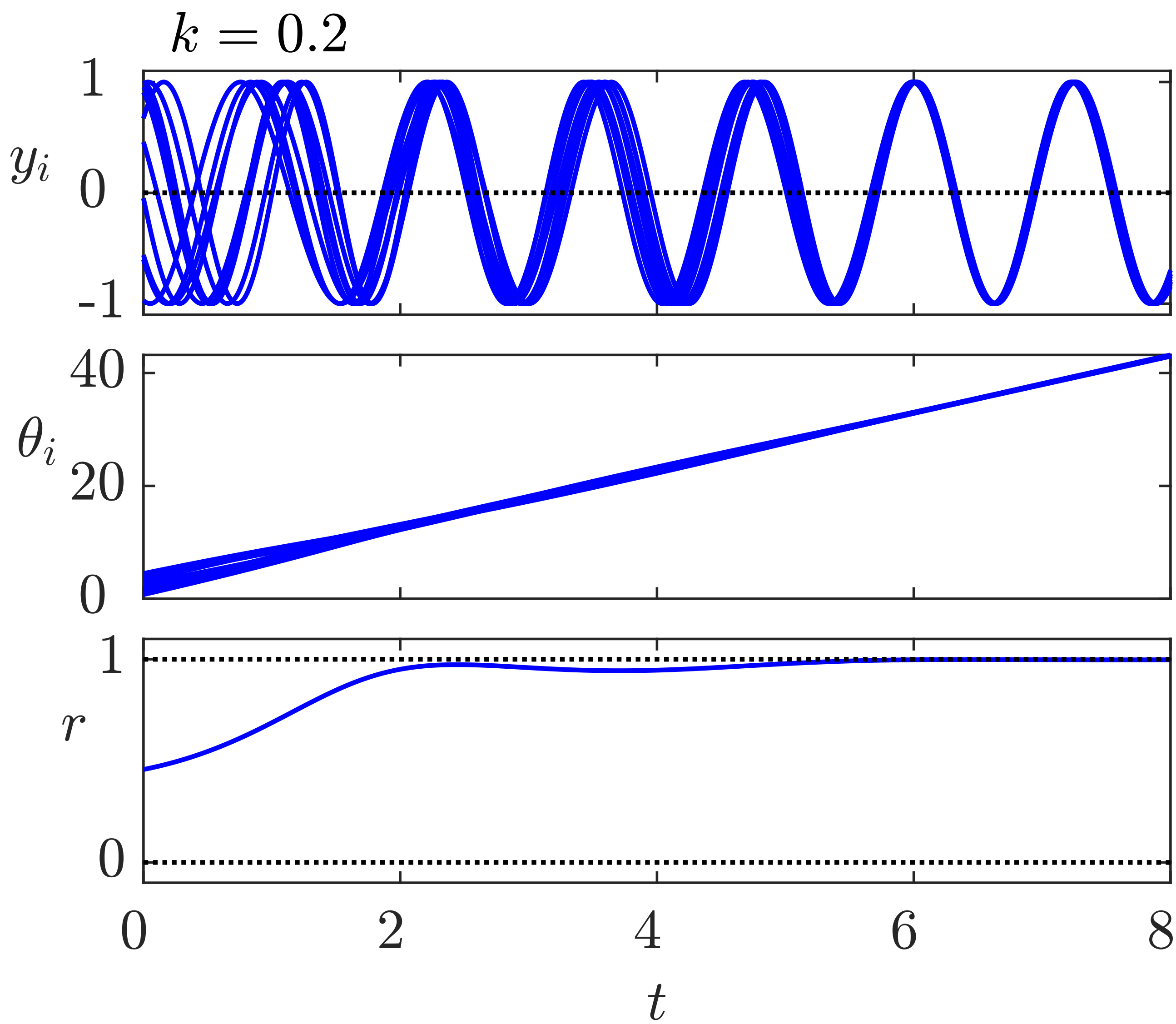

Fig. 4.71: Synchronisation of ten extended oscillators with nonlinear all-to-all couplings and coupling strength $k = 0.2$

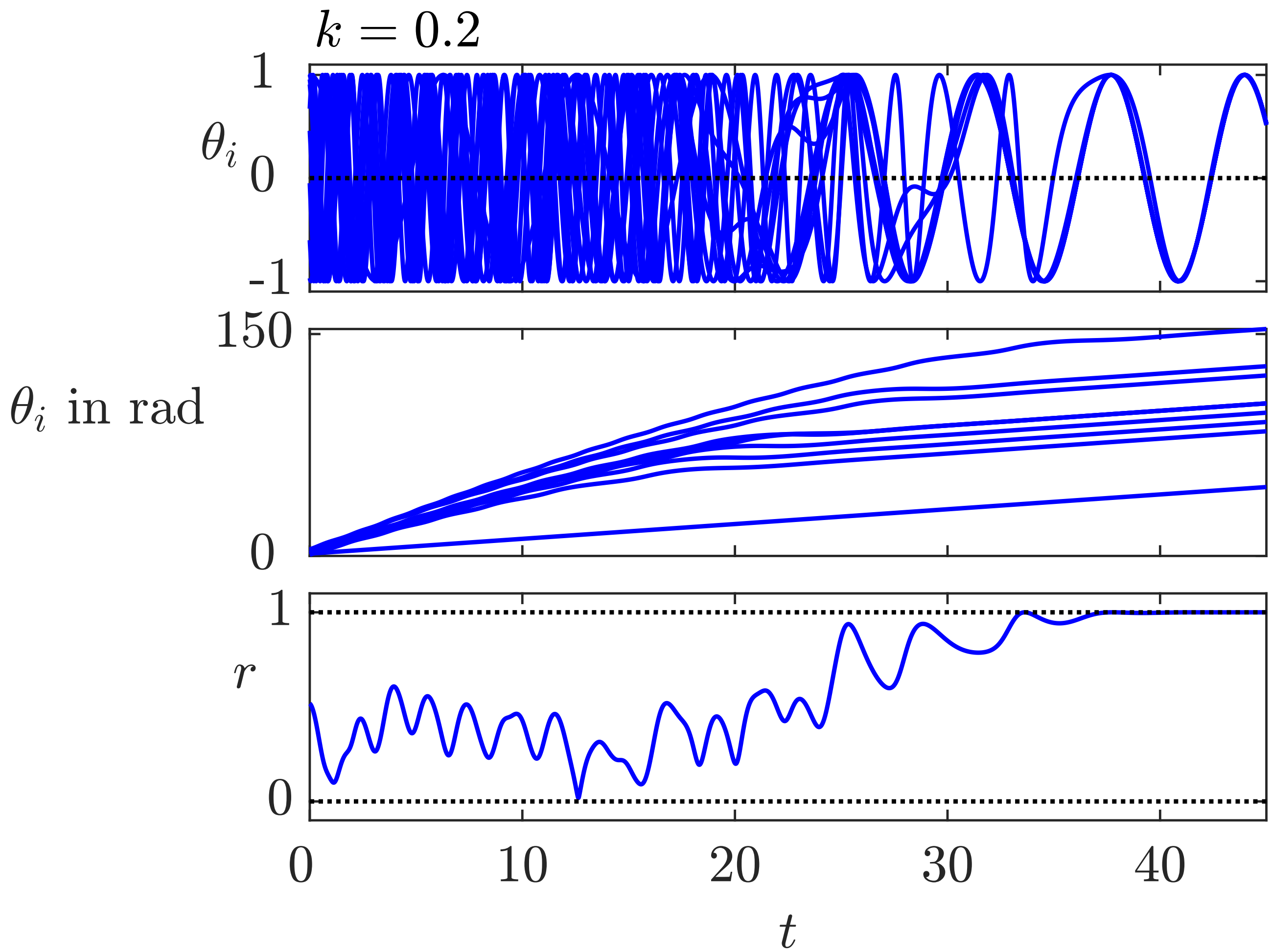

Fig. 4.72: Synchronisation of ten Kuramoto oscillators with nonlinear star couplings

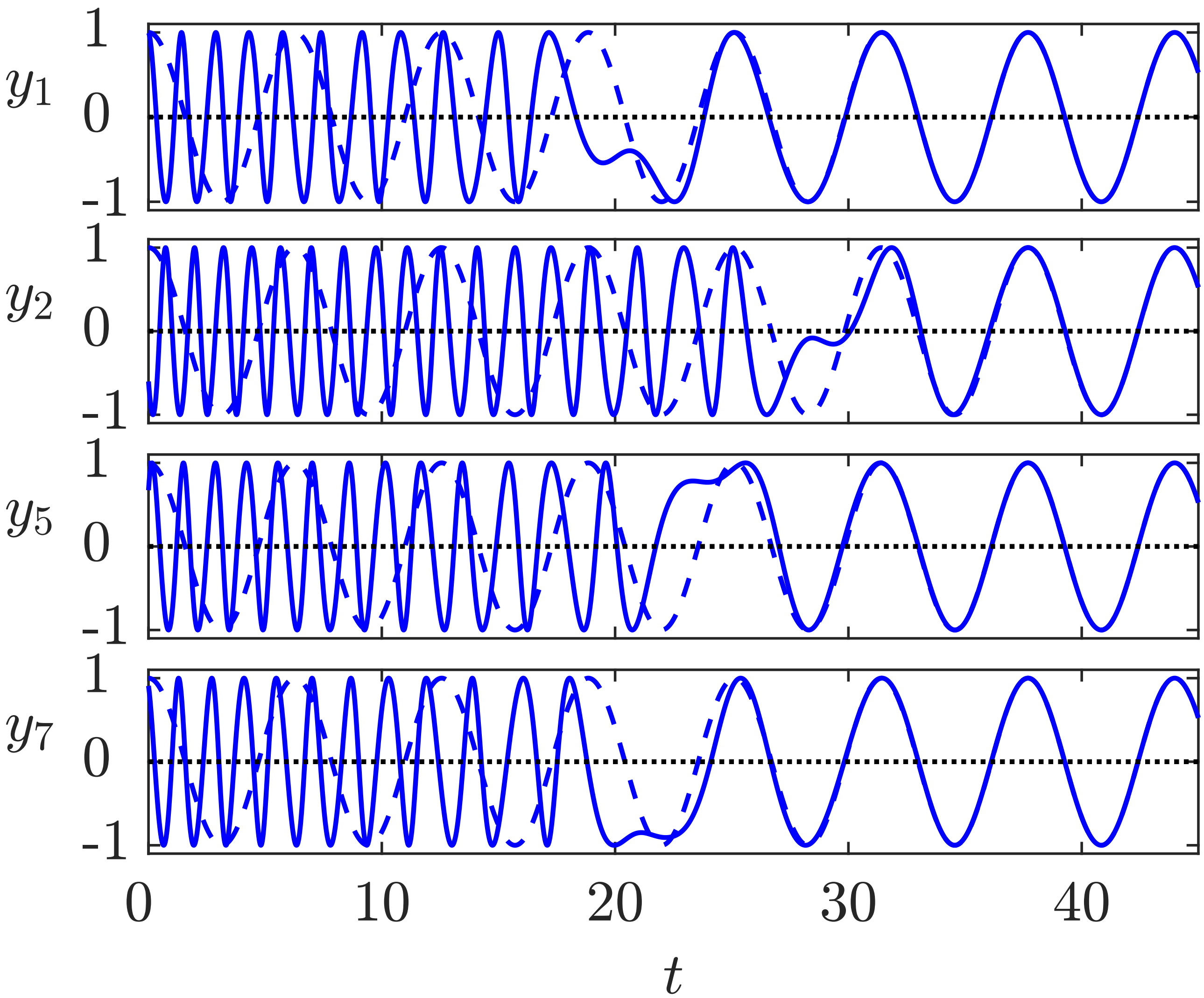

Fig. 4.73: Outputs of four oscillators (detail of Fig. 4.72)

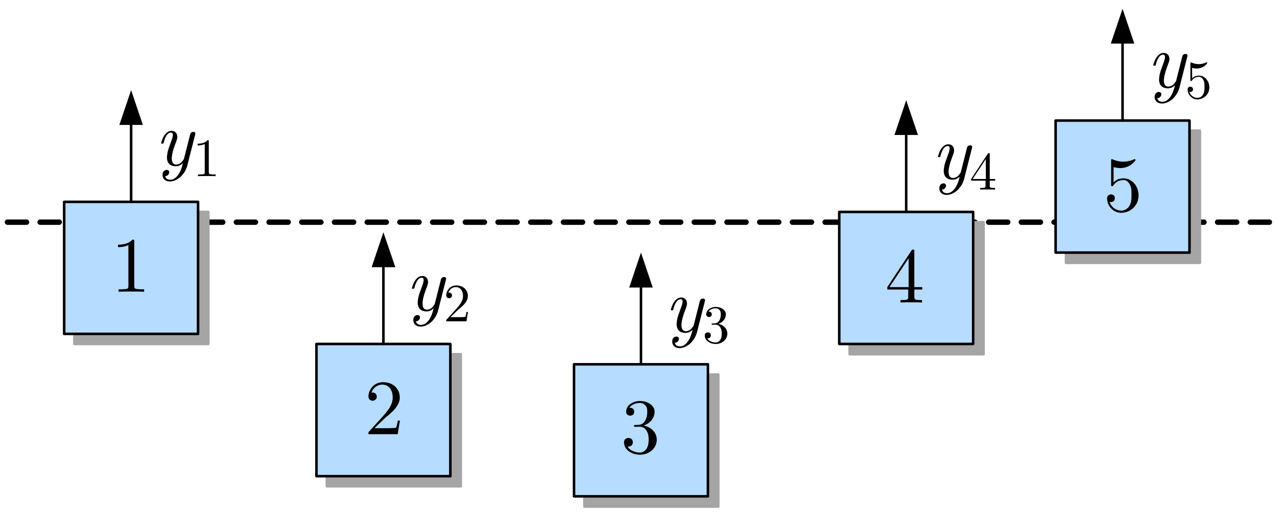

Fig. 4.74: Robot positioning problem

J. LUNZE: *Networked Control of Multi-Agent Systems*, Edition **MoRa** 2022

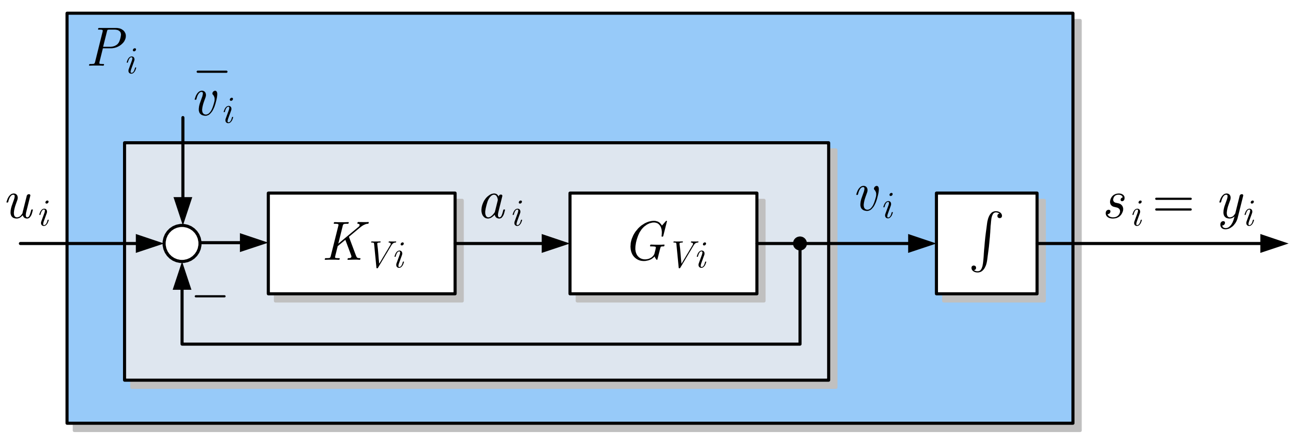

Fig. 4.75: Robot model

J. LUNZE: *Networked Control of Multi-Agent Systems*, Edition **M**o**R**a 2022

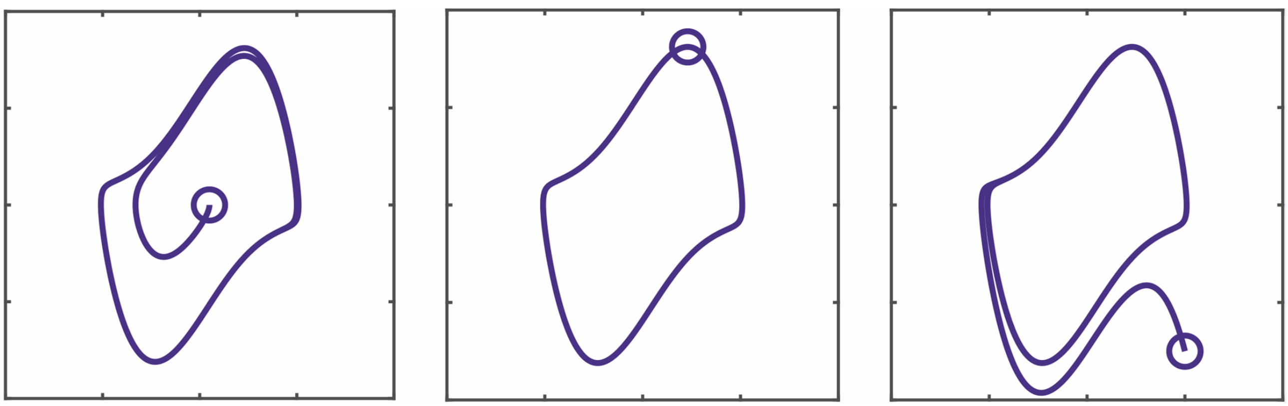

Fig. 4.76: Behaviour of van der Pol oscillators with $\varepsilon = 1.5$

J. LUNZE*: Networked Control of Multi-Agent Systems,* Edition **M**o**R**a 2022

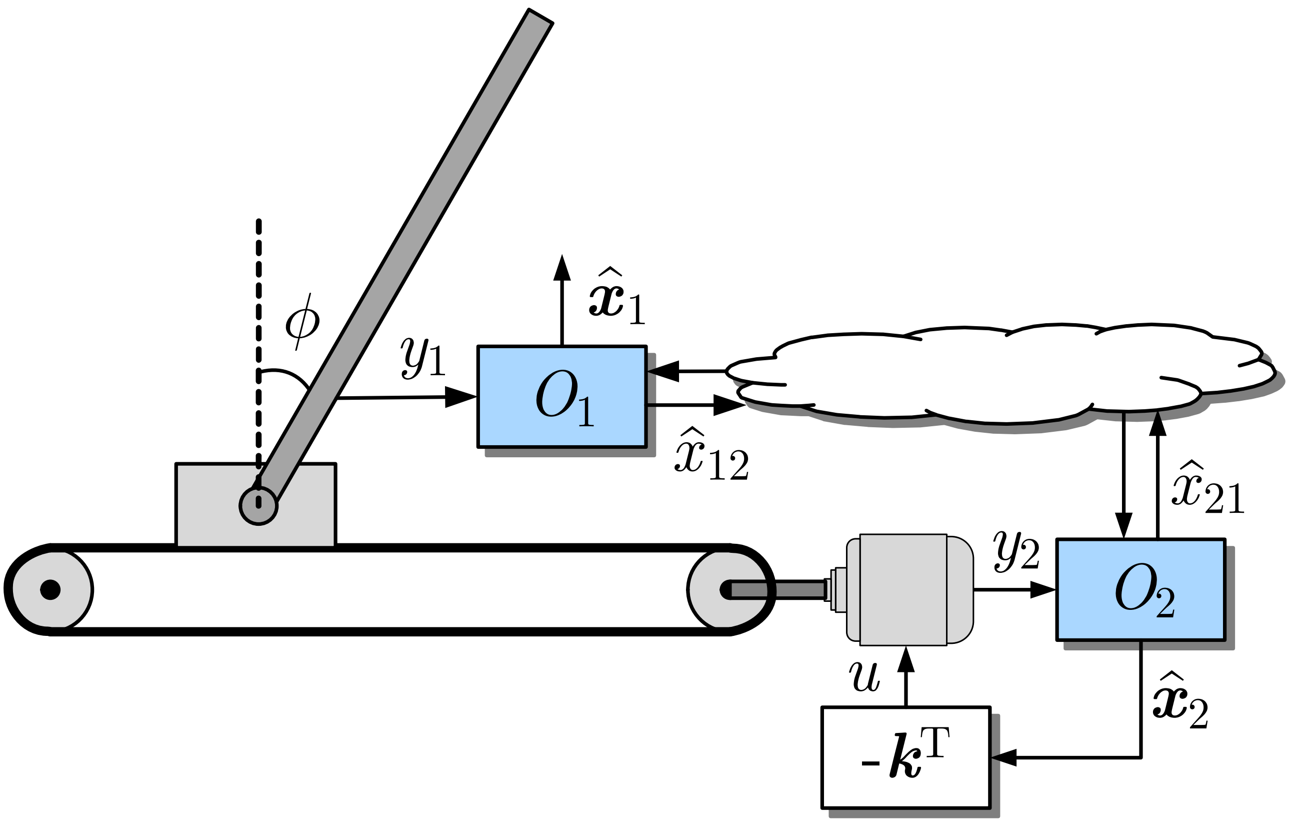

Fig. 4.77: Inverted pendulum with distributed state observers

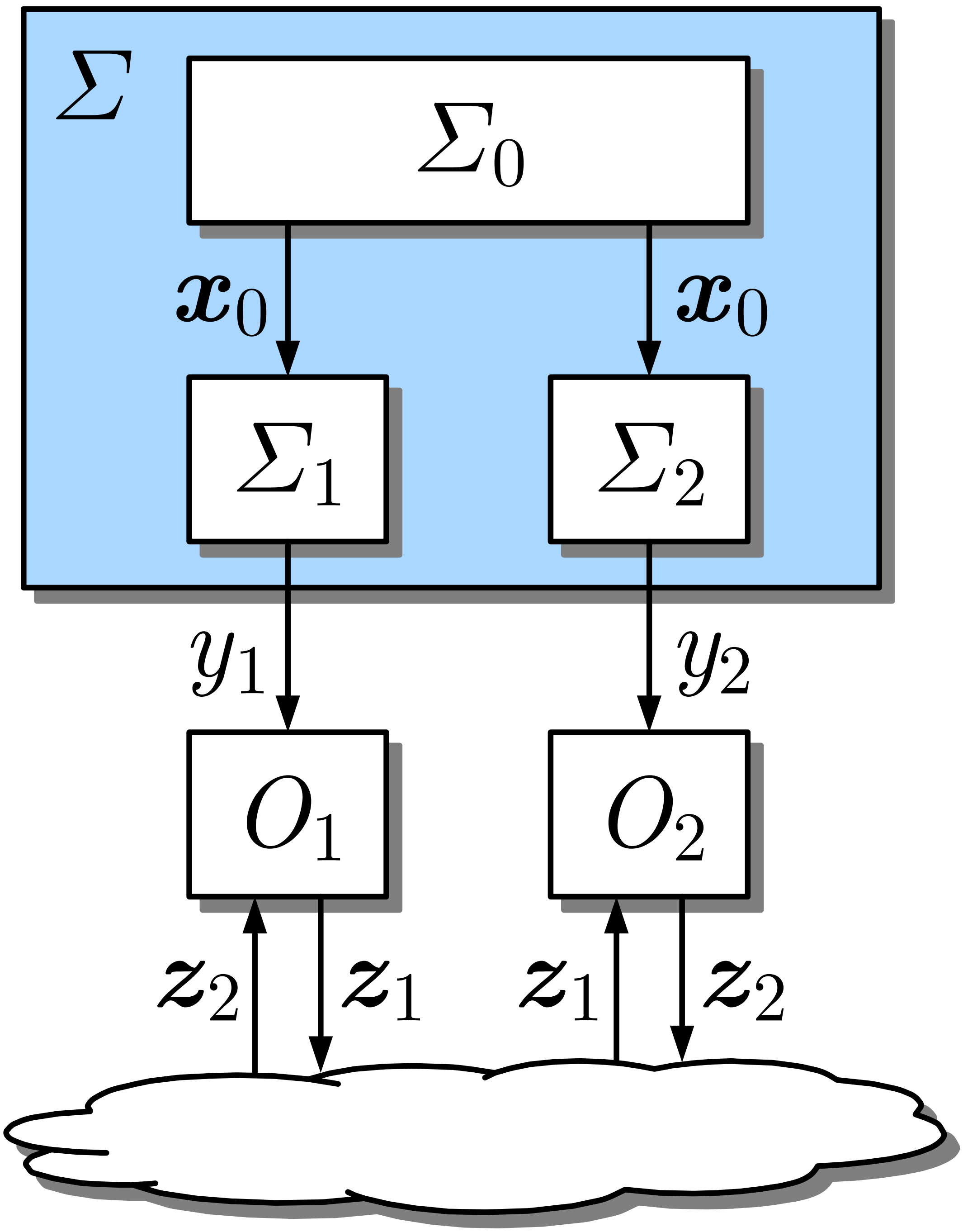

Fig. 4.78. Distributed observers for the system Σ

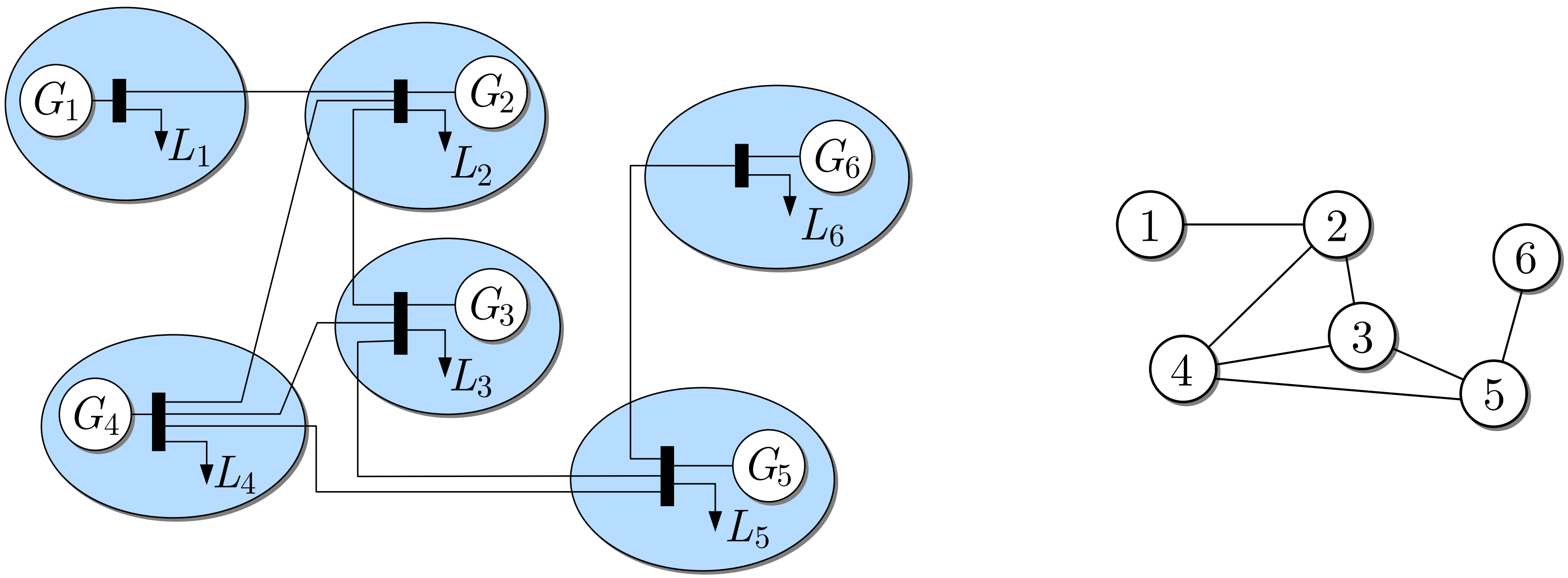

Fig. 4.79. Electrical power network

J. Lunze: *Networked Control of Multi-Agent Systems*, Edition MoRa 2022

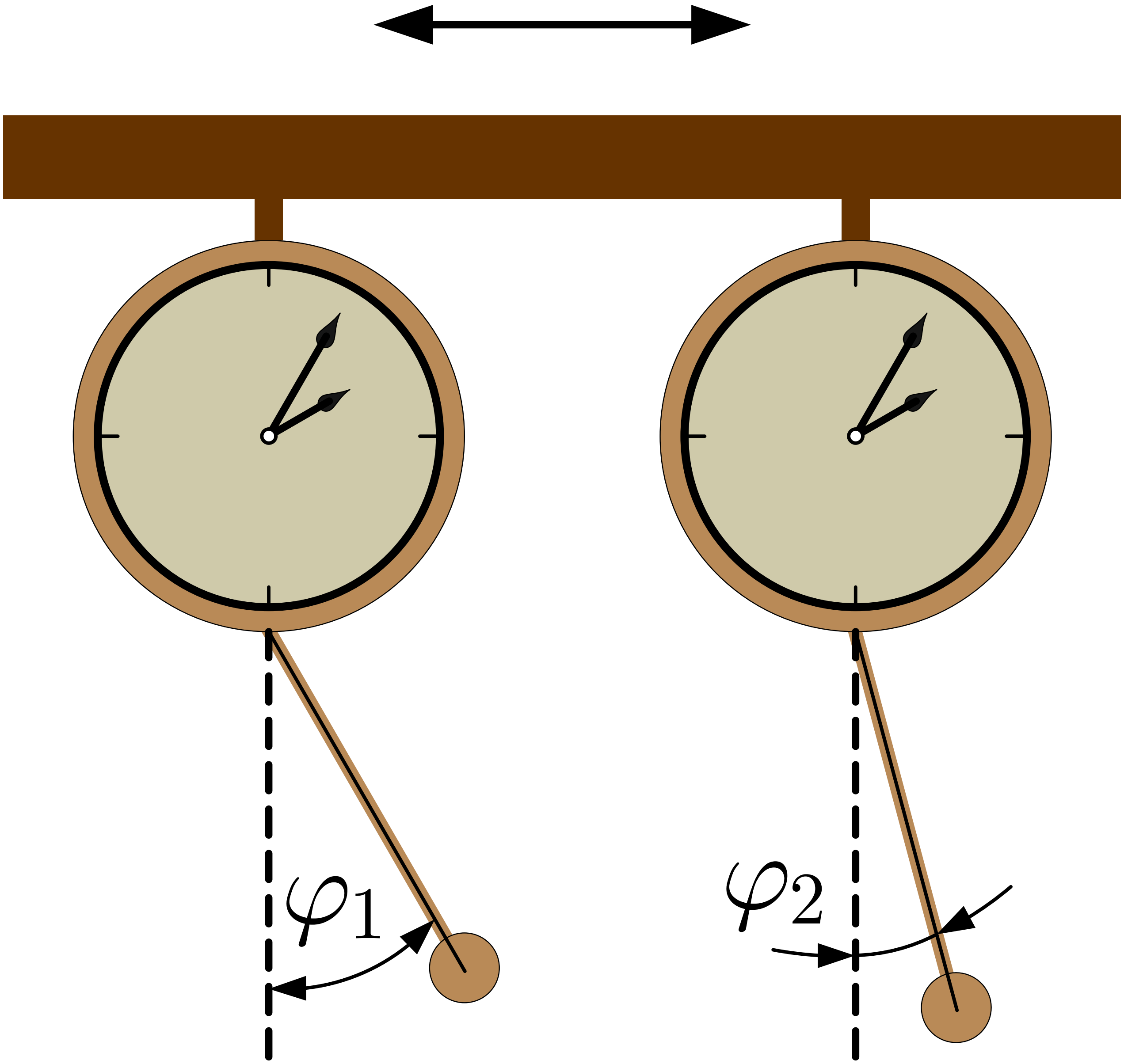

Fig. 4.80: HUYGENS' pendulum experiment

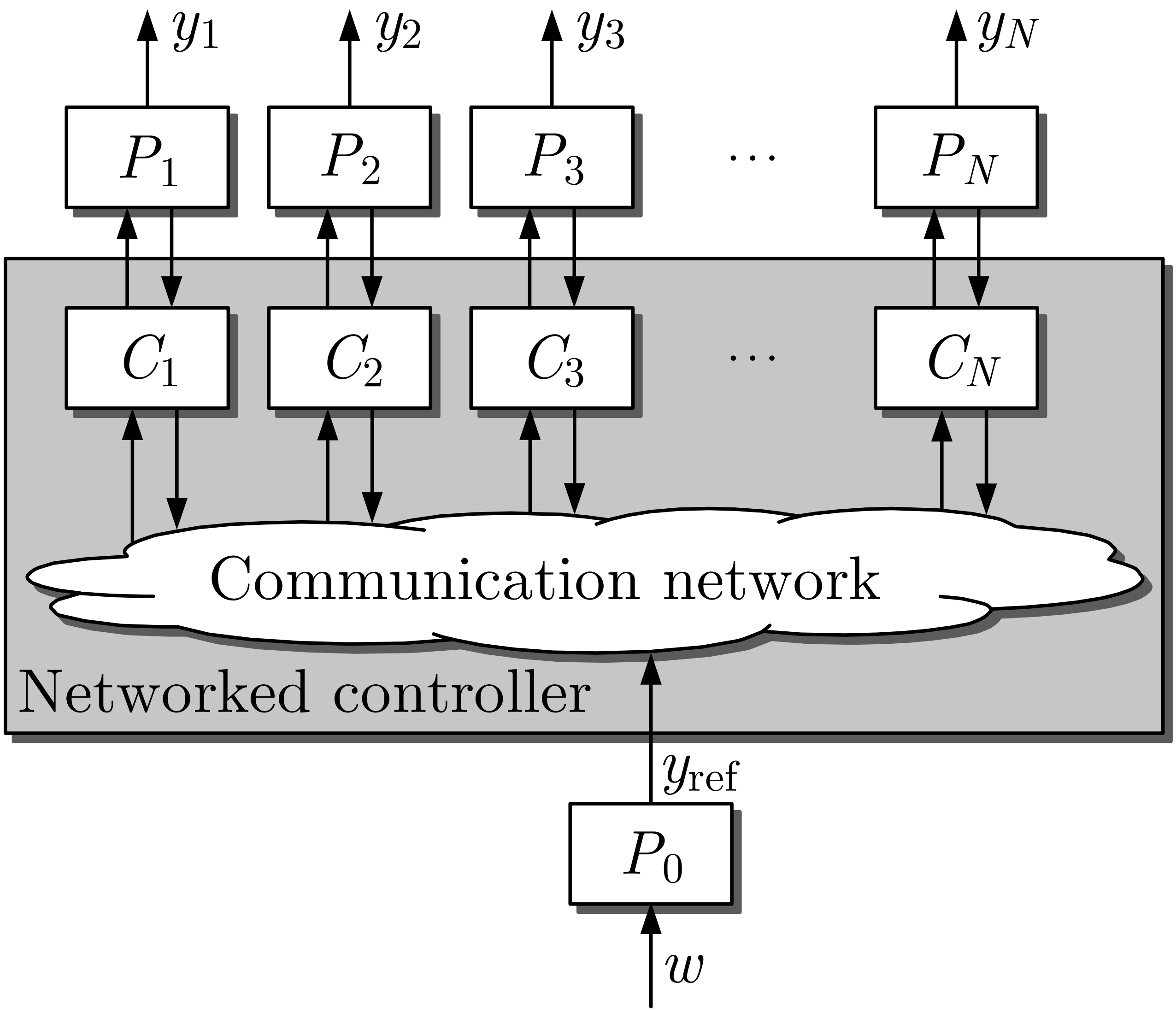

Fig. 5.1: Overall system $\overline{\Sigma}$: Networked control of autonomous agents with a leader-follower structure

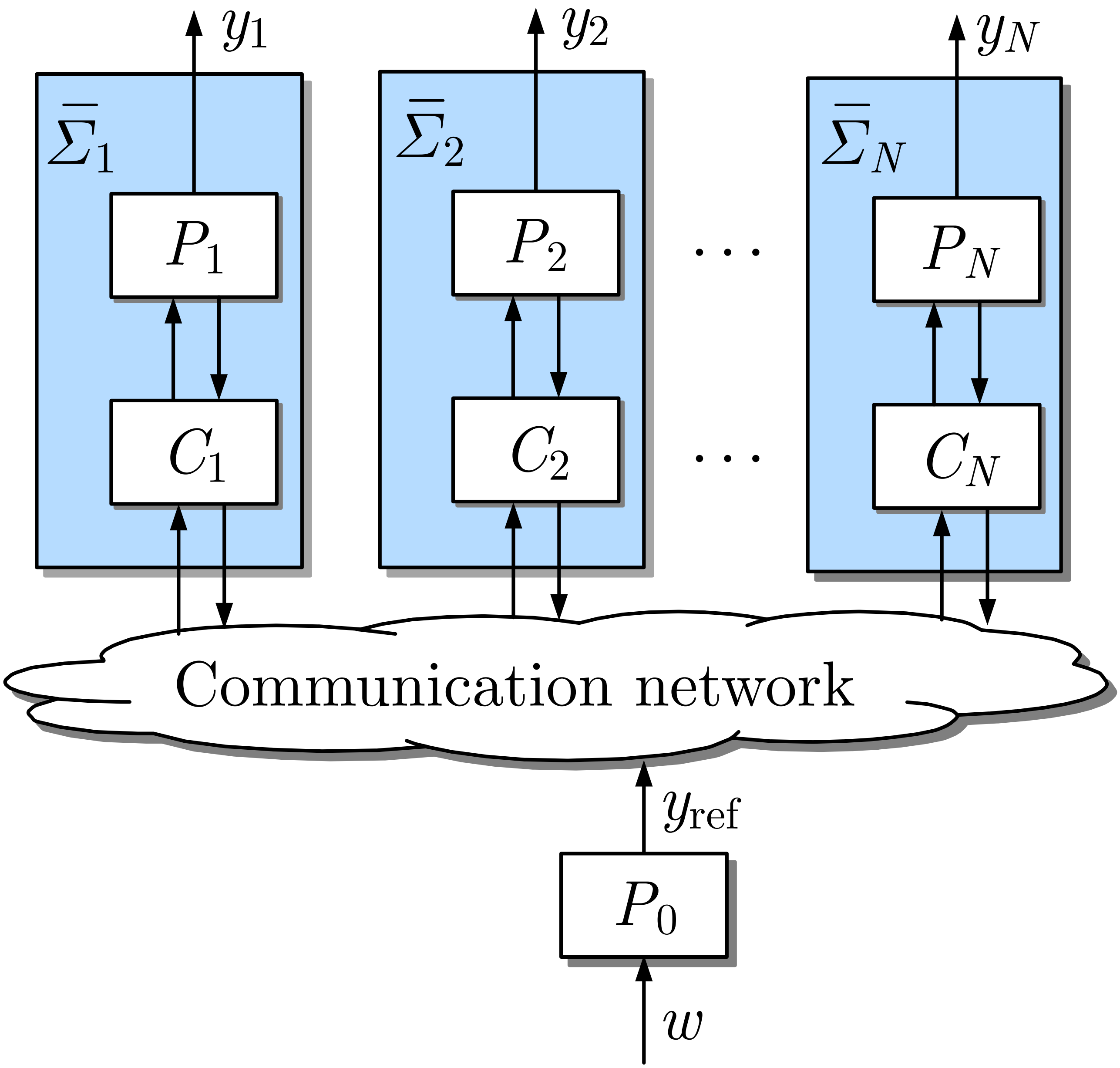

Fig. 5.2: Decomposition of the overall system $\overline{\Sigma}$ with respect to the design steps of Algorithm 5.1

J. LUNZE: *Networked Control of Multi-Agent Systems*, Edition **MoRa** 2022

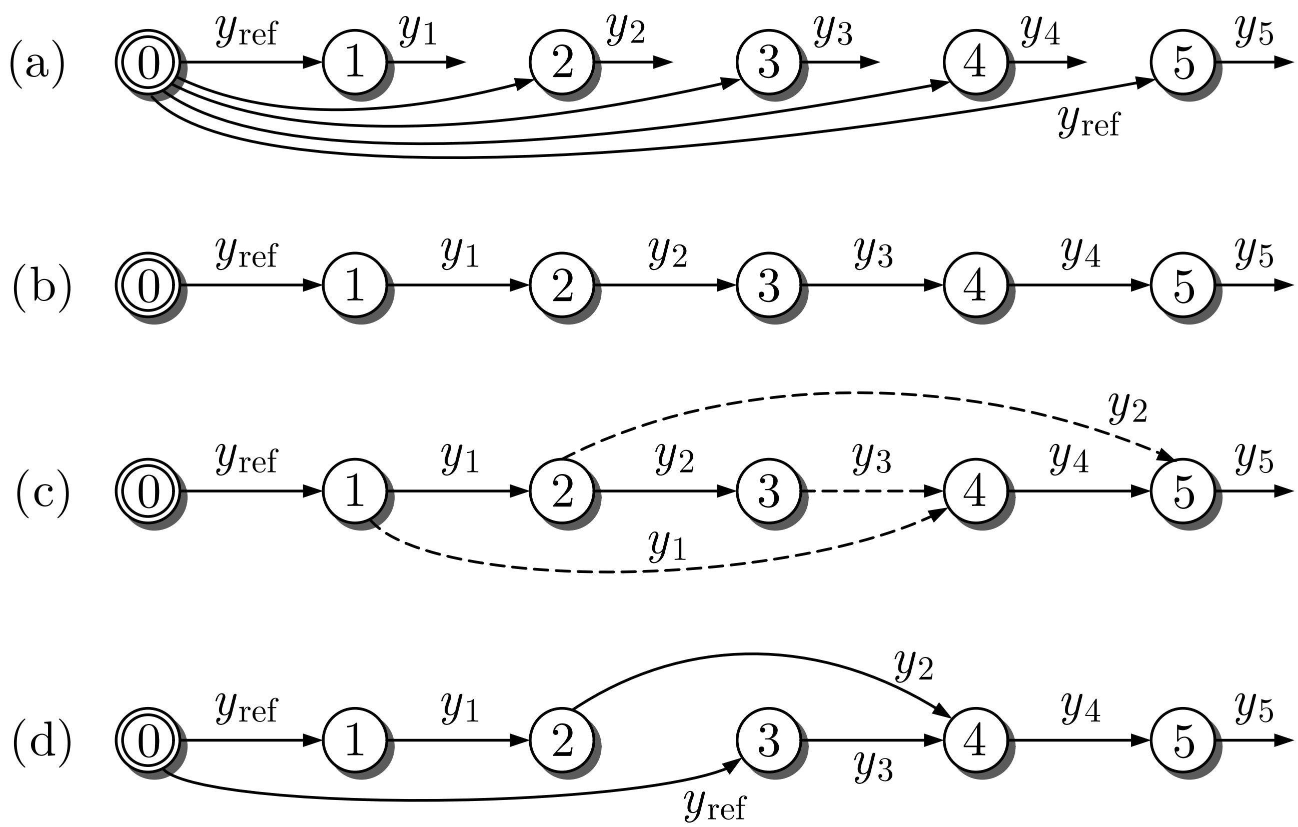

Fig. 5.3: Four communication structures

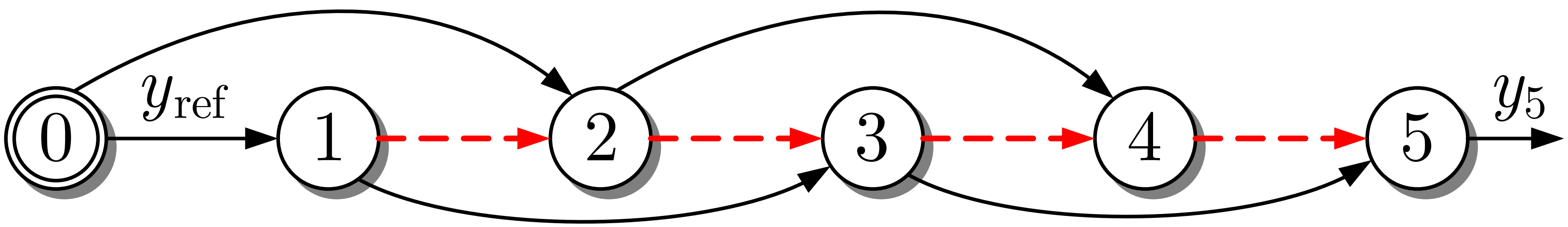

Fig. 5.4. Communication structures

J. Lunze: *Networked Control of Multi-Agent Systems,* Edition MoRa 2022

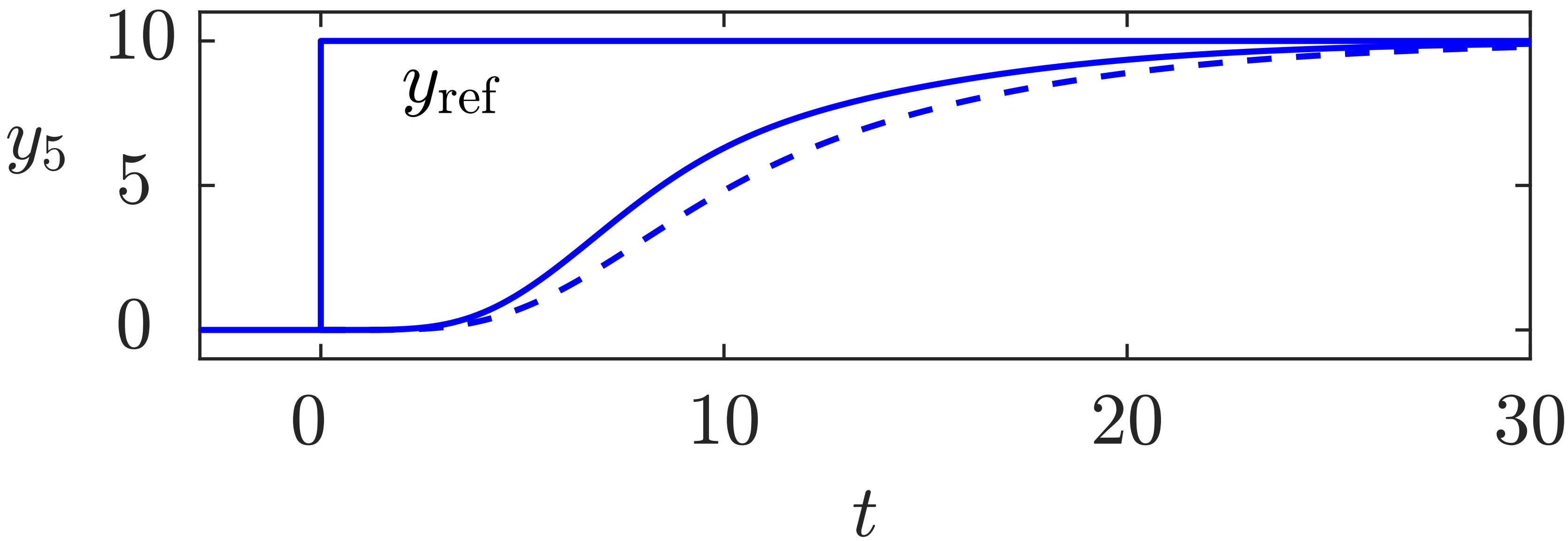

Fig. 5.4. Behaviour of the fifth agent

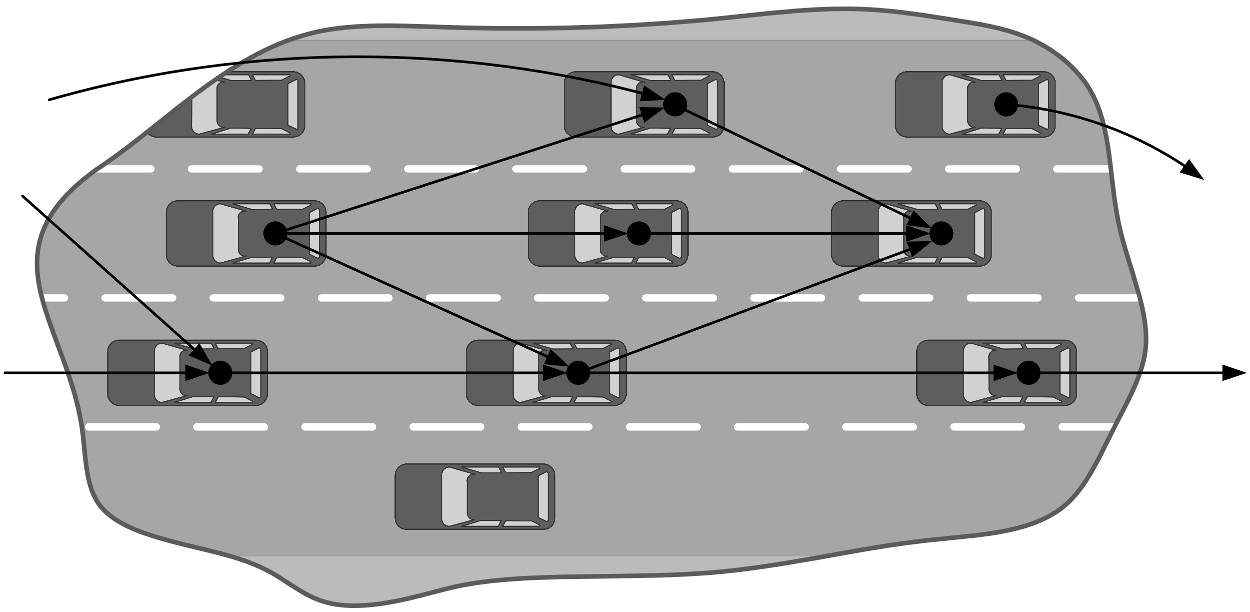

Fig. 5.5: Part of a networked vehicle group on a highway

J. Lunze: *Networked Control of Multi-Agent Systems,* Edition **MoRa** 2022

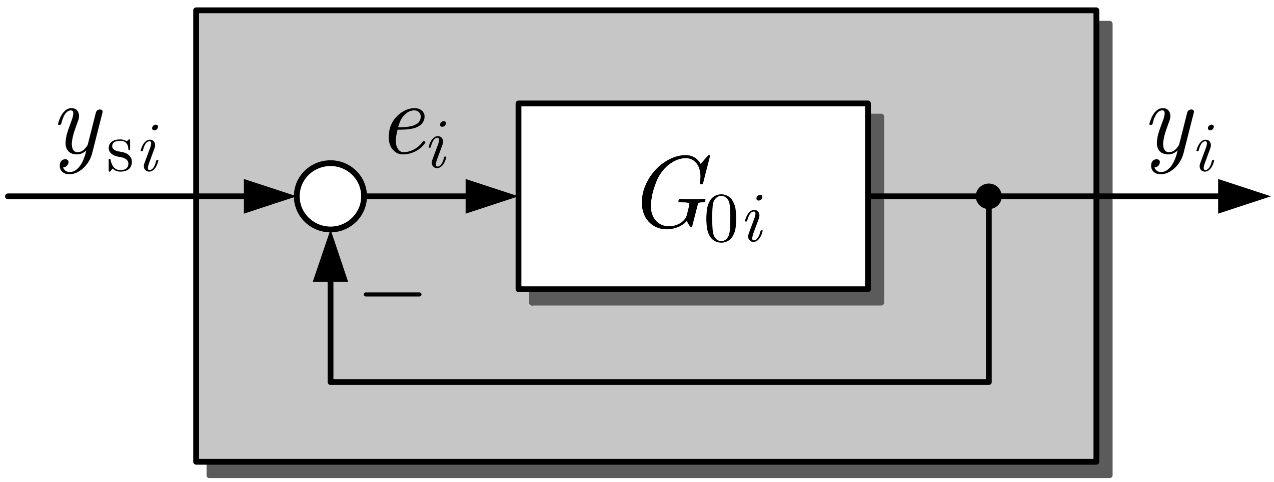

Fig. 5.6: Controlled agent

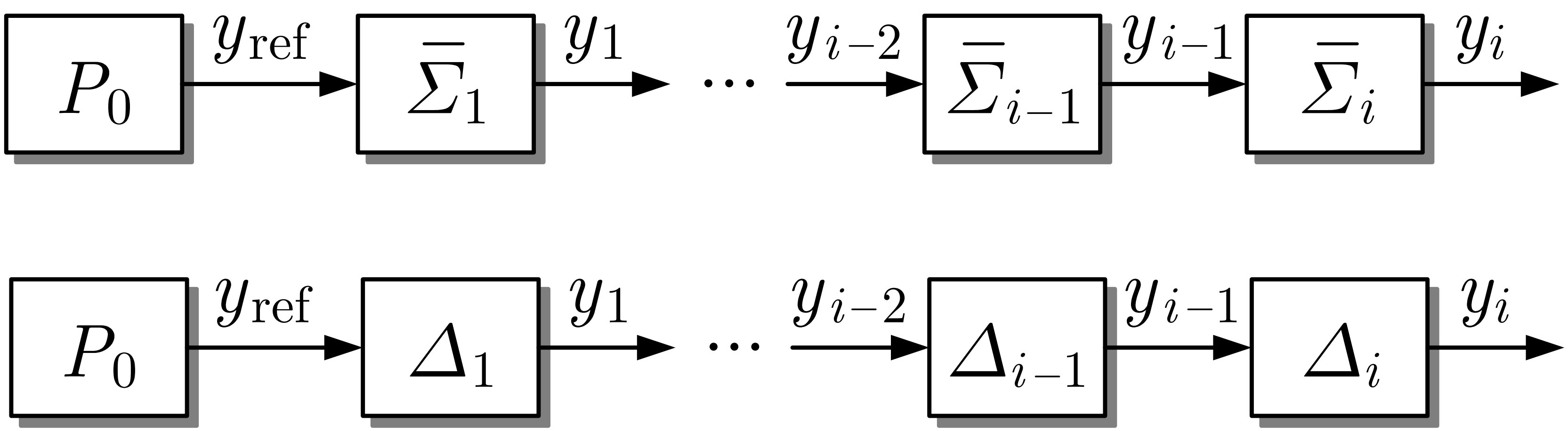

Fig. 5.7. Information flow from the leader towards the i-th agent

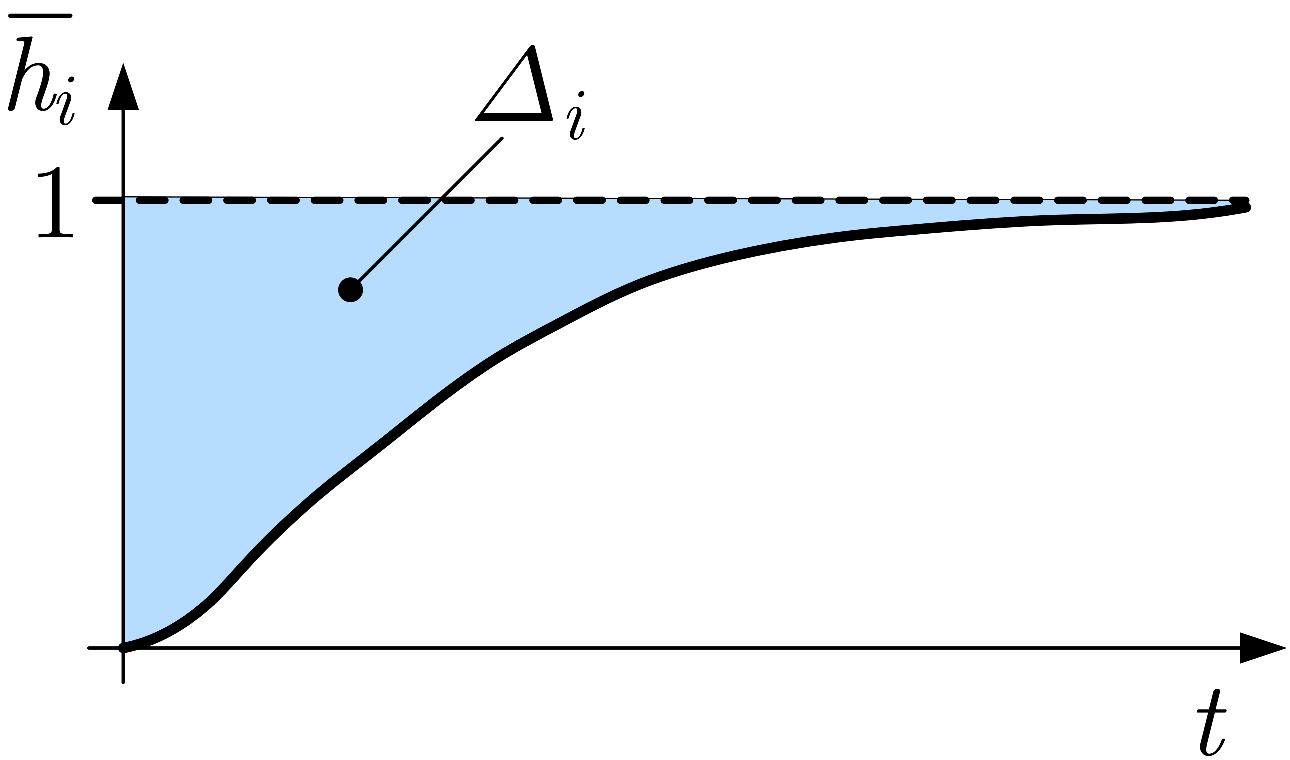

Fig. 5.8: Interpretation of the delay Δ_i

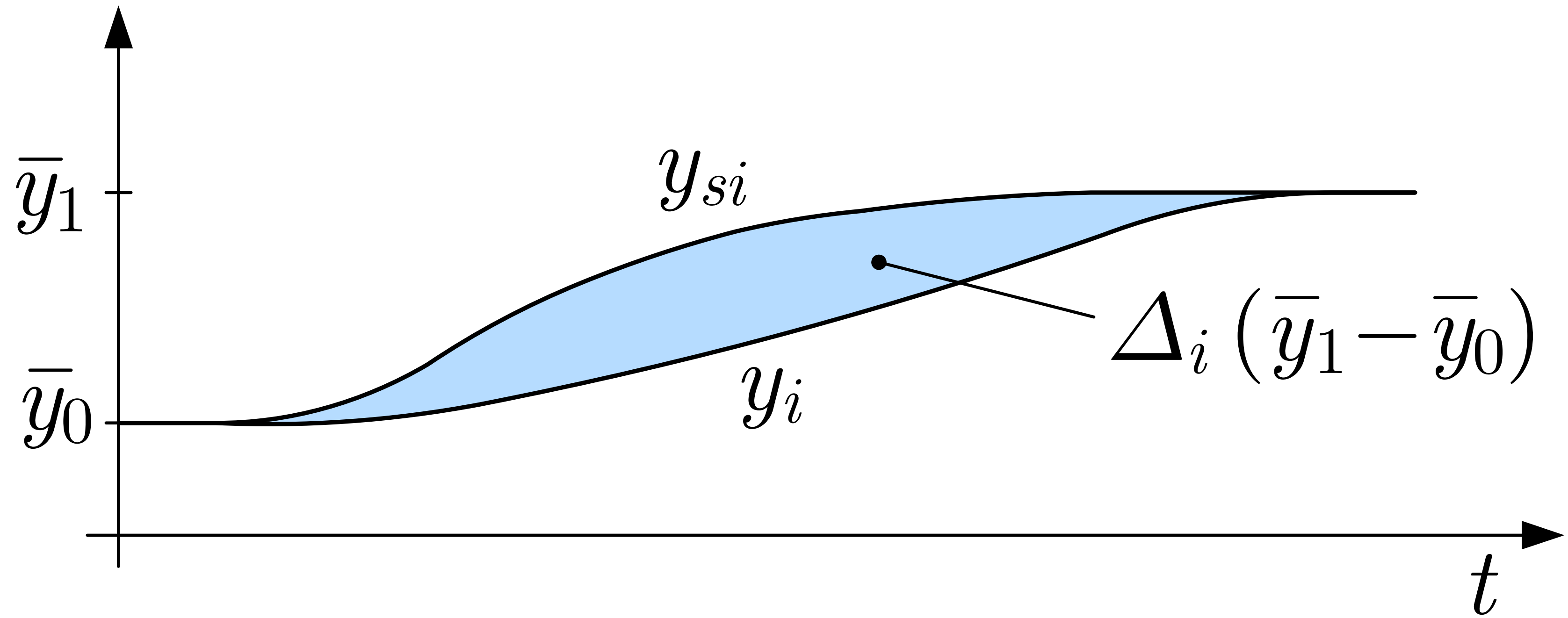

Fig. 5.9. Interpretation of eqn. (5.33)

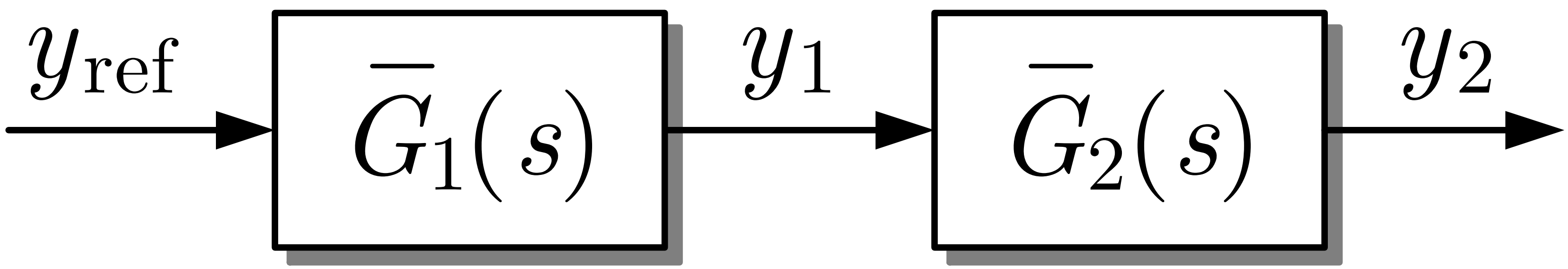

Fig. 5.10. Series connection of two controlled agents

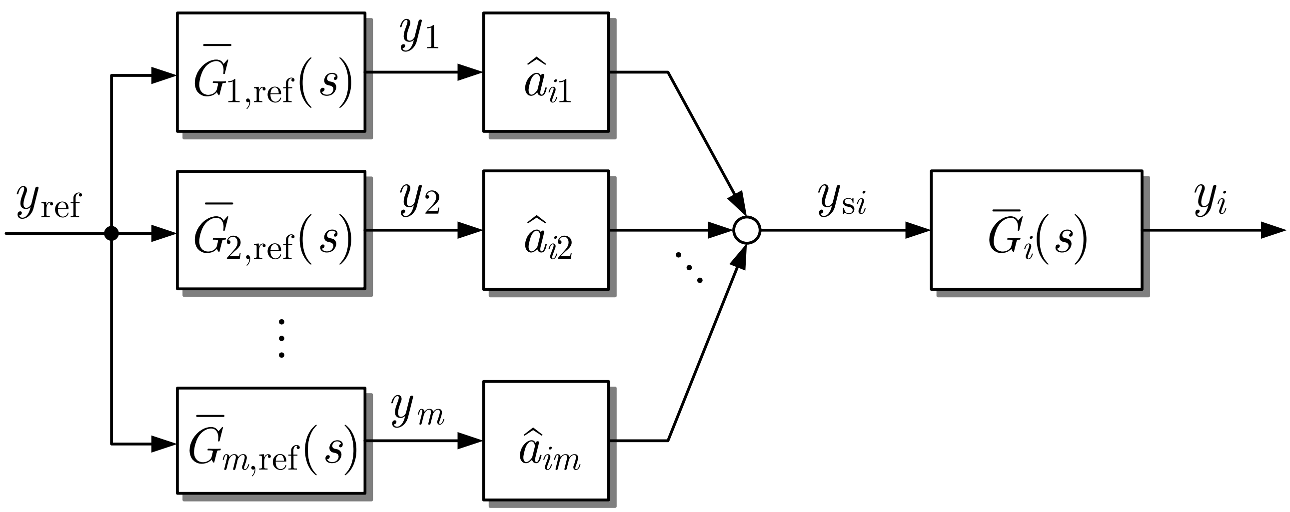

Fig. 5.11: Parallel connection

J. Lunze: *Networked Control of Multi-Agent Systems,* Edition **MoRa** 2022

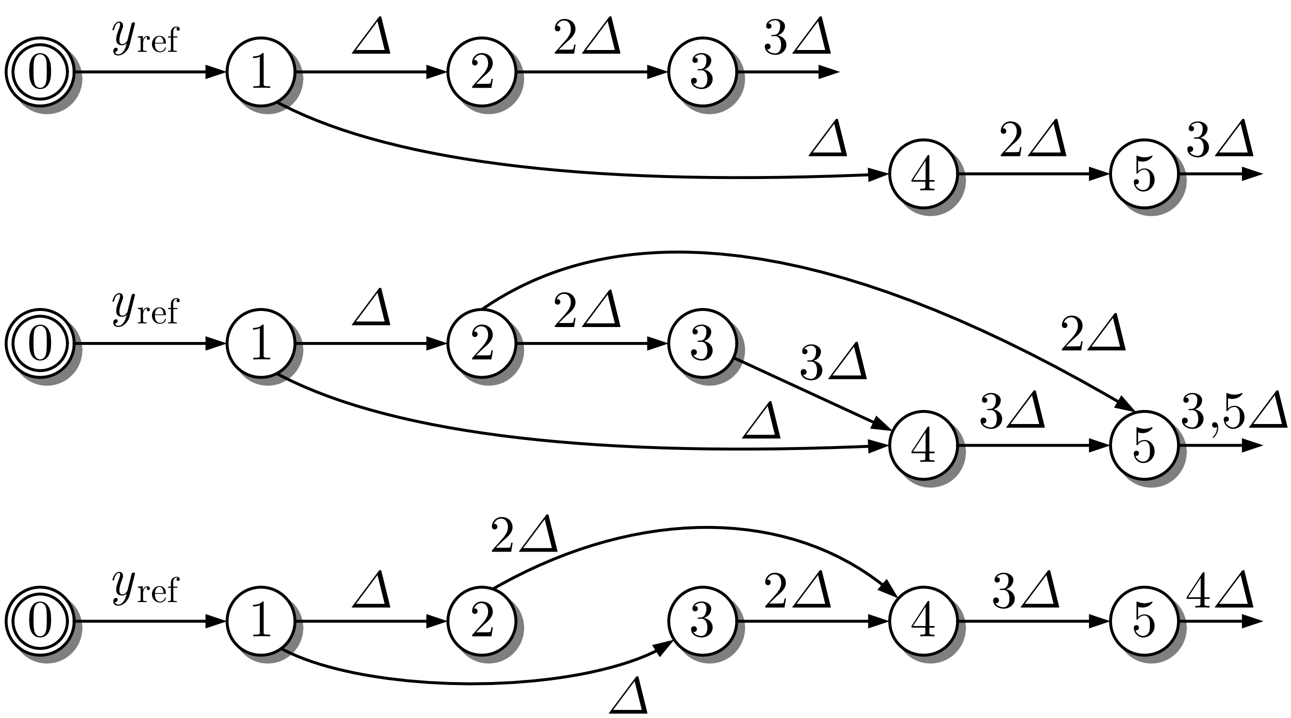

Fig. 5.12: Delay of the three communication structures

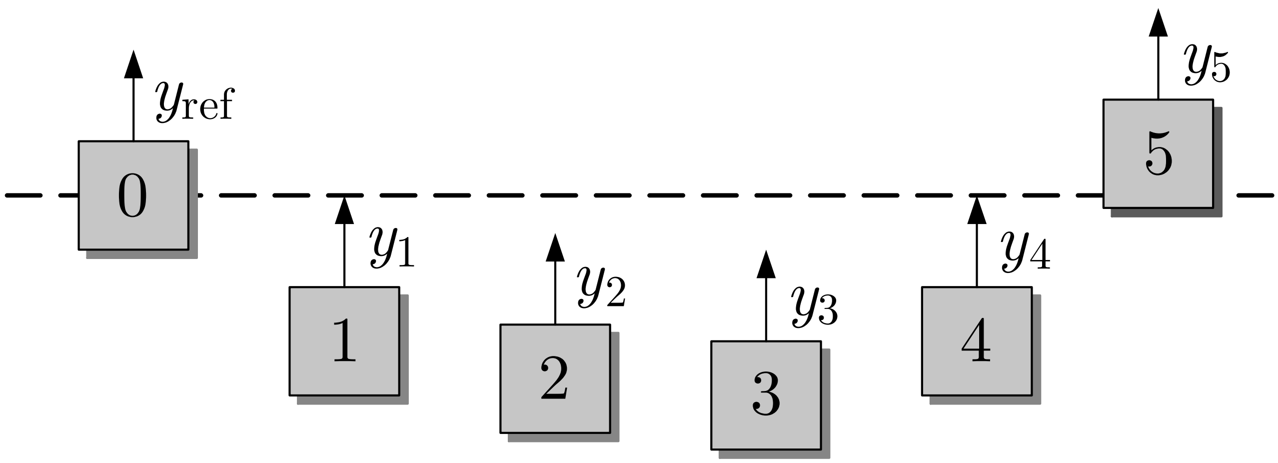

Fig. 5.13: Positioning problem for robots

J. Lunze: *Networked Control of Multi-Agent Systems*, Edition **MoRa** 2022

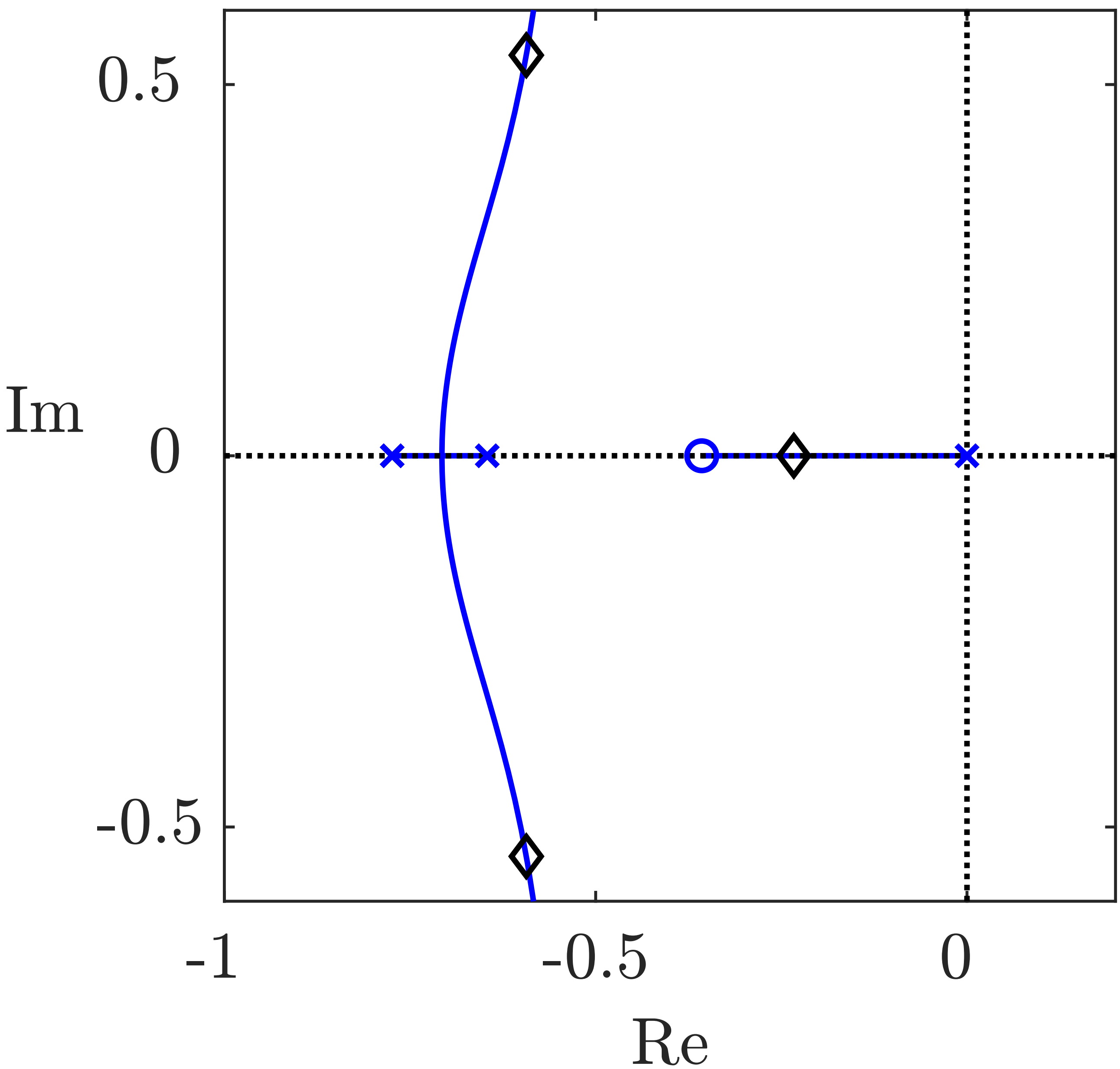

Fig. 5.14: Root locus

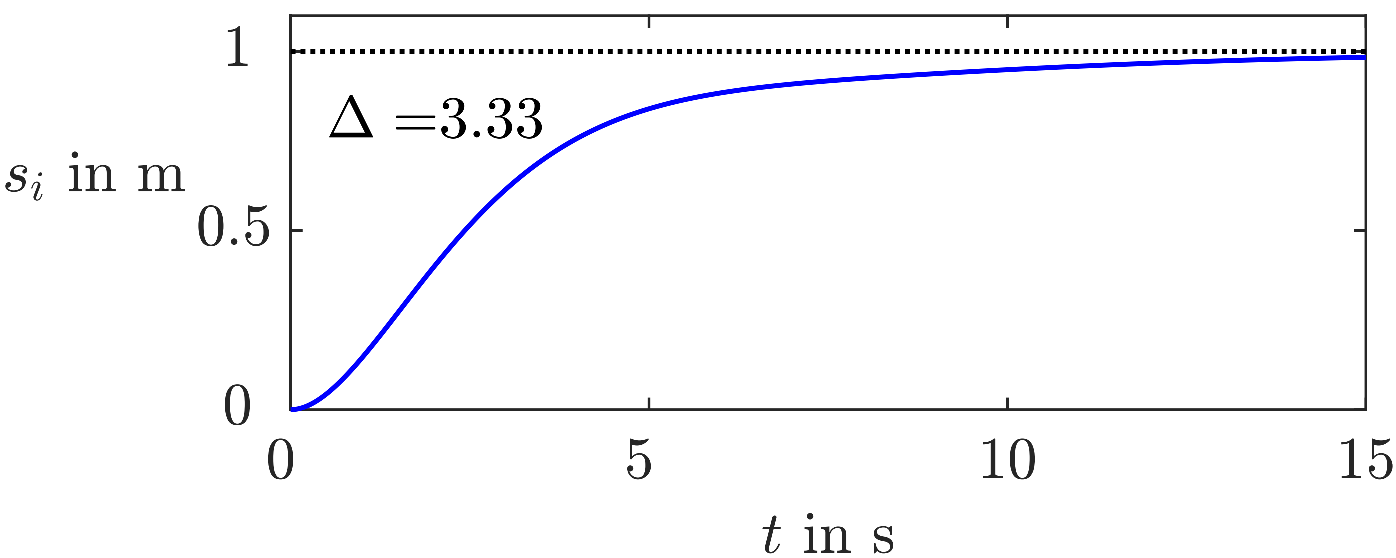

Fig. 5.14: Step response of the controlled robot

J. Lunze: *Networked Control of Multi-Agent Systems,* Edition MoRa 2022

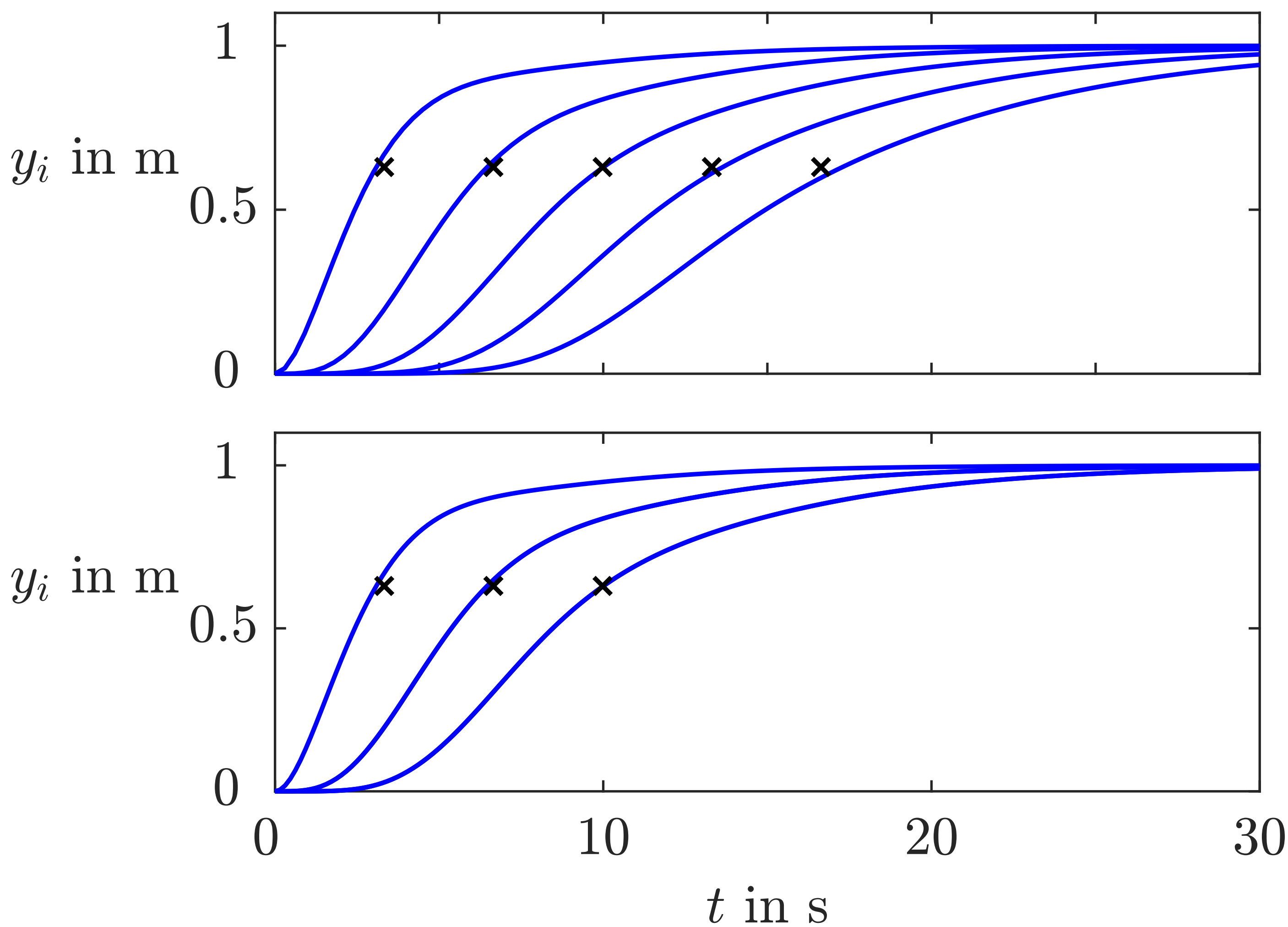

Fig. 5.15: Behaviour of the five robots with neighbouring couplings (top) and with the first communication graph of Fig. 5.12

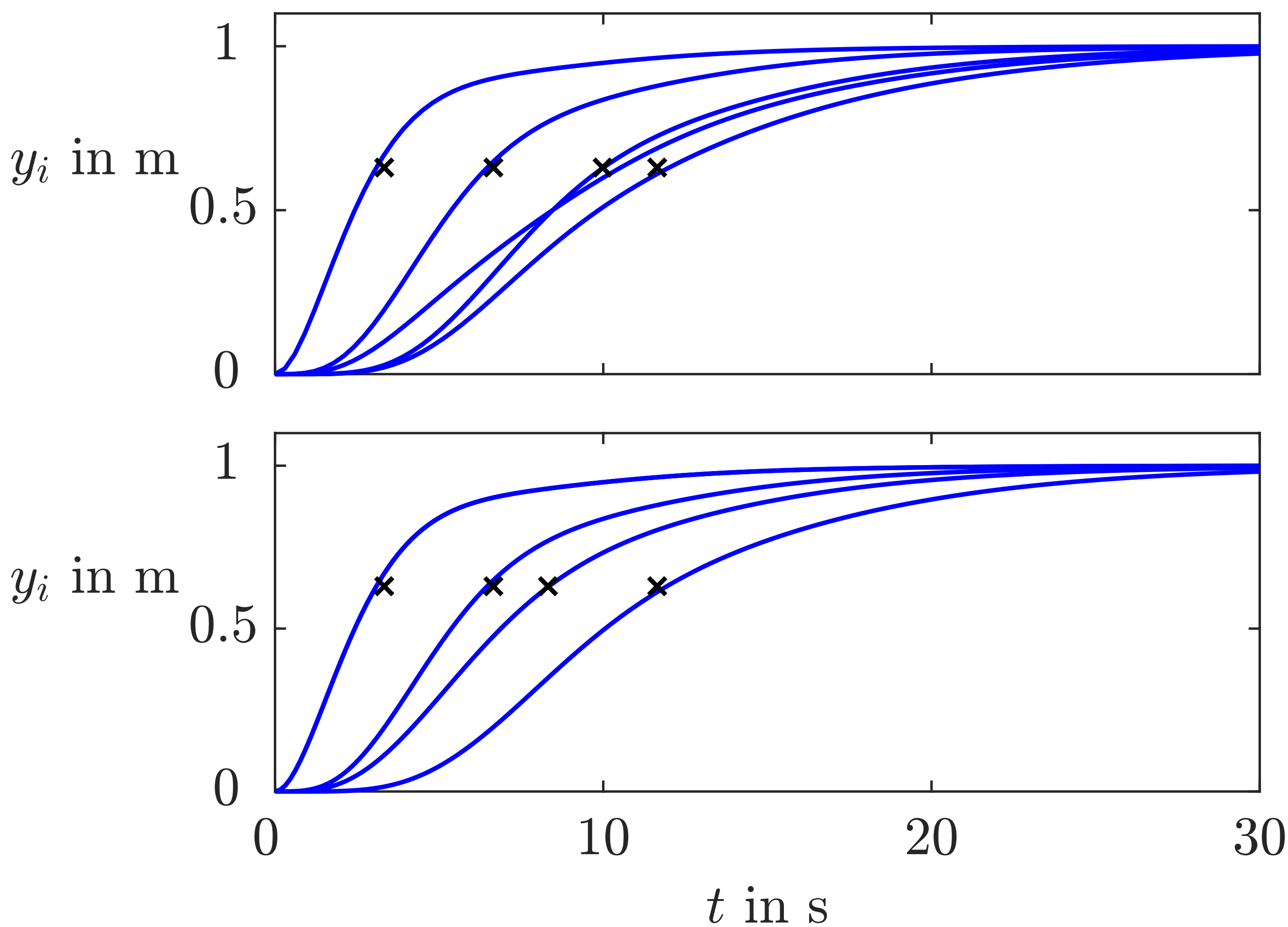

Fig. 5.15: Behaviour of the five robots with two communication graphs of Fig. 5.12

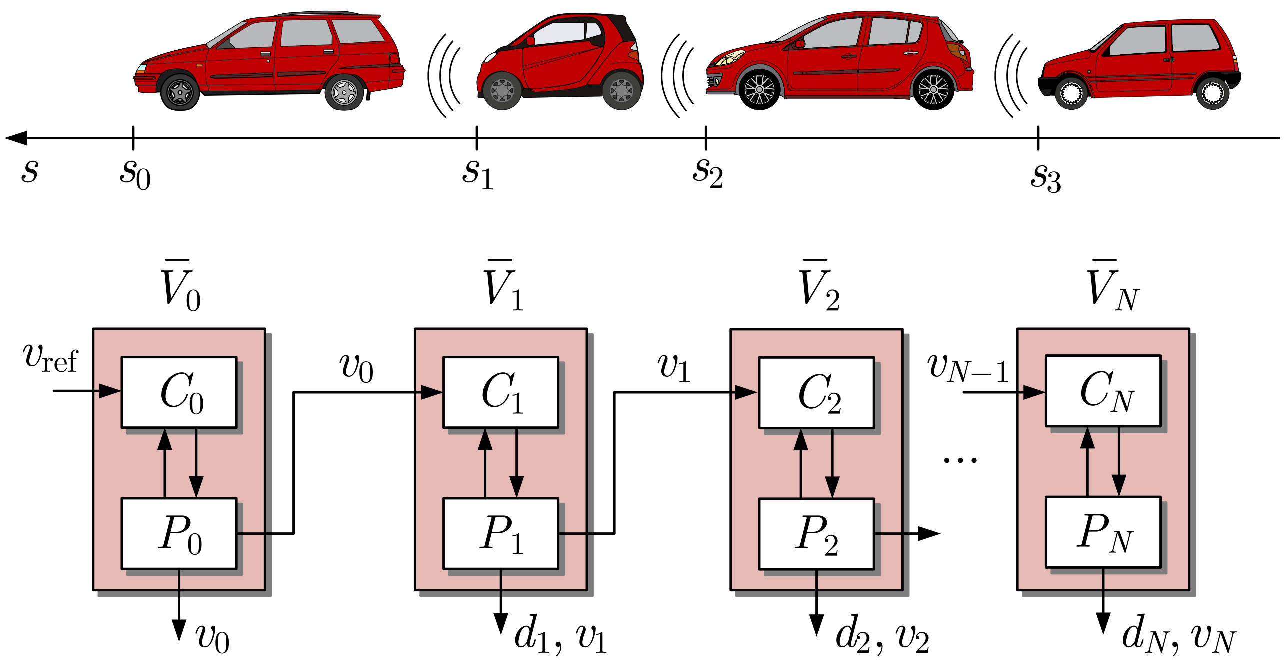

Fig. 5.16: Platoon with adaptive cruise controller

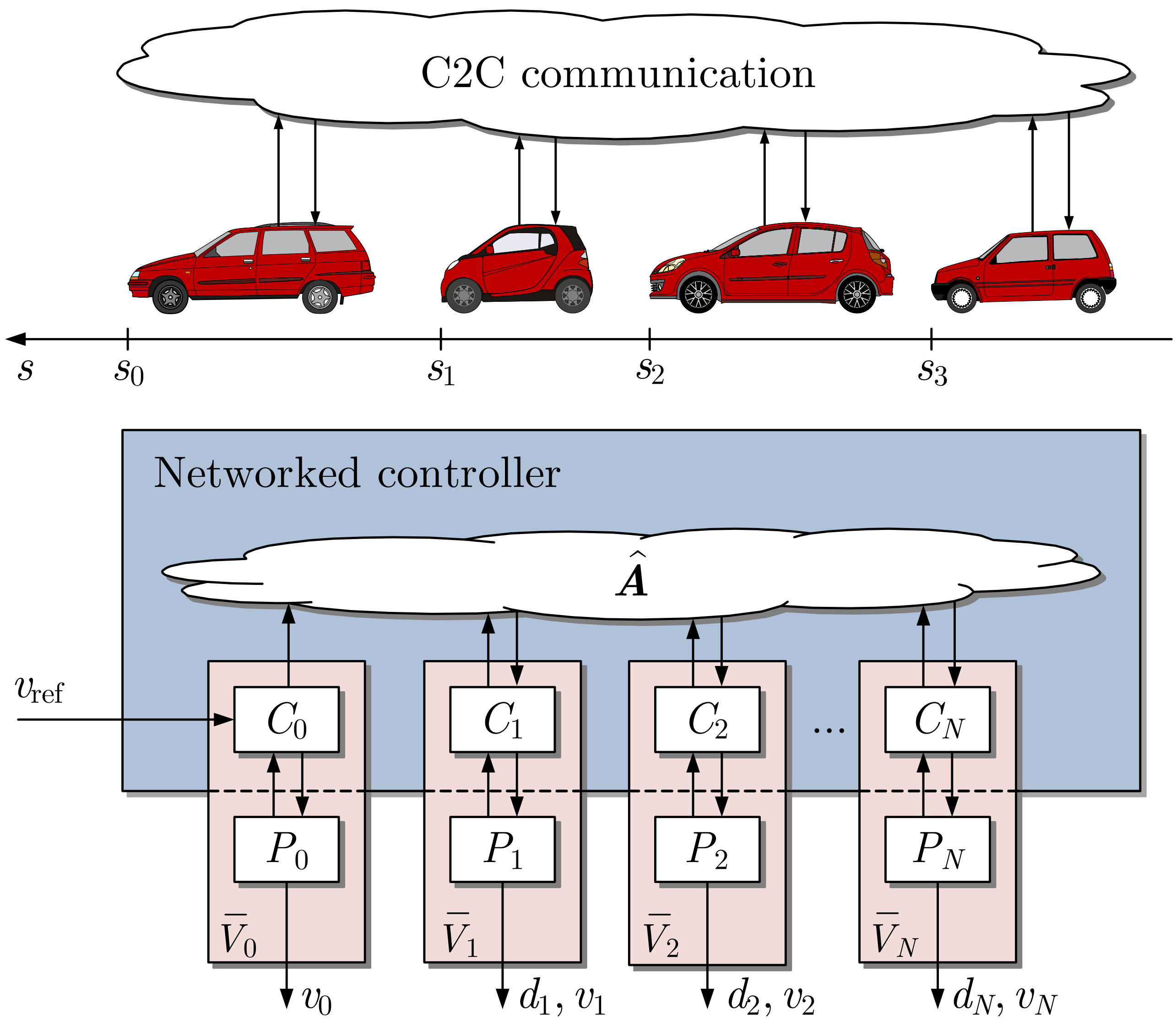

Fig. 5.17: Platoon with cooperative adaptive cruise controller

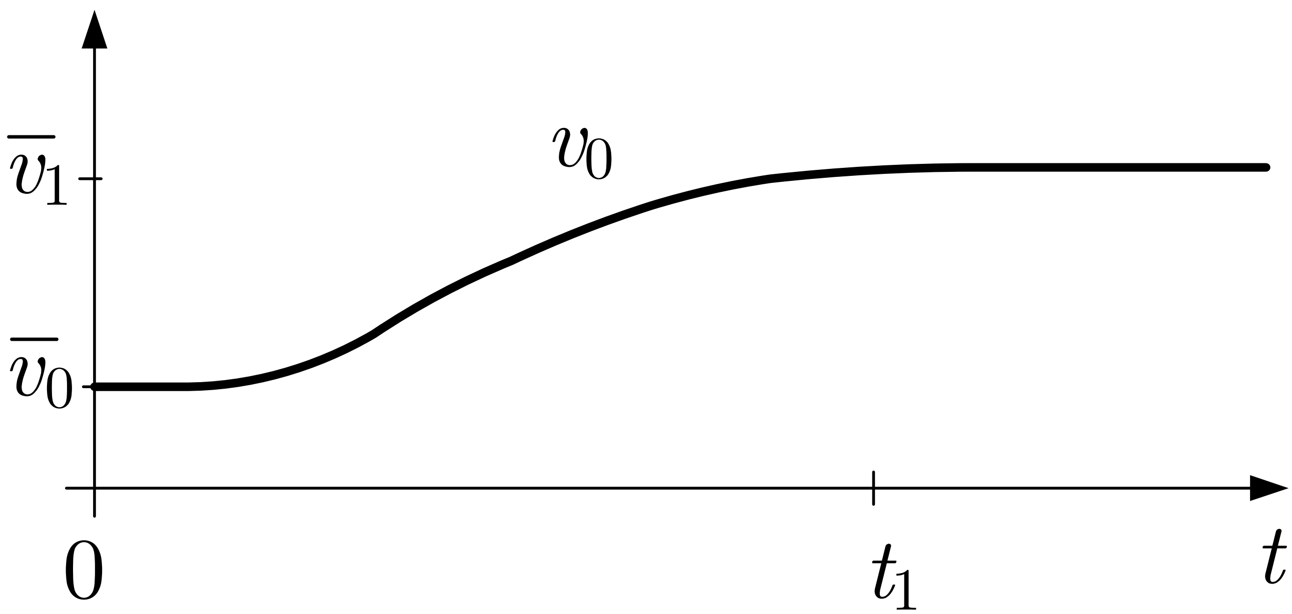

Fig. 5.18: Velocity of the leading vehicle in an acceleration manoeuvre

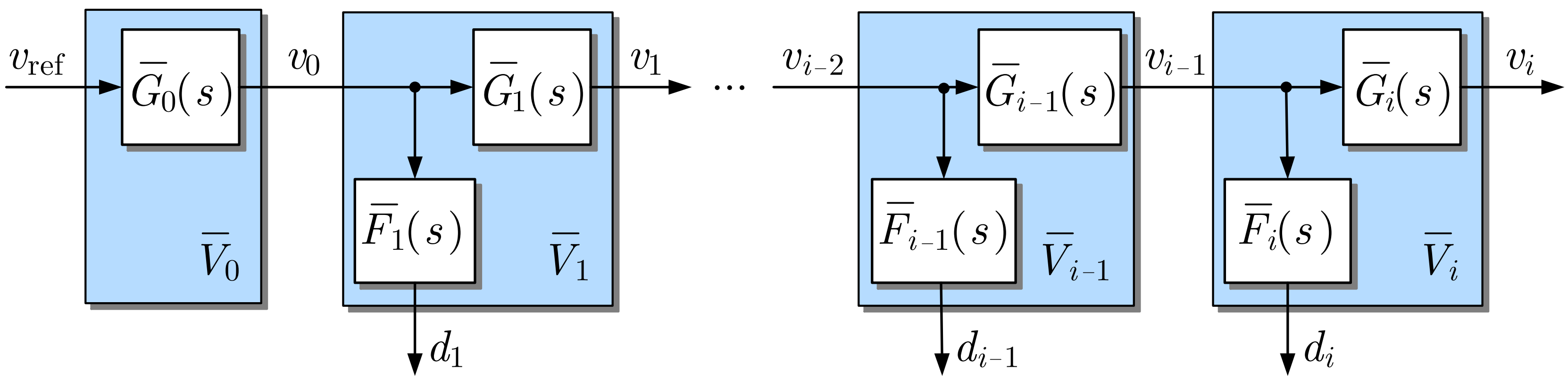

Fig. 5.19. Detailed block diagram of a vehicle platoon with ACC

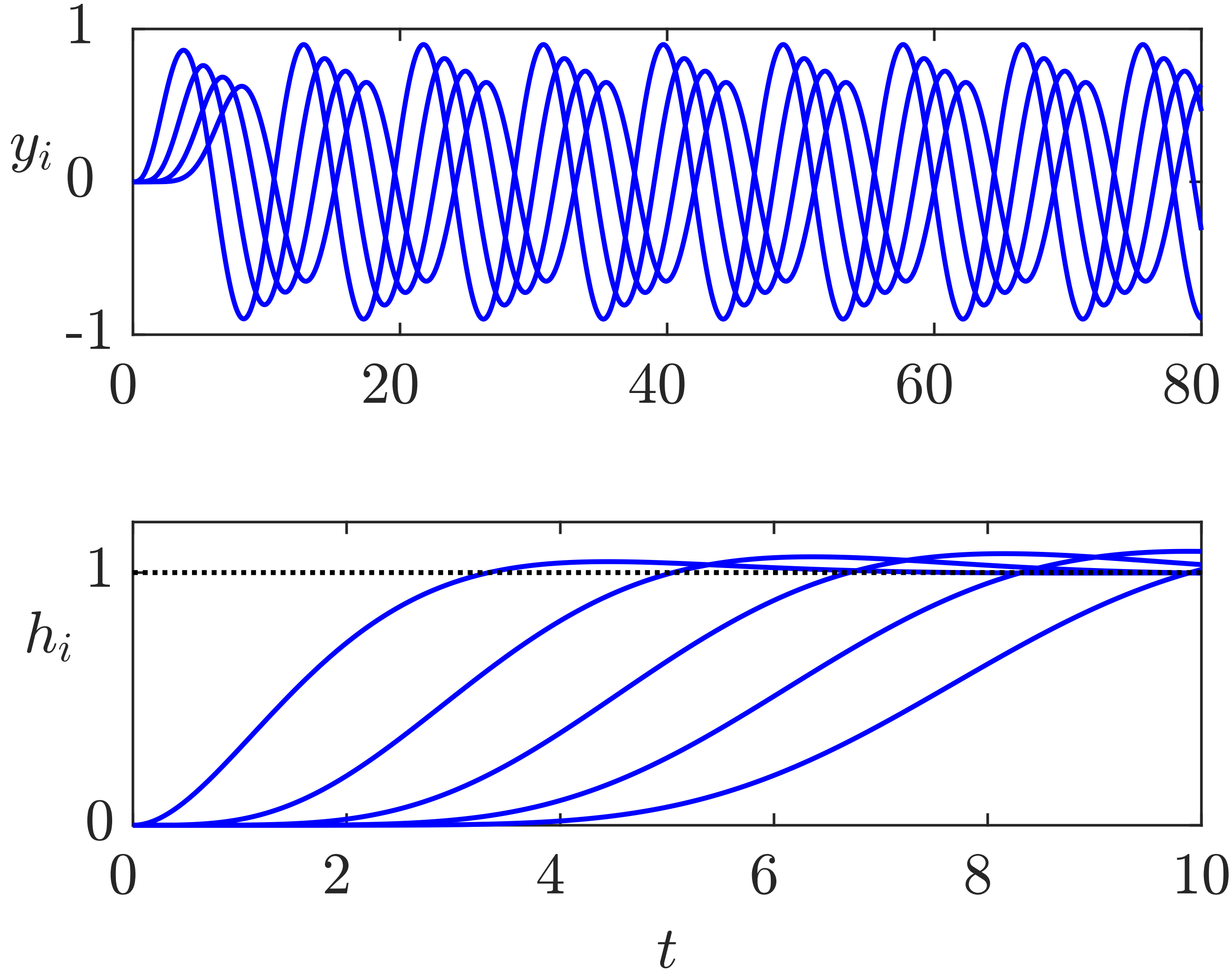

Fig. 5.20: Vehicle outputs $y_1(t)$,..., $y_4(t)$ for sinusoidal input (top) and for step input (bottom)

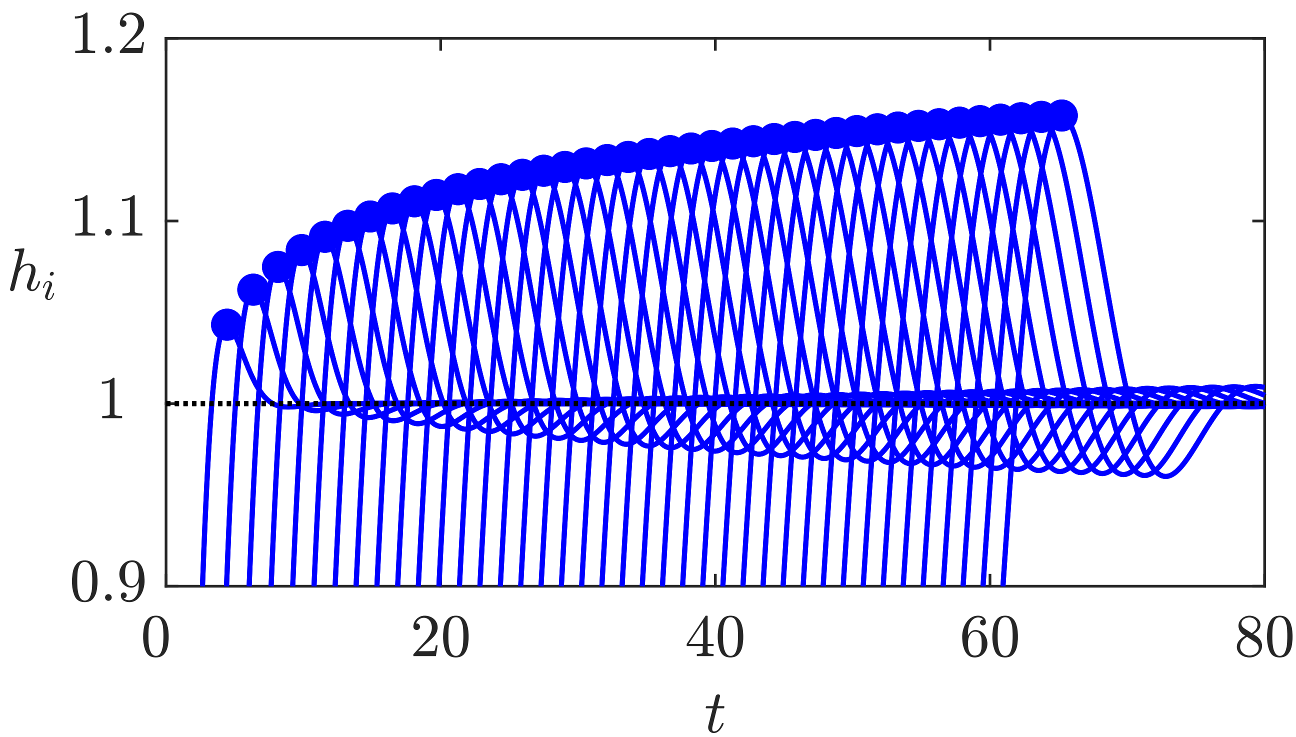

Fig. 5.21: Details of the step responses $y_i(t)$ of $N = 50$ vehicles

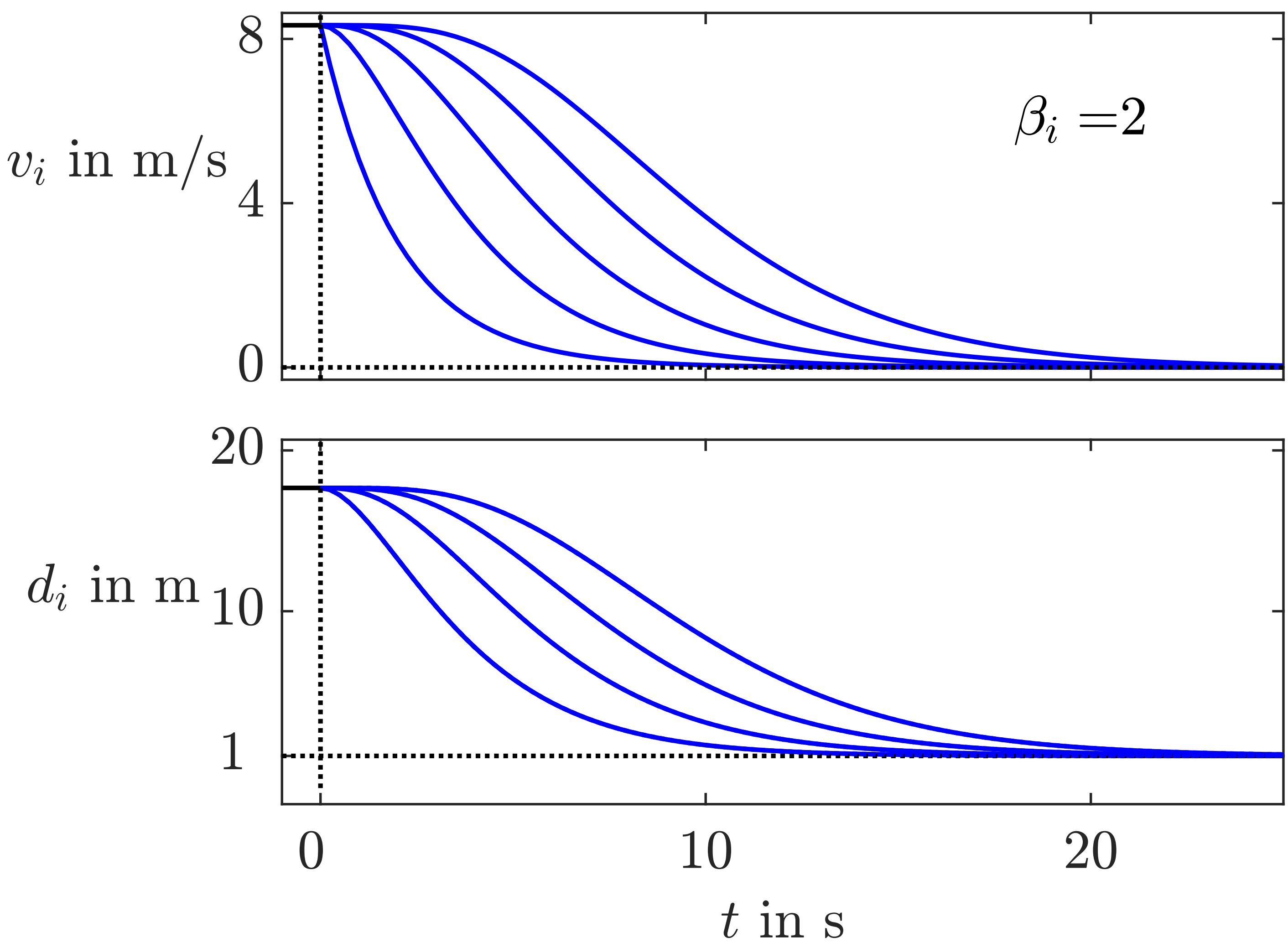

Fig. 5.22: Velocities and vehicle distances in a braking manoeuvre

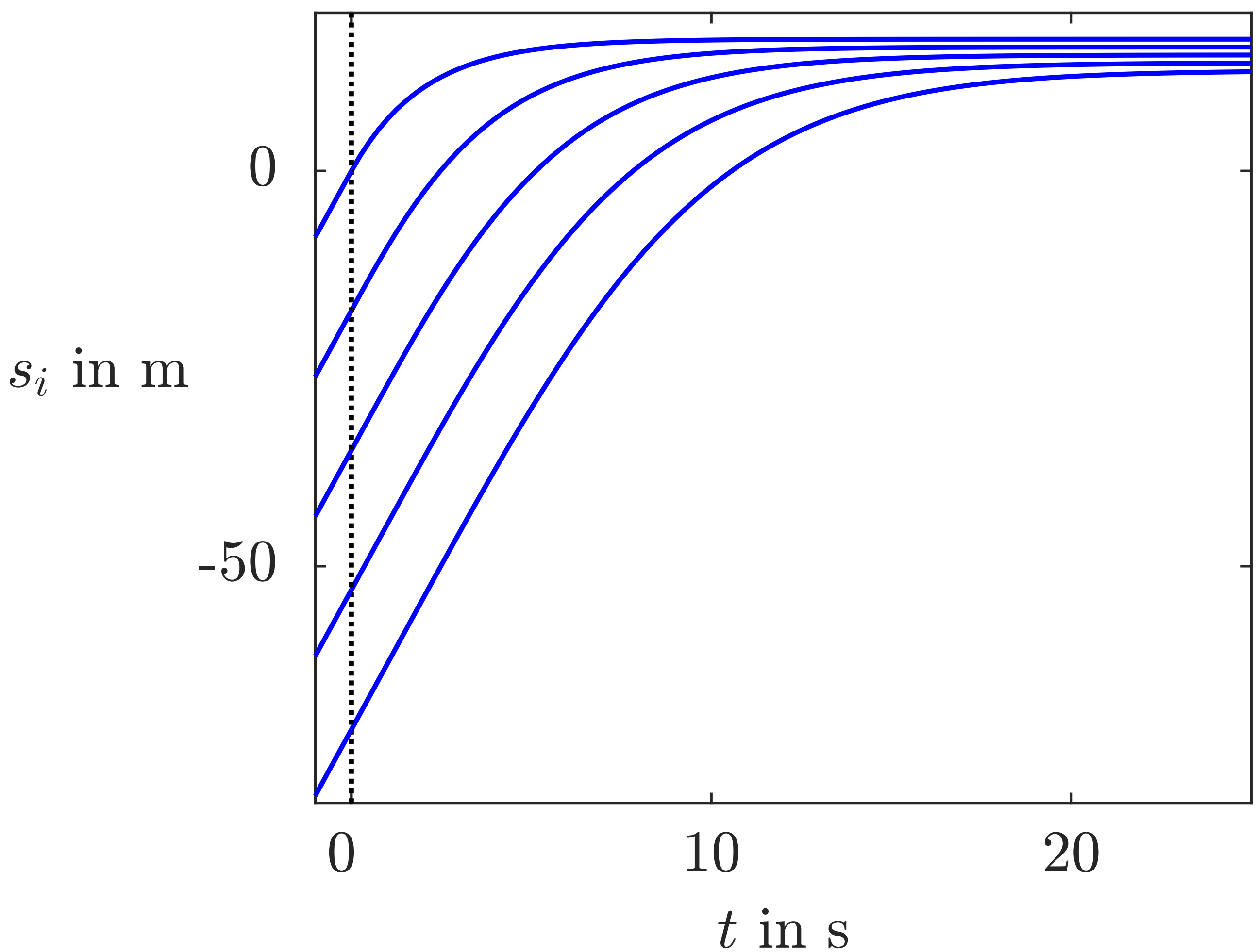

Fig. 5.22: Vehicle positions in a braking manoeuvre

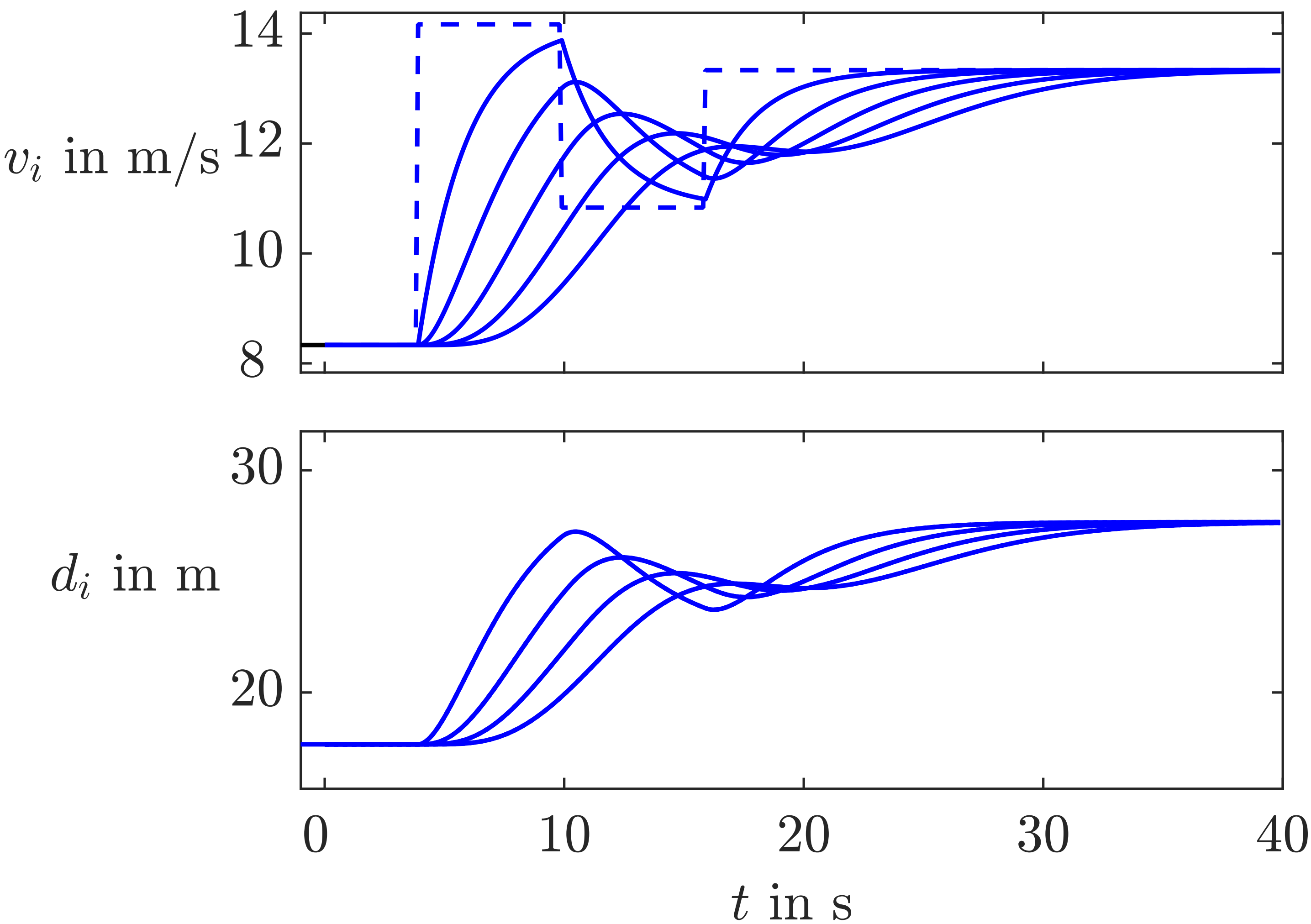

Fig. 5.23: Velocities and vehicle distances for changing command signal $v_{\mathrm{ref}}(t)$ of the leader (dashed line)

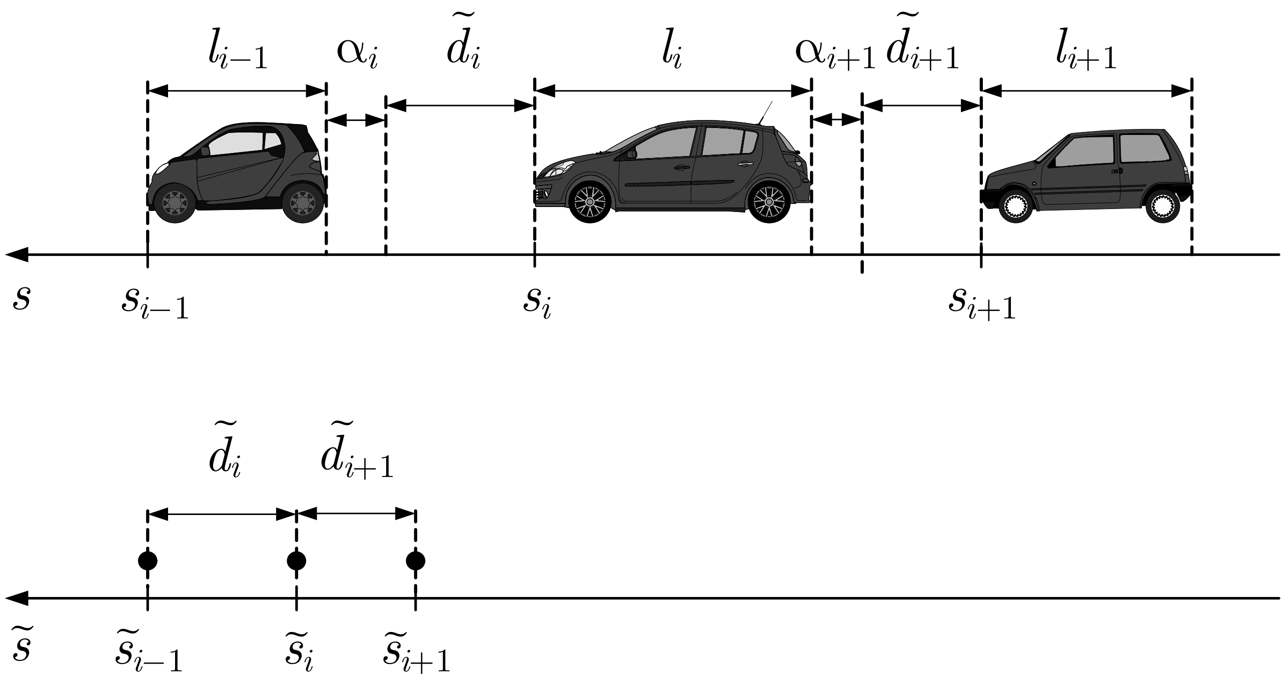

Fig. 5.24: Signals used for modelling the platoon behaviour

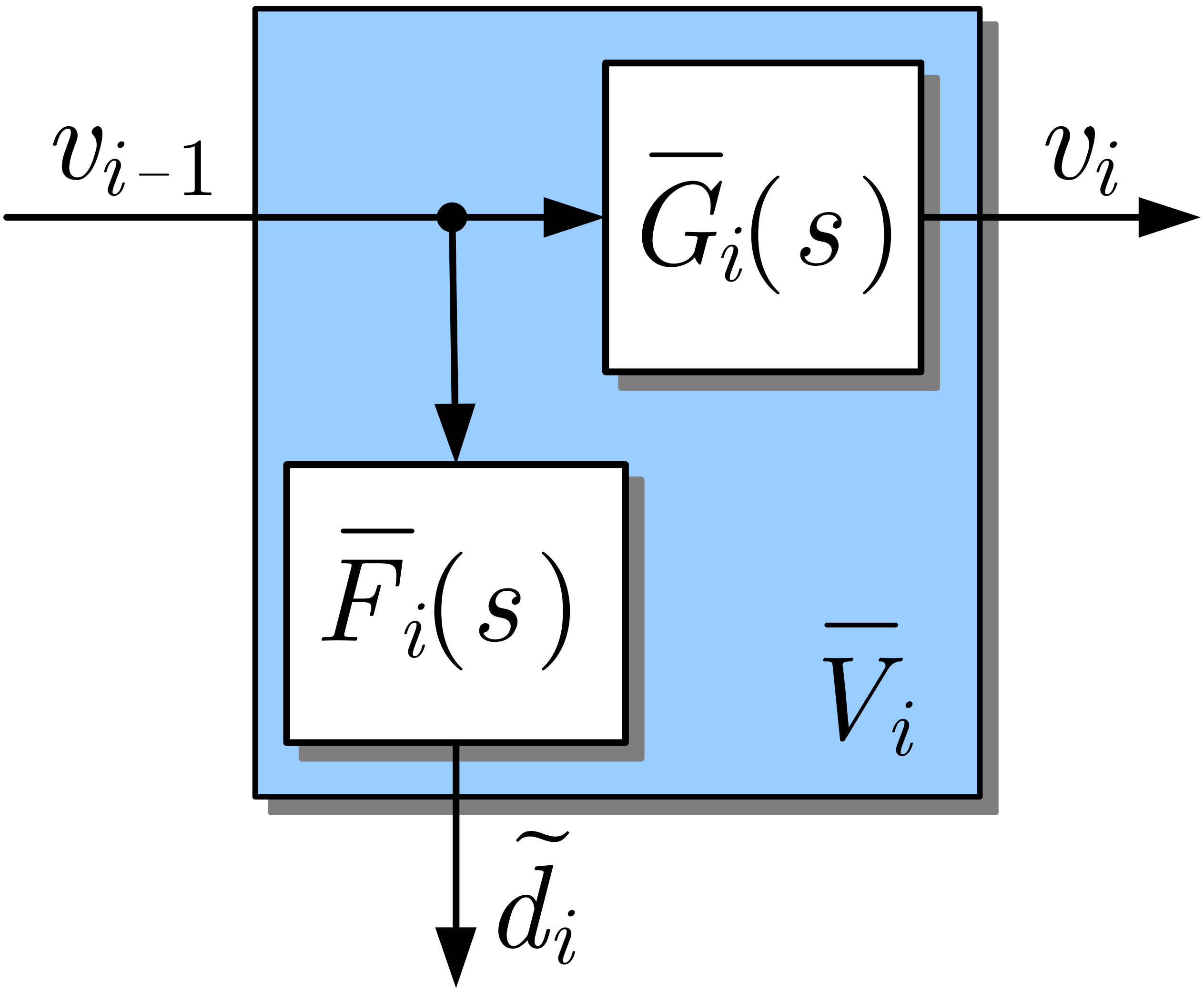

Fig. 5.25: Vehicle model considered

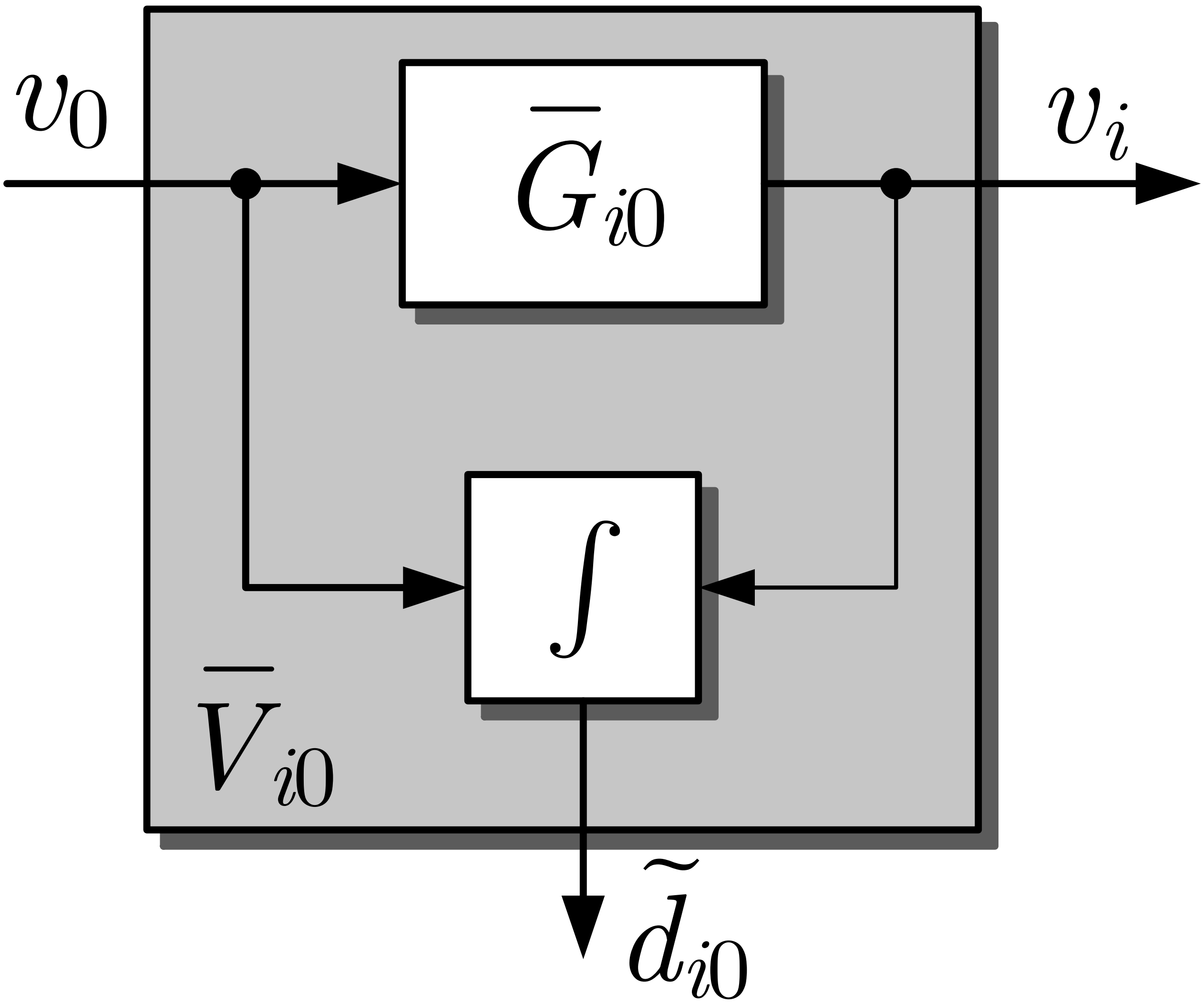

Fig. 5.26: Truncated platoon

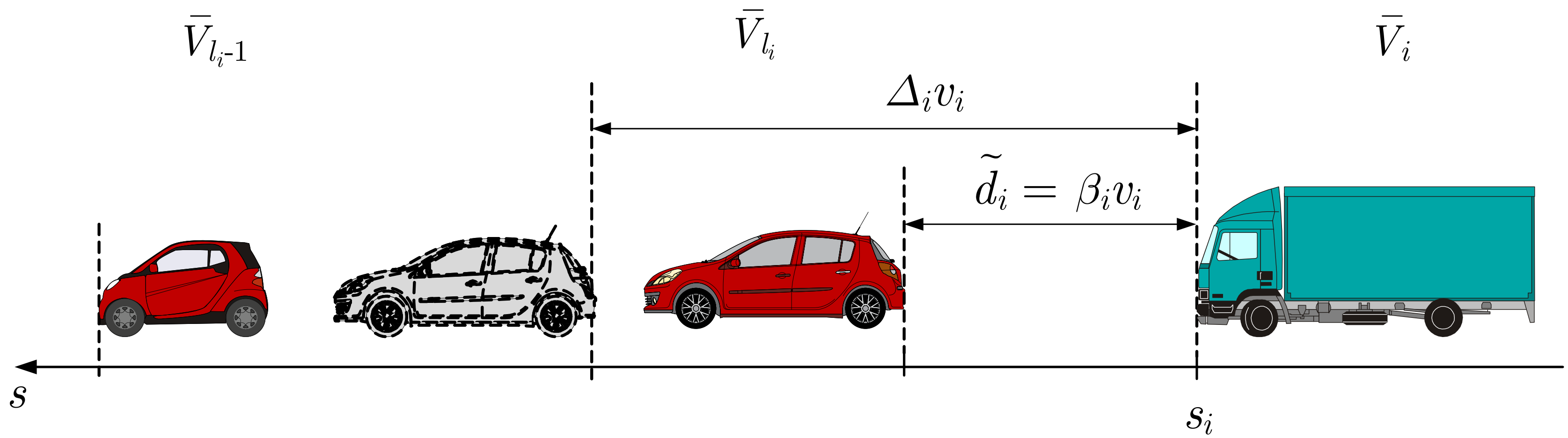

Fig. 5.27. Interpretation of the conditions of Theorem 5.2

J. Lunze: *Networked Control of Multi-Agent Systems,* Edition MoRa 2022

page 313

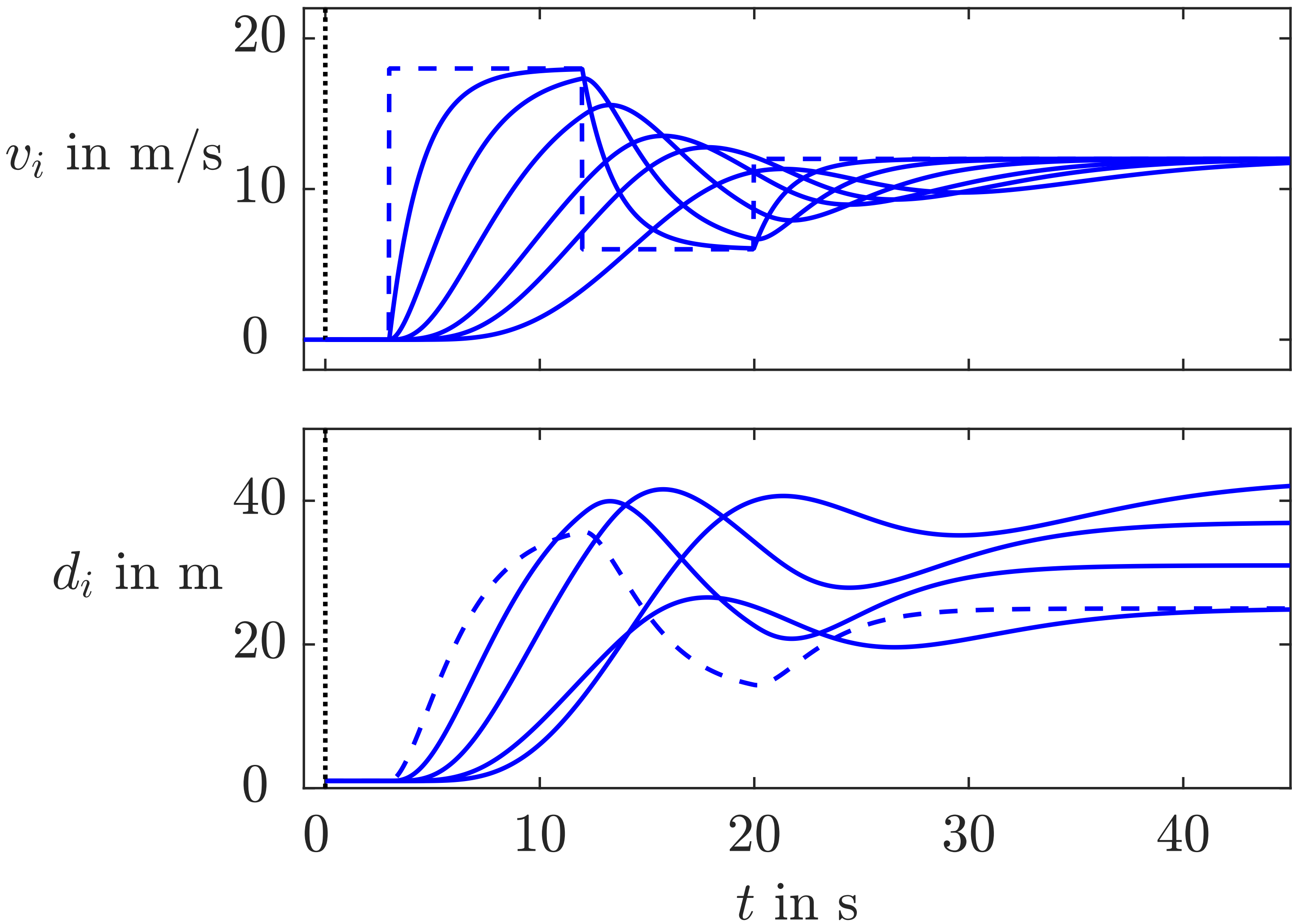

Fig. 5.28: Platoon behaviour with ACC
(velocities $v_0, ..., v_5$; distances $d_1, ..., d_5$)

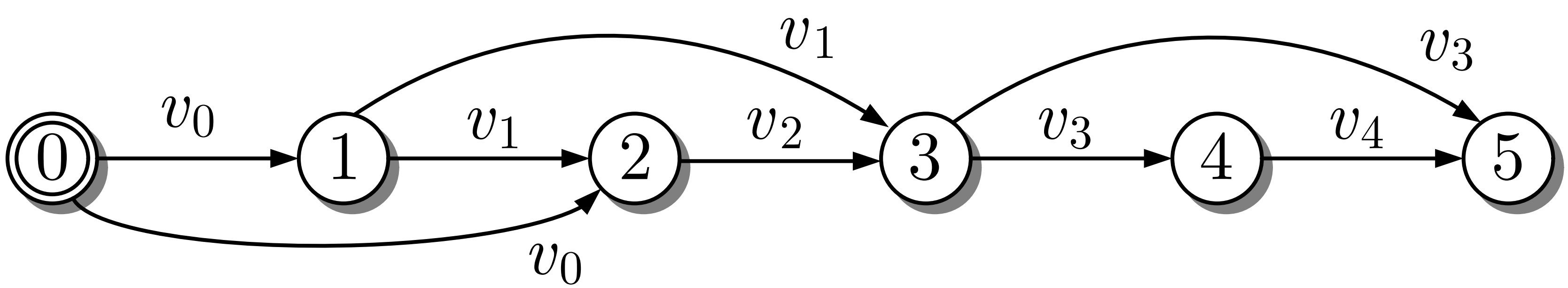

Fig. 5.29. Communication structure of the cooperative adaptive cruise controller of Example 5.8

J. Lunze: *Networked Control of Multi-Agent Systems,* Edition MoRa 2022

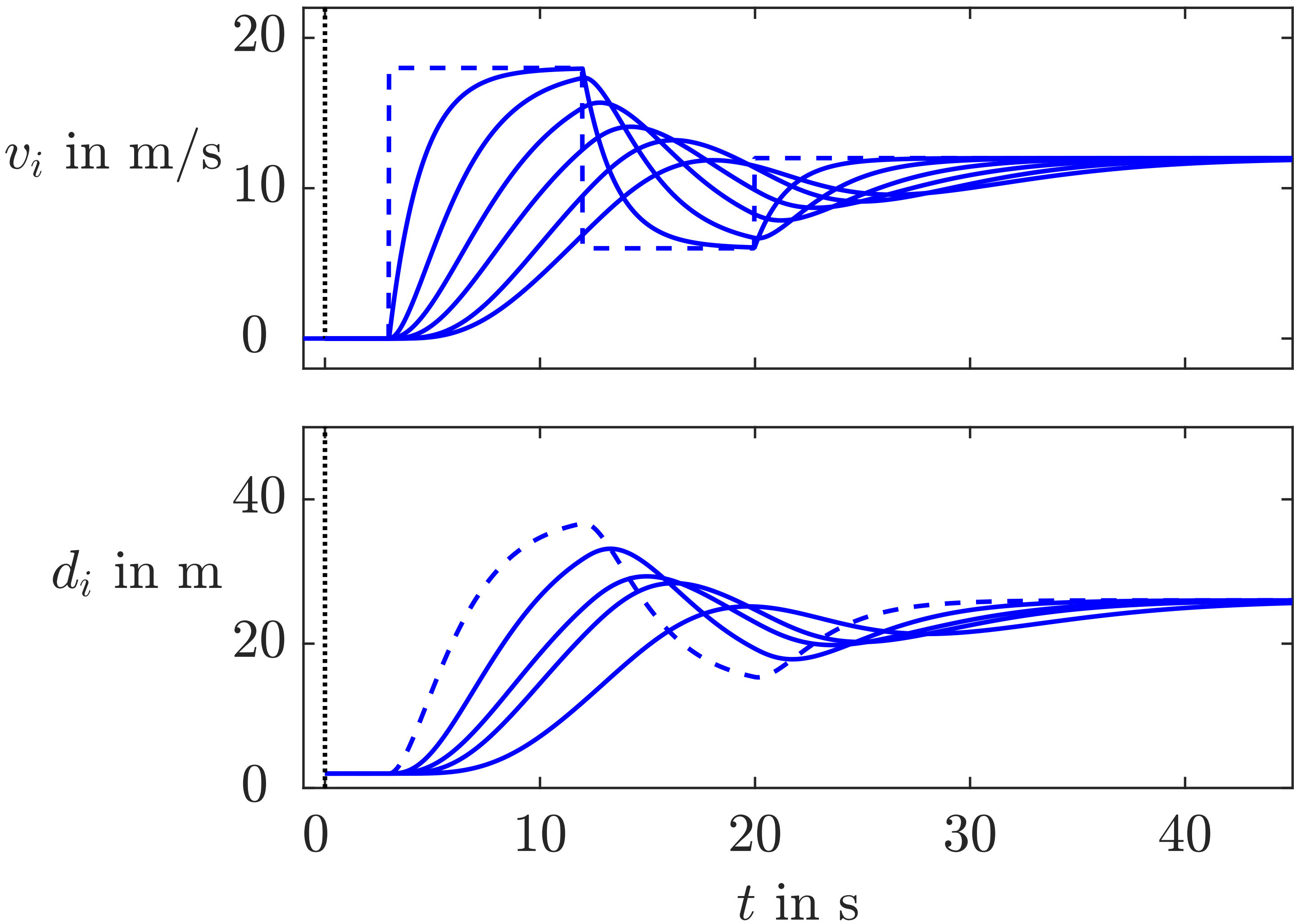

Fig. 5.30: Velocities and distances of the vehicles in a platoon with CACC

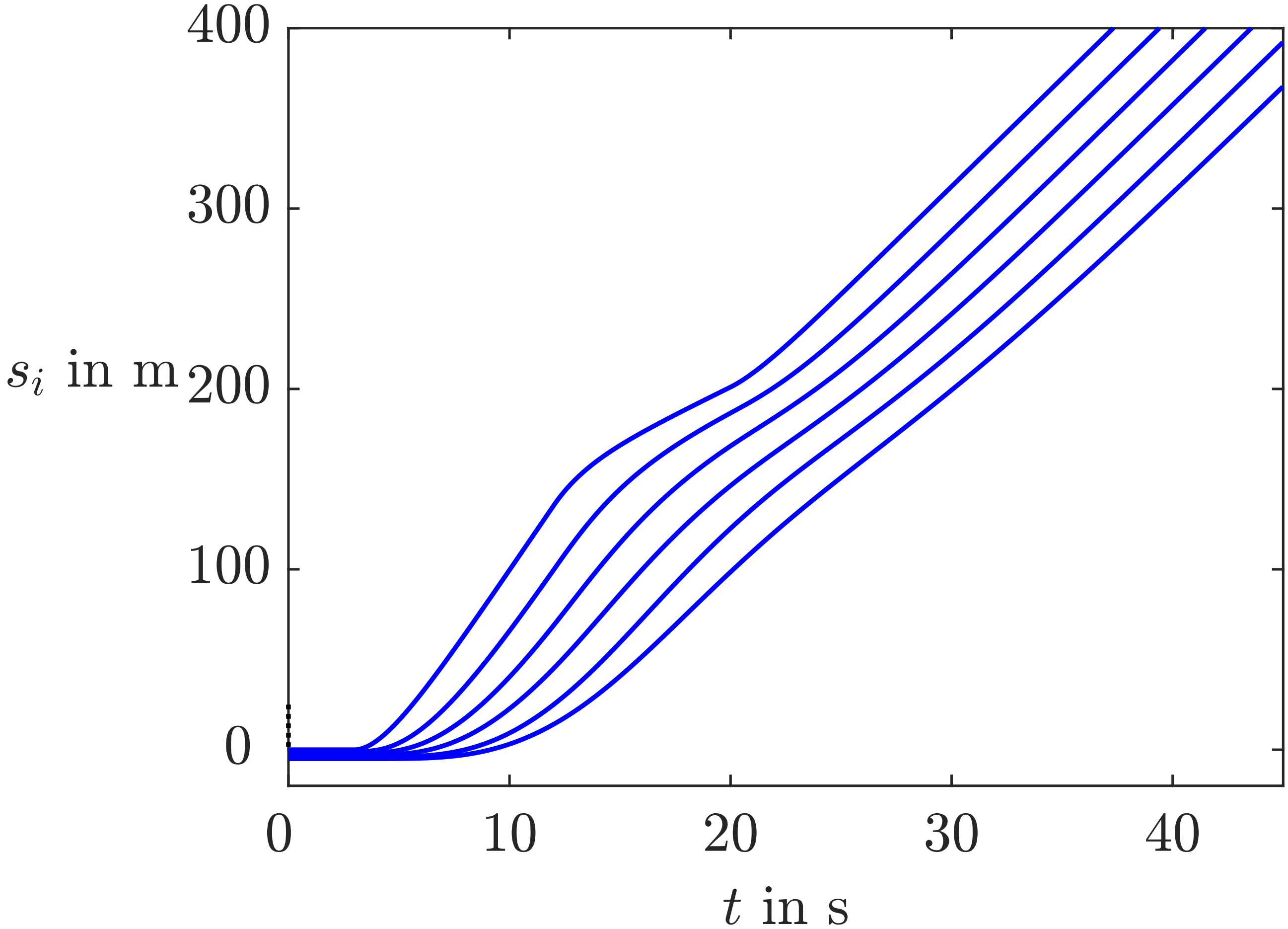

Fig. 5.30: Positions of the vehicles in a platoon with CACC

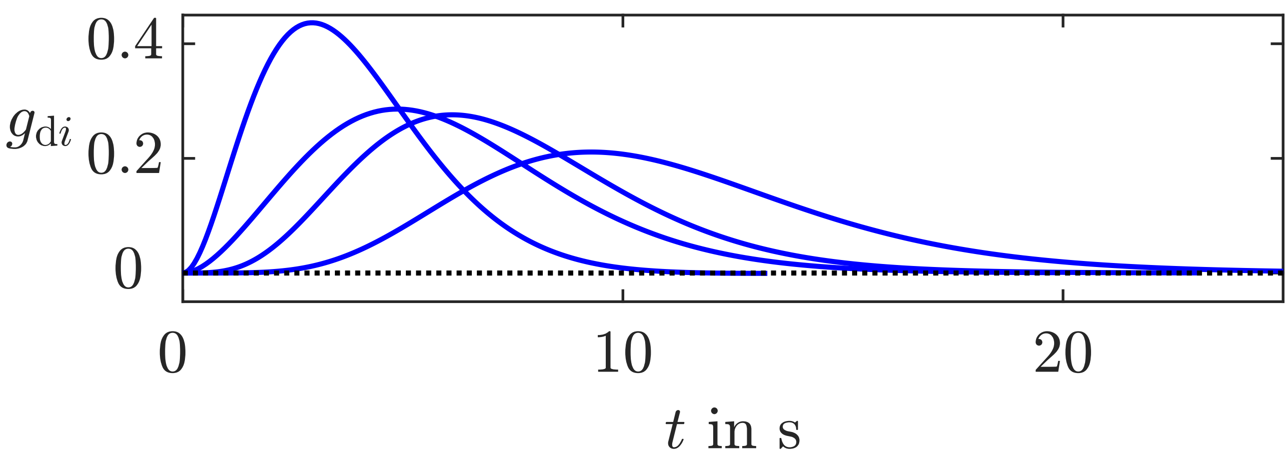

Fig. 5.31: Impulse responses belonging to the transfer functions (5.112), $(i = 2, ..., 5)$

J. Lunze: *Networked Control of Multi-Agent Systems,* Edition **MoRa** 2022

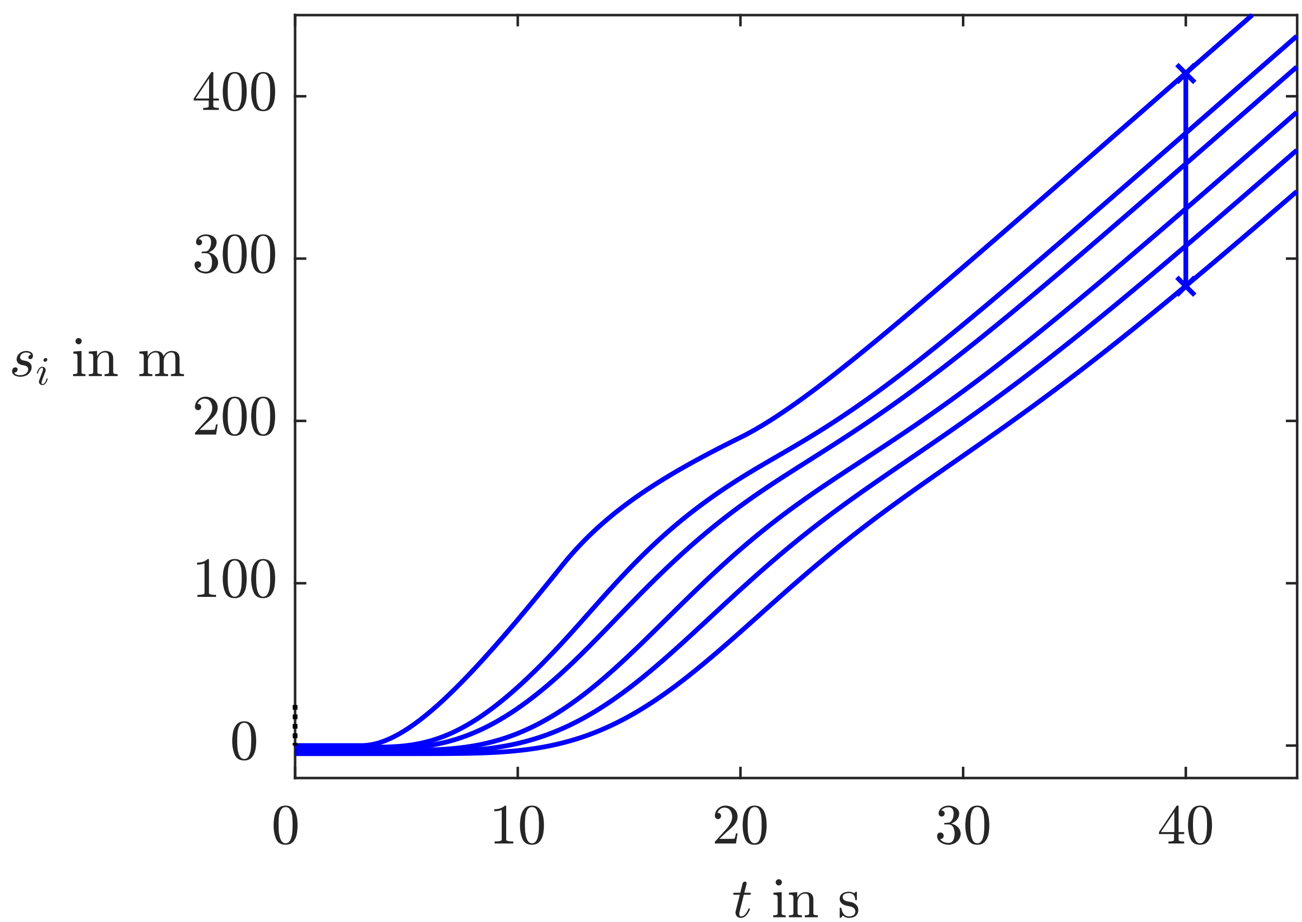

Fig. 5.32: Platoon behaviour with CACC

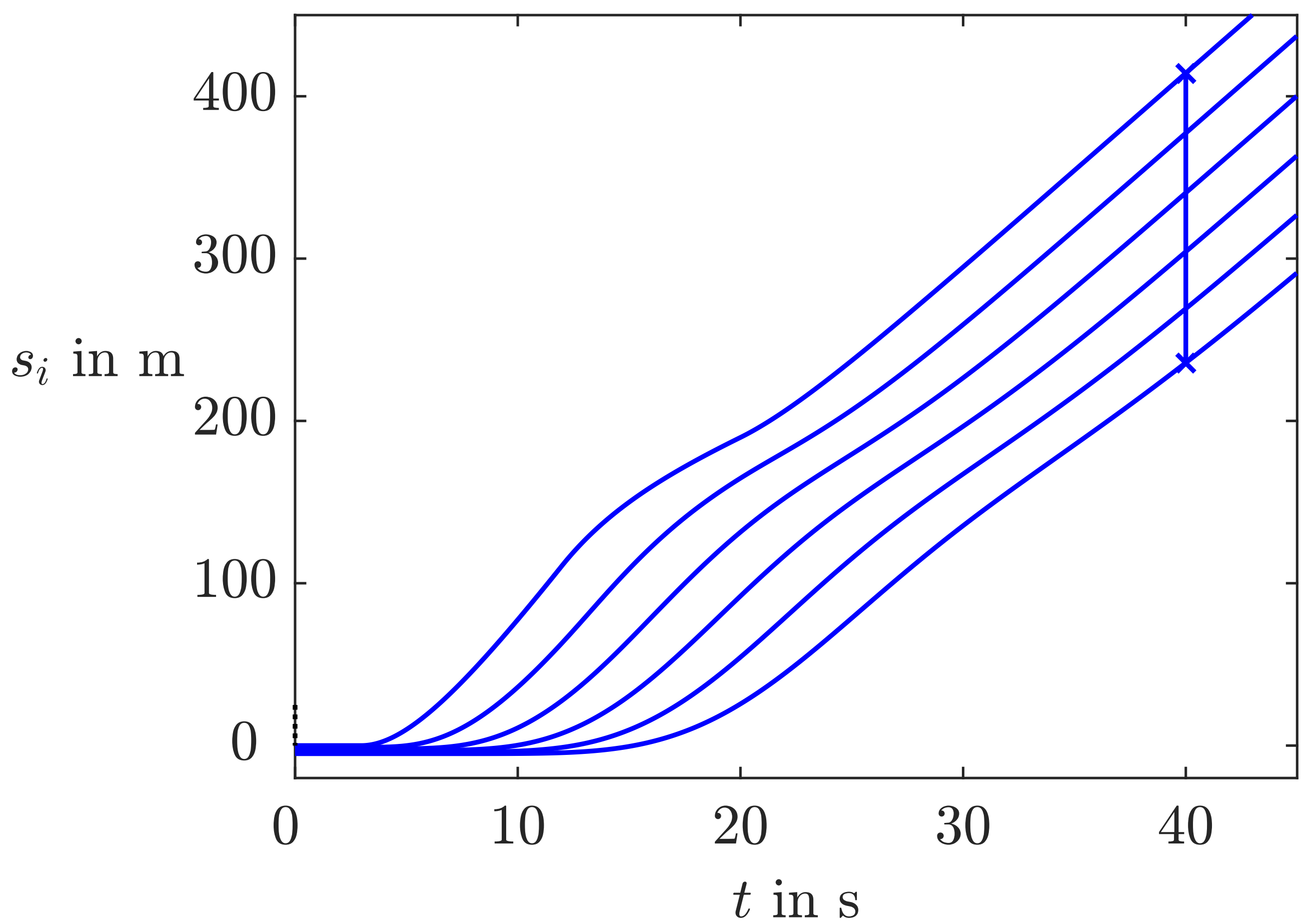

Fig. 5.32: Platoon behaviour with ACC

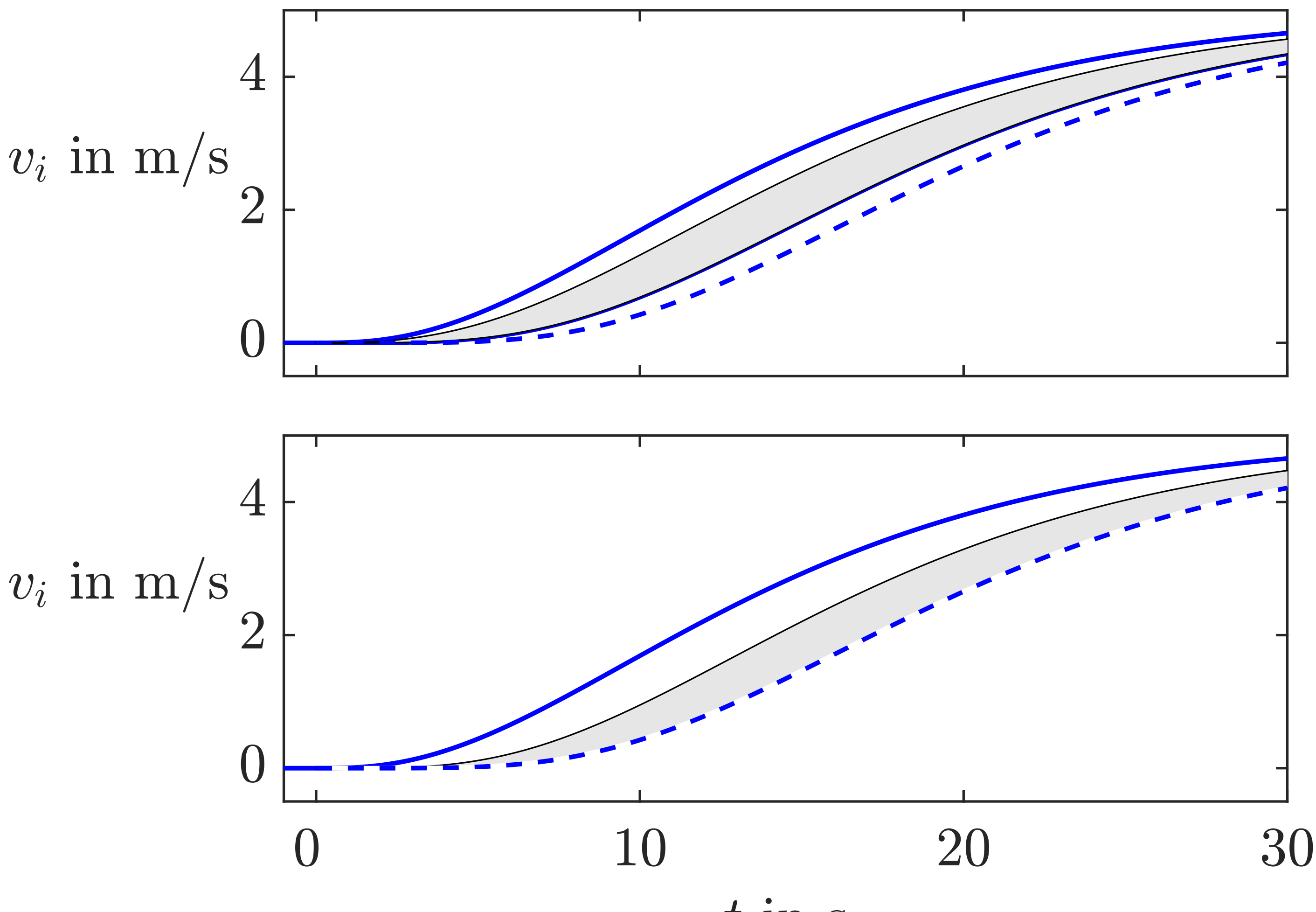

Fig. 5.33: Comparison of the velocity $v_2(t)$ of the second follower (third curve from above) for CACC (top) and ACC (bottom)

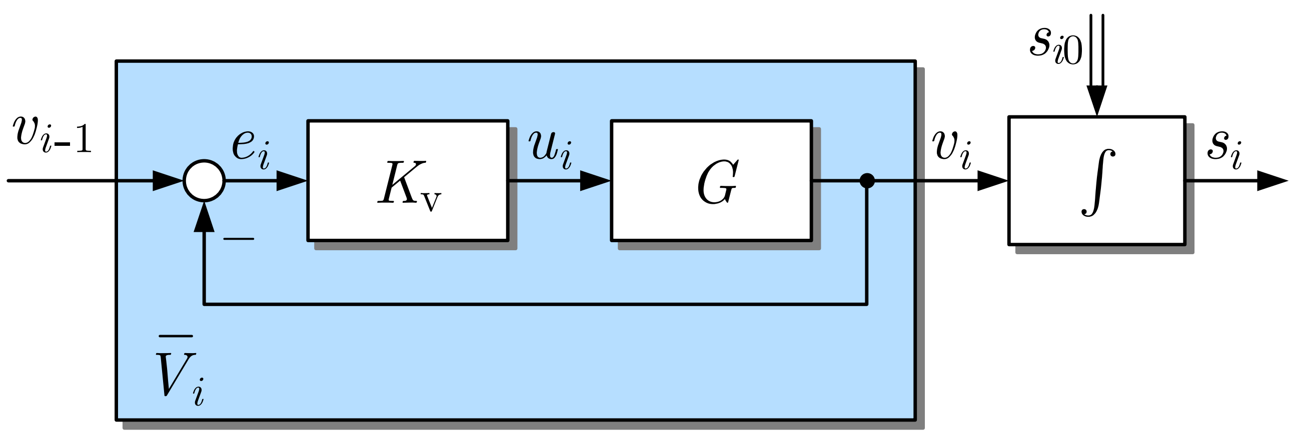

Fig. 5.34: Vehicle with velocity controller

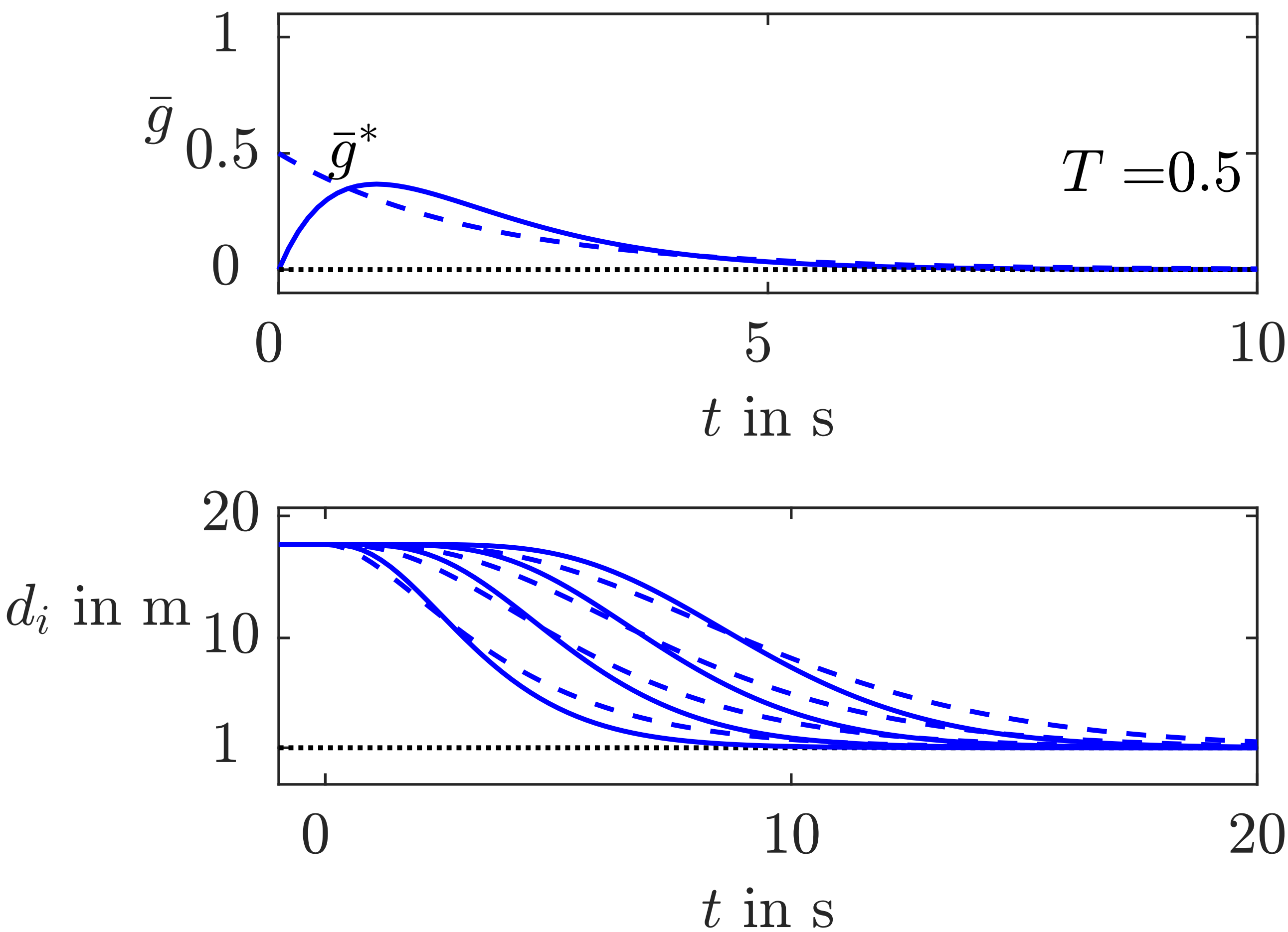

Fig. 5.35: Impulse response and vehicle distance in a braking manoeuvre

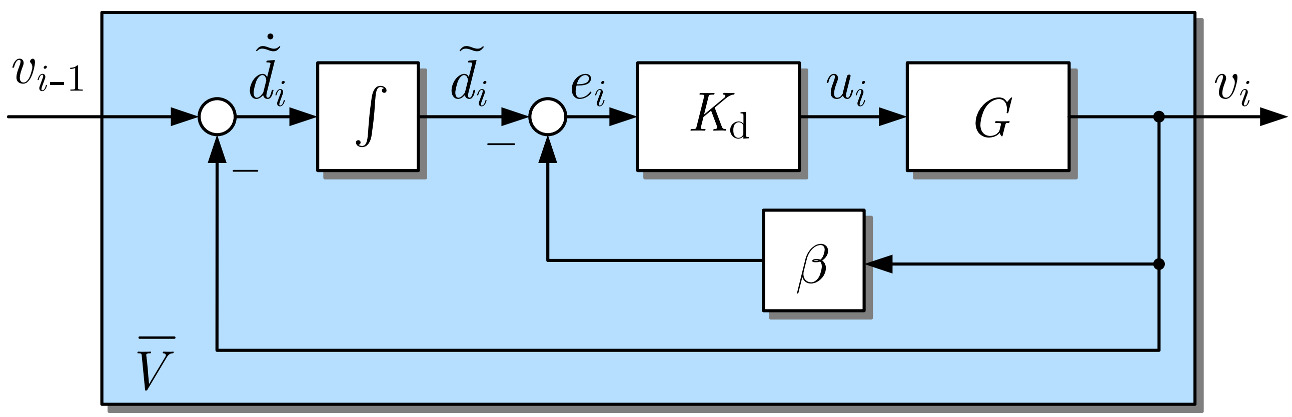

Fig. 5.36: Vehicle with distance controller

J. Lunze: *Networked Control of Multi-Agent Systems*, Edition MoRa 2022

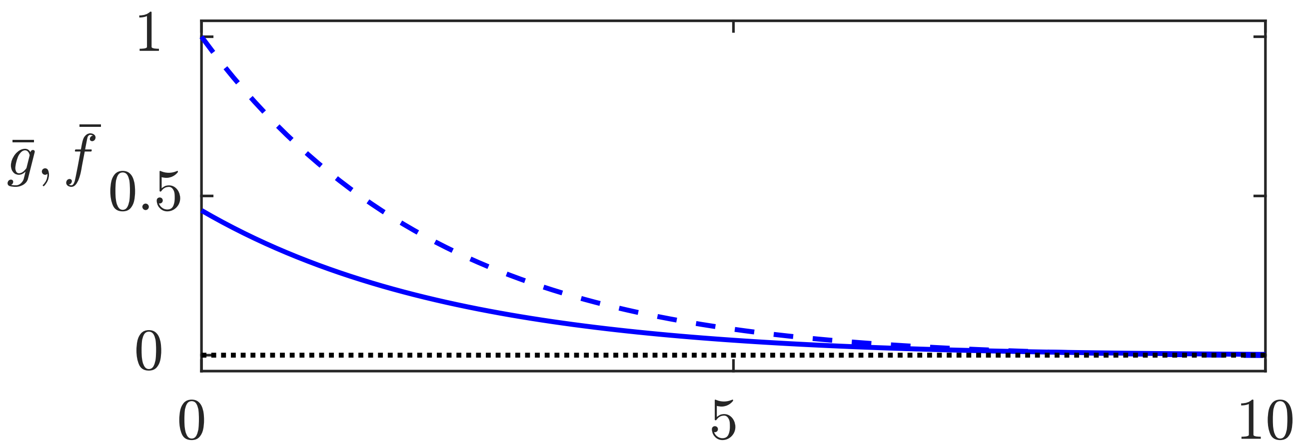

Fig. 5.37: Impulse responses of the controlled vehicles ($\bar{g}$ —, $\bar{f}$ - - -)

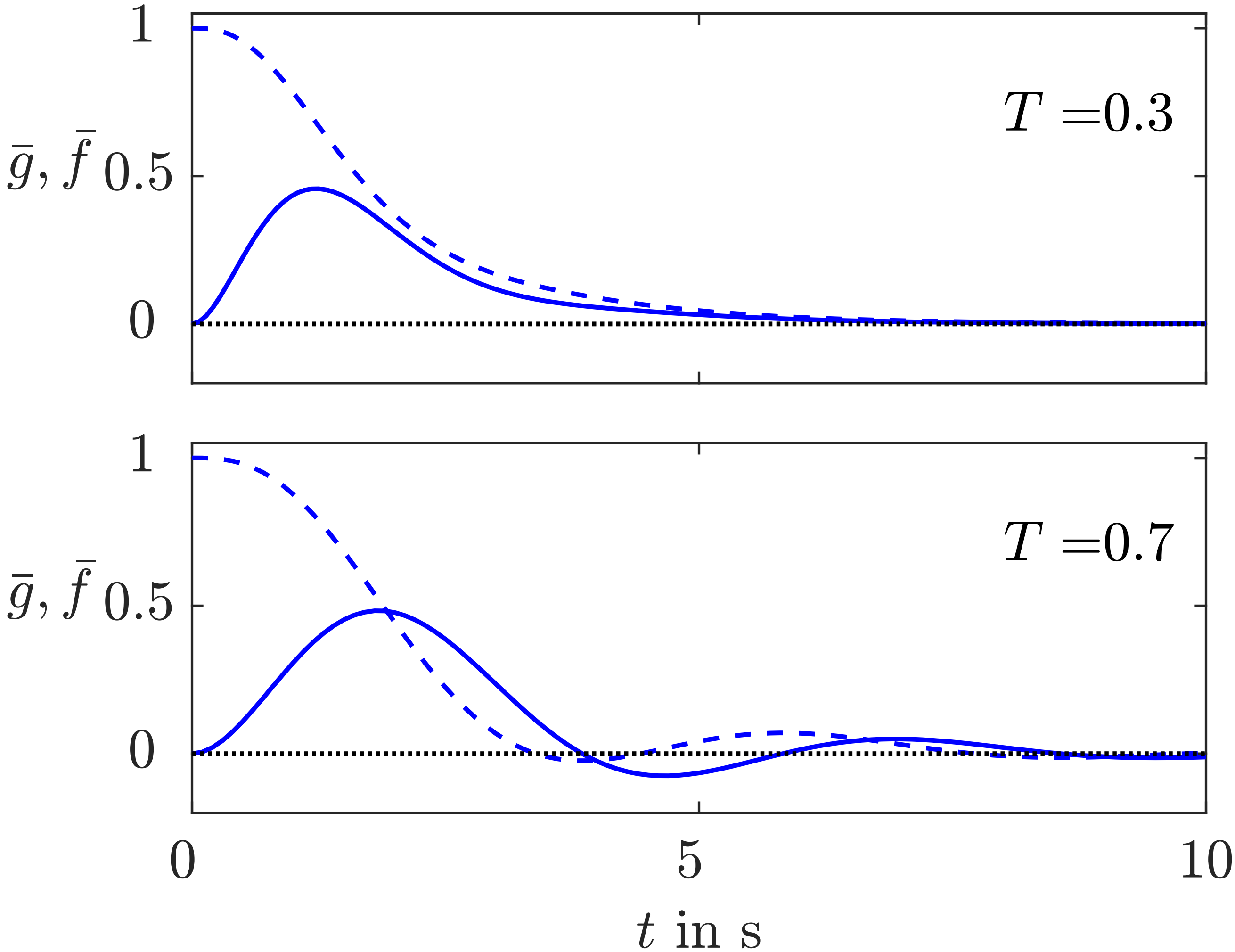

Fig. 5.38: Impulse responses of the controlled vehicle for proportional distance controller

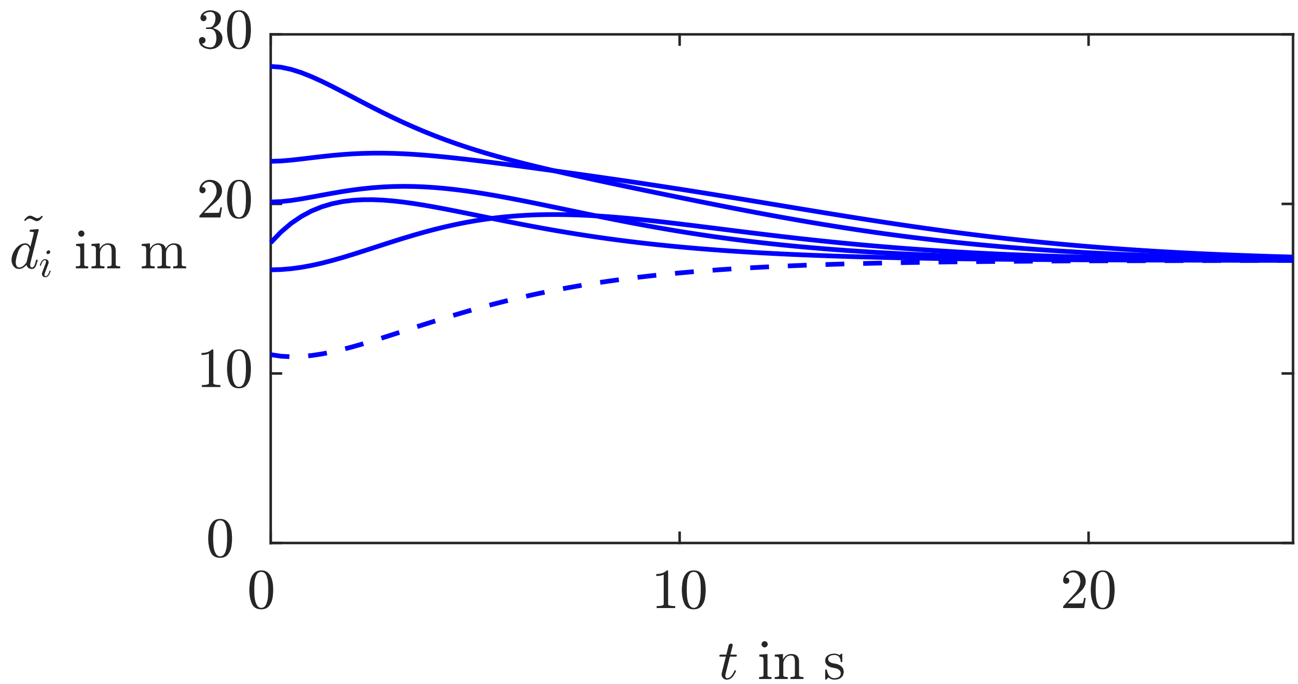

Fig. 5.39: Vehicle distances in a platoon with distance controllers

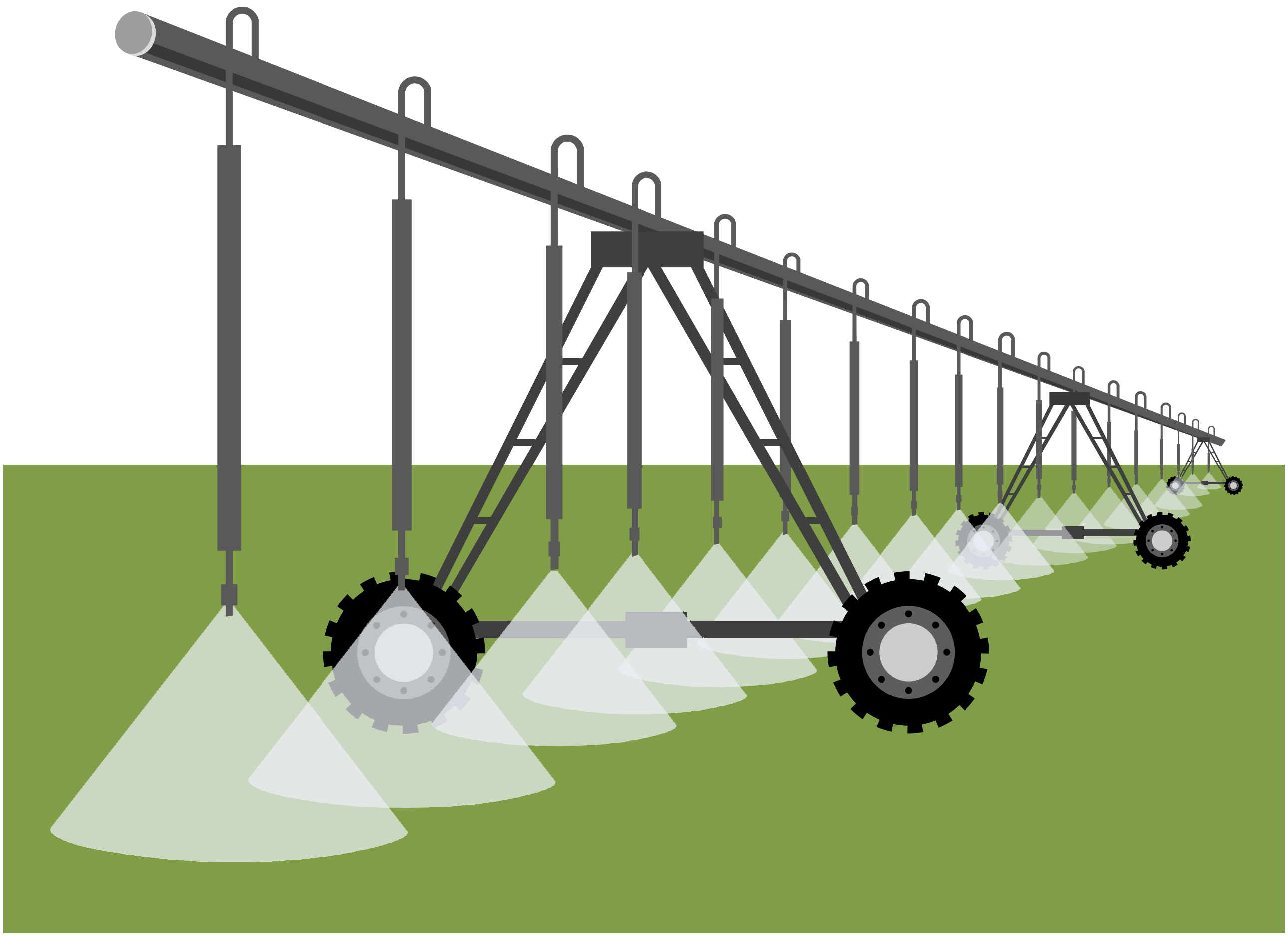

Fig. 5.40: Irrigation system

J. Lunze: *Networked Control of Multi-Agent Systems*, Edition **MoRa** 2022

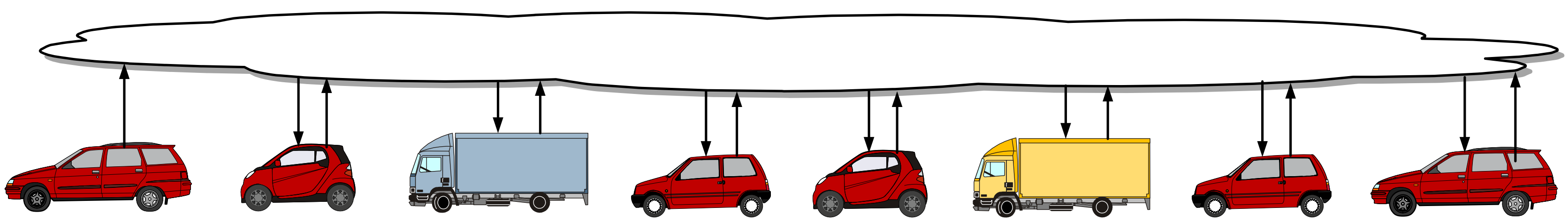

Fig. 5.41. Vehicle platoon

J. Lunze: *Networked Control of Multi-Agent Systems*, Edition MoRa 2022

page 334

Fig. 5.42: μ-split braking manoeuvre

J. Lunze: *Networked Control of Multi-Agent Systems*, Edition **MoRa** 2022

page 335

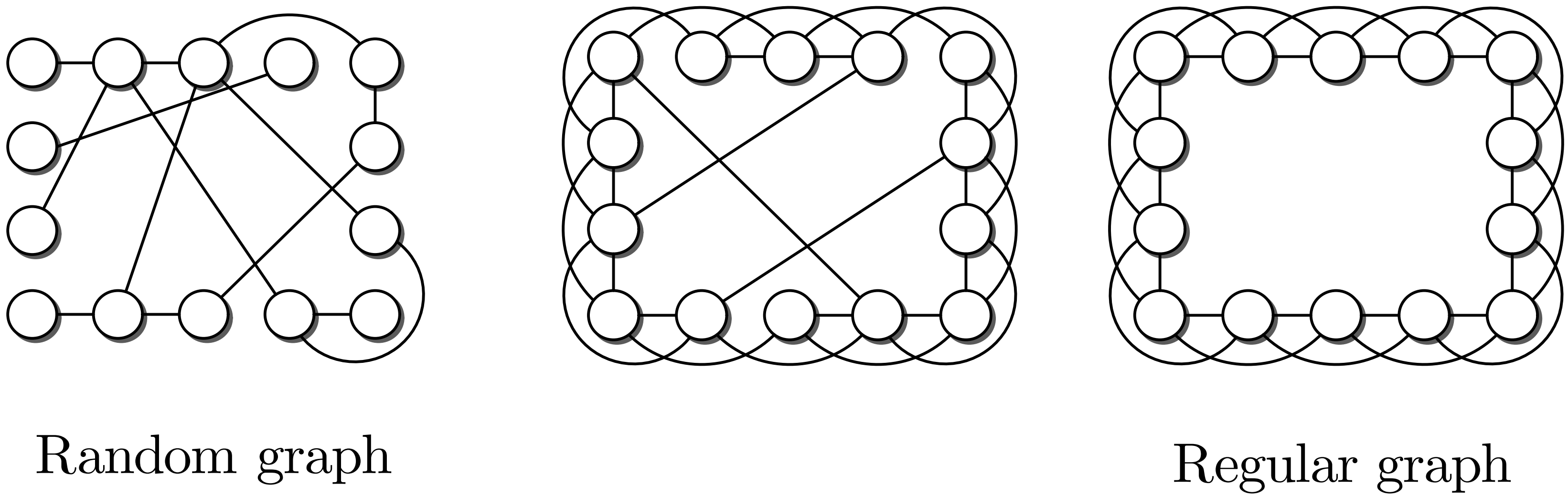

Fig. 6.1. Random graph vs. regular graph

J. Lunze: *Networked Control of Multi-Agent Systems*, Edition **M**o**R**a 2022

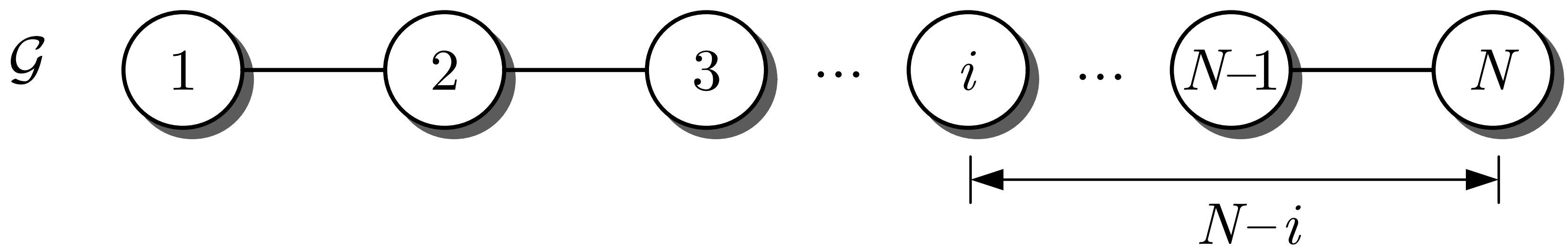

Fig. 6.2. Determination of the characteristic path length of a path graph

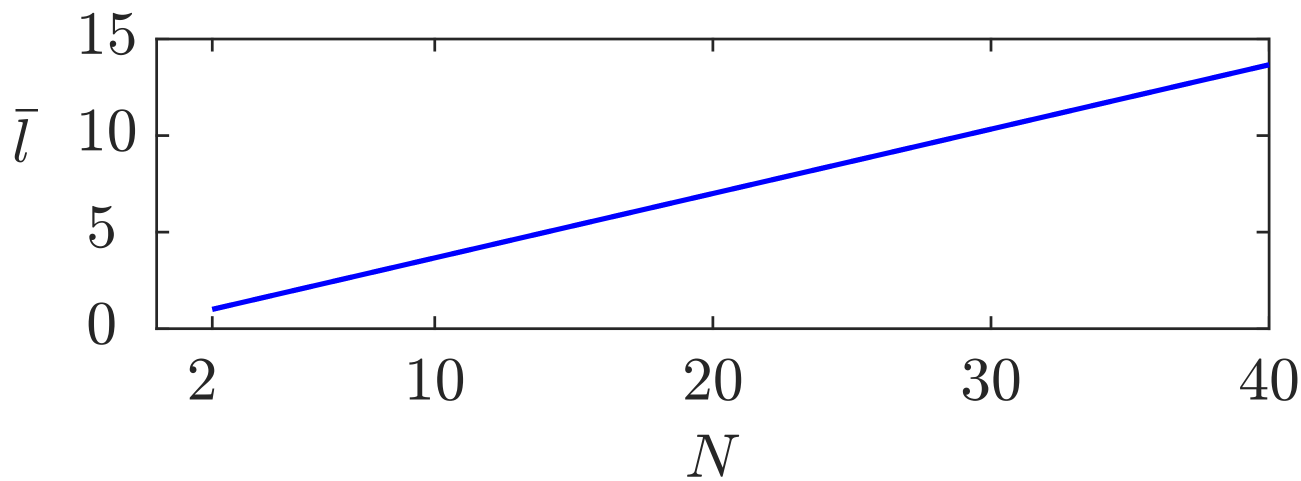

Fig. 6.3: Characteristic path length of the undirected path graph

J. LUNZE: *Networked Control of Multi-Agent Systems,* Edition MoRa 2022

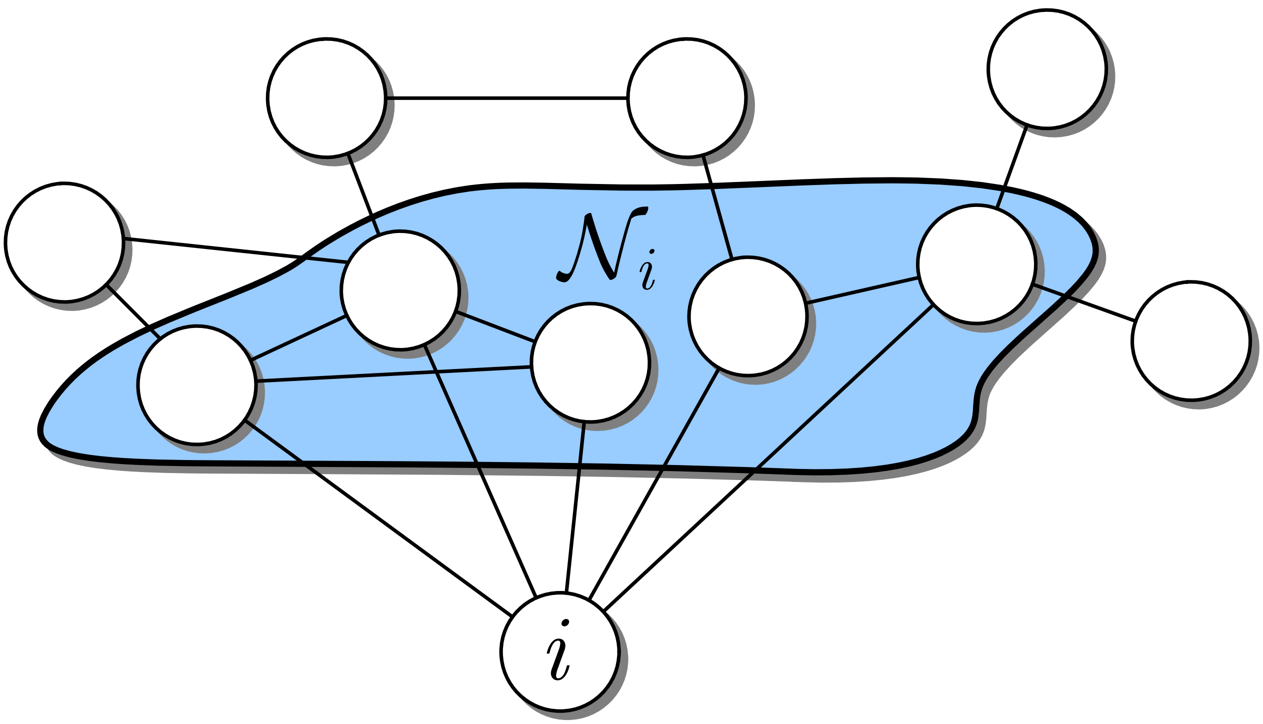

Fig. 6.4: Vertex i and its set $\mathcal{N}_i$ of neighbours

J. Lunze: *Networked Control of Multi-Agent Systems,* Edition **M**o**R**a 2022

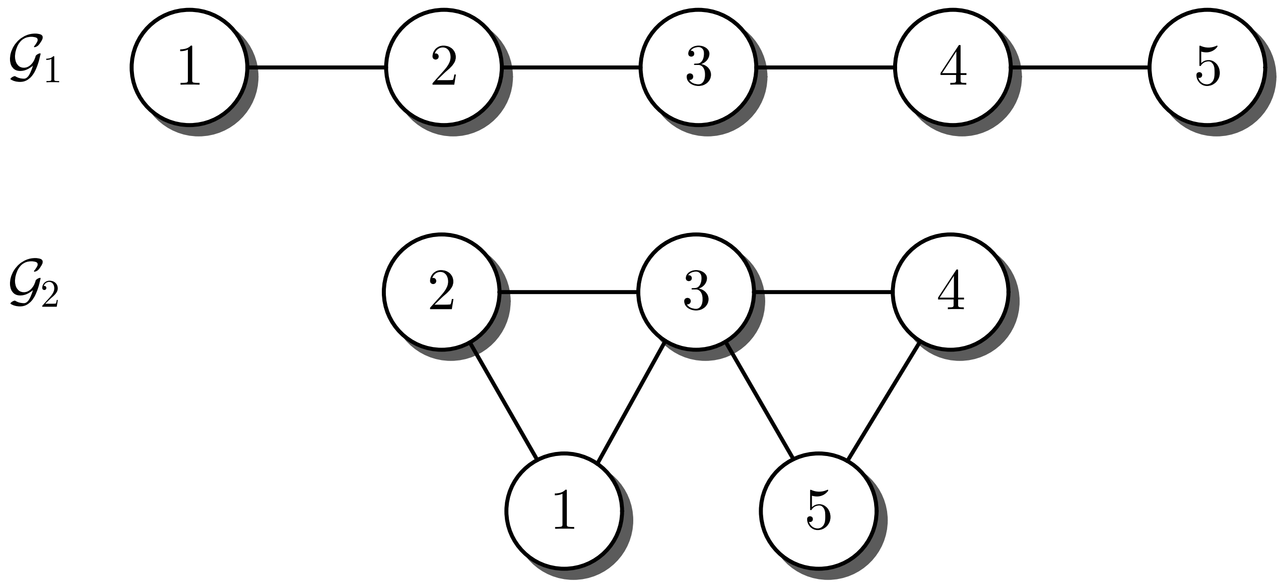

Fig. 6.5: Two graphs with quite different clustering coefficients

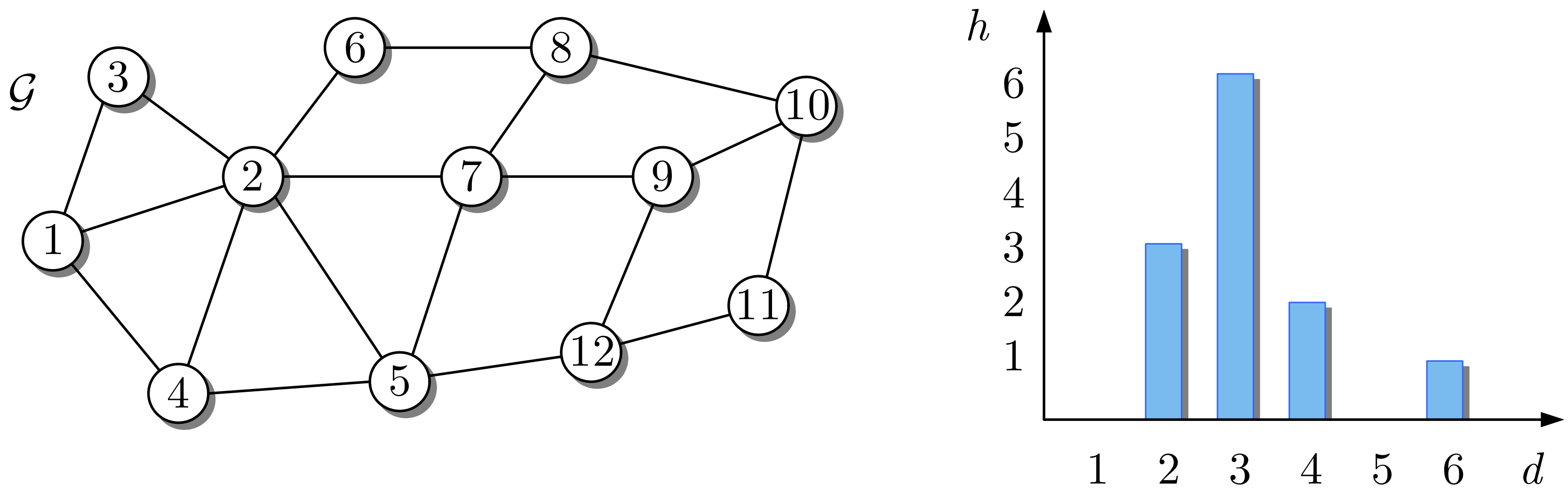

Fig. 6.6. Example graph with bar chart

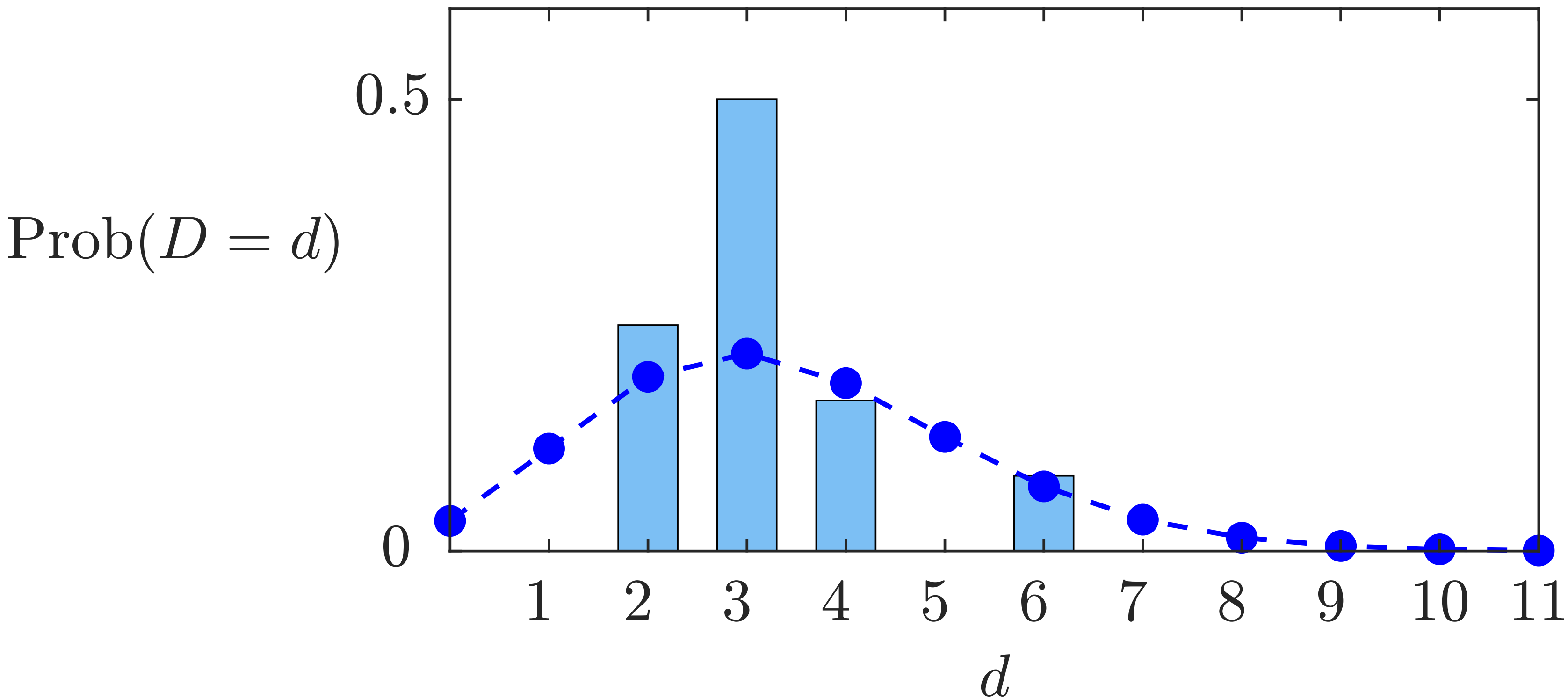

Fig. 6.7. Relative frequencies of the vertex degrees of the graph of Fig. 6.6 and Poisson degree distribution of a random graph

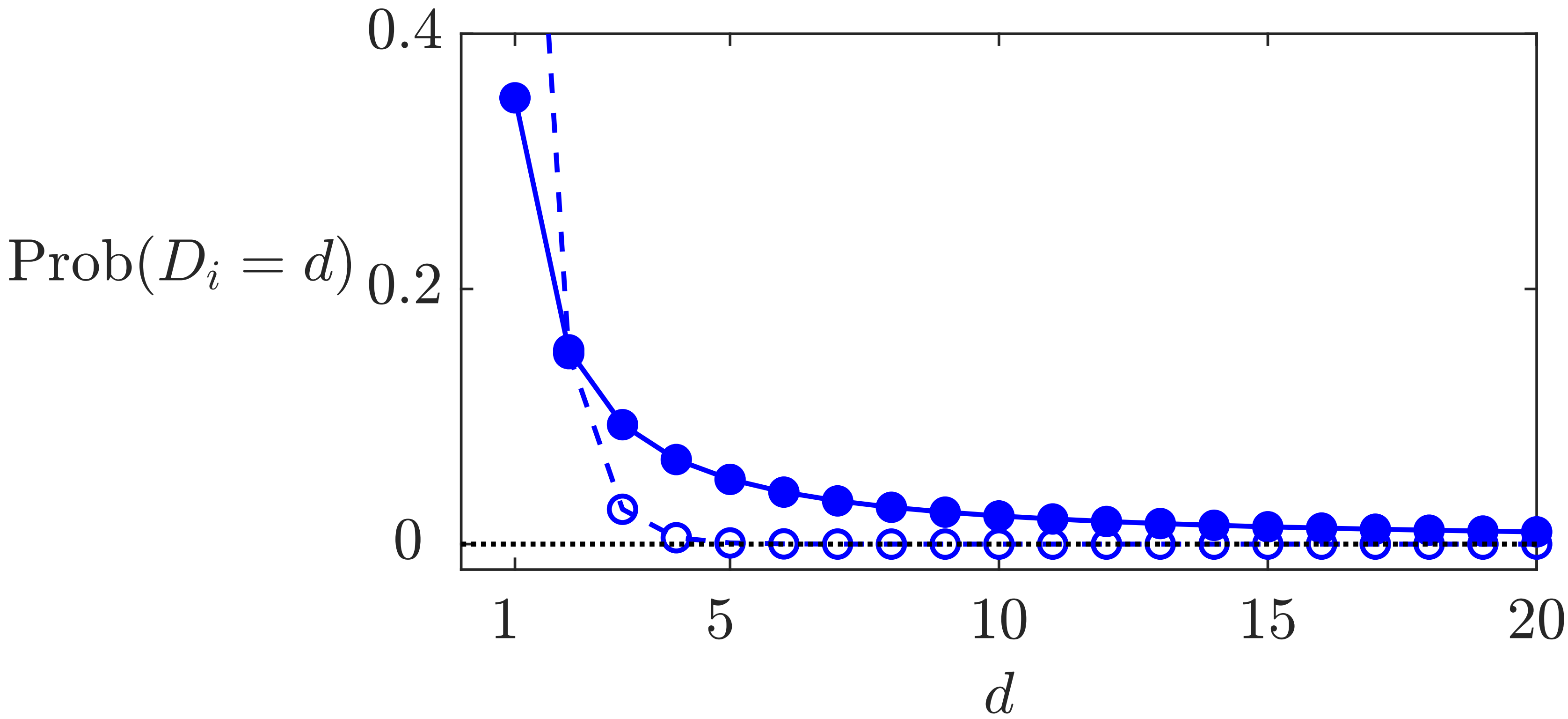

Fig. 6.8. Comparison of an exponential probability distribution -o-o- with a power-law probability distribution -•-•-

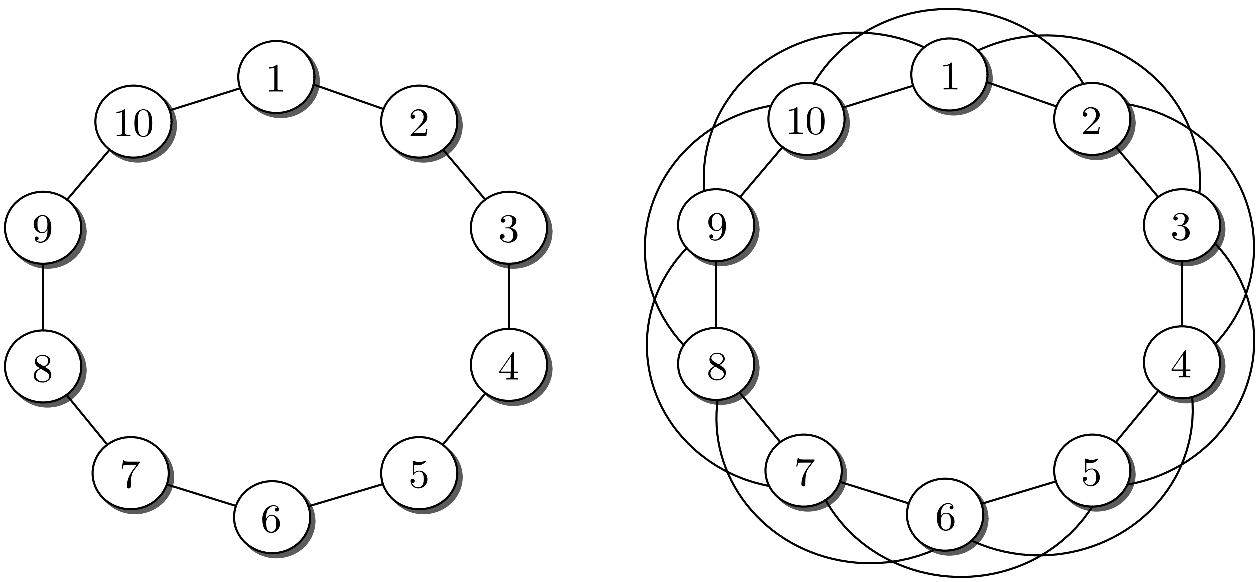

Fig. 6.9: 2–regular and 4–regular graph

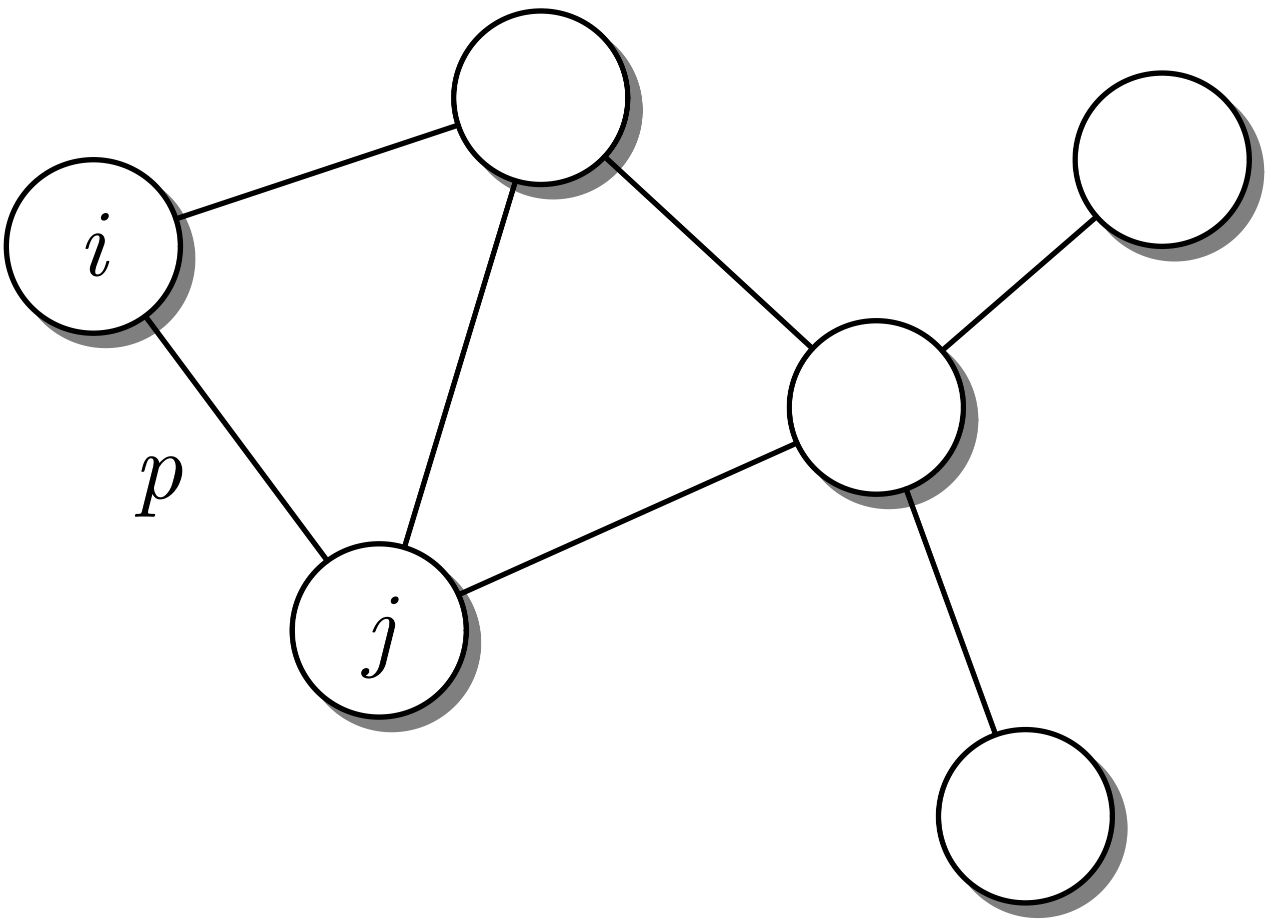

Fig. 6.10: Random graph

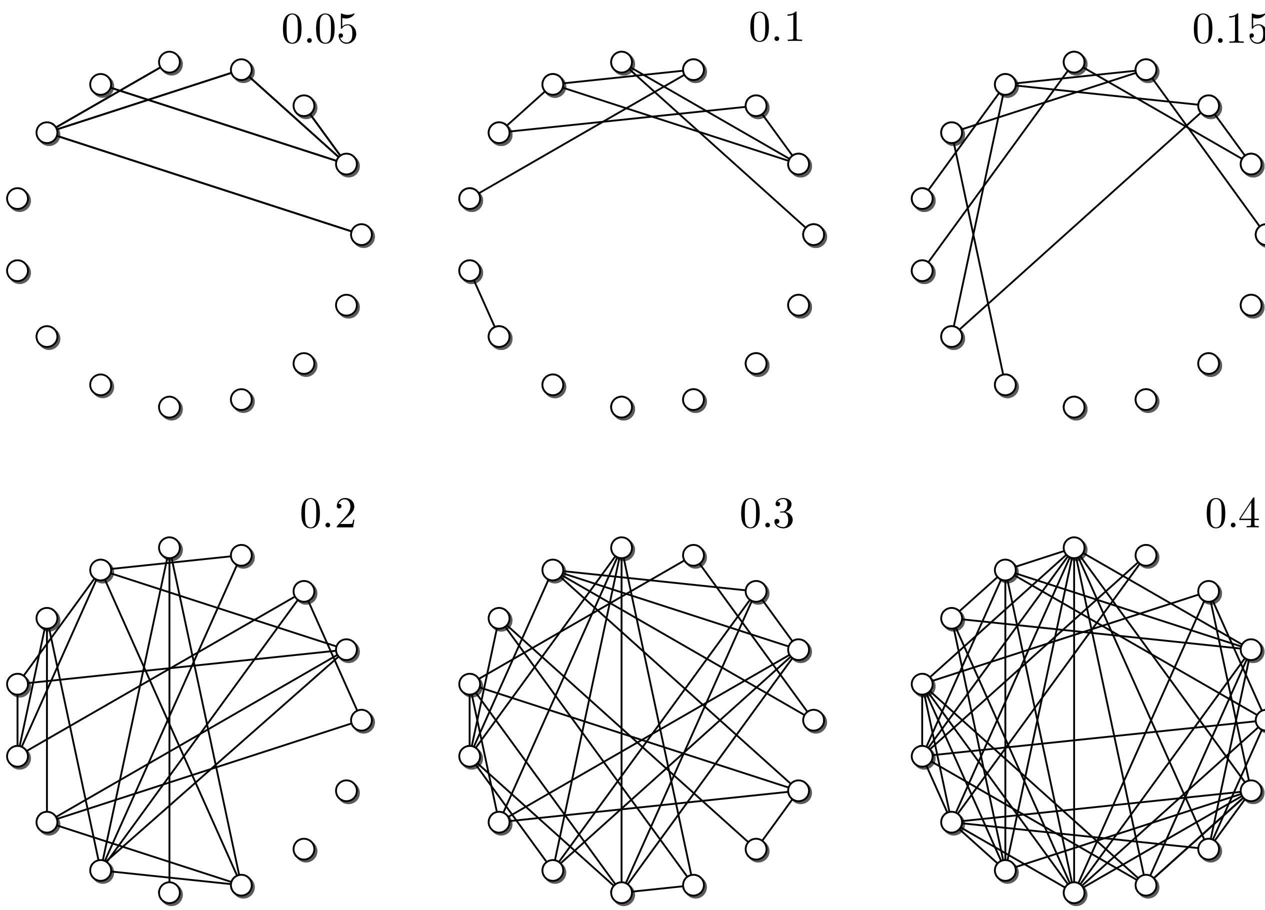

Fig. 6.11: Random graphs for six values of the connection probability p

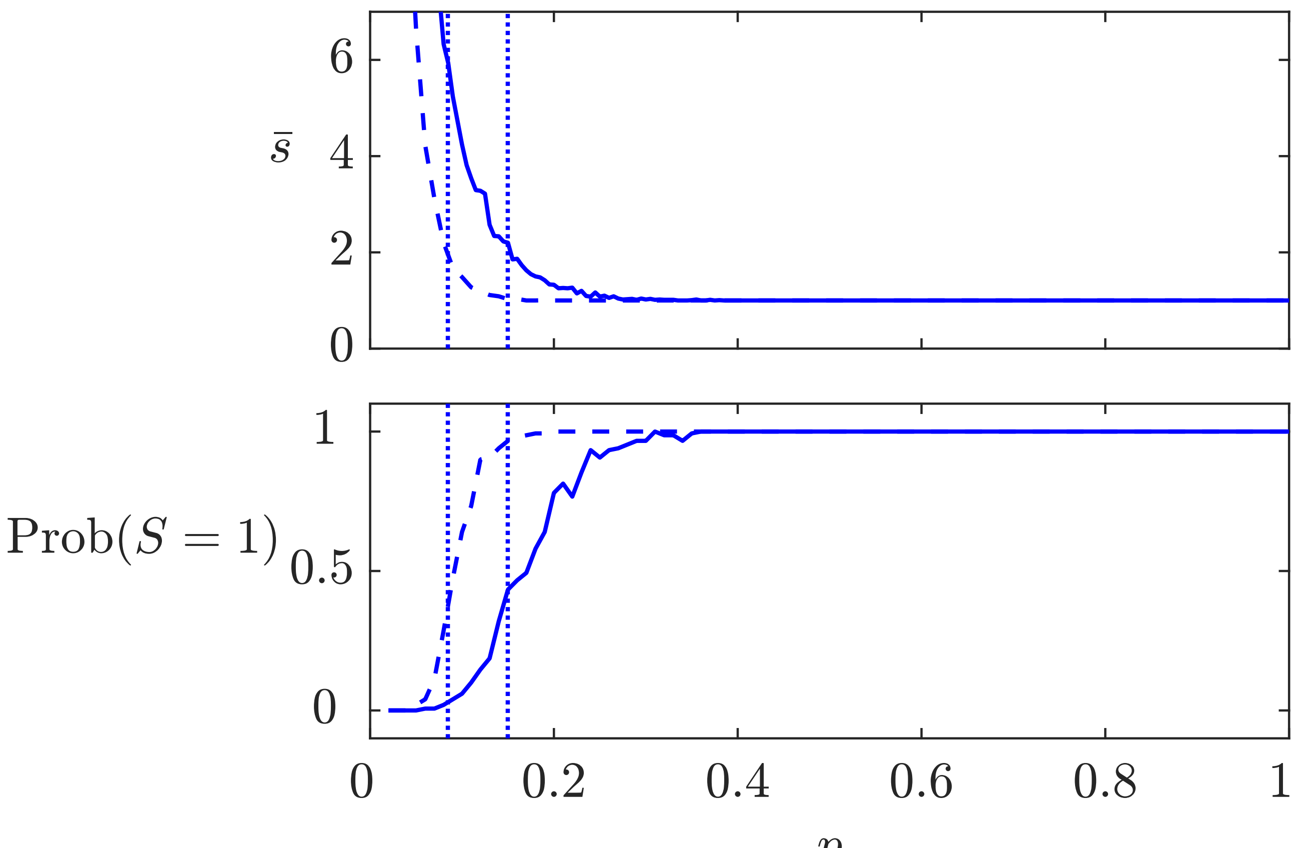

Fig. 6.12: Characteristic number $\bar{s}$ of connected components and probability for the graph to be a single connected component

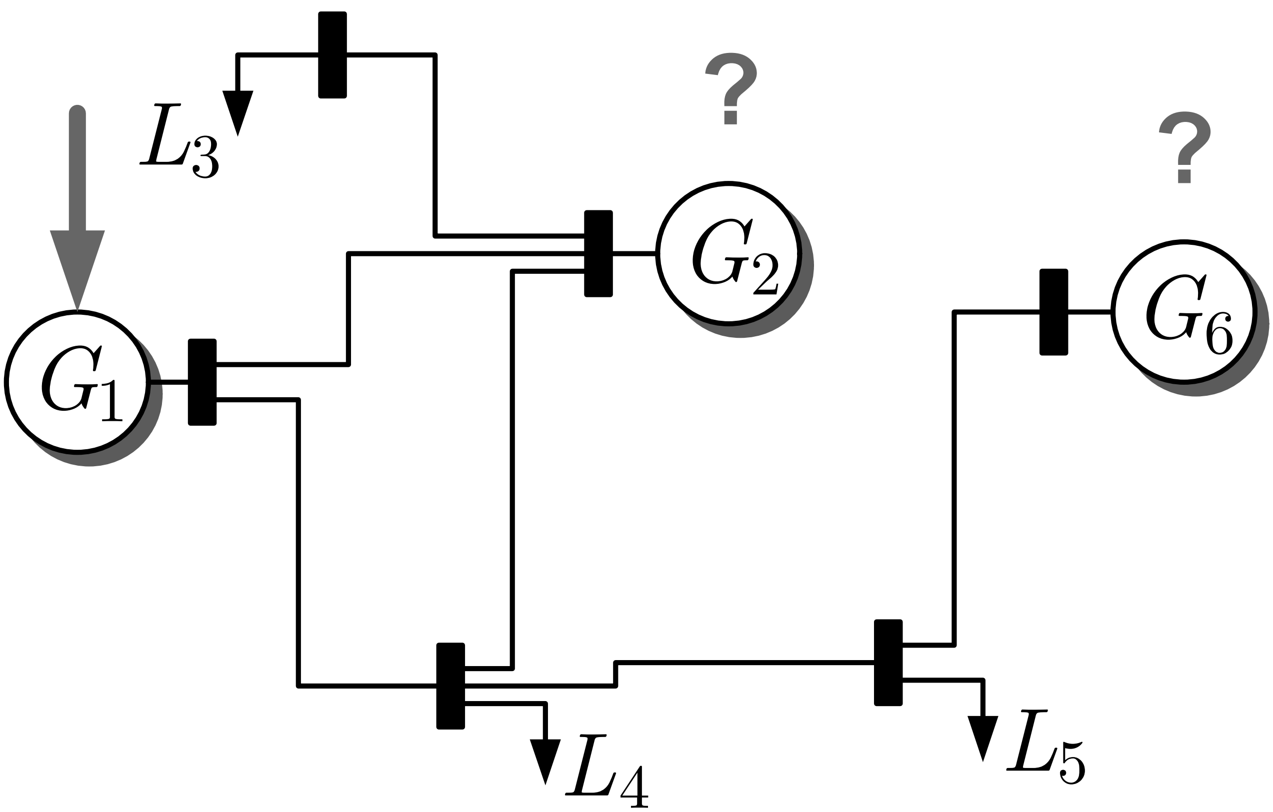

Fig. 6.13: Electrical power network

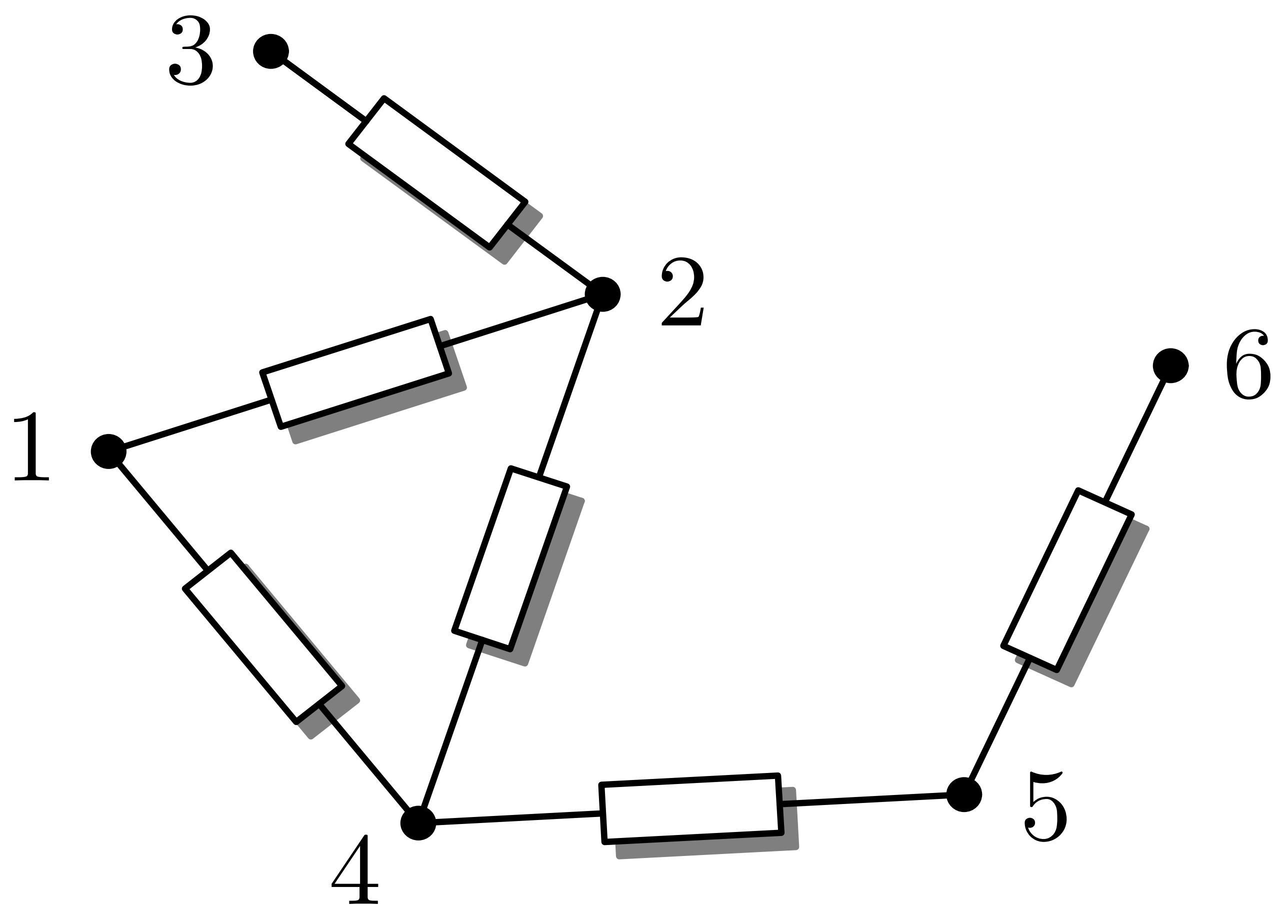

Fig. 6.13: Electrical power network

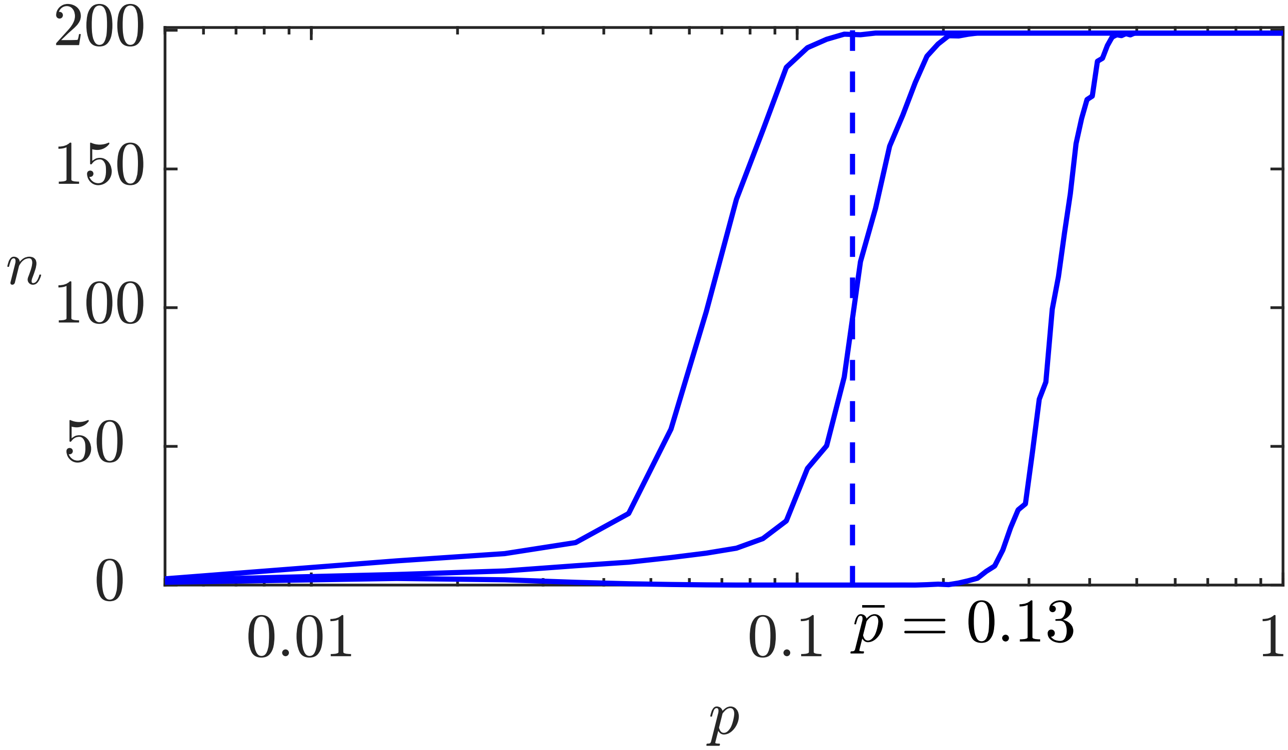

Fig. 6.14: Disturbance behaviour of the electrical power network

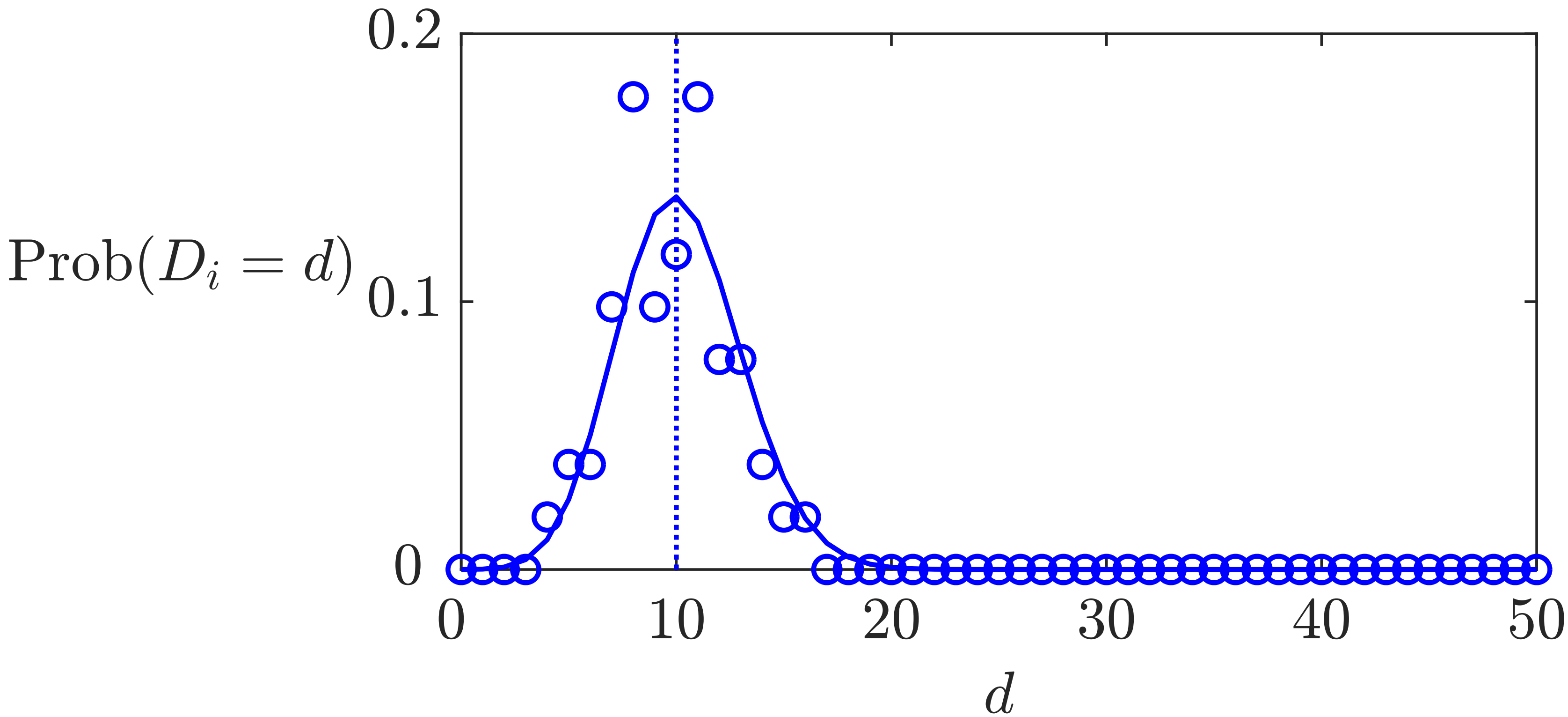

Fig. 6.15. Degree distribution of a random graph with $N = 51$ vertices and connection probability $p = 0.2$

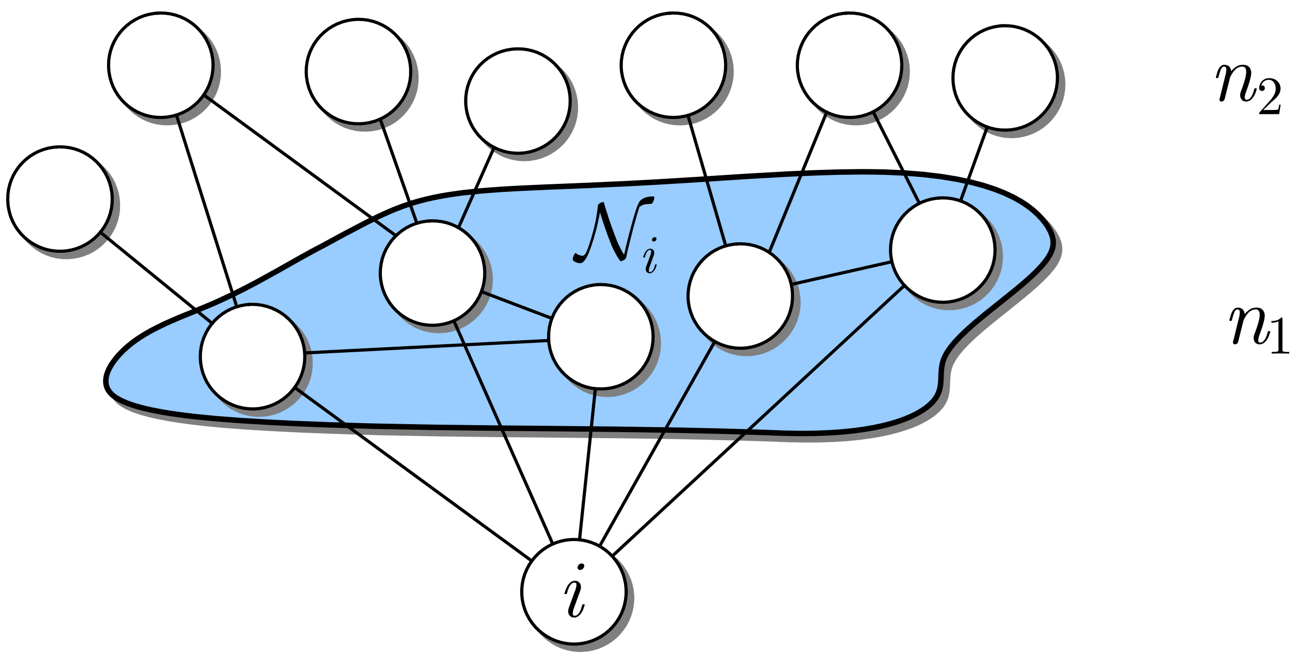

Fig. 6.16: Estimation of the number of vertices that are reachable from i on paths of length $l = 1, 2$

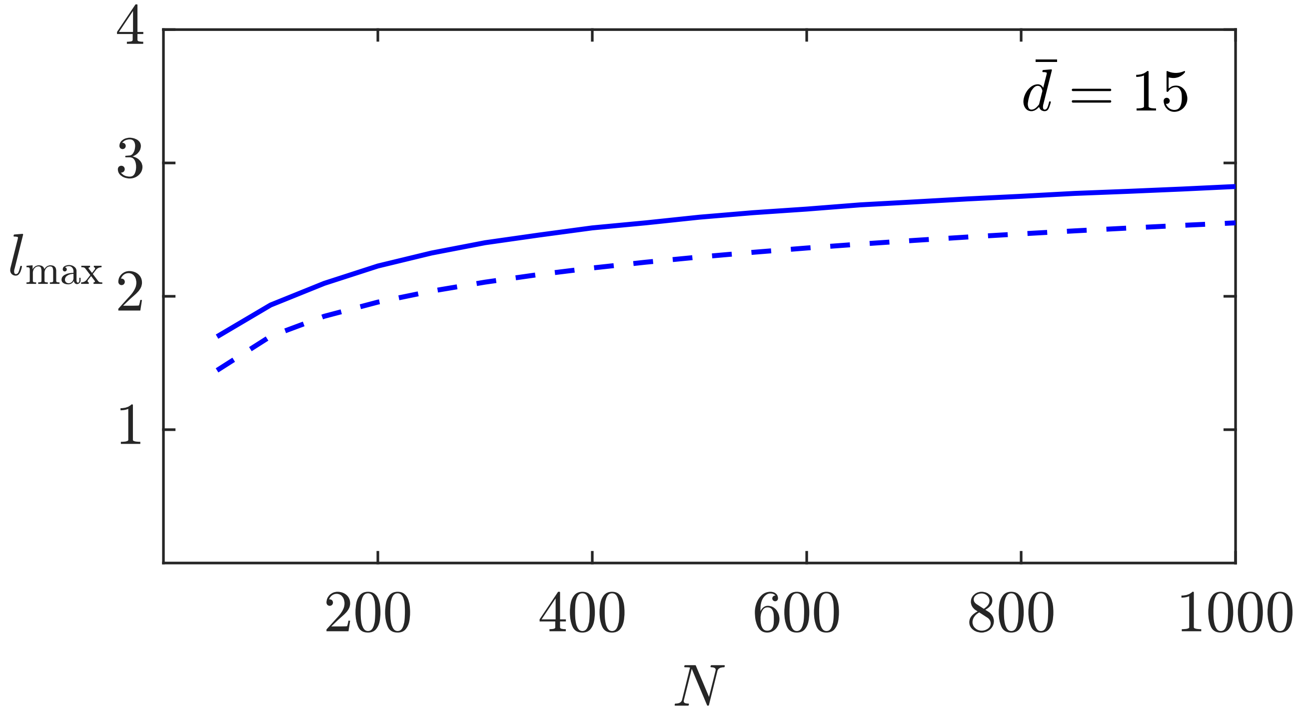

Fig. 6.17: Diameter of random graphs

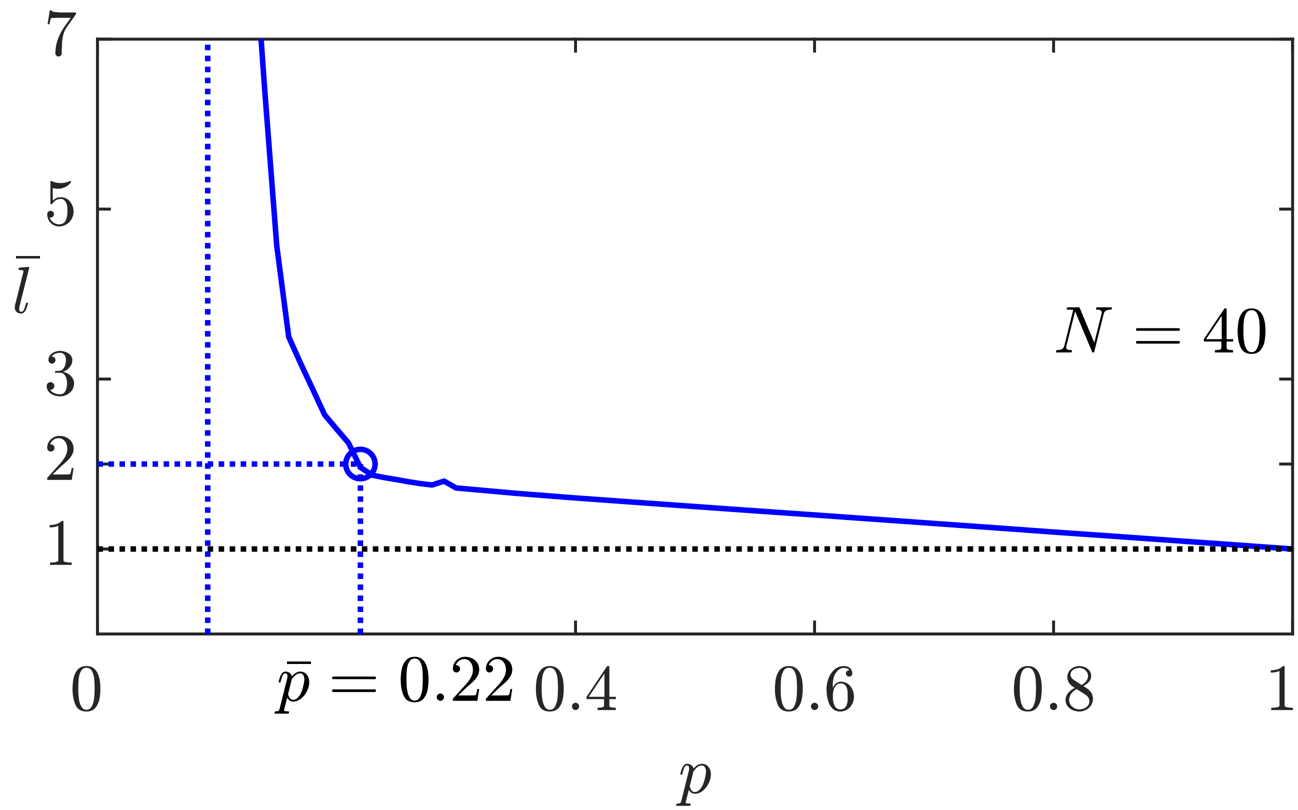

Fig. 6.18: Characteristic path length of random graphs determined numerically for 600 realisations

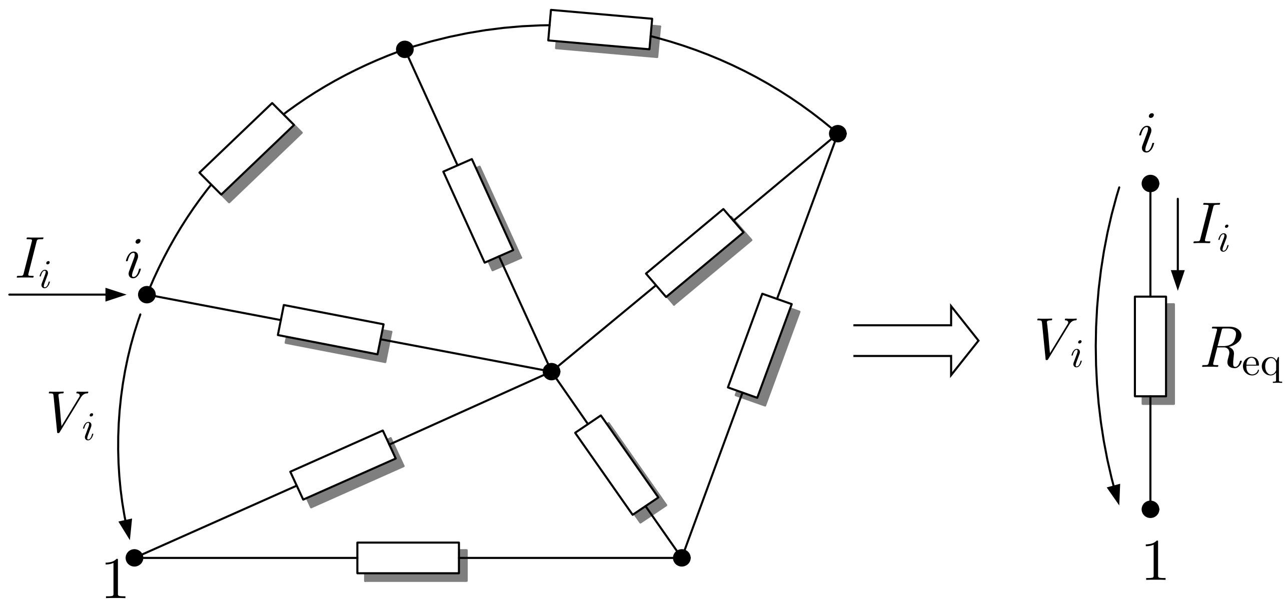

Fig. 6.19: Electrical network

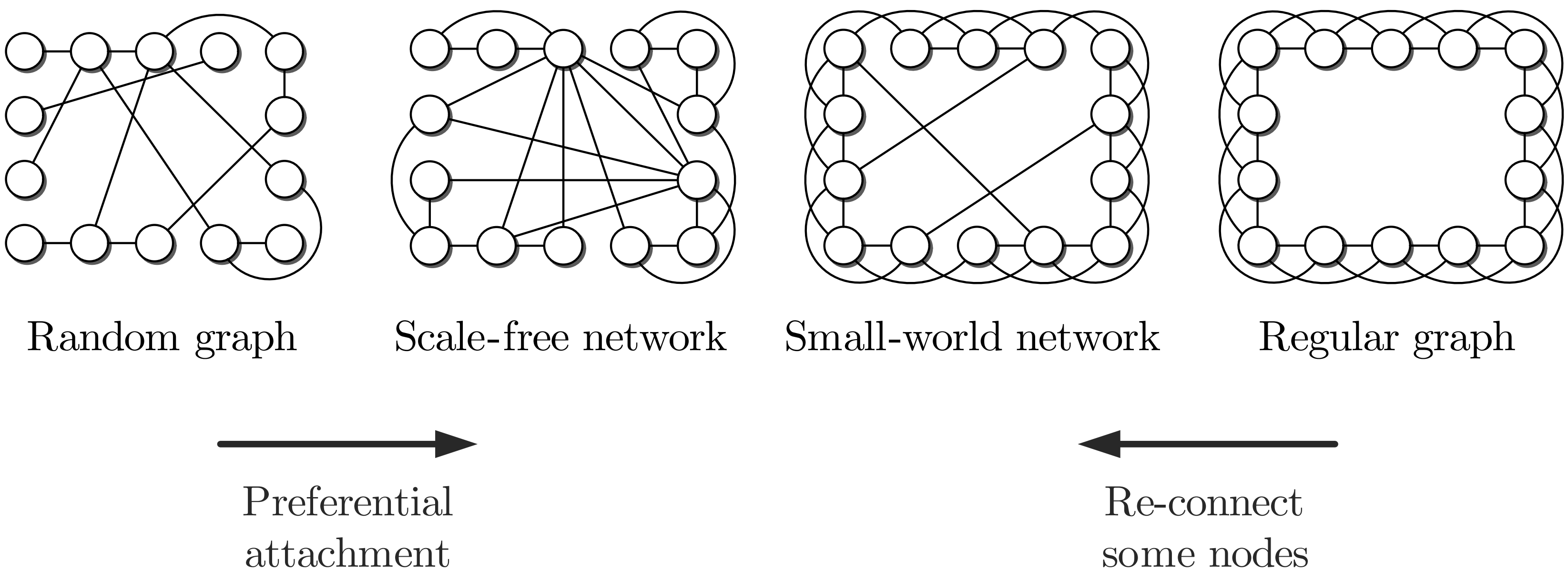

Fig. 6.20. Four generative network models

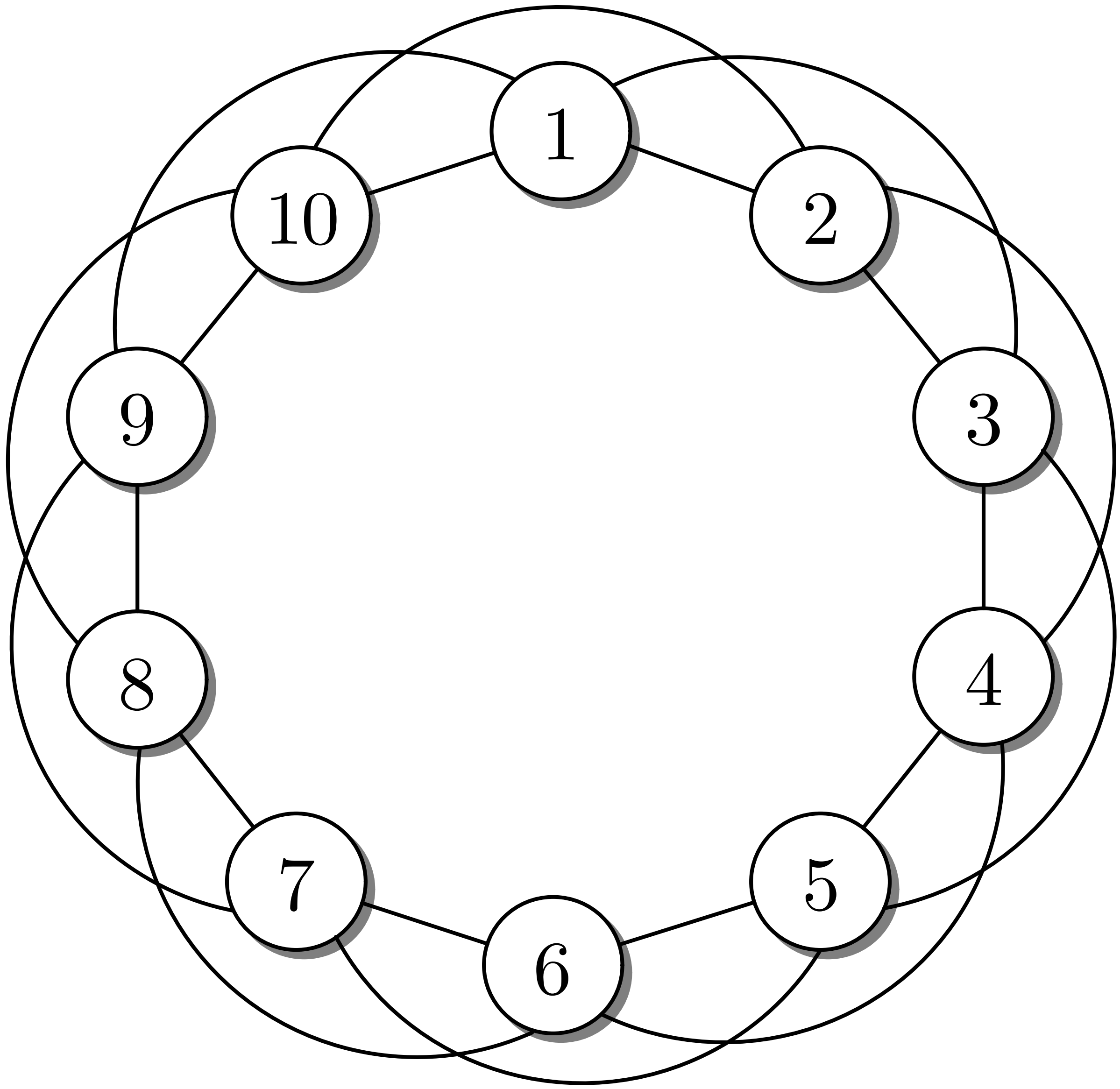

Fig. 6.21: Regular graph

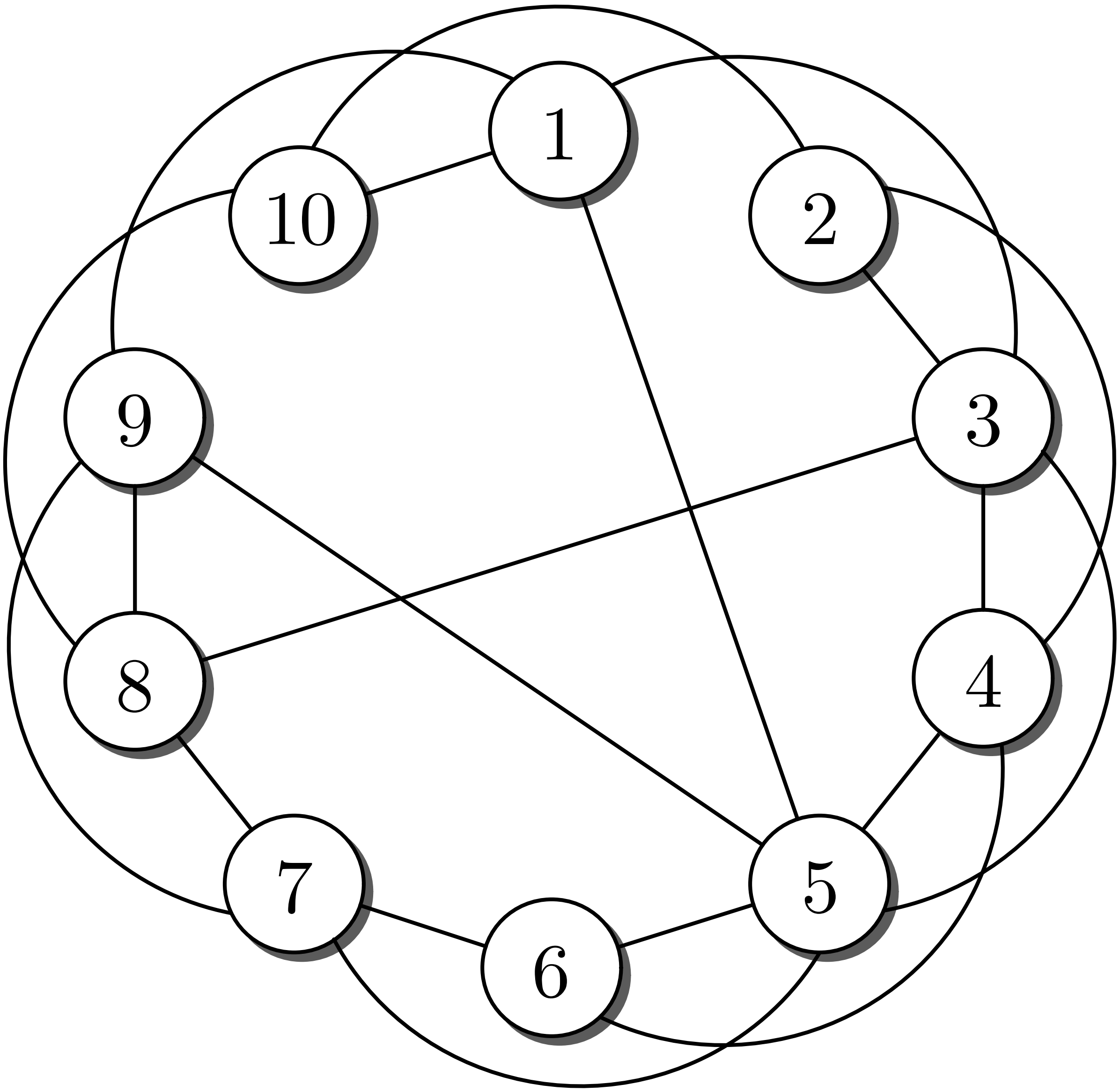

Fig. 6.21: Small-world network

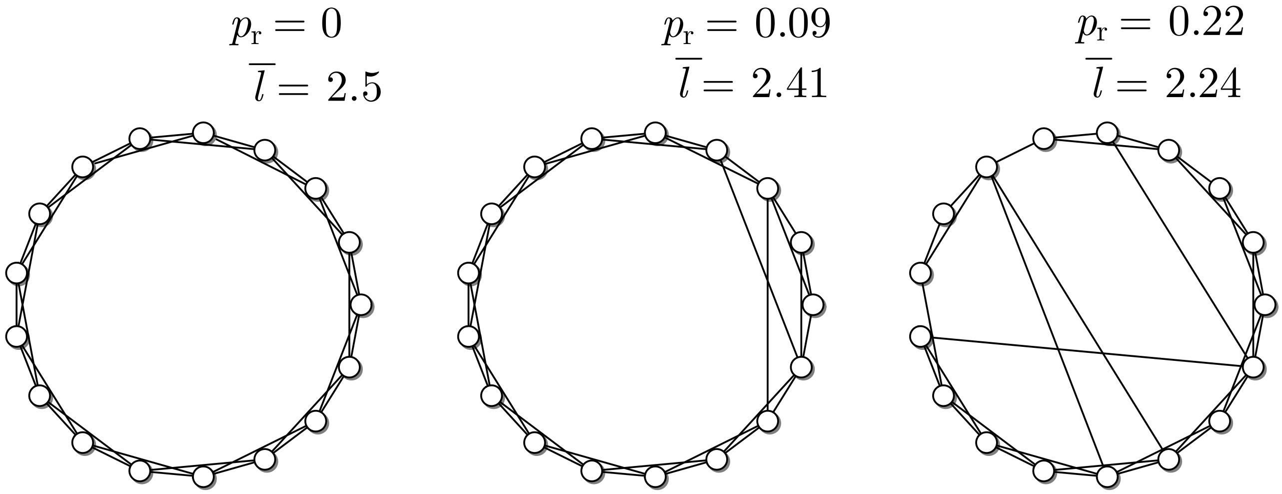

Fig. 6.22: Small-world networks for three re-connection probabilities p_r

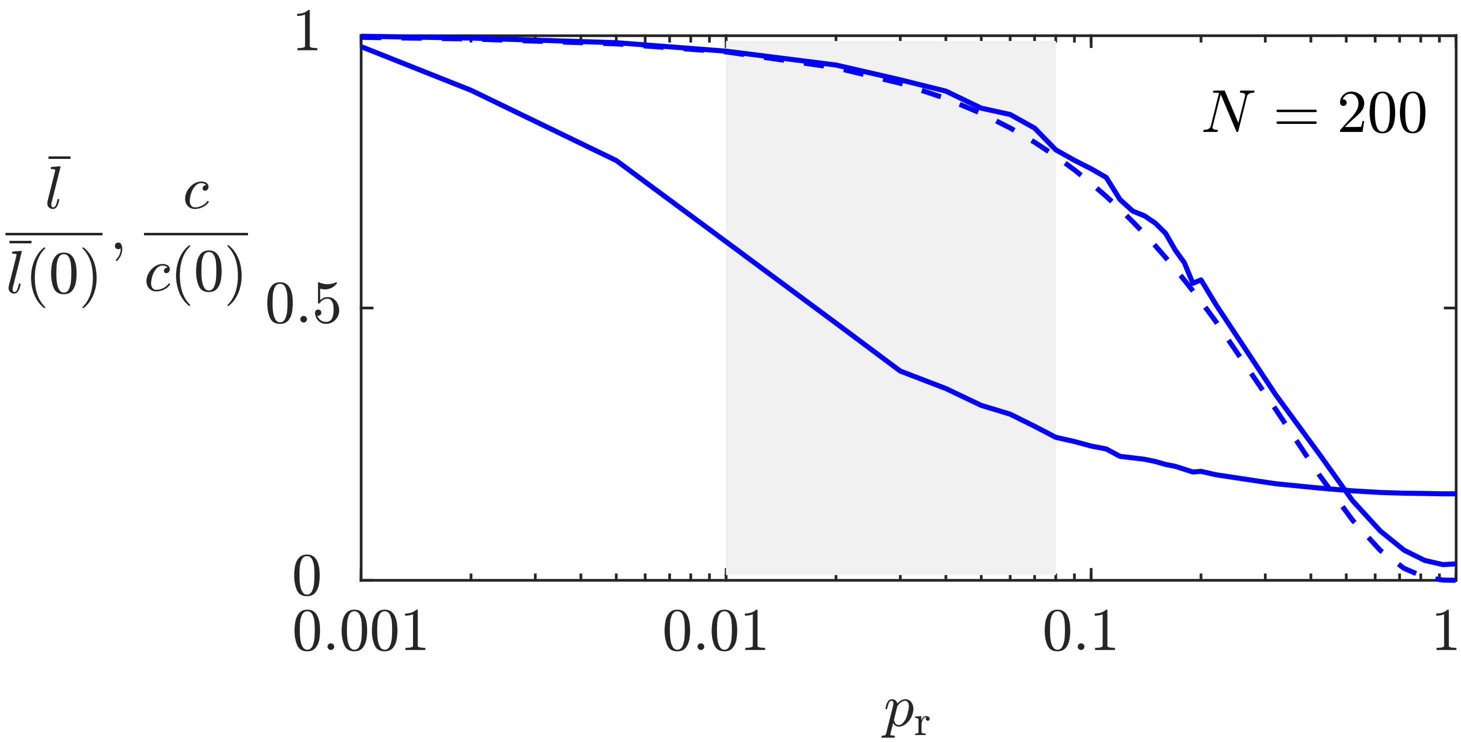

Fig. 6.23: Characteristic path length and clustering coefficient of small-world networks in dependence upon the re-connection probability p_{r}

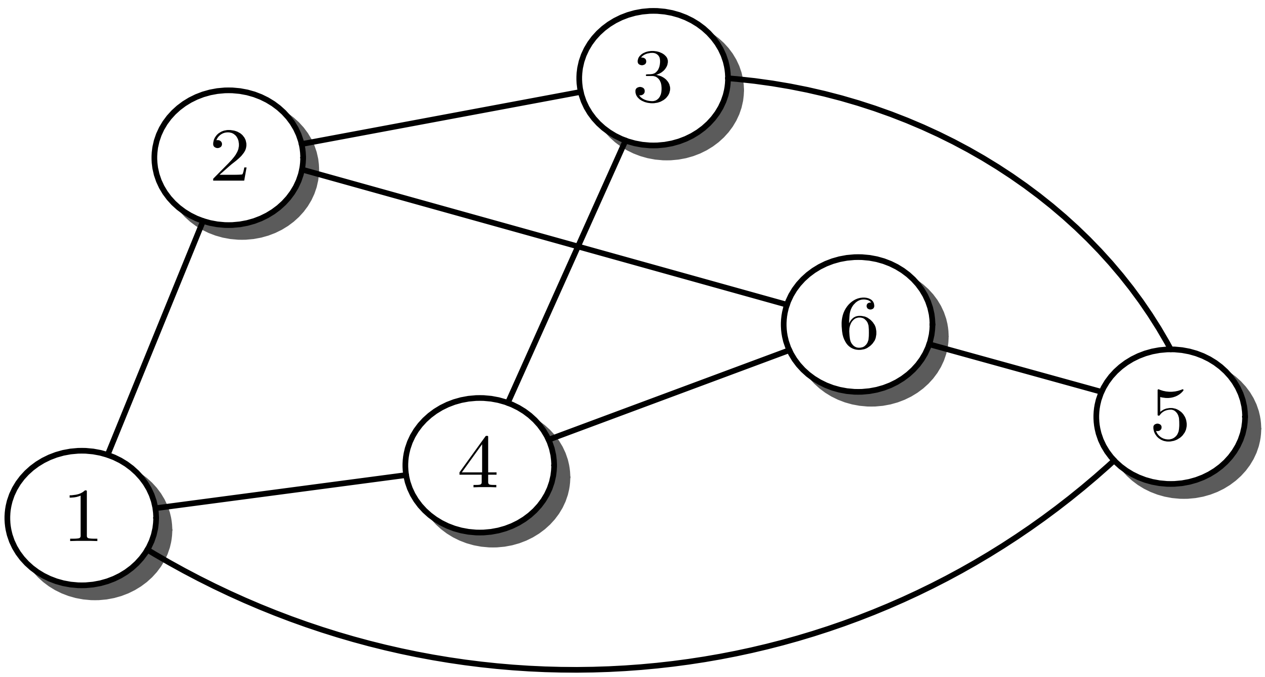

Fig. 6.24: Initial graph $\mathcal{G}_6$ used in the examples

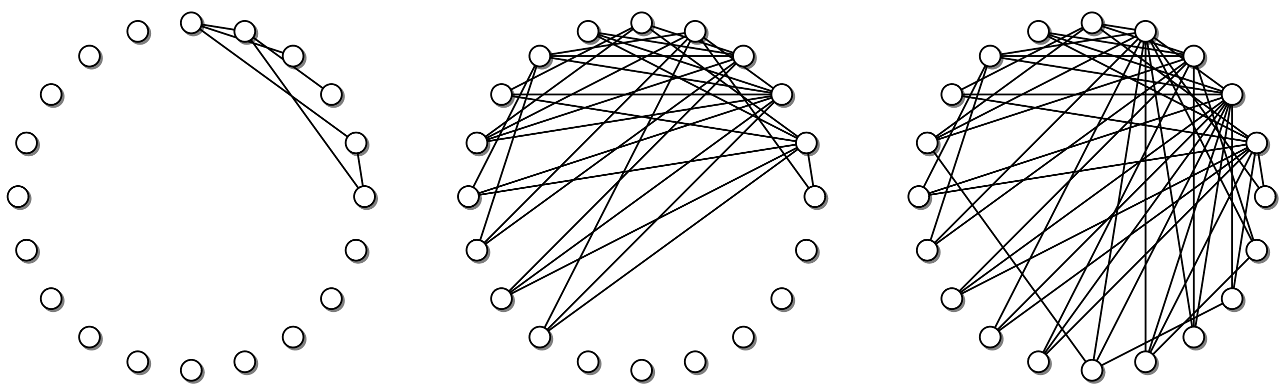

Fig. 6.25: Scale-free networks: initial graph (left), intermediate graph (middle) and final graph (right)

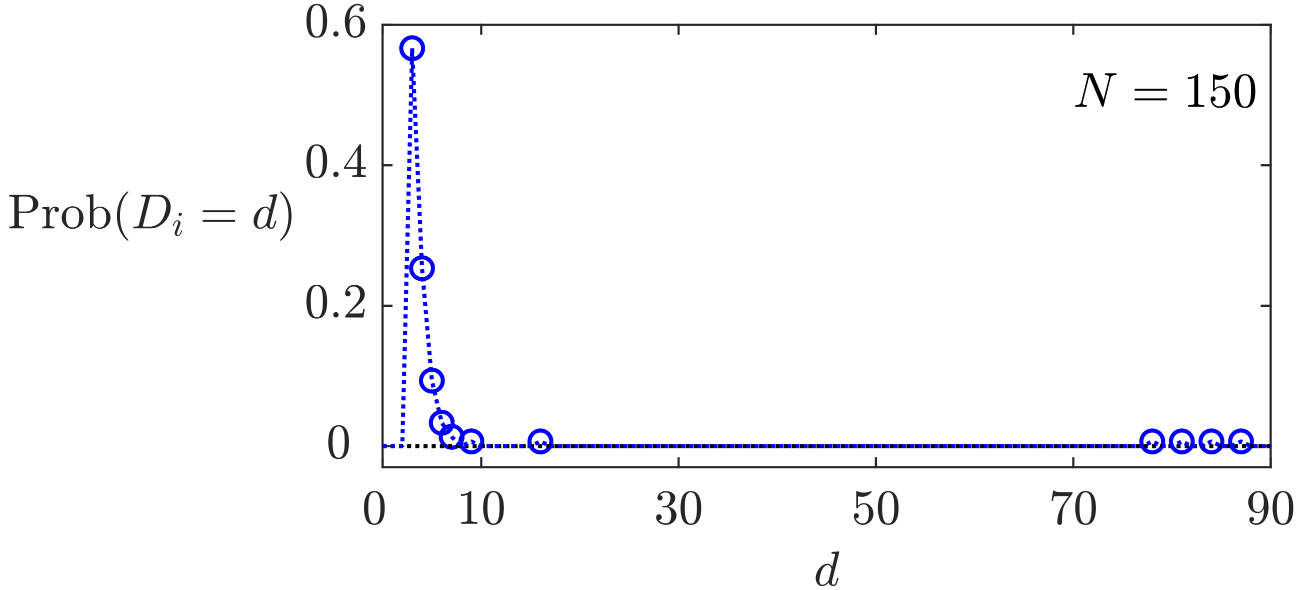

Fig. 6.26: Degree distribution of a scale-free network (only non-zero values are shown by the circles)

Fig. 6.27: Part of the plan of the bike-renting stations in Paris

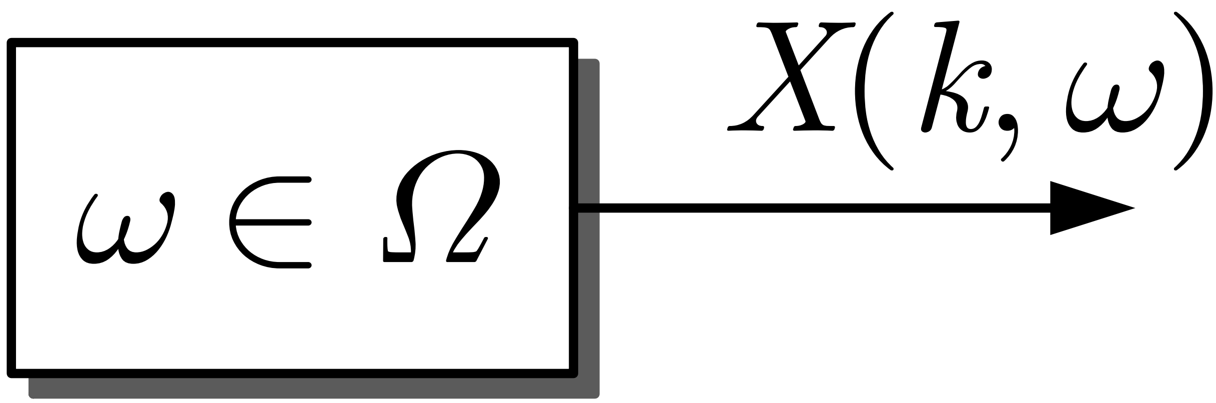

Fig. 7.1: Generation of a random sequence

J. Lunze: *Networked Control of Multi-Agent Systems,* Edition **MoRa** 2022

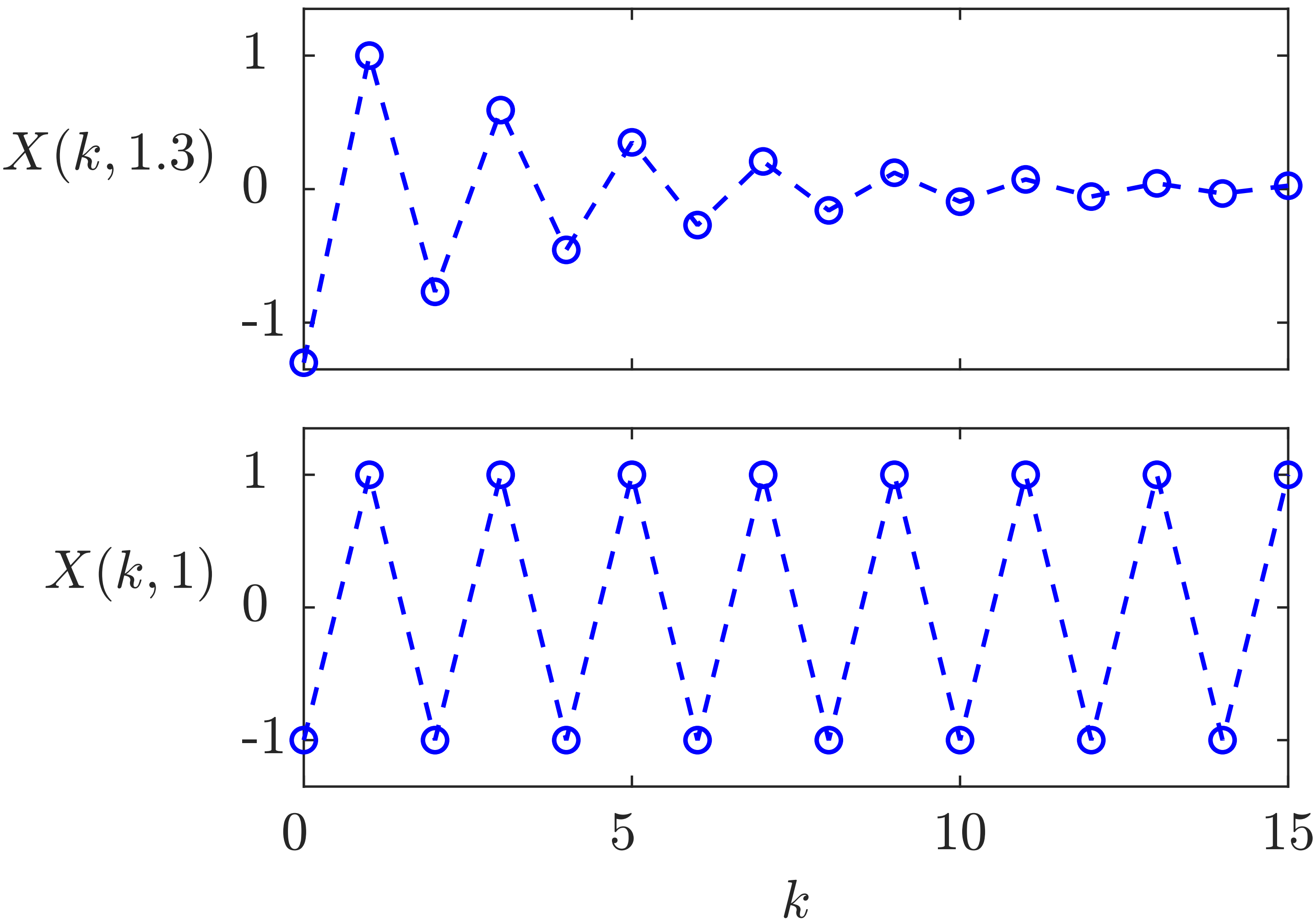

Fig. 7.2: Random sequences considered in Example 7.2

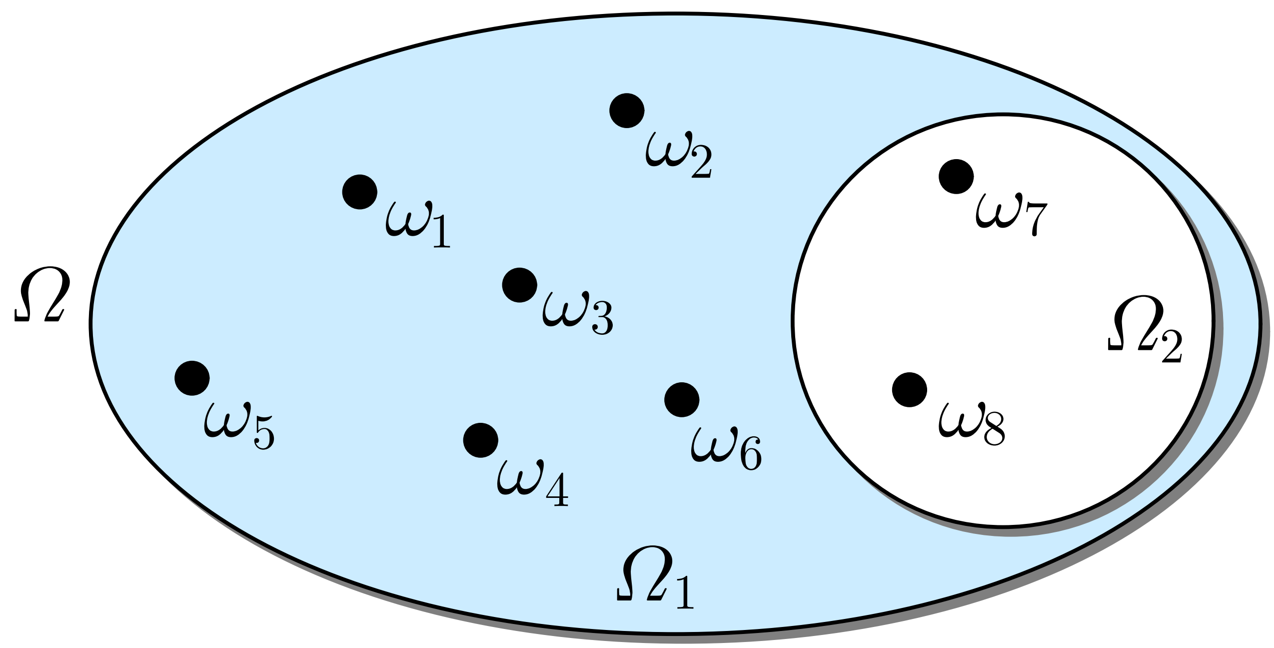

Fig. 7.3: Decomposition of the sample space

J. Lunze: *Networked Control of Multi-Agent Systems*, Edition **MoRa** 2022

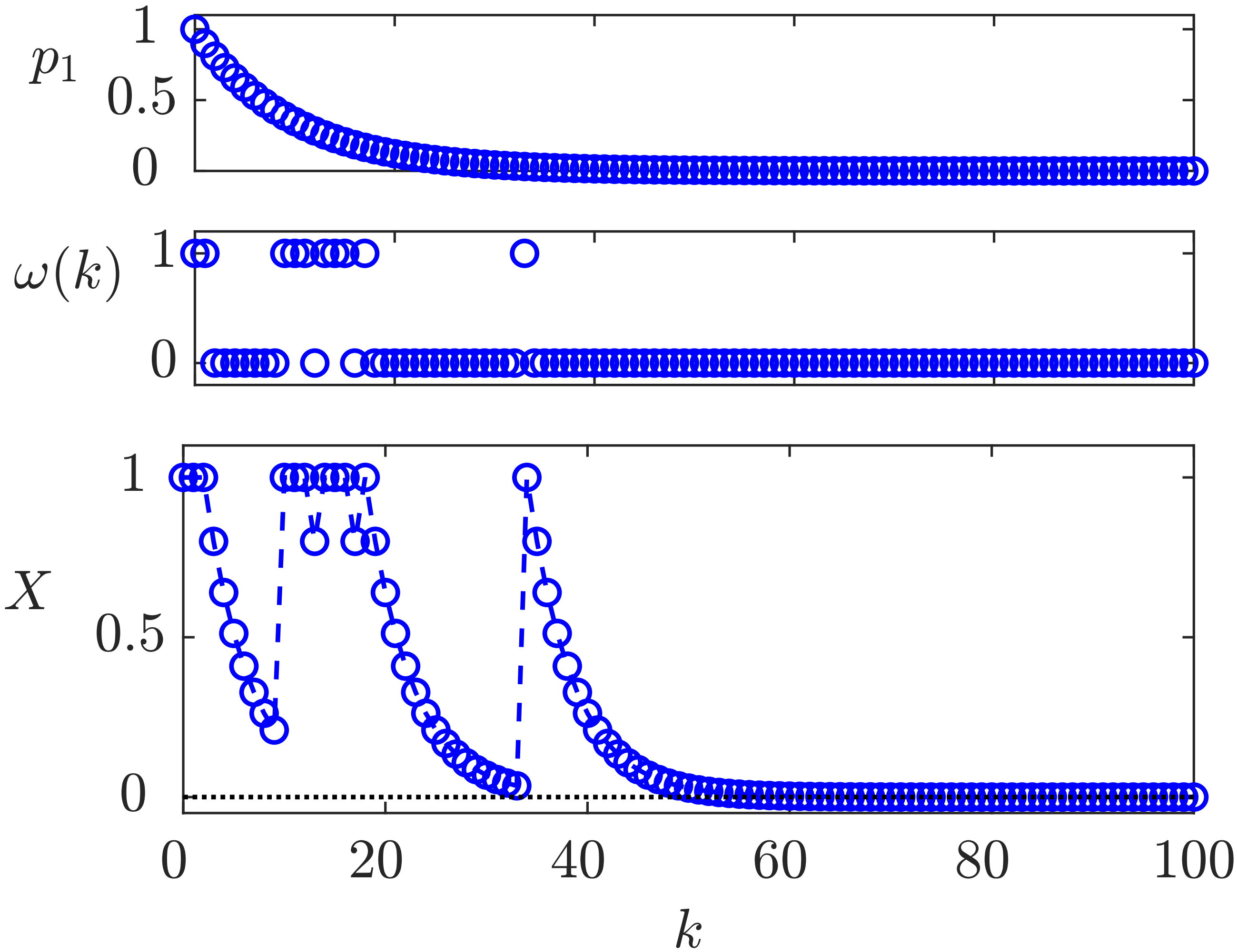

Fig. 7.4: Probability distribution (7.12), outcome $\omega(k)$ of the experiment and the realisation of the sequence $\{X(k, \omega)\}$

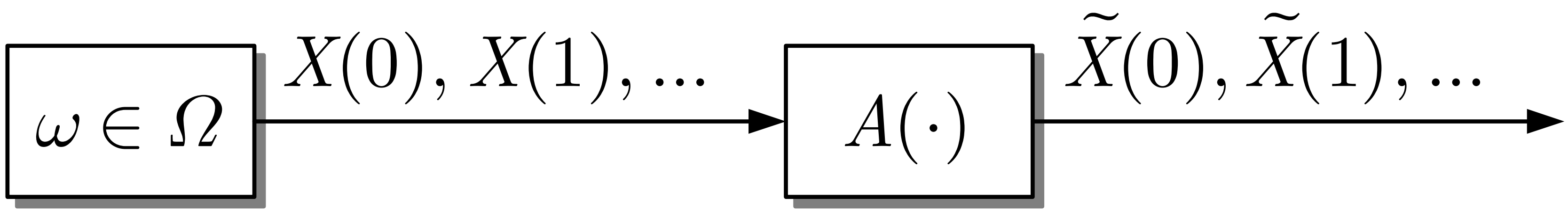

Fig. 7.5. Example for the convergence in probability

J. LUNZE: *Networked Control of Multi-Agent Systems,* Edition MoRa 2022

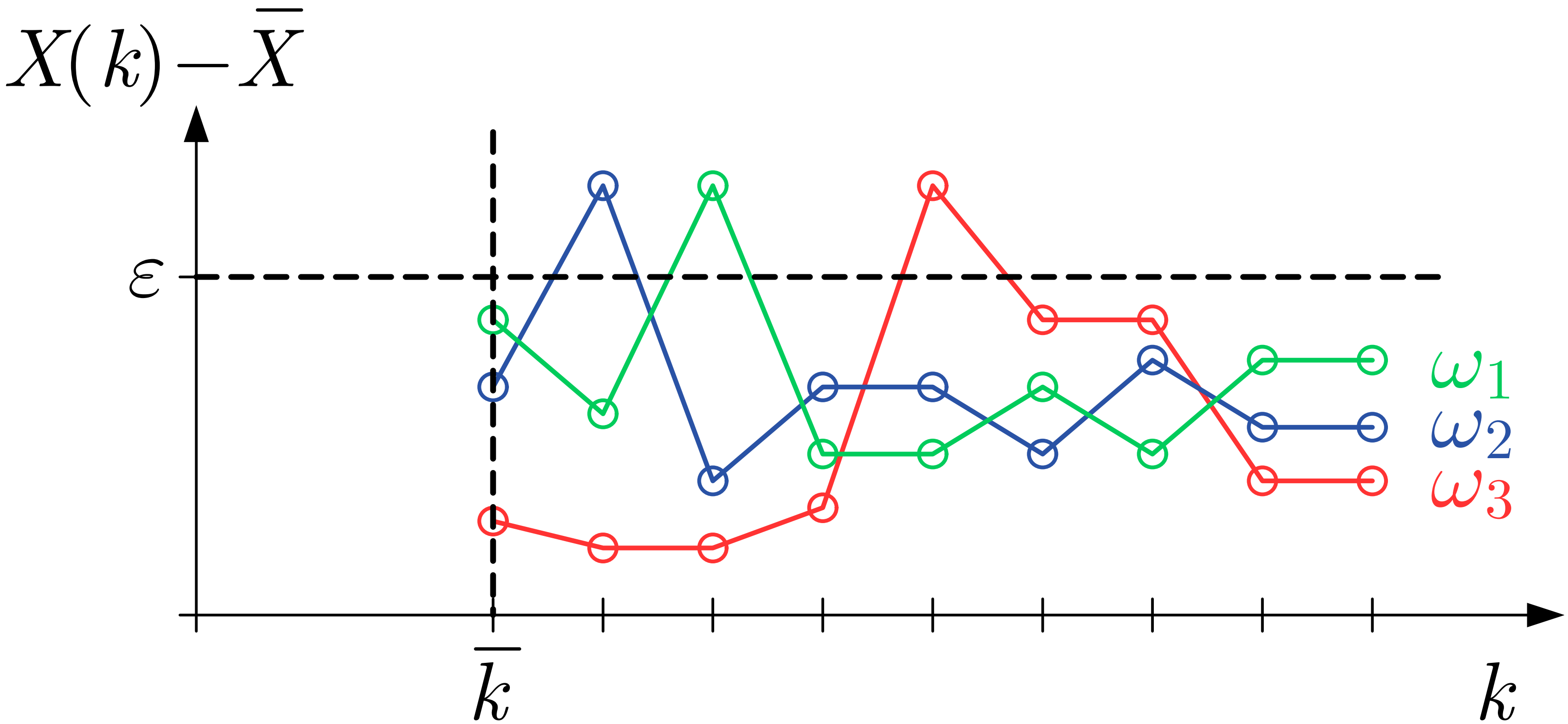

Fig. 7.6. Three realisations of a random sequence

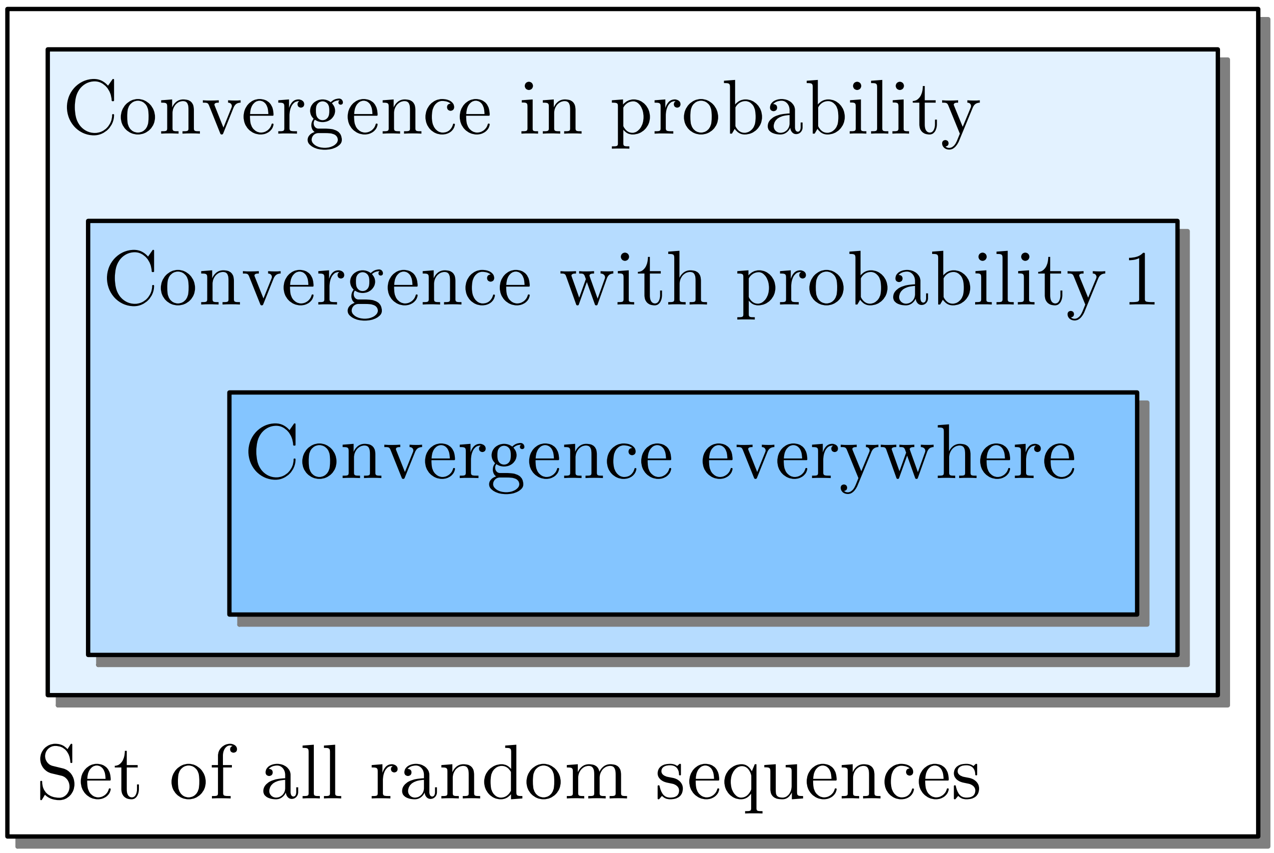

Fig. 7.7: Relations among the convergence notions

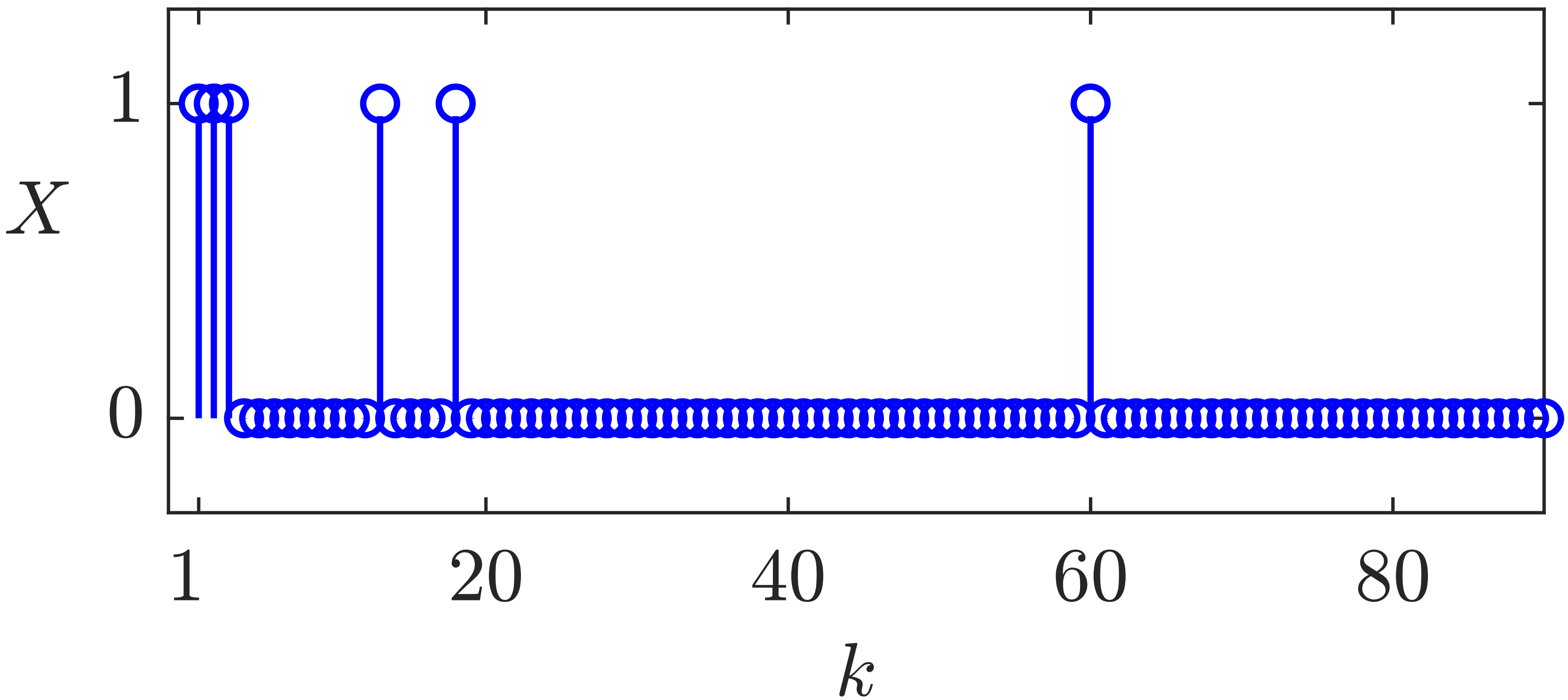

Fig. 7.8. **Realisation of the random sequence (7.20)**

J. Lunze: *Networked Control of Multi-Agent Systems*, Edition MoRa 2022

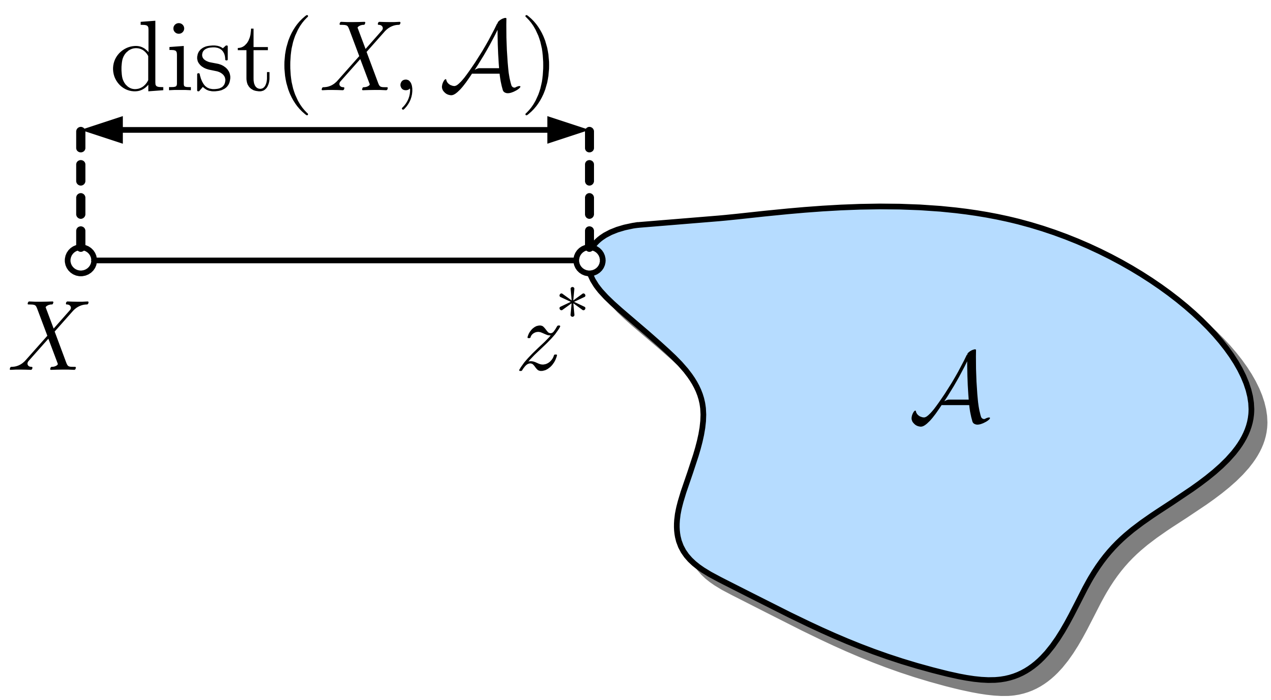

Fig. 7.9: Definition of dist

J. Lunze: *Networked Control of Multi-Agent Systems,* Edition **M**o**R**a 2022

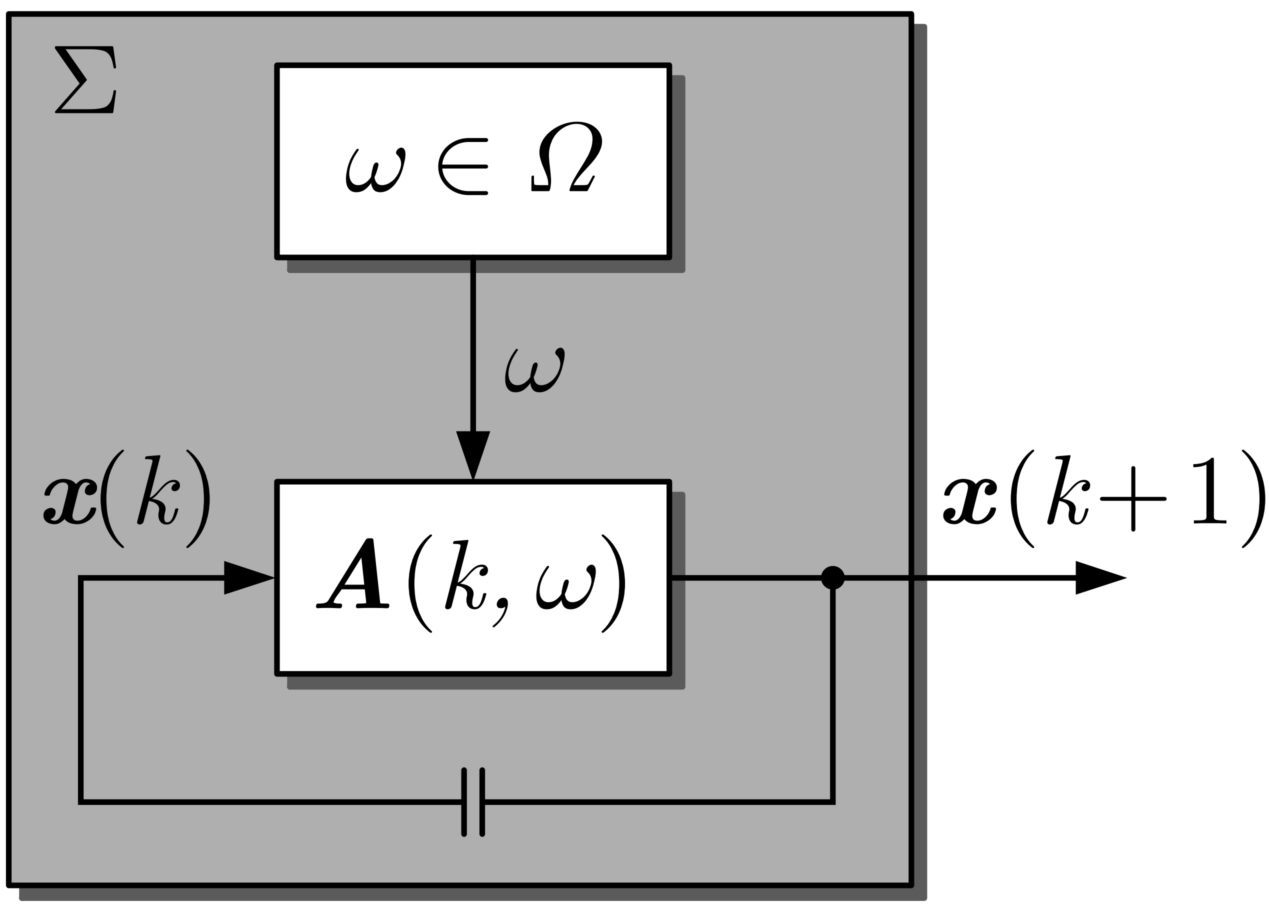

Fig. 7.10: Linear dynamical system with random matrix A

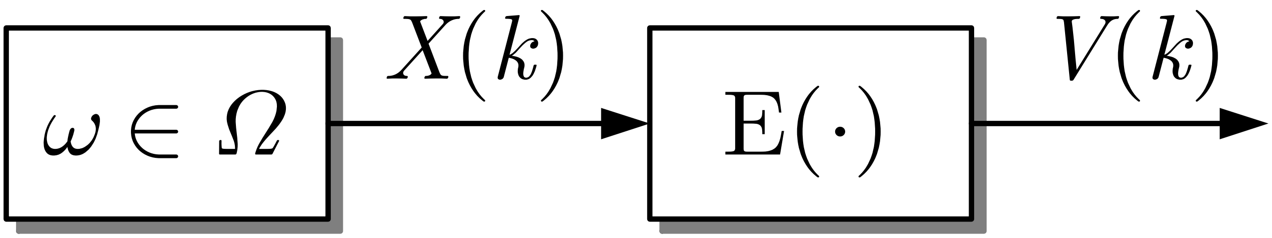

Fig. 7.11: Generation of a martingale sequence

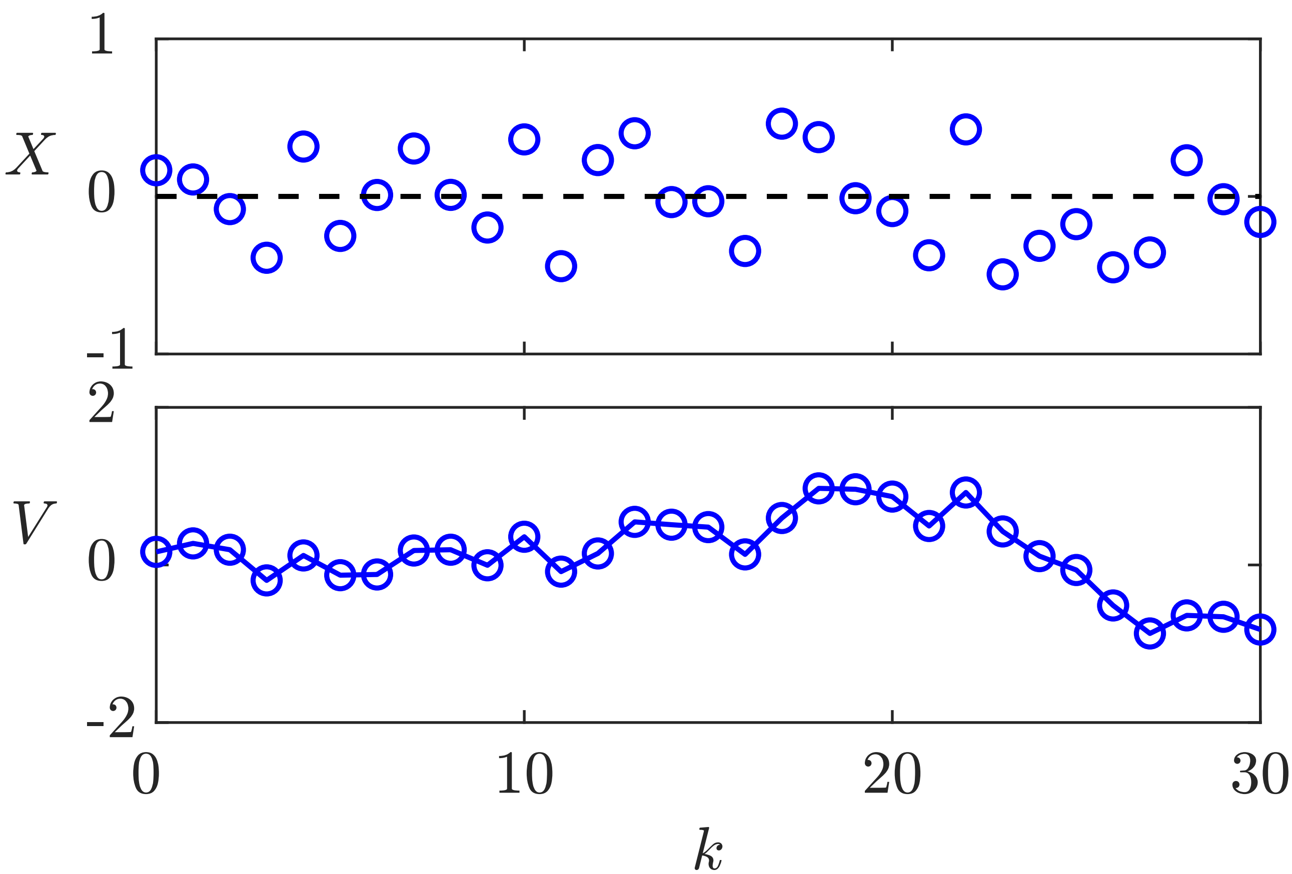

Fig. 7.12: Martingale

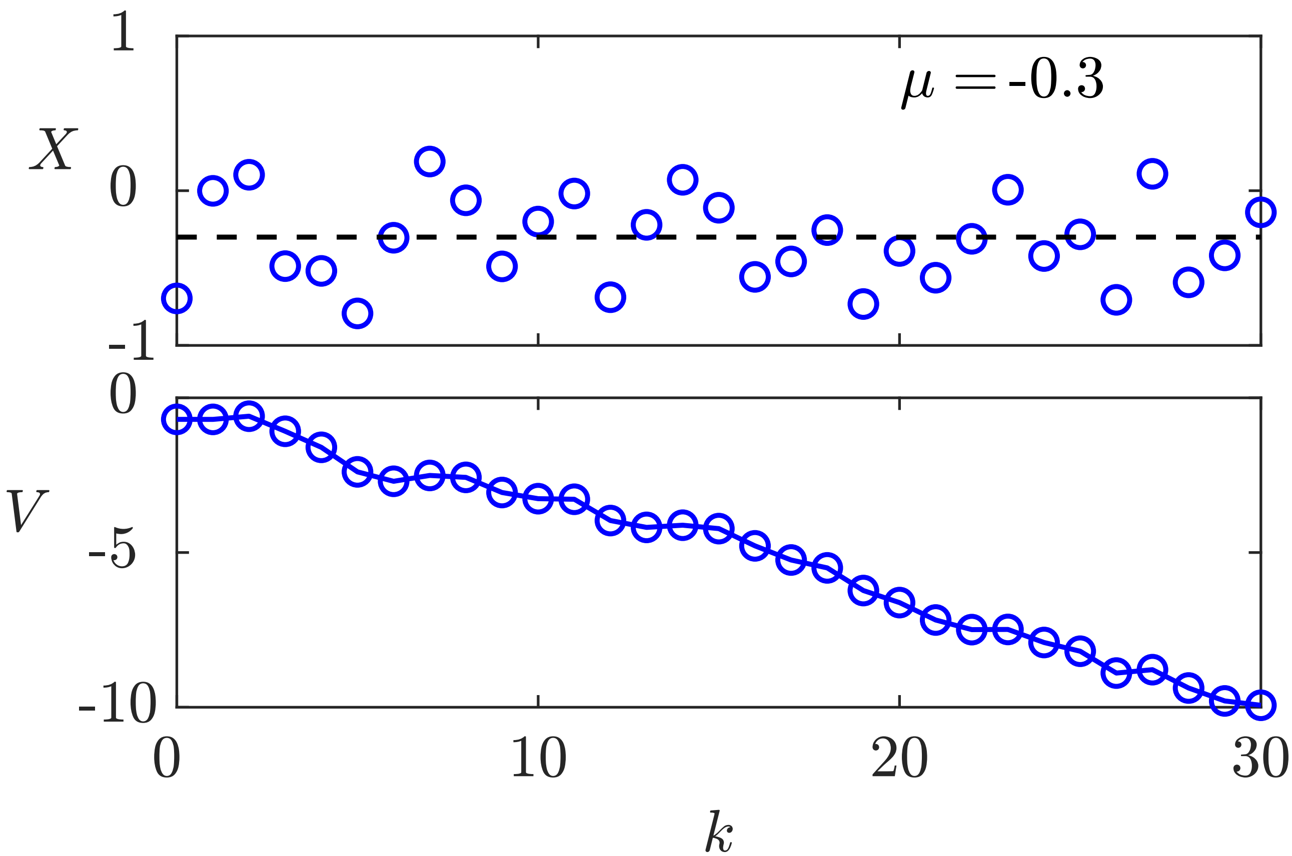

Fig. 7.12: Supermartingale

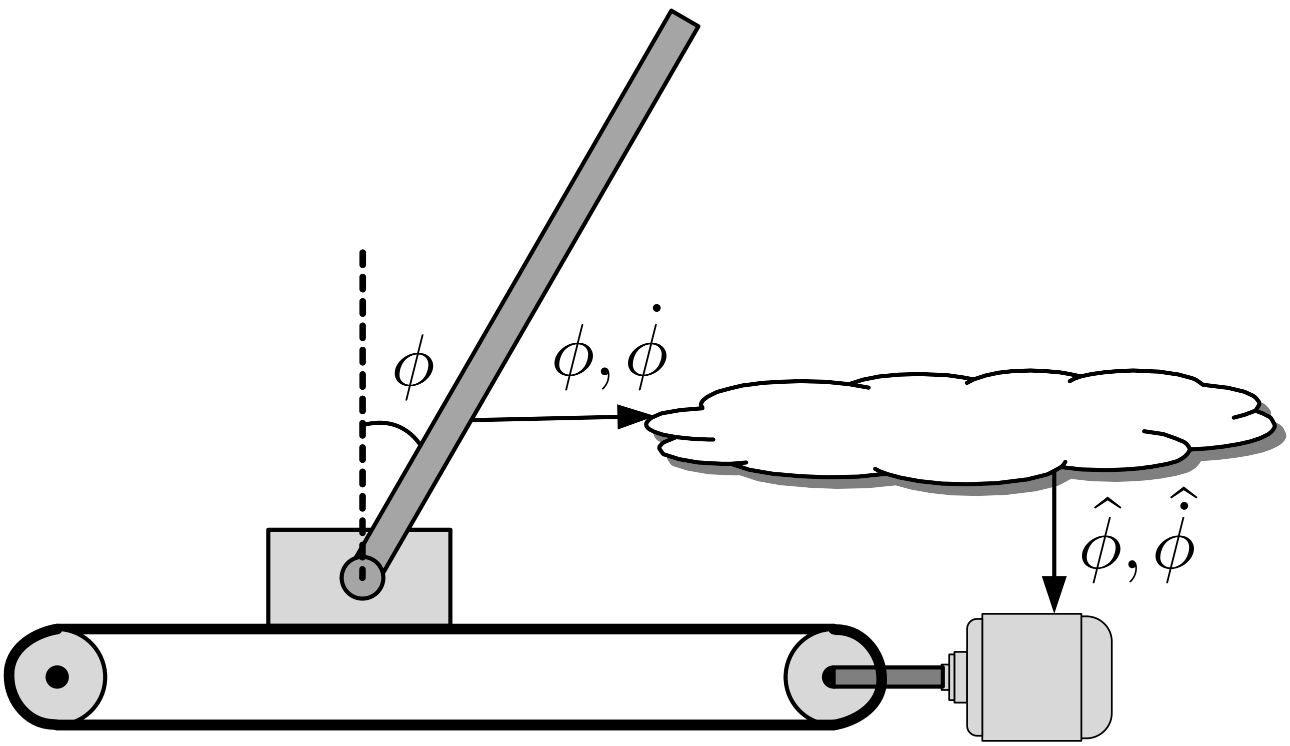

Fig. 7.13: Networked control of an inverted pendulum

J. LUNZE: *Networked Control of Multi-Agent Systems*, Edition **MoRa** 2022

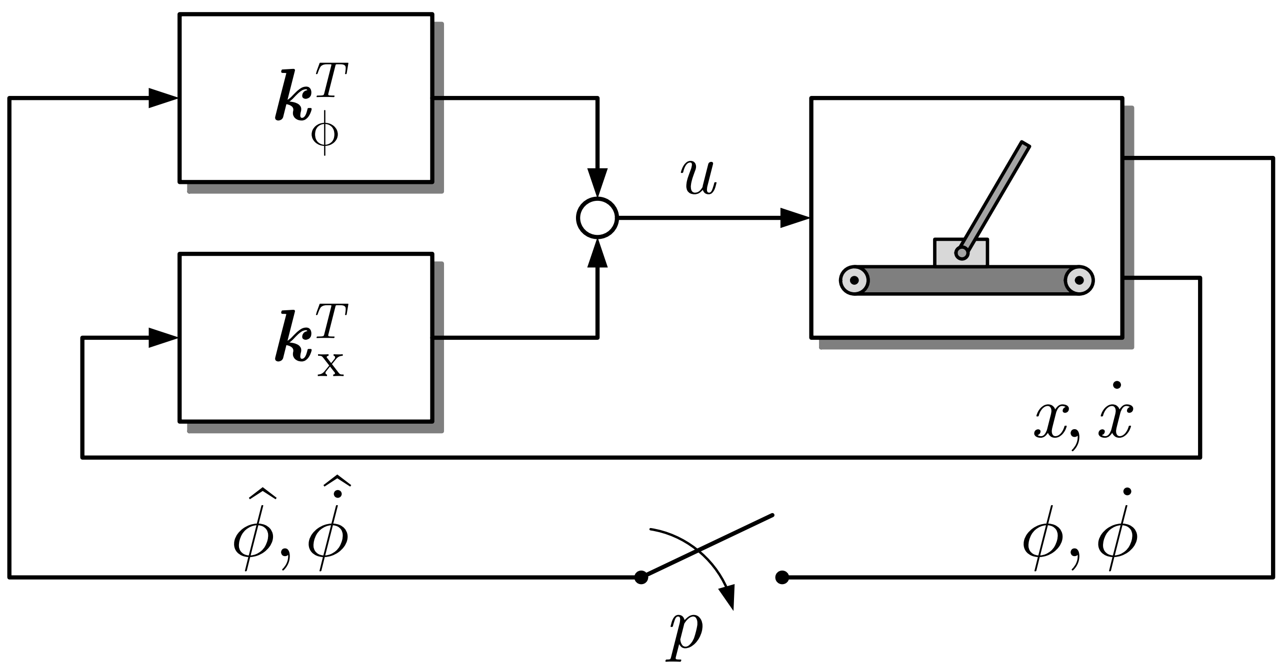

Fig. 7.14: Block diagram of the controlled pendulum

J. Lunze: *Networked Control of Multi-Agent Systems*, Edition **MoRa** 2022

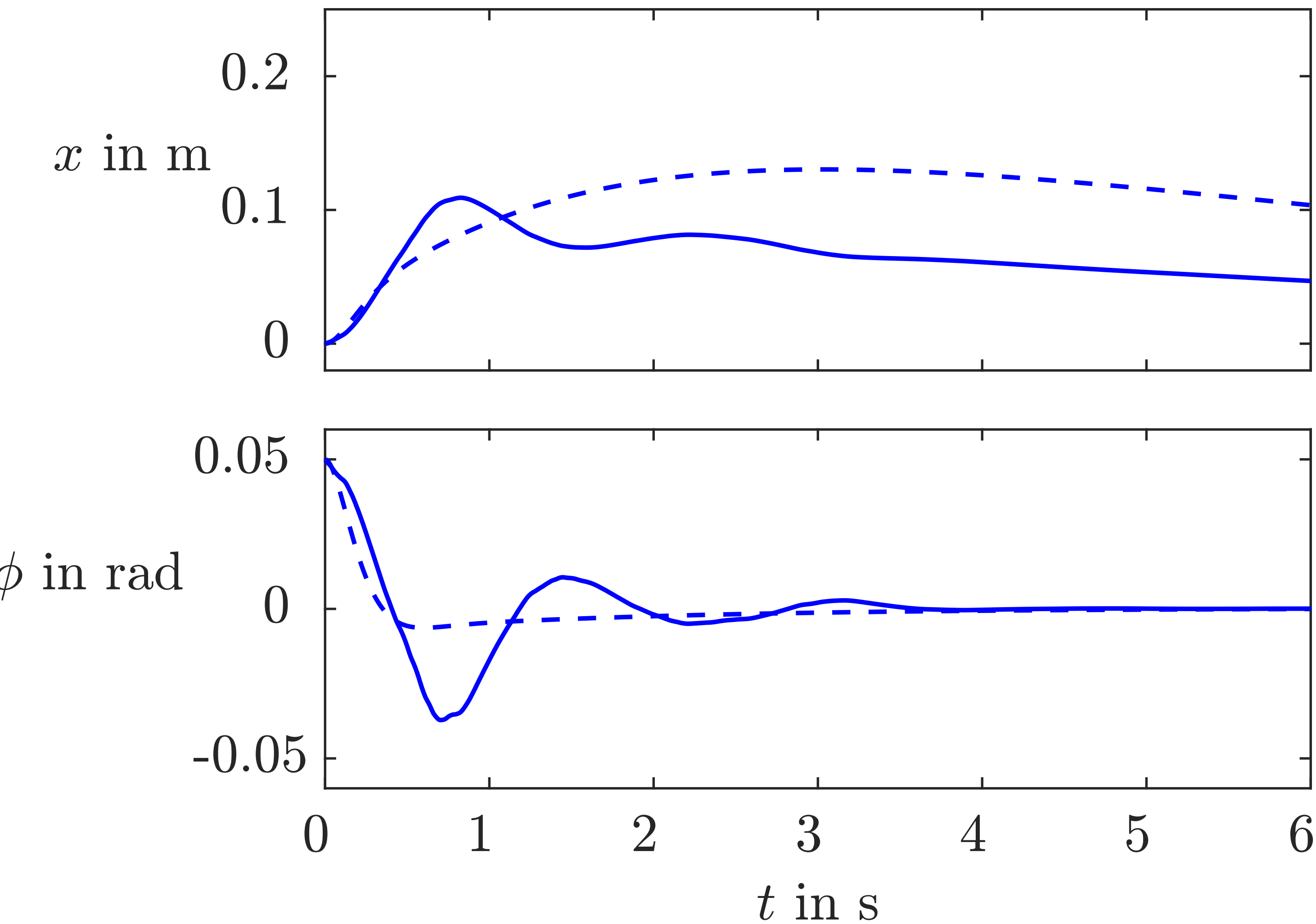

Fig. 7.15: Pendulum behaviour for the networked controller (—) compared with the behaviour for the controller with permanent data transfer (- - -)

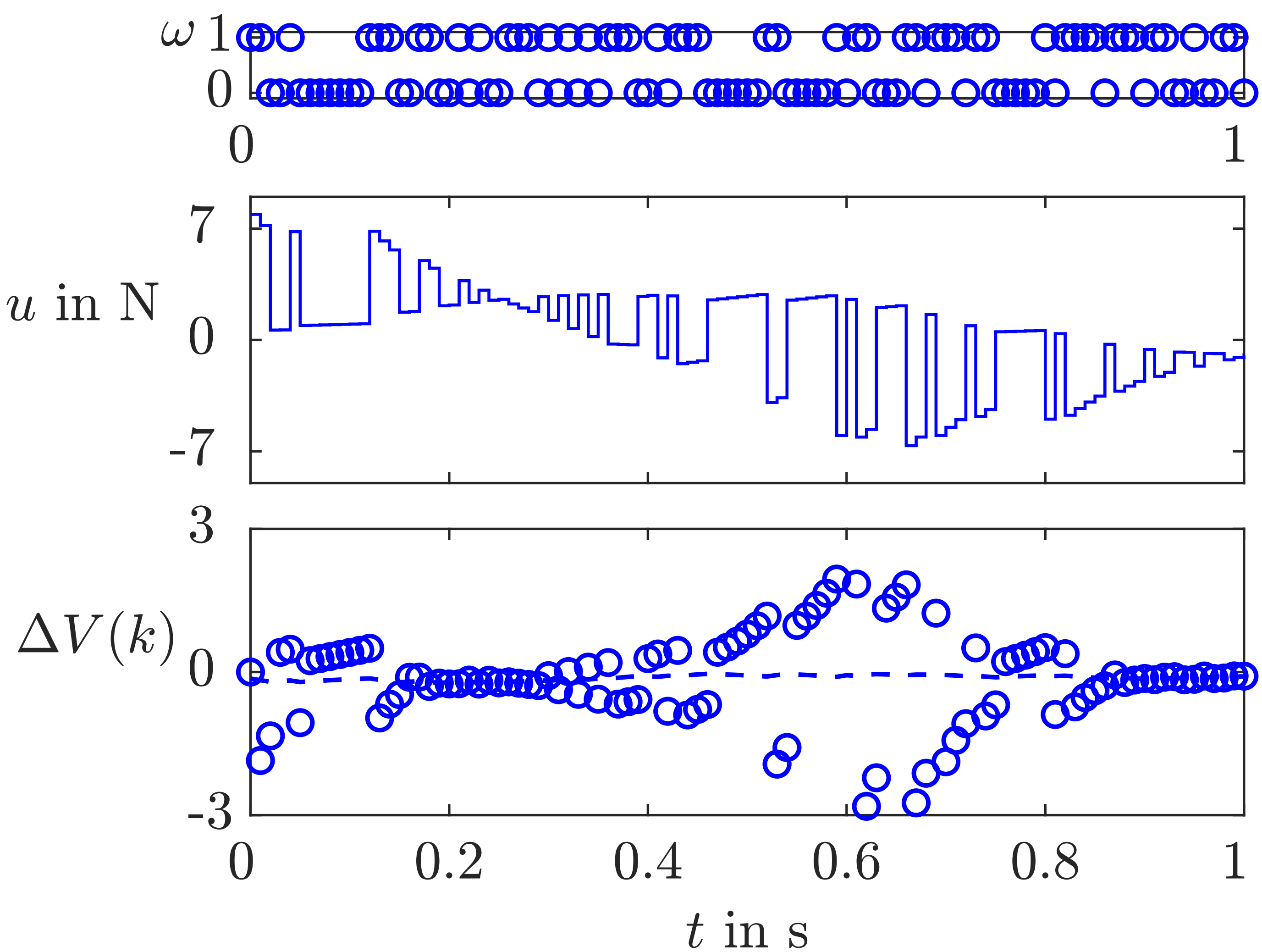

Fig. 7.16: Details of Fig. 7.15

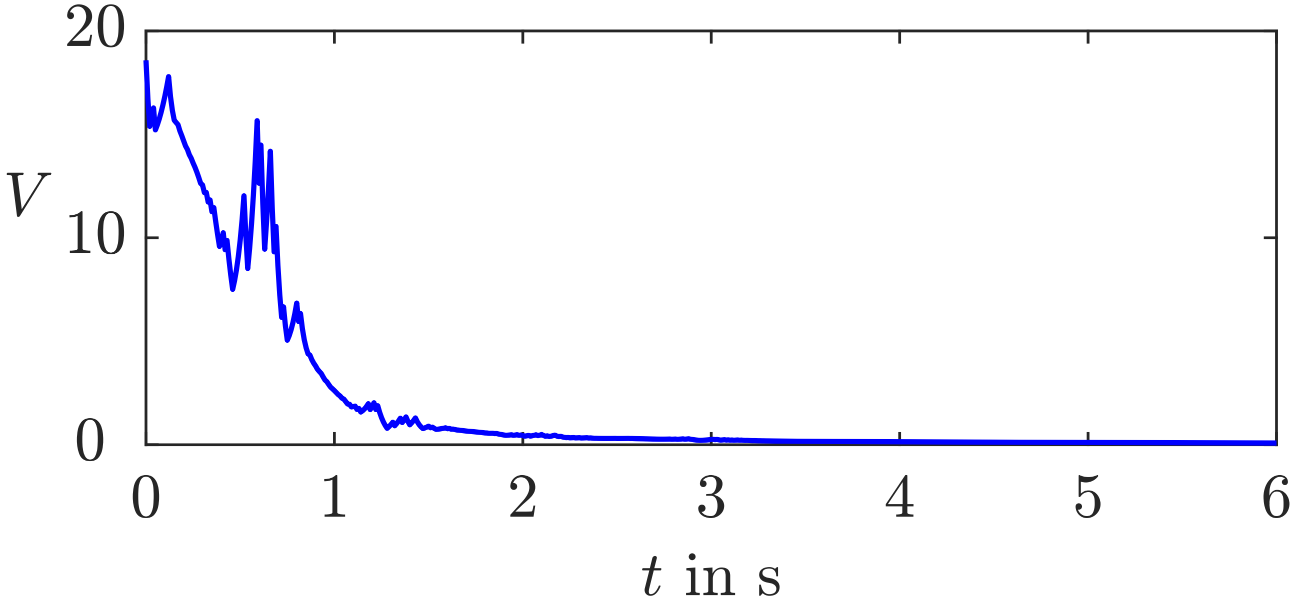

Fig. 7.17: Lyapunov function of the inverted pendulum

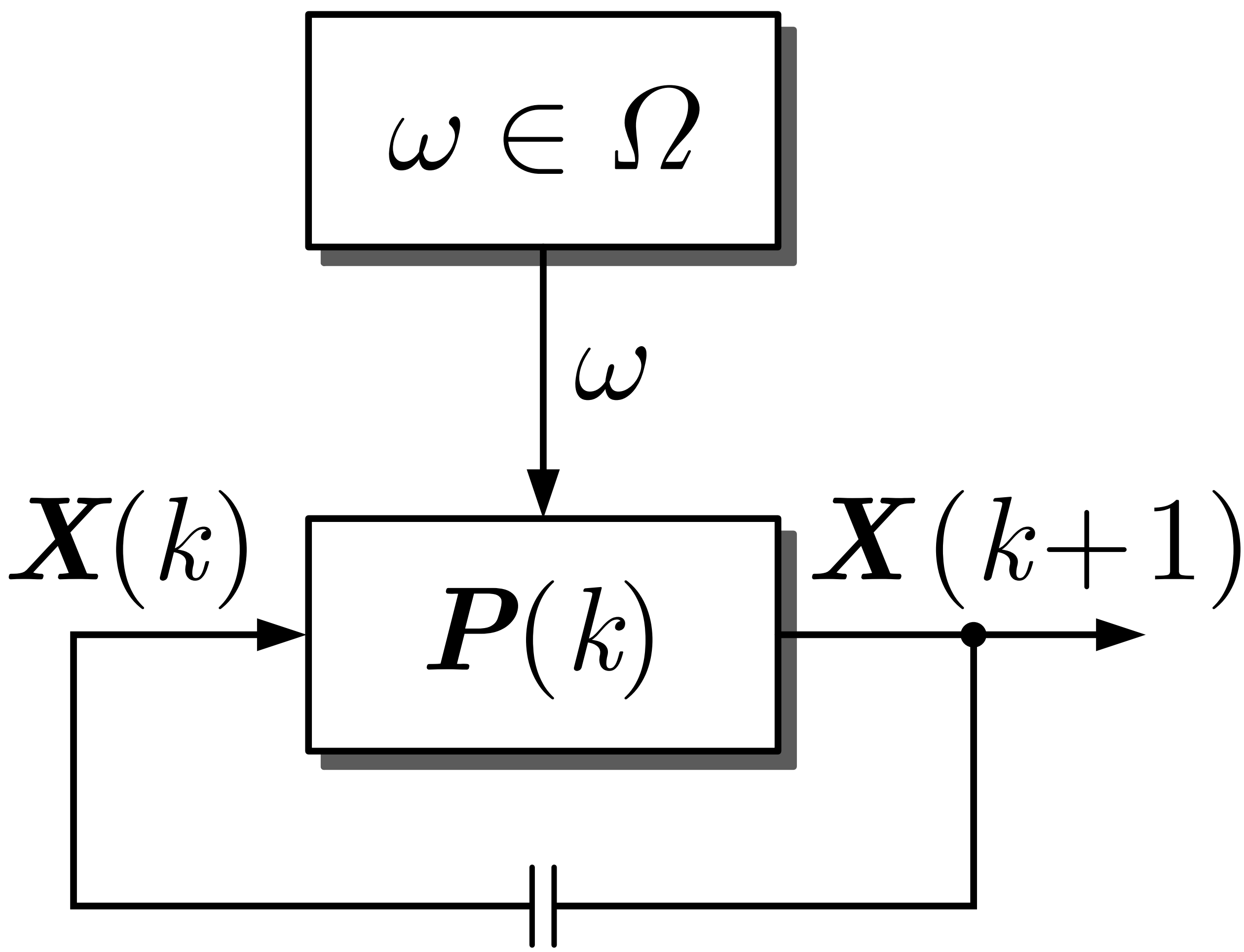

Fig. 7.18: Consensus dynamics with random matrix P

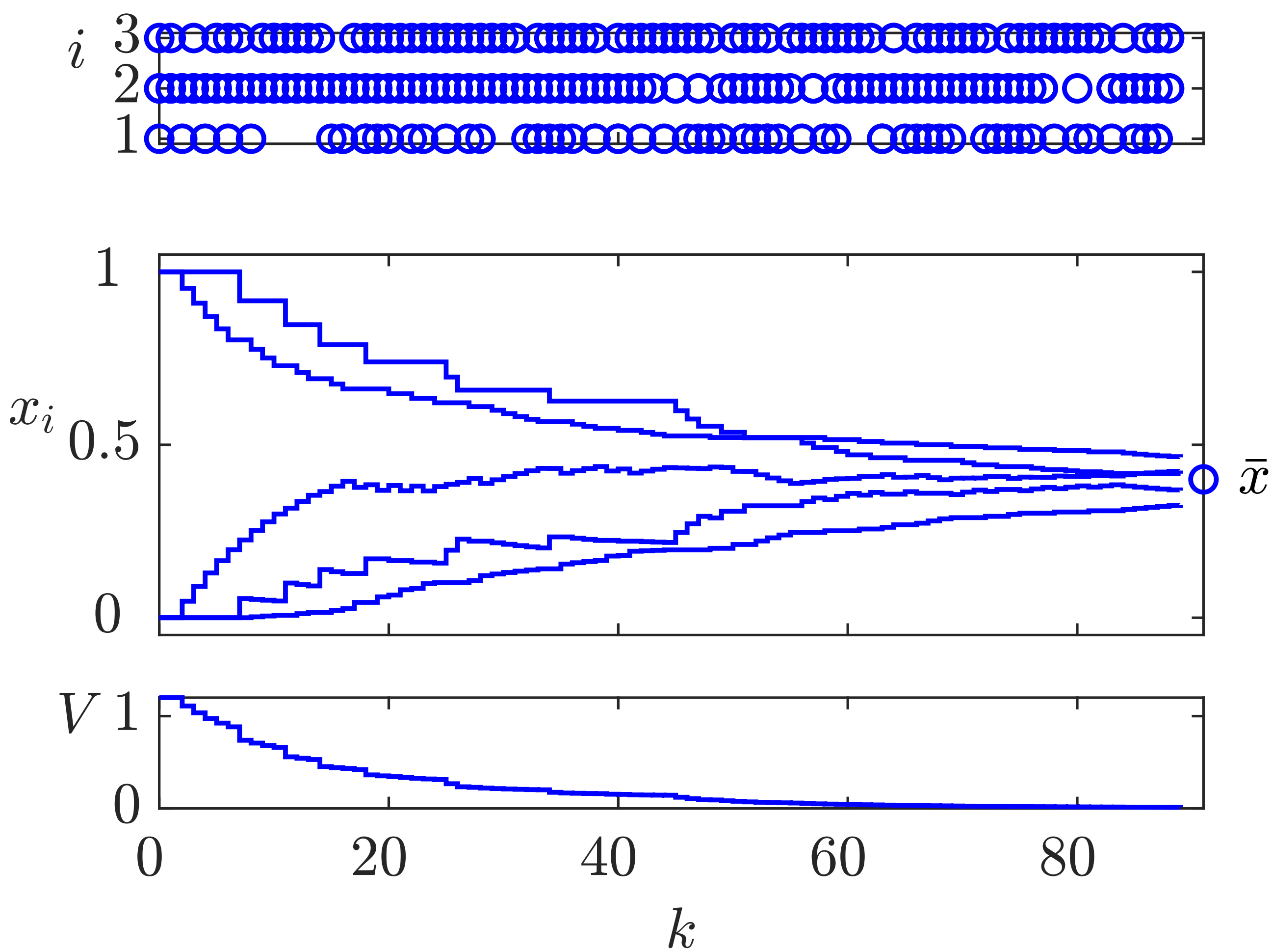

Fig. 7.19: Random agreement

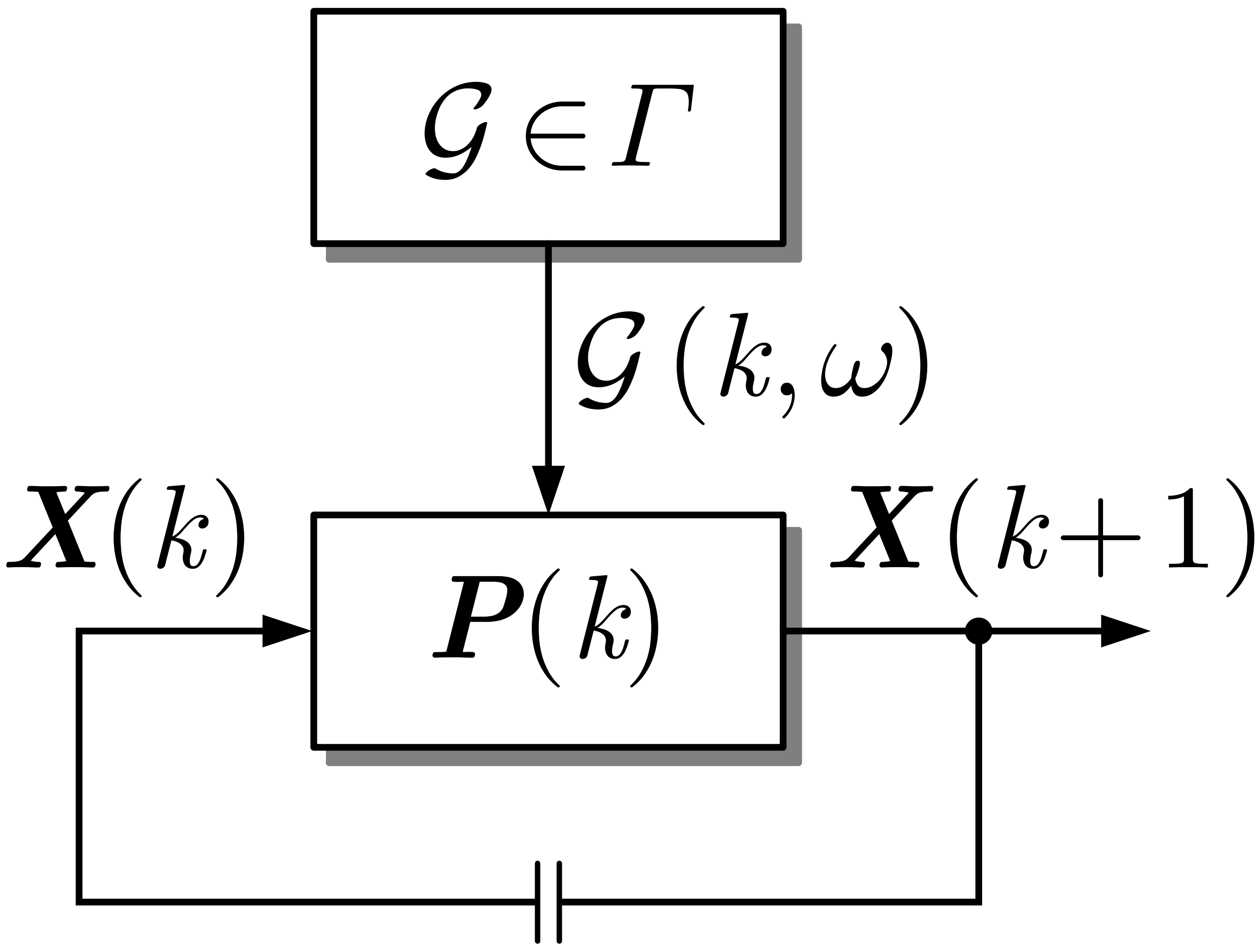

Fig. 7.20: Consensus dynamics with random communication graph

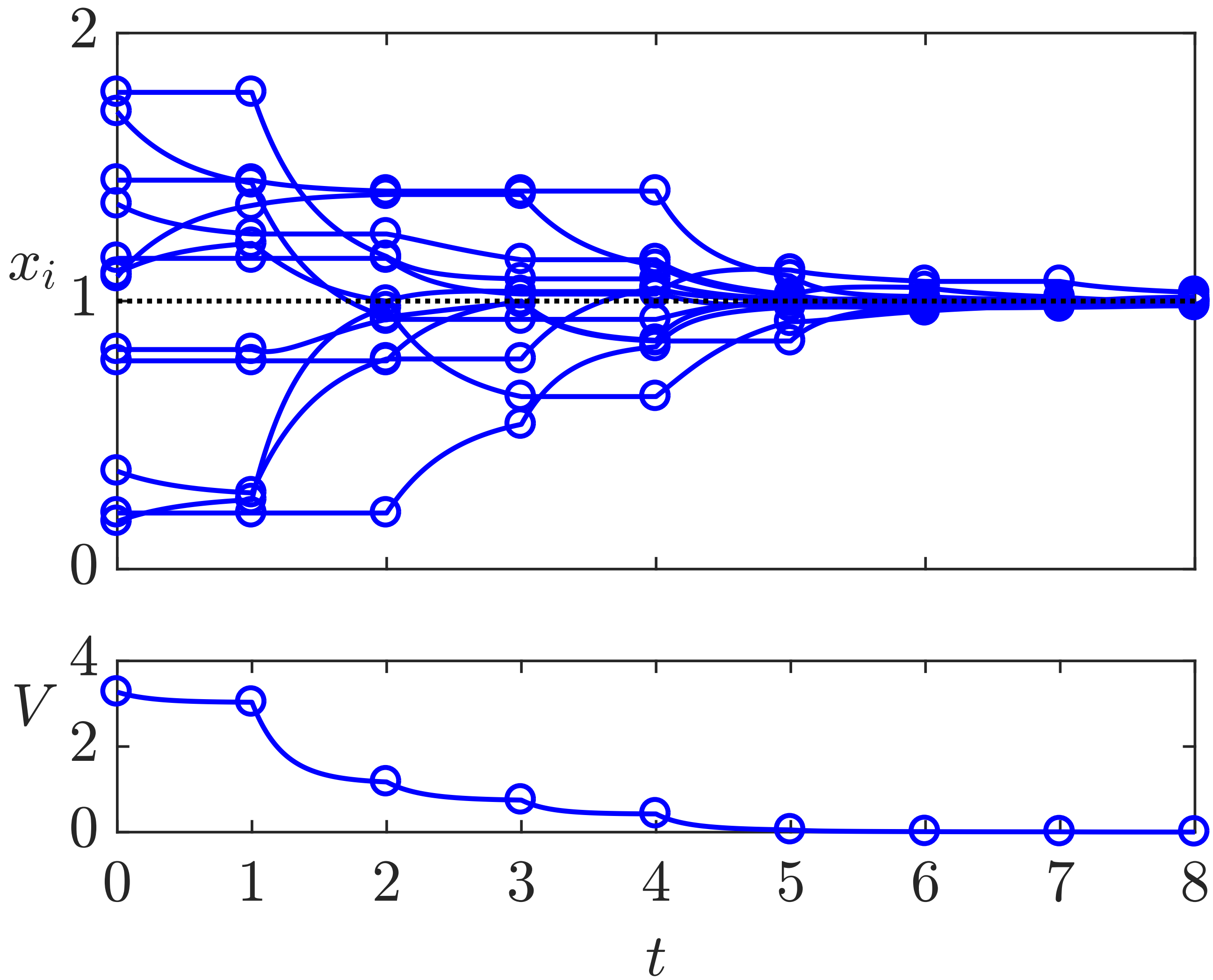

Fig. 7.21: Behaviour of a system with $N = 12$ **agents and Erdös-Rényi communication graph with probability** $p = 0.08$

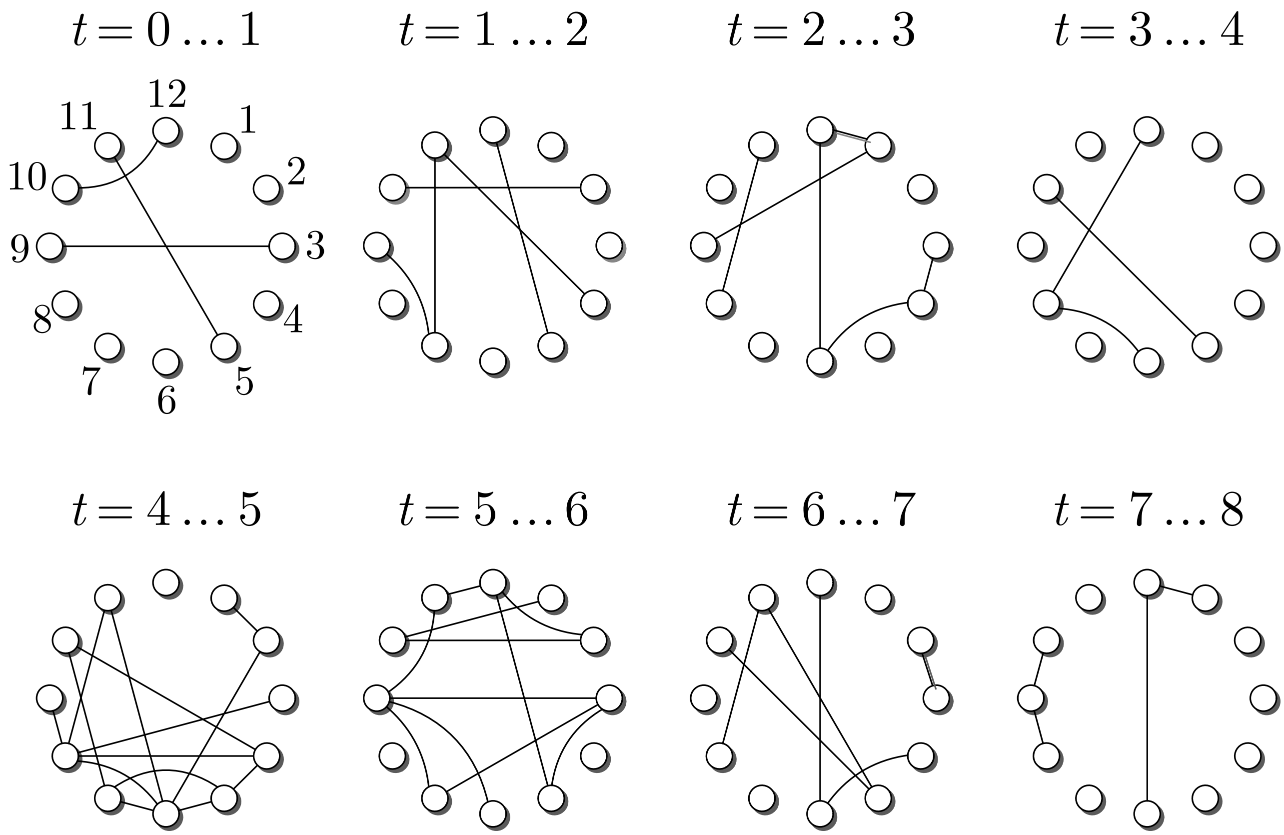

Fig. 7.22: Communication networks used in the example in the time interval $[0, 8]$

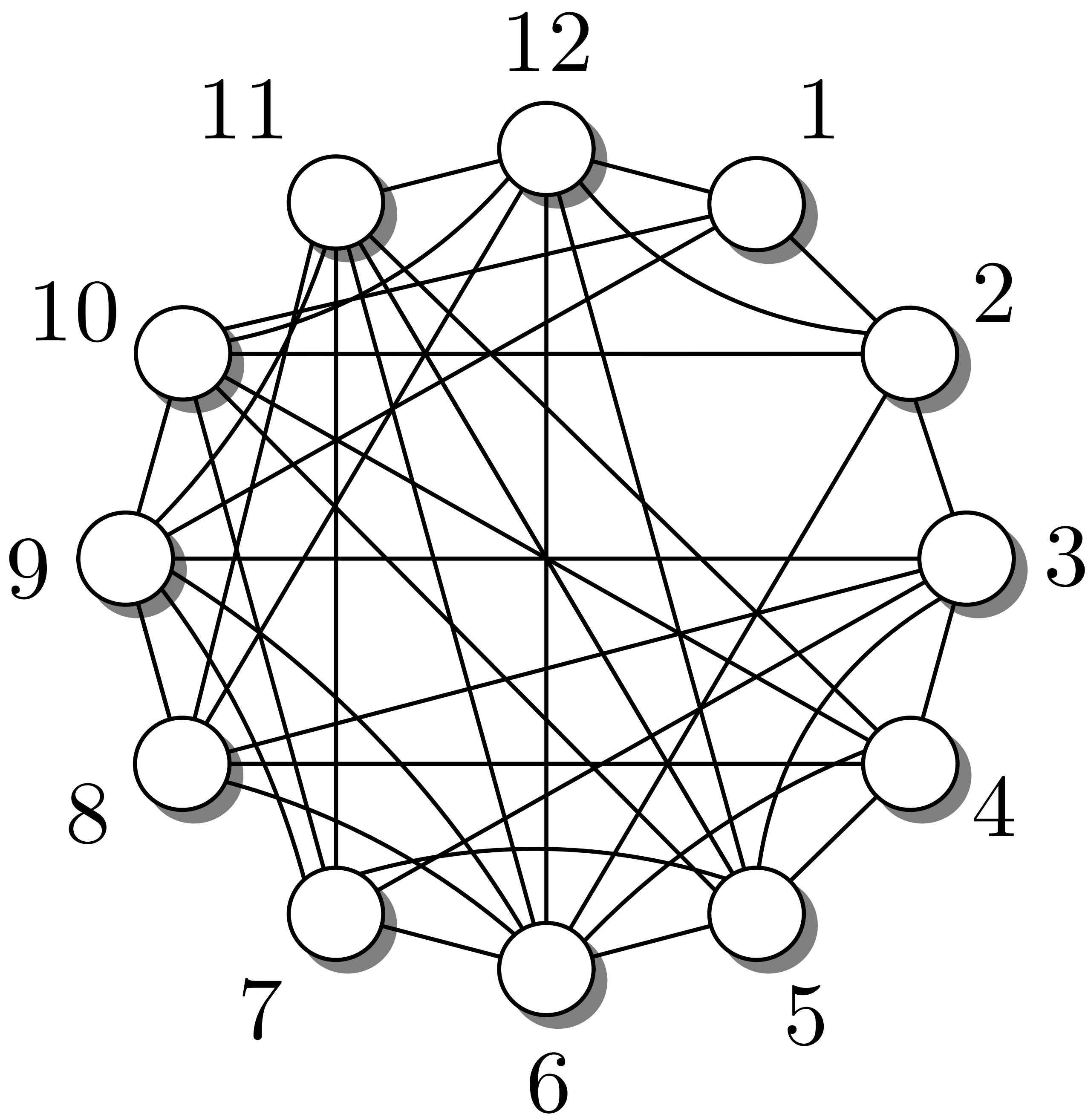

Fig. 7.22: Union of the graphs

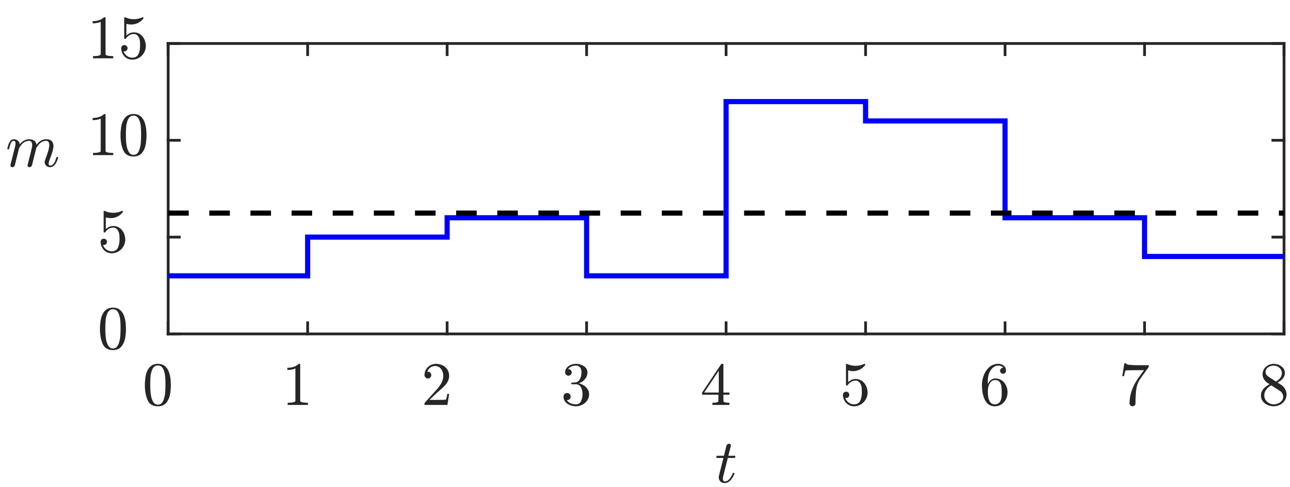

Fig. 7.23: Number of edges in the communication graph

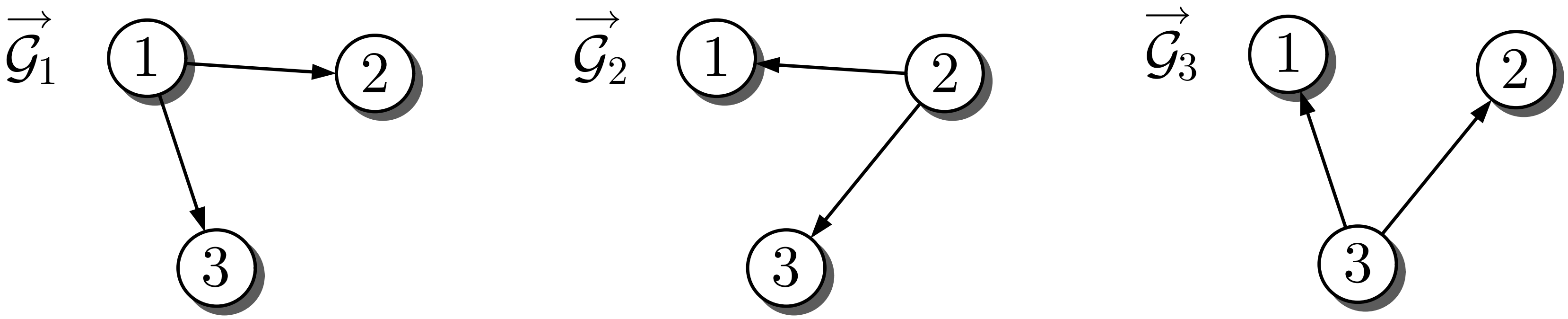

Fig. 7.24. Communication structure in broadcast communication

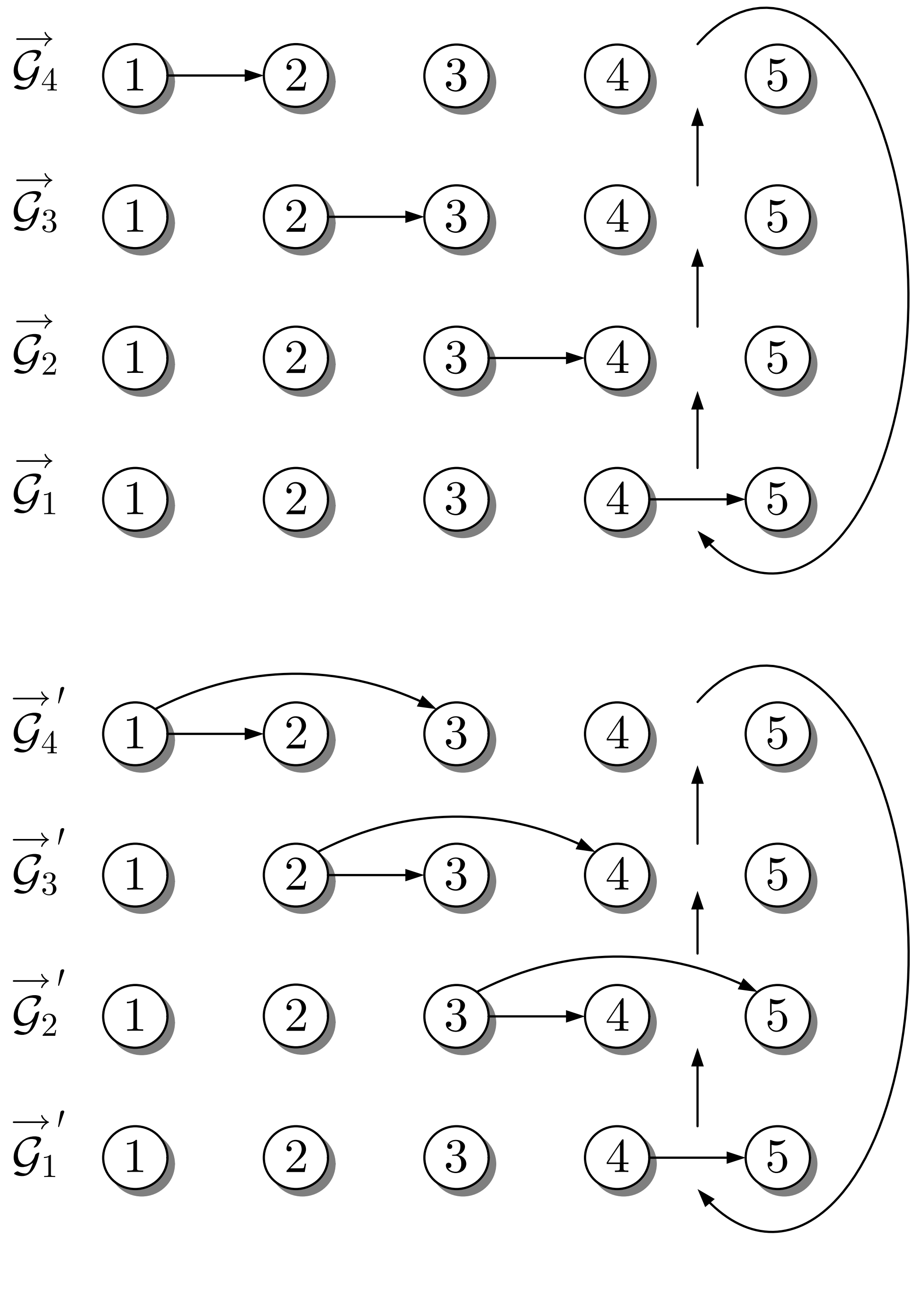

Fig. 7.25. Gossiping in a vehicle string

Fig. 7.26: Dice throwing

J. Lunze: *Networked Control of Multi-Agent Systems*, Edition **MoRa** 2022

page 427

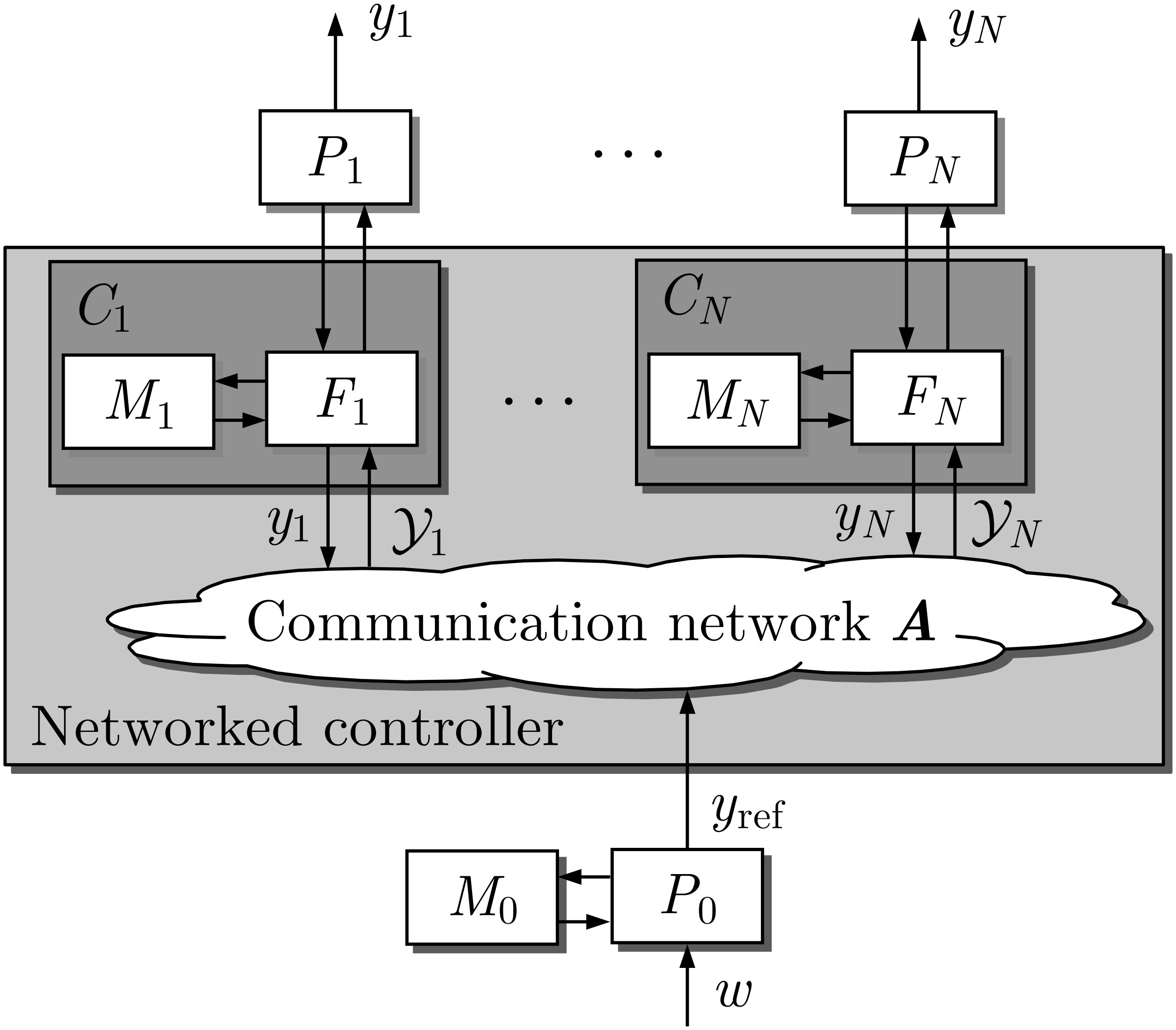

Fig. 8.1: Self-organising multi-agent system

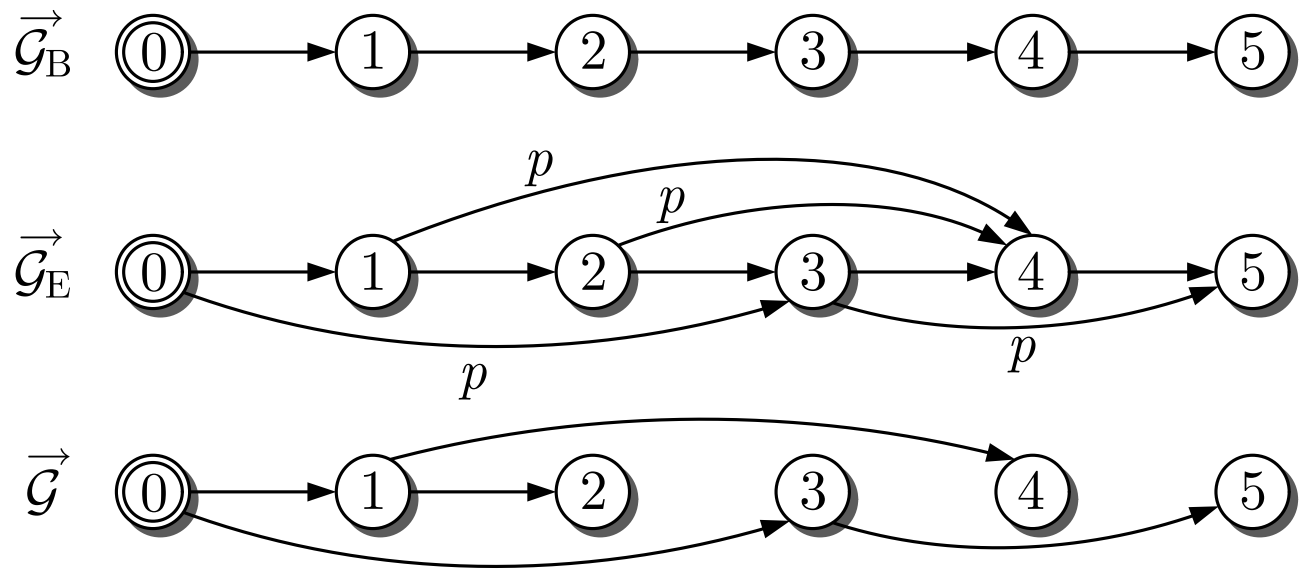

Fig. 8.2: Communication graphs

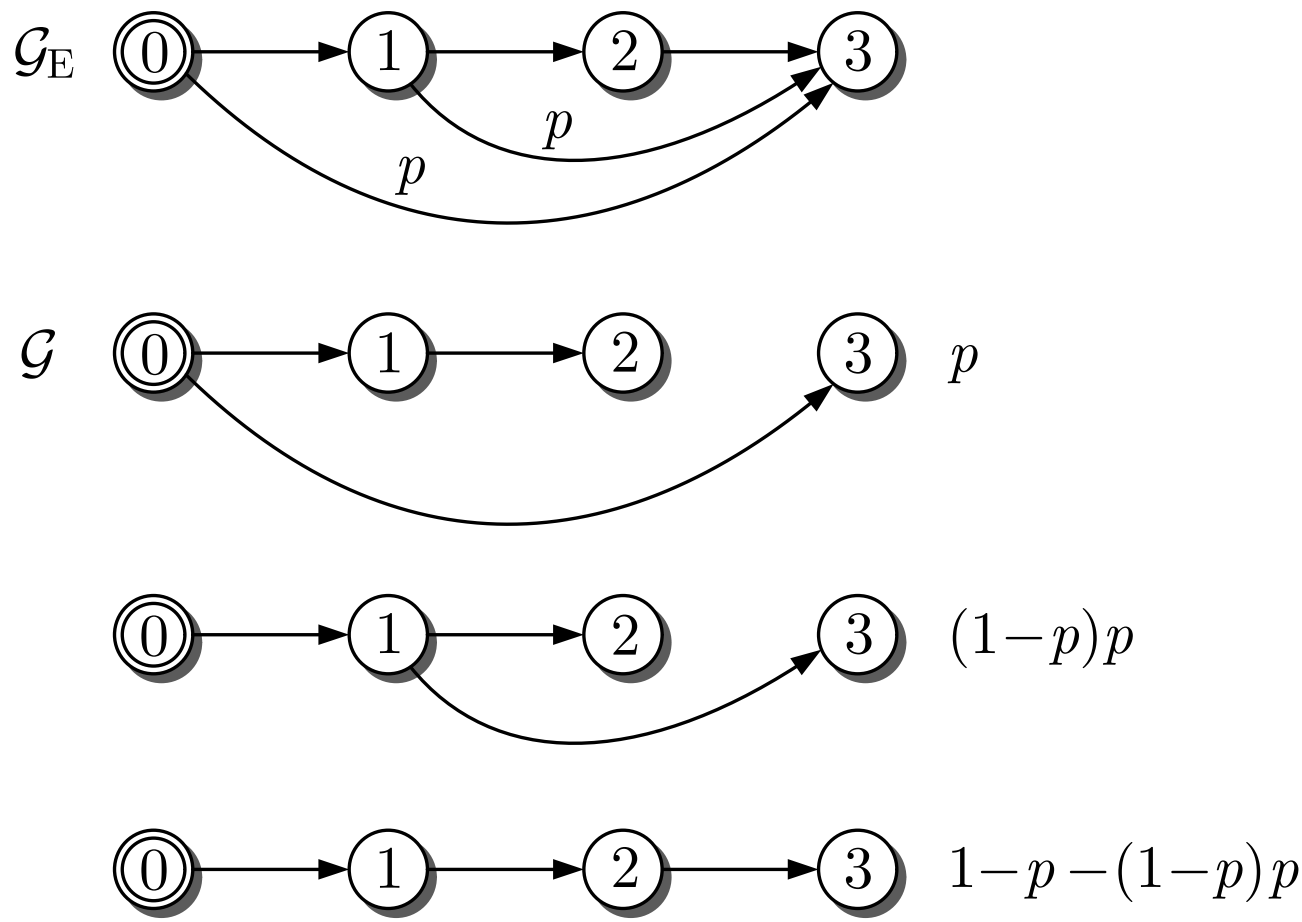

Fig. 8.3: Determination of v_3

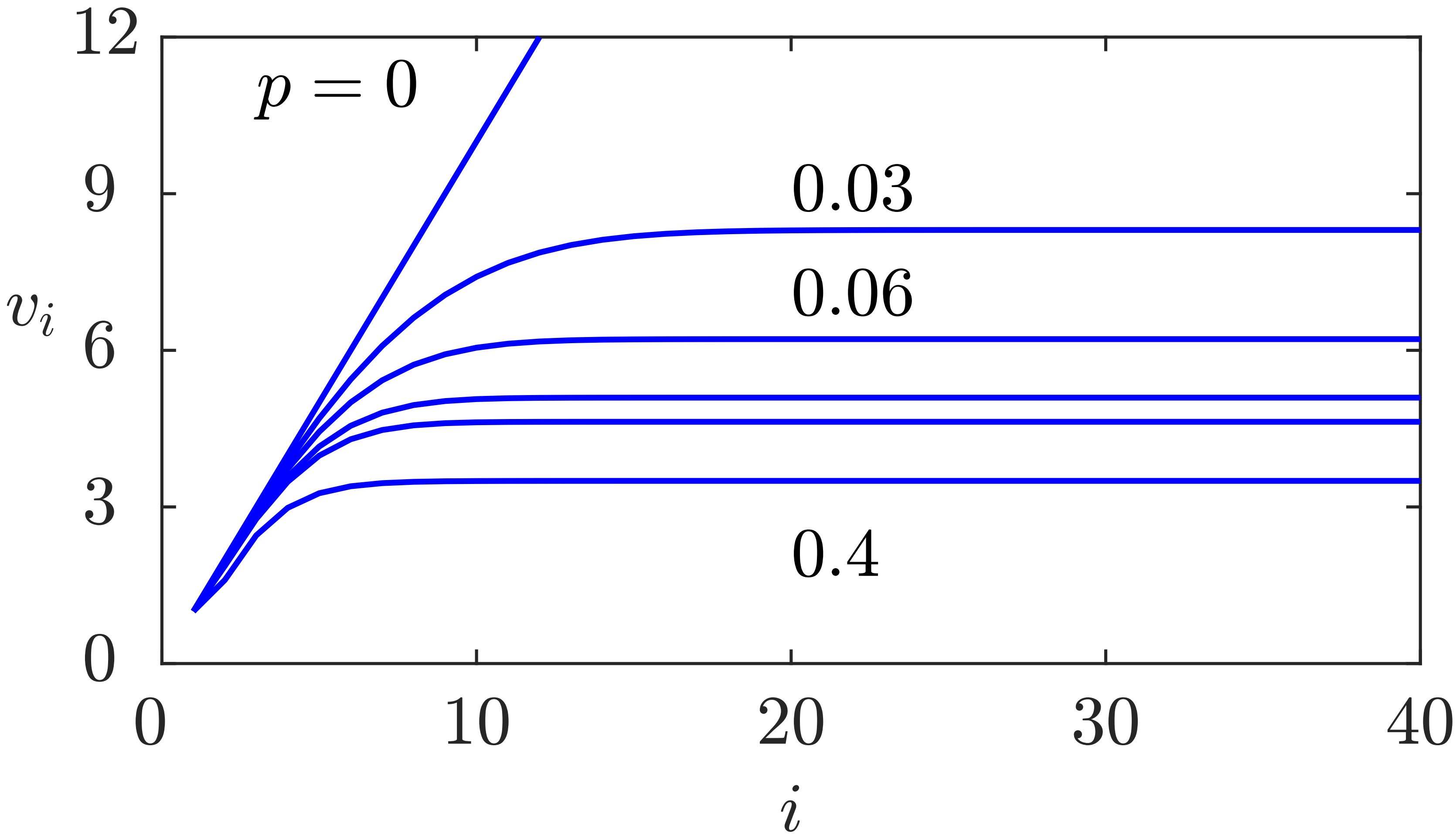

Fig. 8.4. Expected path length v_i for 40 agents with parameters $p \in \{0, 0.03, 0.06, 0.1, 0.13, 0.4\}$

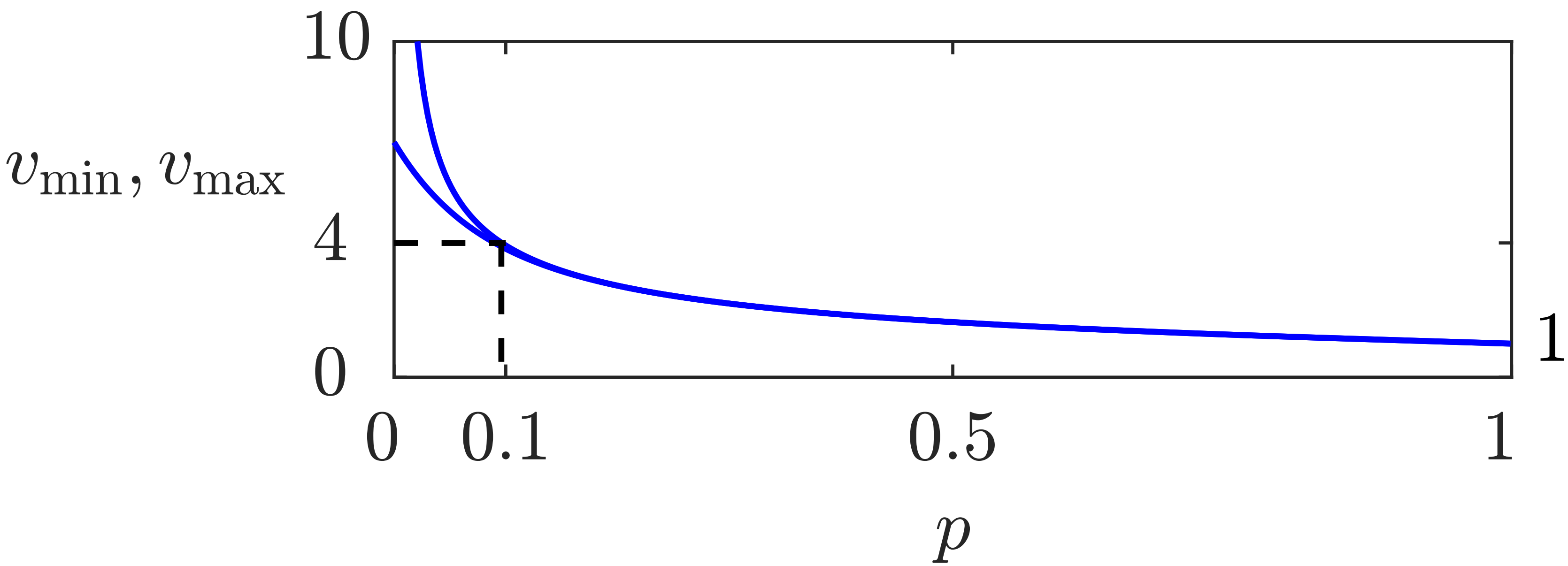

Fig. 8.5. Interval for the upper bound $\bar{v}$

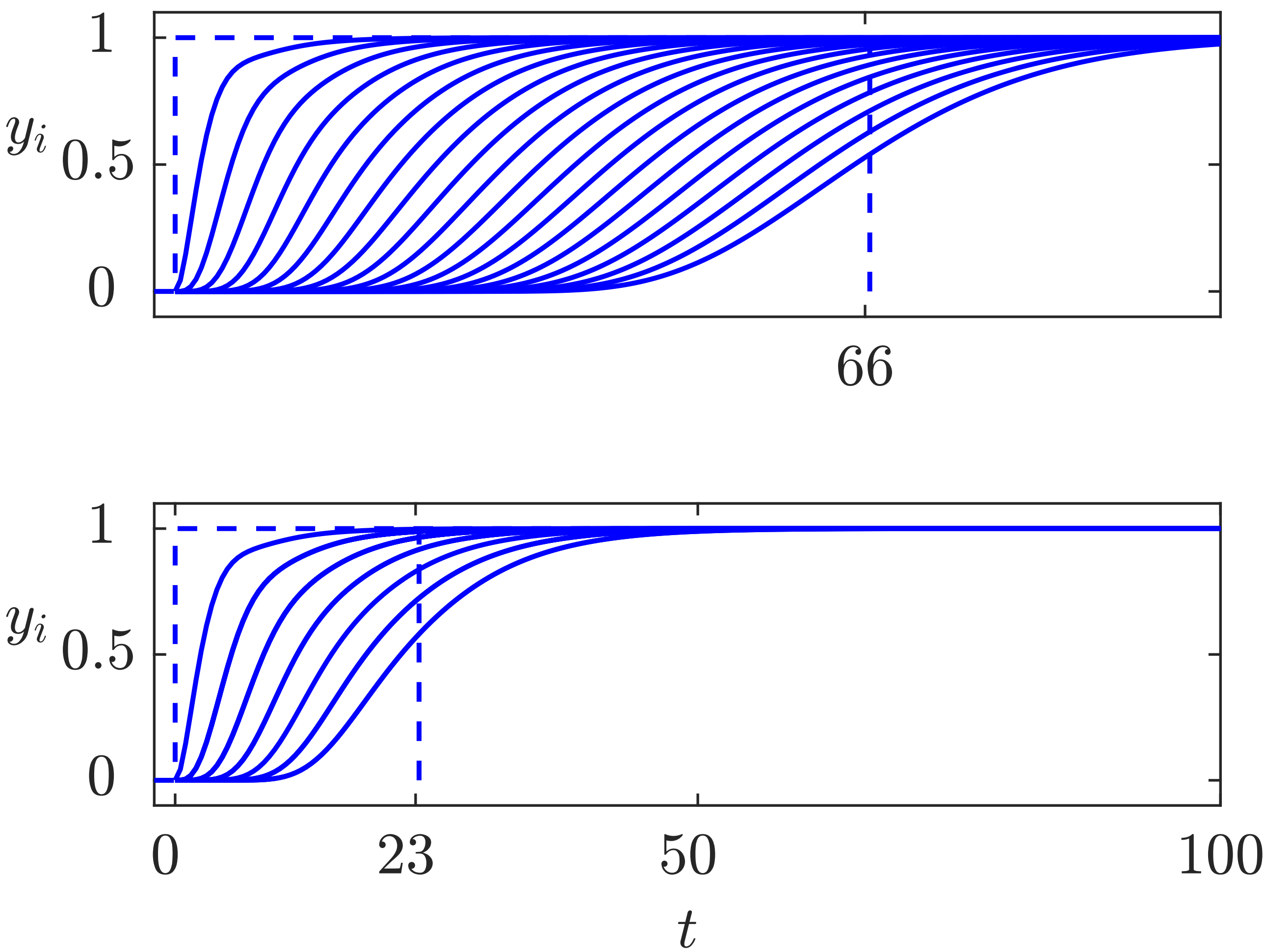

Fig. 8.6: Performance of 21 robots with path connection (above) and with the effective communication graph (below)

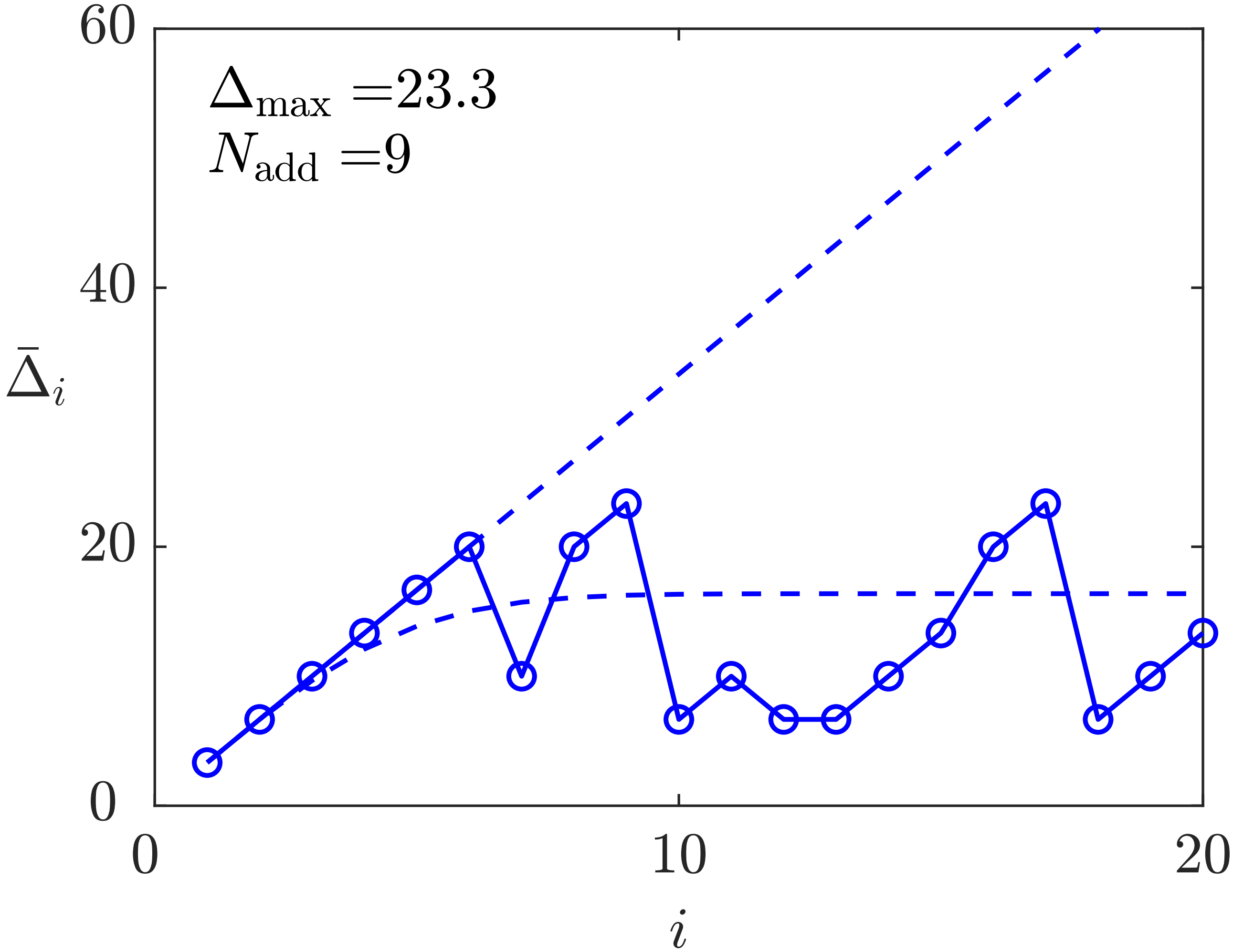

Fig. 8.7: Delay of the robot formation in two experiments with the same connection probability $p = 0.1$ **(I)**

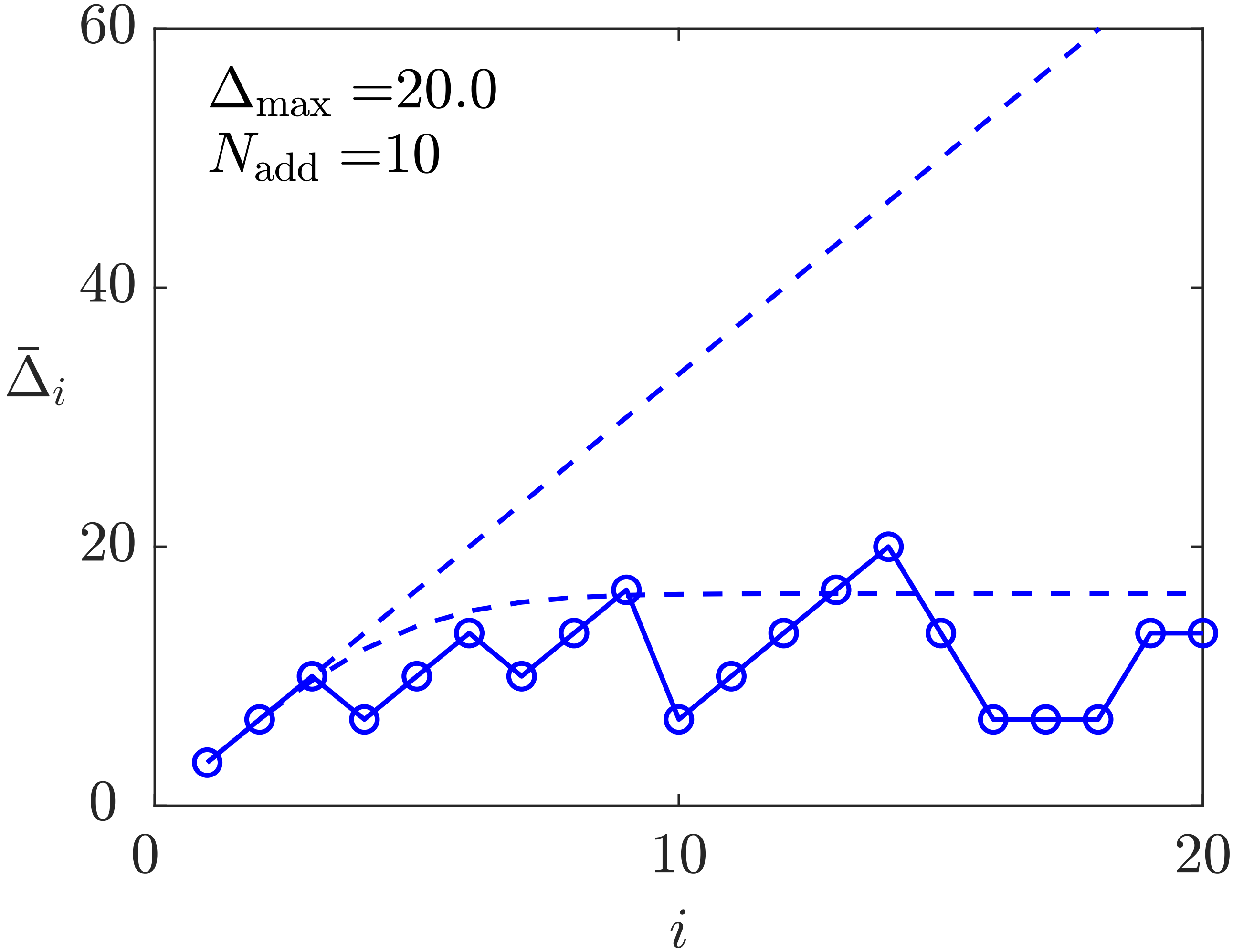

Fig. 8.7: Delay of the robot formation in two experiments with the same connection probability $p = 0.1$ (II)

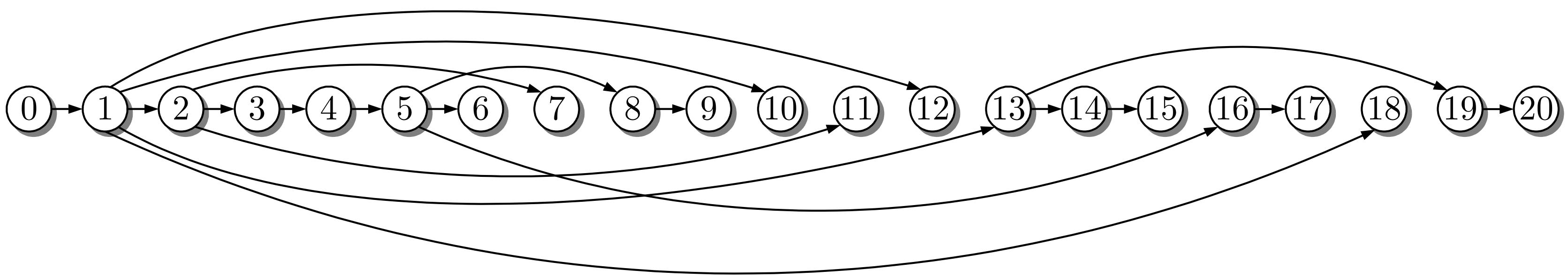

Fig. 8.8. Example of an effective communication graph

J. Lunze: *Networked Control of Multi-Agent Systems*, Edition MoRa 2022

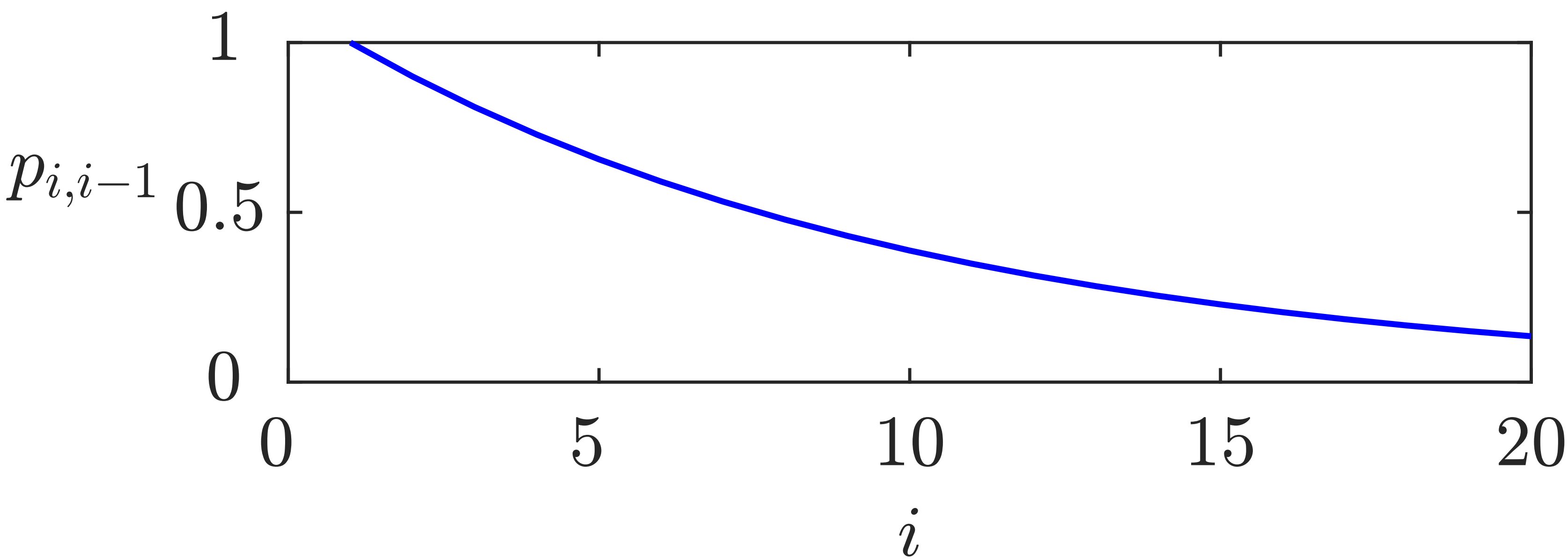

Fig. 8.9. Probability of the edge $(i-1 \rightarrow i)$ to be an edge of the effective communication graph

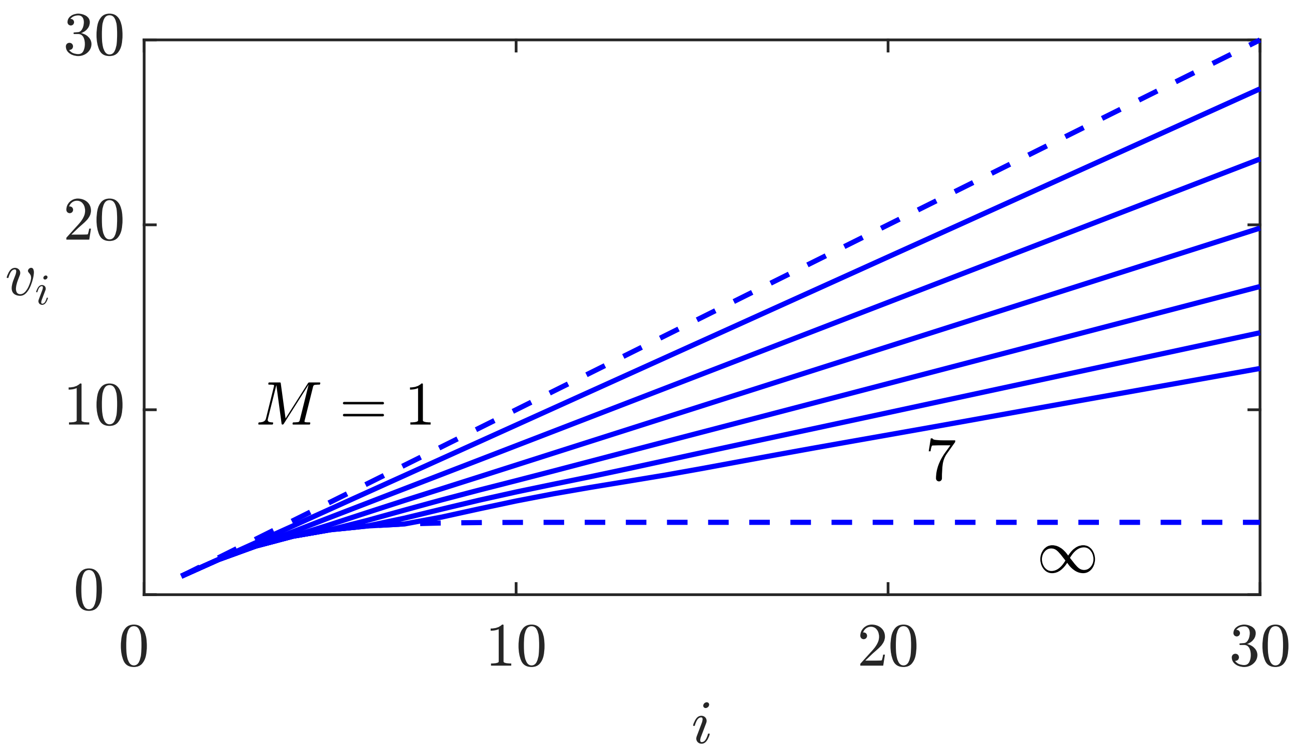

Fig. 8.10: Expected path length v_i for various sizes M of the neighbourhood

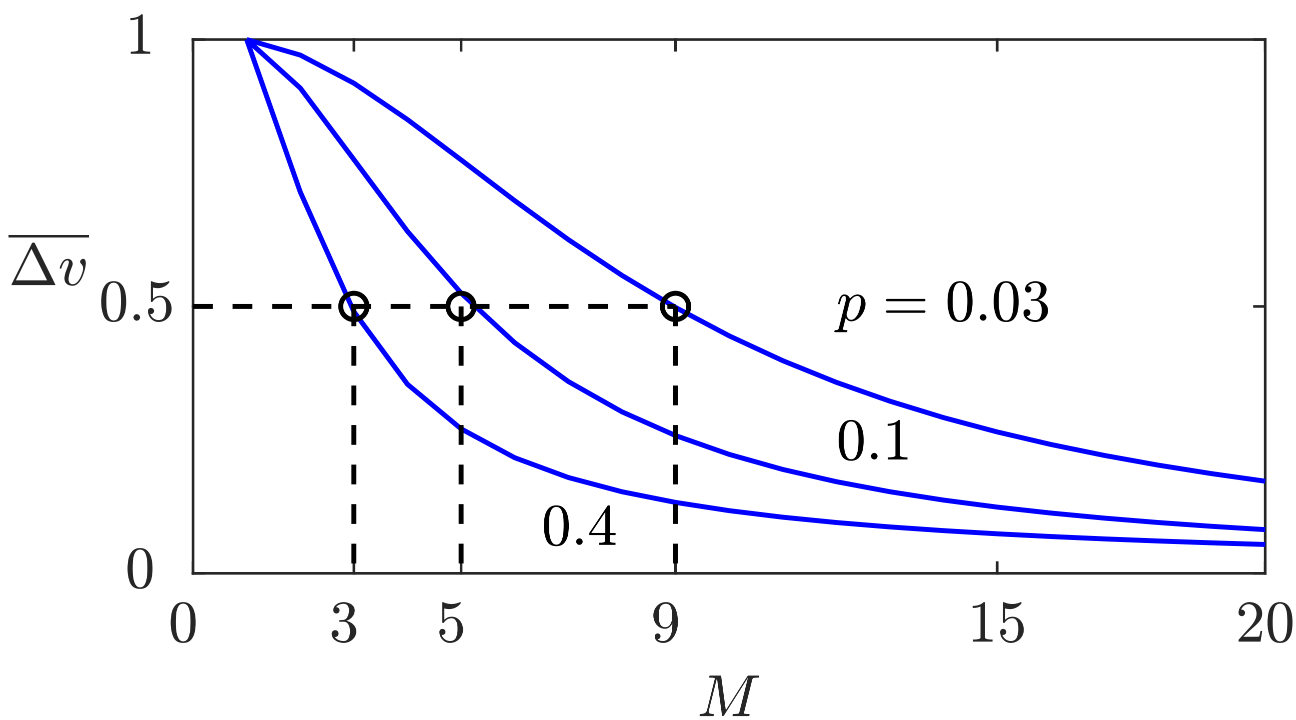

Fig. 8.11: $\overline{\Delta v}$ **in dependence upon the connection probability** $p \in \{0.03, 0.1, 0.4\}$ **and the size** M **of the neighbourhood**

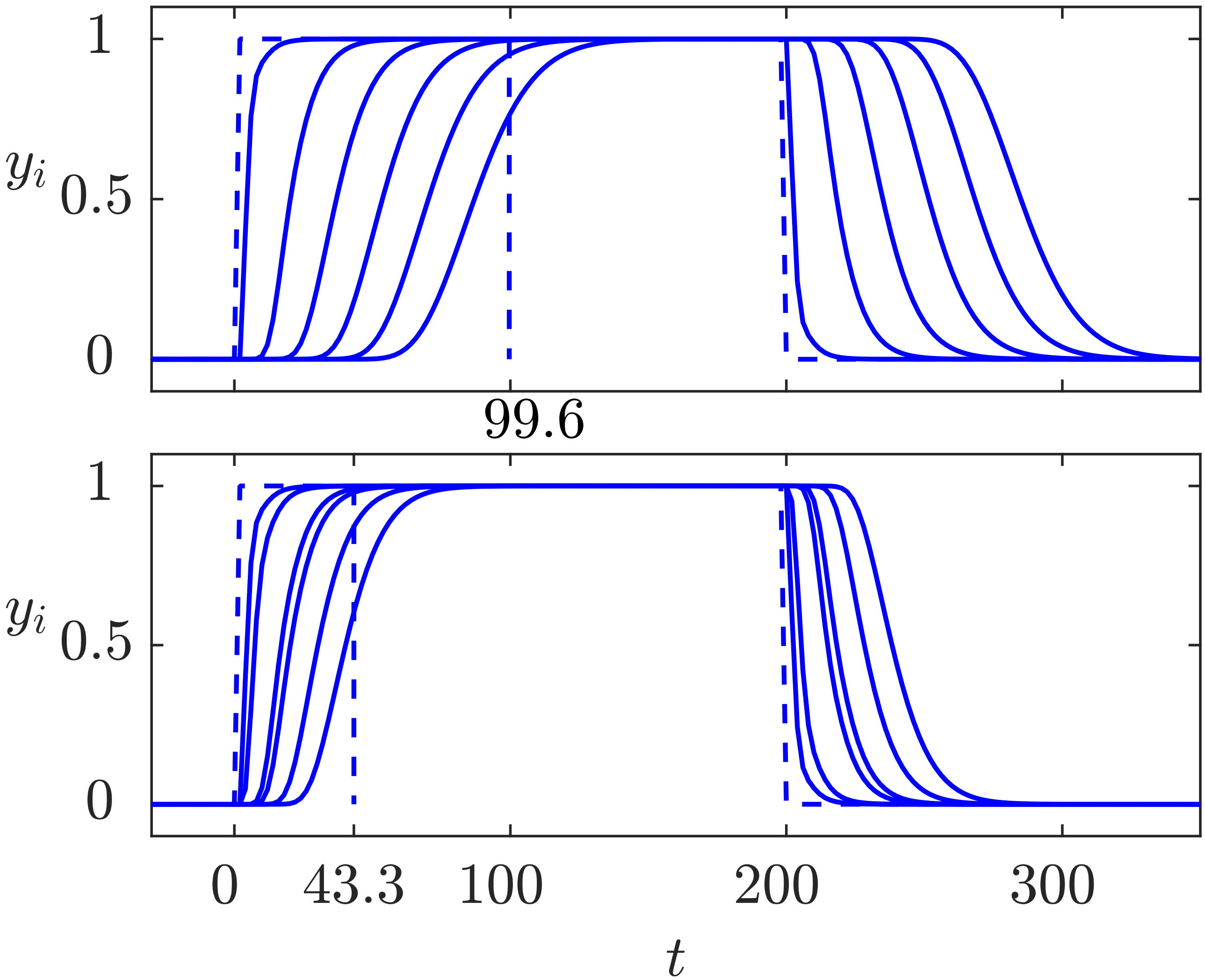

Fig. 8.12: Behaviour of the networked robots with the basic communication structure (above) and with the effective communication structure (below) ($y_i(t)$ is drawn for $i = 1, 6, 11, ..., 26$)

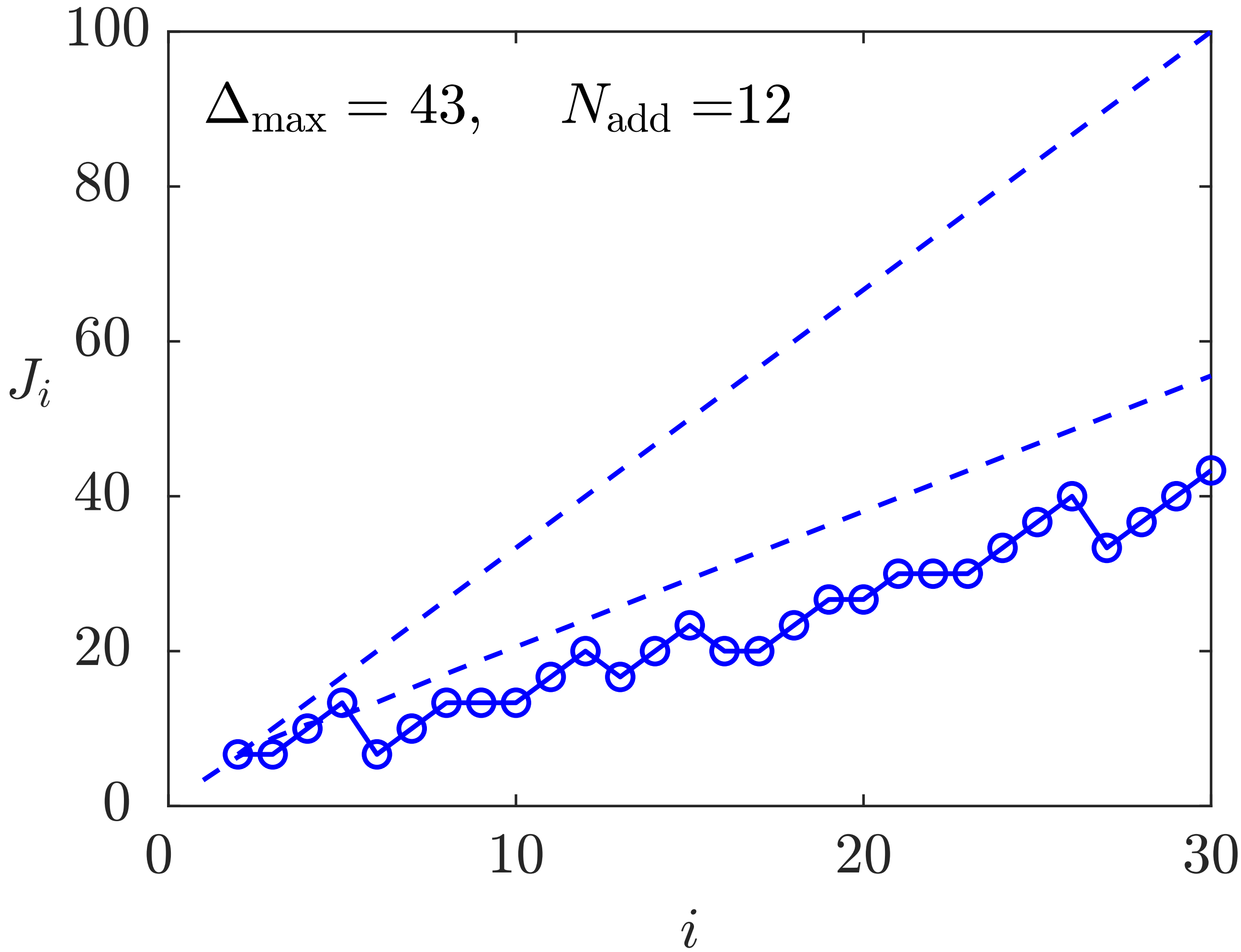

Fig. 8.13: Performance index of the networked robots

J. LUNZE: *Networked Control of Multi-Agent Systems*, Edition **MoRa** 2022

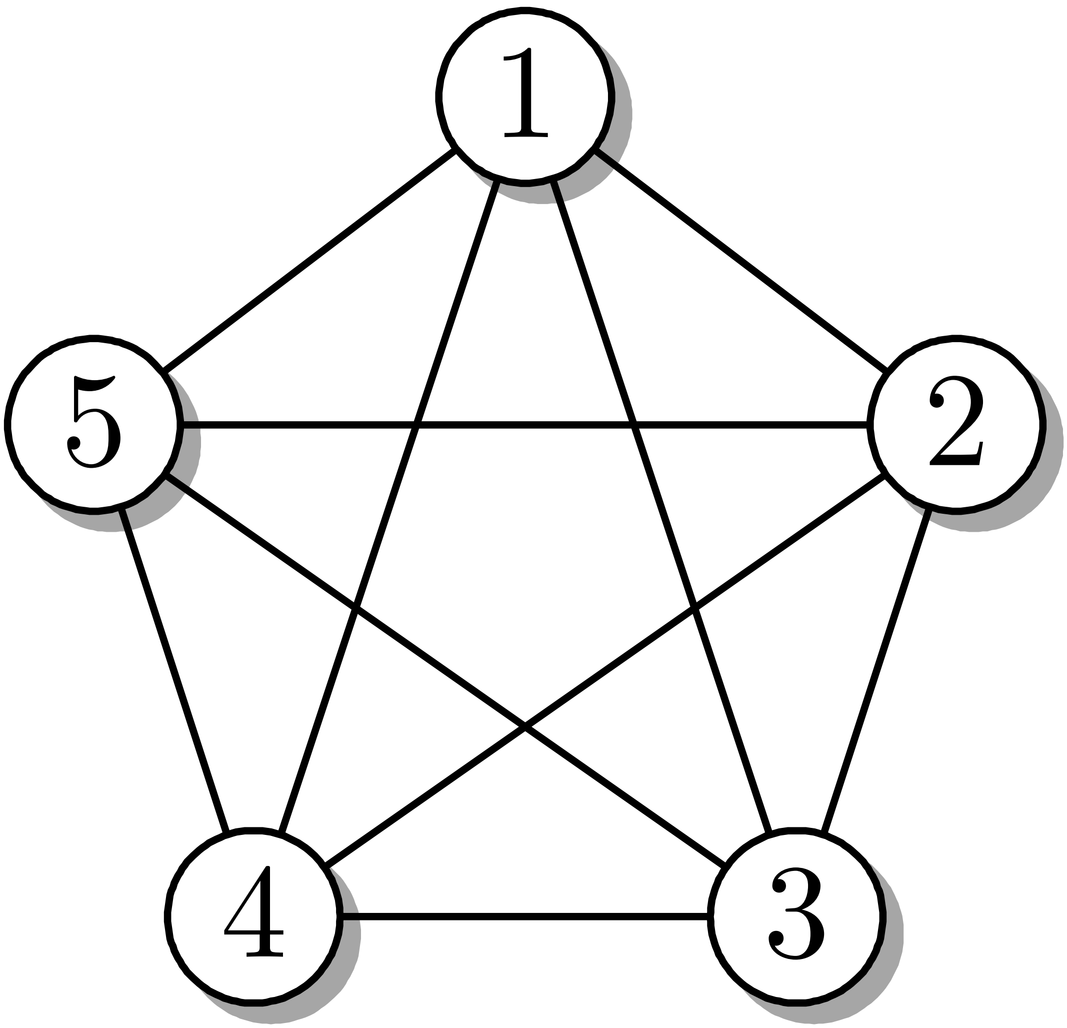

Fig. 8.14: All-to-all communication graph

J. LUNZE: *Networked Control of Multi-Agent Systems,* Edition MoRa 2022

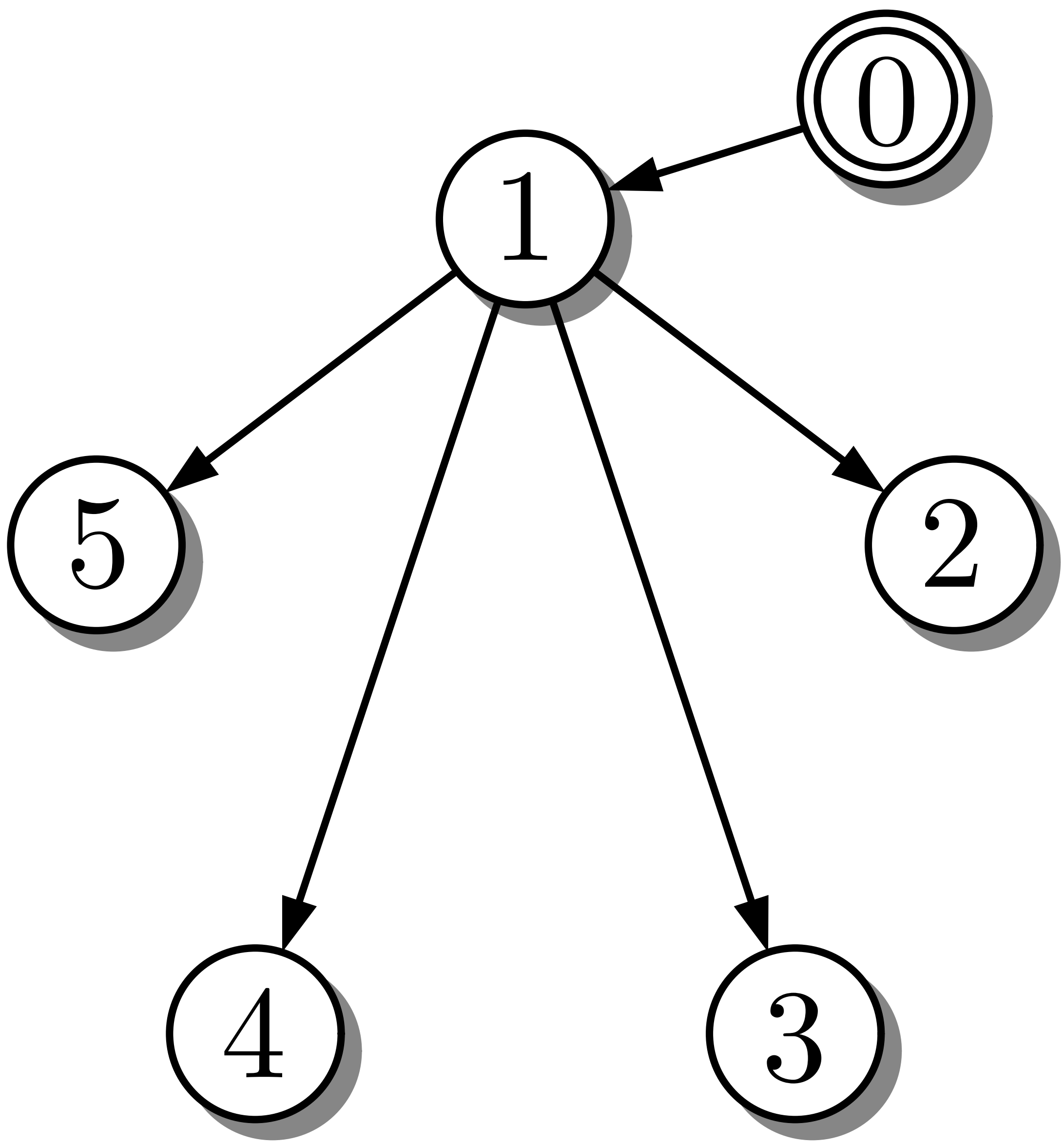

Fig. 8.14: Resulting communication structure for the entry point of the leader at agent $\bar{\Sigma}_1$

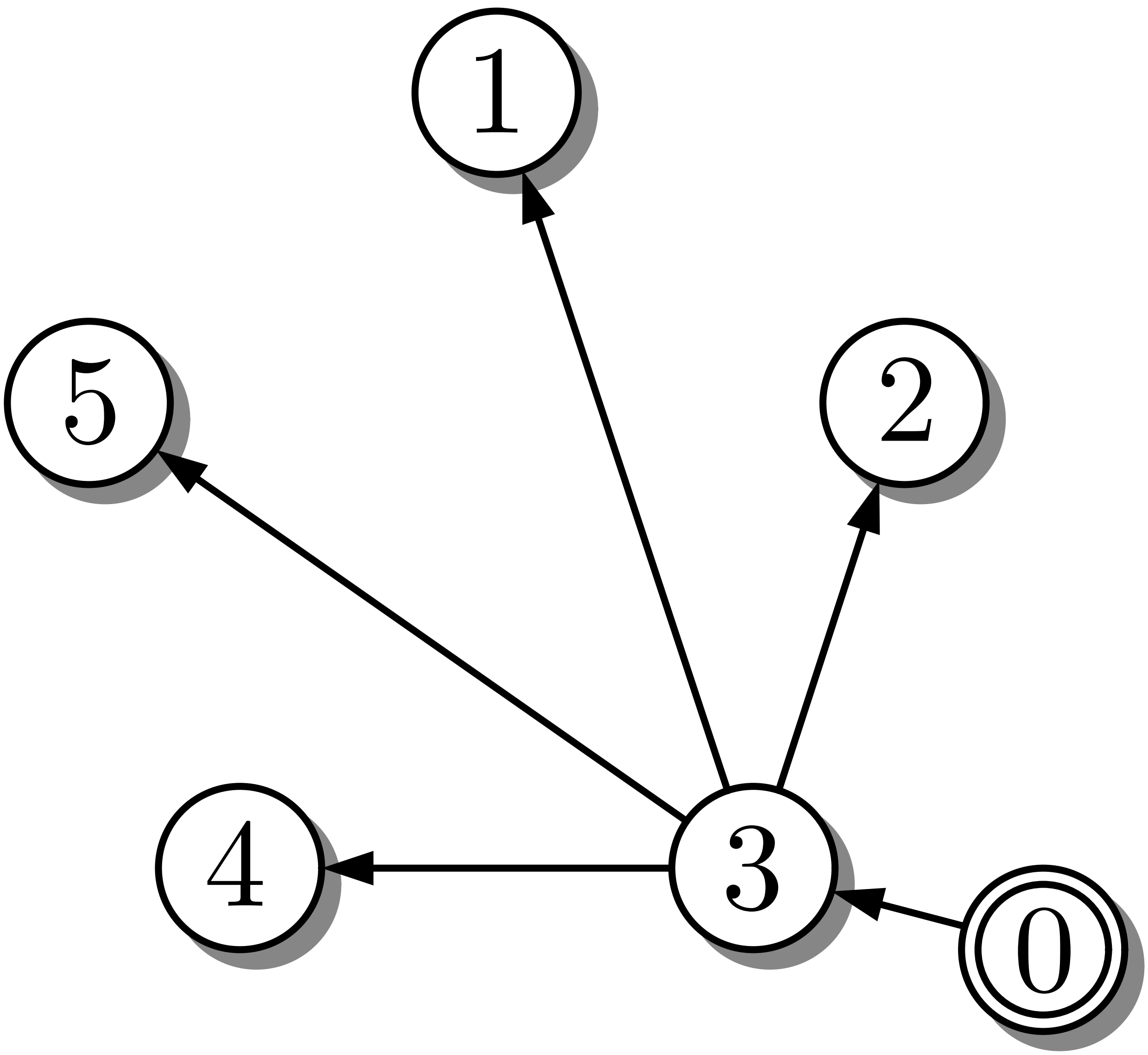

Fig. 8.14: Resulting communication structure for the entry point of the leader at agent $\bar{\Sigma}_3$

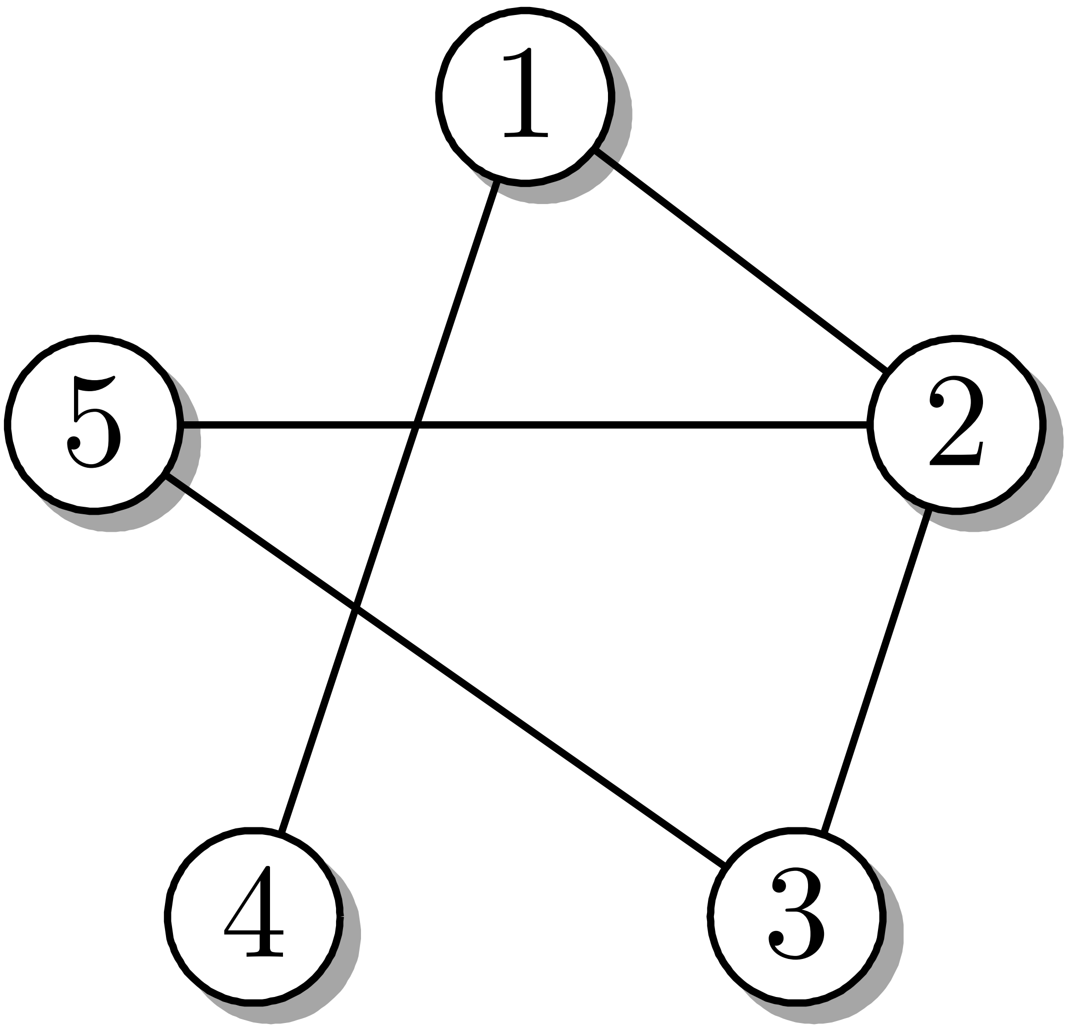

Fig. 8.15: Connected graph

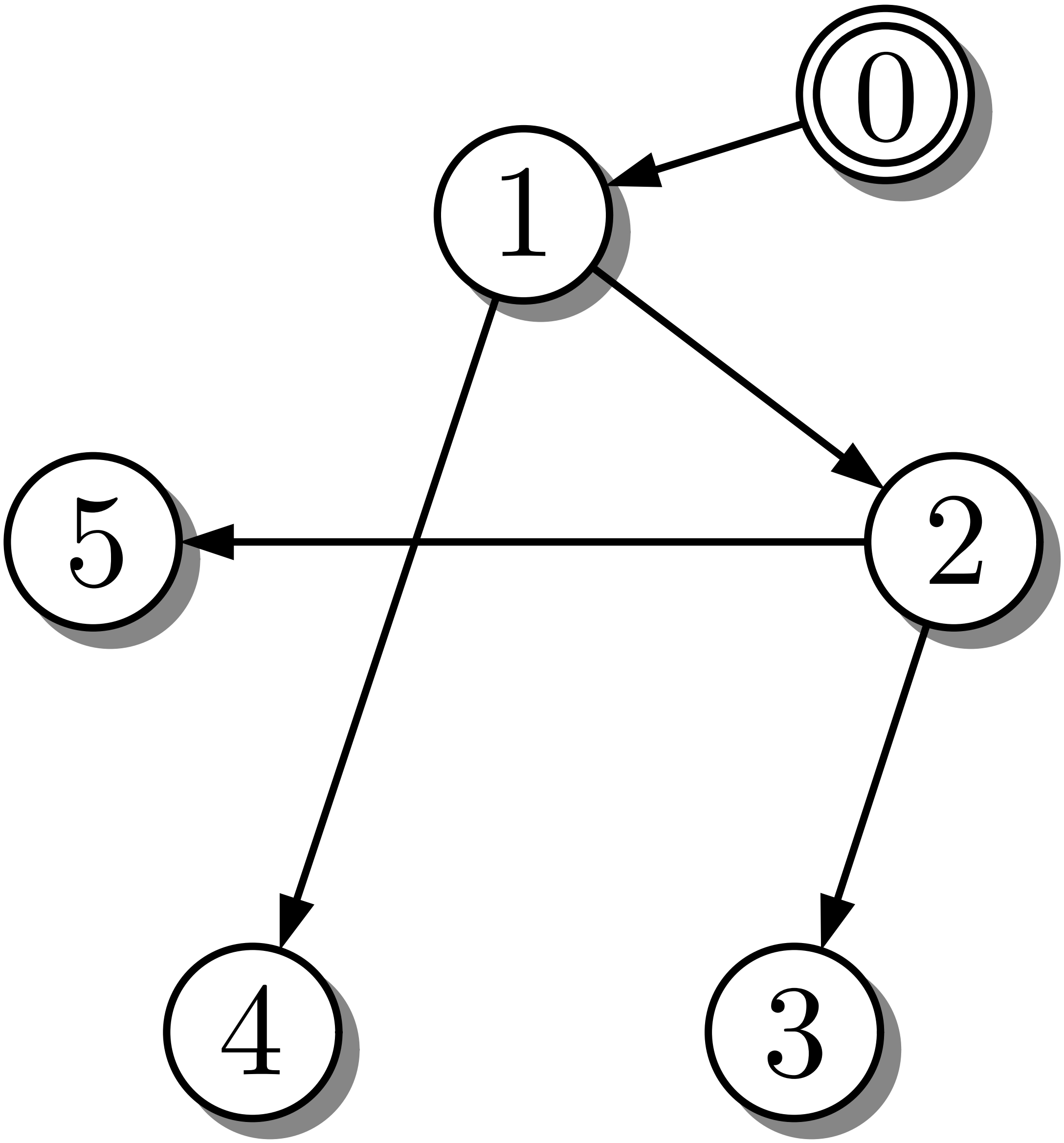

Fig. 8.15: Resulting effective communication graphs for command input at agent 1

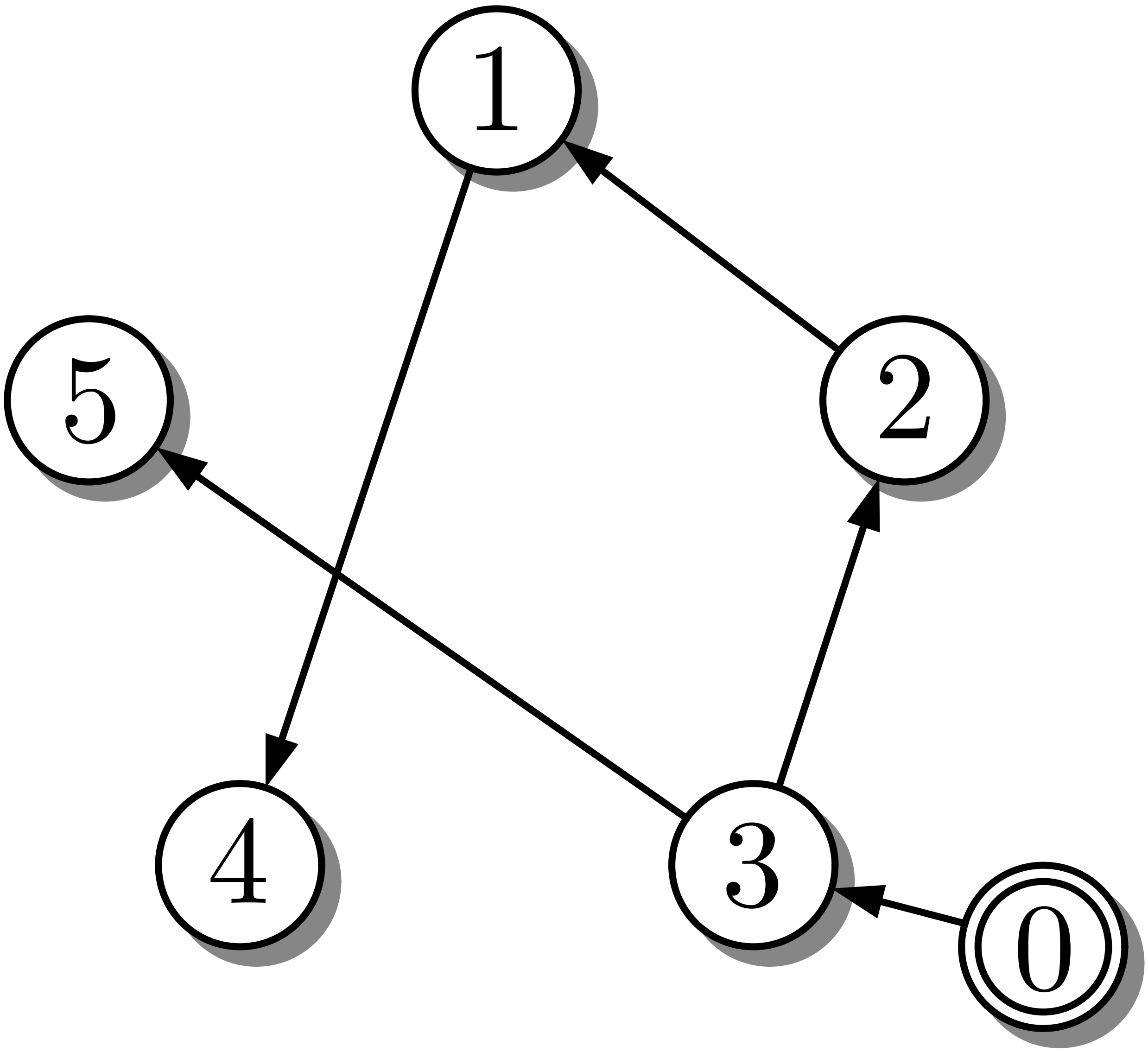

Fig. 8.15: Resulting effective communication graphs for command input at agent 3

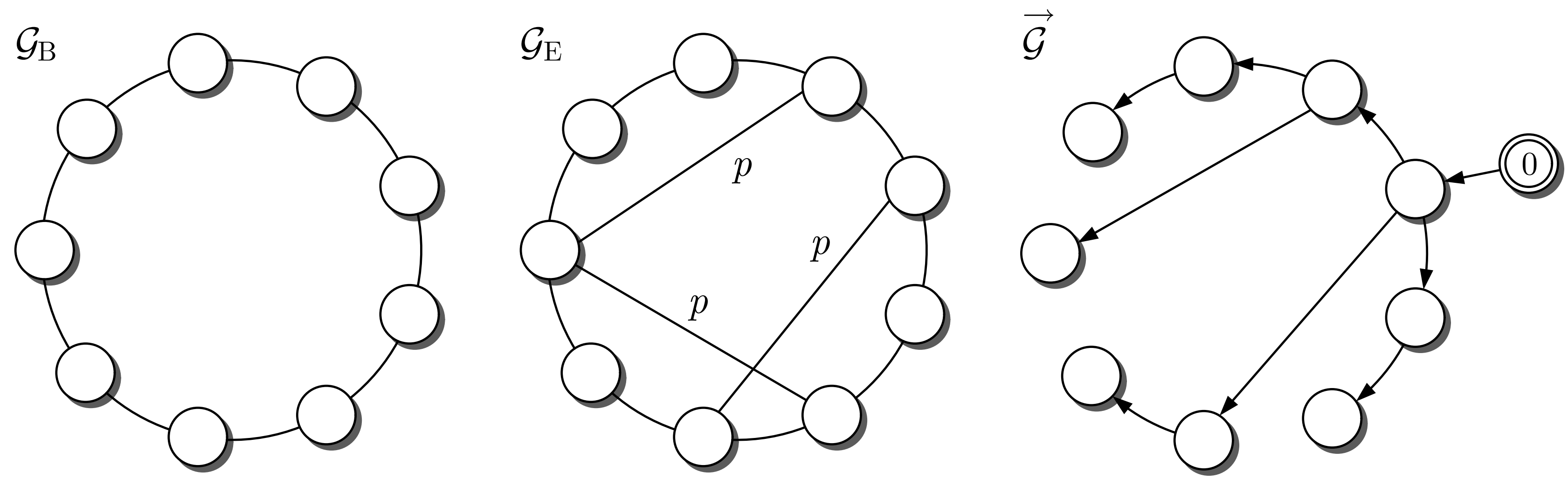

Fig. 8.16. Basic communication graph (left), extended communication graph (middle) and effective communication graph (right)

J. Lunze: *Networked Control of Multi-Agent Systems*, Edition MoRa 2022

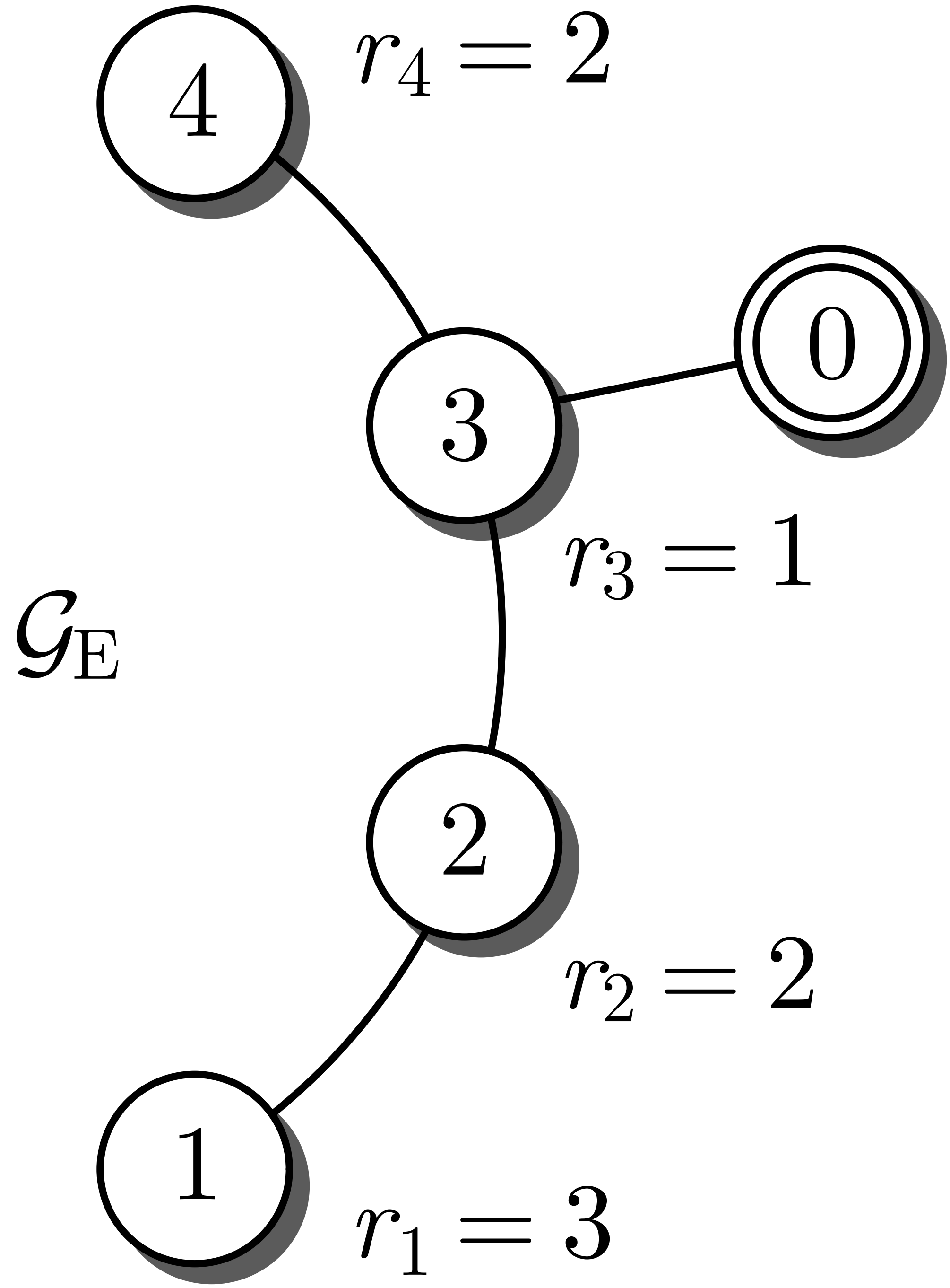

Fig. 8.17. Extended communication graph $\mathcal{G}_\mathrm{E}$ for entry point $l = 3$

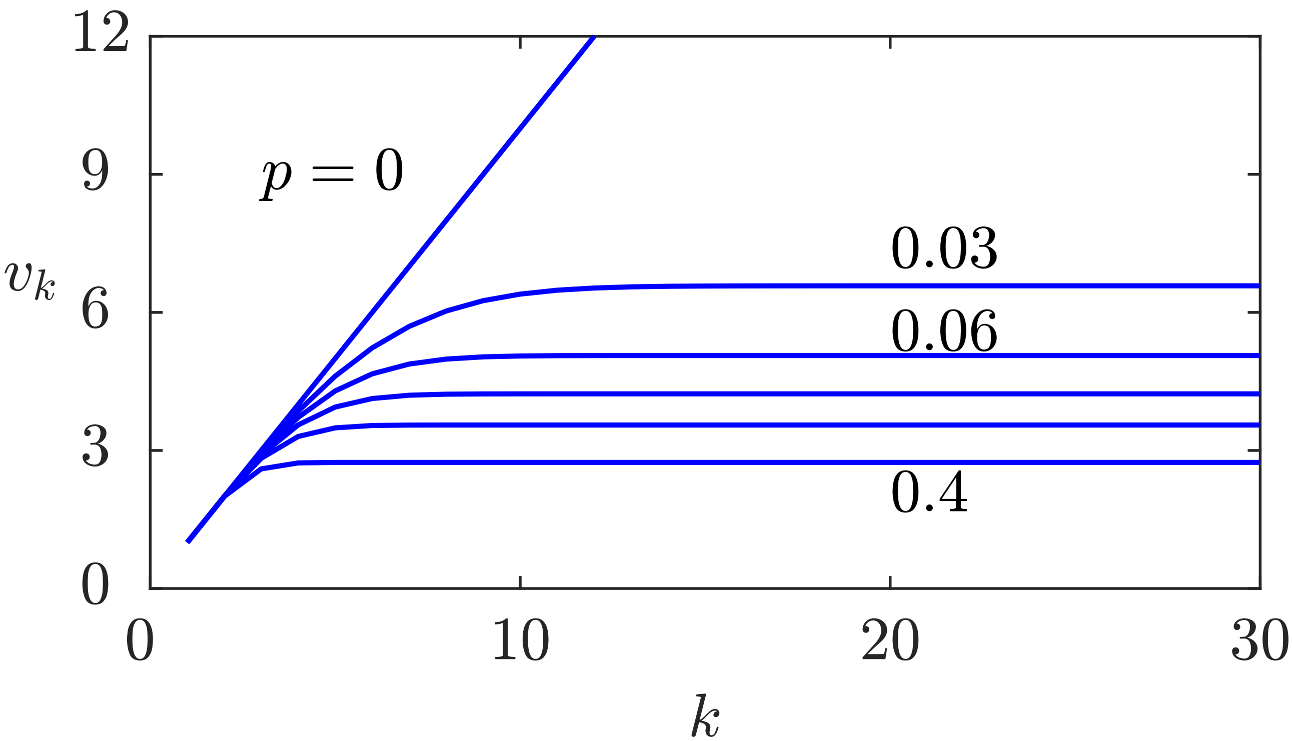

Fig. 8.18: Expected path length v_k for agents with the rank $k = 1, ..., 30$ with probability $p \in \{0, 0.03, 0.06, 0.1, 0.17, 0.4\}$

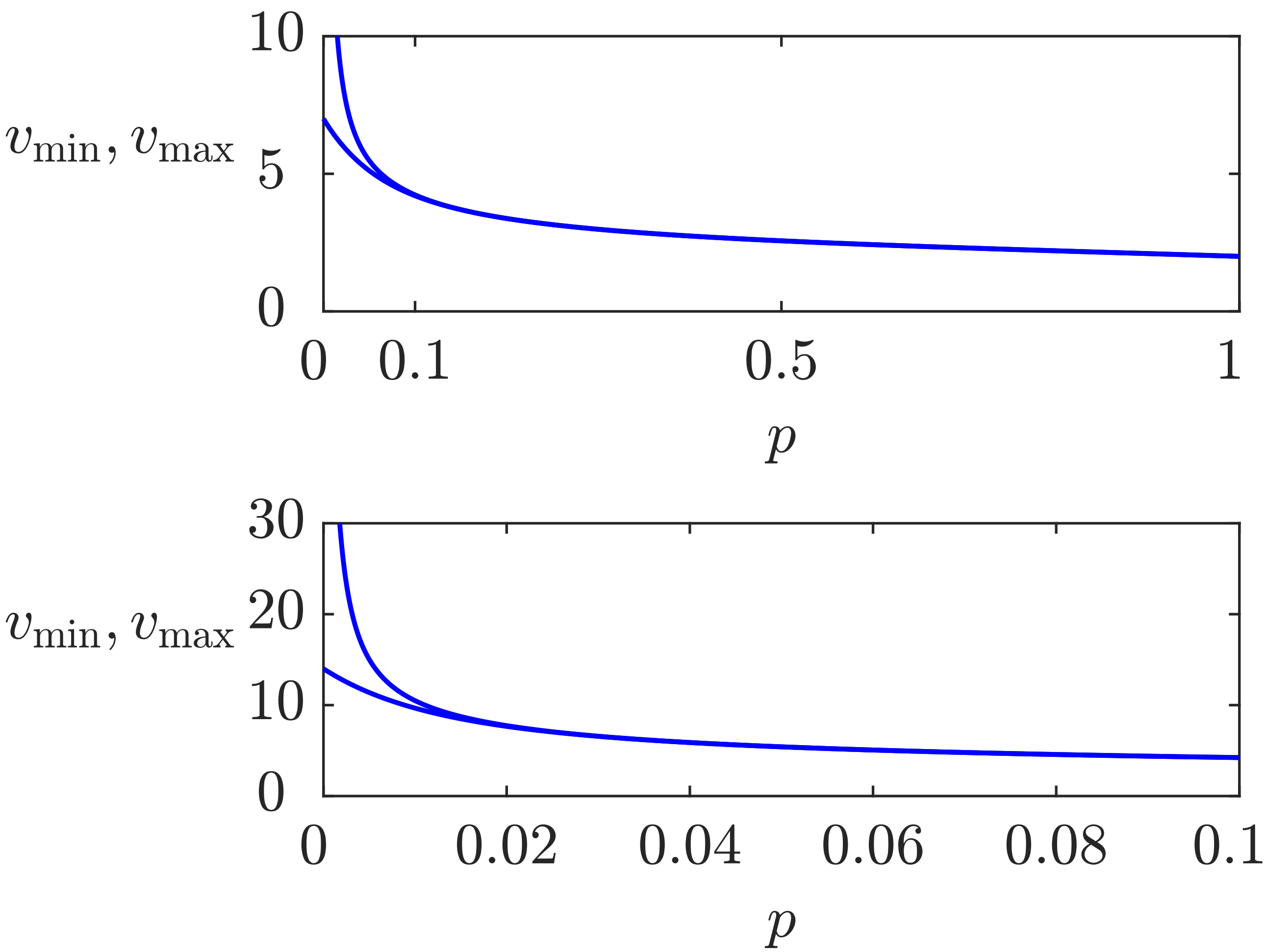

Fig. 8.19: Bound $\bar{v}$ of the expected path length

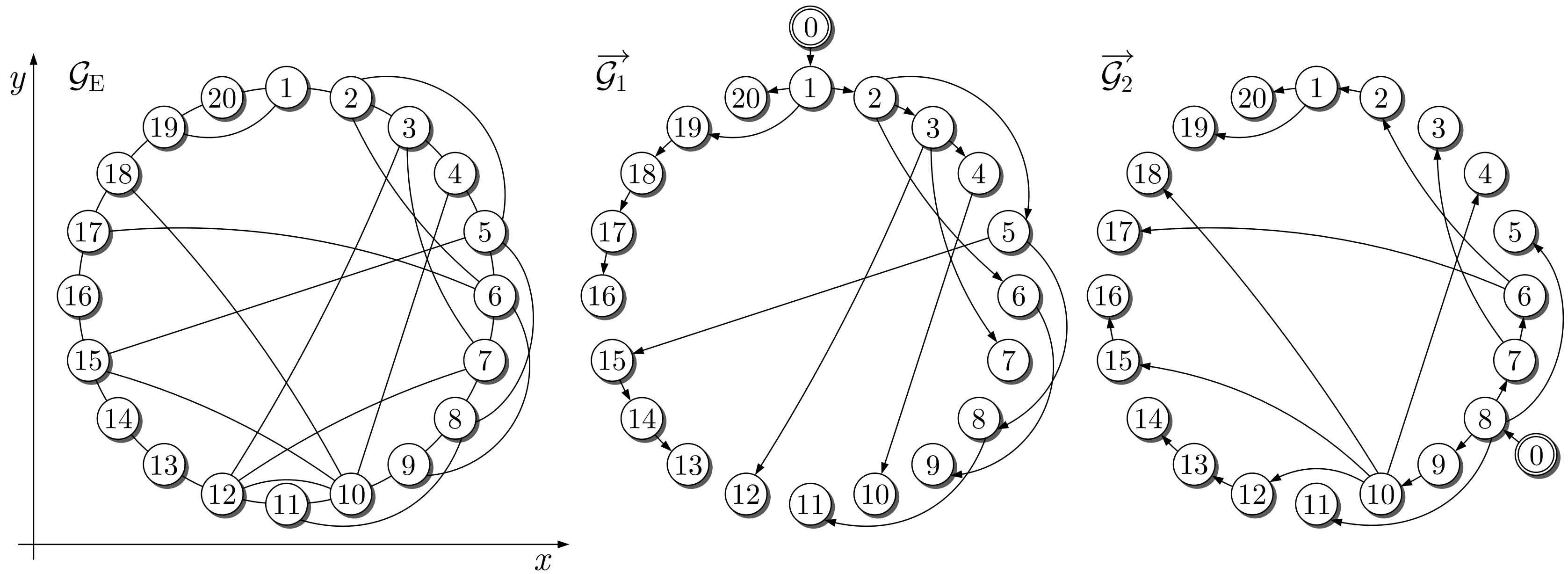

Fig. 8.20. Extended communication graph (left) and two effective communication graphs (middle and right)

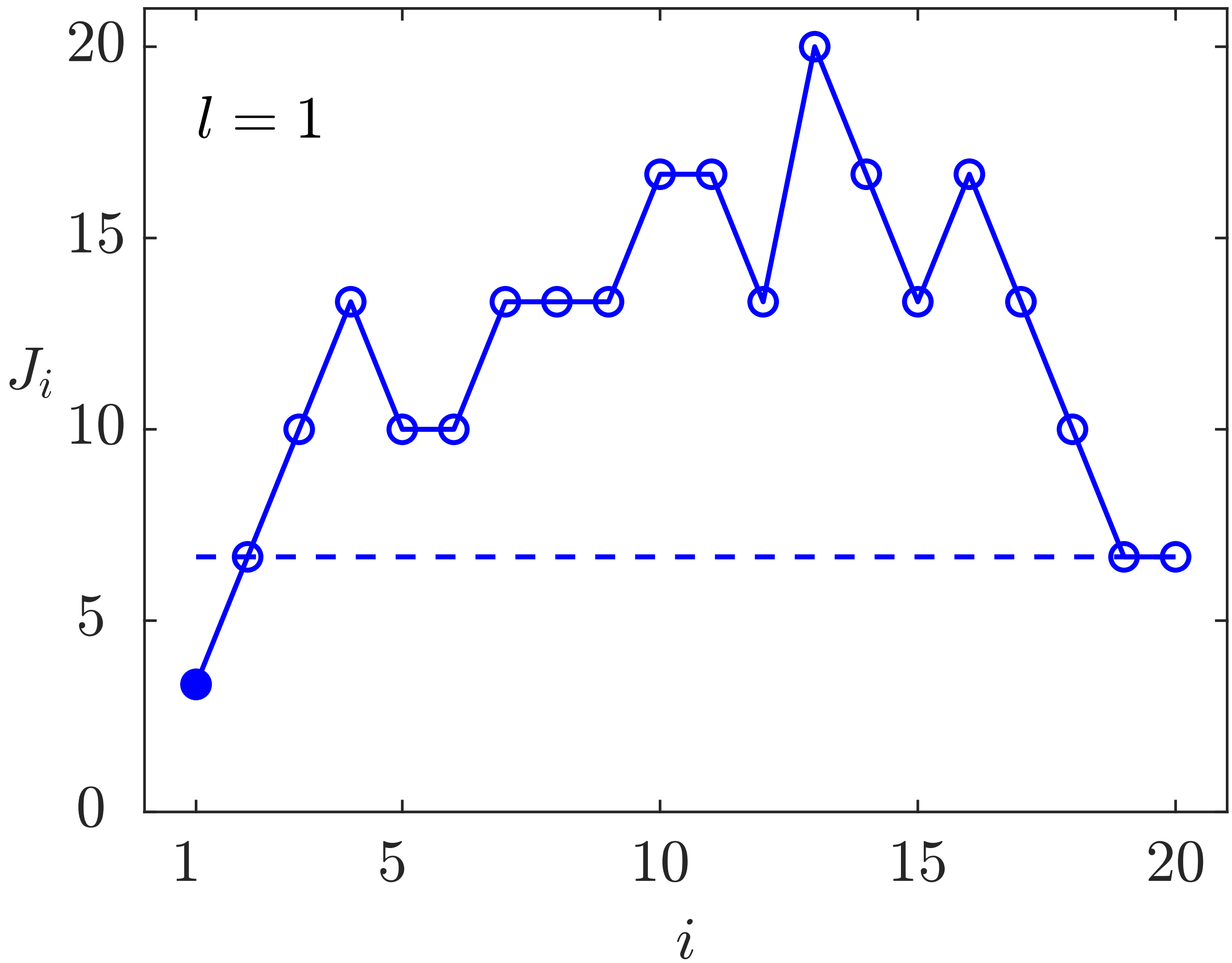

Fig. 8.21: Performance of the robots for two entry points of the leader marked by the filled dots (I)

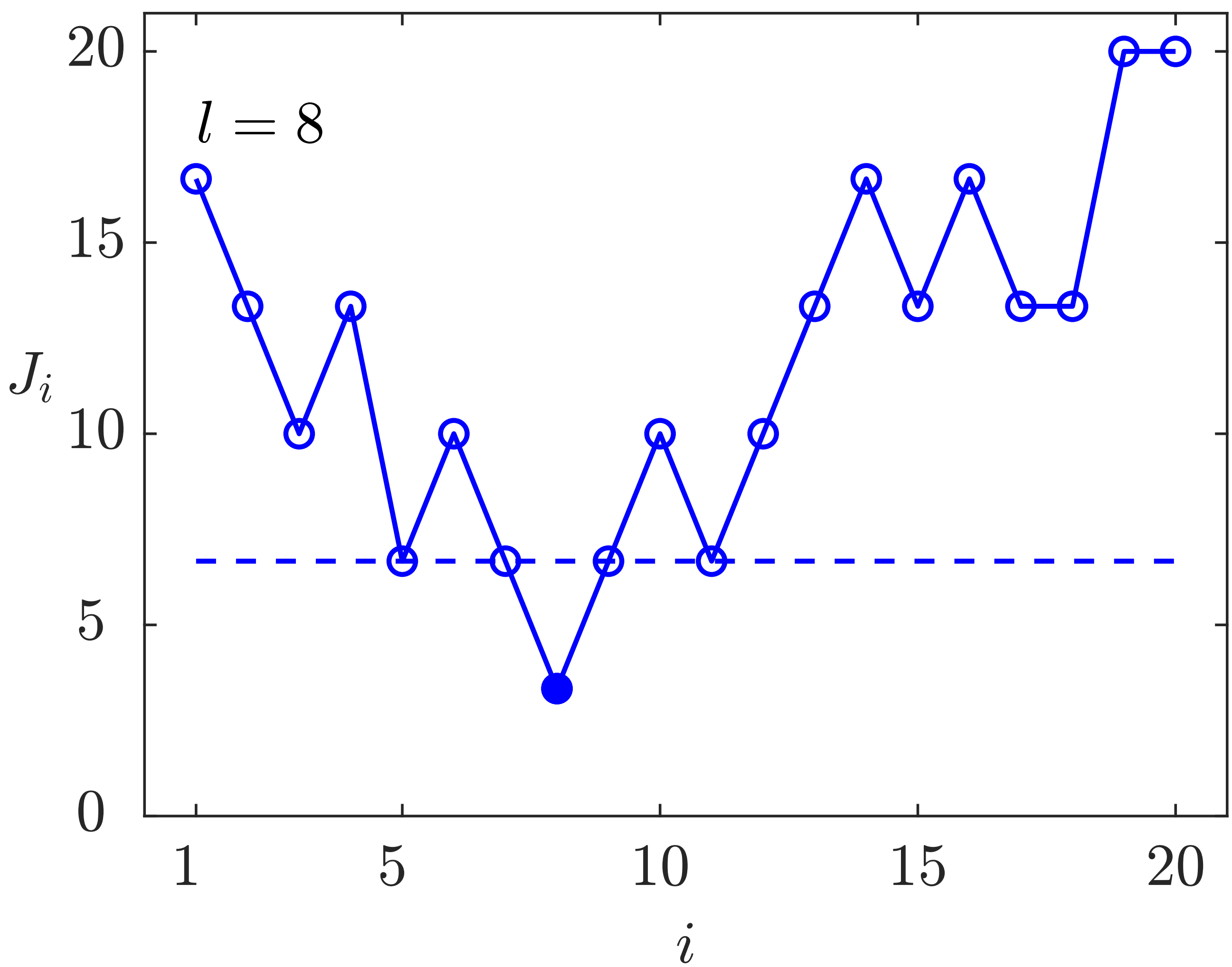

Fig. 8.21: Performance of the robots for two entry points of the leader marked by the filled dots (II)

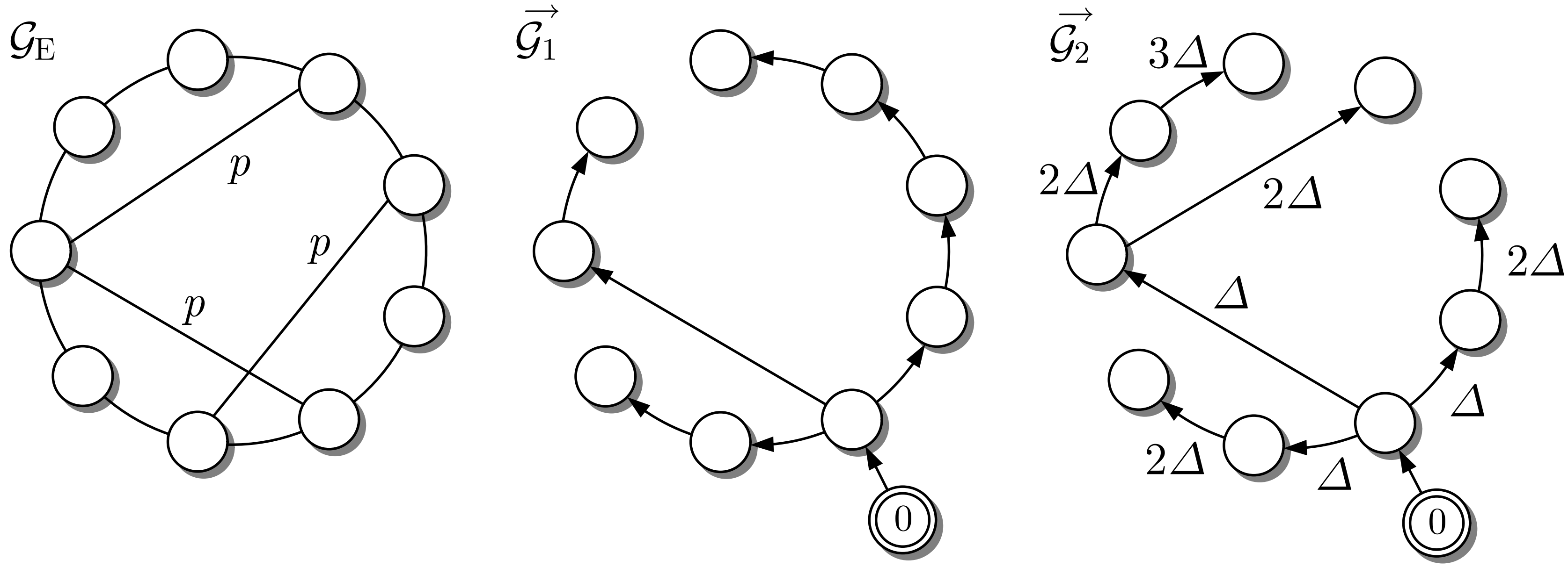

Fig. 8.22. Results of two methods to generate the effective communication graph

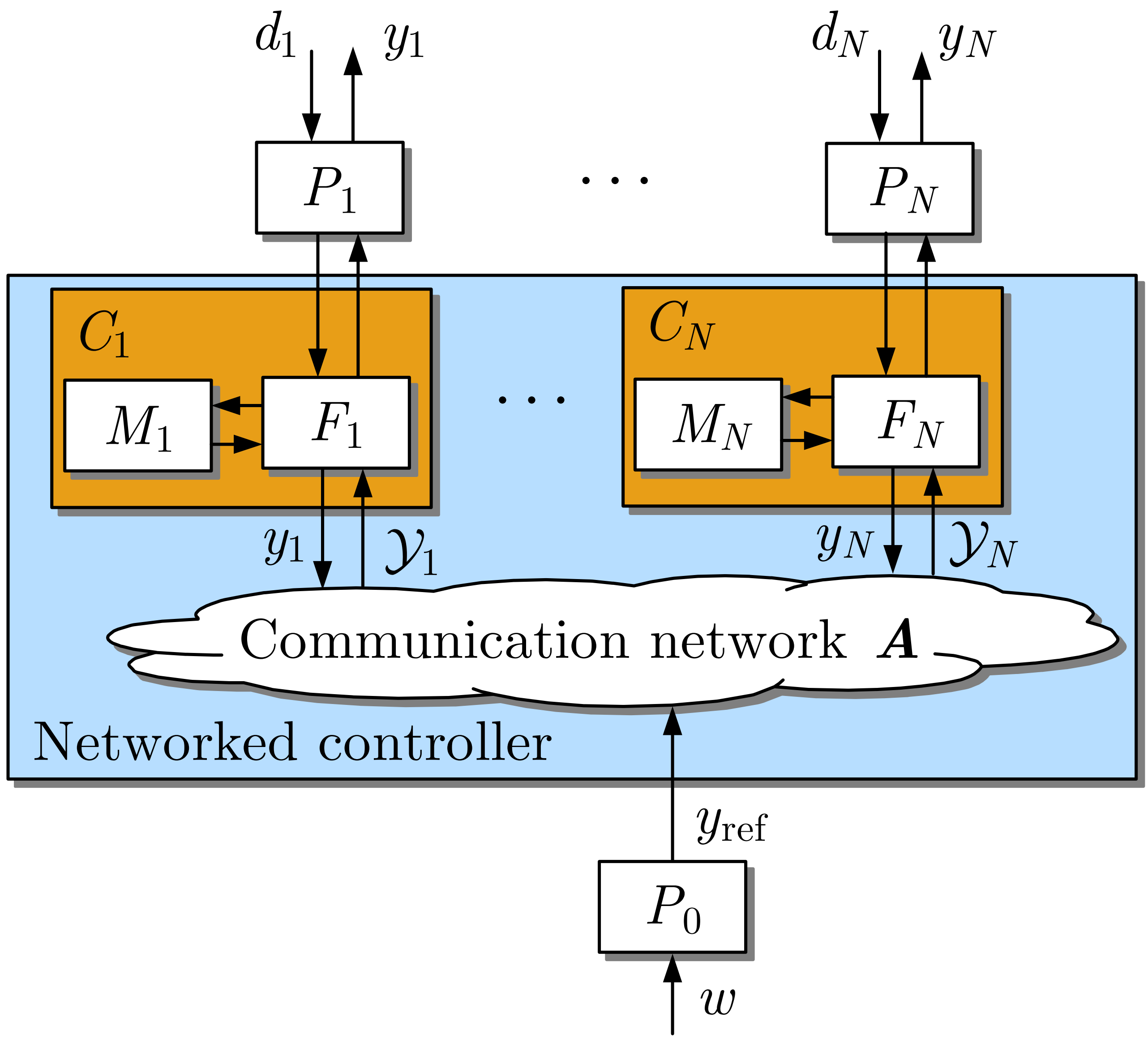

Fig. 8.23: Self-organising disturbance attenuation

J. Lunze: *Networked Control of Multi-Agent Systems*, Edition MoRa 2022

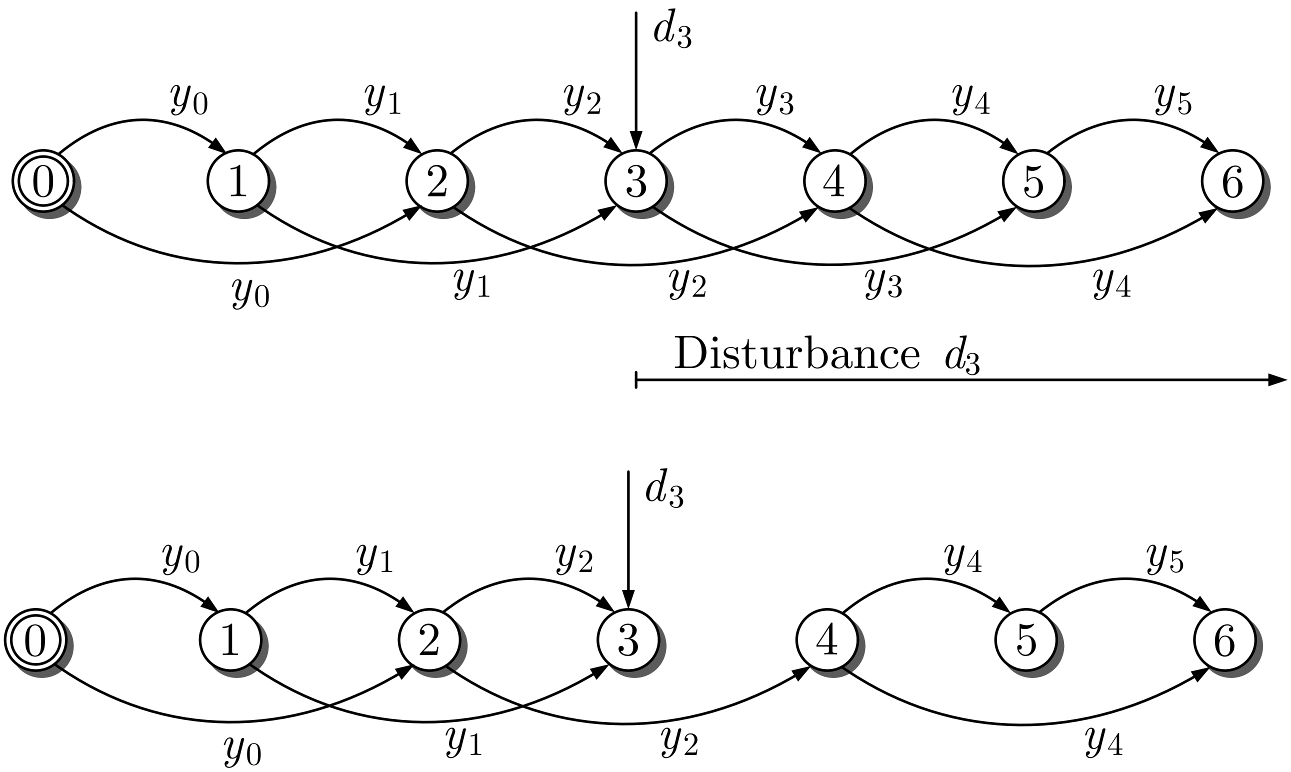

Fig. 8.24: Communication structure of the networked system

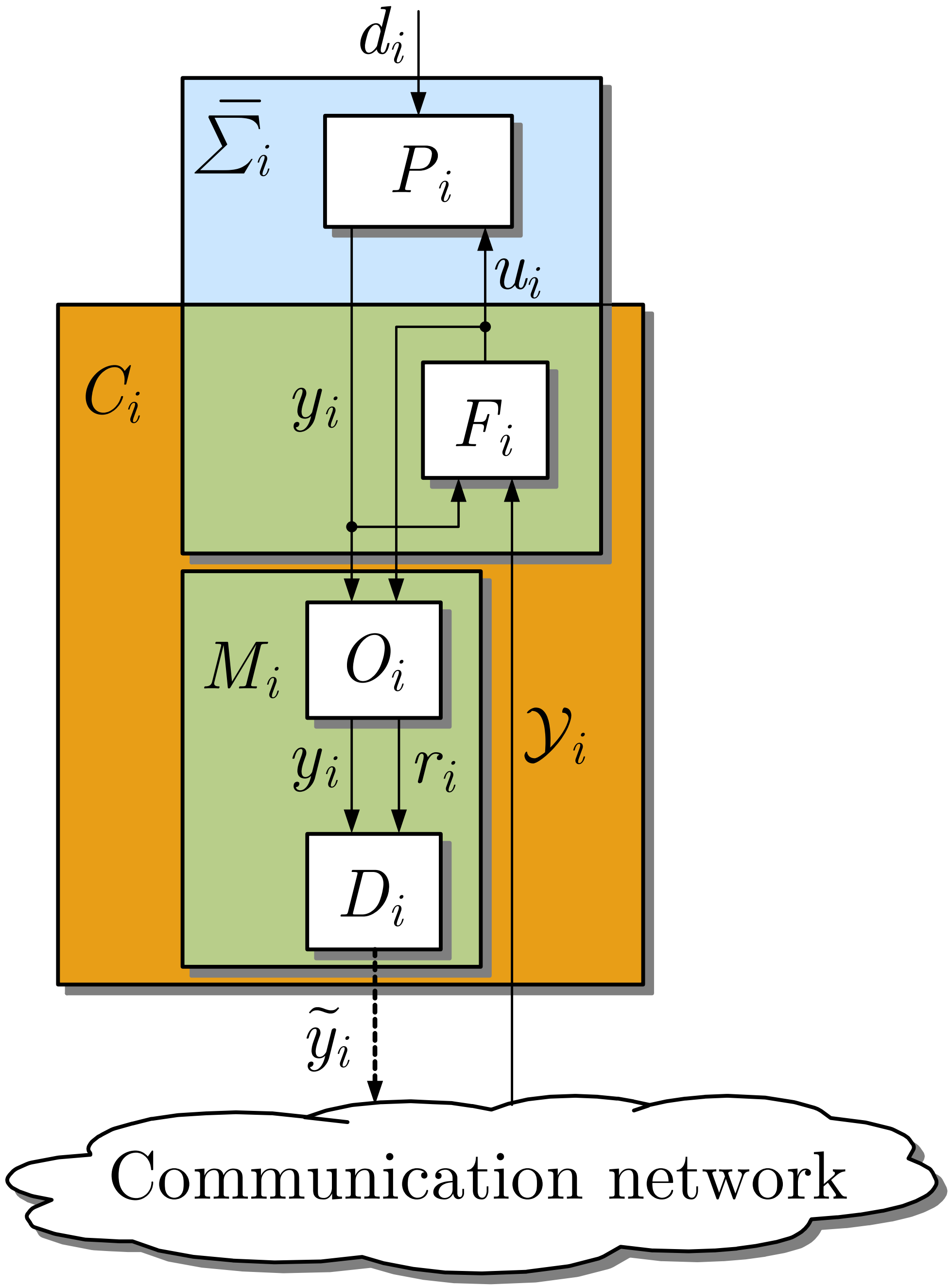

Fig. 8.25. Analysis of a single agent

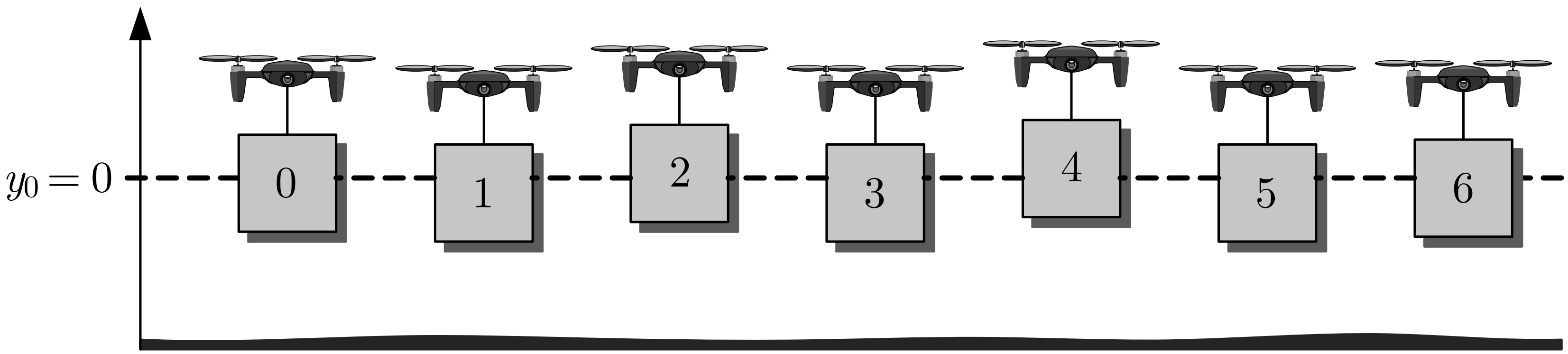

Fig. 8.26. Formation of flying multirotors

J. Lunze: *Networked Control of Multi-Agent Systems*, Edition MoRa 2022

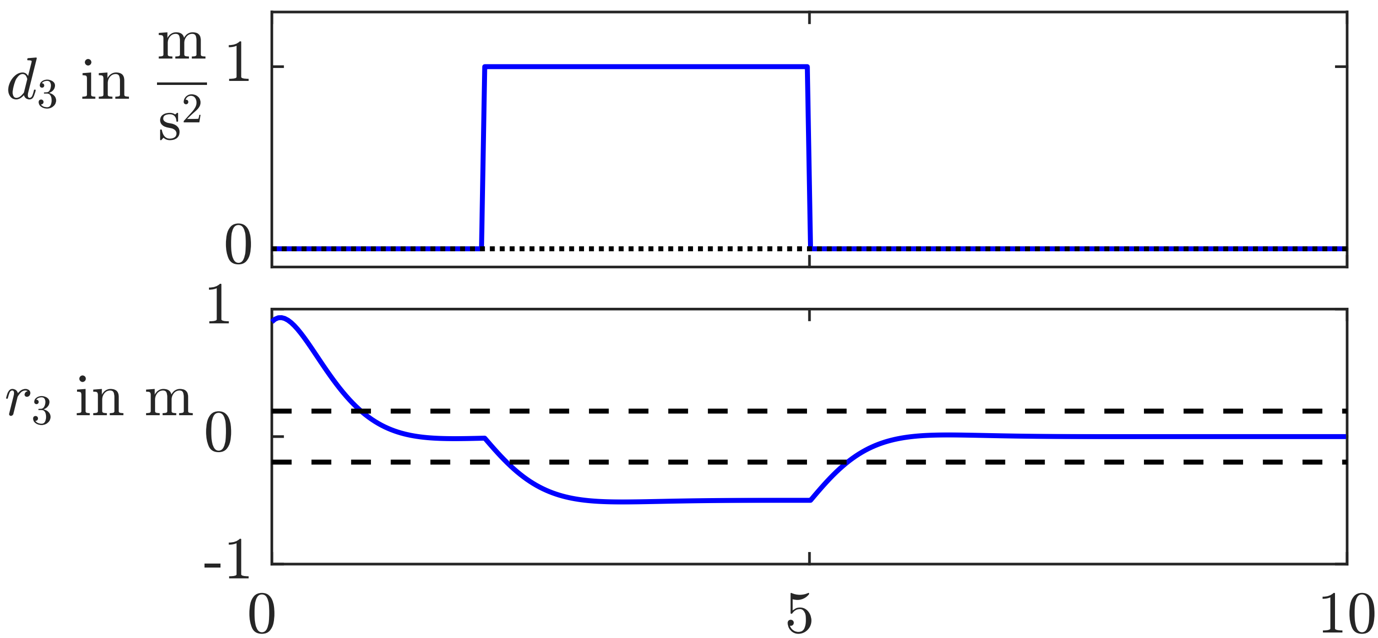

Fig. 8.27: Reconstruction of the disturbance effect on the output $y_3(t)$ of the third multirotor

J. Lunze: *Networked Control of Multi-Agent Systems,* Edition MoRa 2022

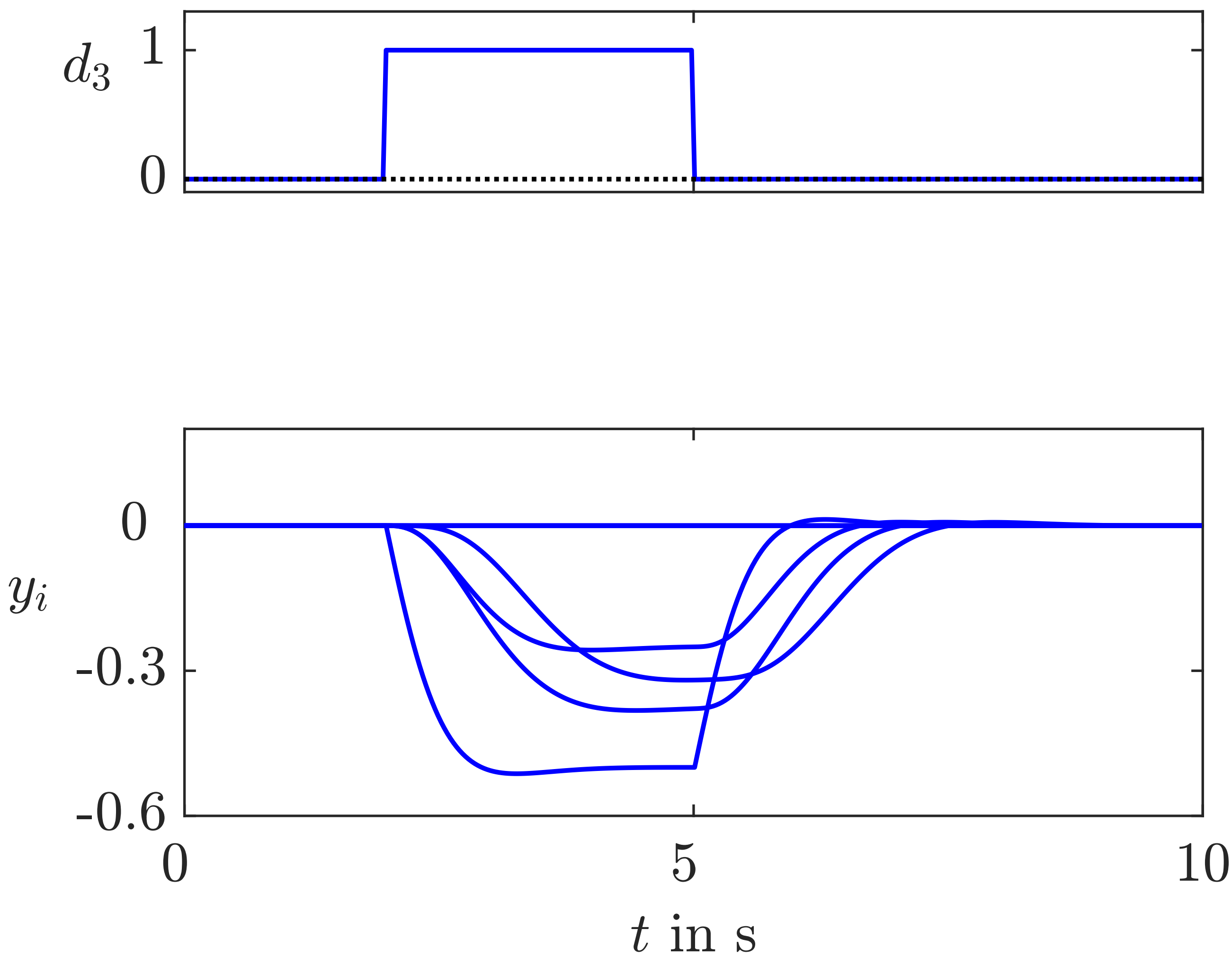

Fig. 8.28: Effect of the disturbance $d_3(t)$ on the whole fleet with complete networked controller

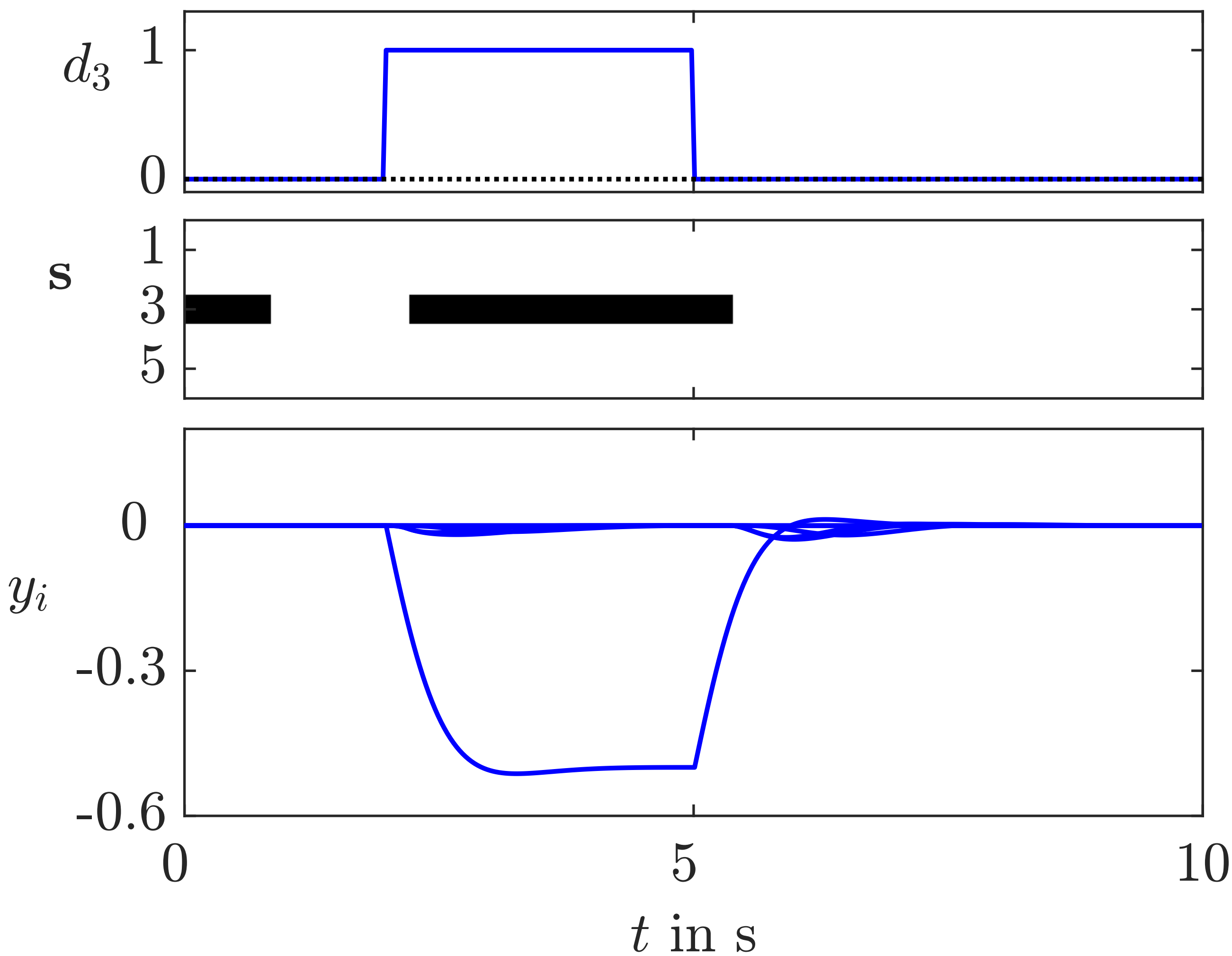

Fig. 8.28: Effect of the disturbance $d_3(t)$ on the whole fleet with switching controller

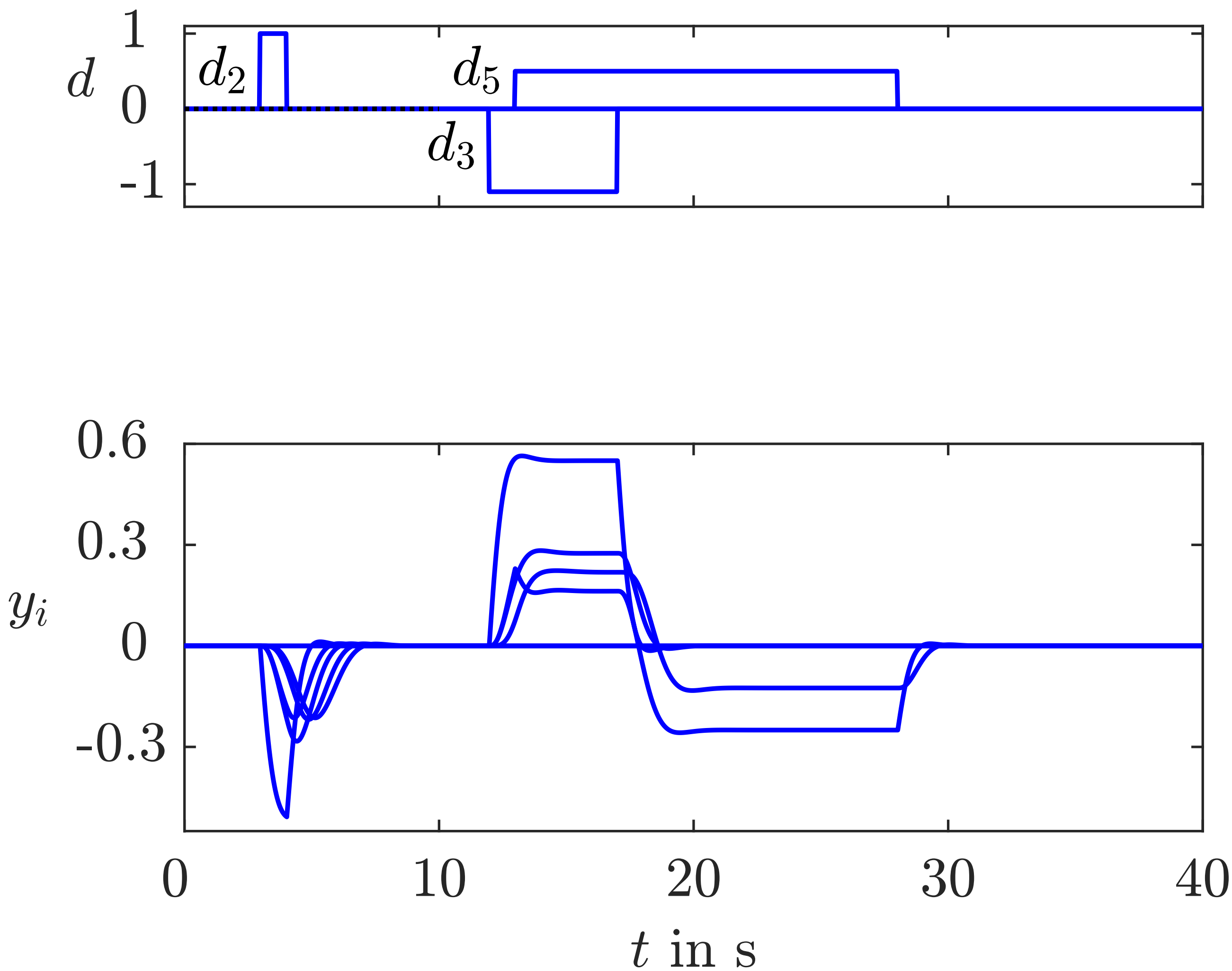

Fig. 8.29: Effect of several disturbances on the multirotor fleet with non-switching controller

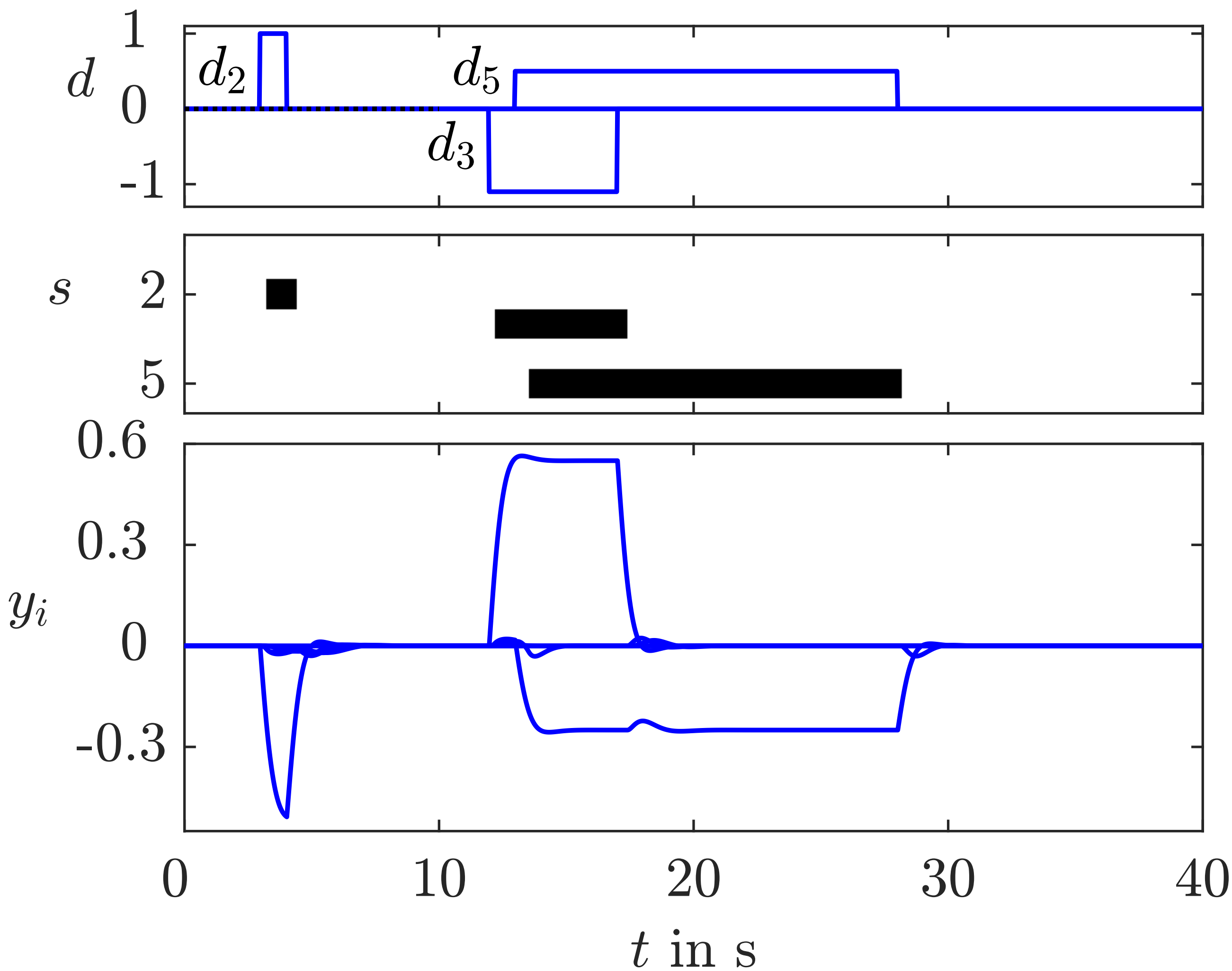

Fig. 8.29: Effect of several disturbances on the multirotor fleet with switching controller

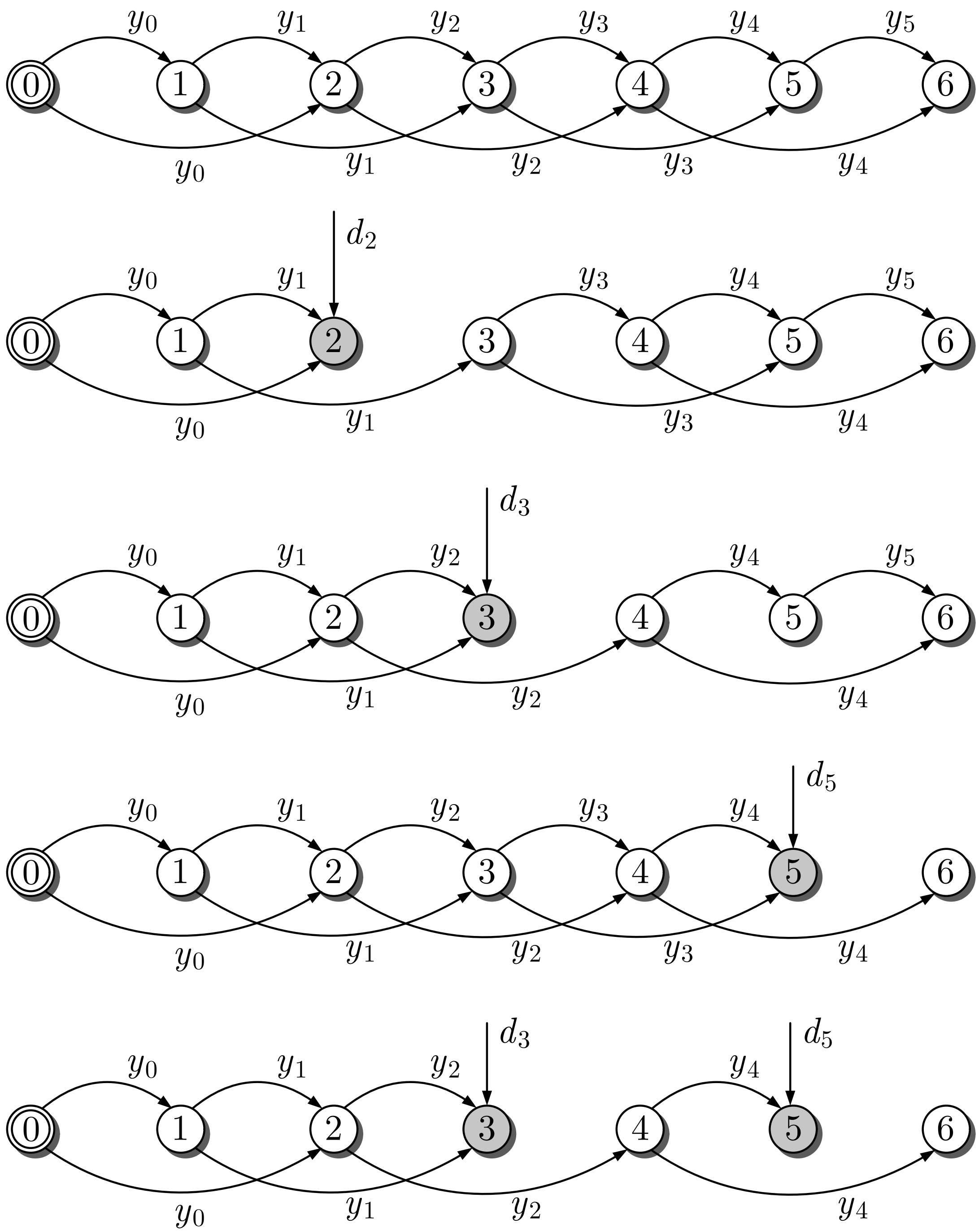

Fig. 8.30. Five structures of the networked controller that appear due to various disturbance situations

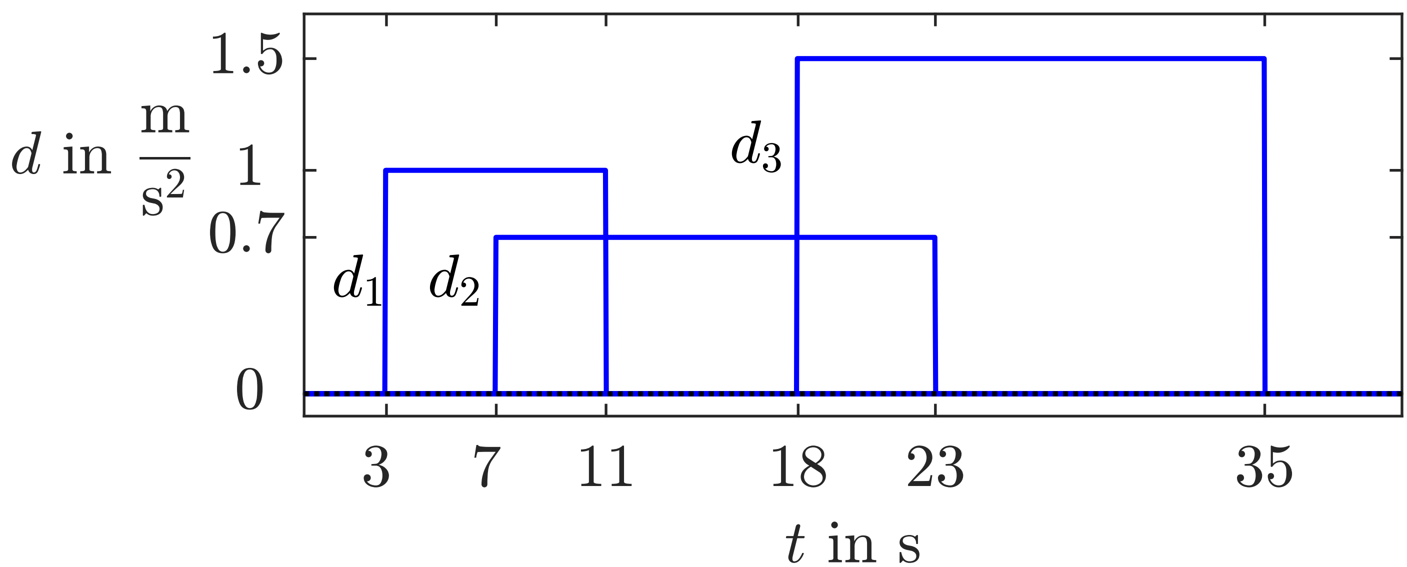

Fig. 8.31: Three piecewise constant disturbances acting on neighbouring multirotors

J. Lunze: *Networked Control of Multi-Agent Systems*, Edition MoRa 2022

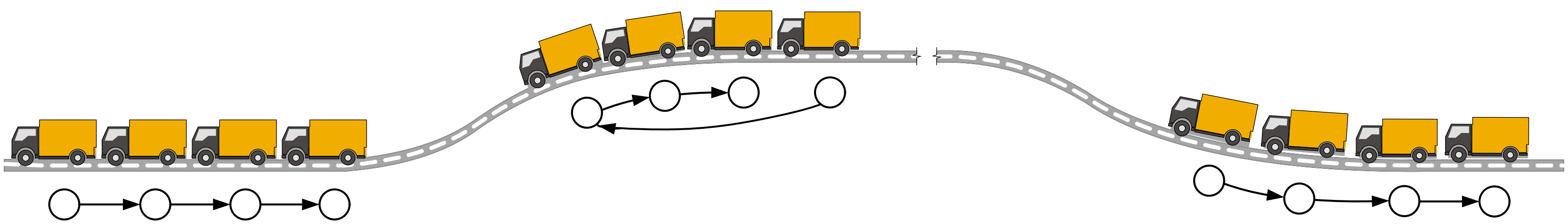

Fig. 8.32. Truck platoon in a hilly terrain

J. Lunze: *Networked Control of Multi-Agent Systems*, Edition MoRa 2022

page 481

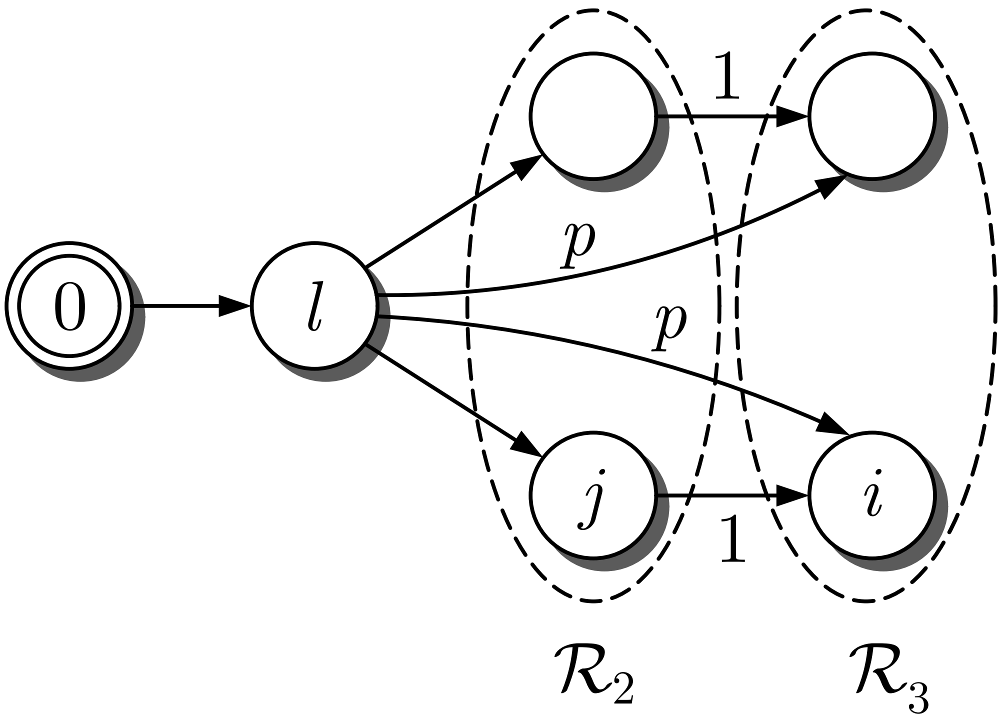

Fig. 8.33: Determination of the expected path length towards agents in the set $\mathcal{R}_3$

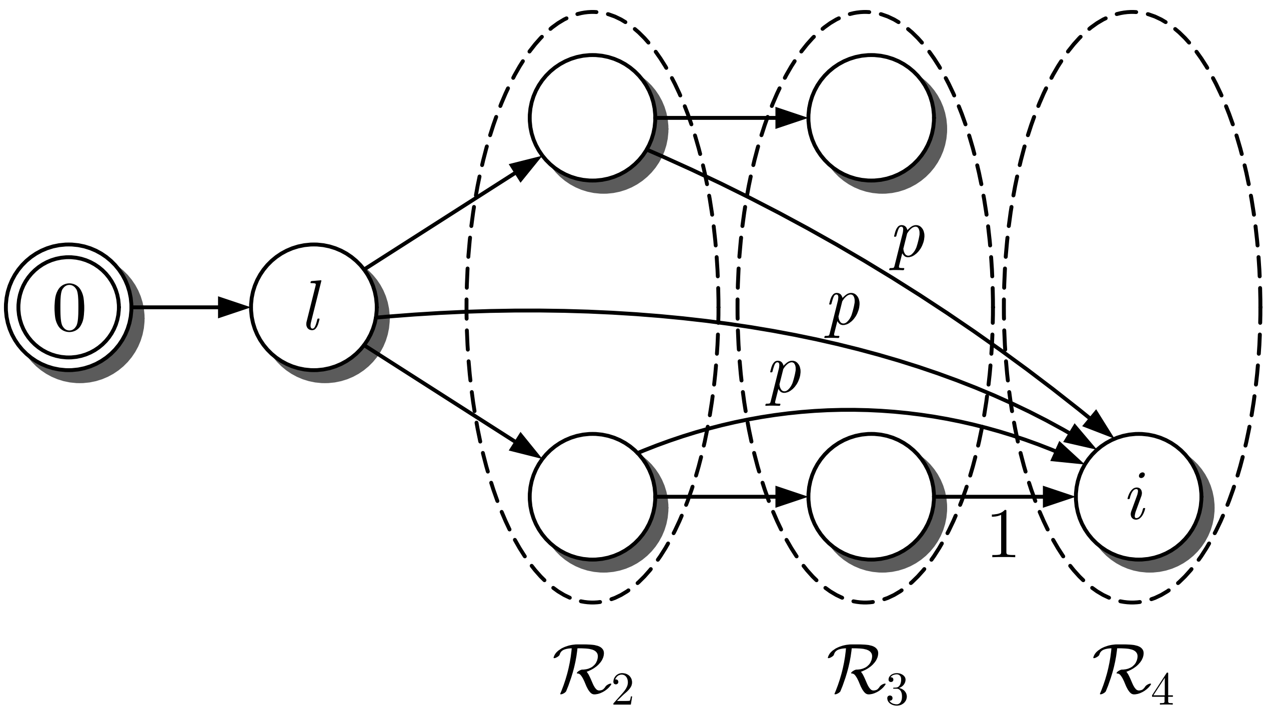

Fig. 8.34: Determination of the expected path length towards agents in the set $\mathcal{R}_4$

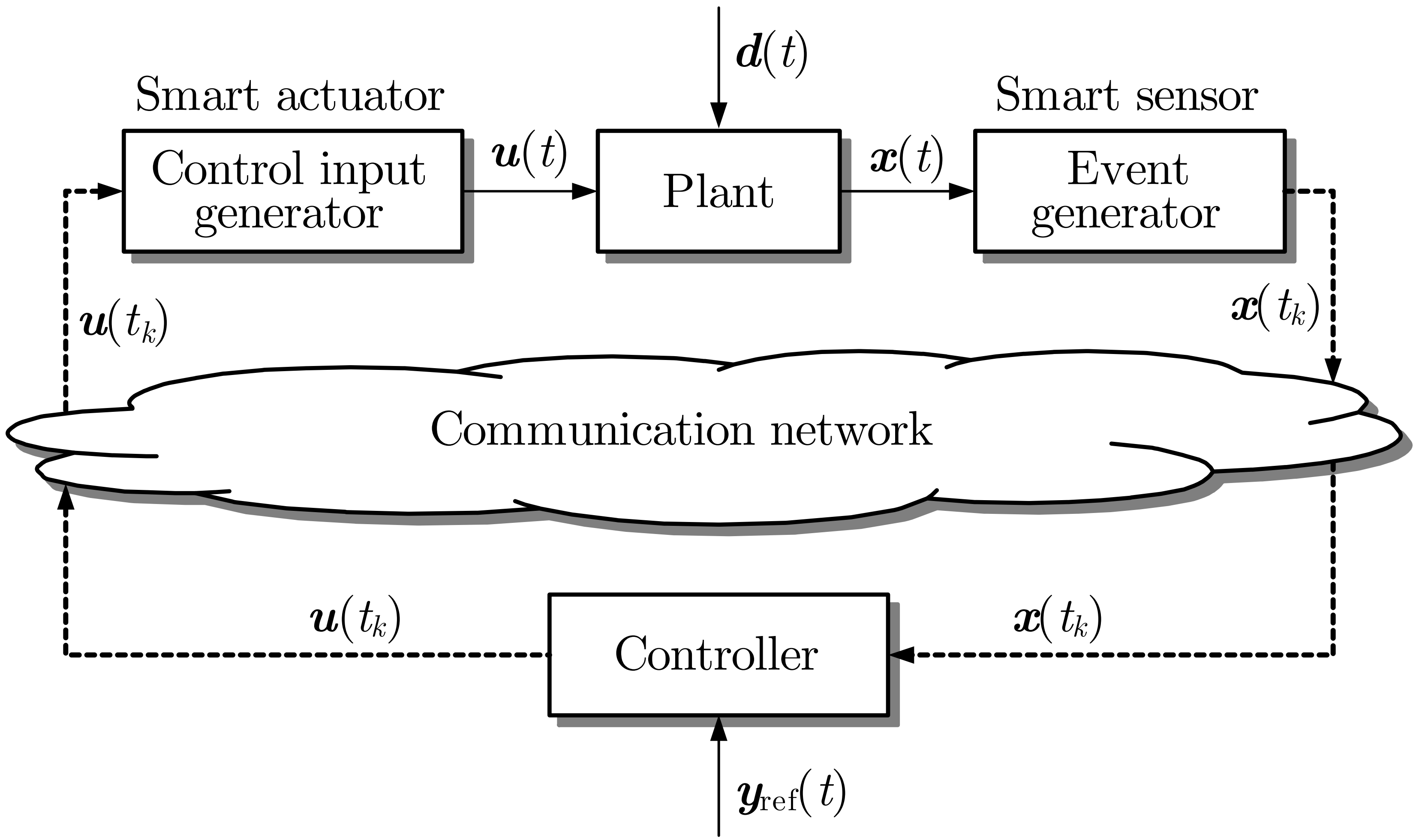

Fig. 9.1. Event-triggered control loop

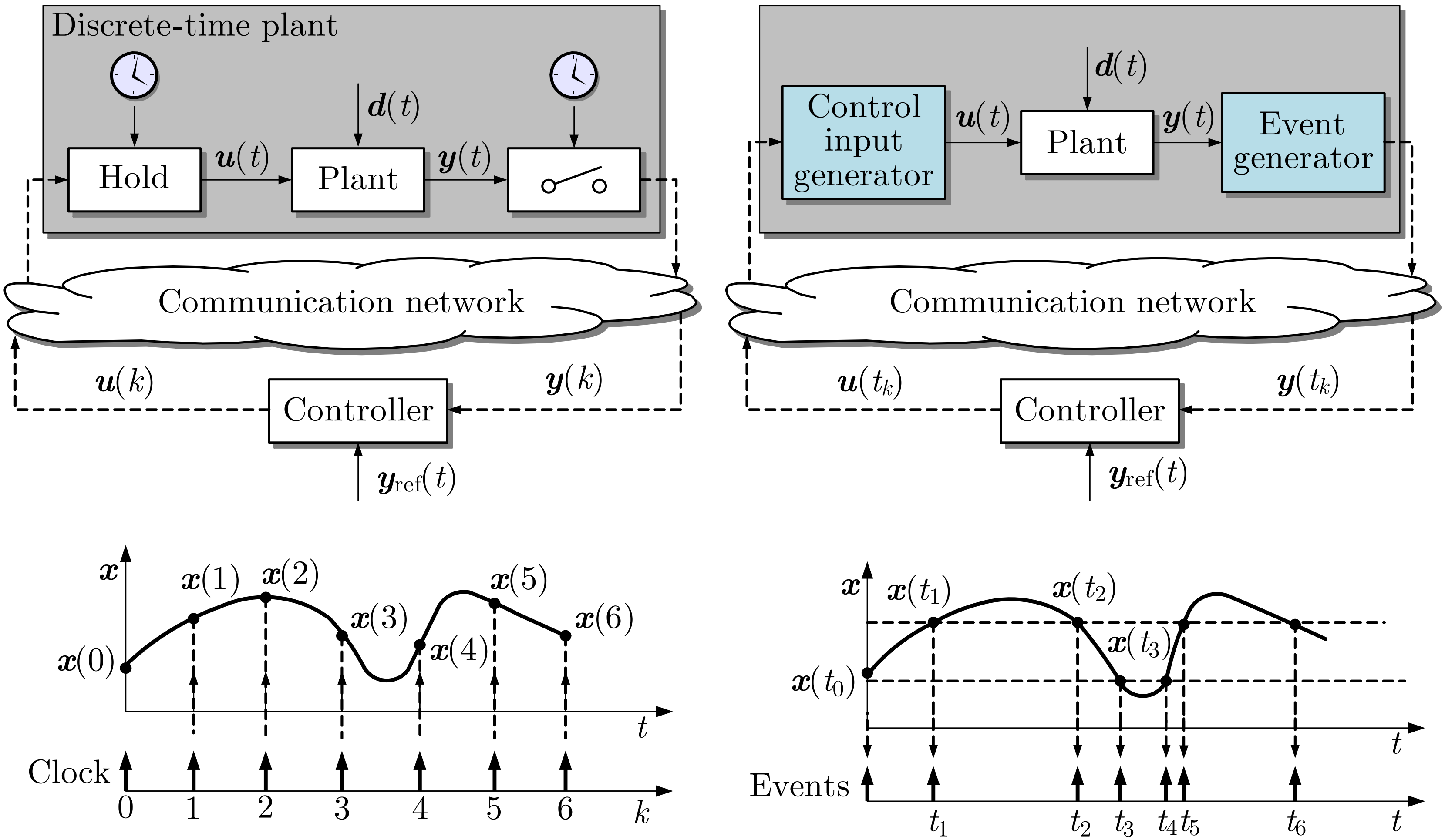

Fig. 9.2. Sampled-data vs. event-triggered control loop

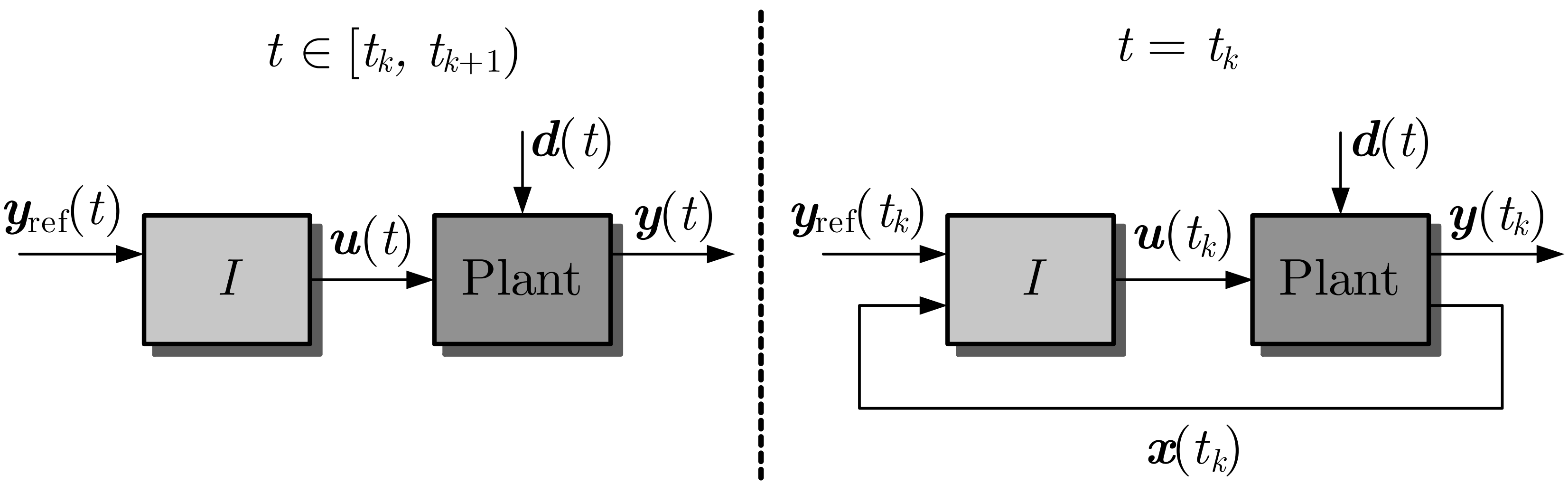

Fig. 9.3. Open-loop control vs. closed-loop control

J. Lunze: *Networked Control of Multi-Agent Systems,* Edition MoRa 2022

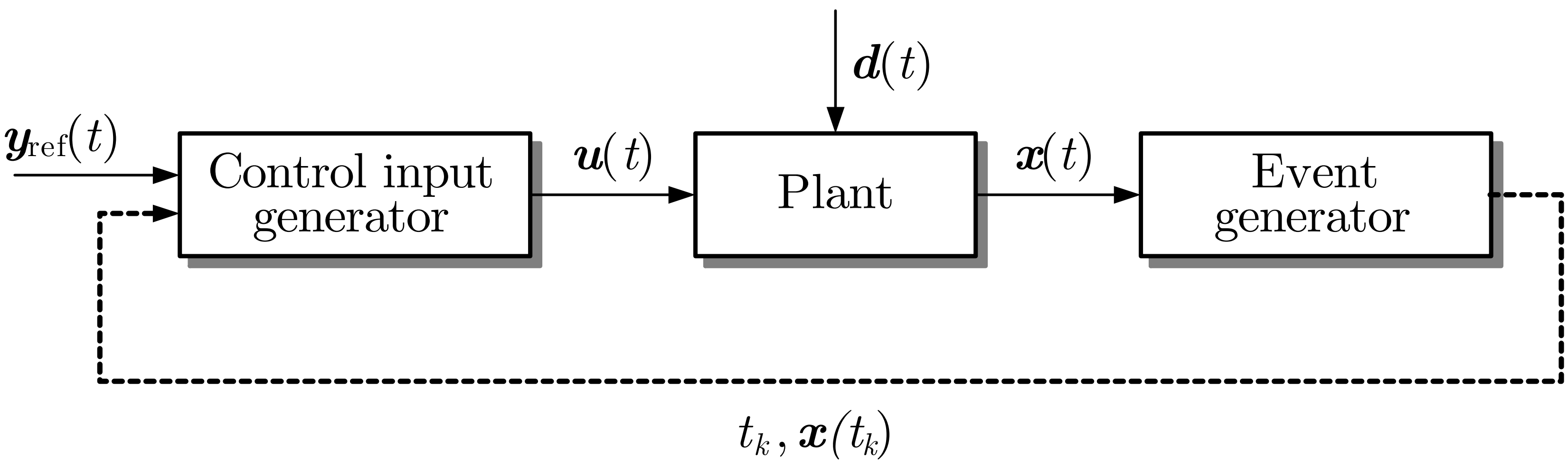

Fig. 9.4. Simplified event-triggered control loop

J. Lunze: *Networked Control of Multi-Agent Systems*, Edition MoRa 2022

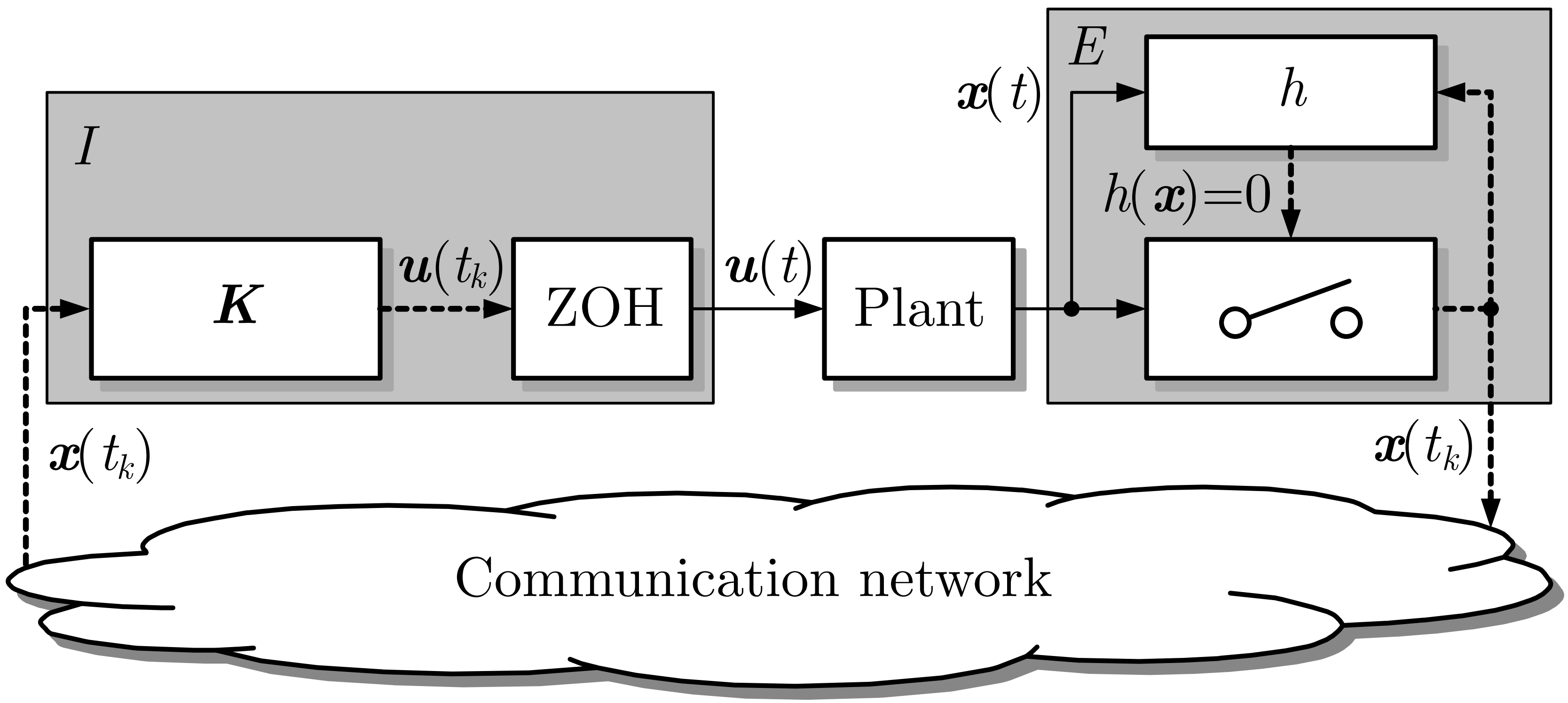

Fig. 9.5. Event-triggered control loop showing the event generation mechanism

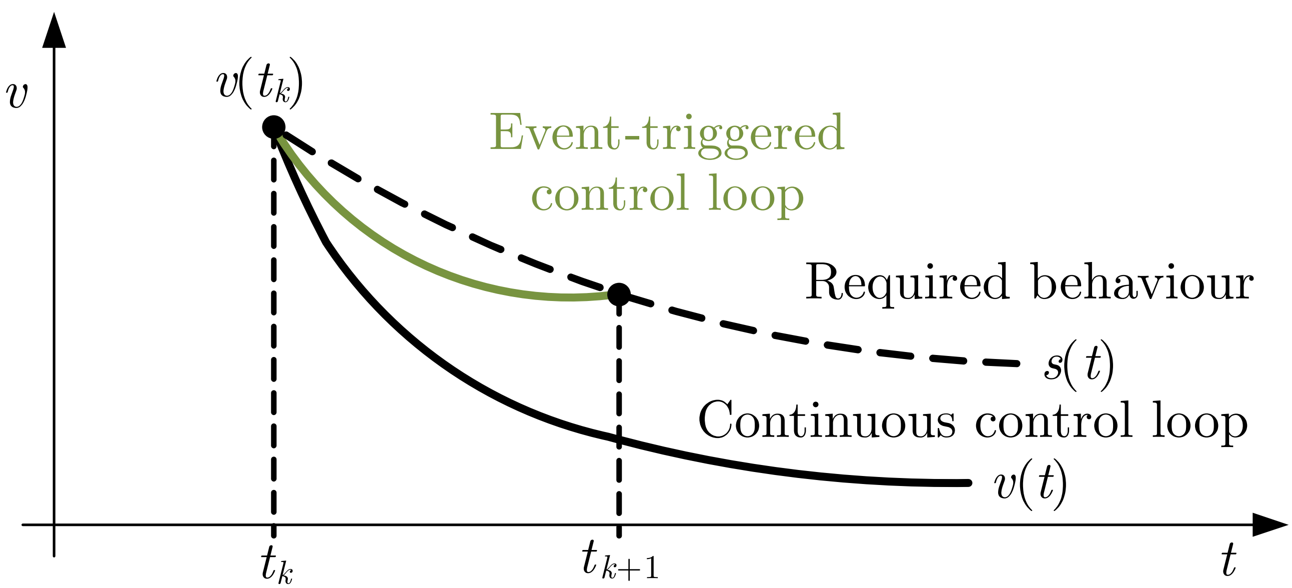

Fig. 9.6: Determination of the next sampling instant

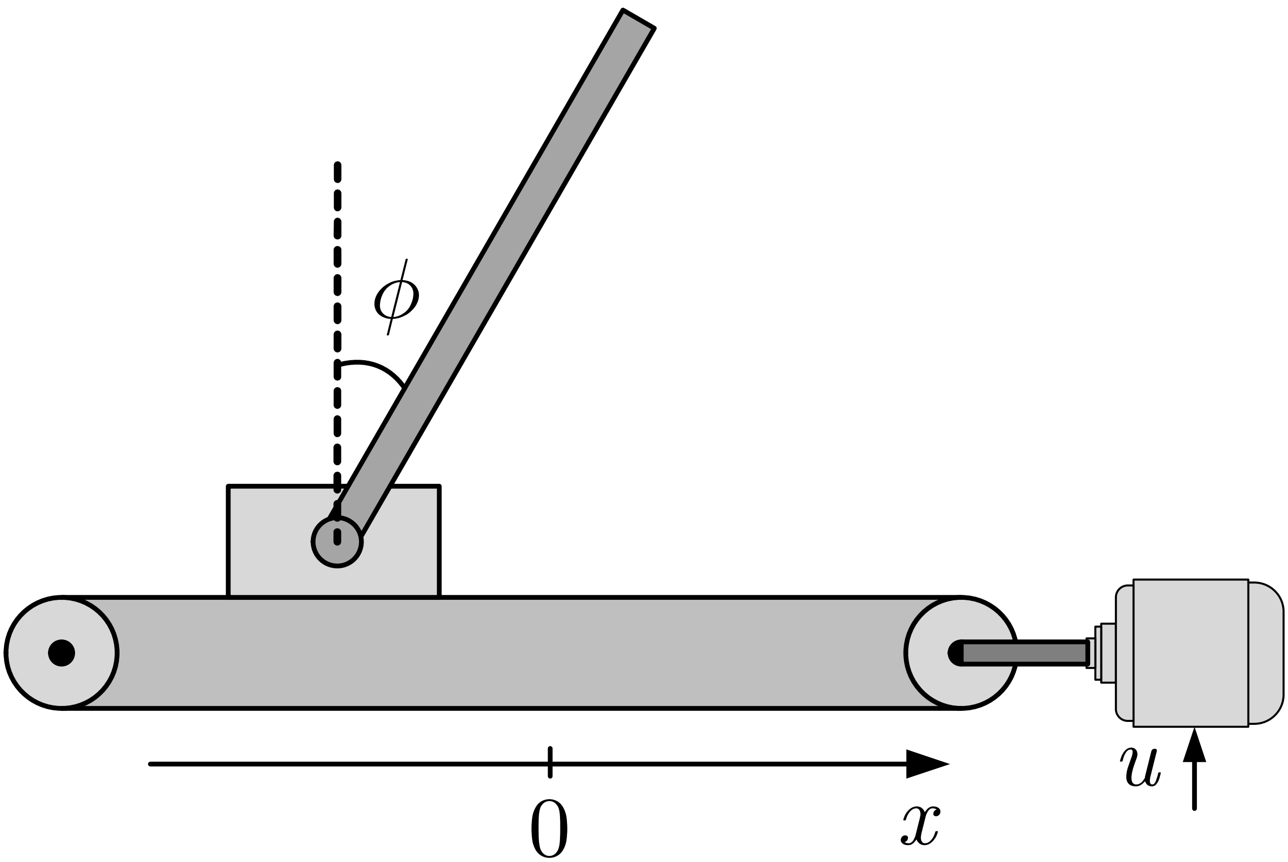

Fig. 9.7: Inverted pendulum

J. Lunze: *Networked Control of Multi-Agent Systems*, Edition MoRa 2022

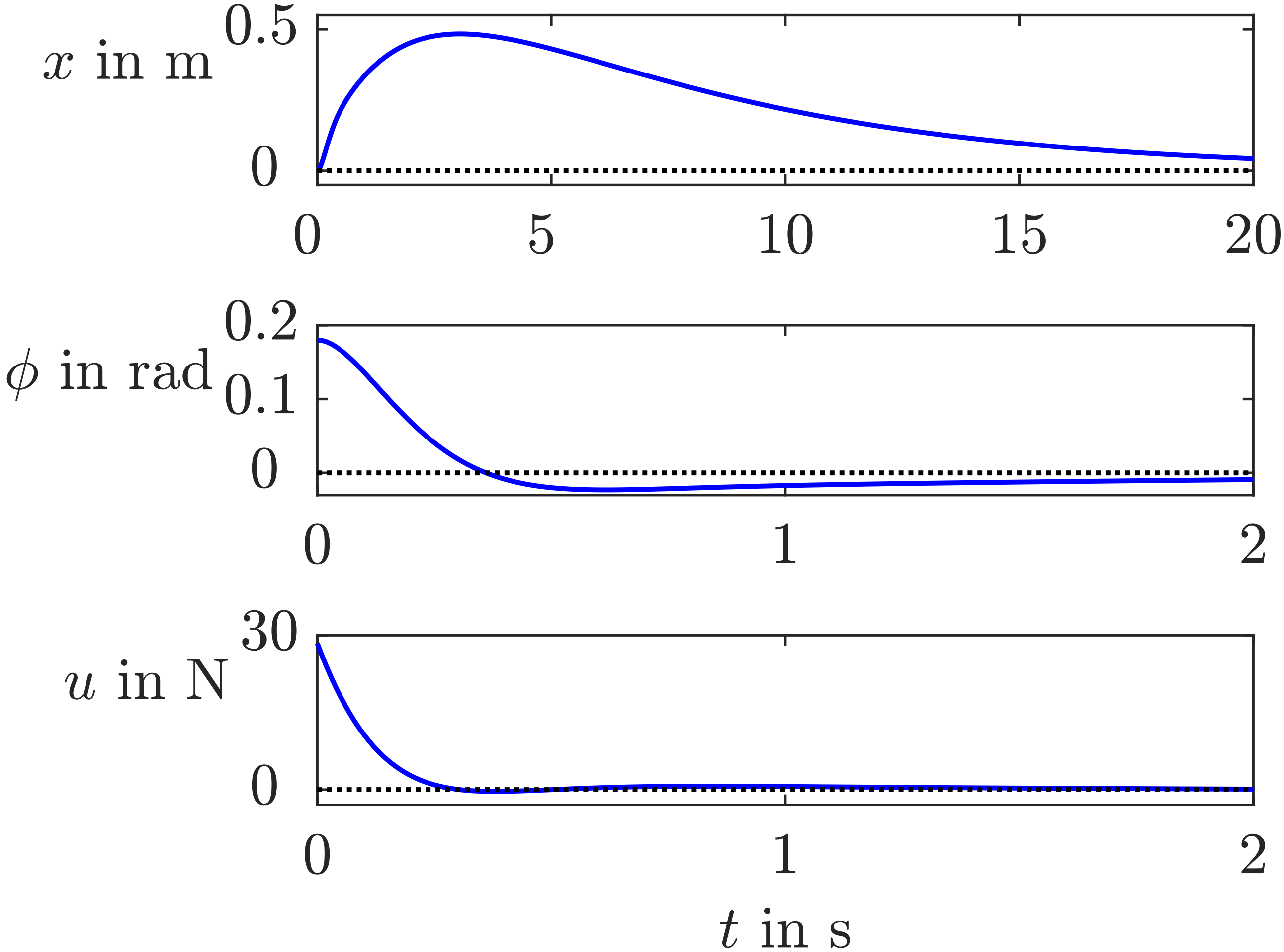

Fig. 9.8: Behaviour of the pendulum with continuous state-feedback controller

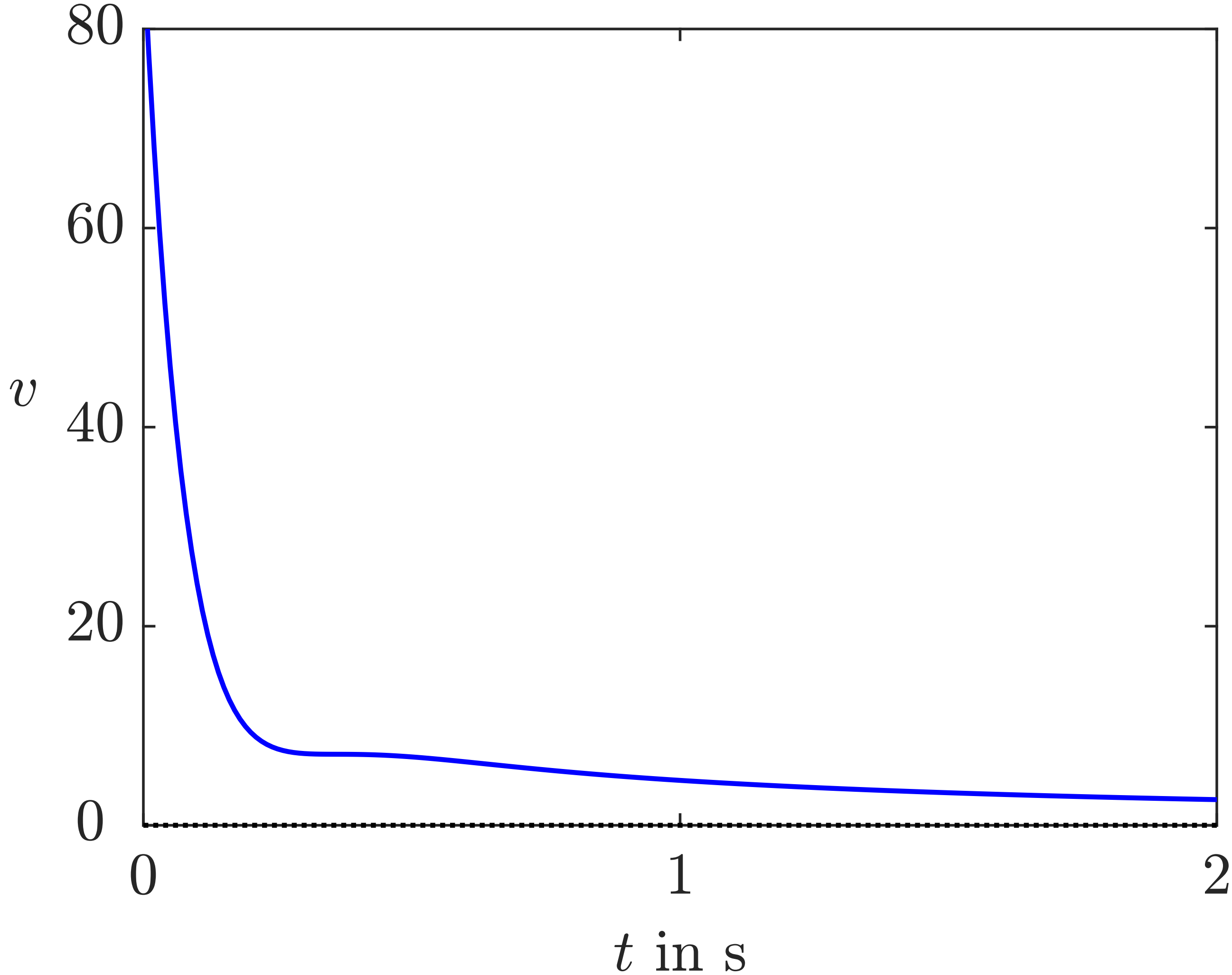

Fig. 9.8: Behaviour of the pendulum with continuous state-feedback controller

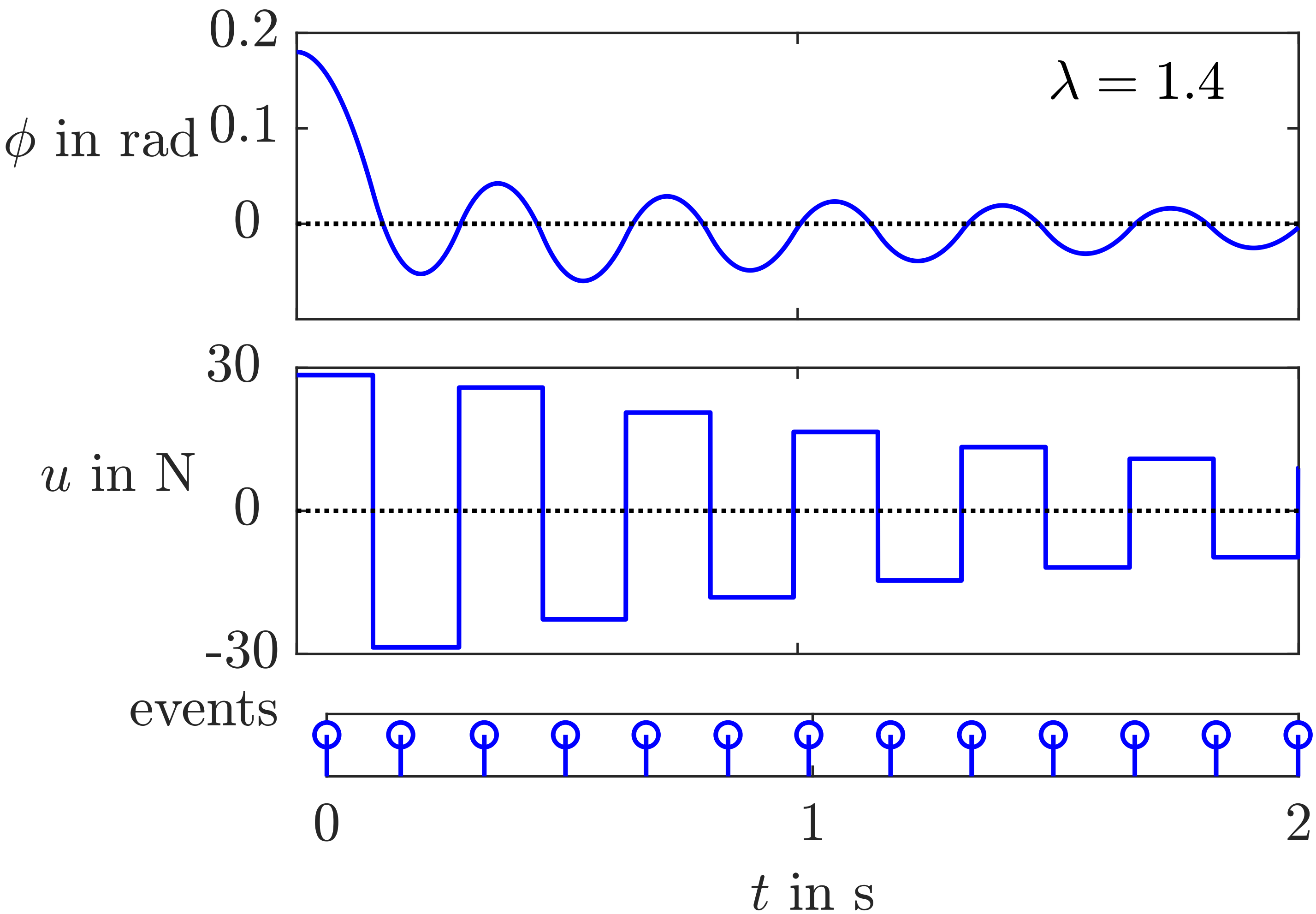

Fig. 9.9: Pendulum with event-triggered control

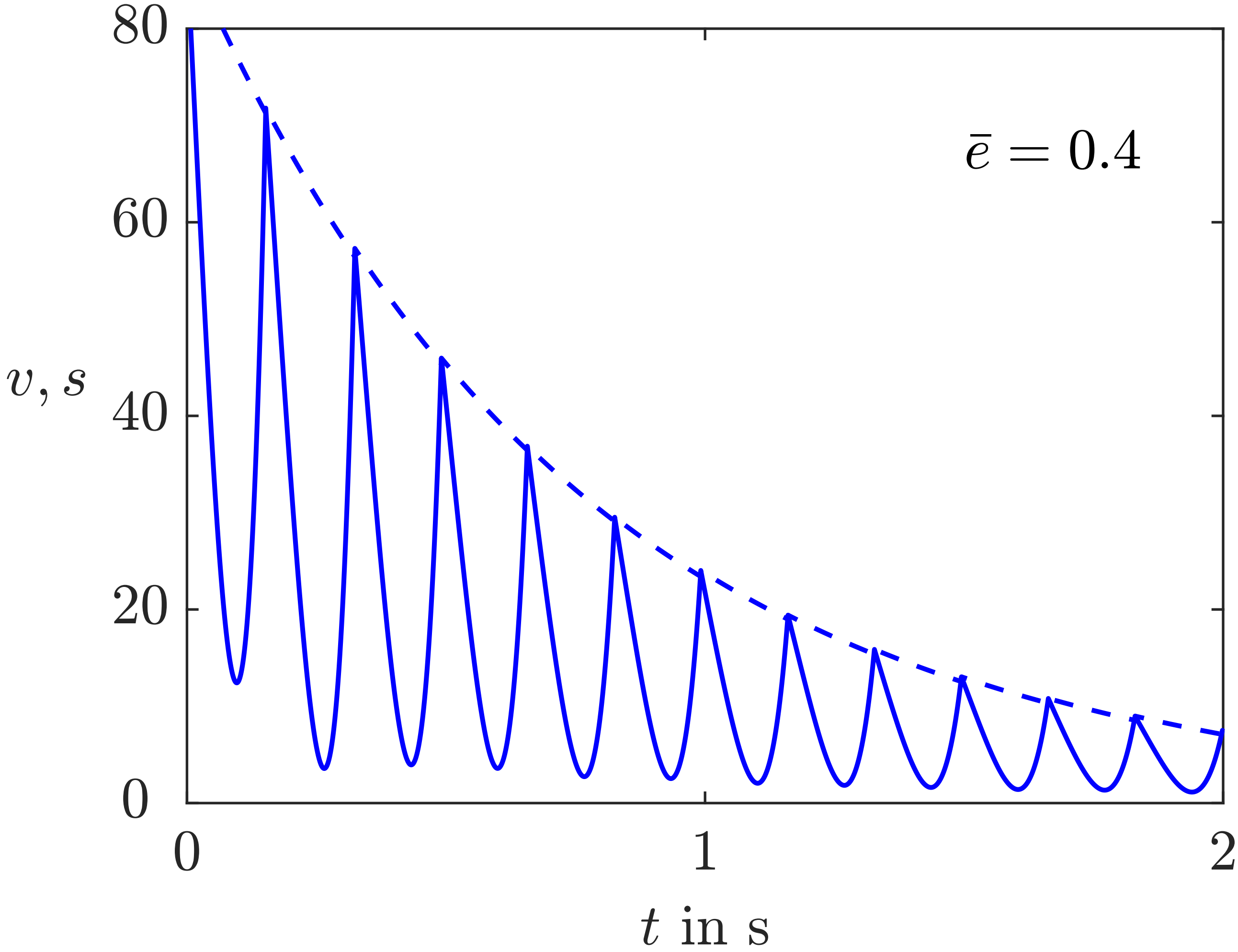

Fig. 9.9: Pendulum with event-triggered control

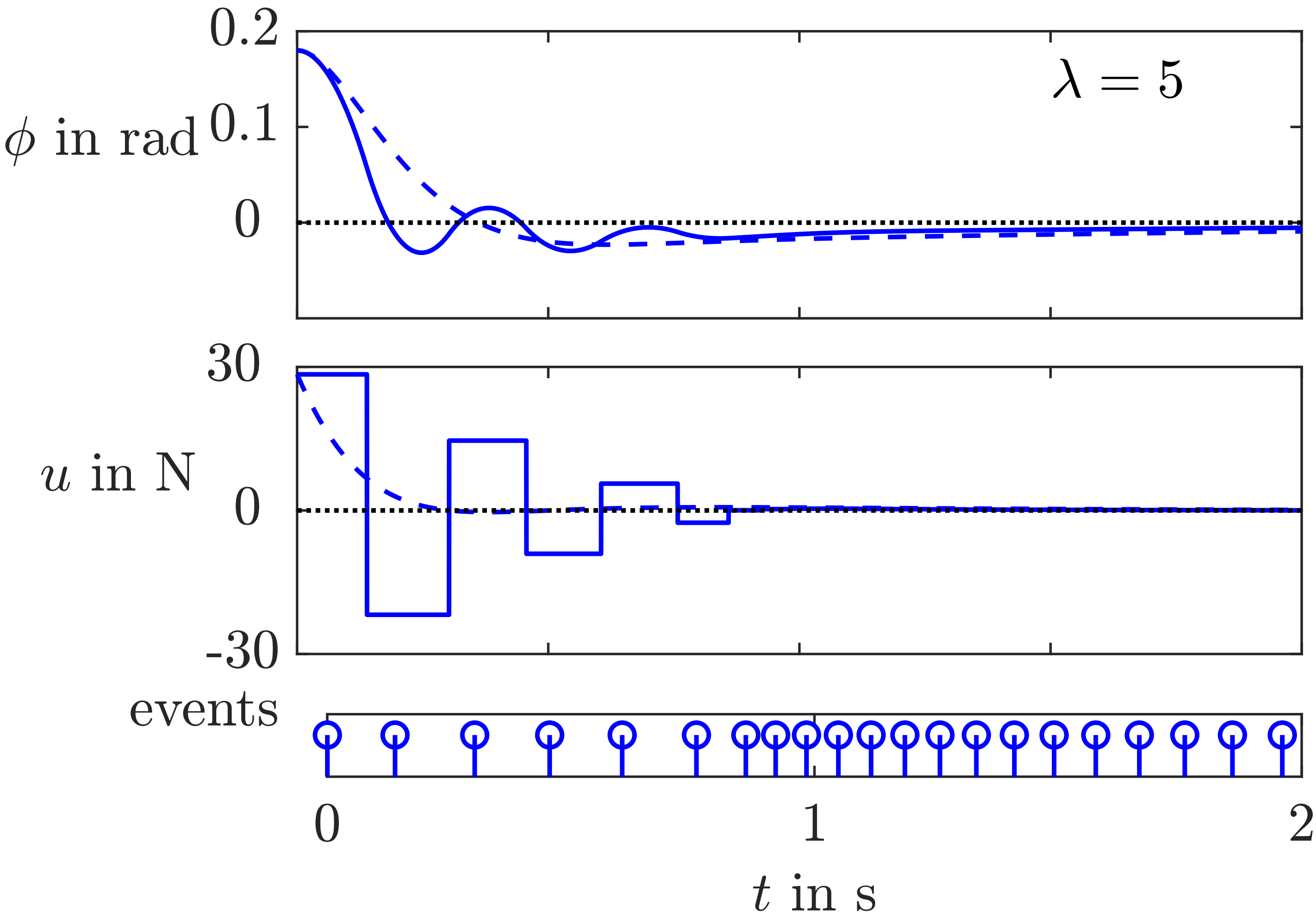

Fig. 9.10: Pendulum behaviour for continuous control (- -) and for event-triggered control (—)

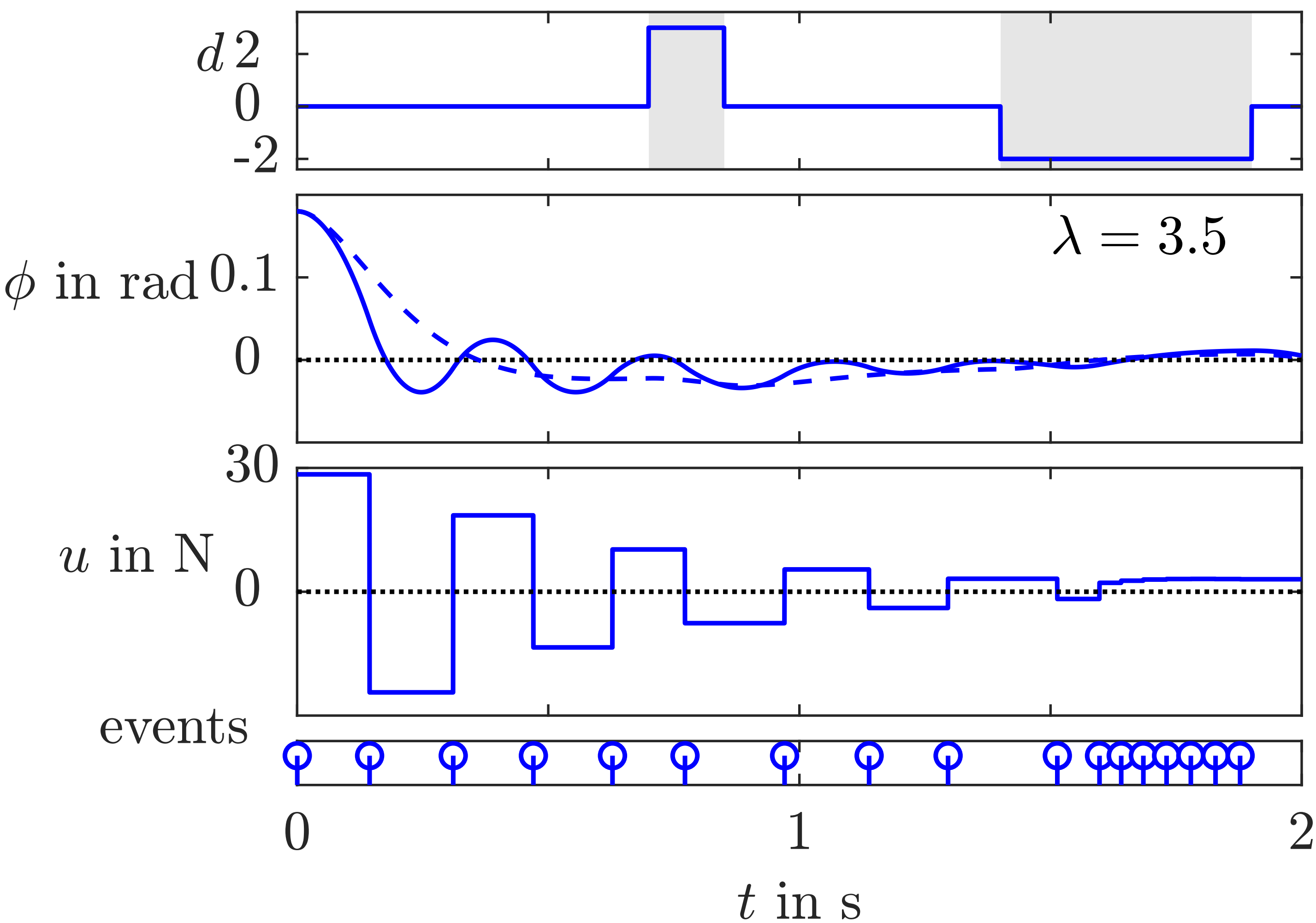

Fig. 9.11: Disturbed pendulum: in the two time intervals marked an external disturbance occurs

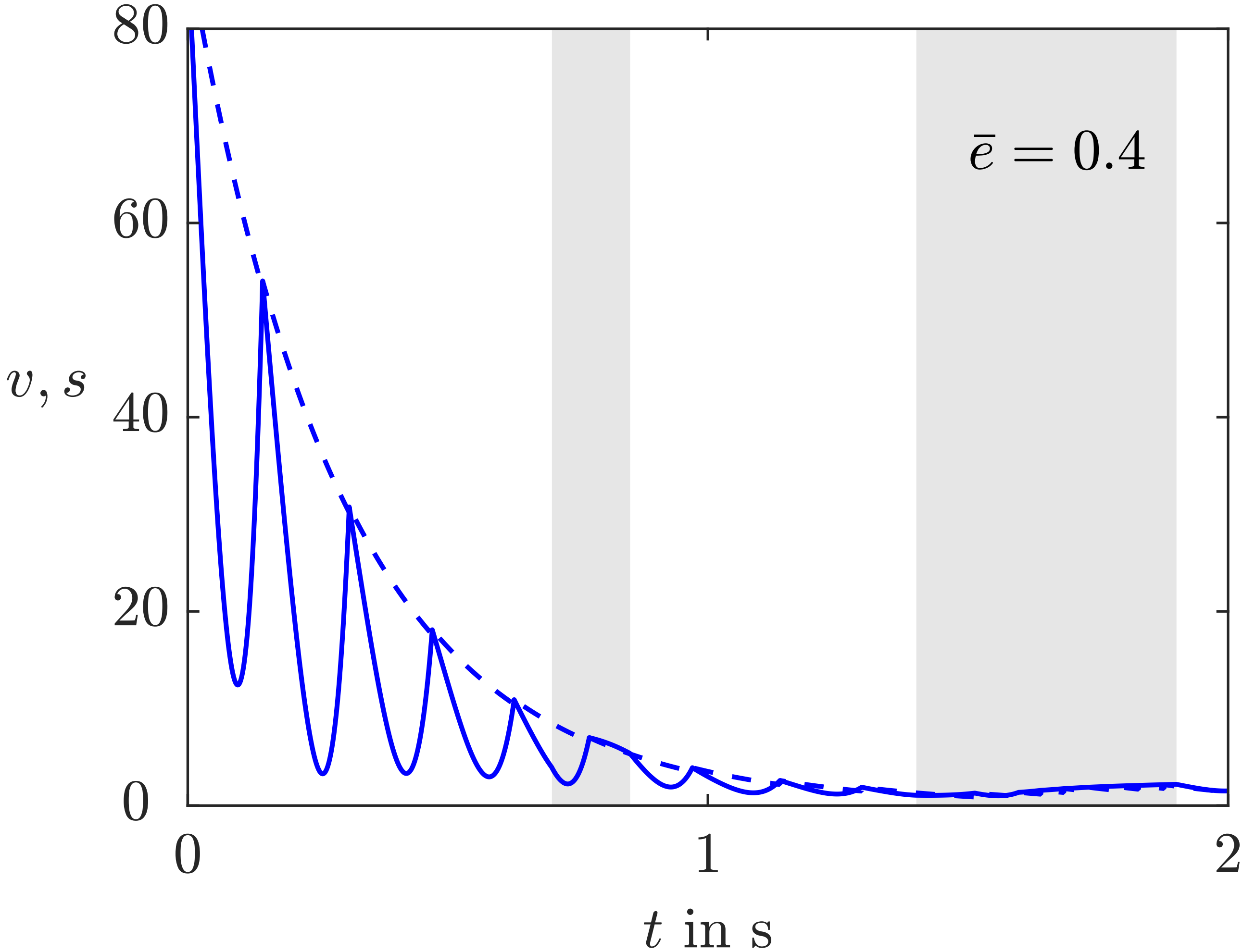

Fig. 9.11: Disturbed pendulum: in the two time intervals marked an external disturbance occurs

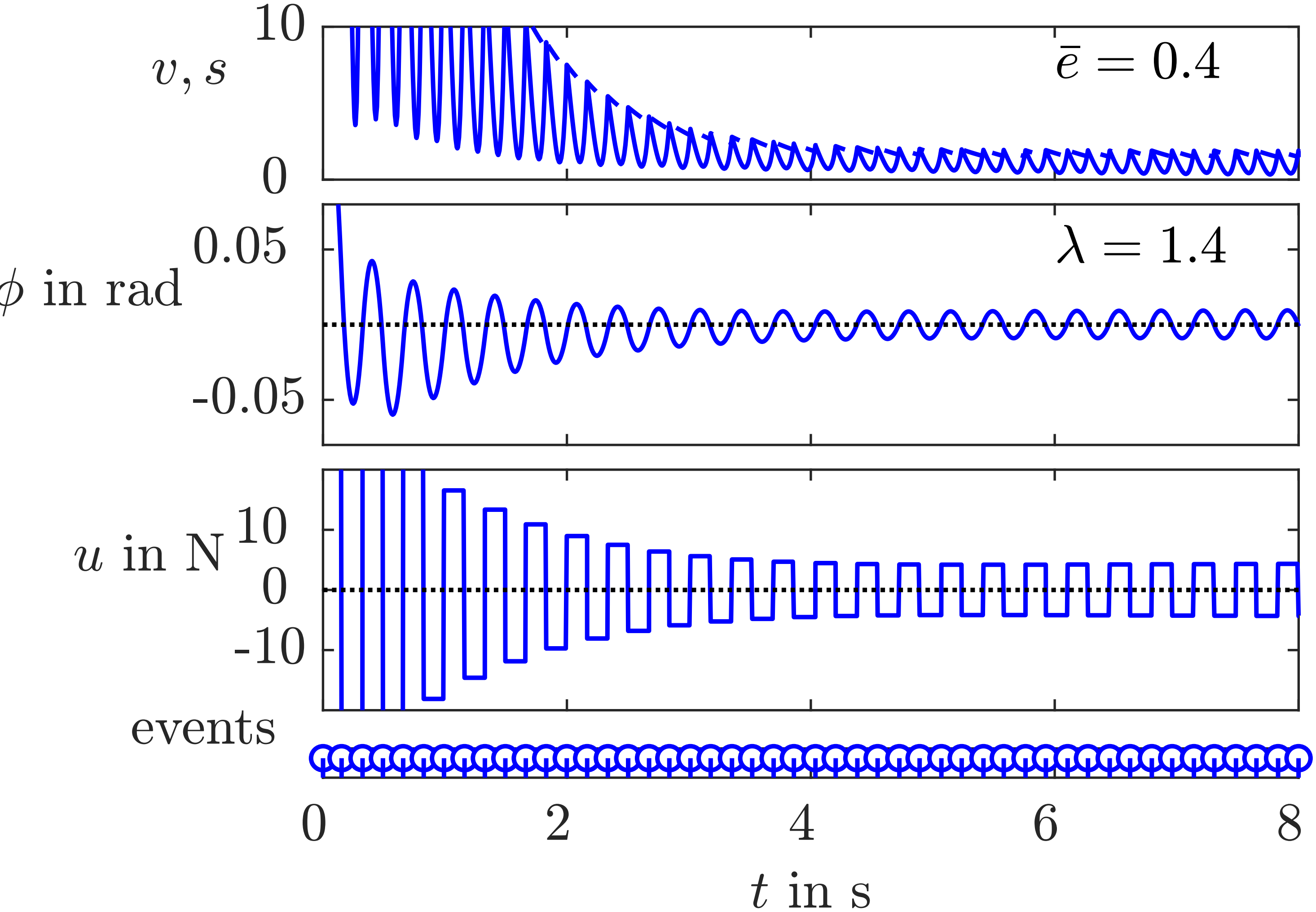

Fig. 9.12: Behaviour of the event-triggered pendulum for a long time horizon

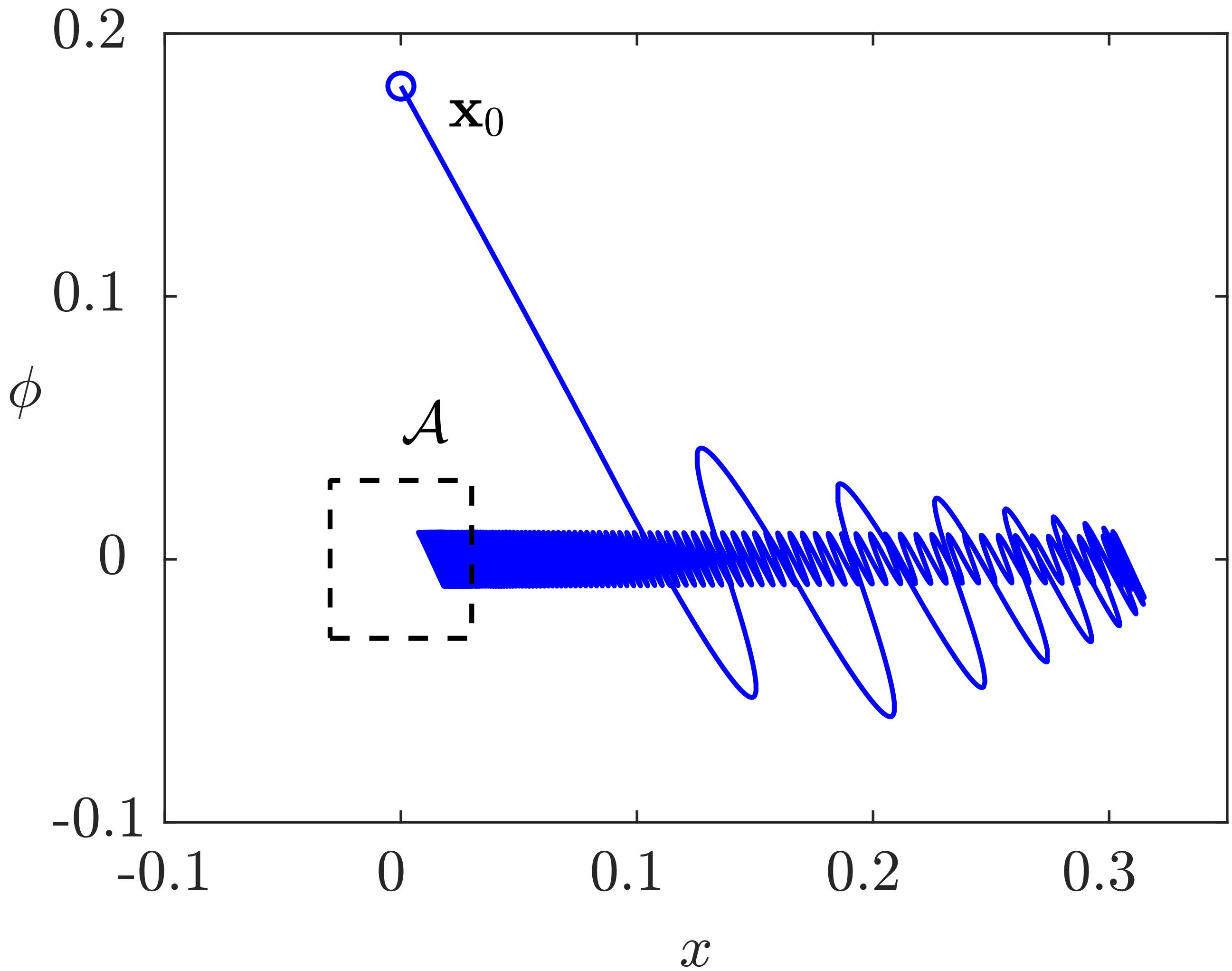

Fig. 9.12: Behaviour of the event-triggered pendulum for a long time horizon

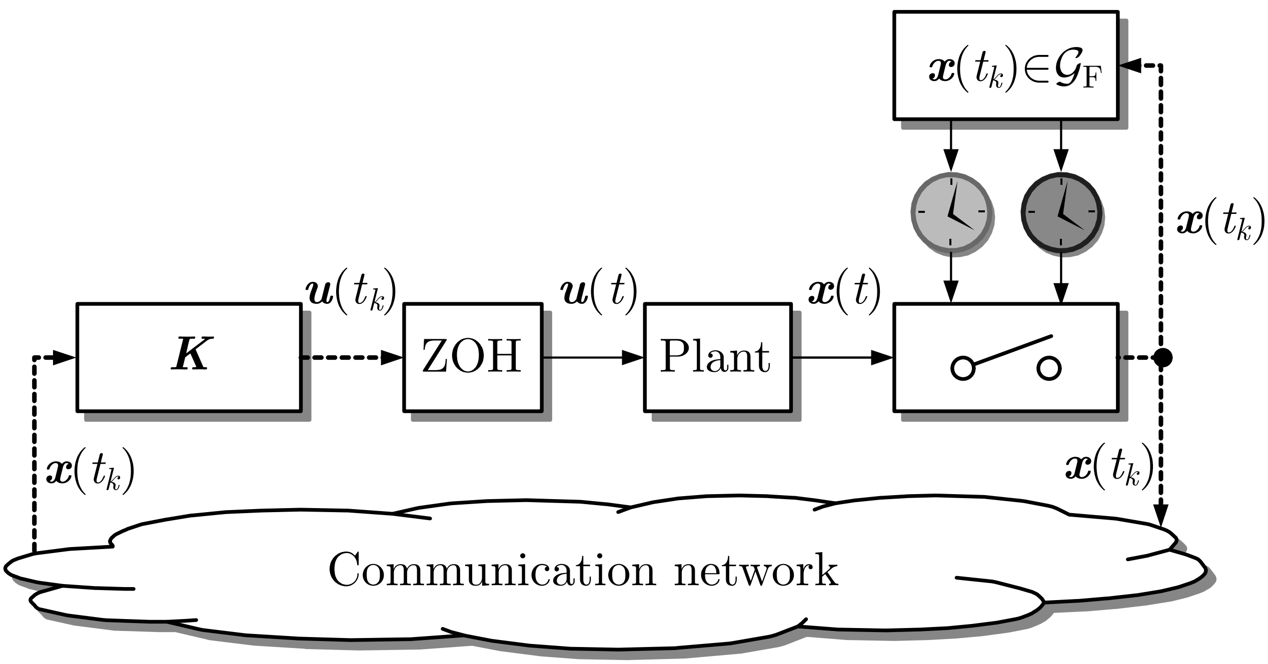

Fig. 9.13: Event-triggered sampling rate selection

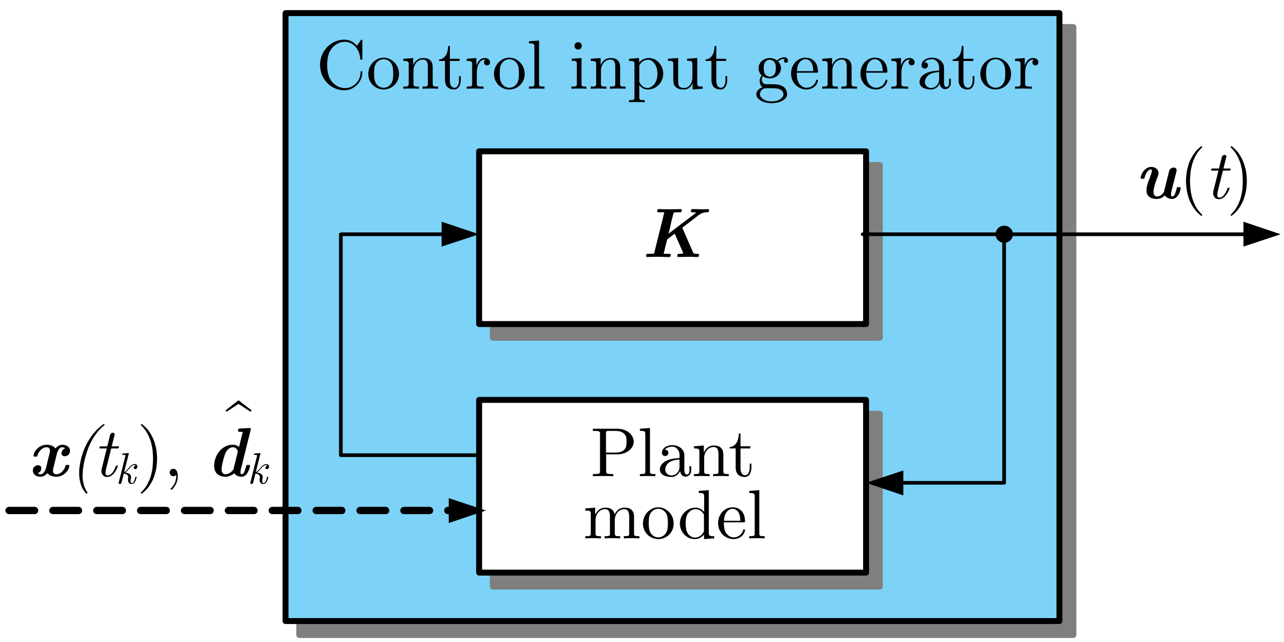

Fig. 9.14: Control input generator

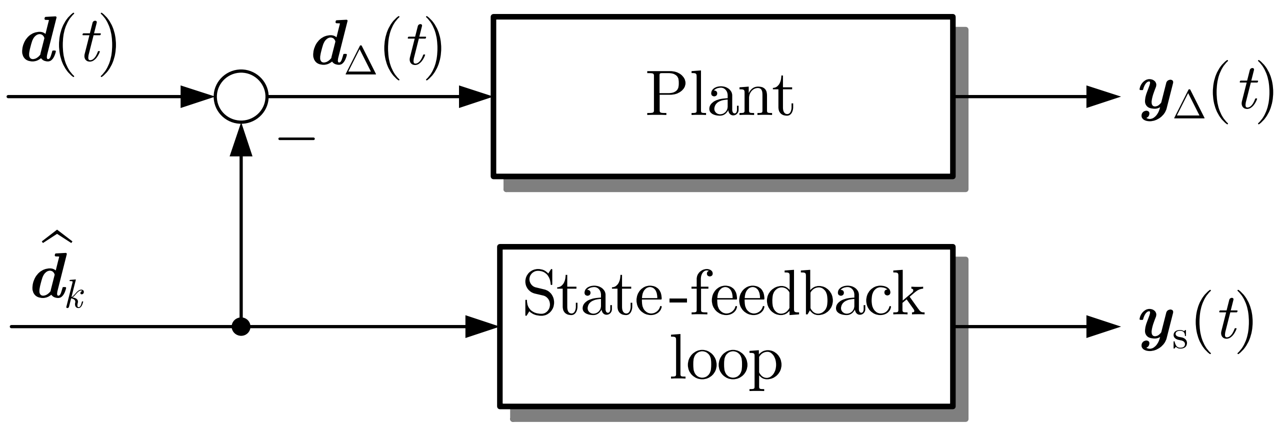

Fig. 9.15: Interpretation of eqn. (9.25)

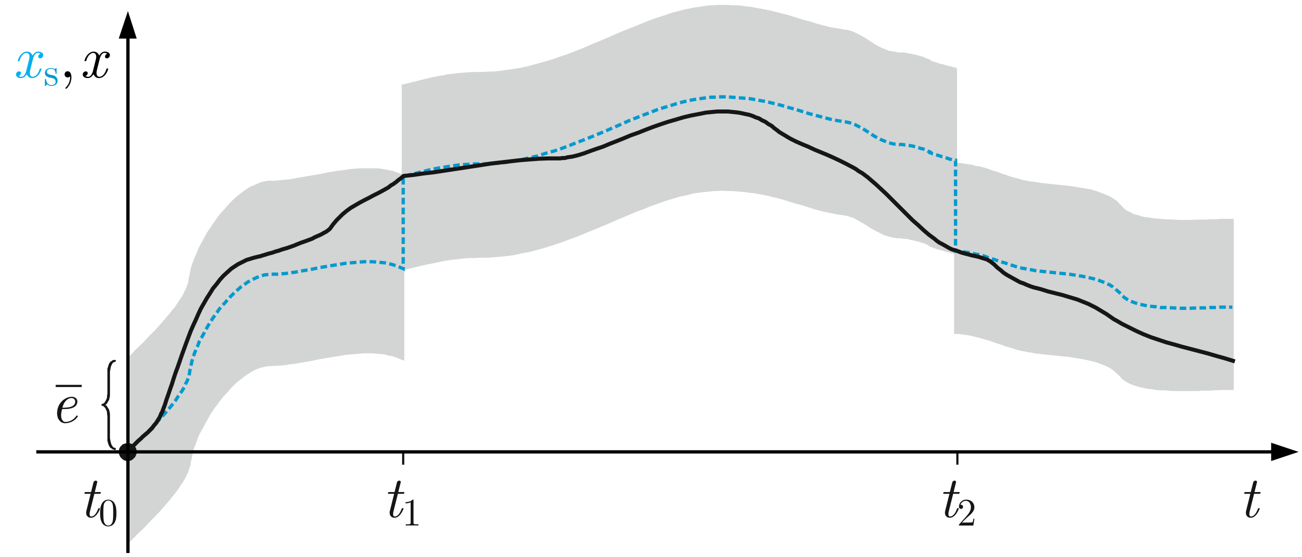

Fig. 9.16: Behaviour of the event-triggered control loop

J. Lunze: *Networked Control of Multi-Agent Systems,* Edition MoRa 2022

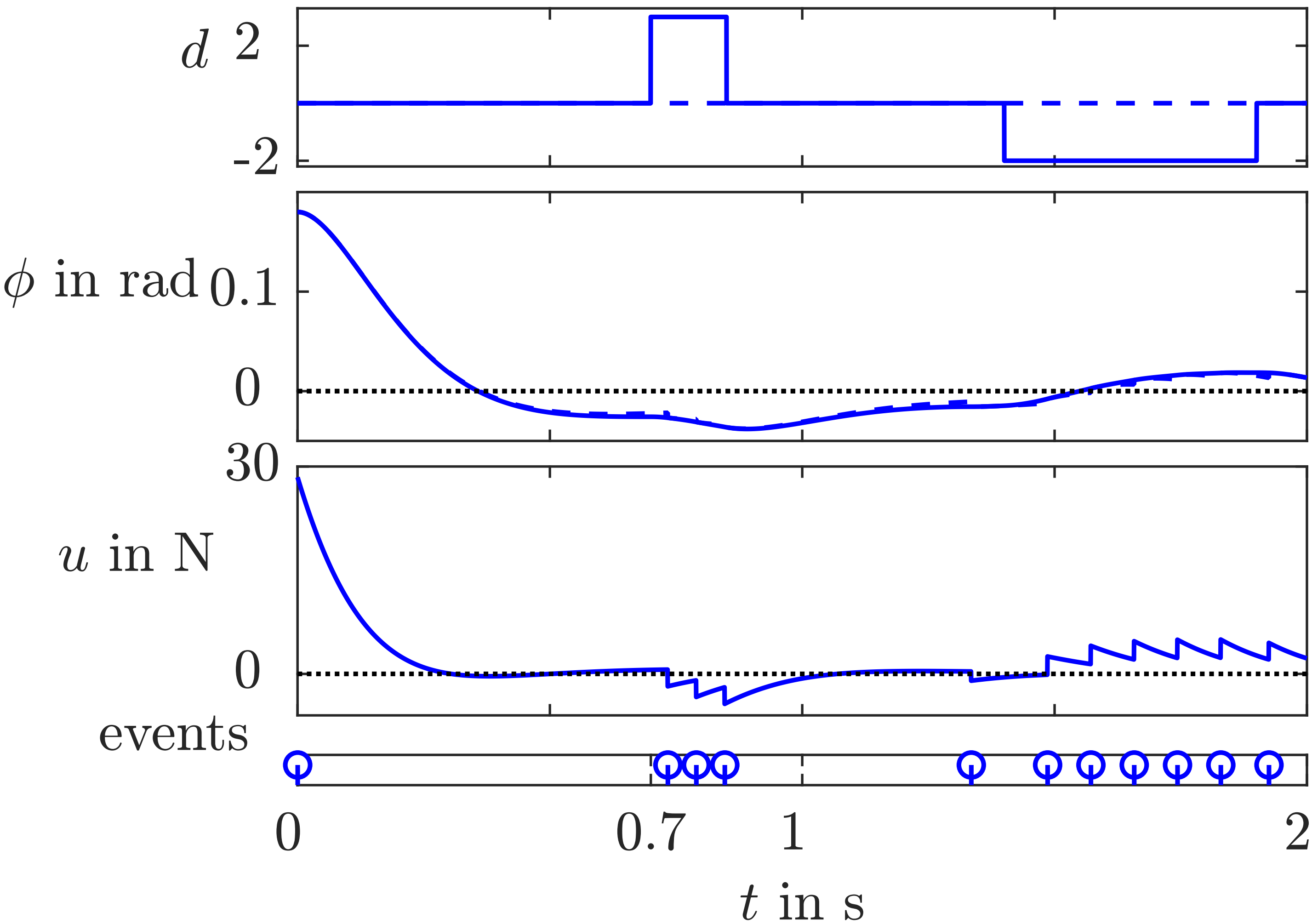

Fig. 9.17: Event-triggered disturbance attenuation of the inverted pendulum without disturbance estimation

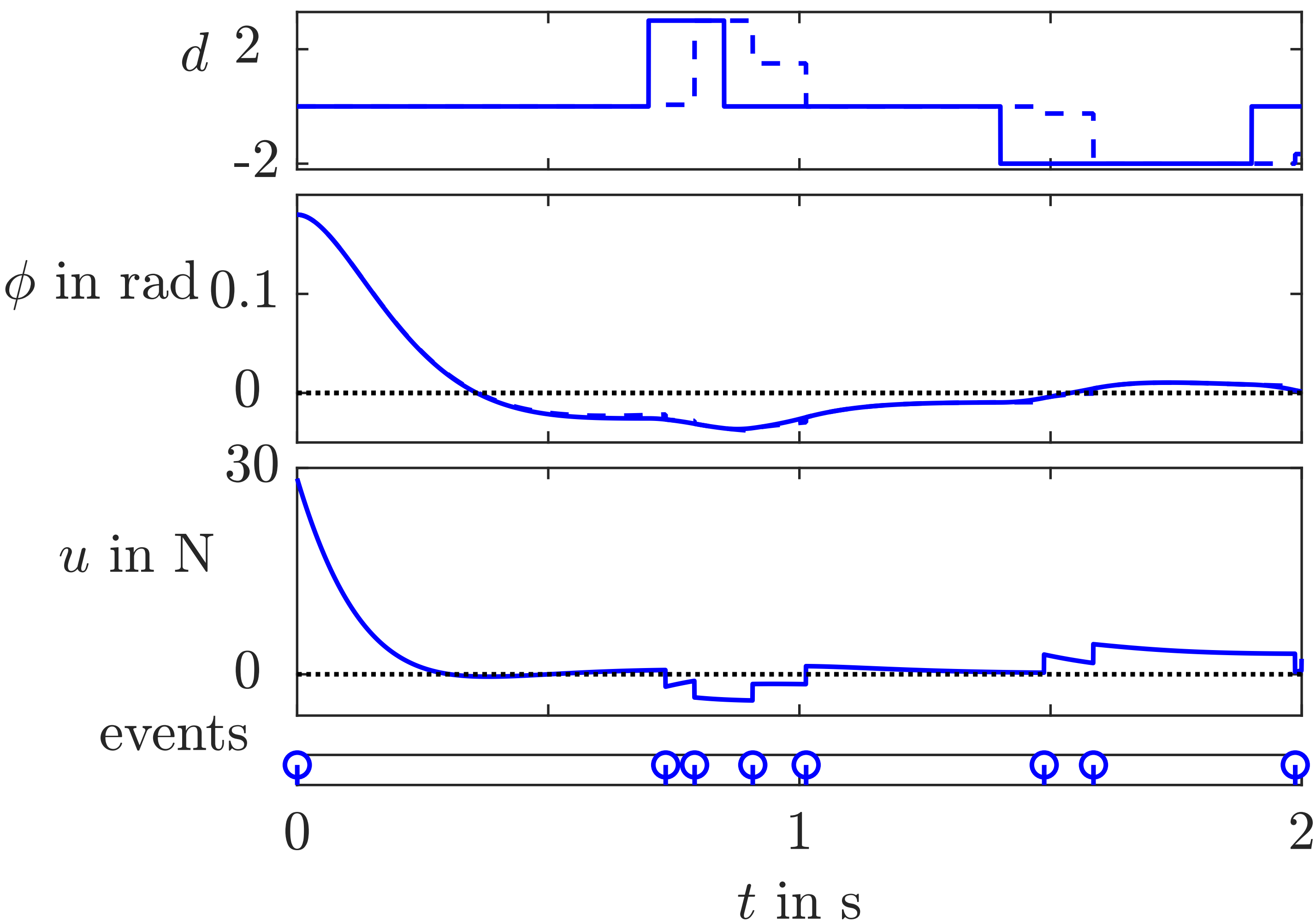

Fig. 9.18: Pendulum behaviour with disturbance estimation

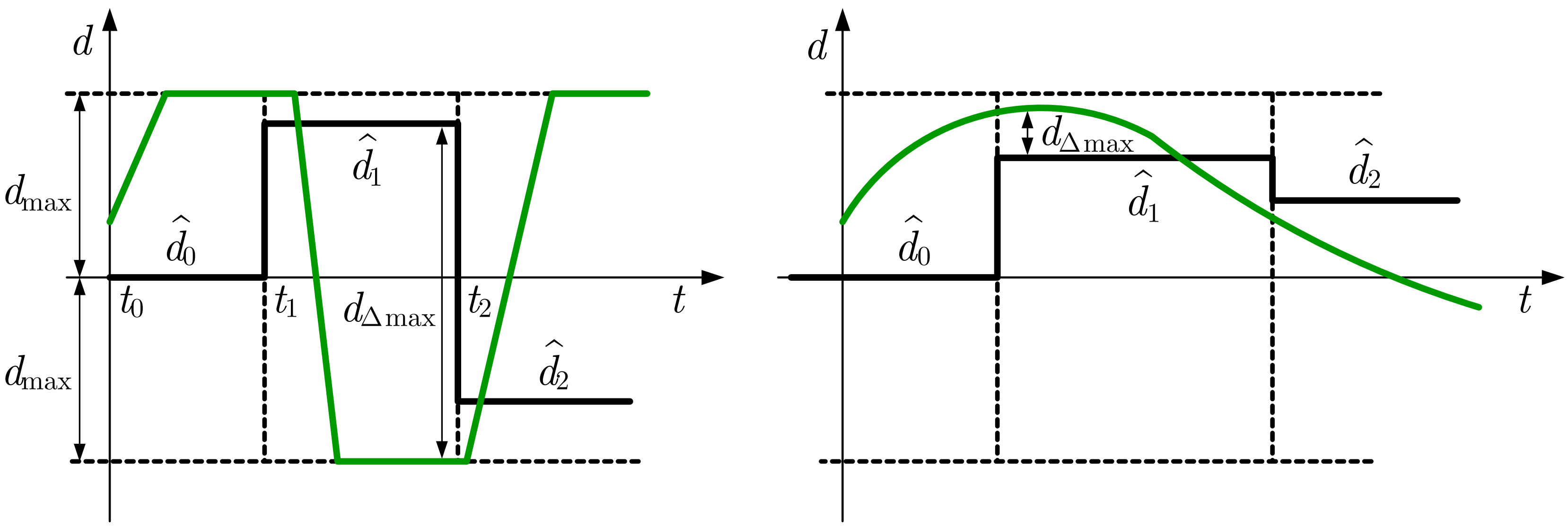

Fig. 9.19. Relation between the maximum disturbance bounds $d_{\max}$ and $d_{\Delta\max}$

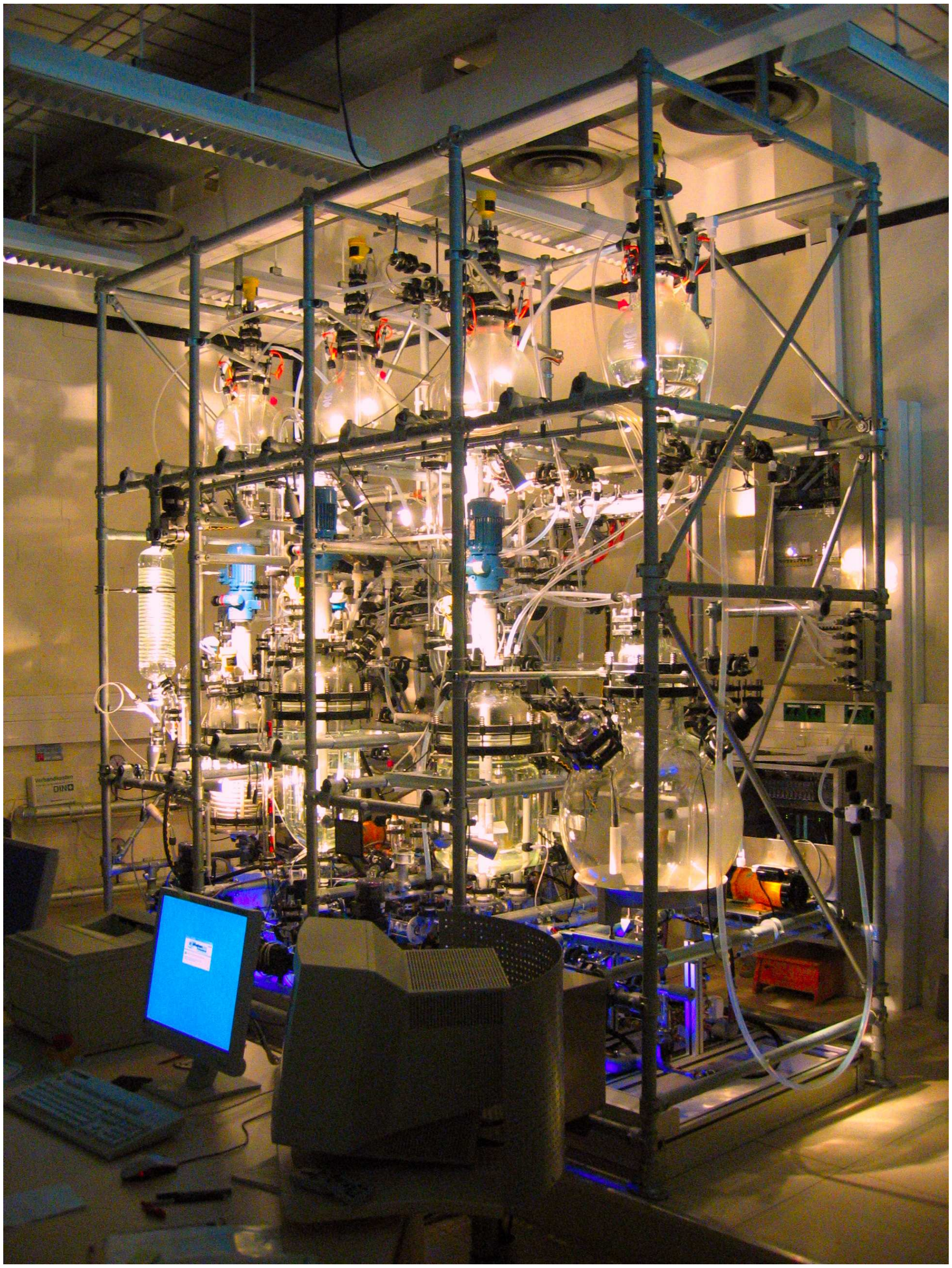

Fig. 9.20. Prototype plant VERA

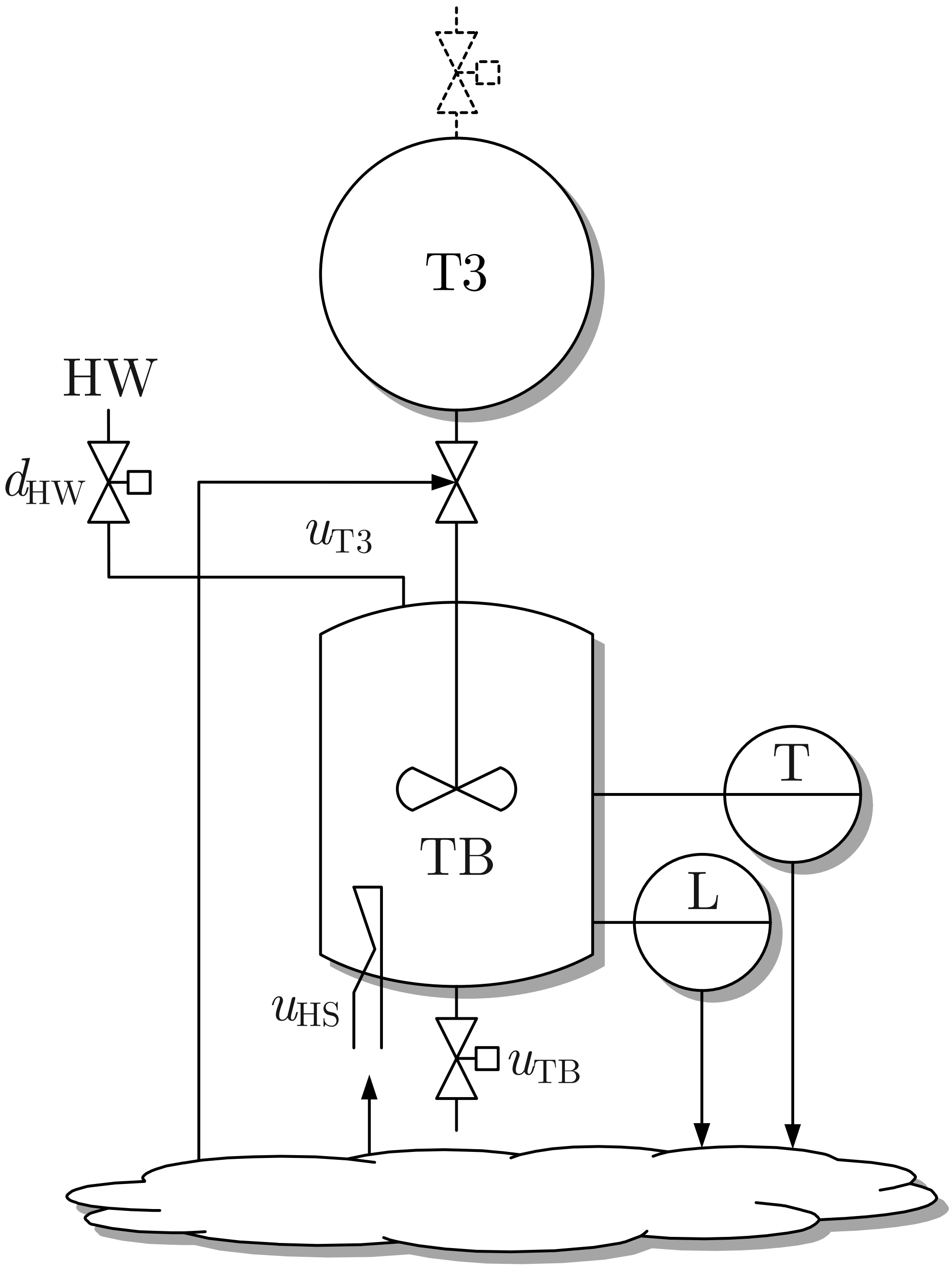

Fig. 9.20. Thermofluid process

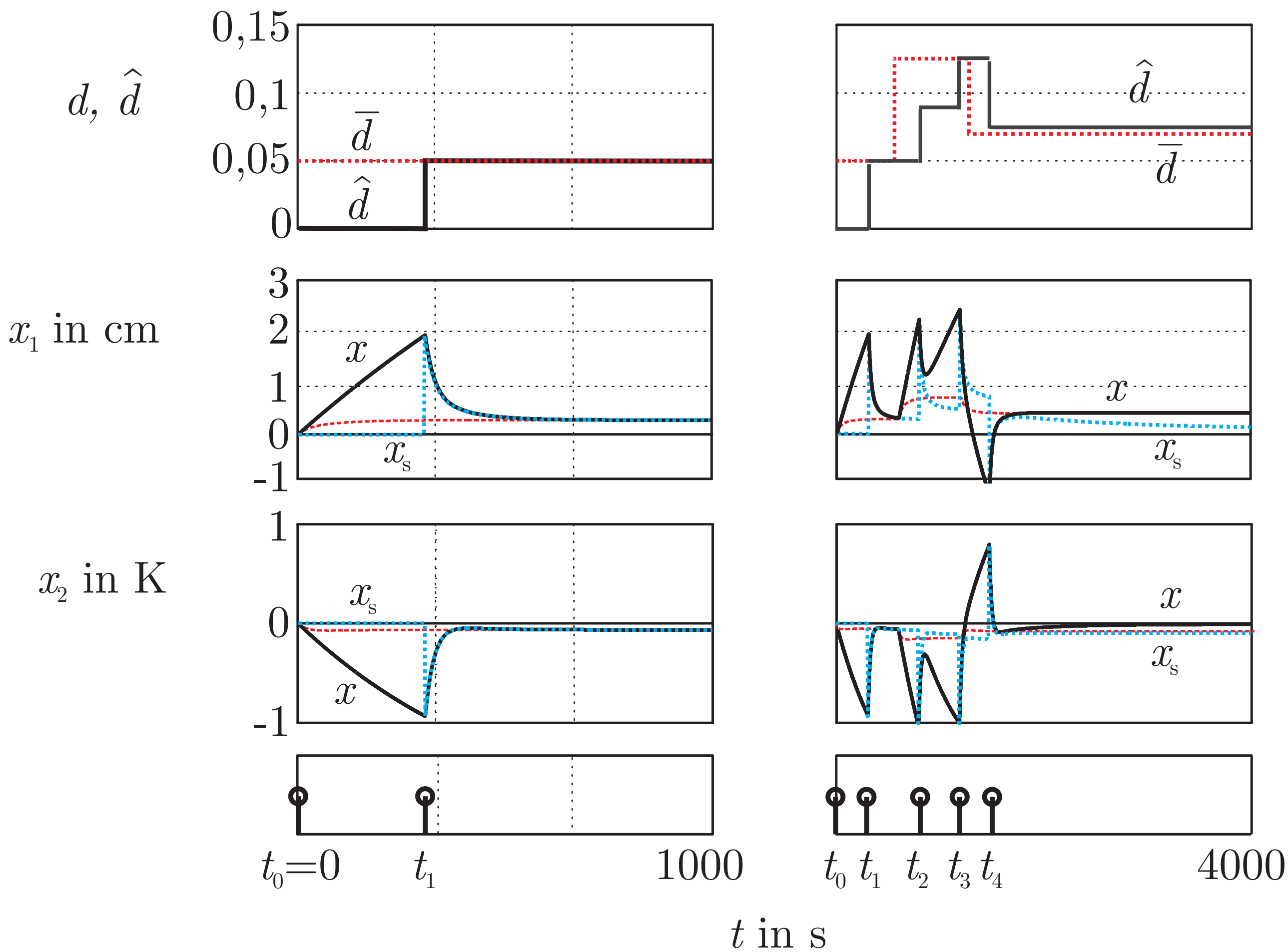

Fig. 9.21: Simulation results for two disturbance scenarios

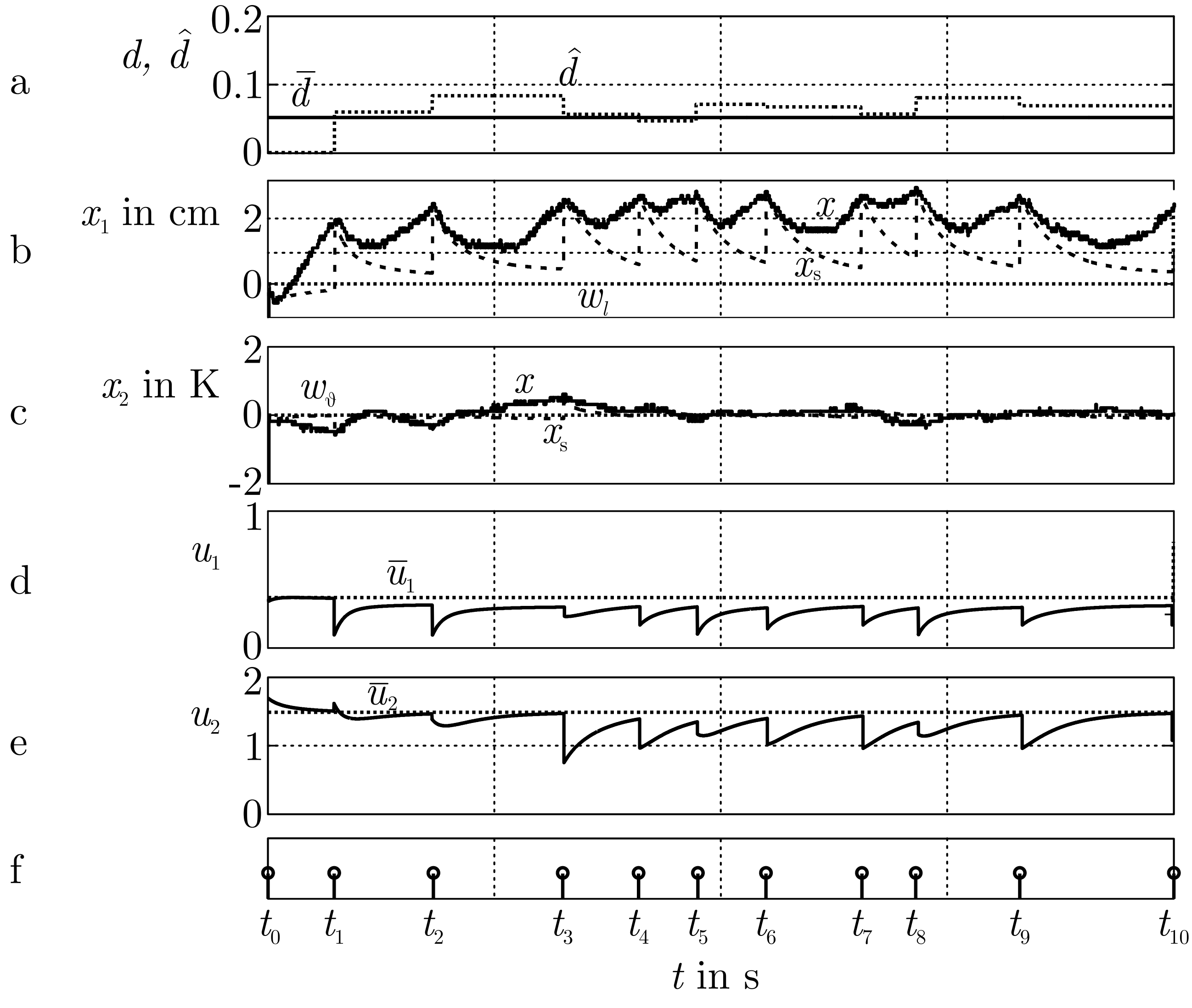

Fig. 9.22: Experimental results of the process subject to an unknown inflow

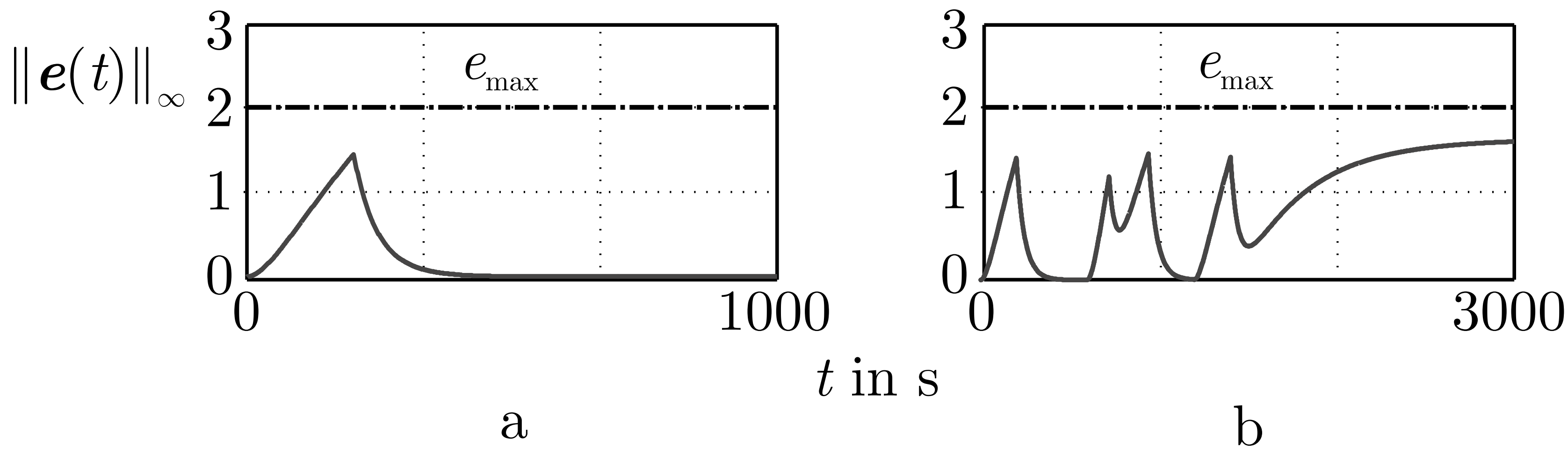

Fig. 9.23. Difference between the states of the event-triggered control loop and the continuous control loop

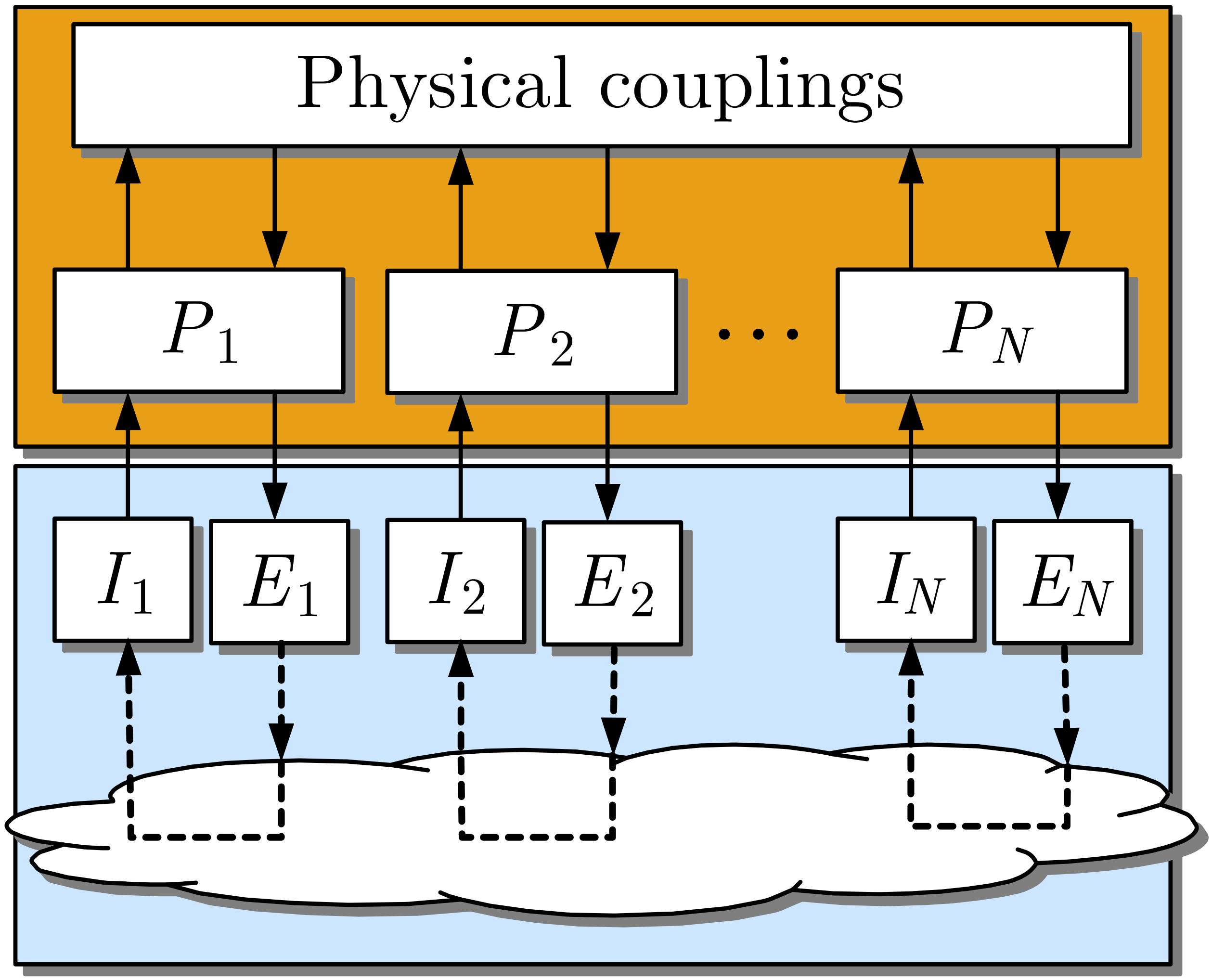

Fig. 9.24: Decentralised event-based control

J. LUNZE: *Networked Control of Multi-Agent Systems*, Edition MoRa 2022

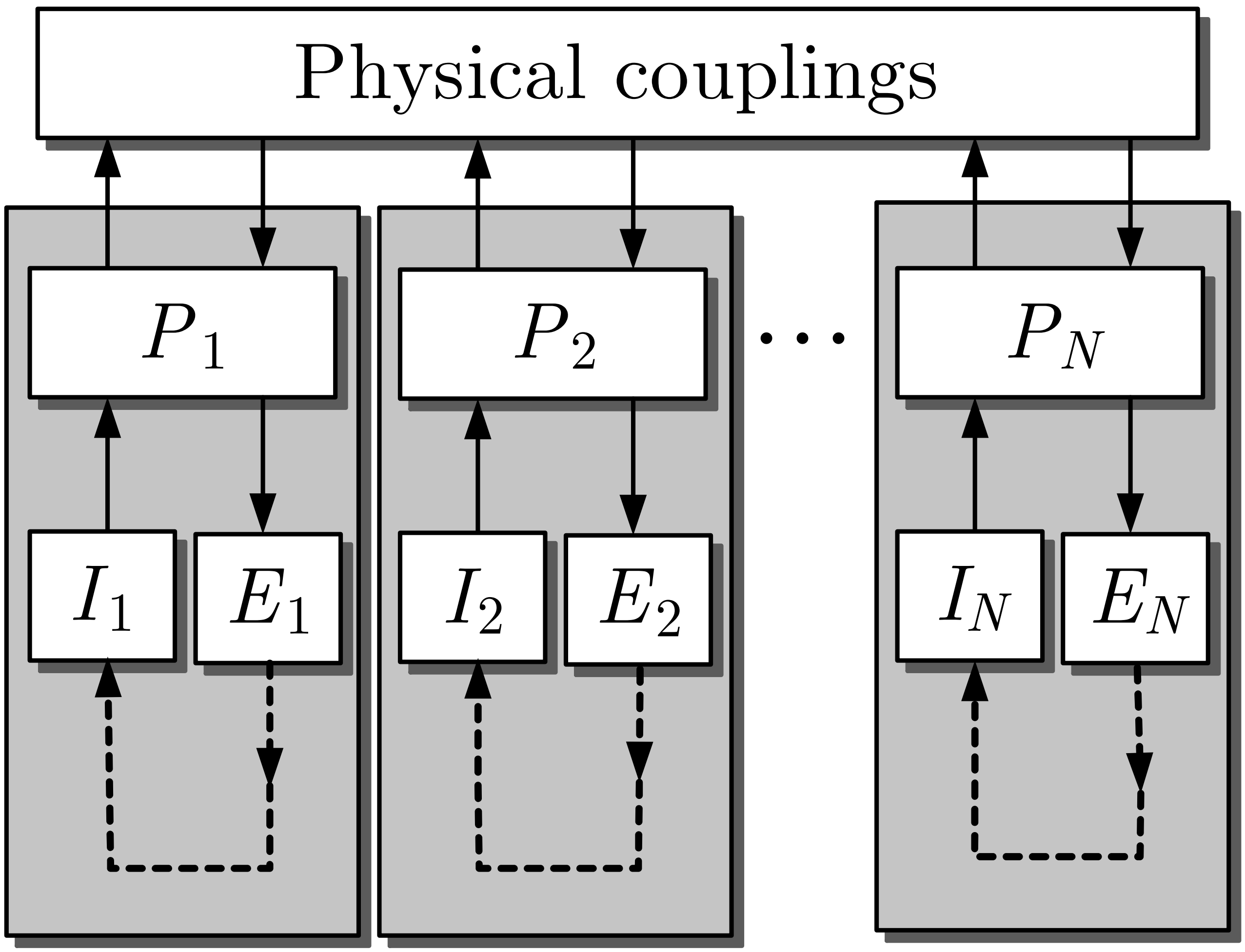

Fig. 9.24: Decentralised event-based control

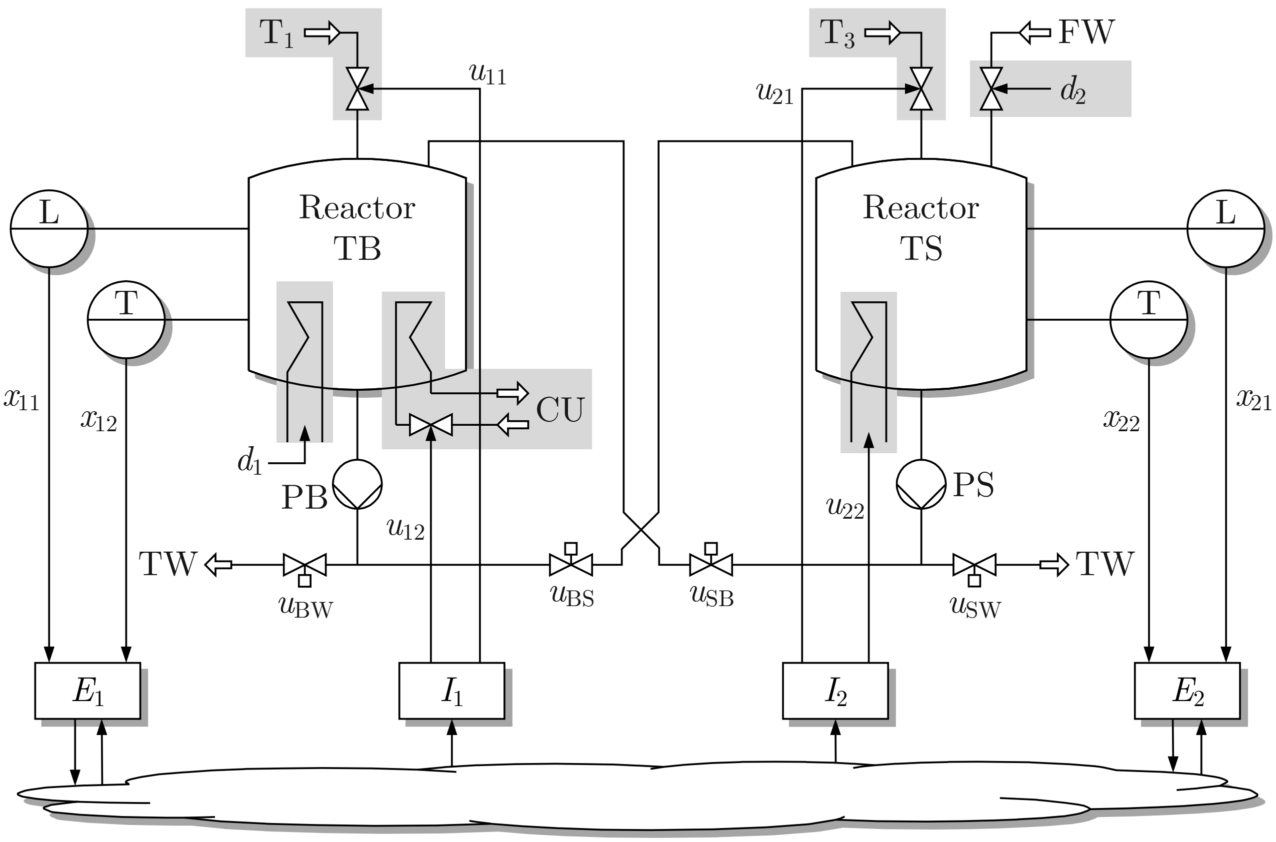

Fig. 9.25: Experimental setup of the thermo-fluid process used in this example

J. LUNZE: *Networked Control of Multi-Agent Systems*, Edition **M**o**R**a 2022

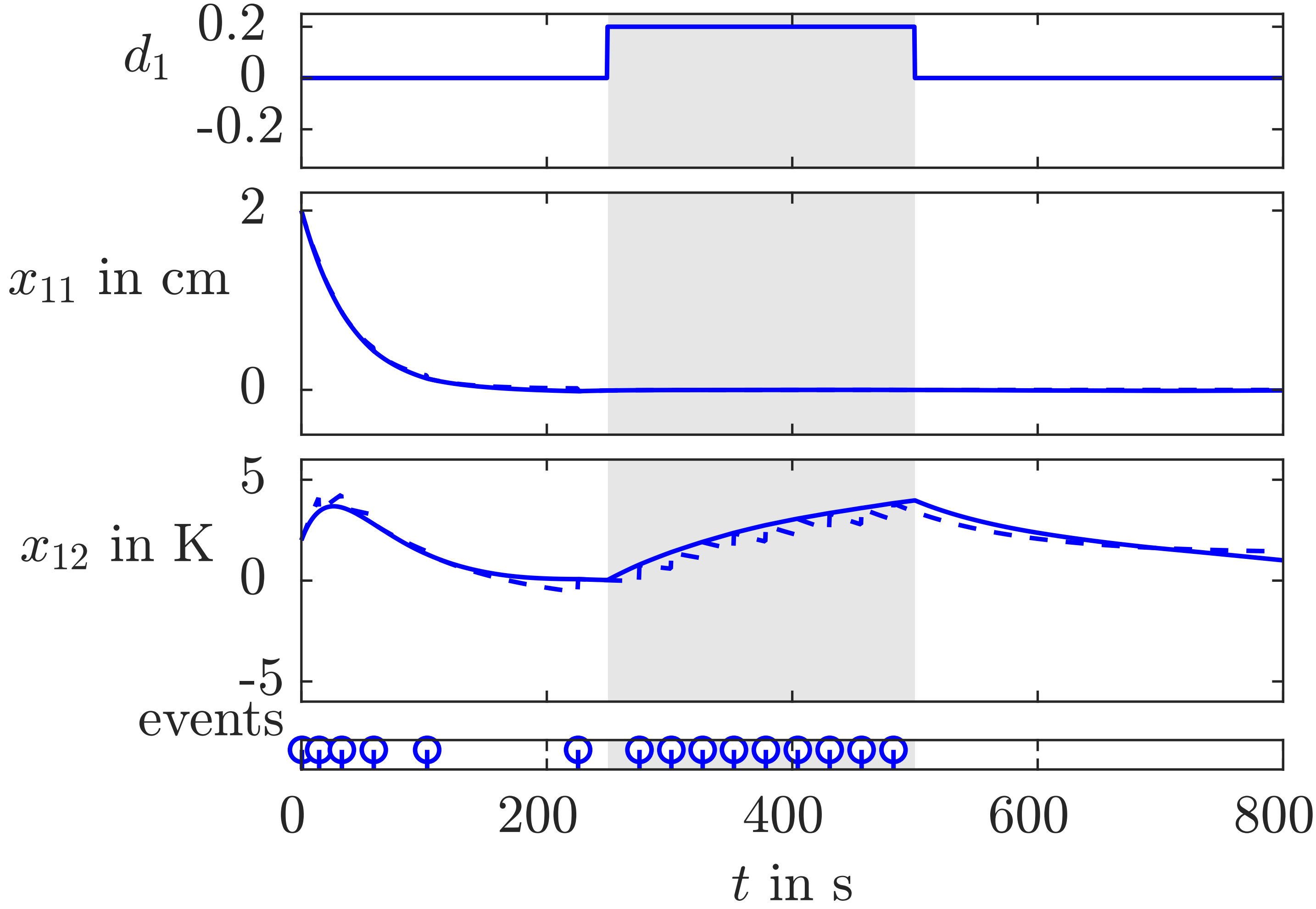

Fig. 9.26: Behaviour of the overall system with event-triggered decentralised control

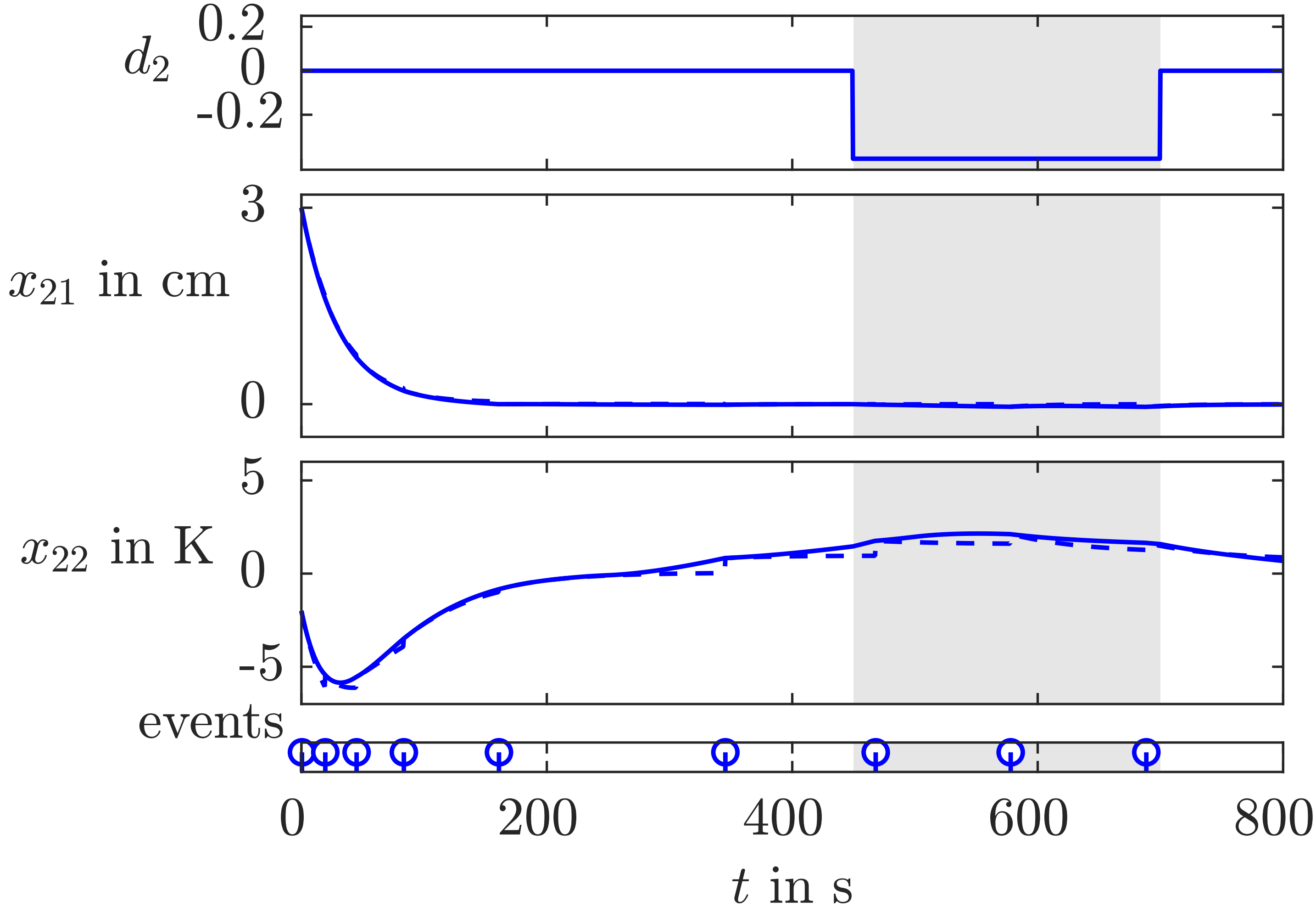

Fig. 9.26: Behaviour of the overall system with event-triggered decentralised control

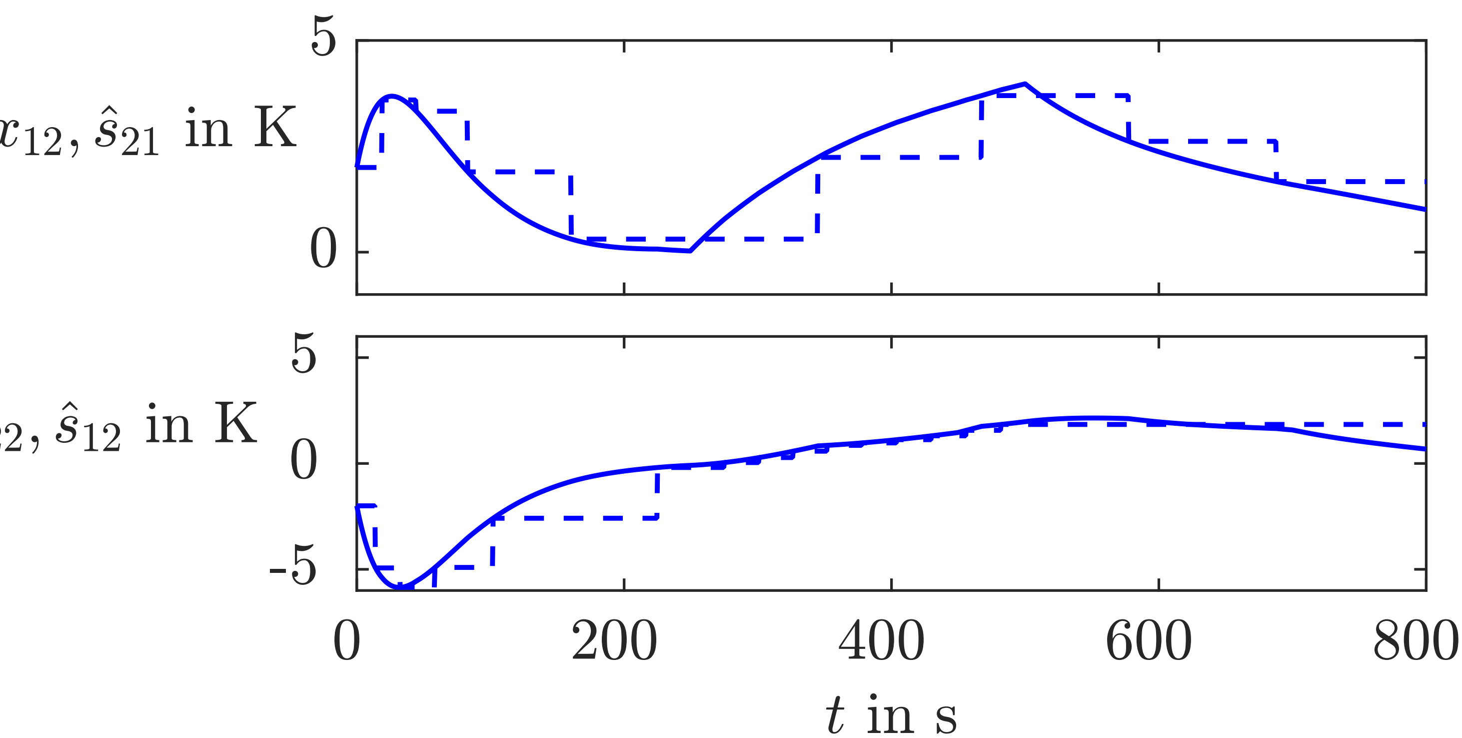

Fig. 9.27: Coupling signals

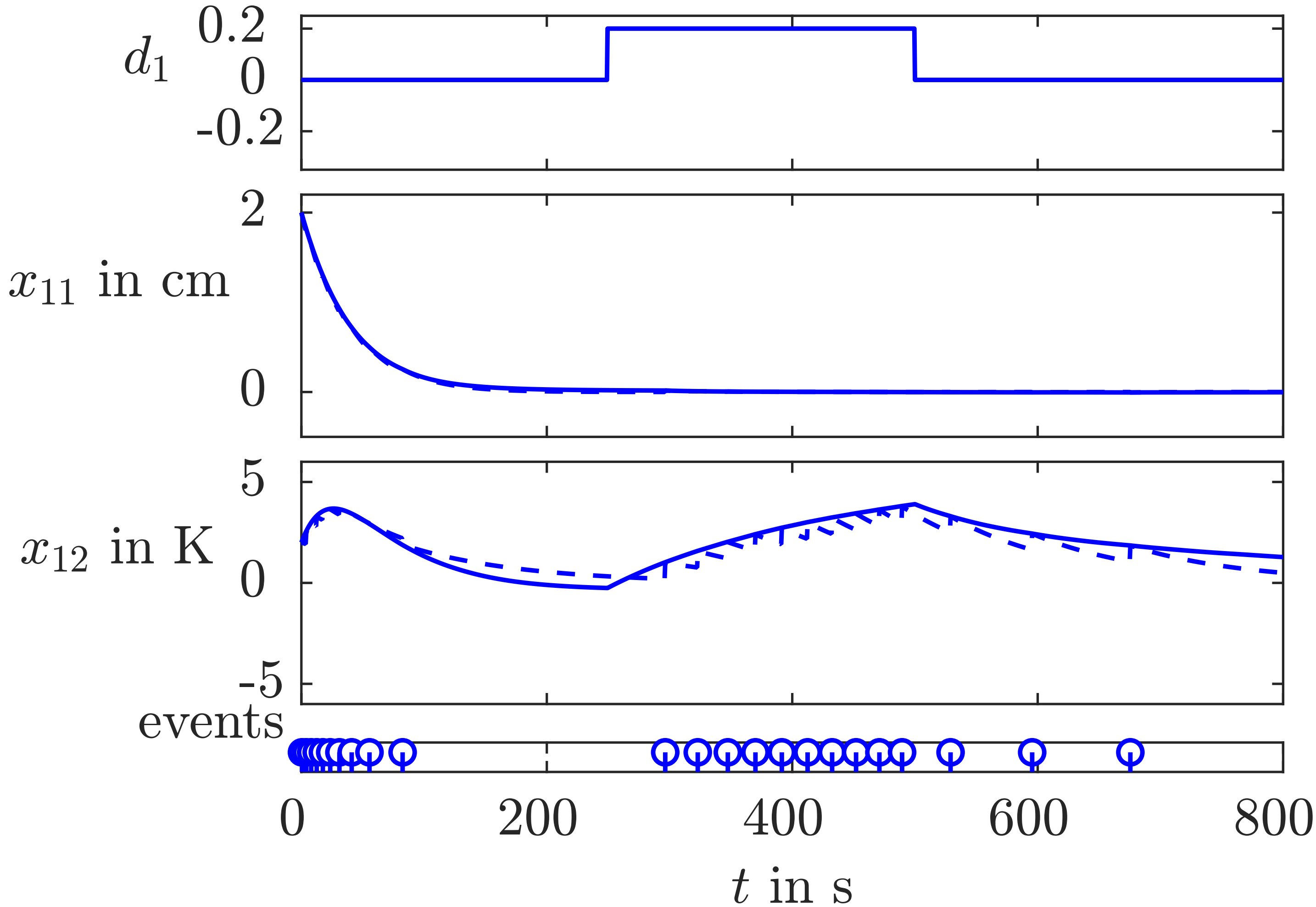

Fig. 9.28: Decentralised event-triggered control without approximate coupling signals (I)

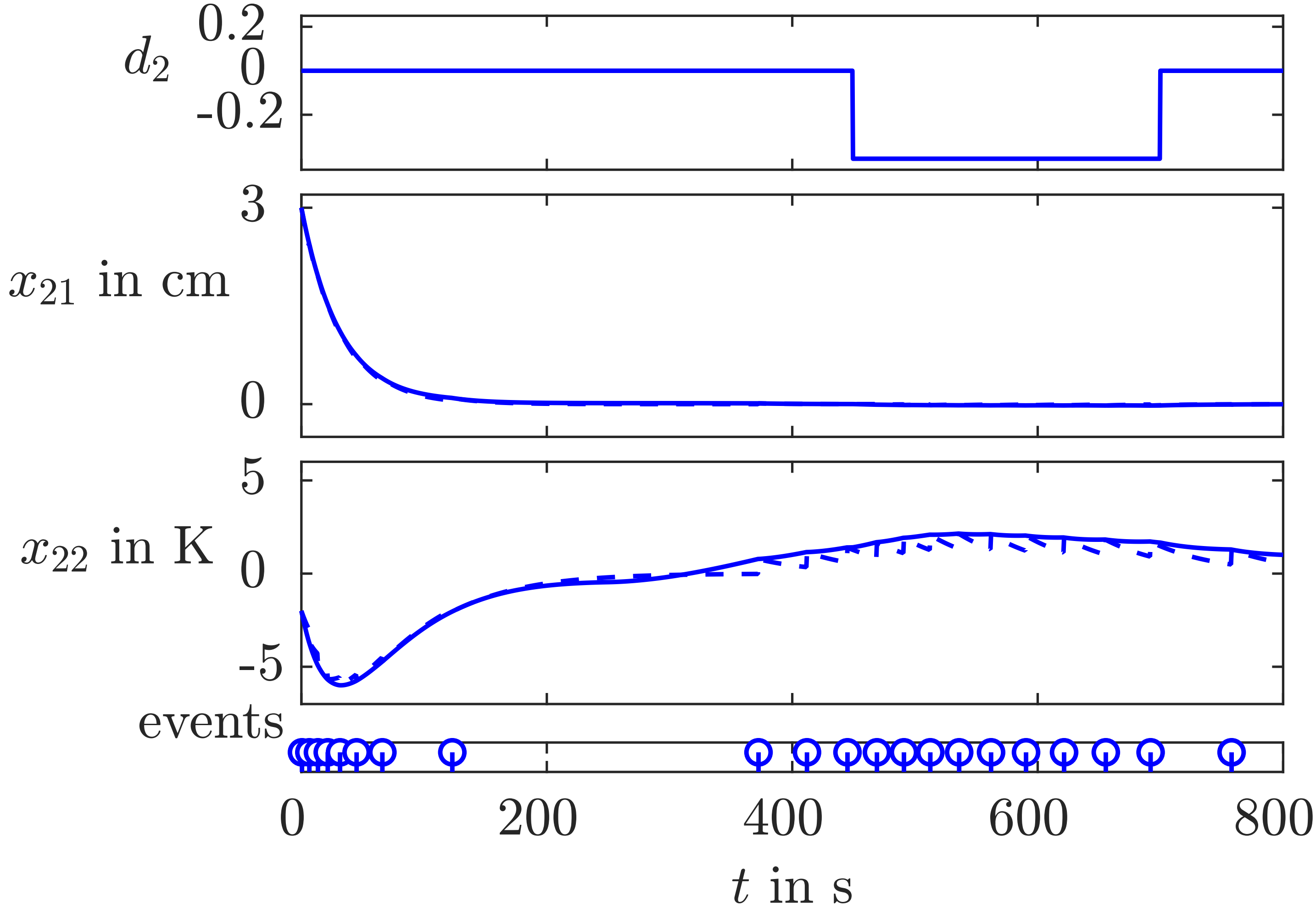

Fig. 9.28: Decentralised event-triggered control without approximate coupling signals (II)

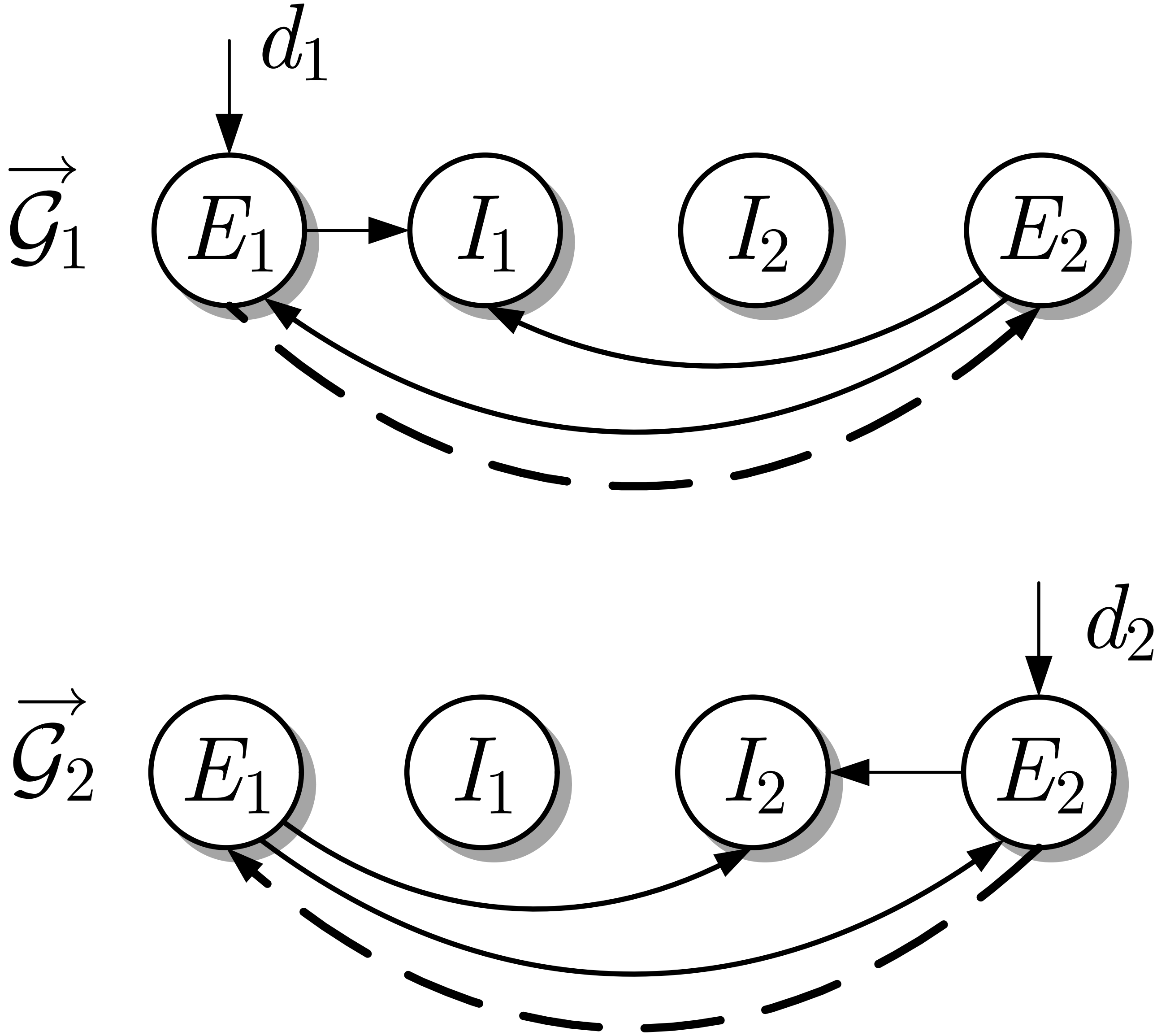

Fig. 9.29: Two communication structures that occur for two disturbance situations

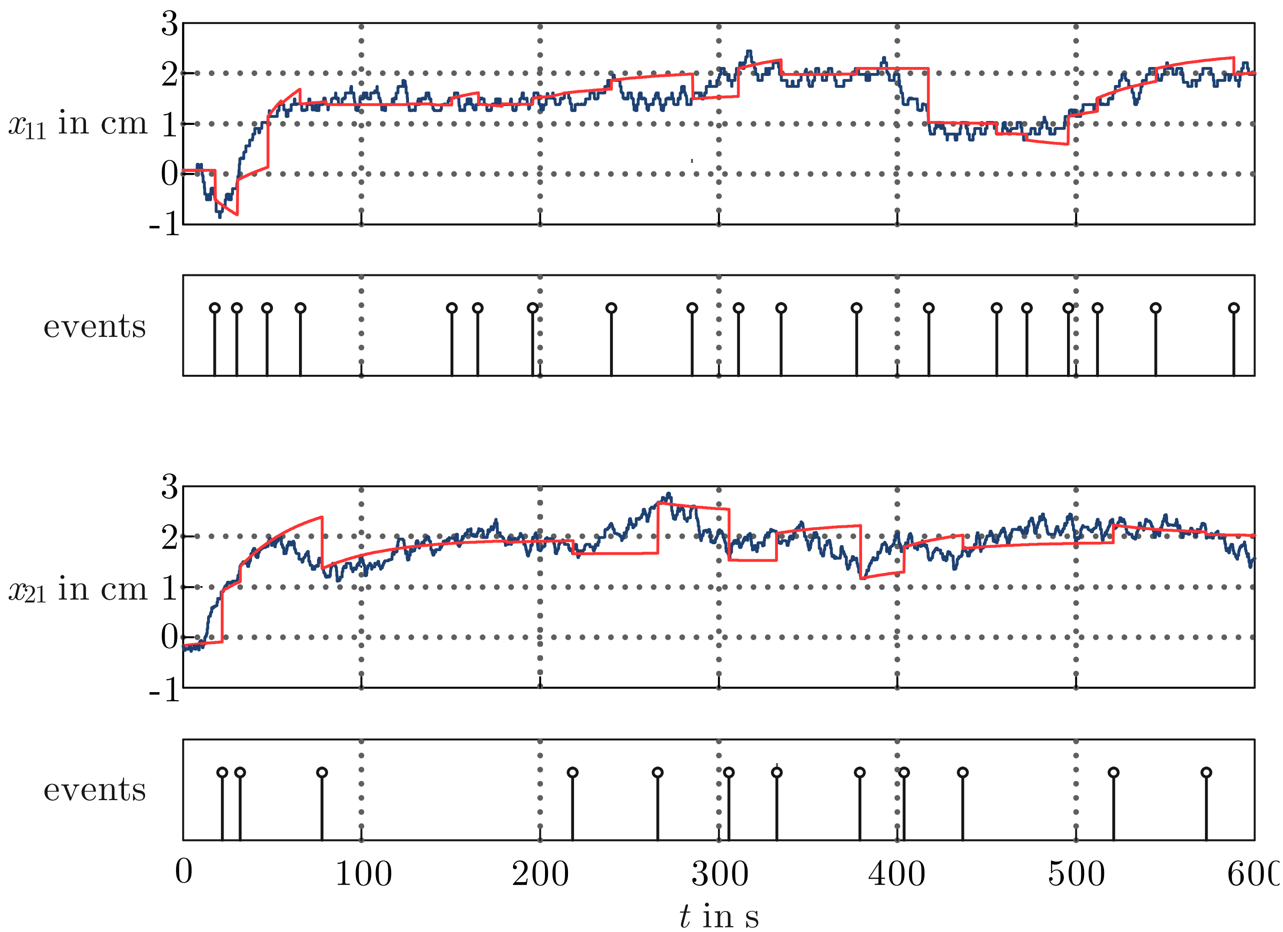

Fig. 9.30: Behaviour of the thermo-fluid process with decentralised event-based control

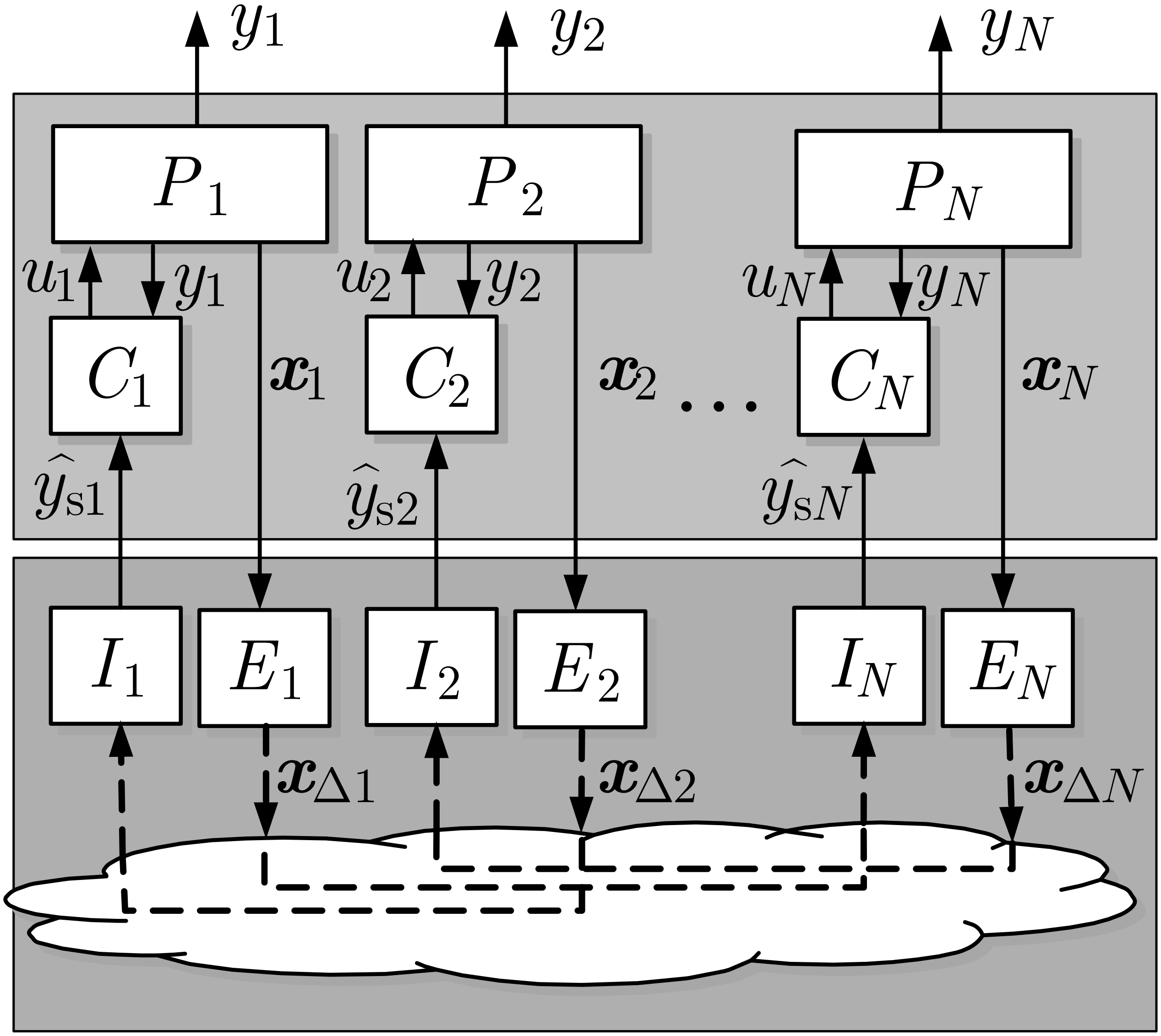

Fig. 9.31: Structure of the event-triggered multi-agent system

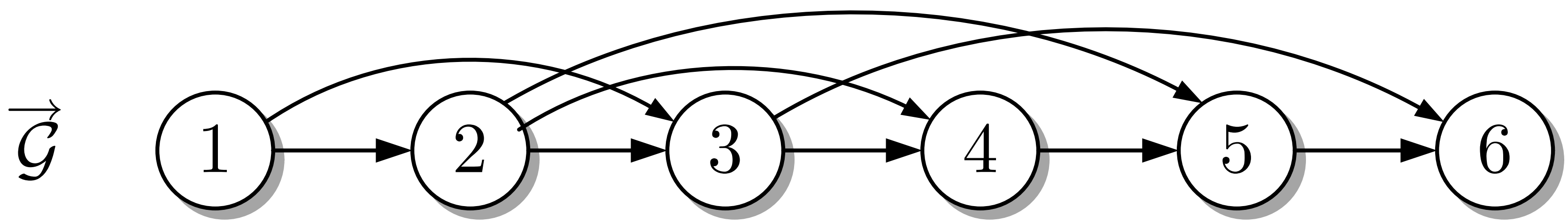

Fig. 9.32. Communication graph used to solve the robot position problem

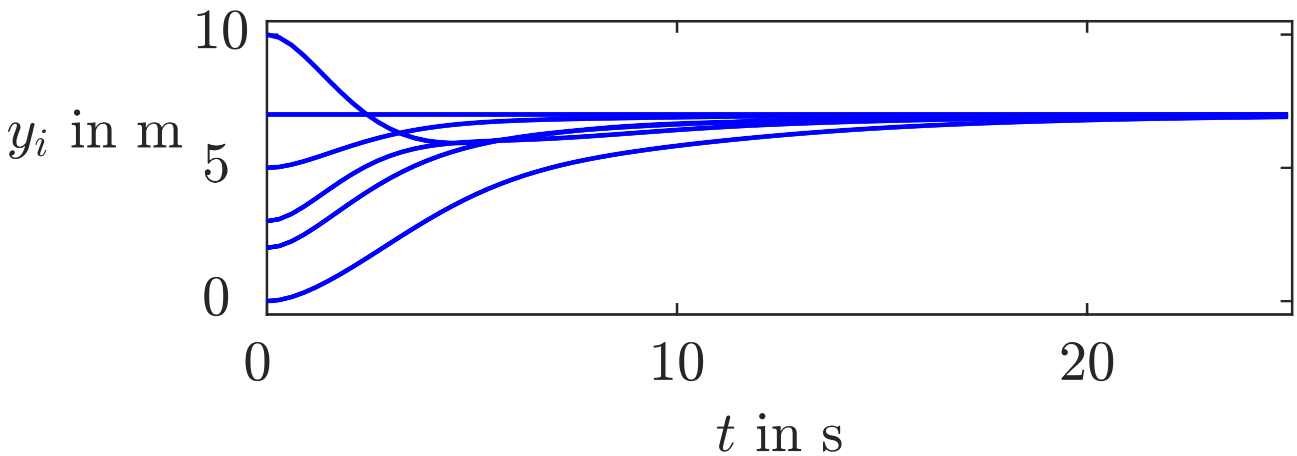

Fig. 9.33: Synchronisation by means of a continuous networked controller

J. LUNZE: *Networked Control of Multi-Agent Systems,* Edition MoRa 2022

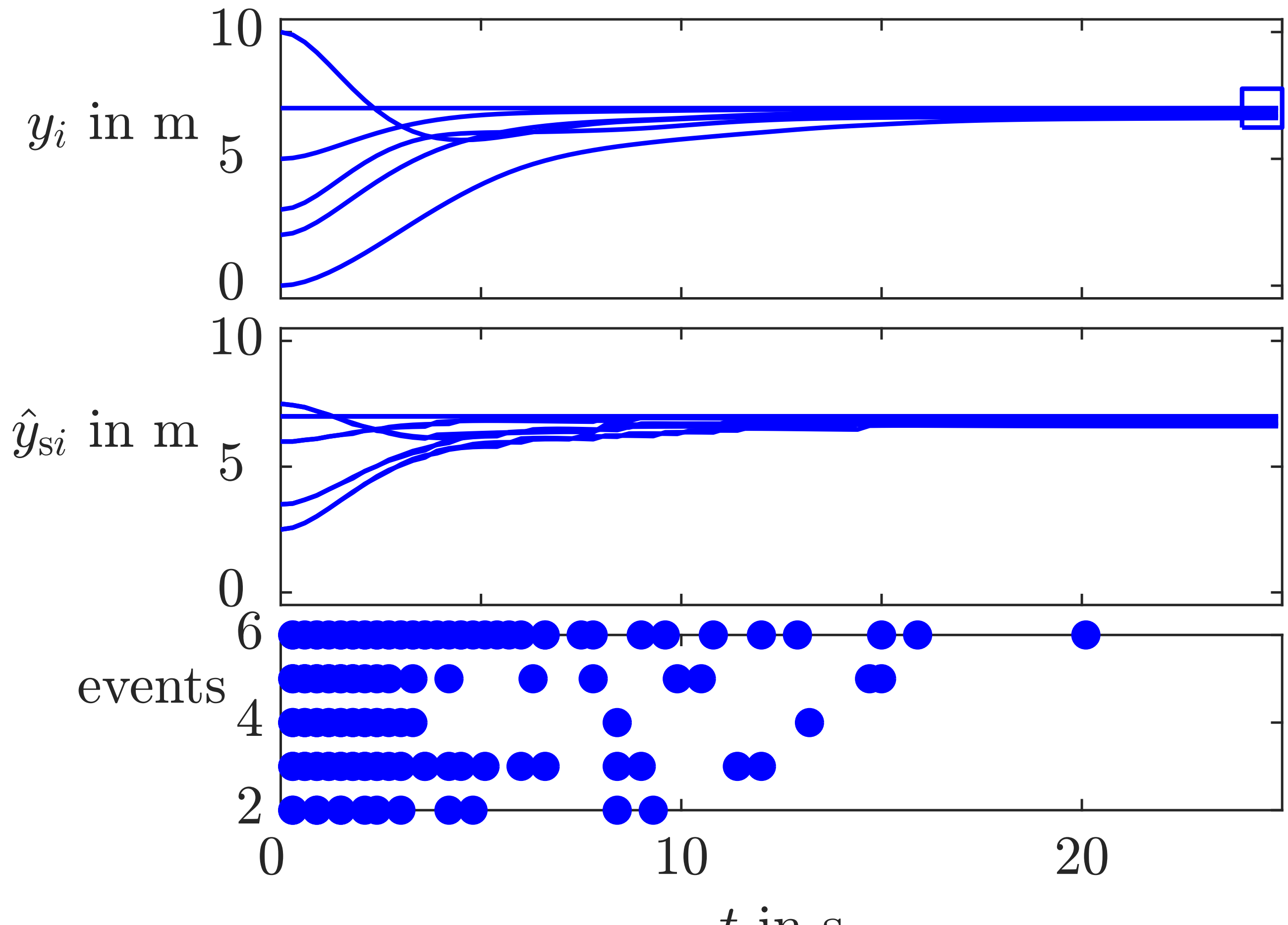

Fig. 9.34: Synchronisation by means of an event-triggered networked controller

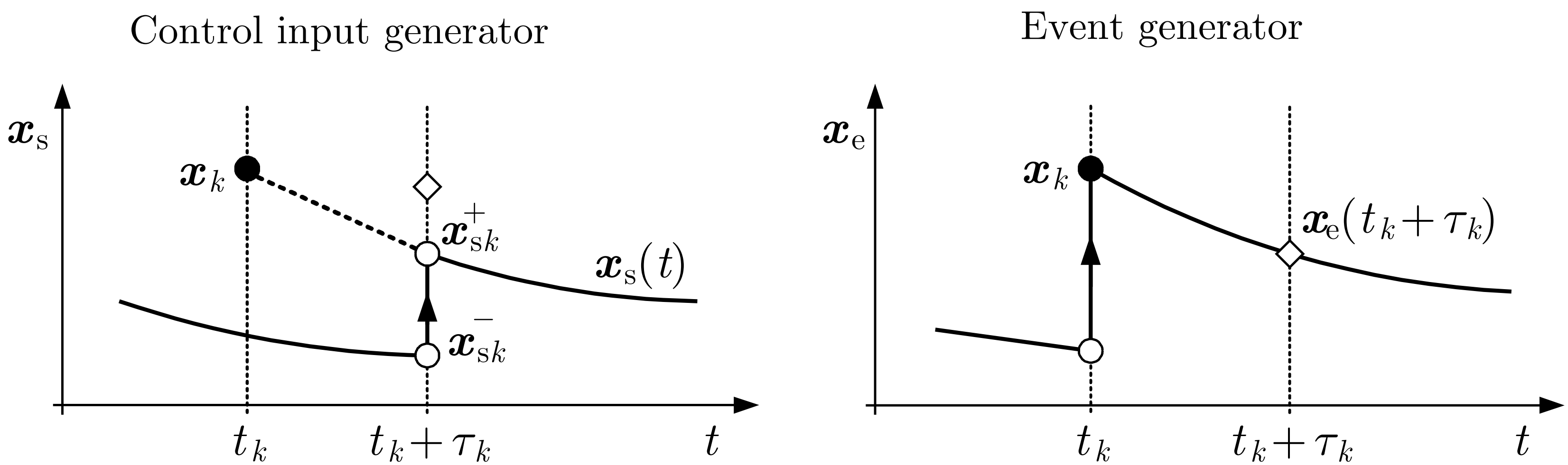

Fig. 9.35. State reset at time t_k or $t_k + \tau_k$

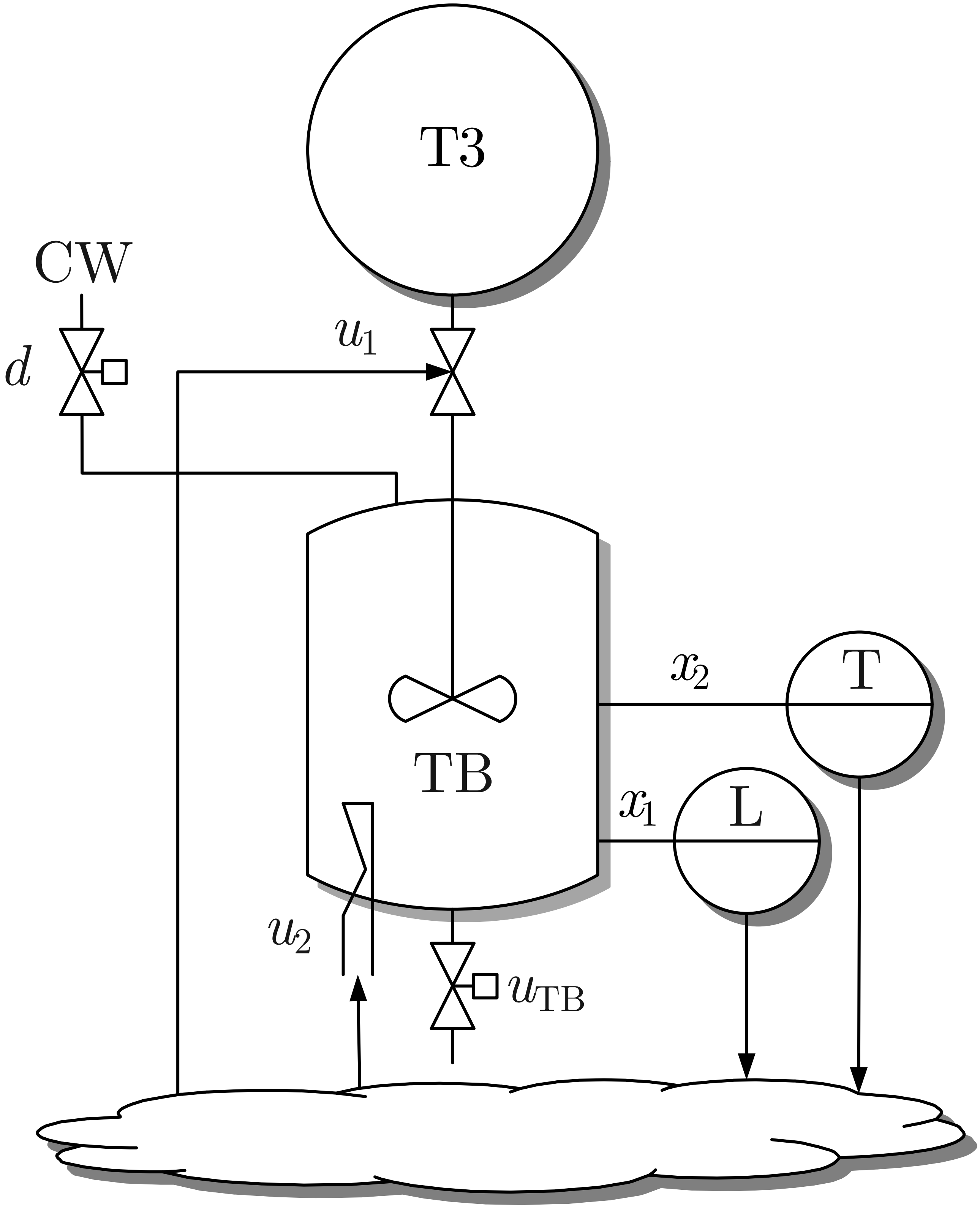

Fig. 9.36: A thermo-fluid process

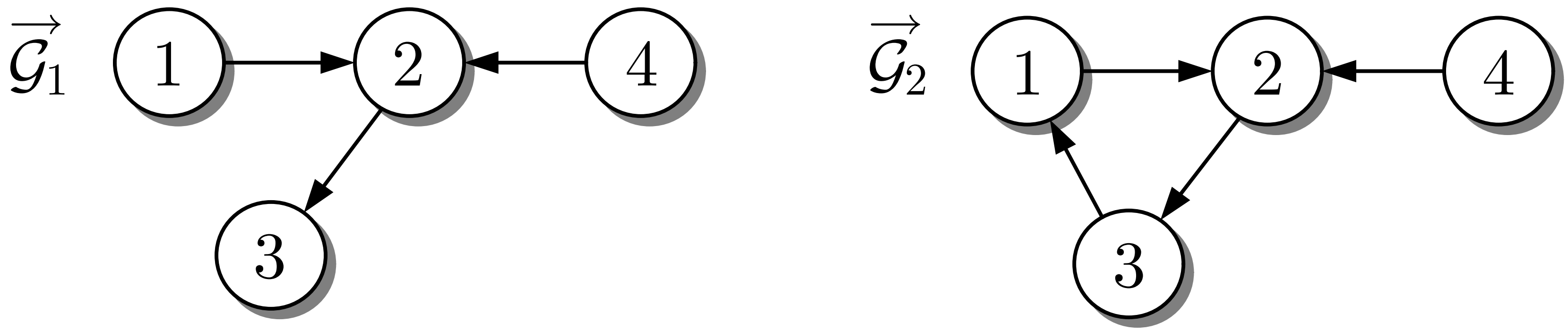

Fig. A1.1. A tree and a general graph with oriented edges

J. Lunze: *Networked Control of Multi-Agent Systems*, Edition MoRa 2022

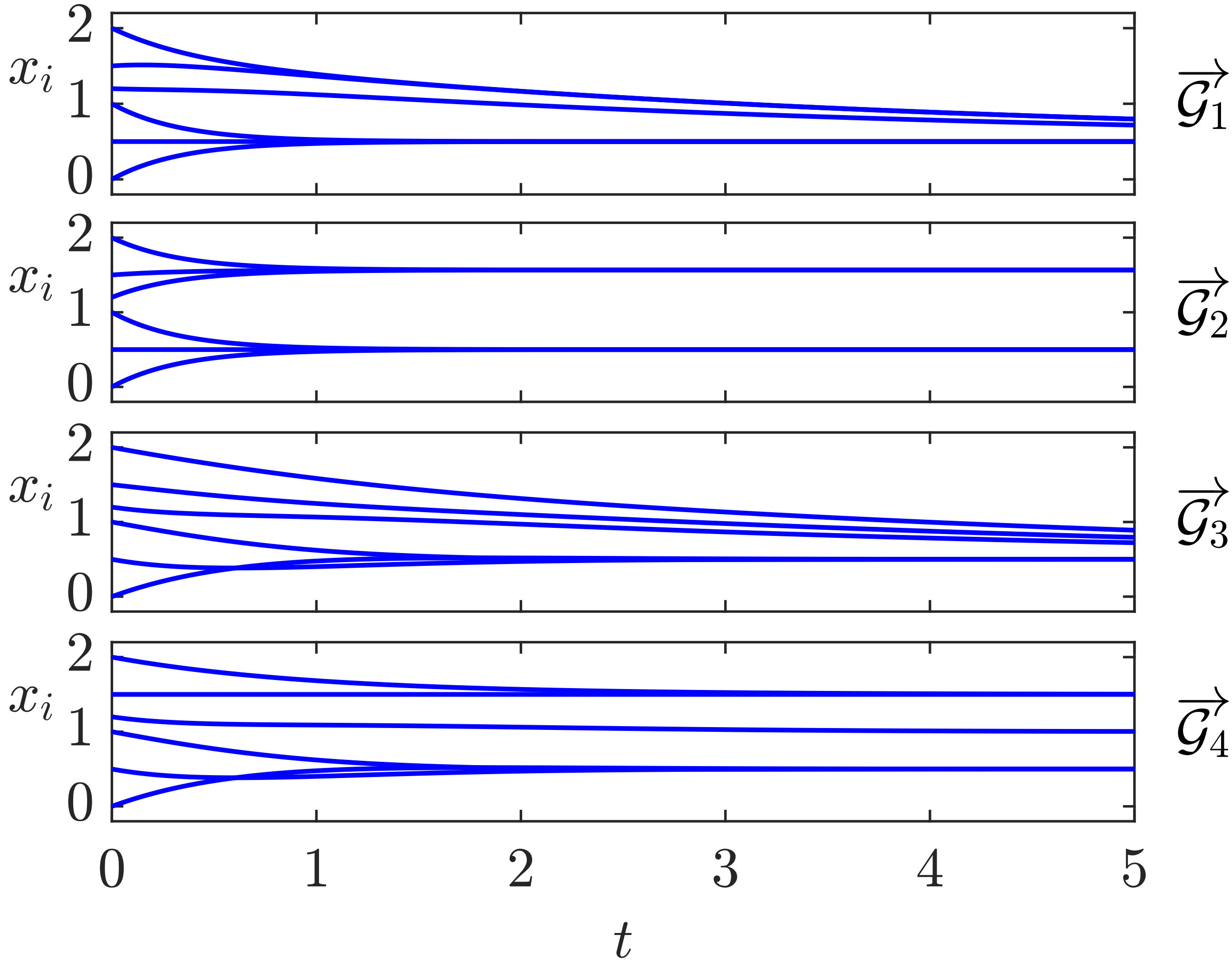

Fig. A1.2: Behaviour of the systems with the graphs shown in Fig. 3.7

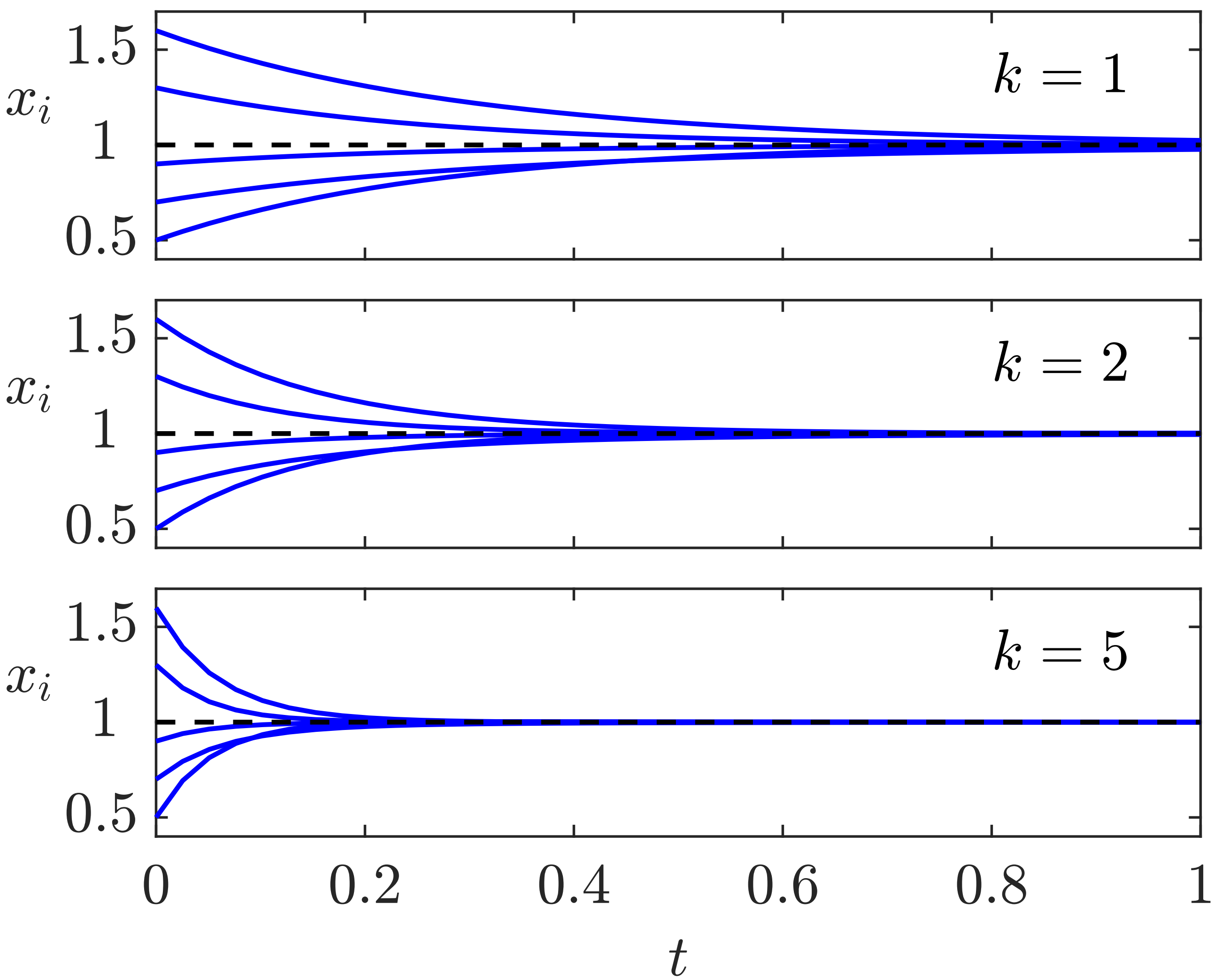

Fig. A1.3: Behaviour of the system with feedback gain $k = 1$ (top), $k = 2$ (middle) and $k = 5$ (bottom)

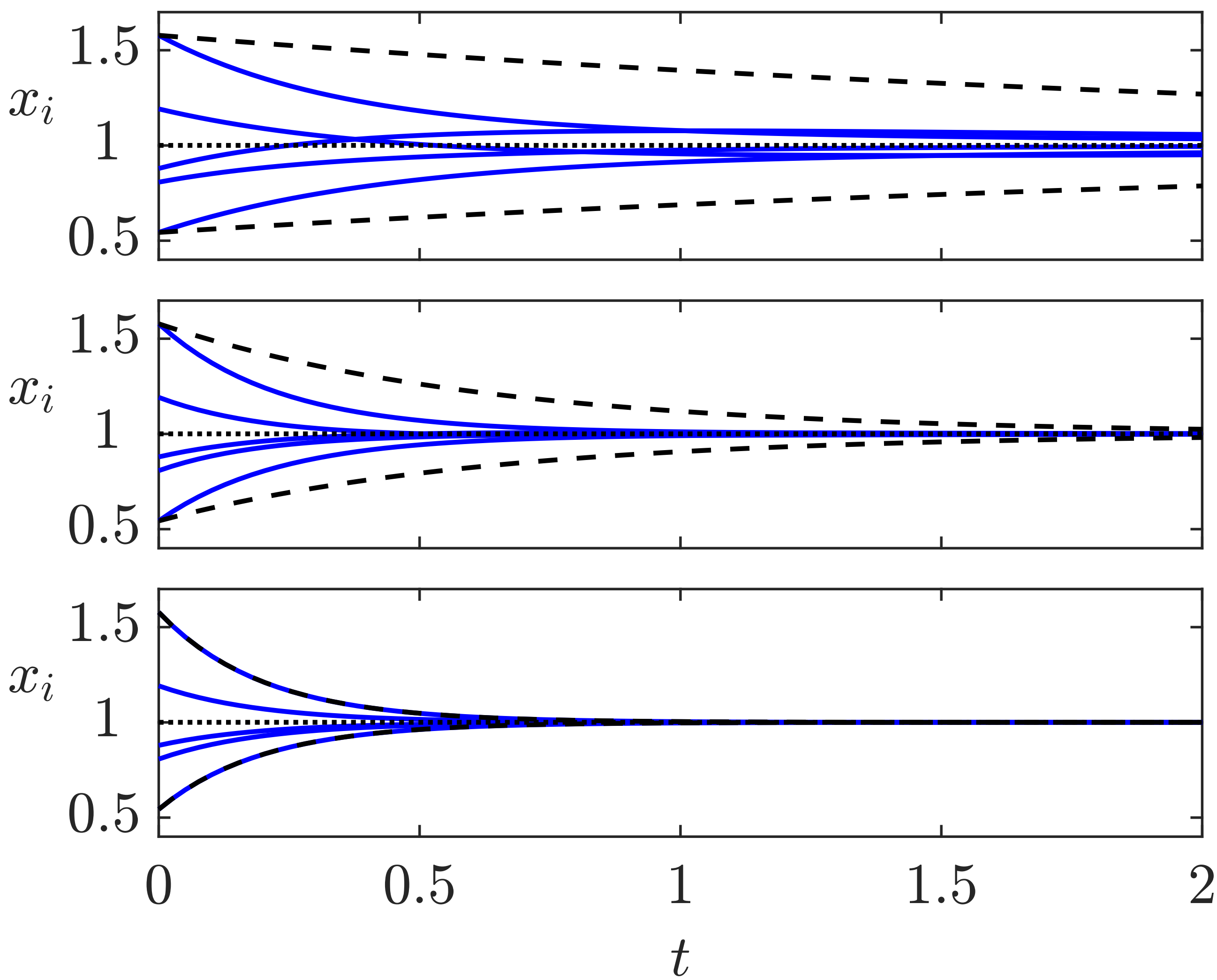

Fig. A1.4: Behaviour of the three systems

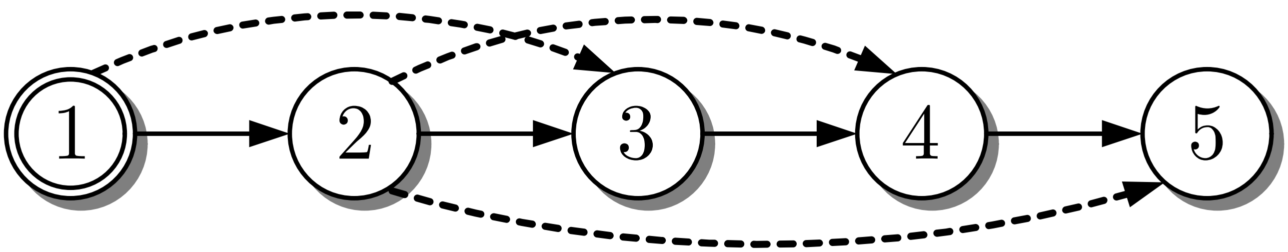

Fig. A1.5: Directed path graph with additional edges

J. Lunze: *Networked Control of Multi-Agent Systems,* Edition **MoRa** 2022

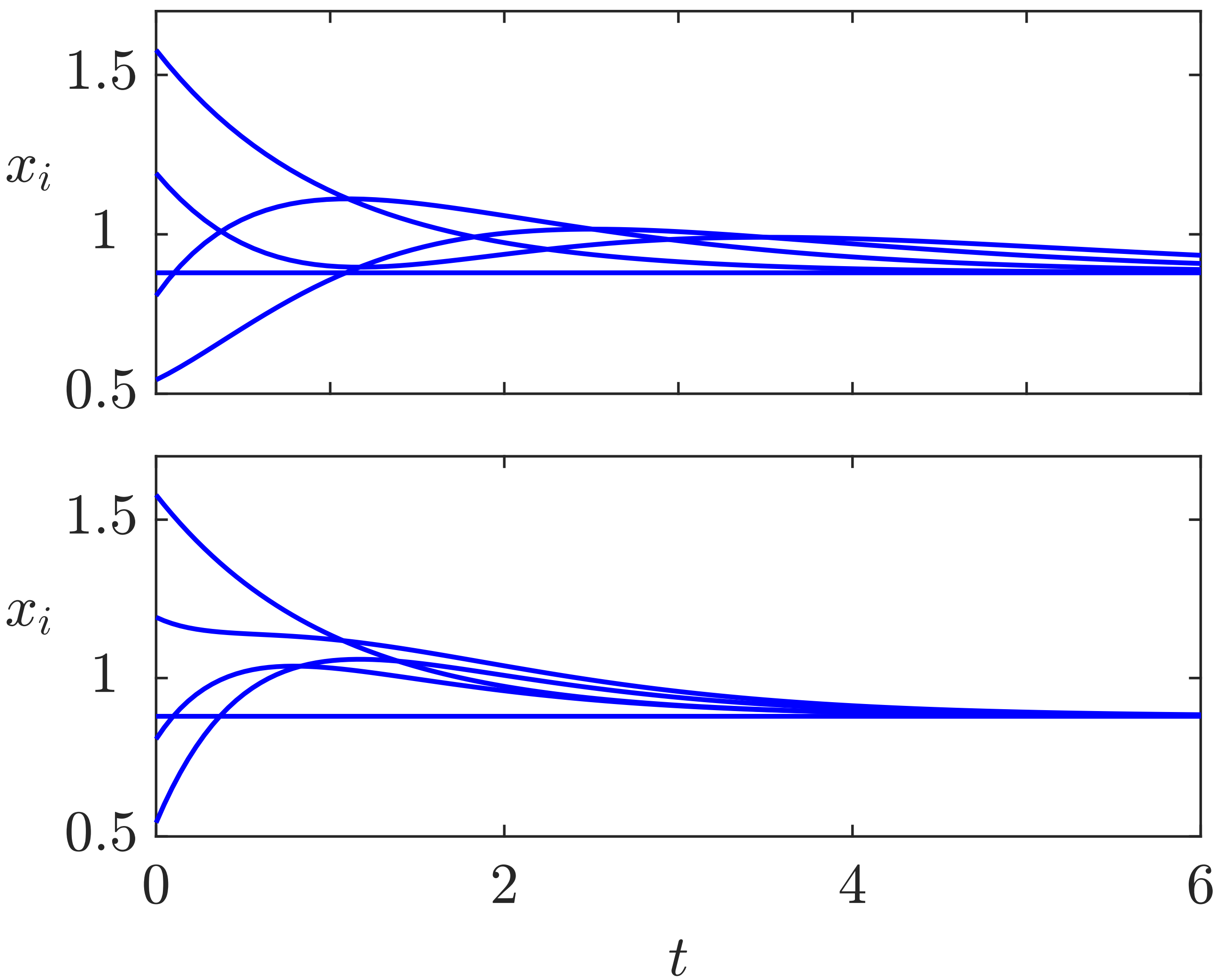

Fig. A1.6: Consensus behaviour for the path graph (top) and the graph with additional edges (bottom)

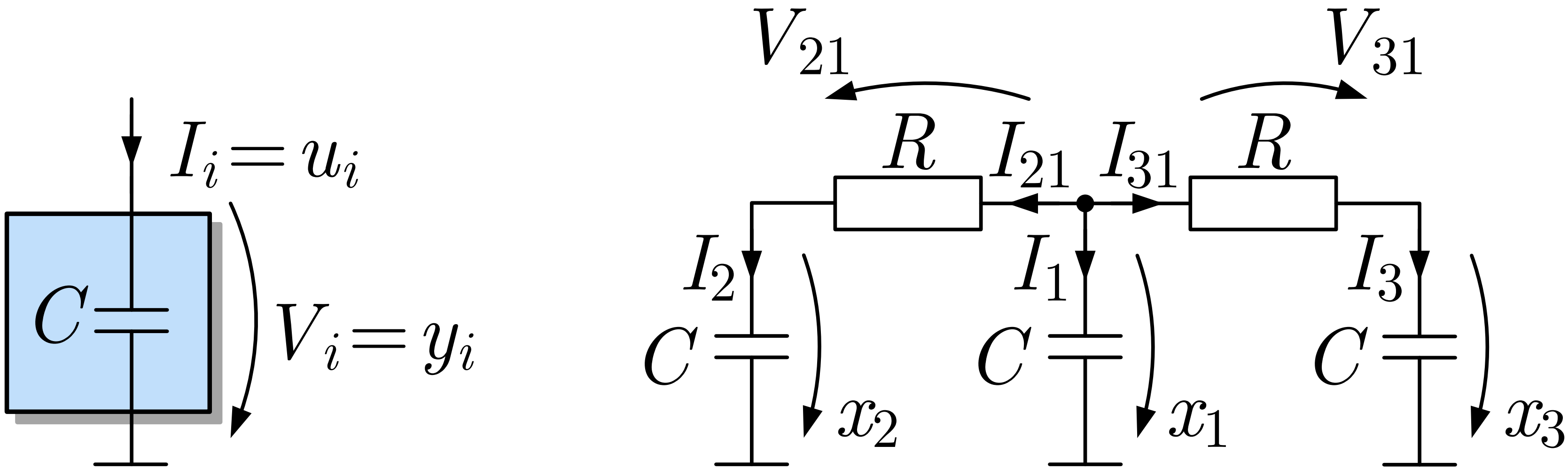

Fig. A1.7. Signals used to model a capacitor agent (left) and a part of the network (right)

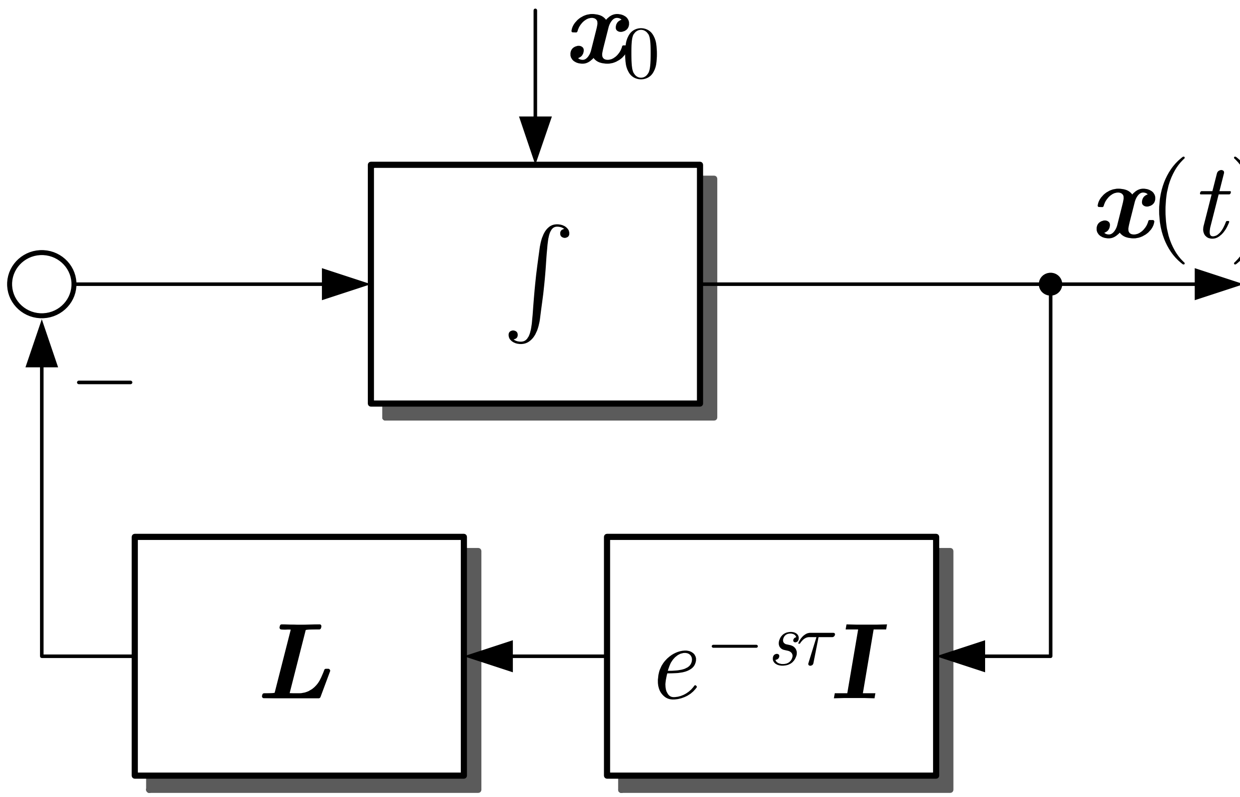

Fig. A1.8: Structure of the consensus system with time delay

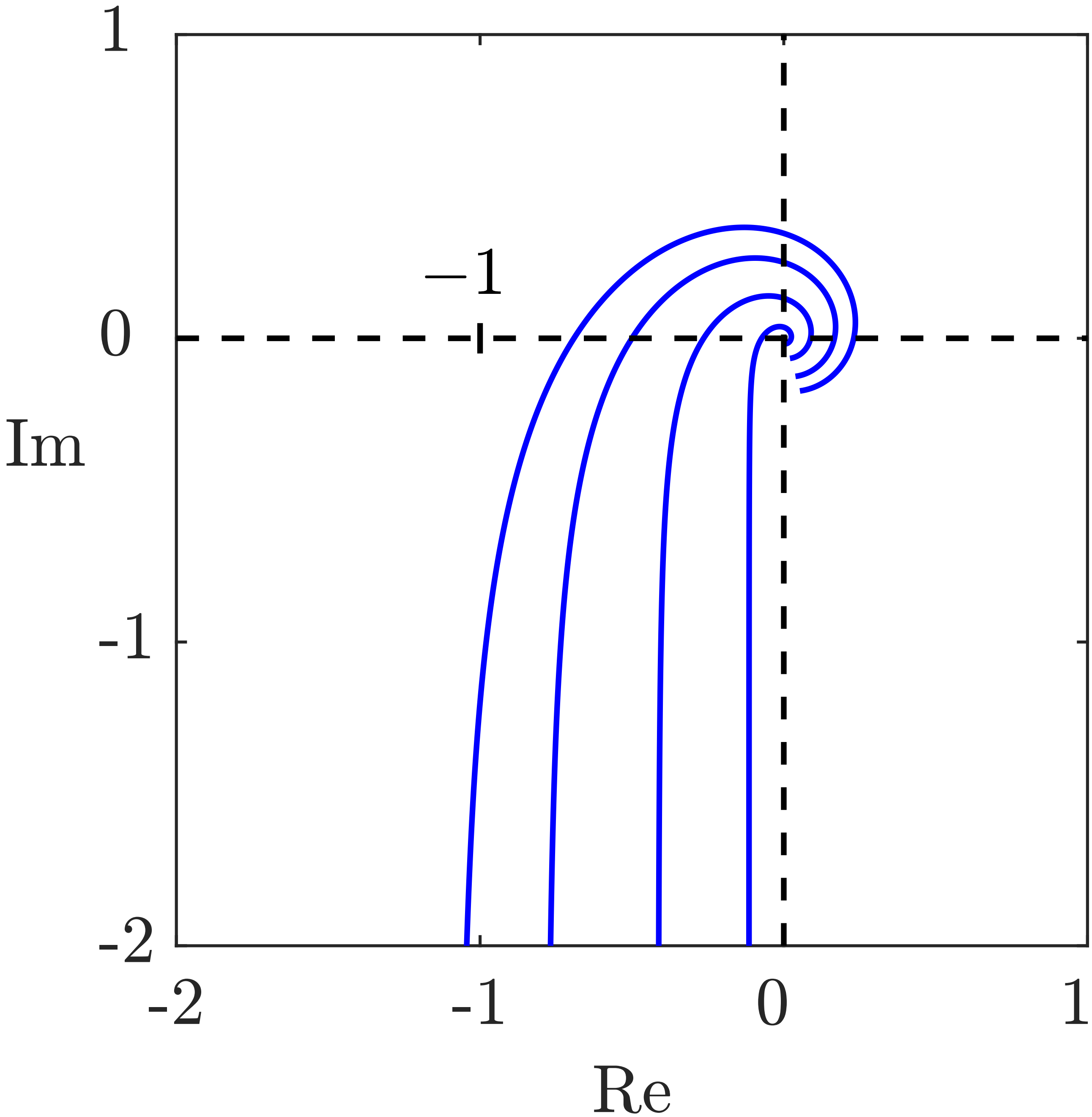

Fig. A1.9: Nyquist plot of the transfer functions (A1.11)

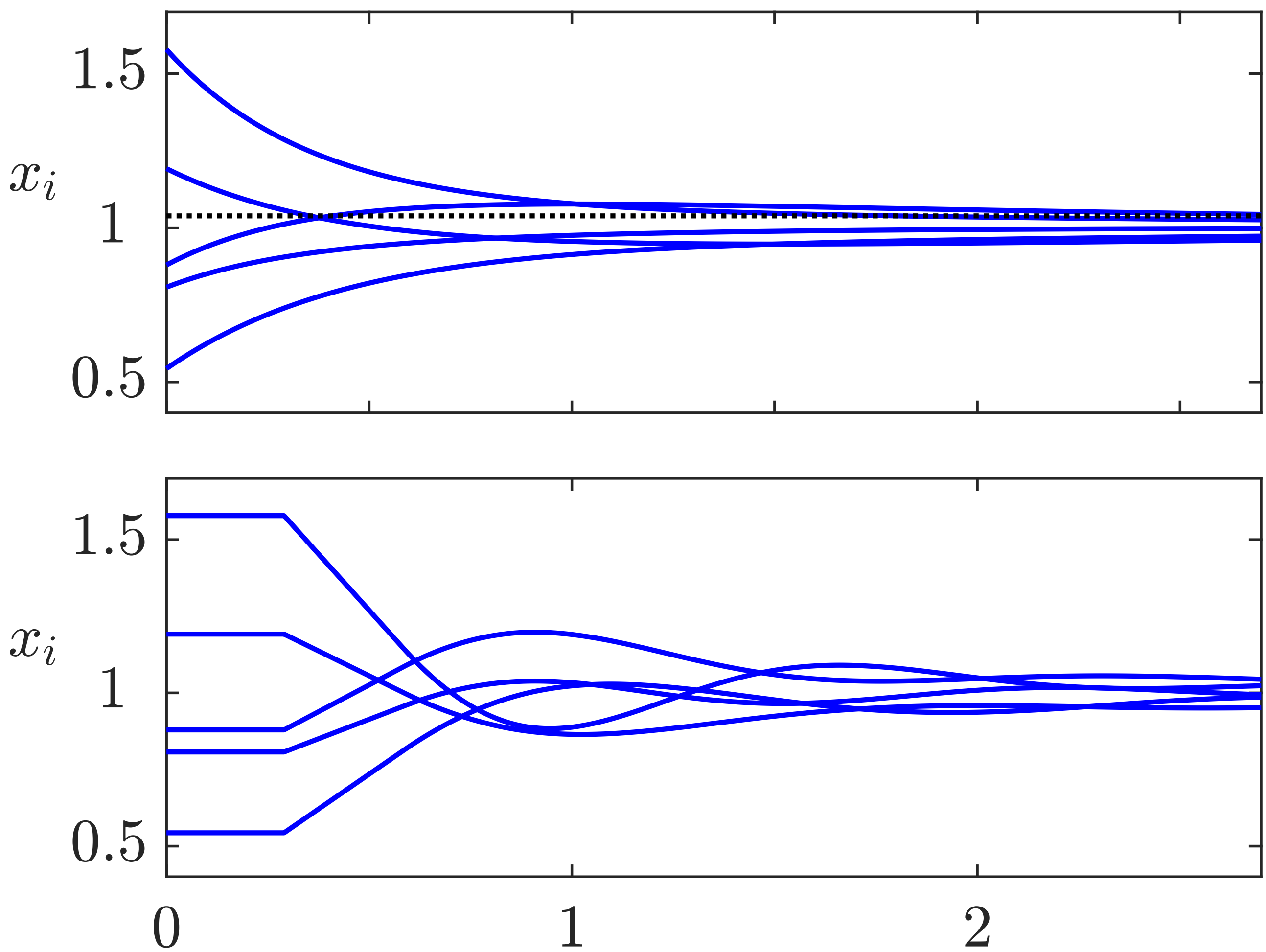

Fig. A1.10: Comparison of the consensus behaviour of the system without delay (top) and with delay $\tau = 0.3$ (bottom)

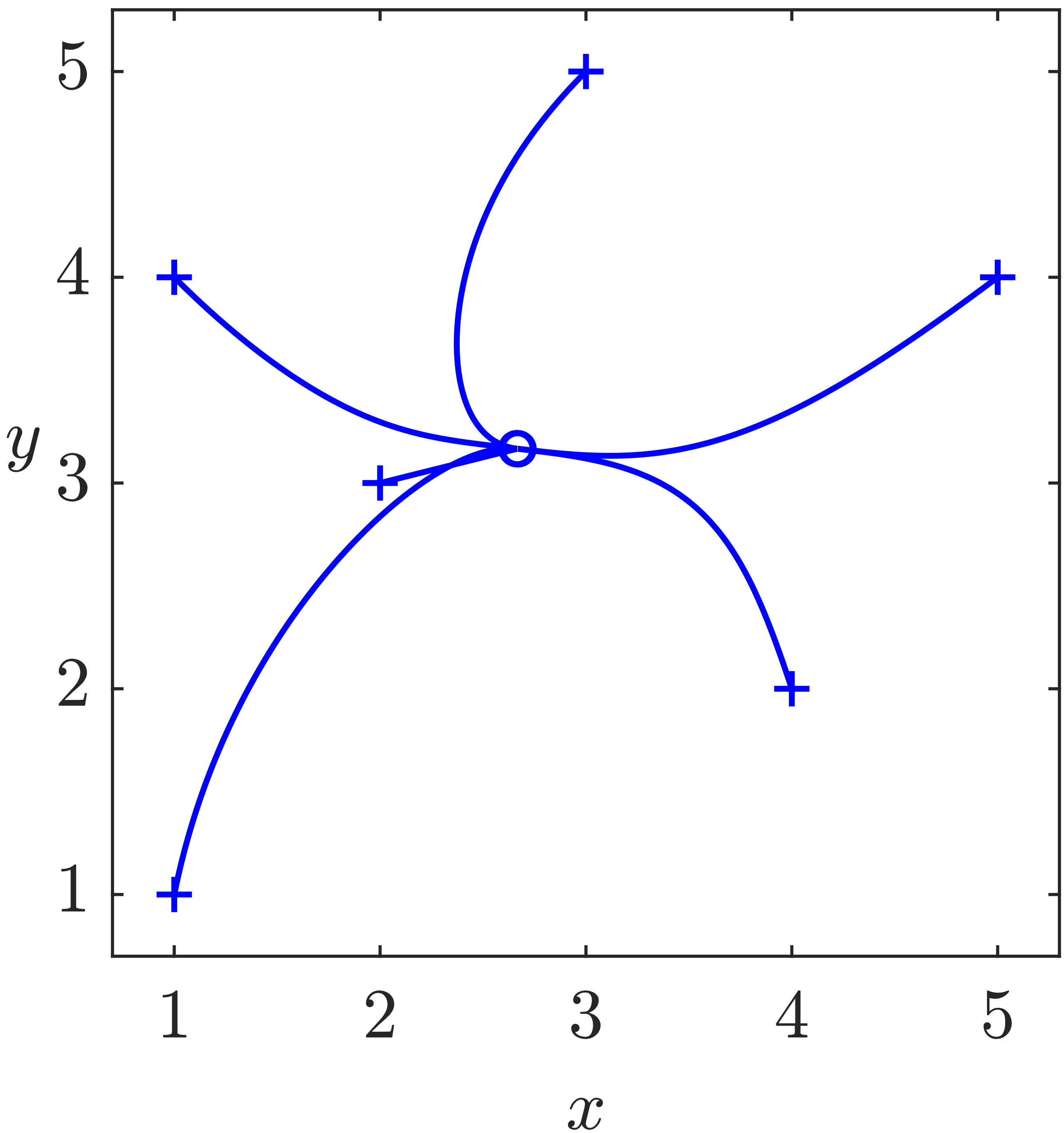

Fig. A1.11: Rendezvous of six robots

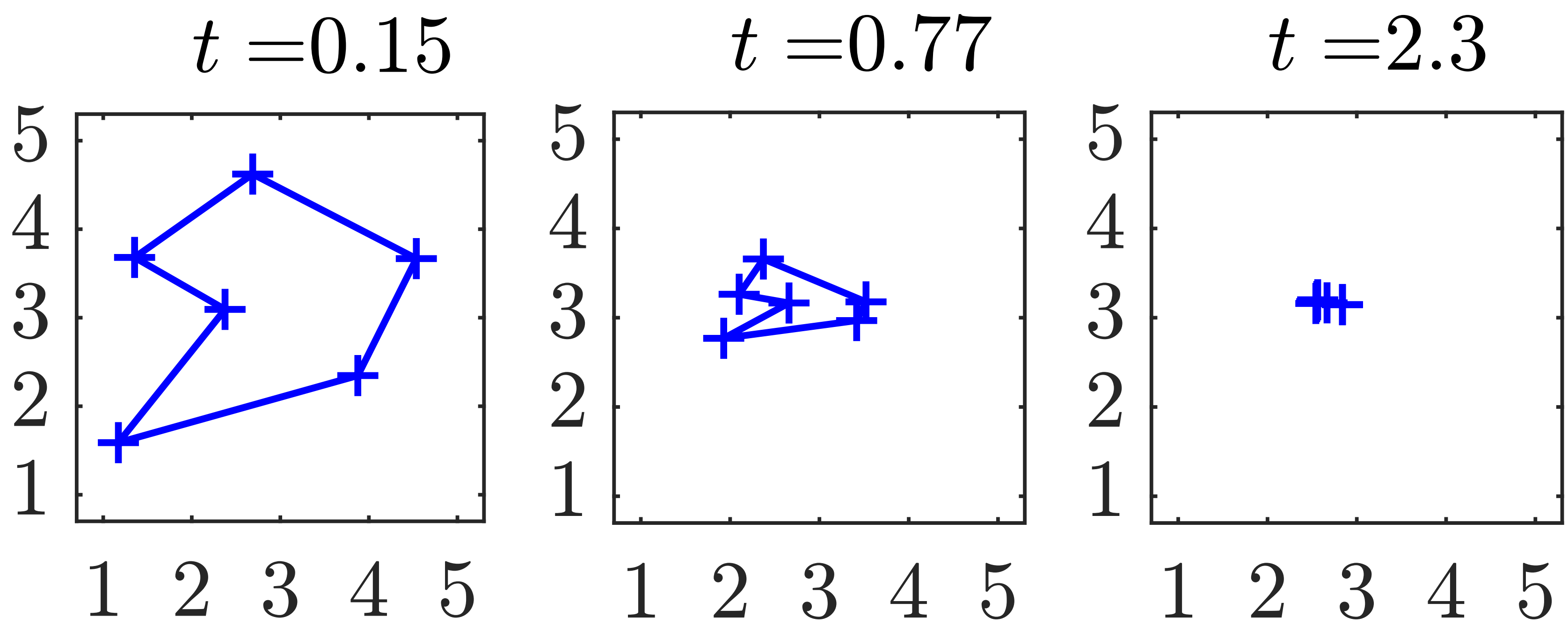

Fig. A1.12. Robot positions at three time points

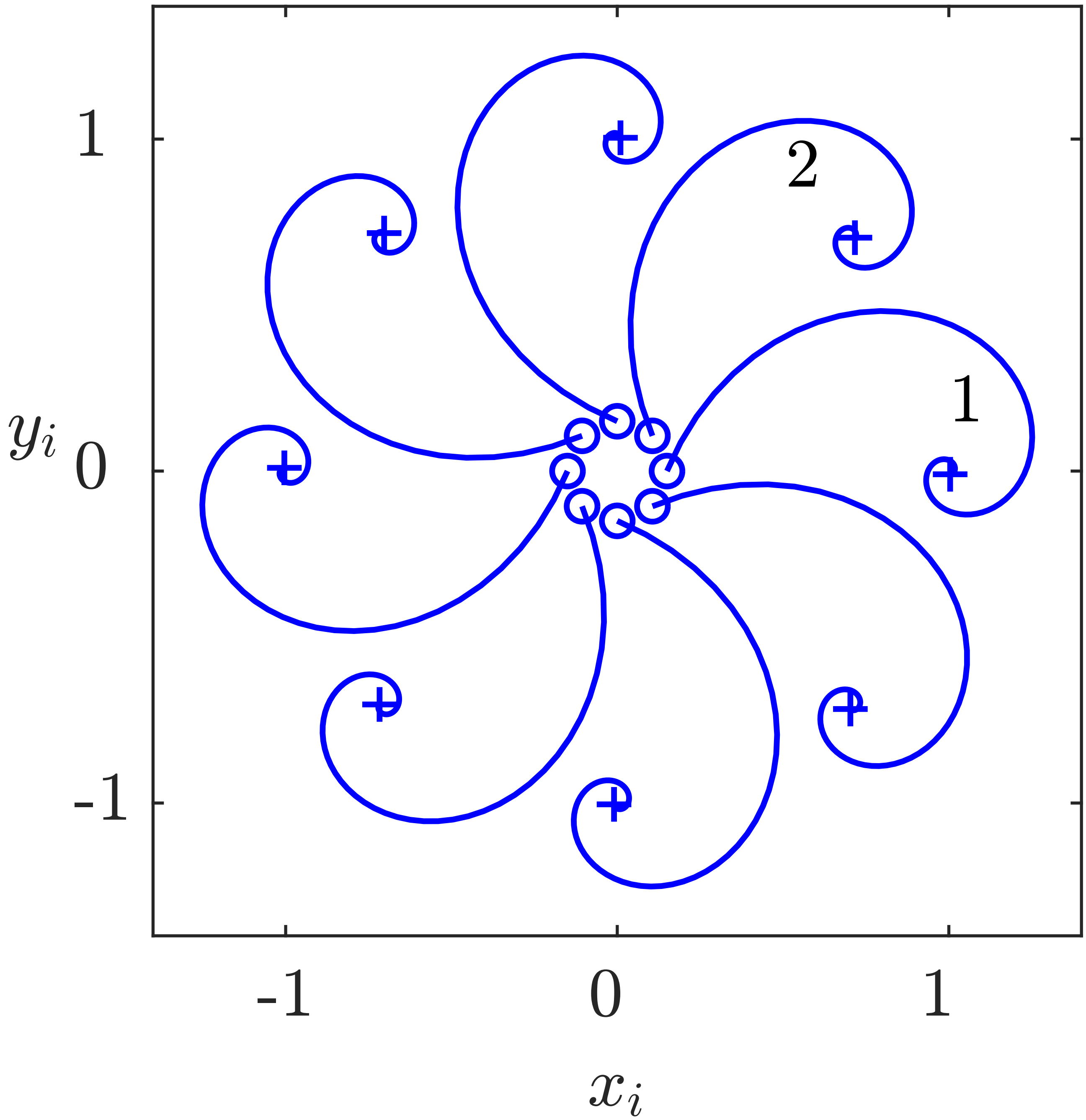

Fig. A1.13: Behaviour of the robots with ring communication structure

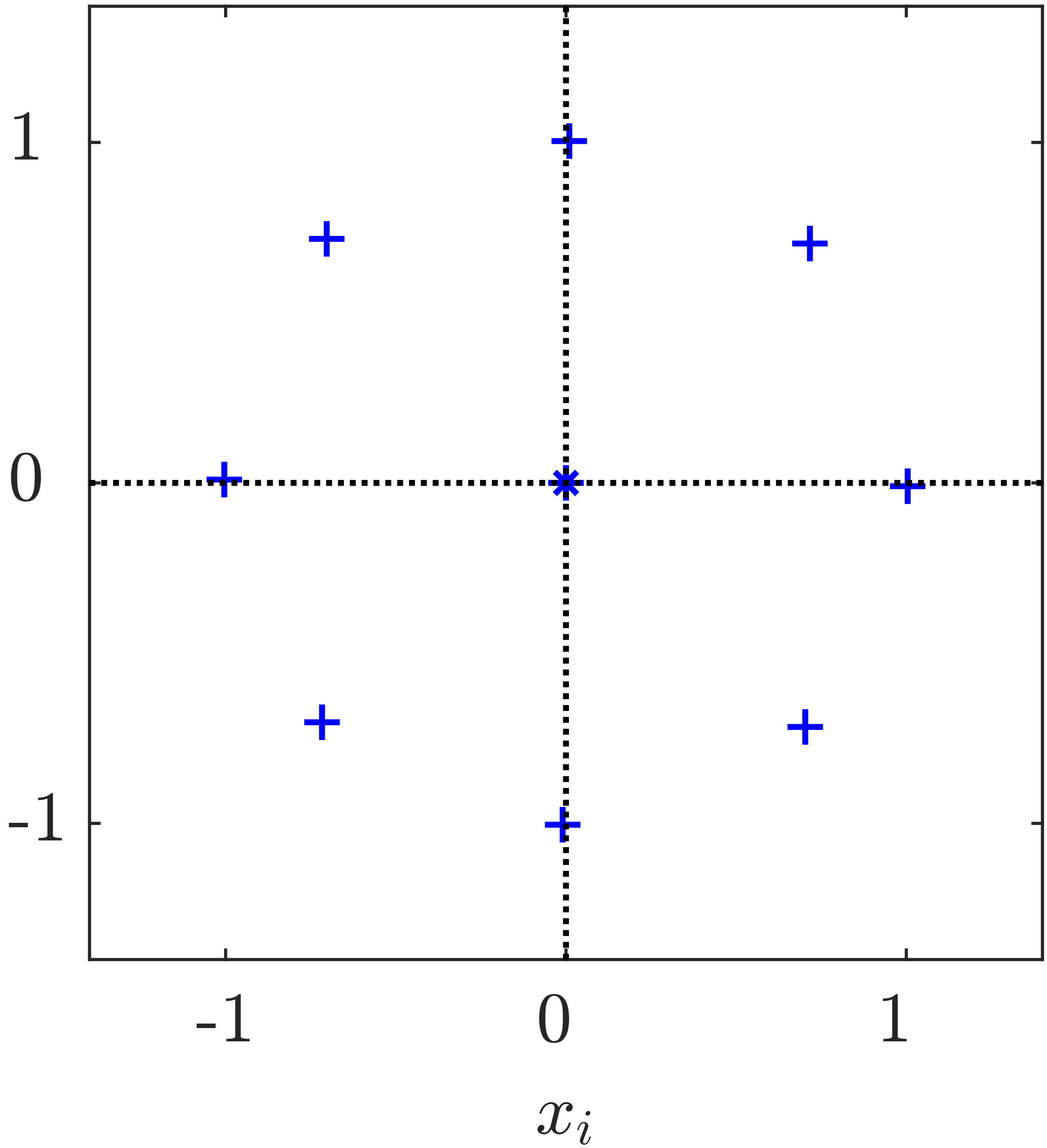

Fig. A1.13: Behaviour of the robots with ring communication structure

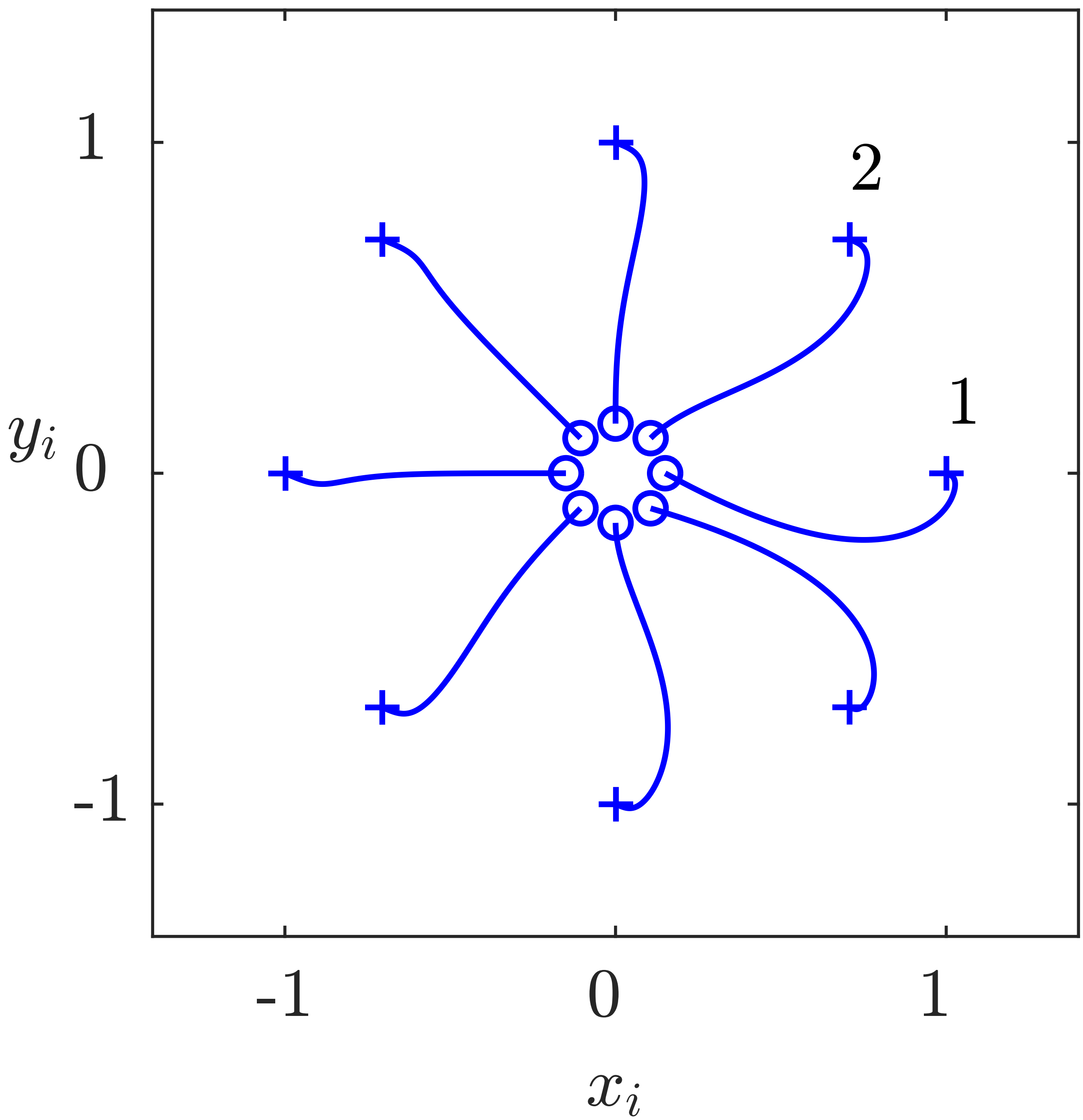

Fig. A1.14: Behaviour of the robots with neighbouring couplings

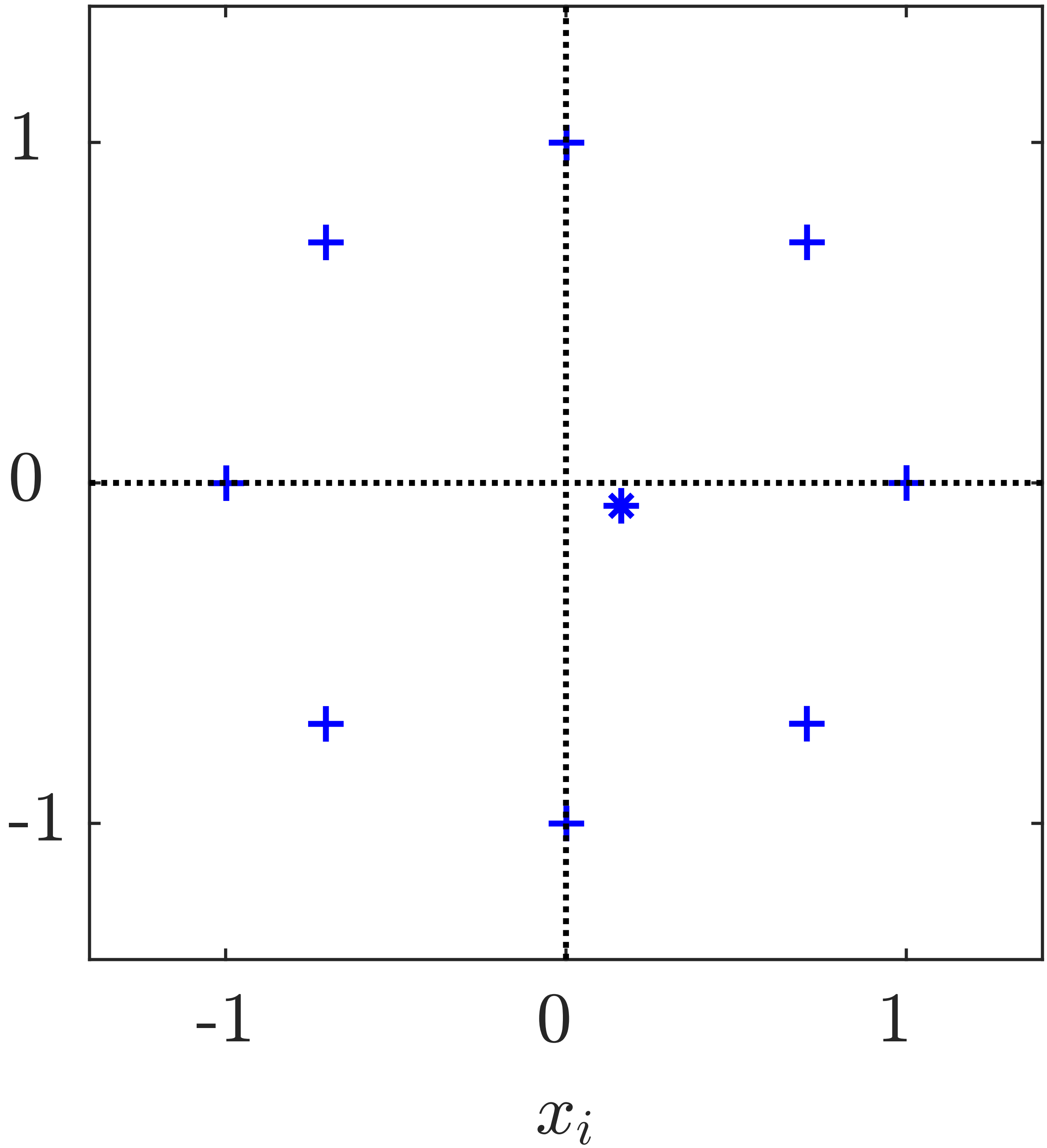

Fig. A1.14: Behaviour of the robots with neighbouring couplings

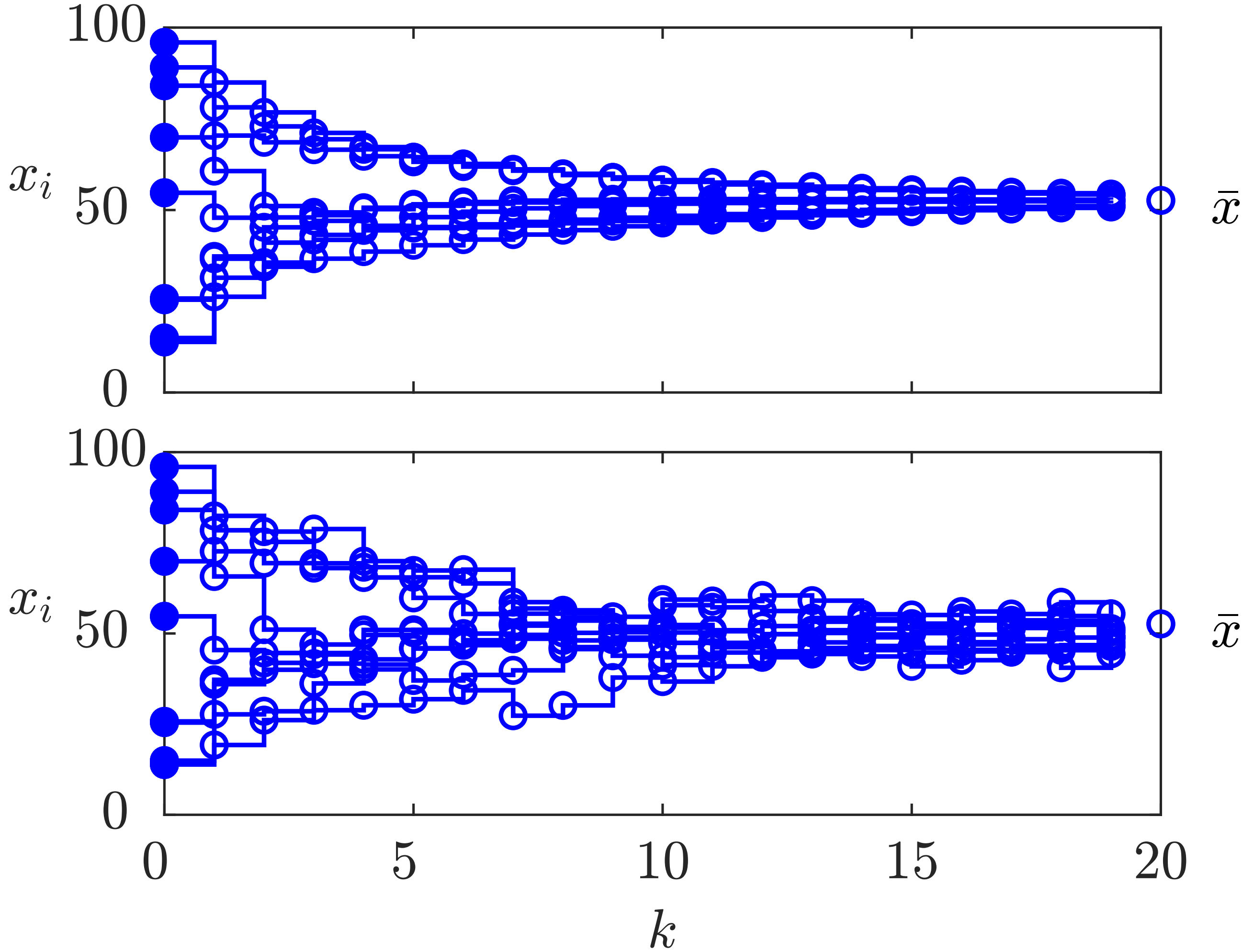

Fig. A1.15: Load-balancing of multiprocessors

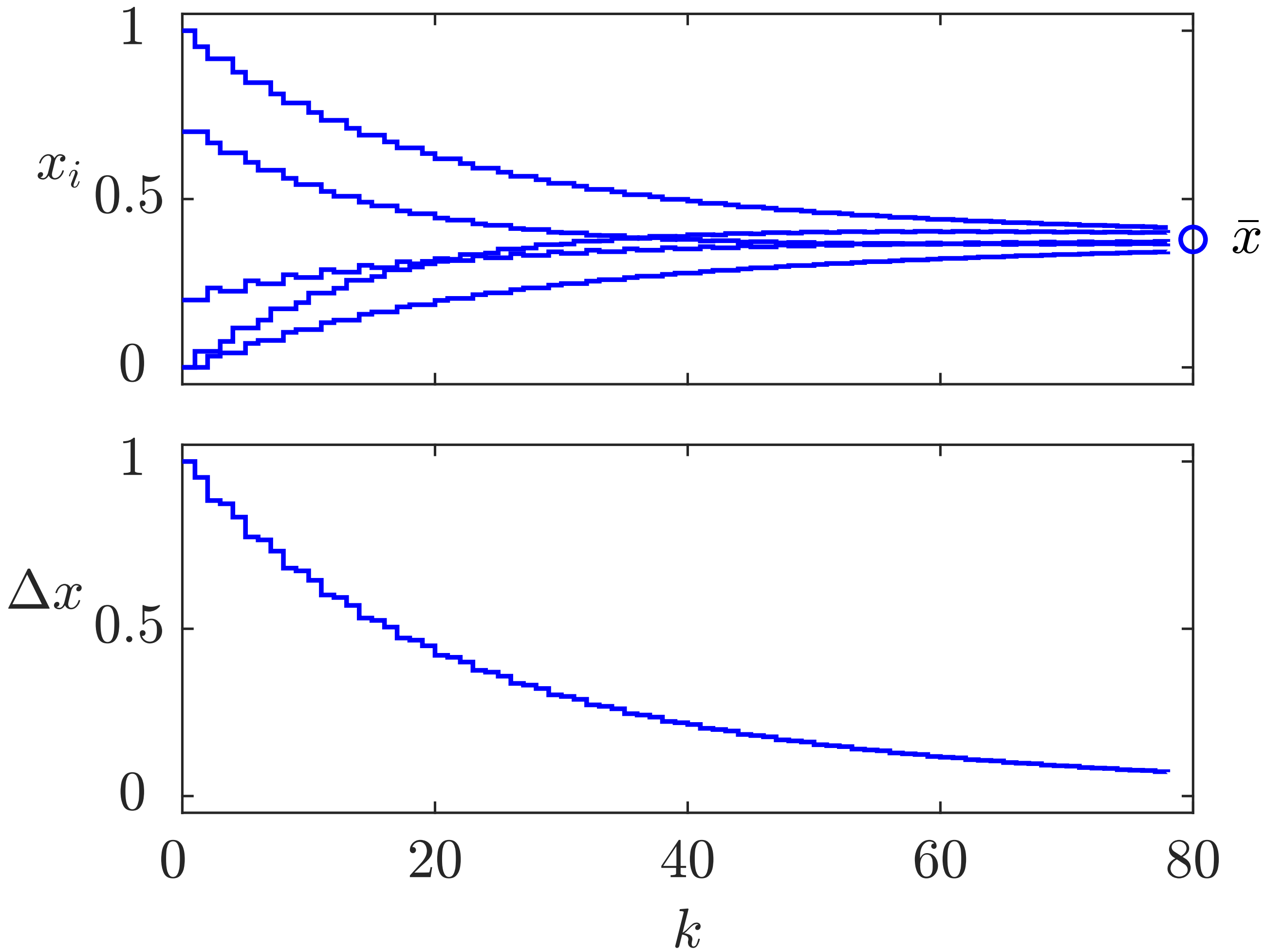

Fig. A1.16: Result of the gossiping algorithm

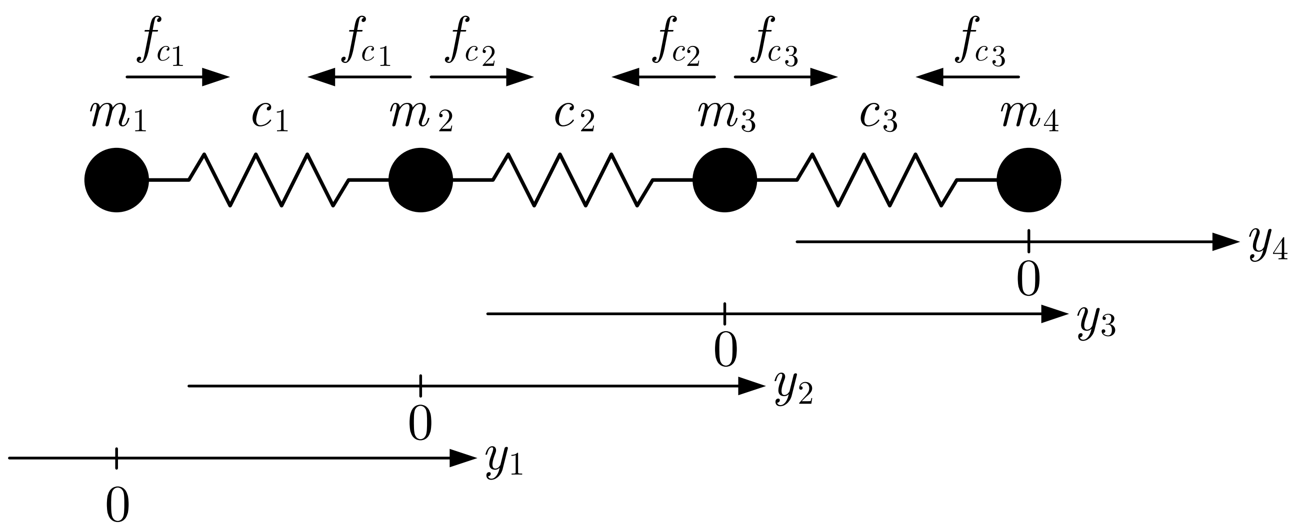

Fig. A1.17: Spring-mass system with forces

J. LUNZE: *Networked Control of Multi-Agent Systems,* Edition **M**o**R**a 2022

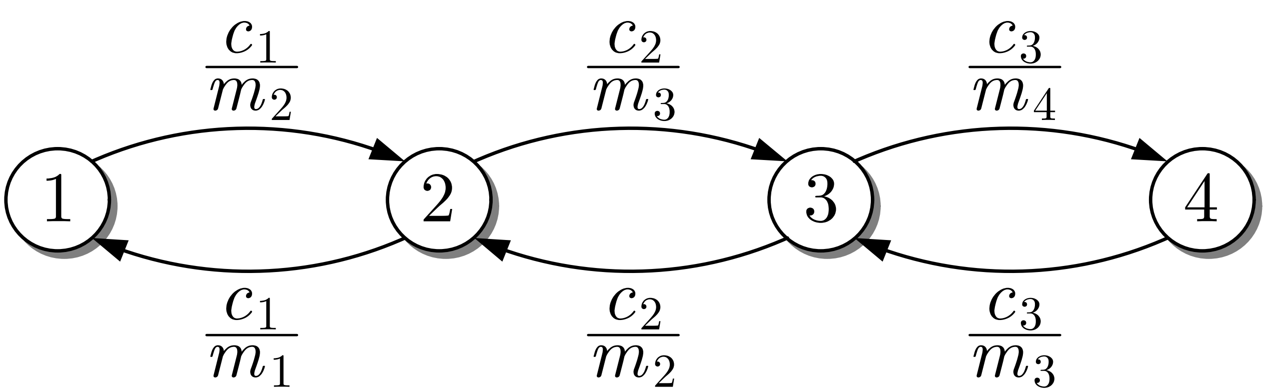

Fig. A1.18: Graph of the spring-mass system

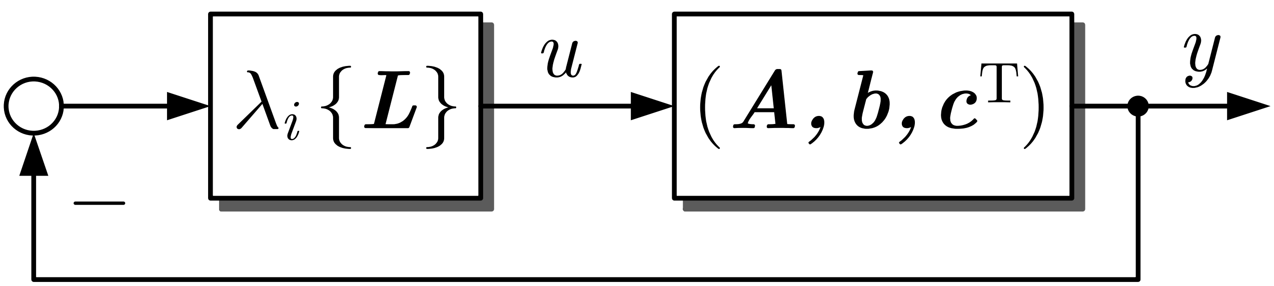

Fig. A1.19: Interpretation of the synchronisation condition

J. Lunze: *Networked Control of Multi-Agent Systems*, Edition MoRa 2022

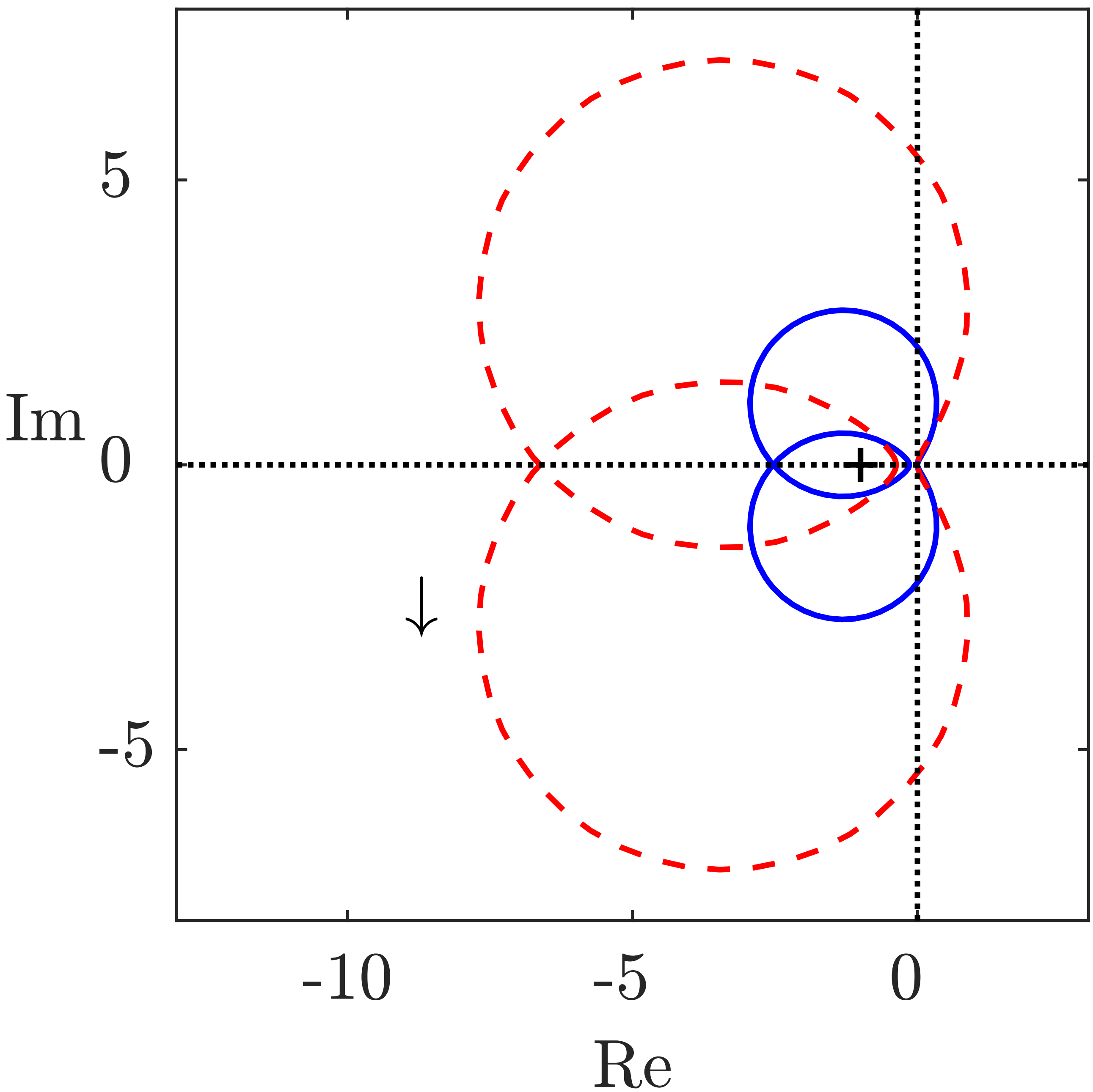

Fig. A1.20: Nyquist plot for the oscillator example

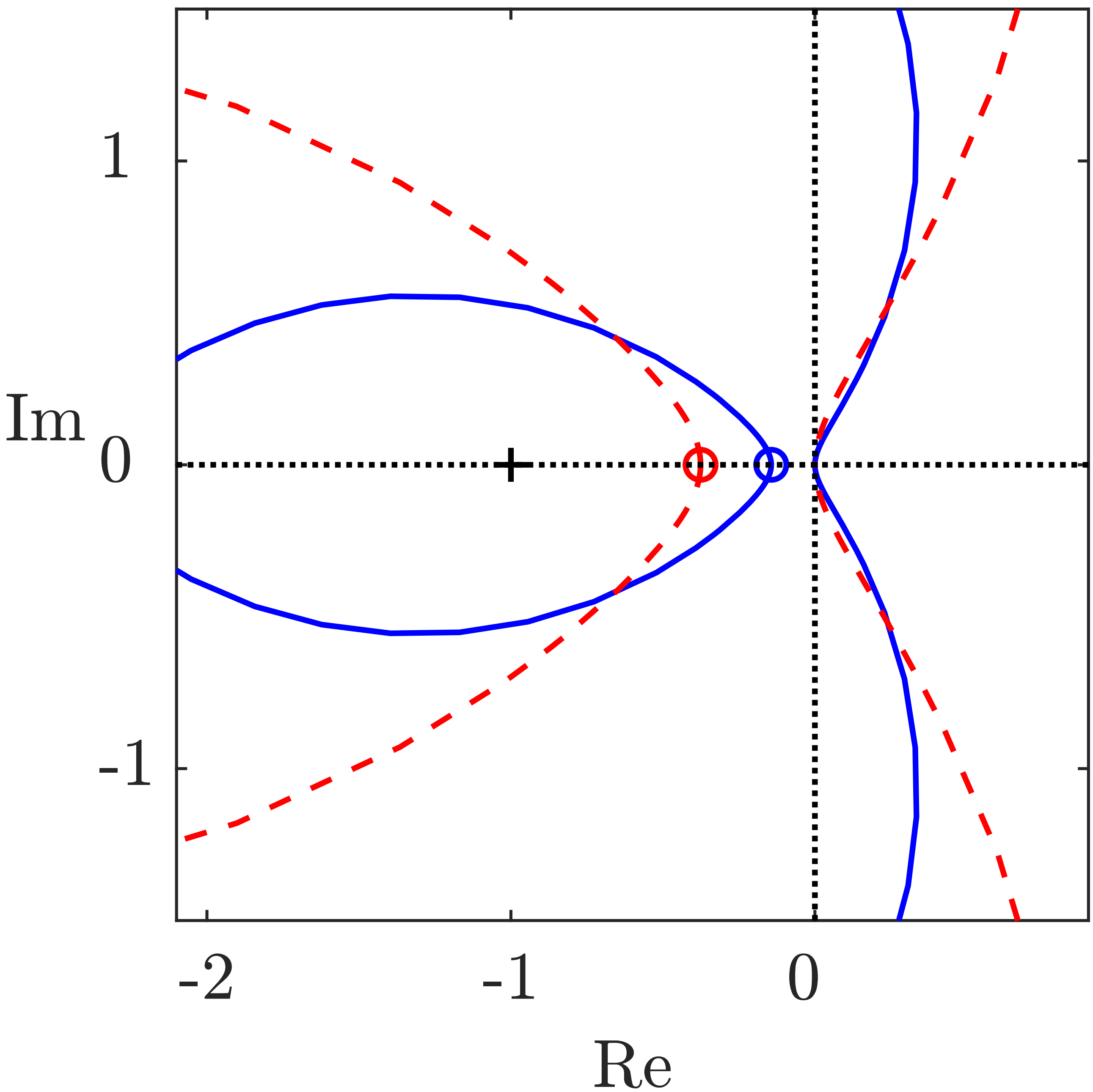

Fig. A1.20: Nyquist plot for the oscillator example

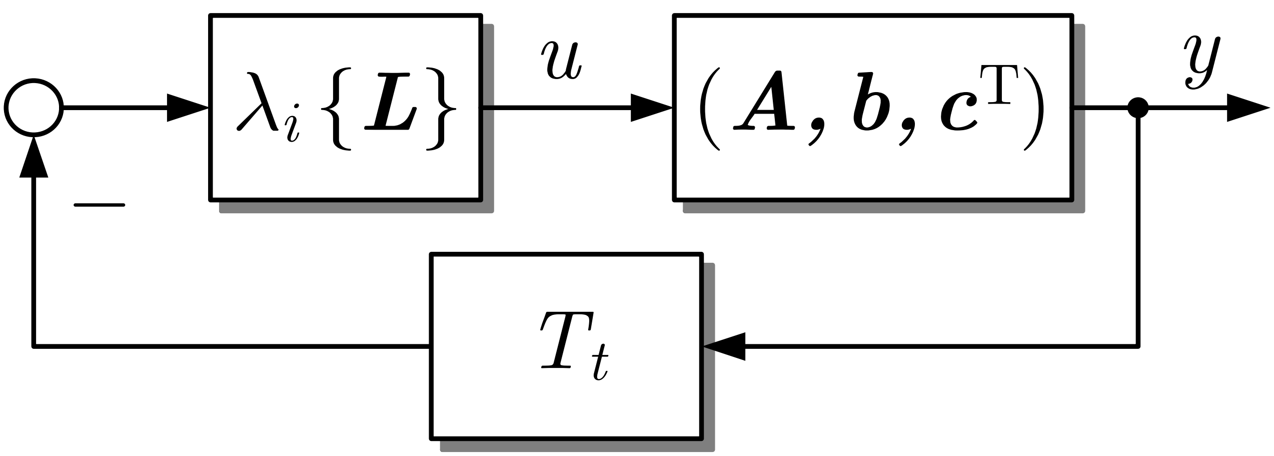

Fig. A1.21: Synchronisation with communication time delay

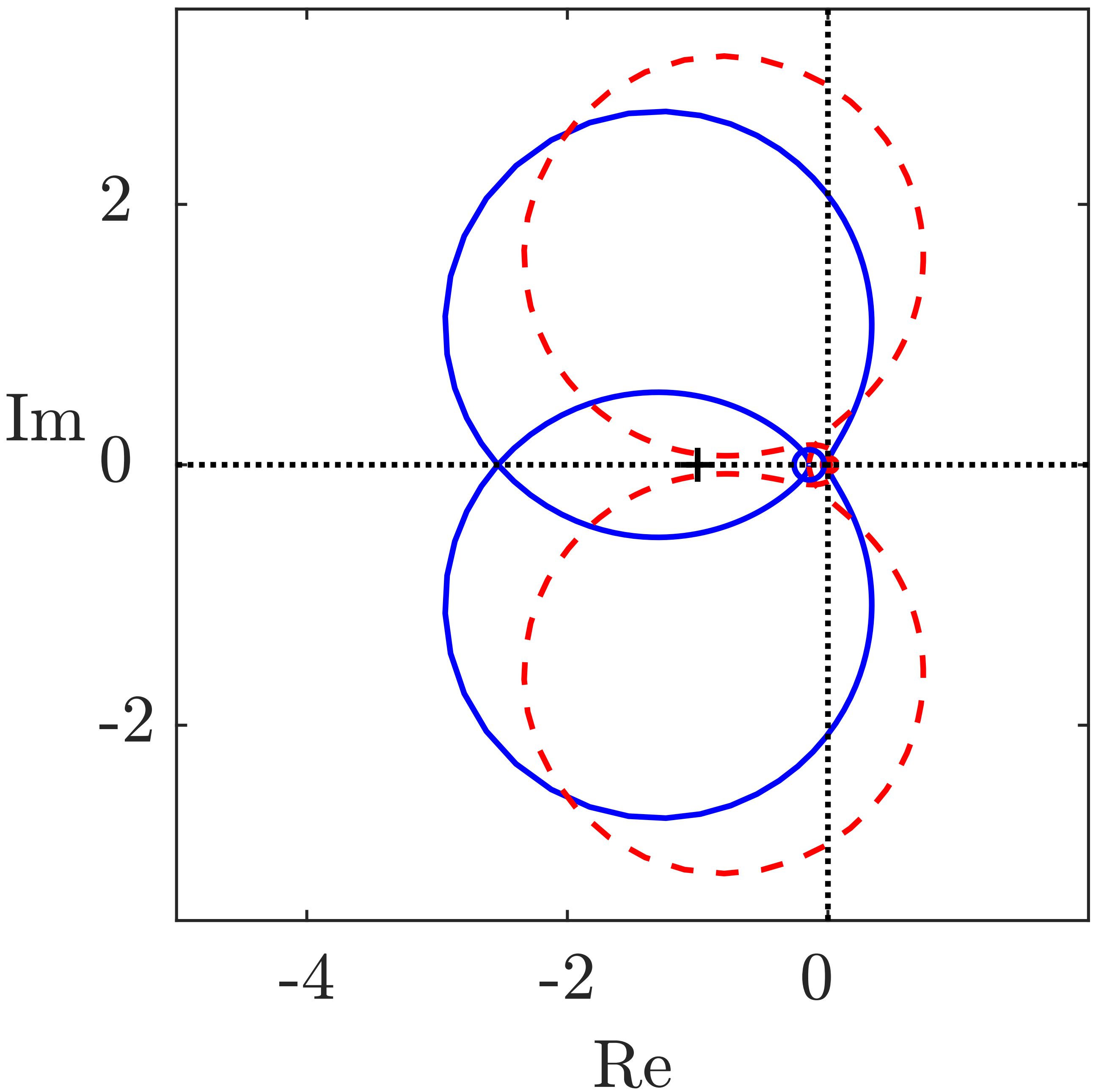

Fig. A1.22: Nyquist plot without and with time delay

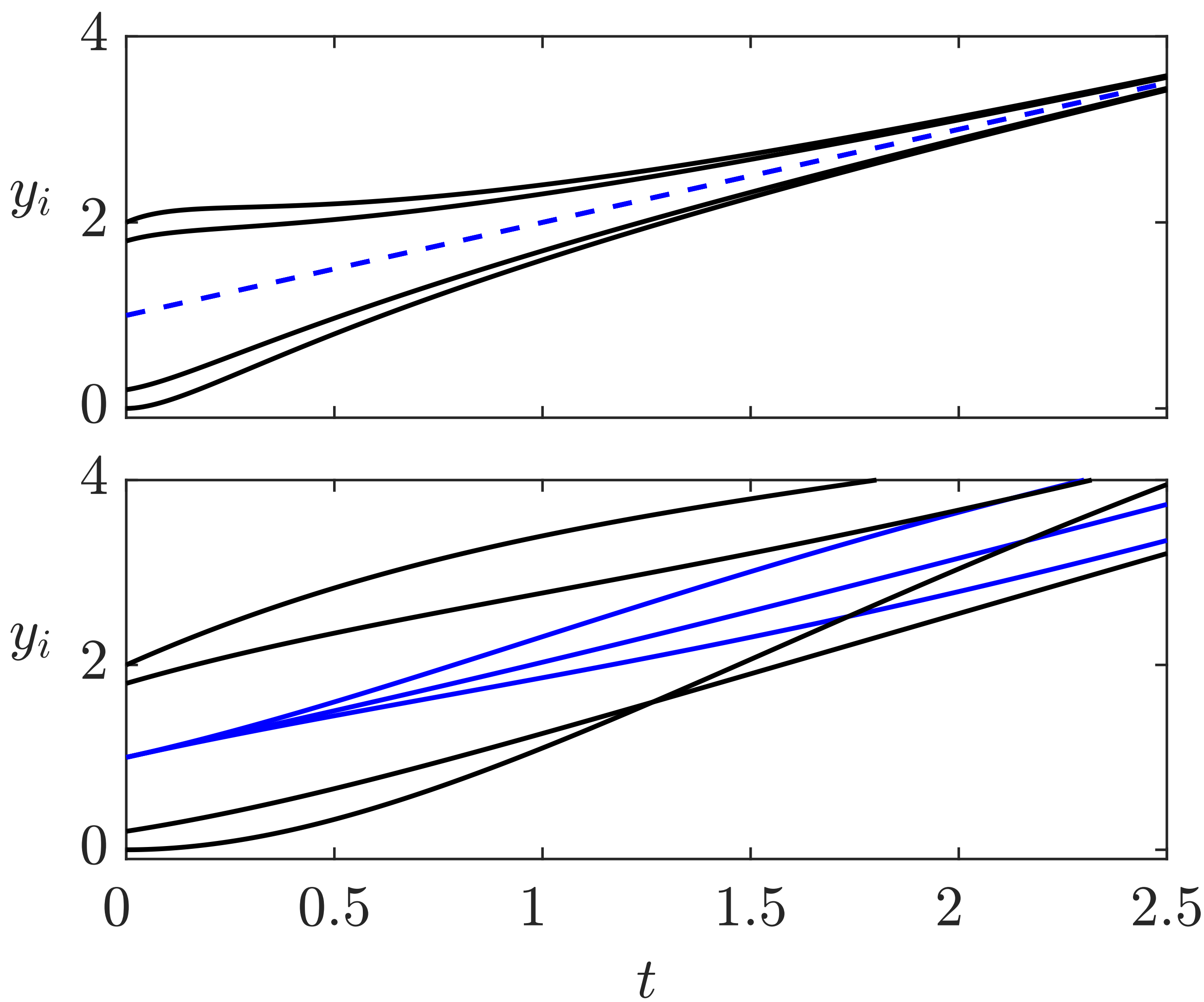

Fig. A1.23: Behaviour of the completely coupled network (top) and a network with path graph (bottom) with $N = 7$

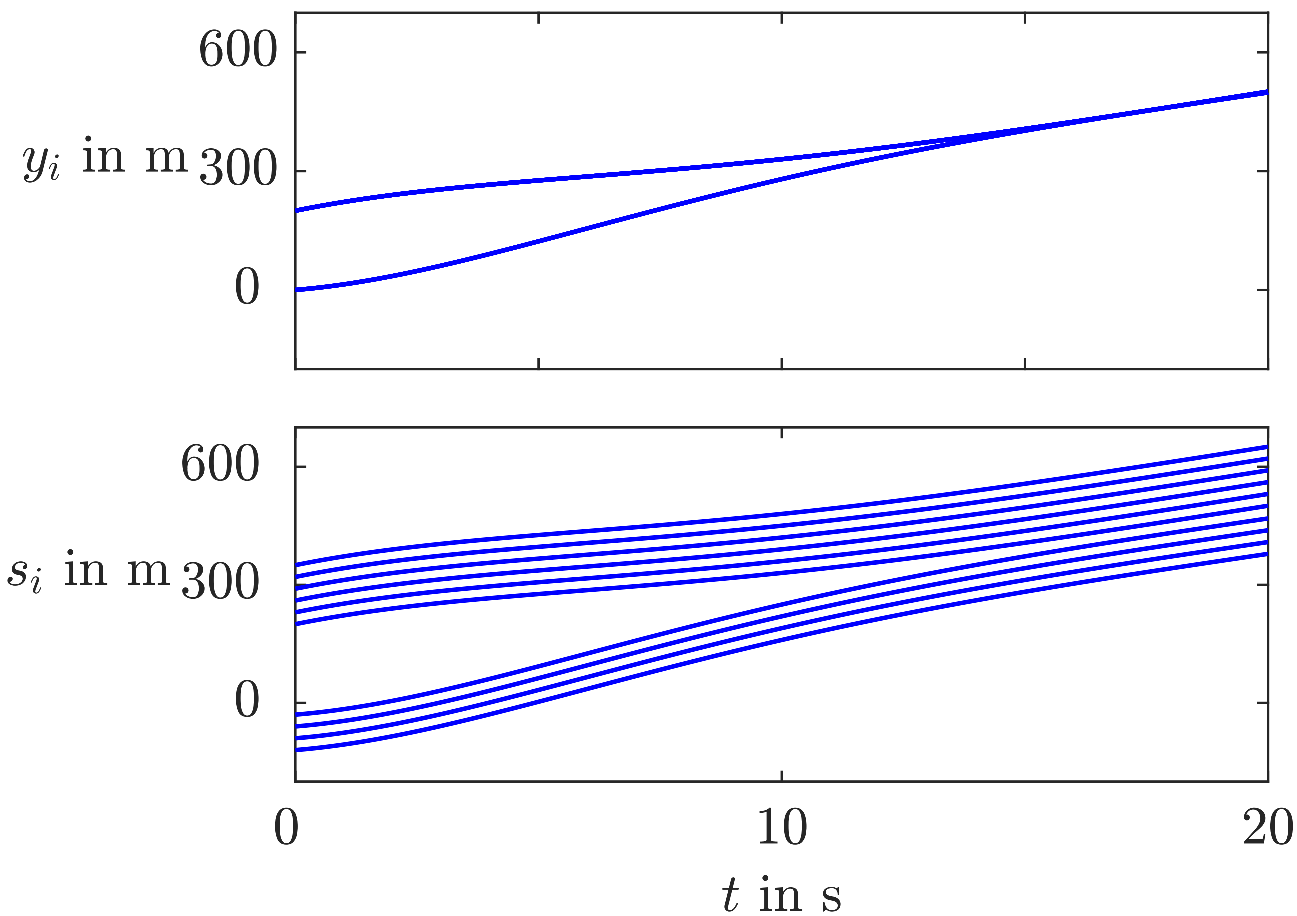

Fig. A1.24: Synchronisation behaviour of the platoon (top) and vehicle trajectories (bottom)

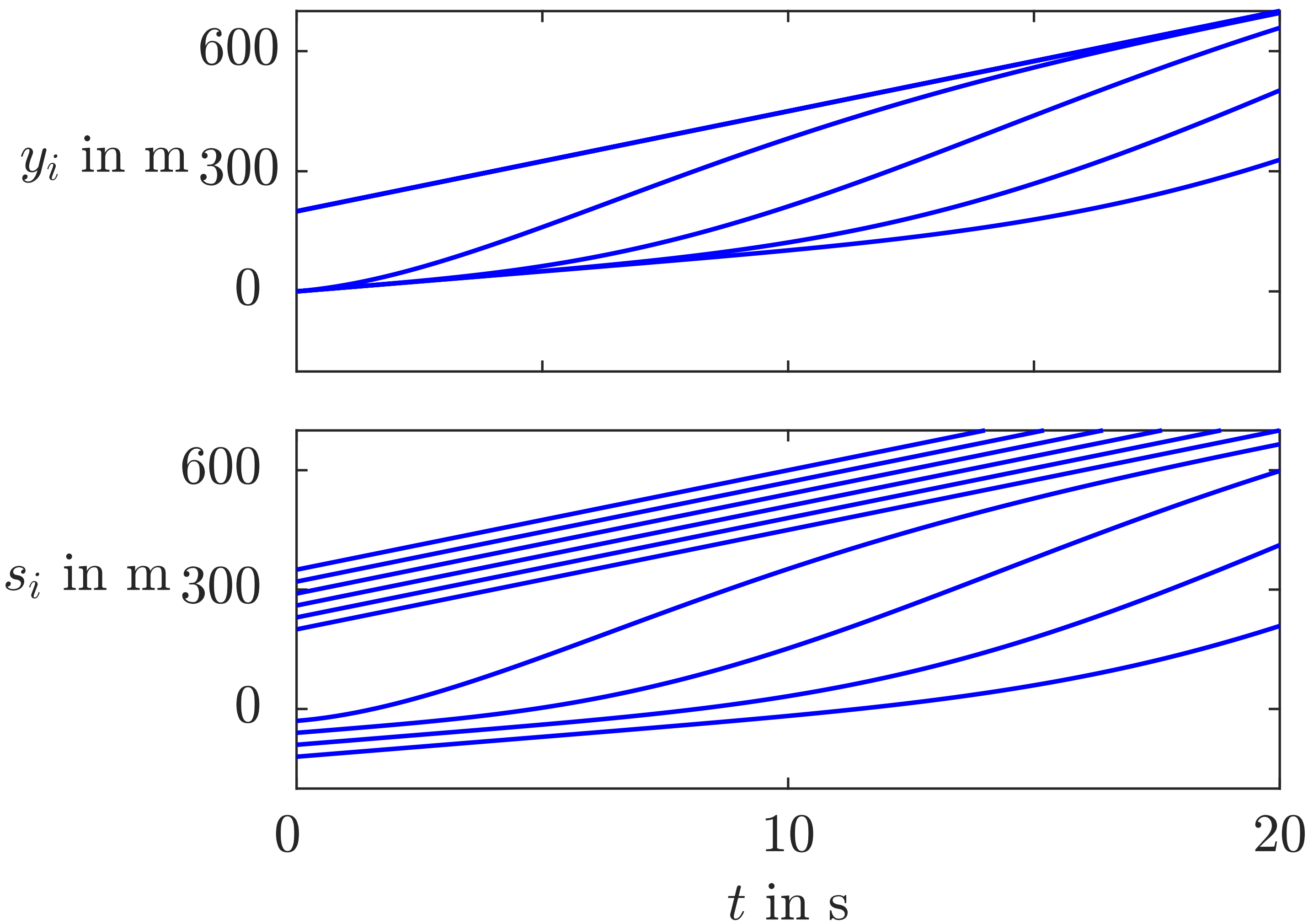

Fig. A1.25: Platoon (top) and vehicle trajectories (bottom) for vehicles with ACC

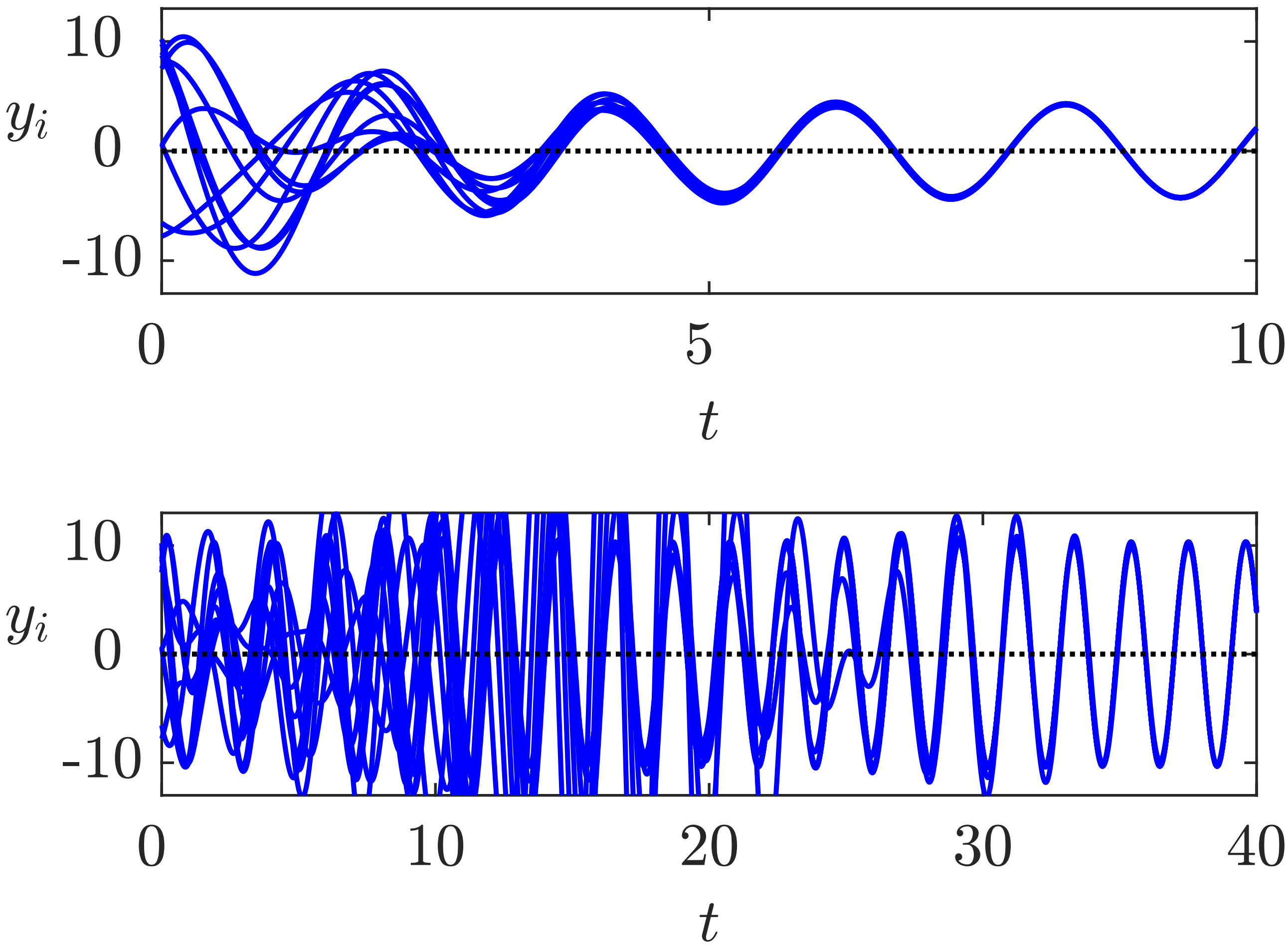

Fig. A1.26: Synchronisation behaviour of ten oscillators with complete couplings (top) and with path graph couplings (bottom)

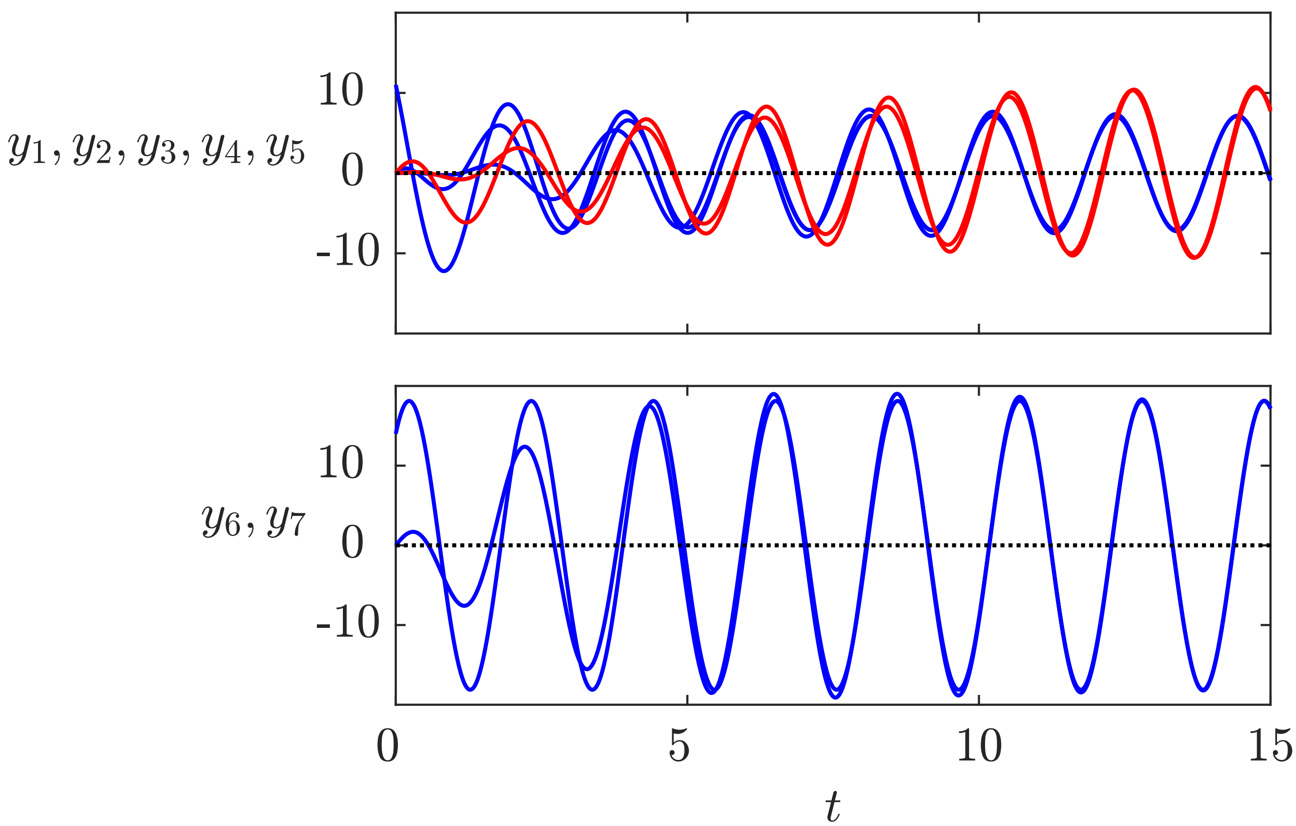

Fig. A1.27: Cluster synchronisation of seven harmonic oscillators

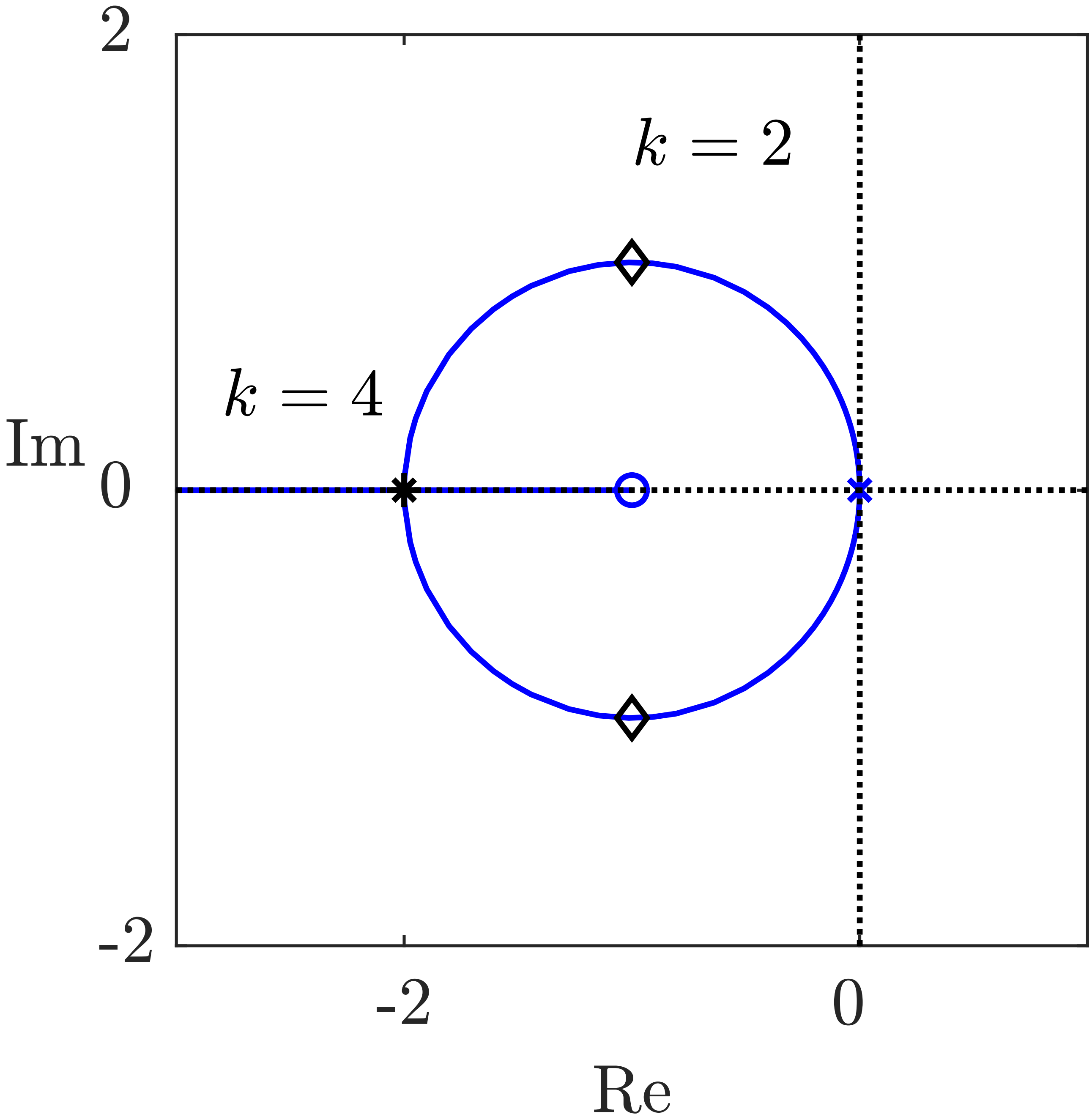

Fig. A1.28: Root locus of the double integrator system

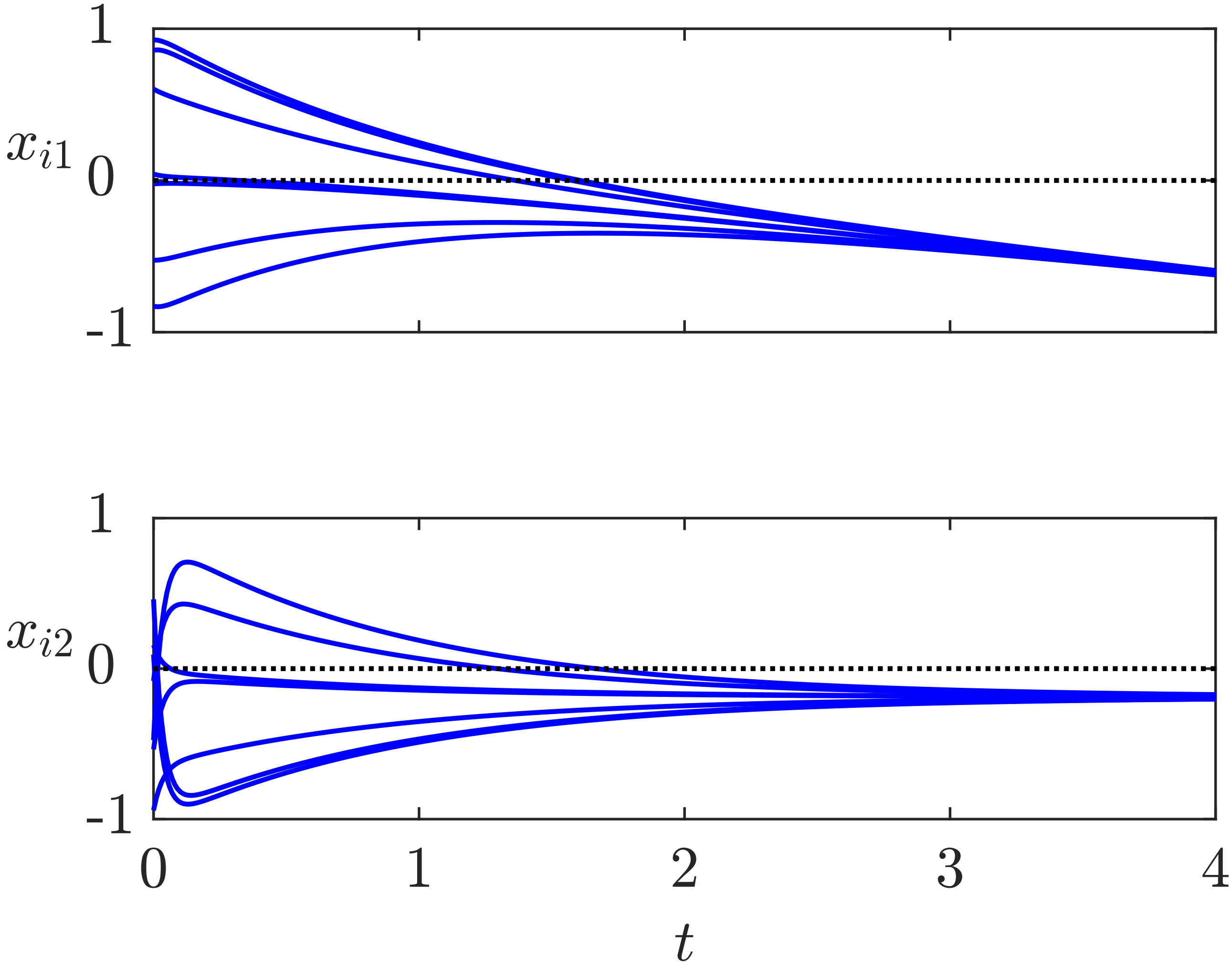

Fig. A1.29: Behaviour of seven synchronised double-integrator agents

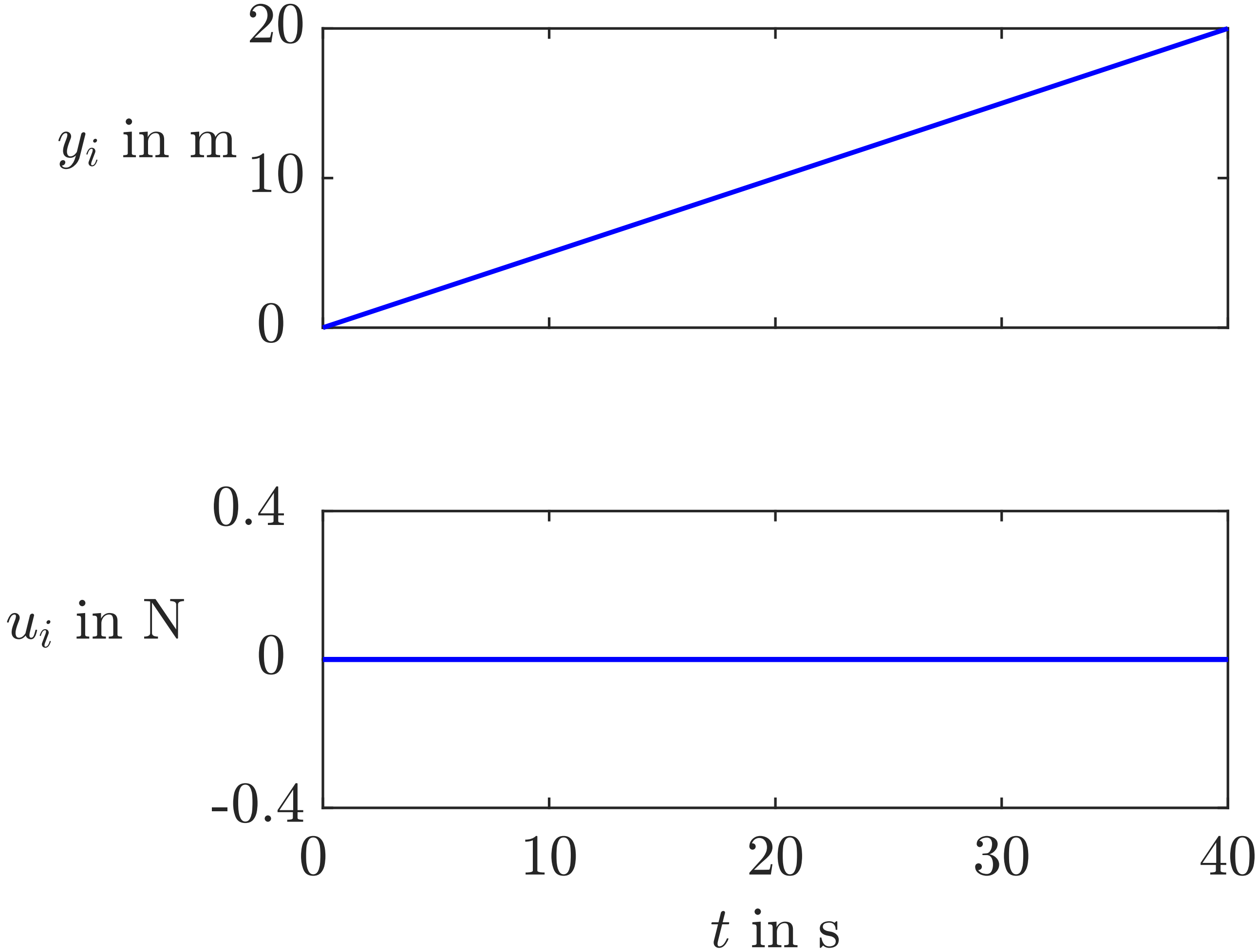

Fig. A1.30: Synchronous behaviour of the spring-mass system

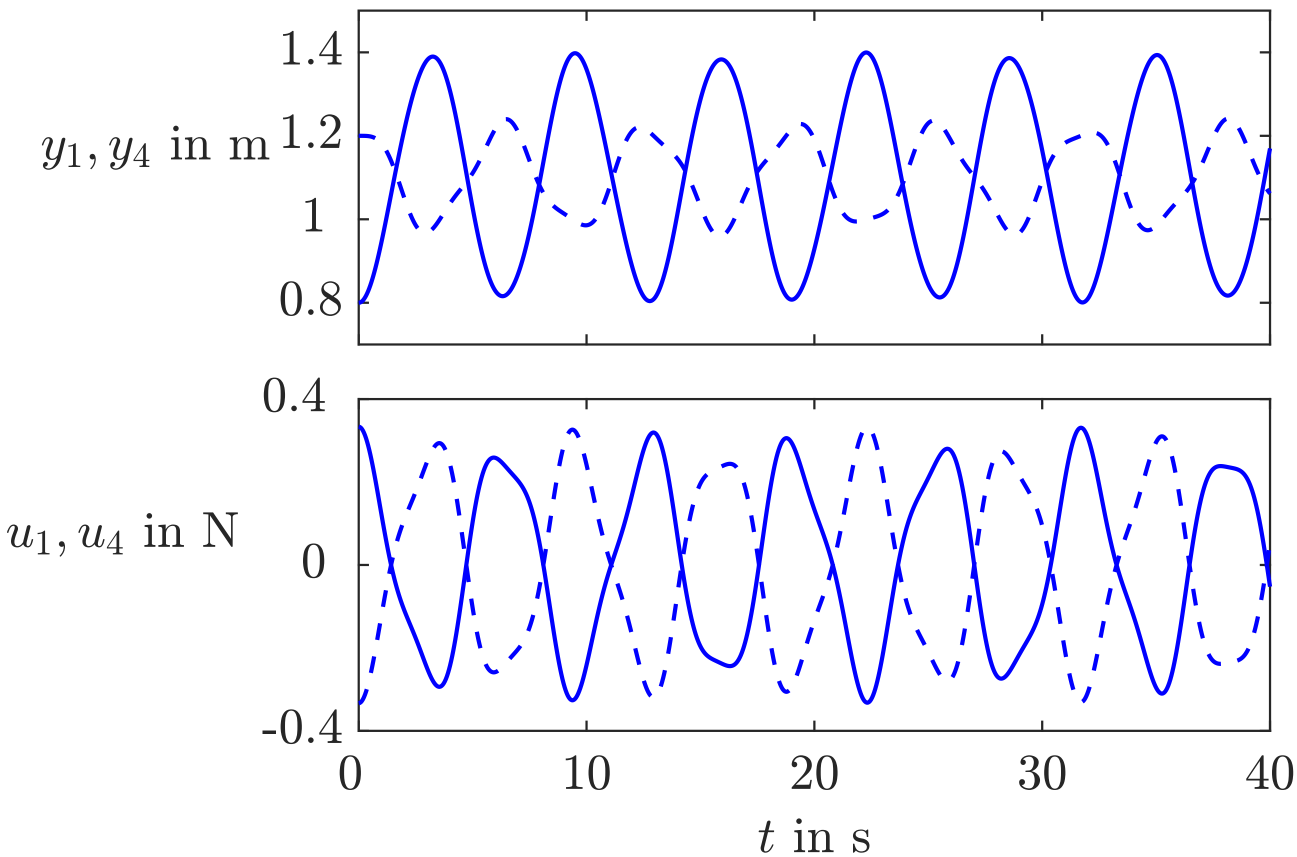

Fig. A1.31: Oscillating movement of the spring-mass system
(— y_1, u_1, - - - y_4, u_4)

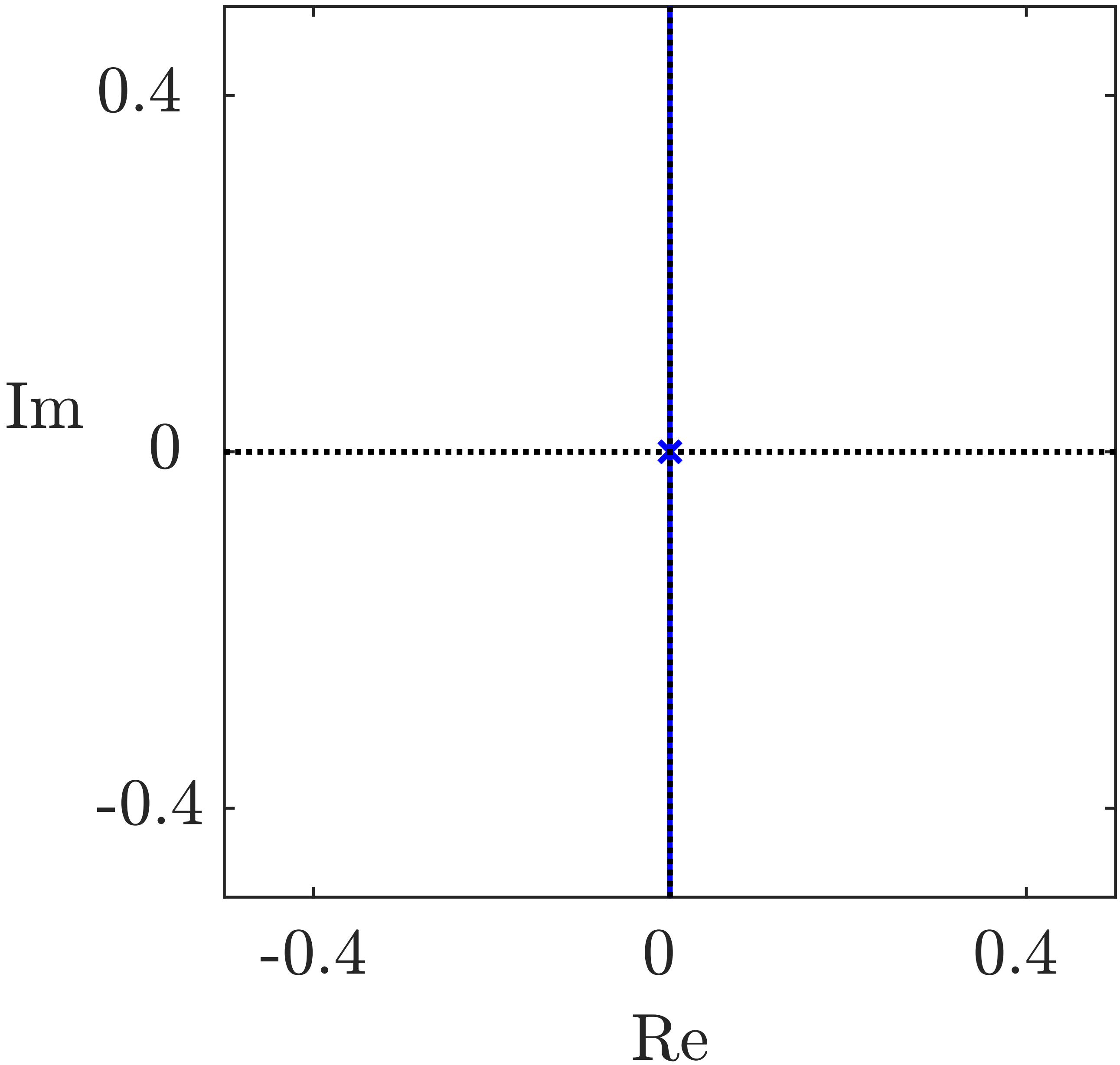

Fig. A1.32: Root locus of the agent model

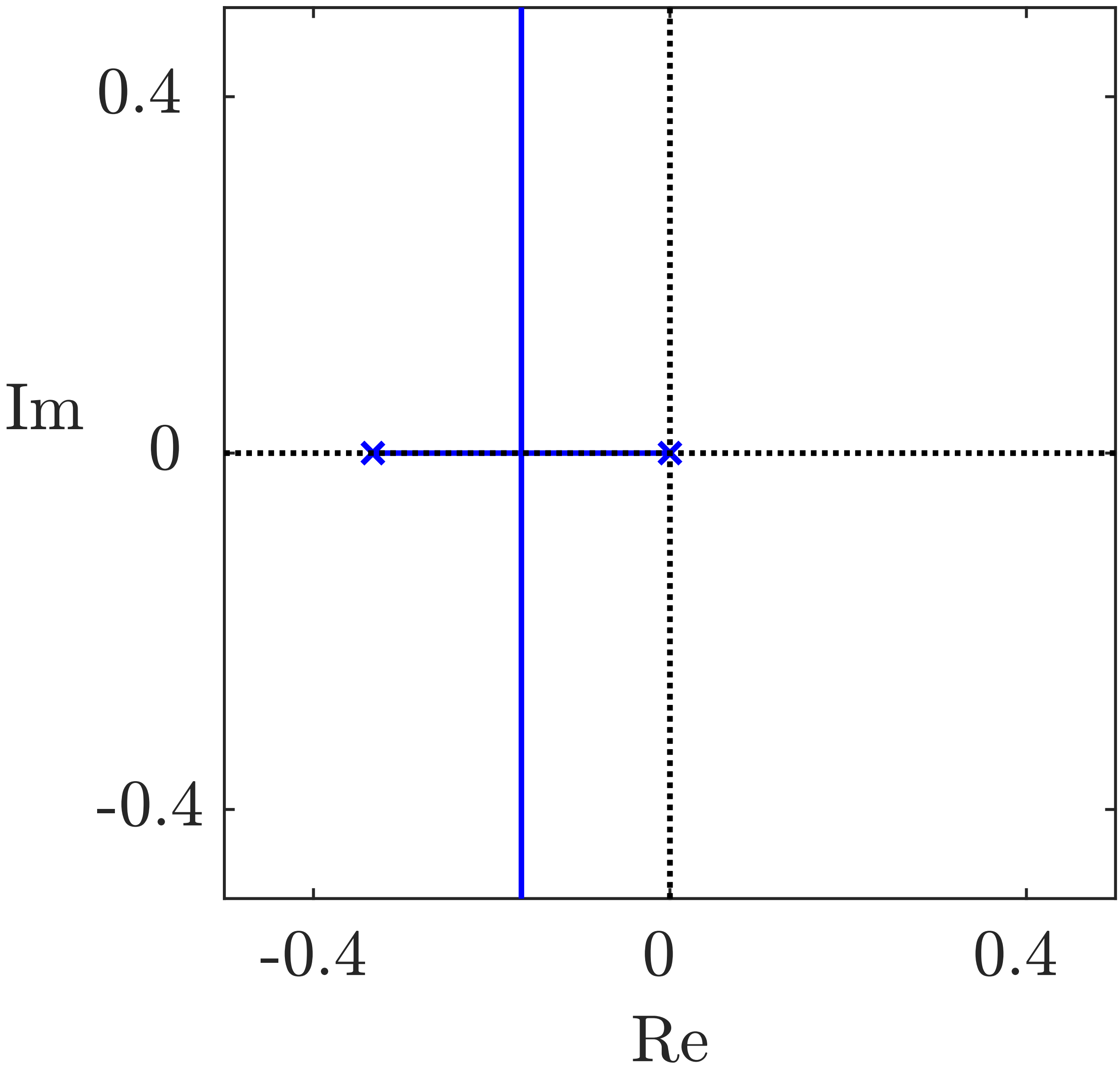

Fig. A1.32: Root locus of the extended model (A1.30)

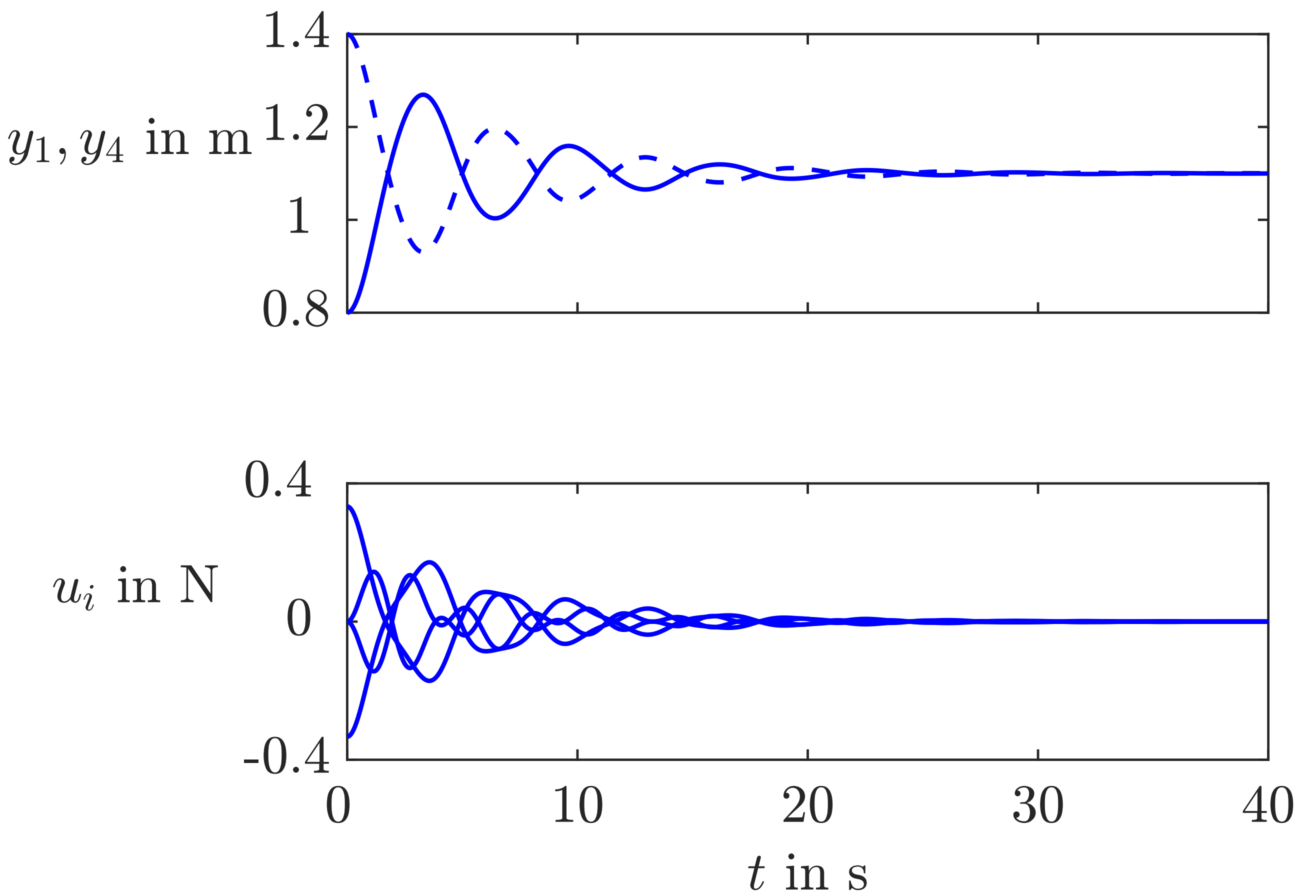

Fig. A1.33: Synchronous behaviour of the spring-mass system

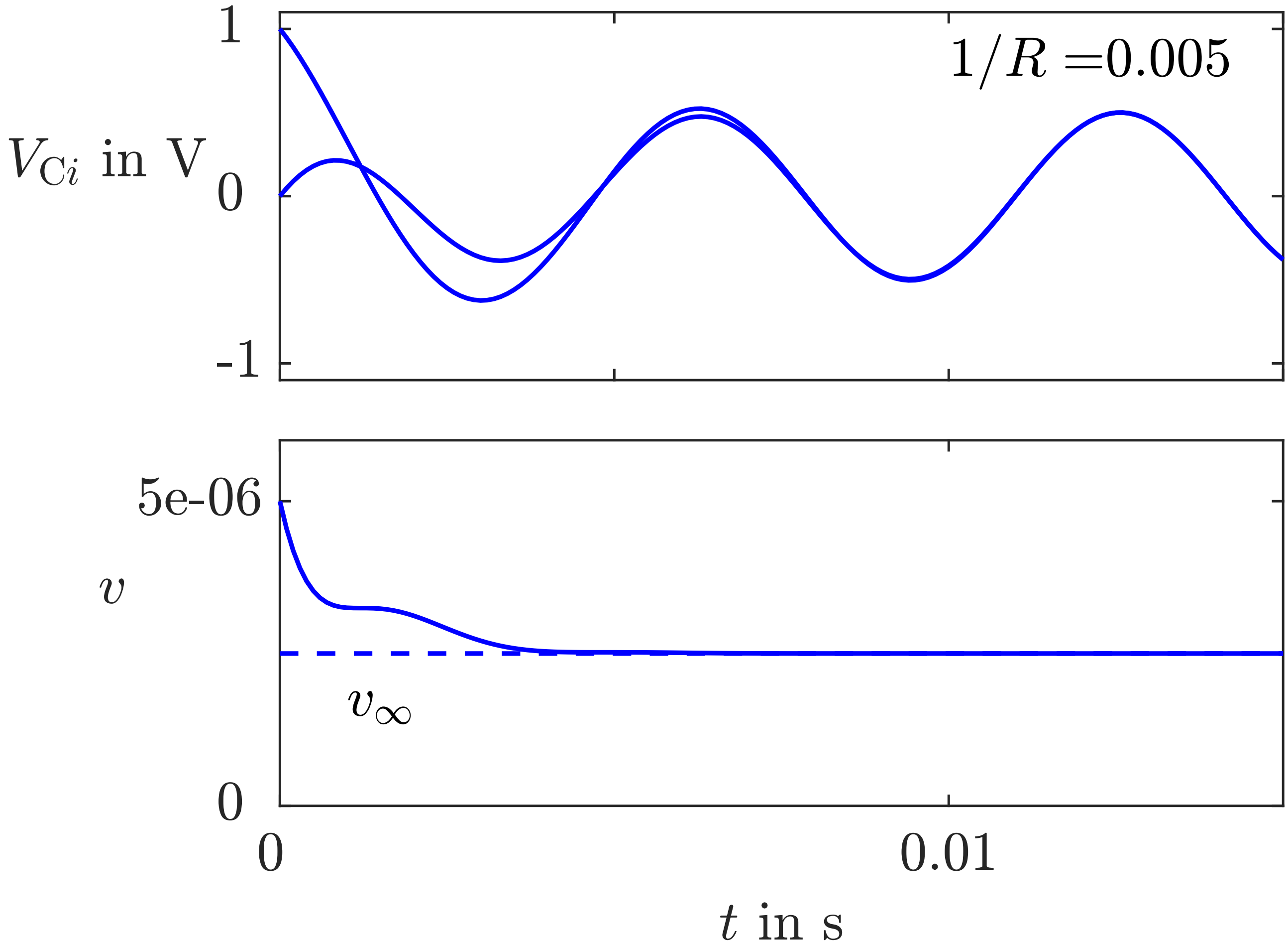

Fig. A1.34: Trajectories and Lyapunov function of an oscillator network with two oscillators

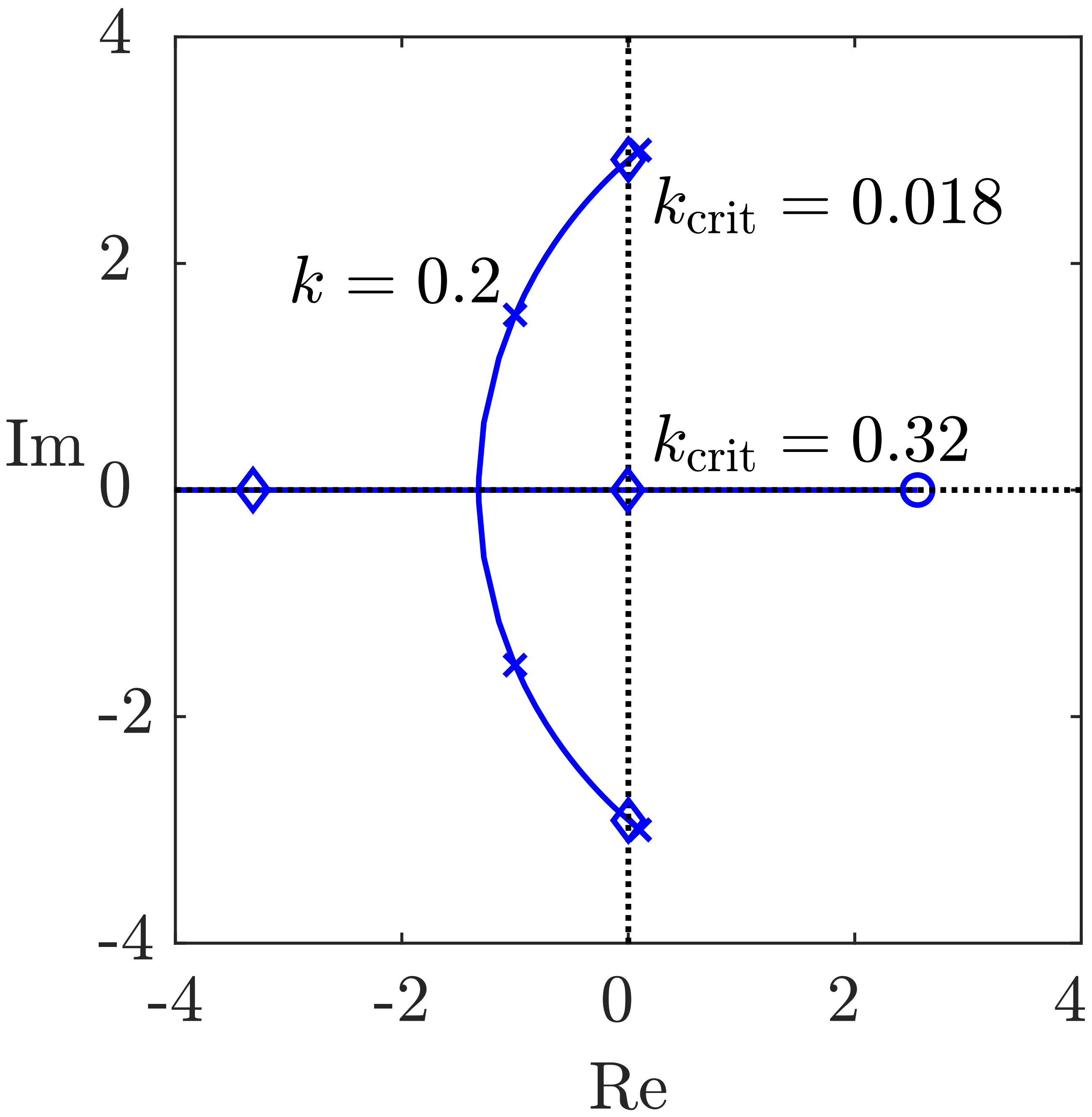

Fig. A1.35: Root locus of the oscillator

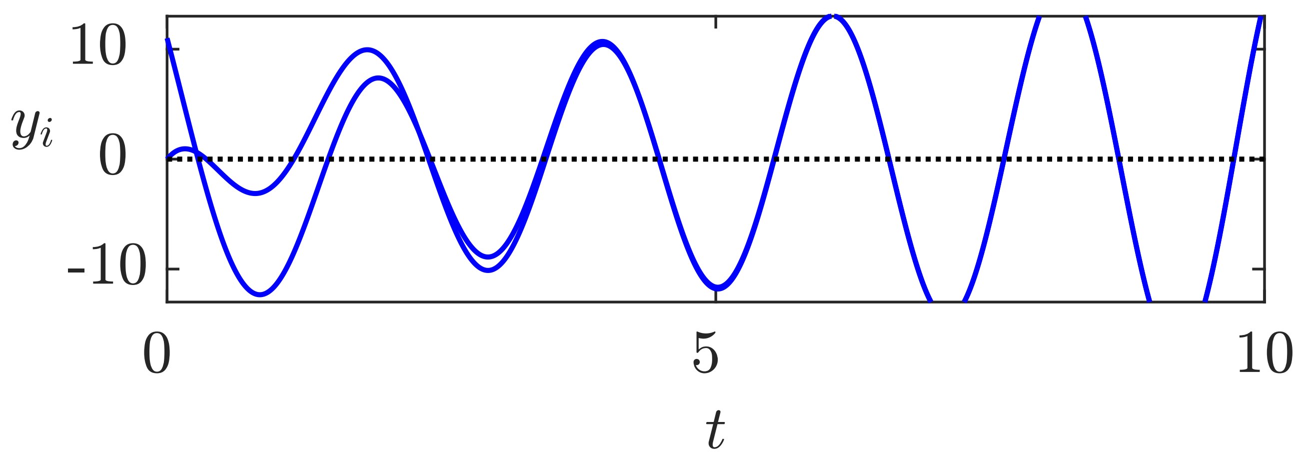

Fig. A1.36: Synchronisation behaviour for $k = 0.1$

J. Lunze: *Networked Control of Multi-Agent Systems,* Edition **M**o**R**a 2022

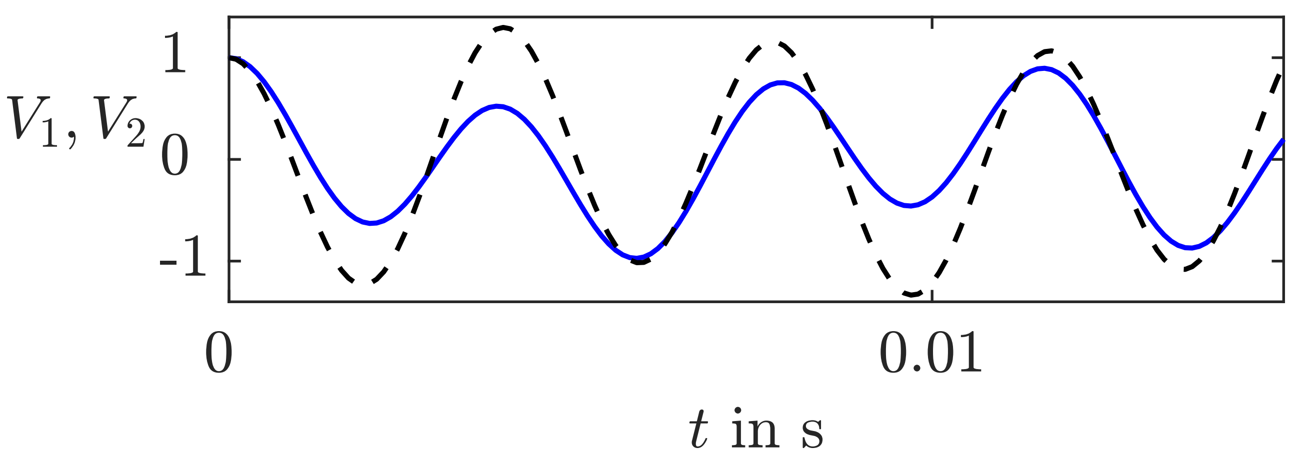

Fig. A1.37: Behaviour of a subsystem

J. LUNZE: *Networked Control of Multi-Agent Systems,* Edition MoRa 2022

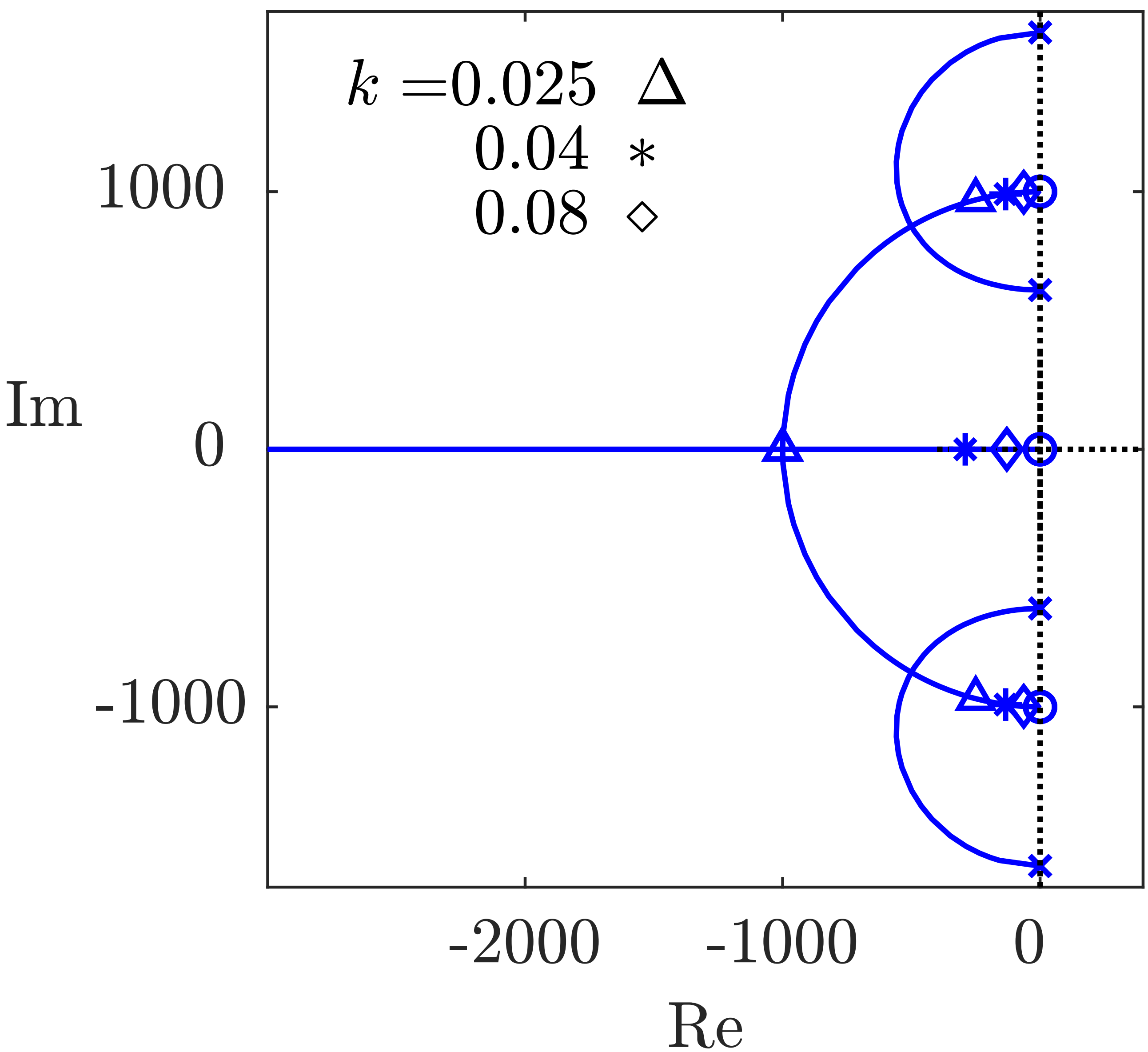

Fig. A1.38: Root locus of the oscillator with respect to $(V_1(t), I_1(t))$

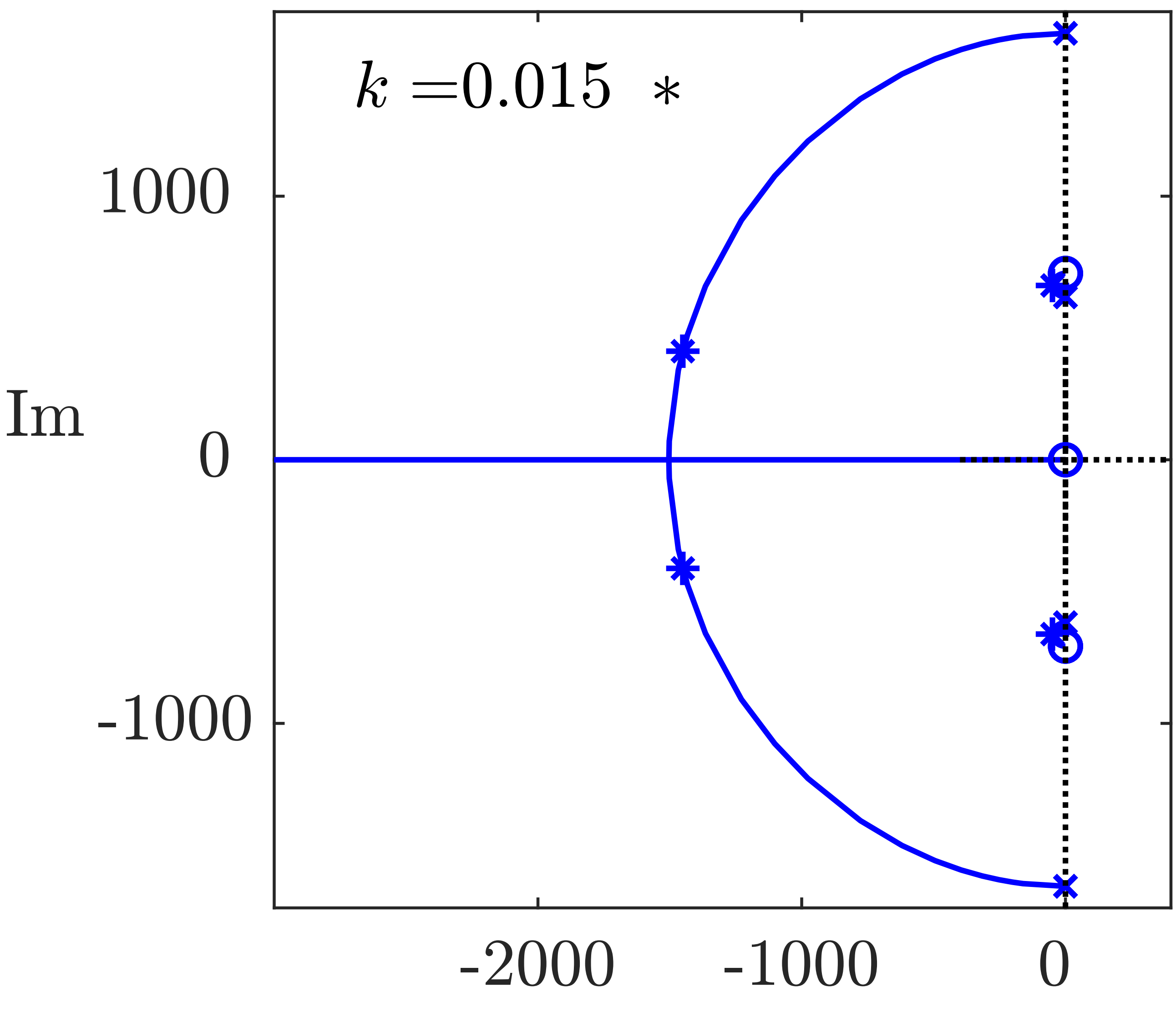

Fig. A1.38: Root locus of the oscillator with respect to $(V_2(t), I_2(t))$

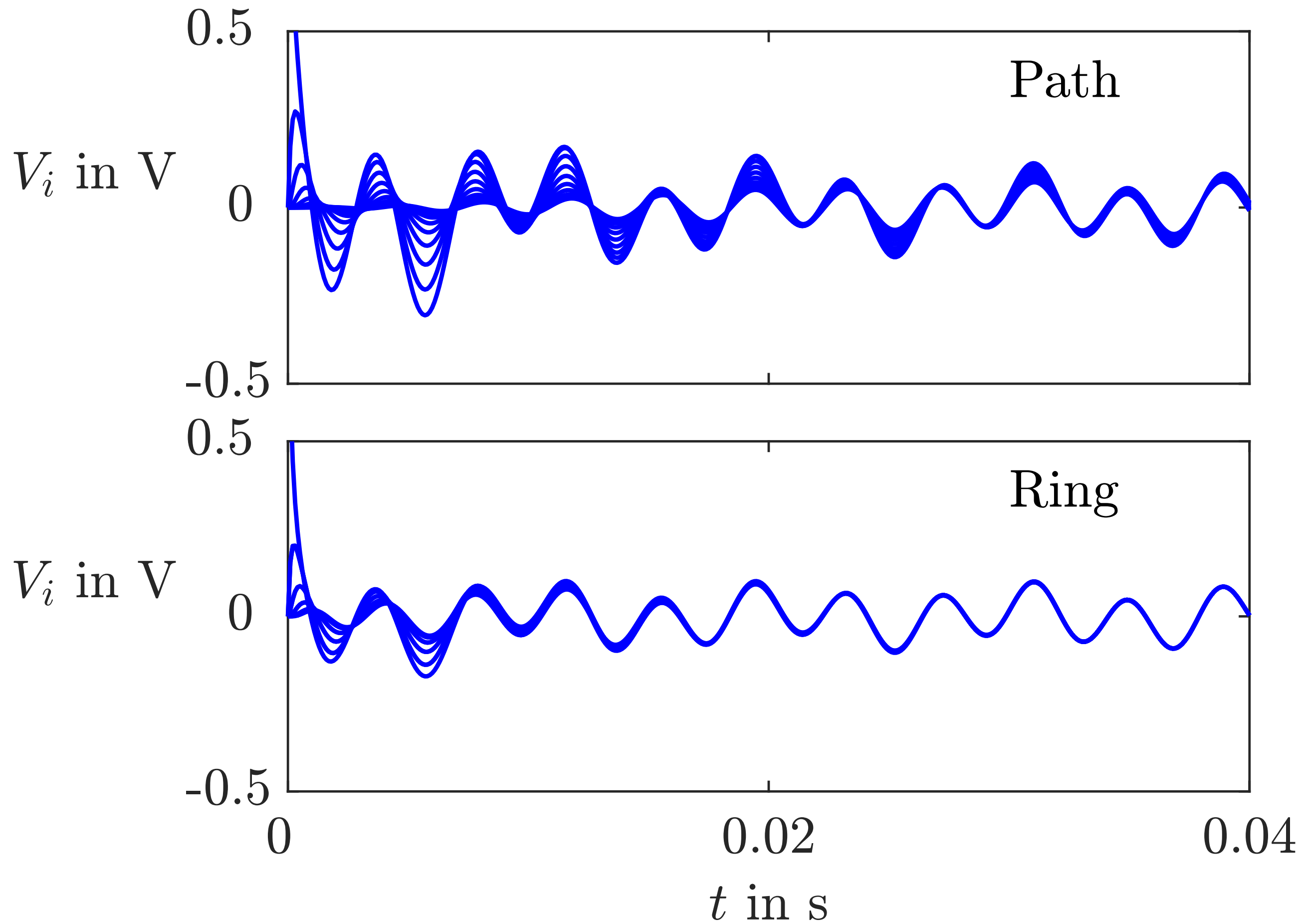

Fig. A1.39: Behaviour of the two networks with $N = 10$ oscillators

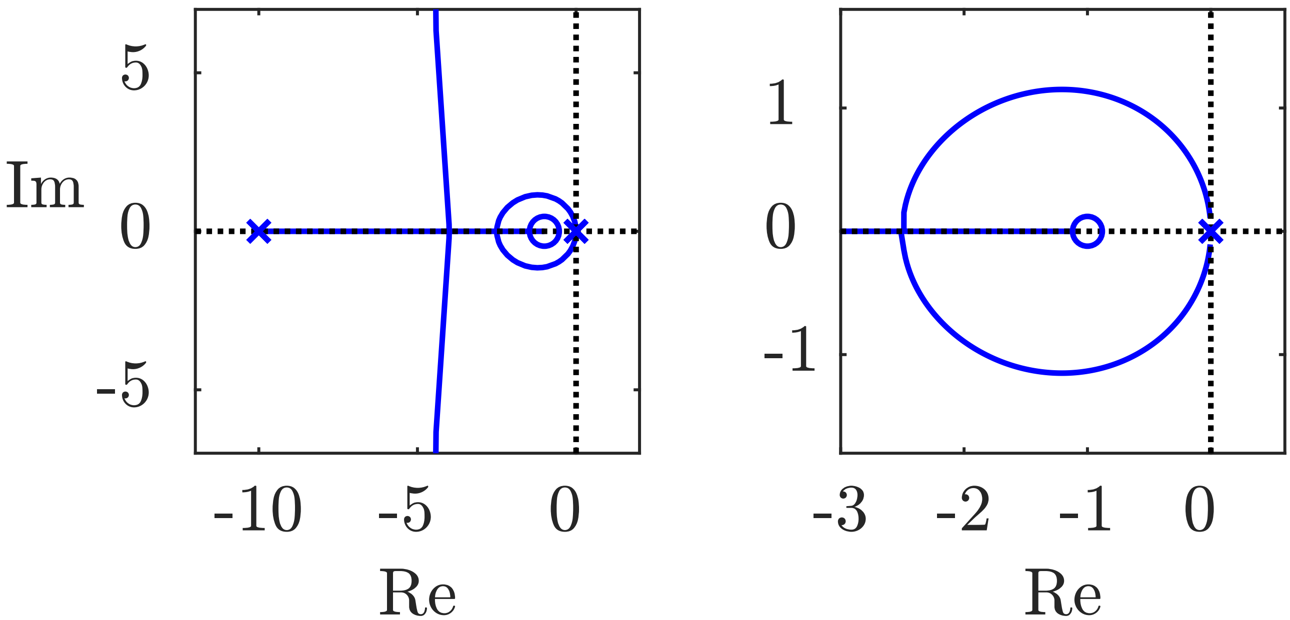

Fig. A1.40: Root loci of the extended closed-loop agent in two scales

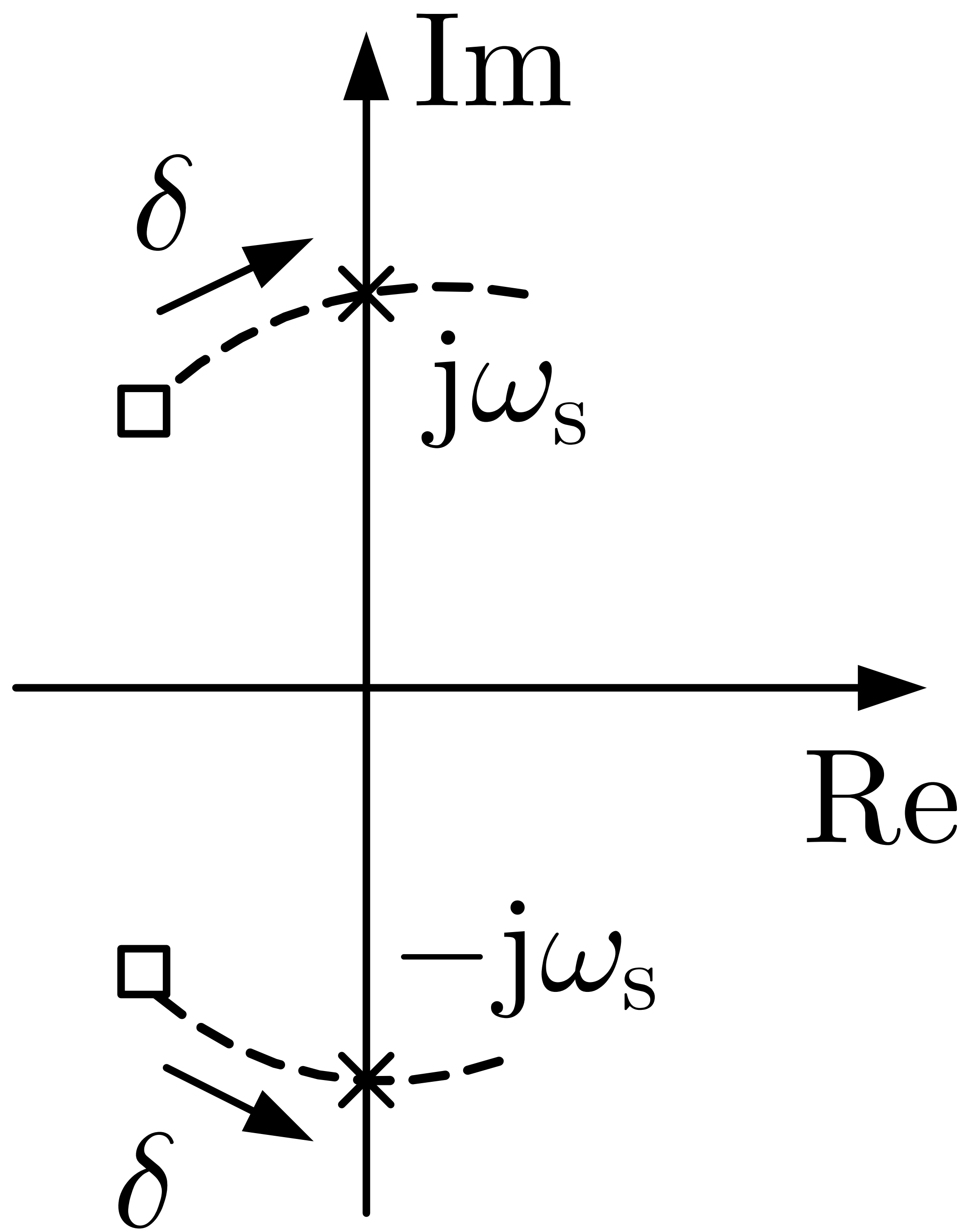

Fig. A1.41. Eigenvalues of the coupled oscillators in dependence upon δ

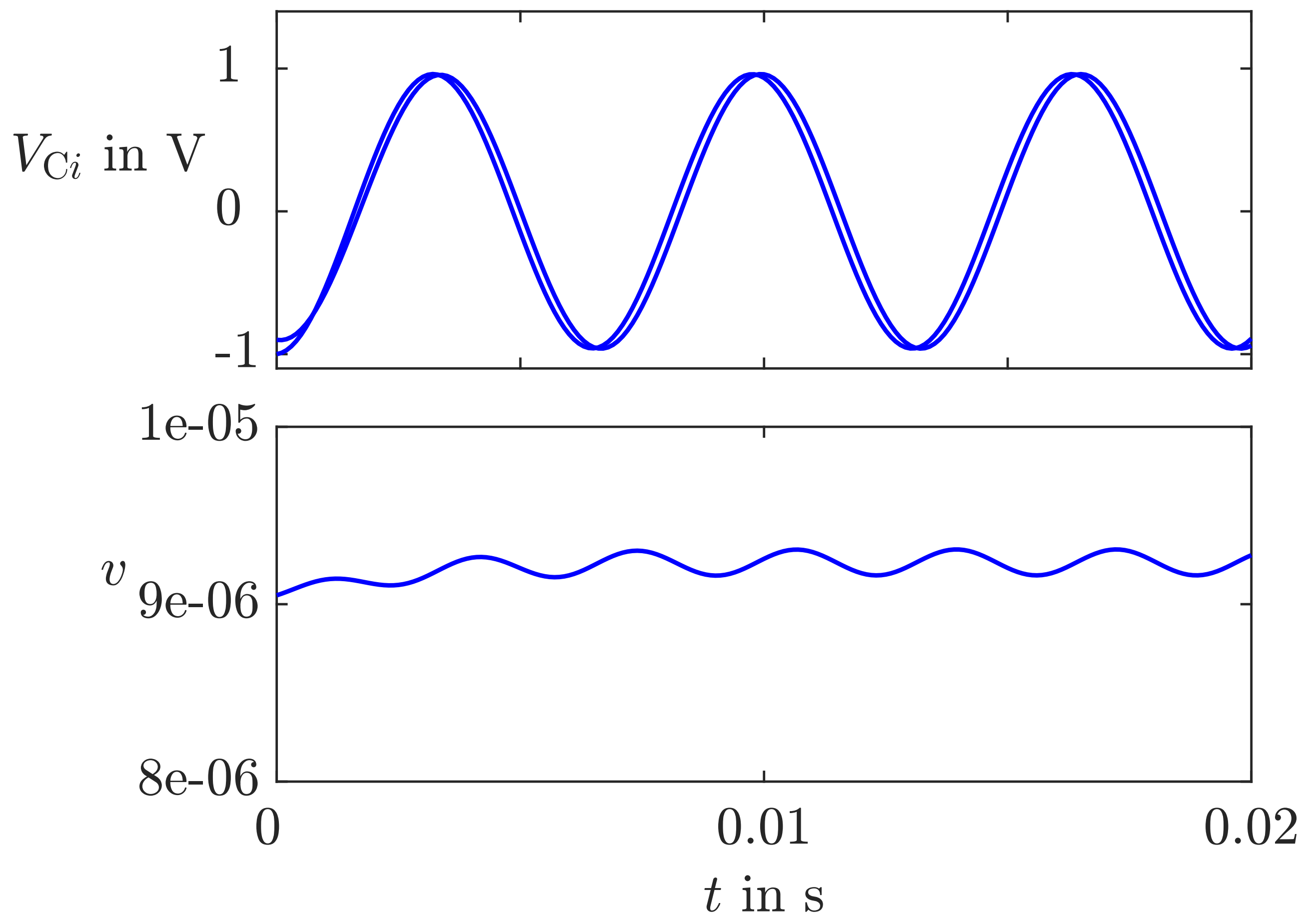

Fig. A1.42: Behaviour of the coupled oscillators for $\delta = 3.817$

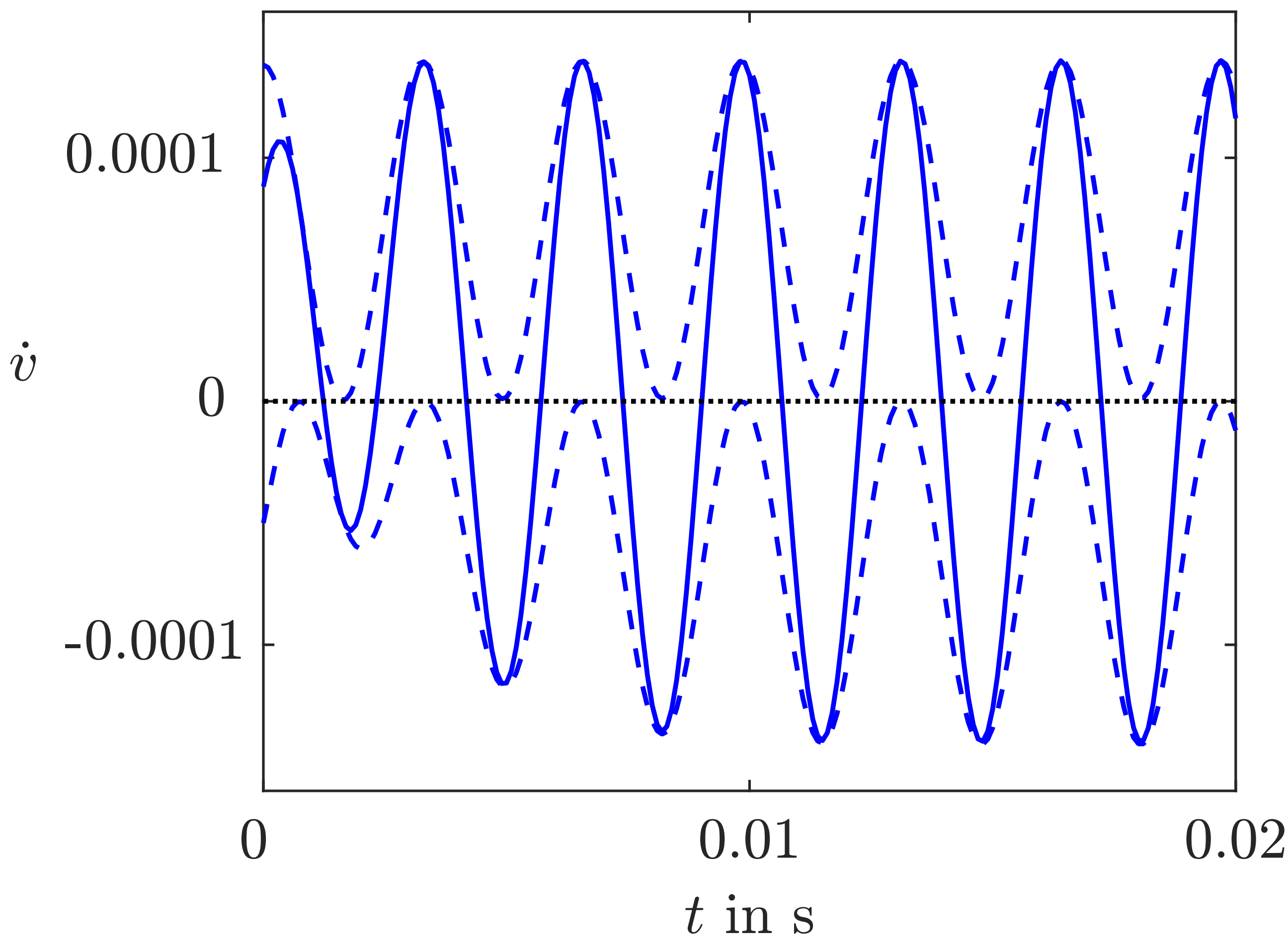

Fig. A1.42: Change of the internal power for $\delta = 3.817$

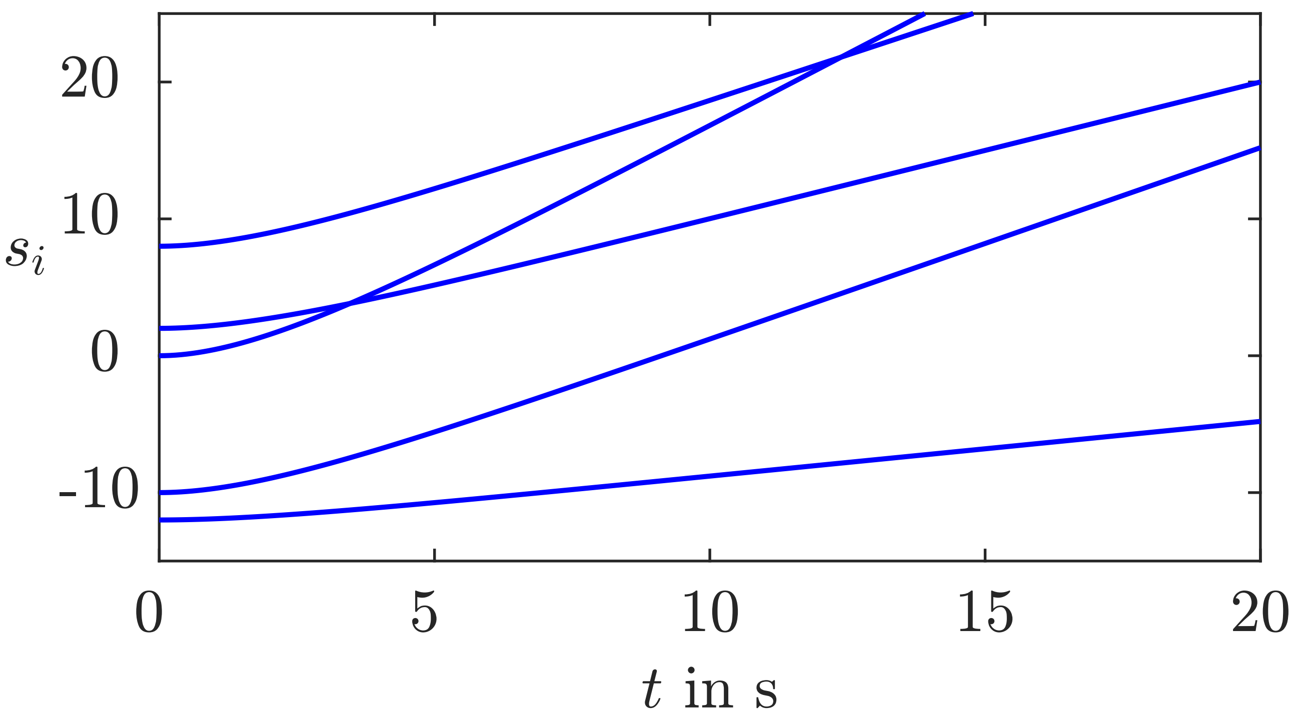

Fig. A1.43: Behaviour of five robots without networked controller

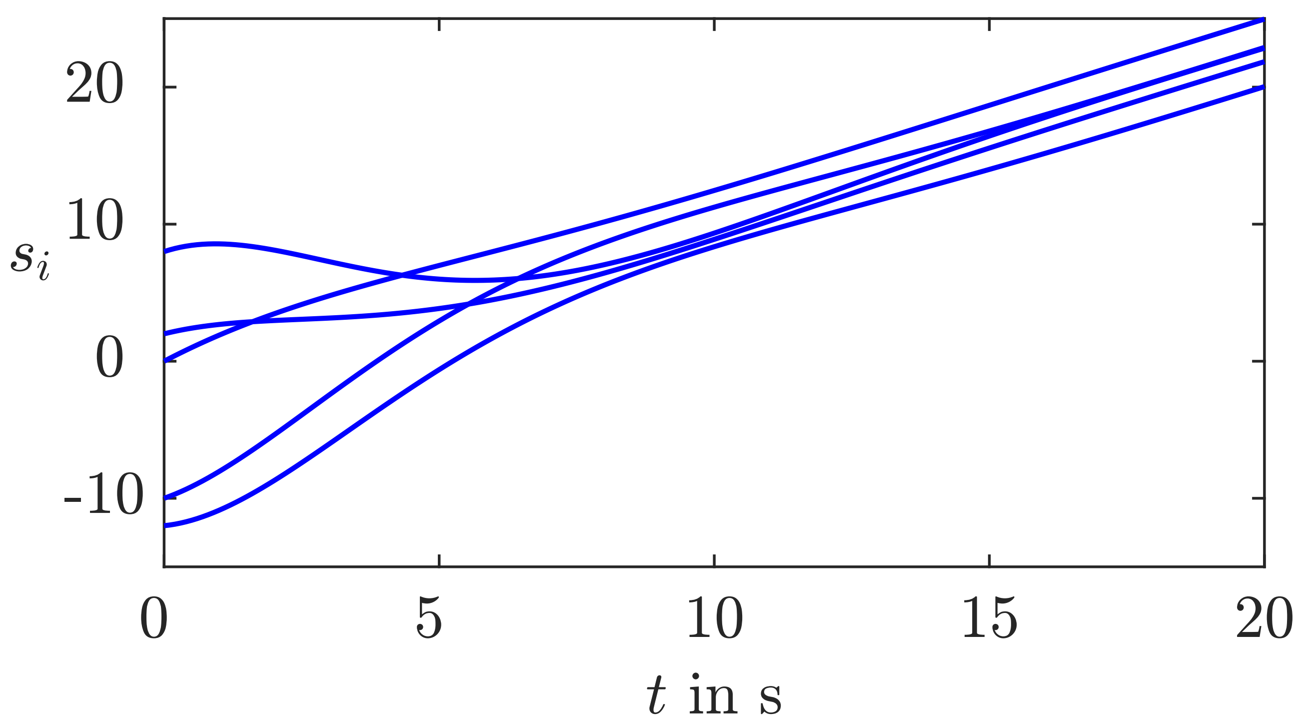

Fig. A1.43: Behaviour of five robots with networked controller

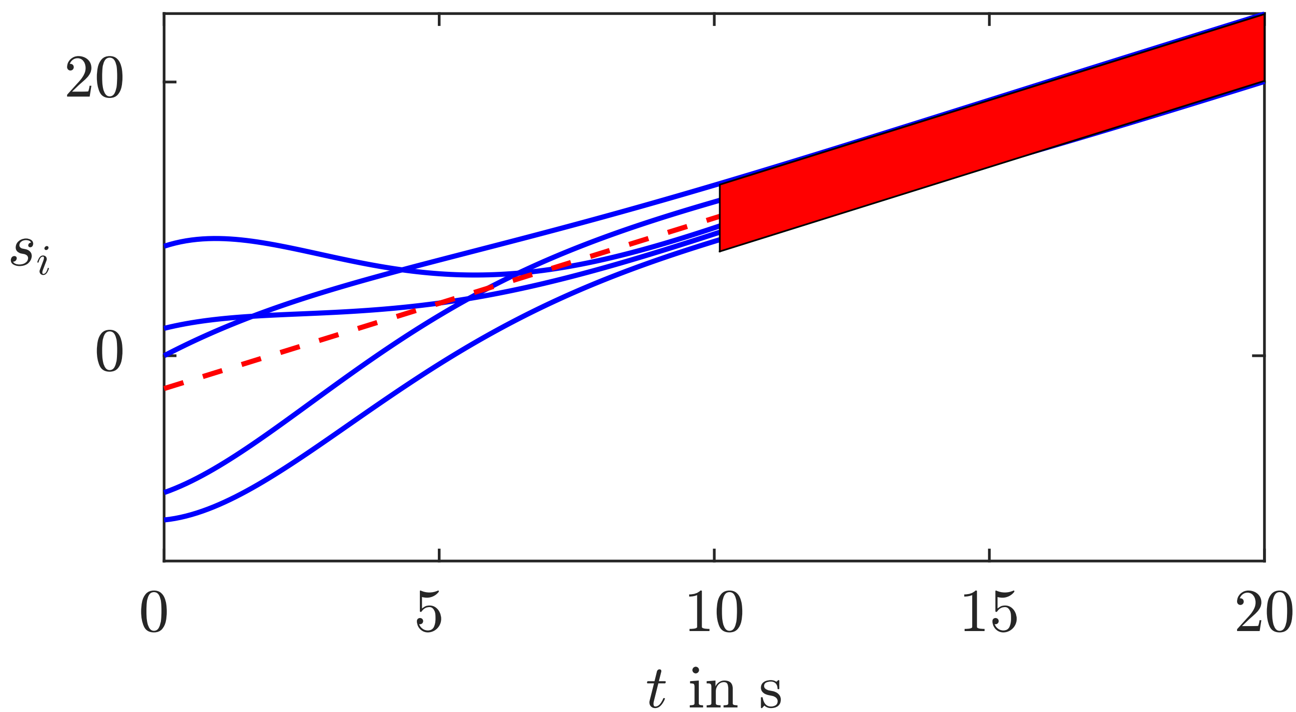

Fig. A1.44: Practical synchronisation of five robots

J. LUNZE: *Networked Control of Multi-Agent Systems,* Edition **MoRa** 2022

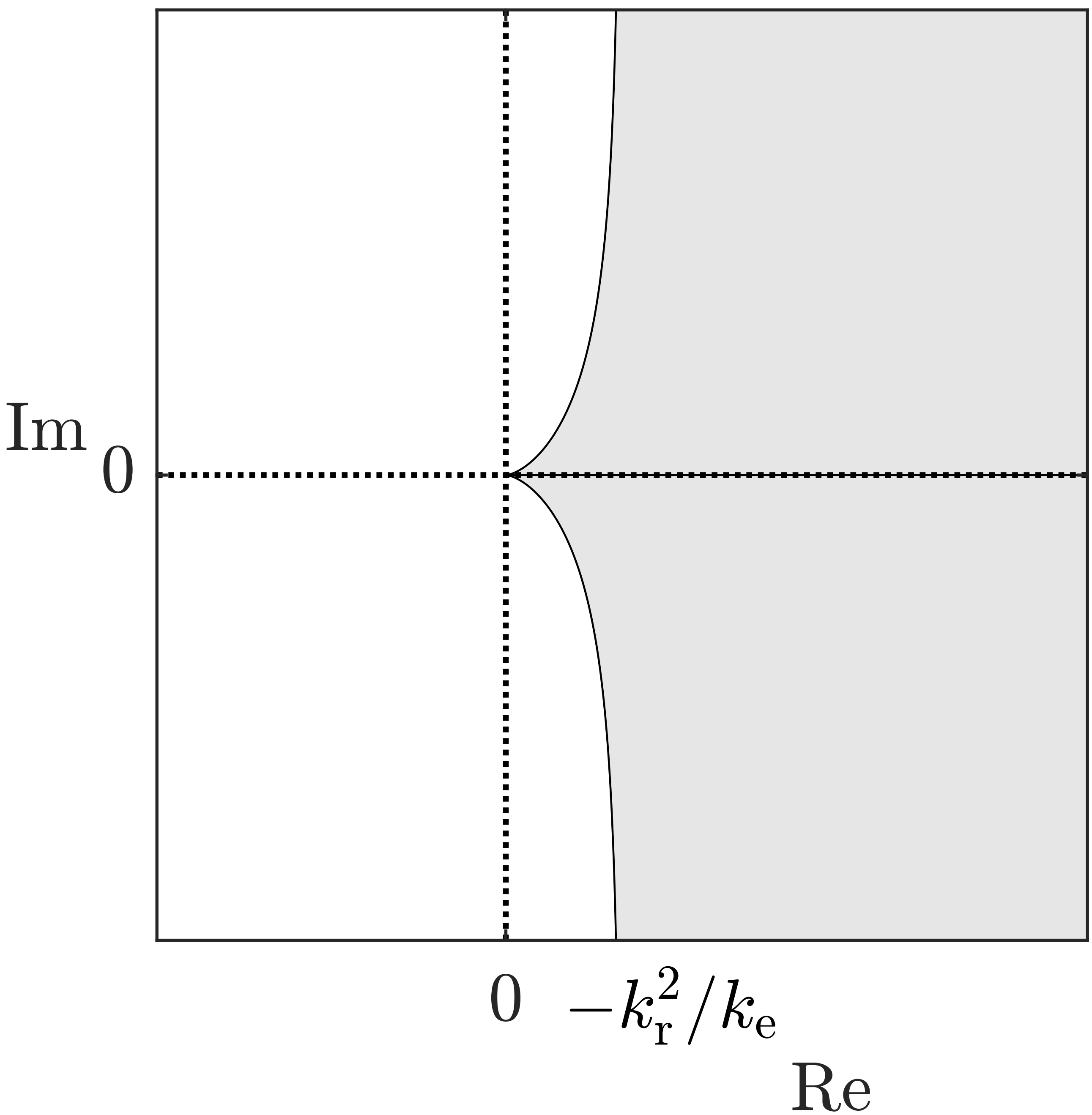

Fig. A1.45: Stability region of the extended Kuramoto oscillator networks

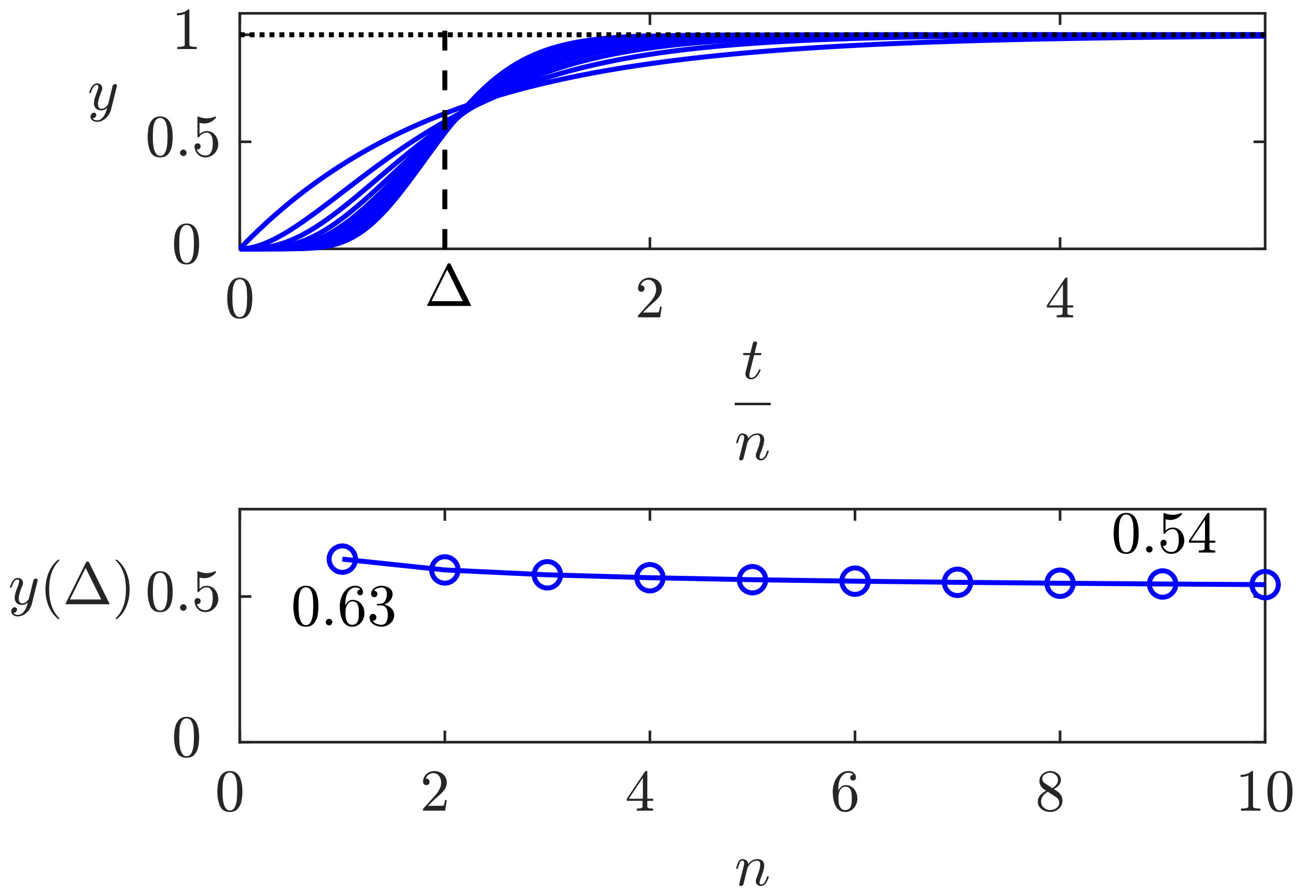

Fig. A1.46: Step responses of lag systems (5.46) with $T_1 = 1$

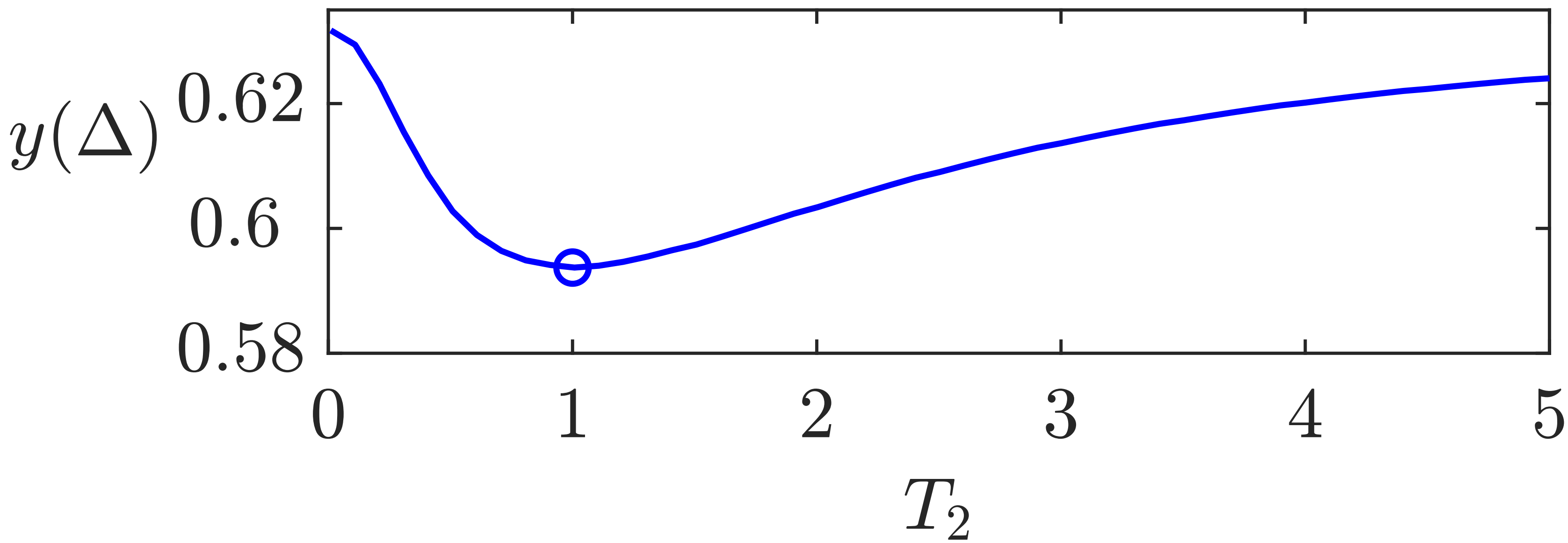

Fig. A1.47. Output $y(\Delta)$ for a second-order system (5.47) with $T_1 = 1$ and $T_2 \in [0, 5]$

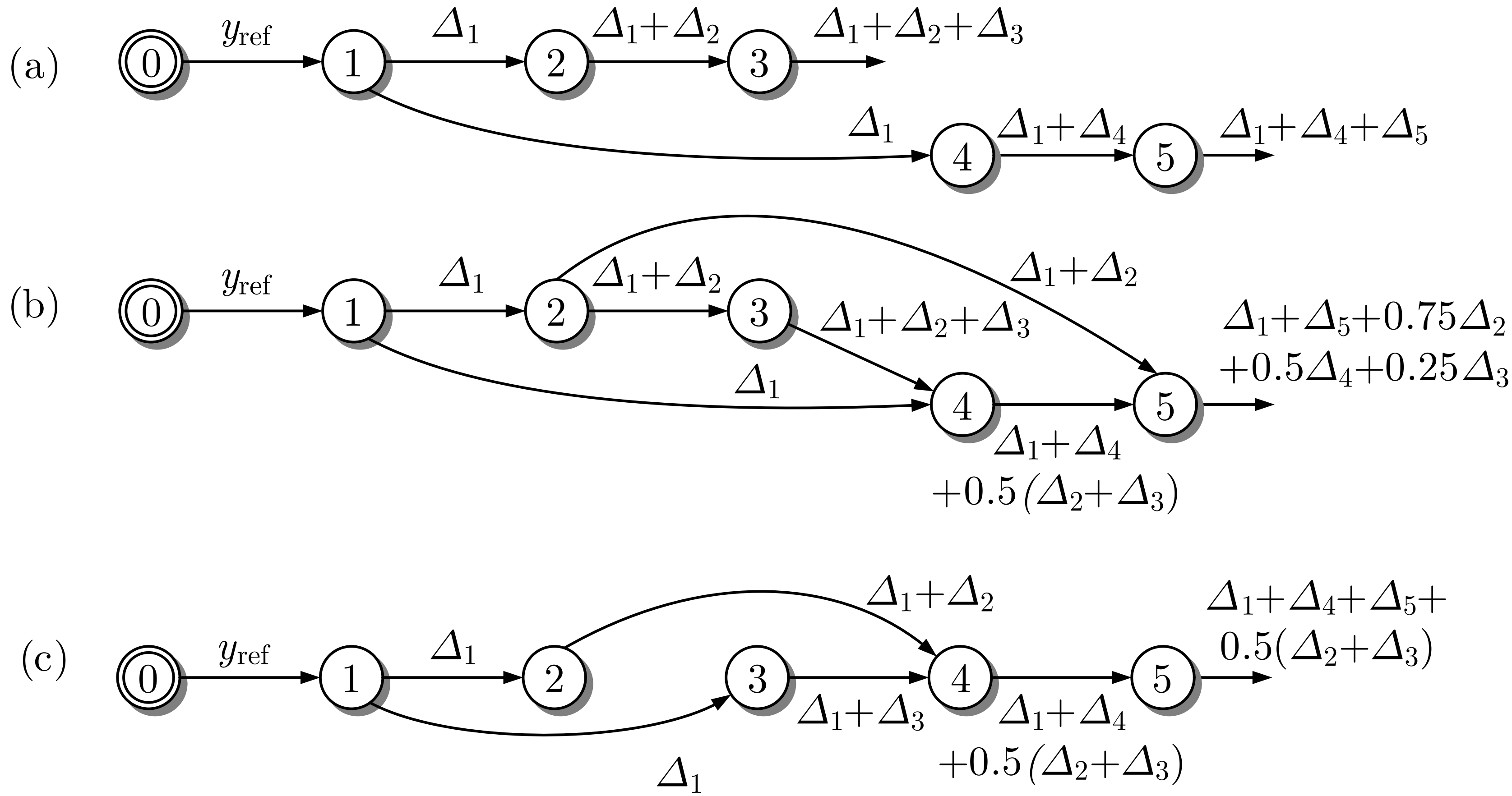

Fig. A1.48. Delay of three communication structures

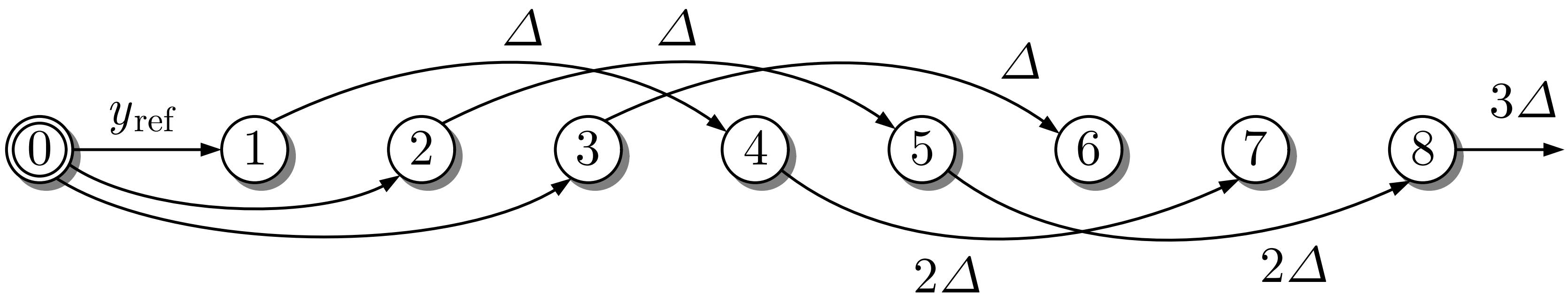

Fig. A1.49. Communication structure that ensures the quickest transient behaviour

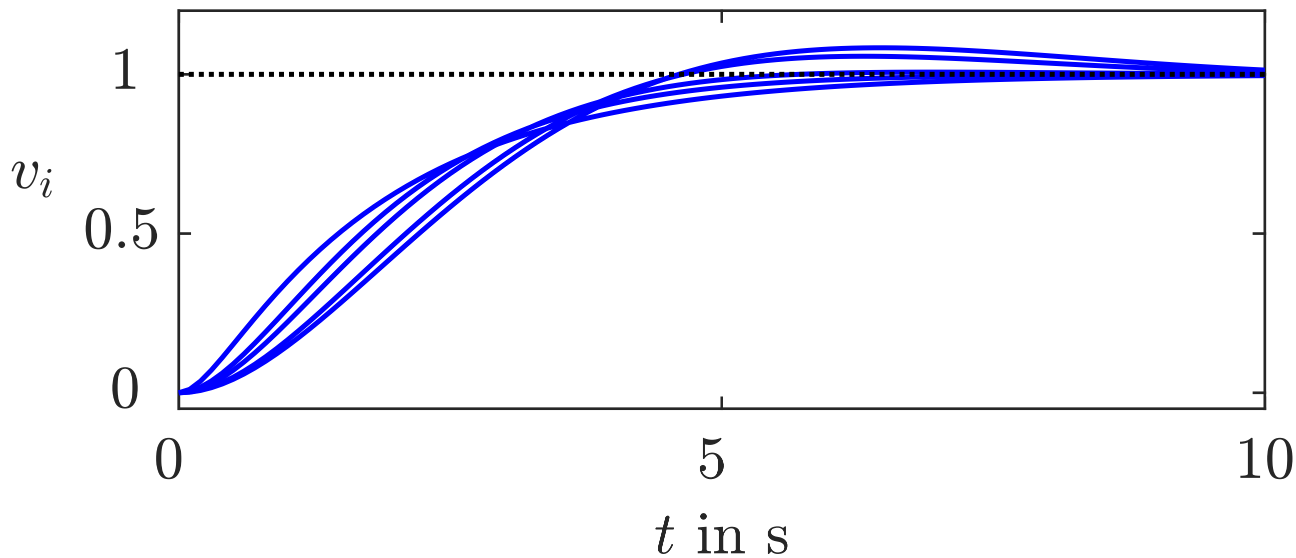

Fig. A1.50: Step responses of the ten controlled vehicles (velocities in $\frac{\mathrm{m}}{\mathrm{s}}$) for $T_i \in [0.2, 1.3]$

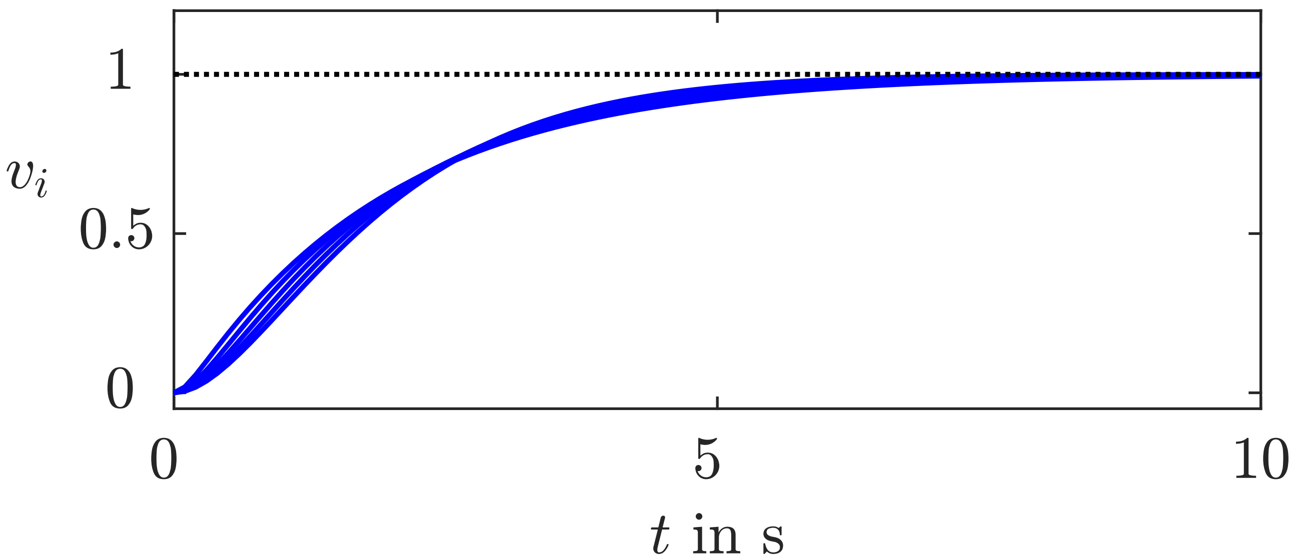

Fig. A1.50: Step responses of the ten controlled vehicles (velocities in $\frac{\text{m}}{\text{s}}$) for $T_i \in [0.1, 0.5]$

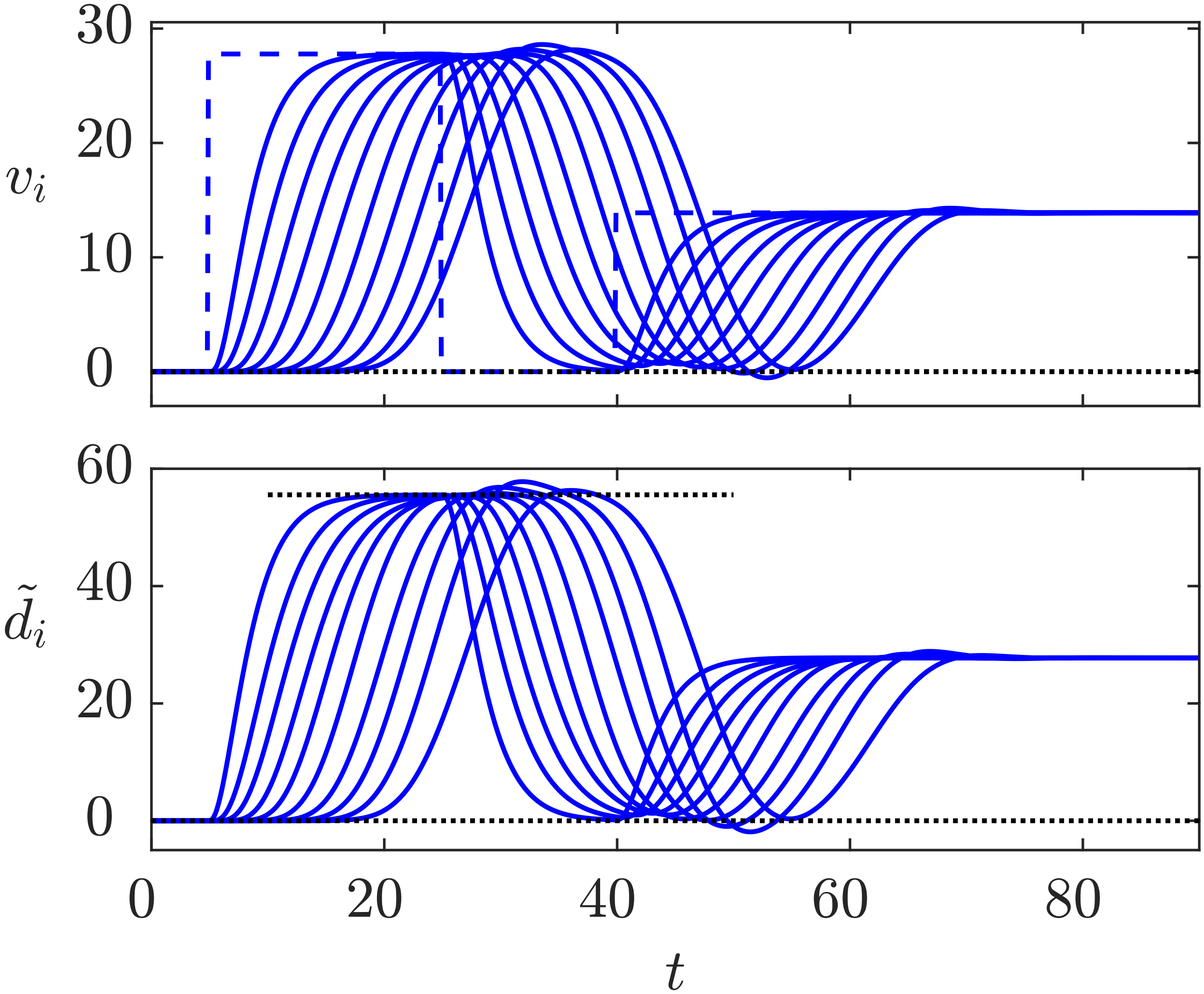

Fig. A1.51: Velocities in $\frac{\mathrm{m}}{\mathrm{s}}$ and reduced distances in meters of the vehicles

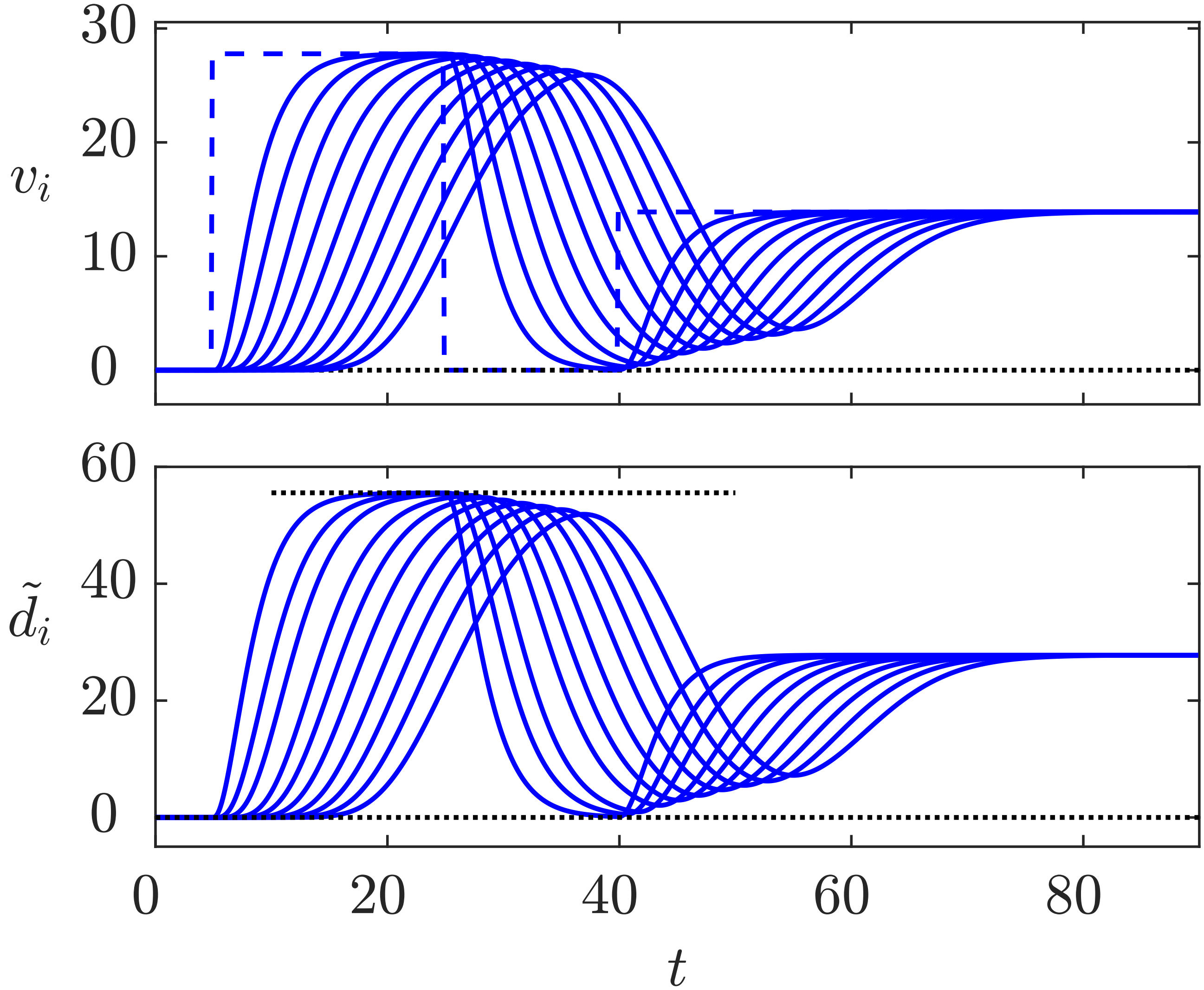

Fig. A1.51: Velocities in $\frac{\mathrm{m}}{\mathrm{s}}$ and reduced distances in meters of the vehicles

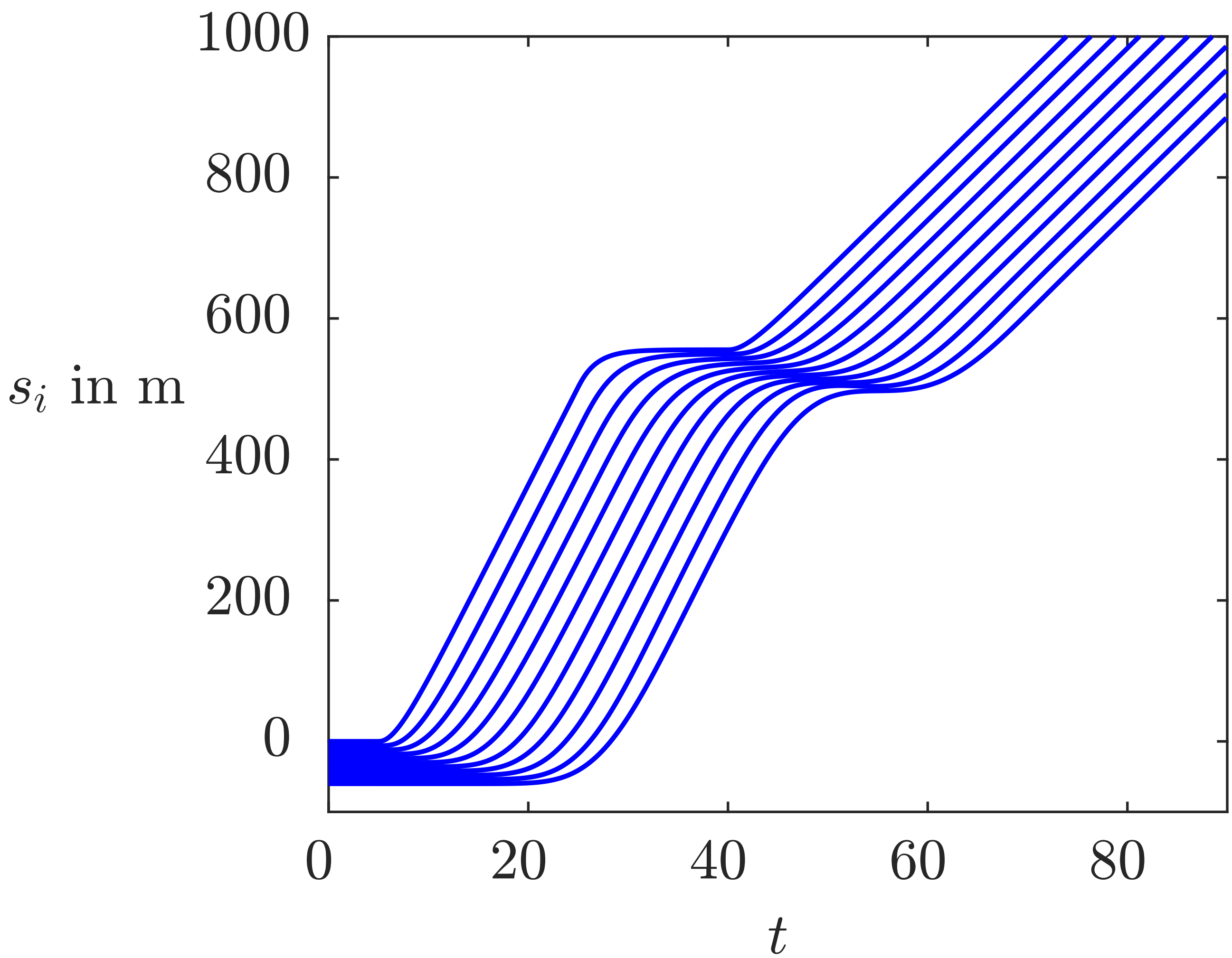

Fig. A1.52: Position of the ten vehicles

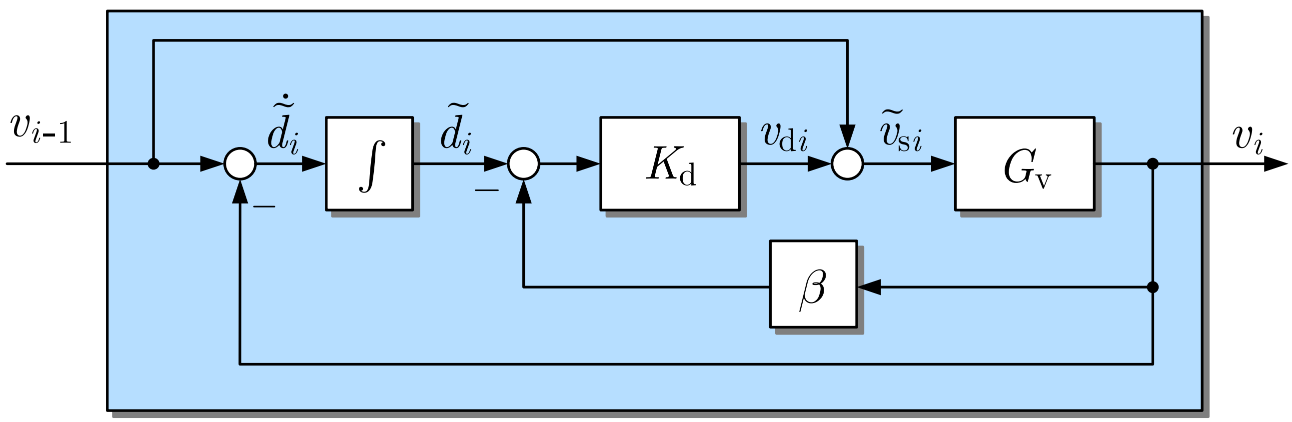

Fig. A1.53: Vehicle with distance and velocity controller

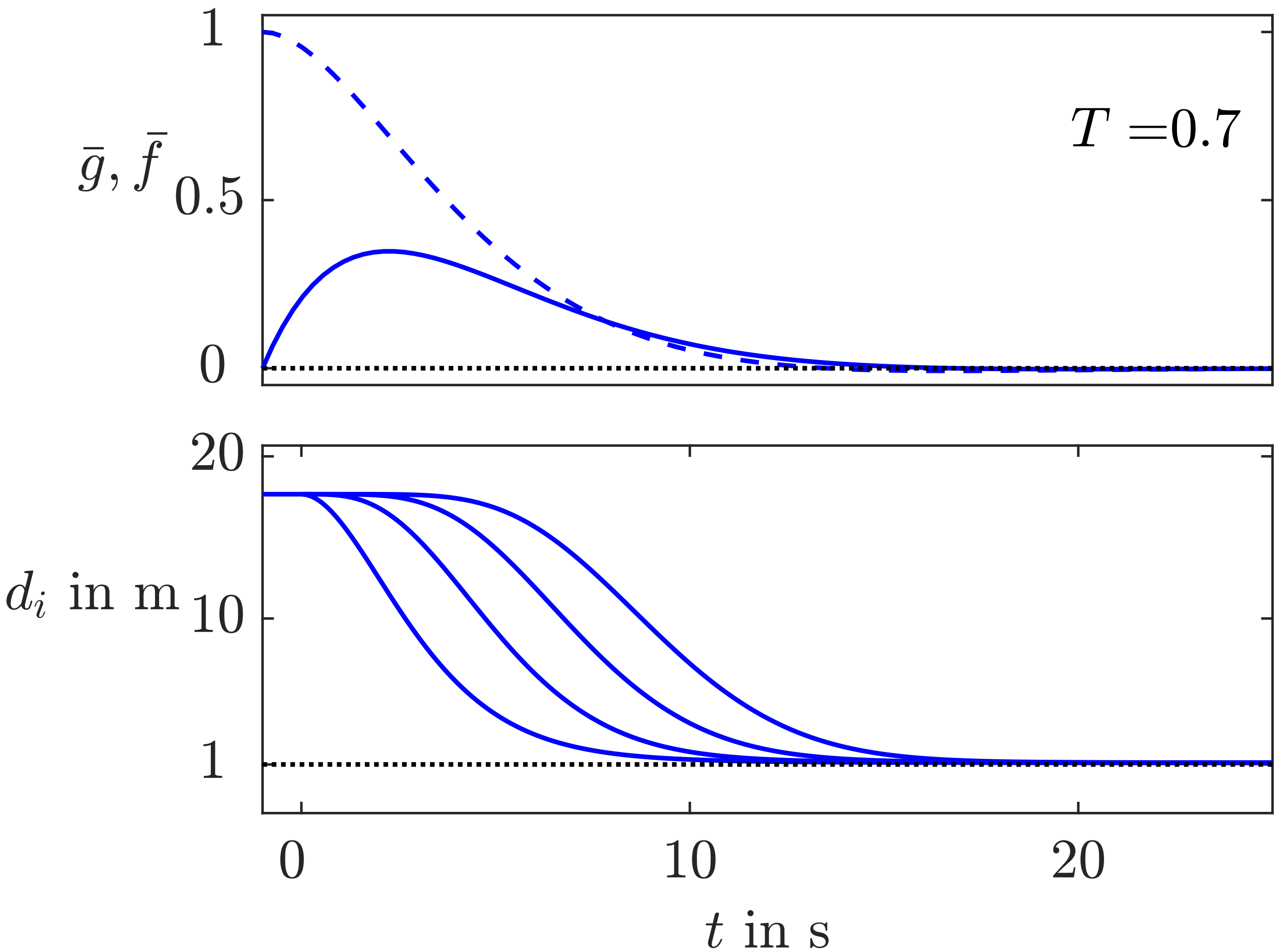

Fig. A1.54: Impulse responses of the controlled vehicle and vehicle distances for proportional distance and velocity controller

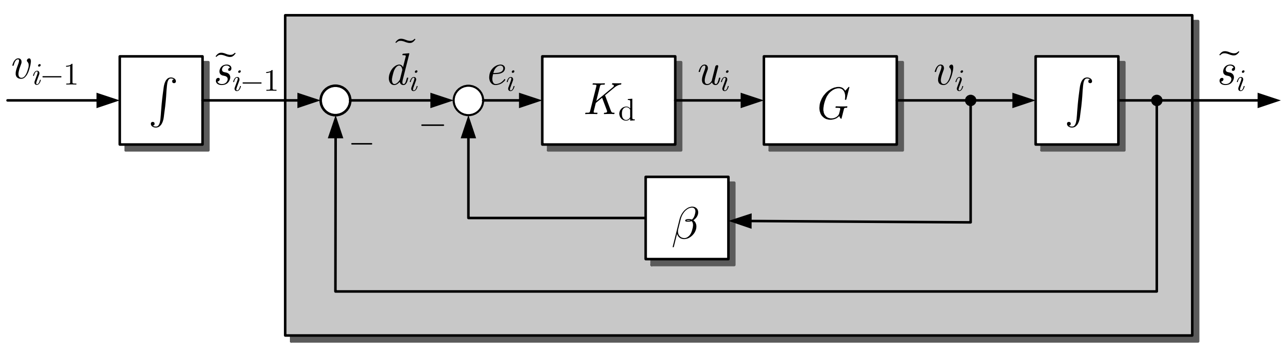

Fig. A1.55: Equivalent re-formulation of Fig. 5.36

J. LUNZE: *Networked Control of Multi-Agent Systems,* Edition **M**o**R**a 2022

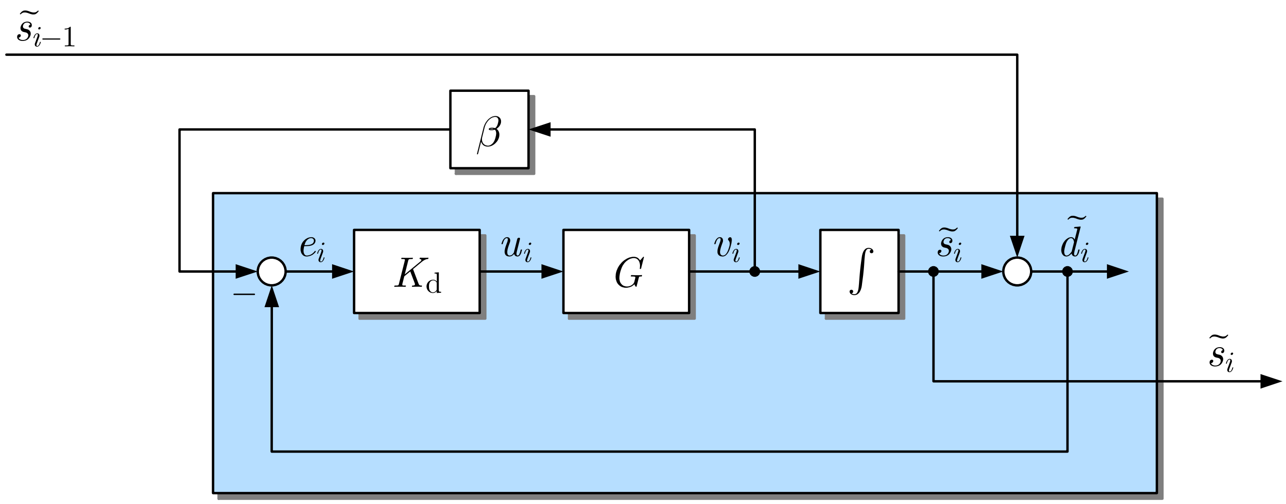

Fig. A1.56: Vehicle with distance controller as a standard feedback loop

J. Lunze: *Networked Control of Multi-Agent Systems,* Edition MoRa 2022

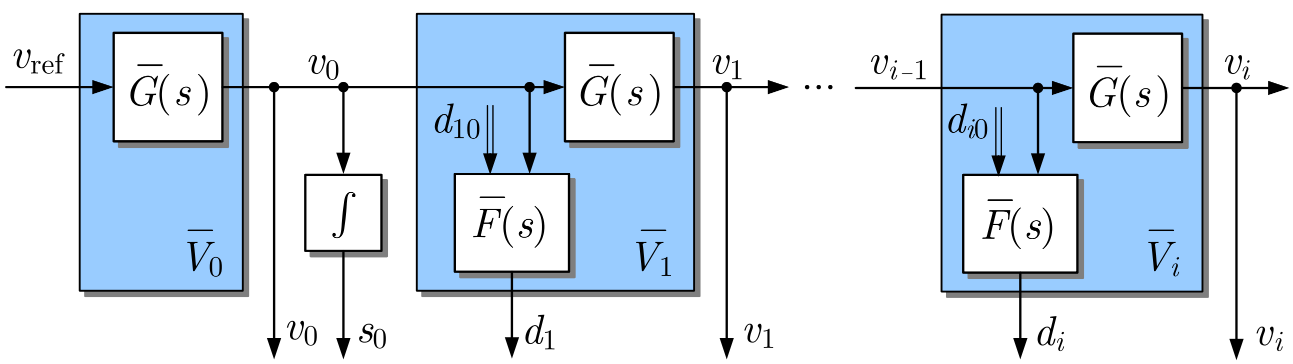

Fig. A1.57: Model of the platoon

J. LUNZE: *Networked Control of Multi-Agent Systems,* Edition **MoRa** 2022

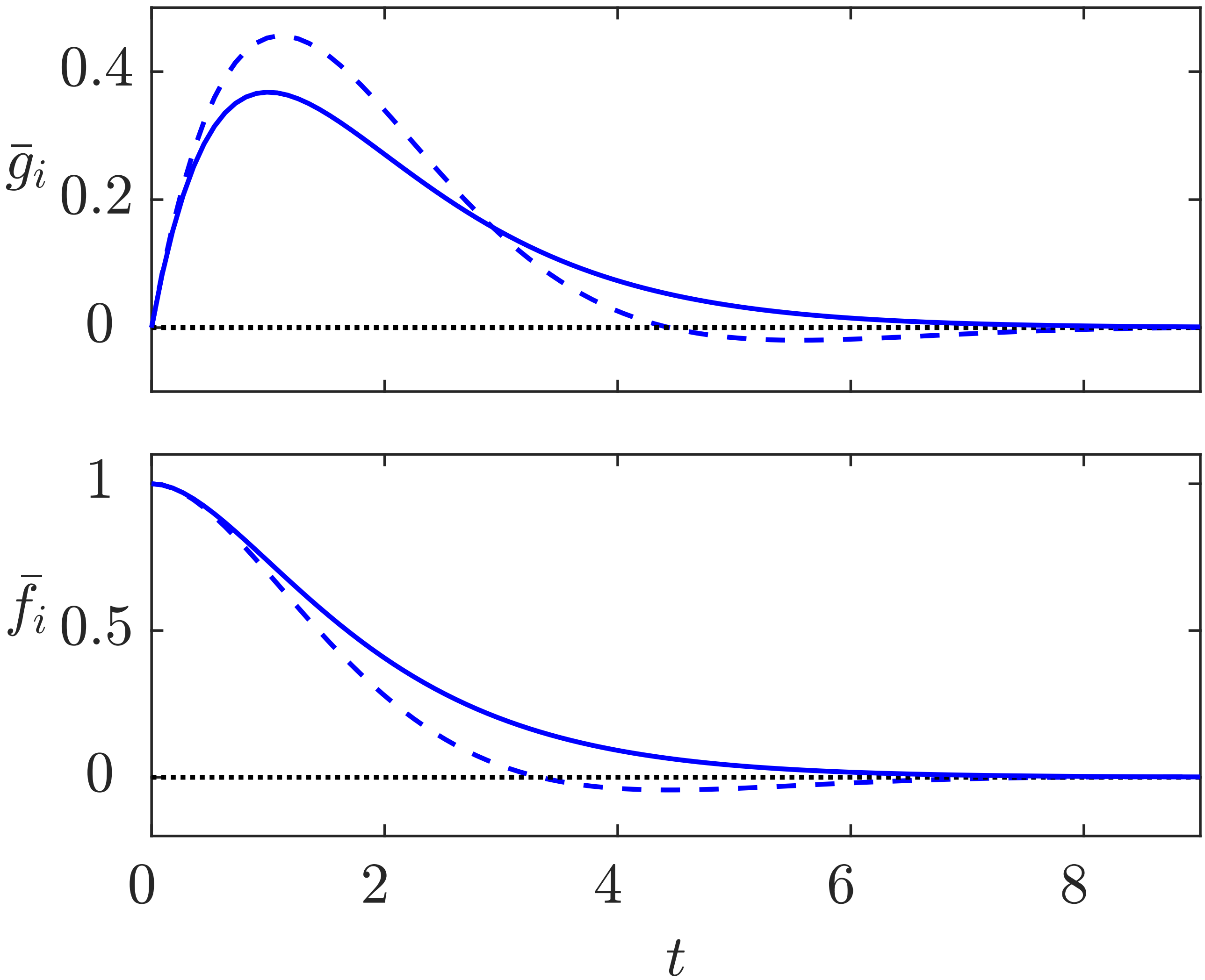

Fig. A1.58: Impulse responses of the controlled vehicles

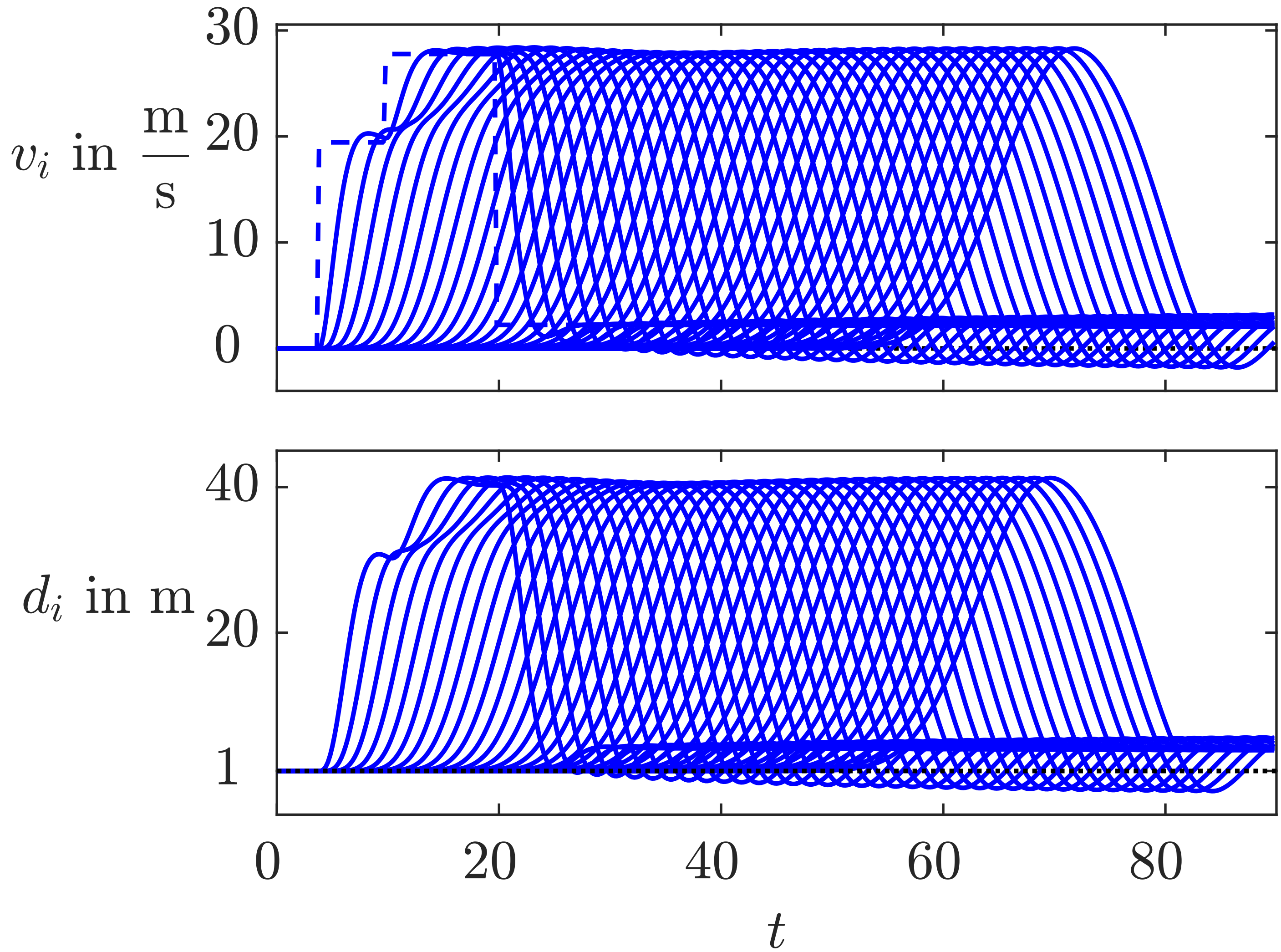

Fig. A1.59: Behaviour of the string stable platoon with $N = 30$ vehicles

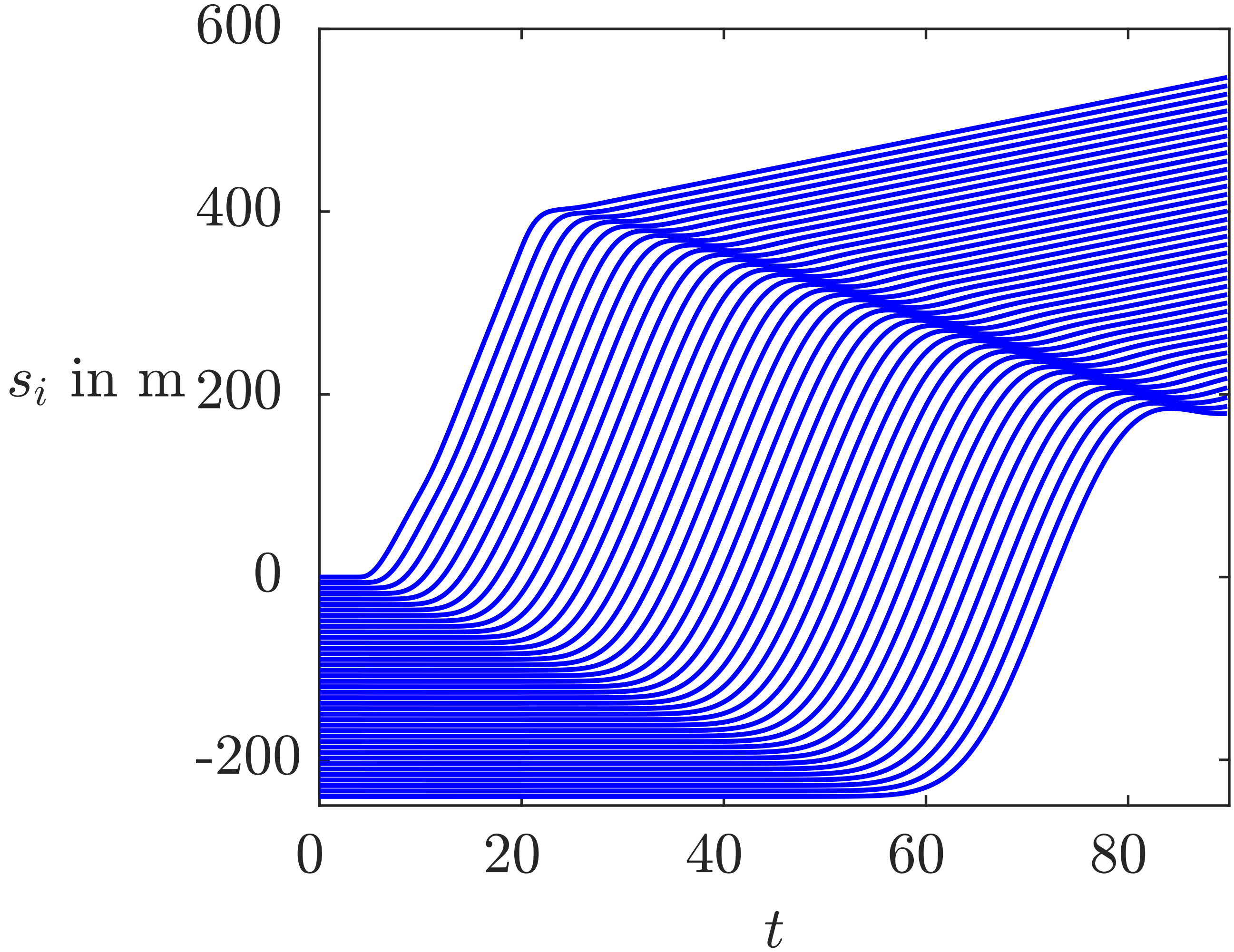

Fig. A1.59: Behaviour of the string stable platoon with $N = 30$ vehicles

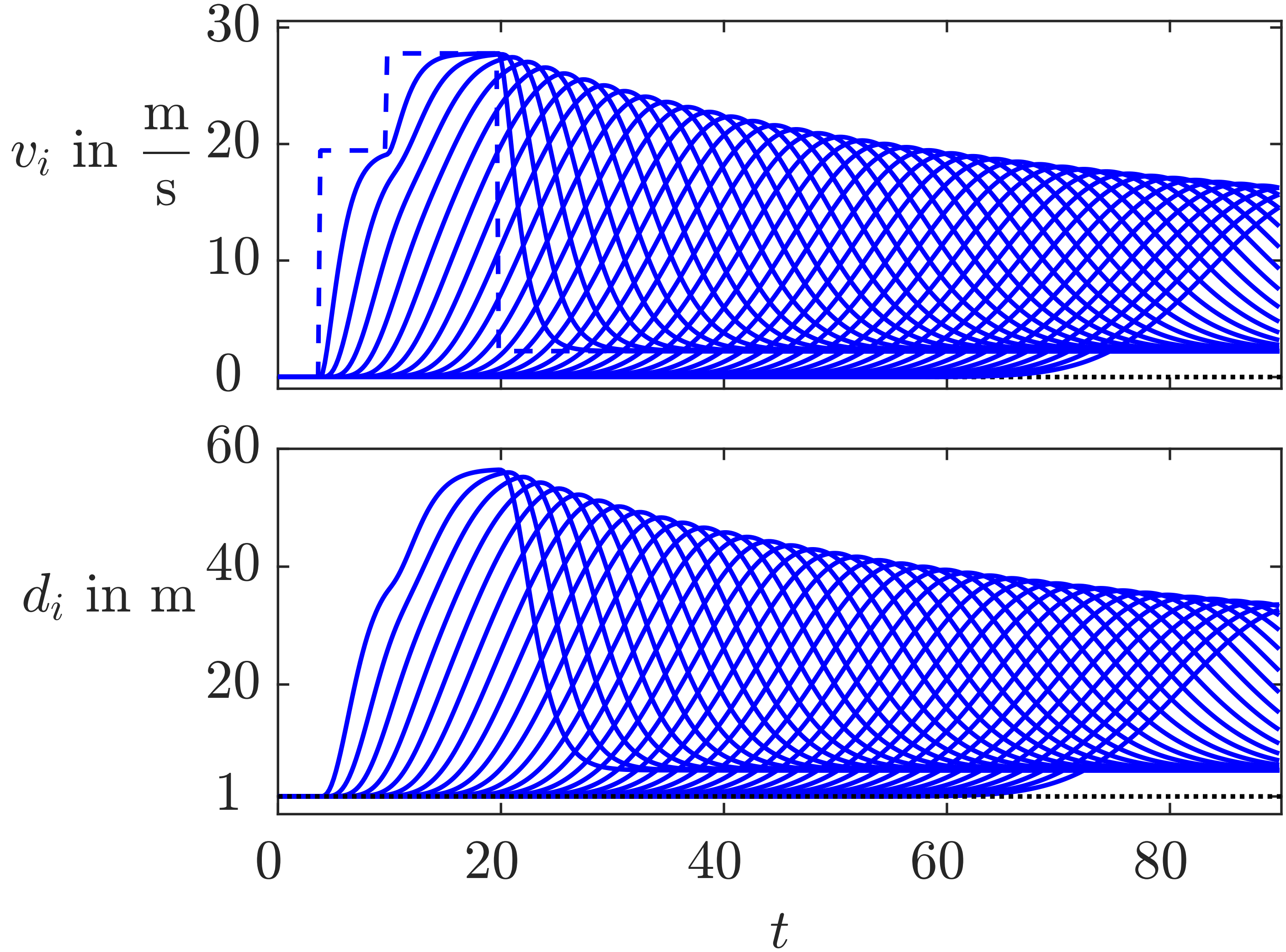

Fig. A1.60: Behaviour of the platoon with guaranteed collision avoidance

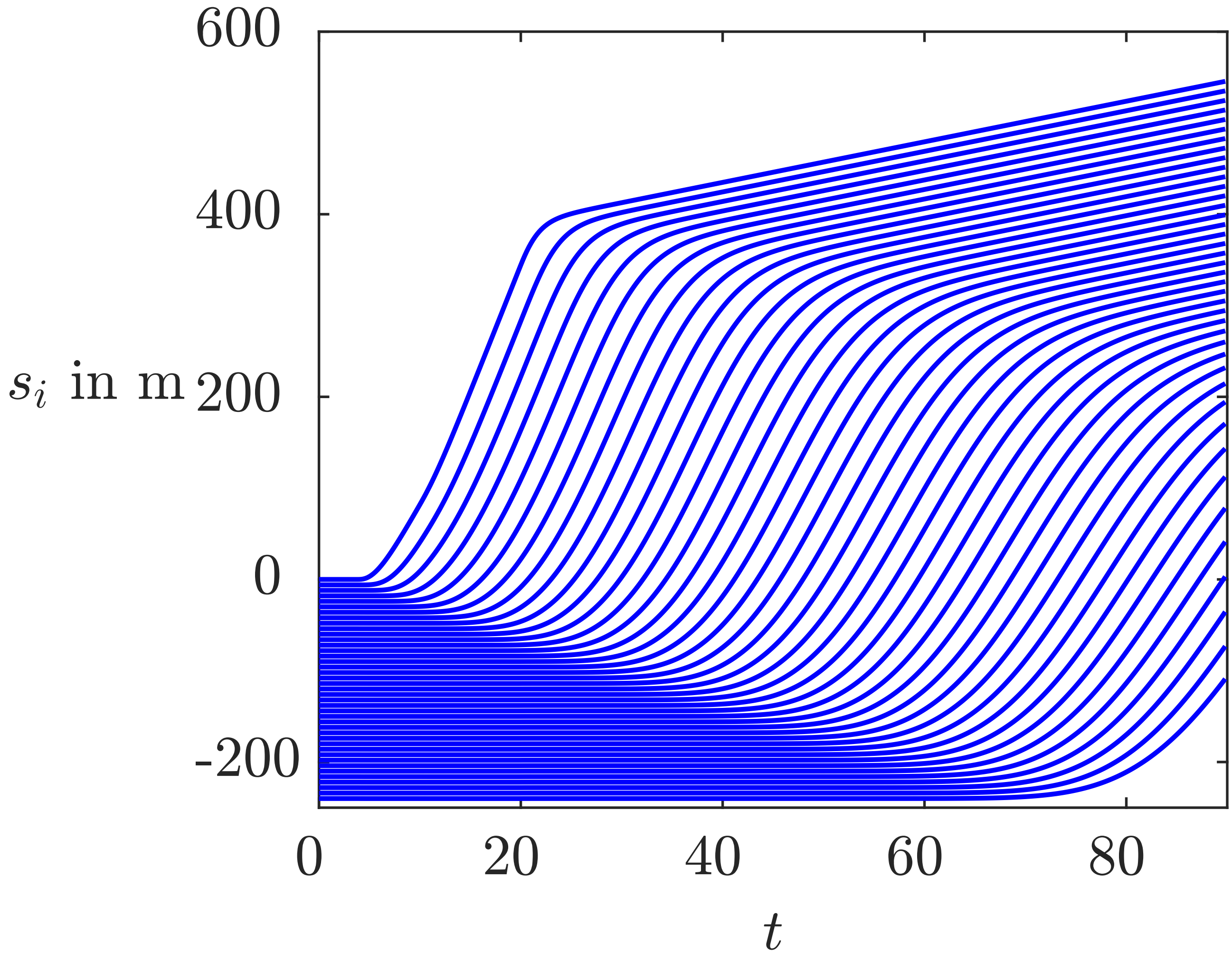

Fig. A1.60: Behaviour of the platoon with guaranteed collision avoidance

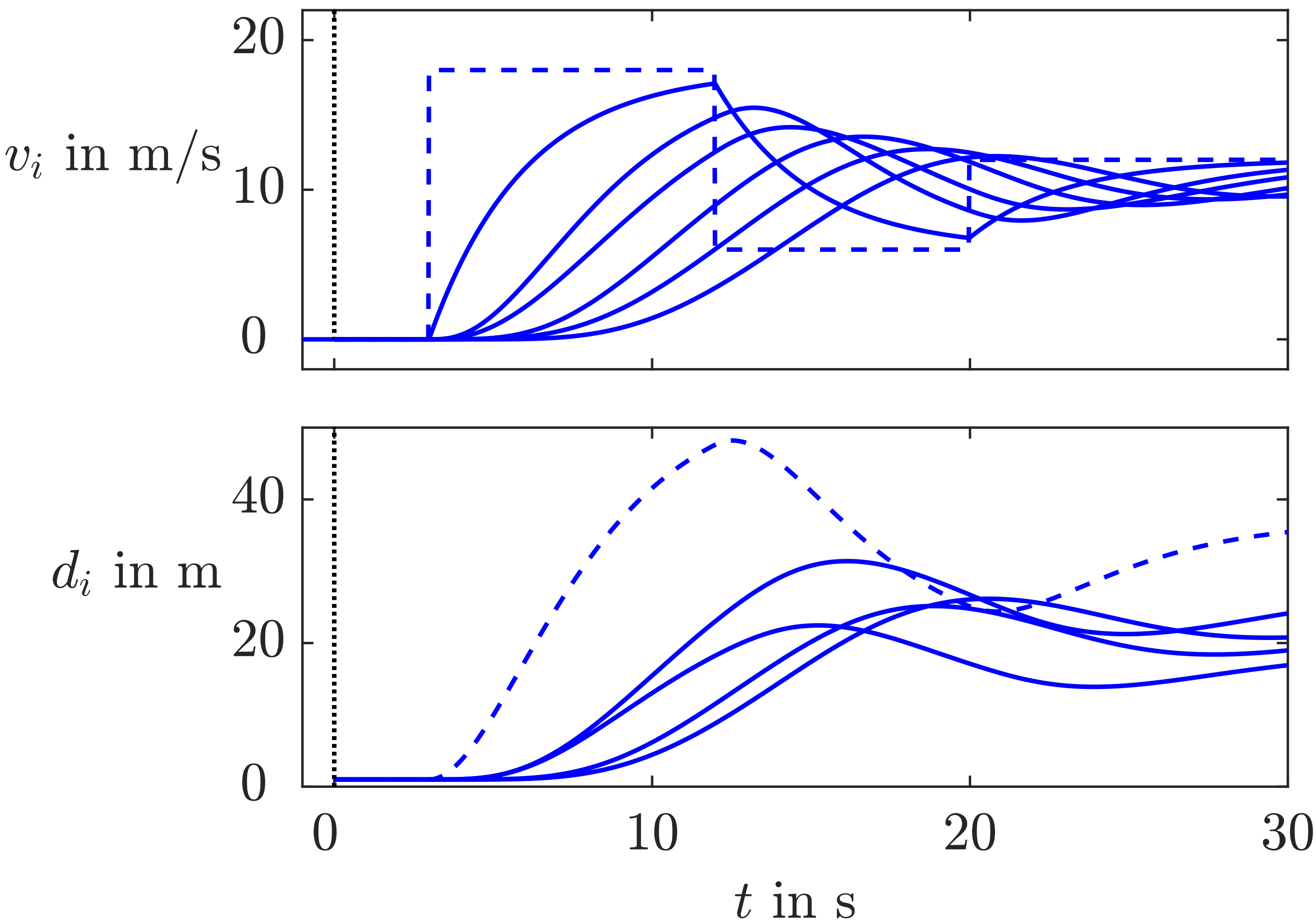

Fig. A1.61: Vehicle velocities and distances in the platoon with CACC (5.117)

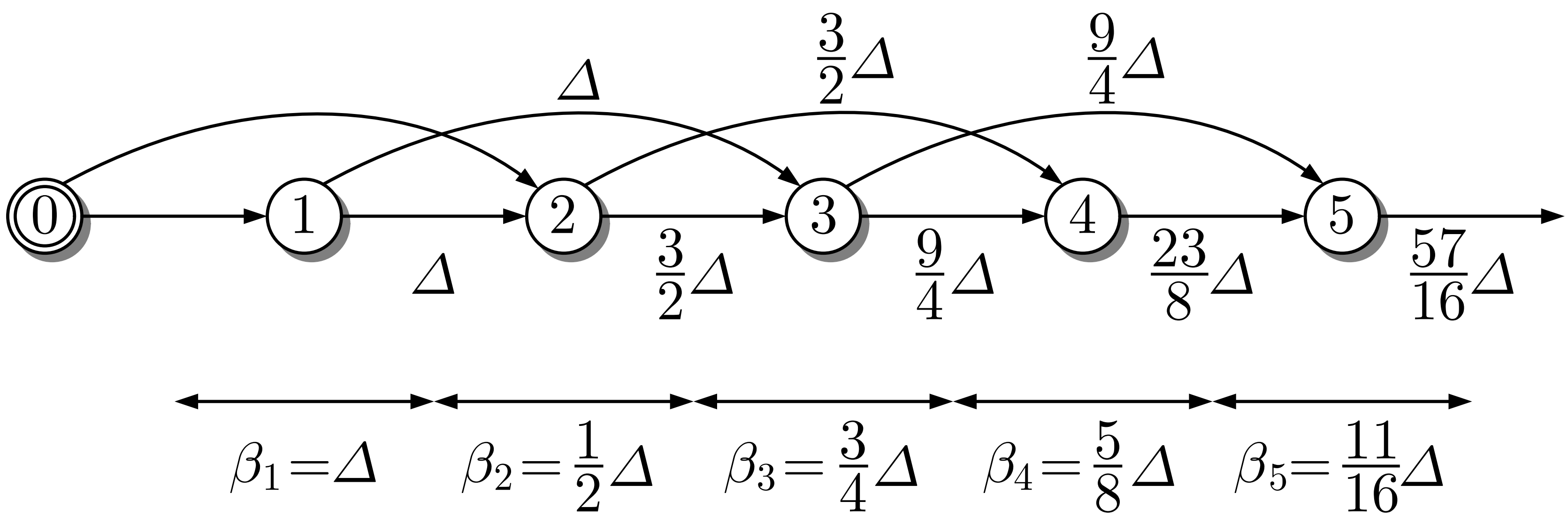

Fig. A1.62. Determination of the time-headway coefficients for vehicles with the same delay D

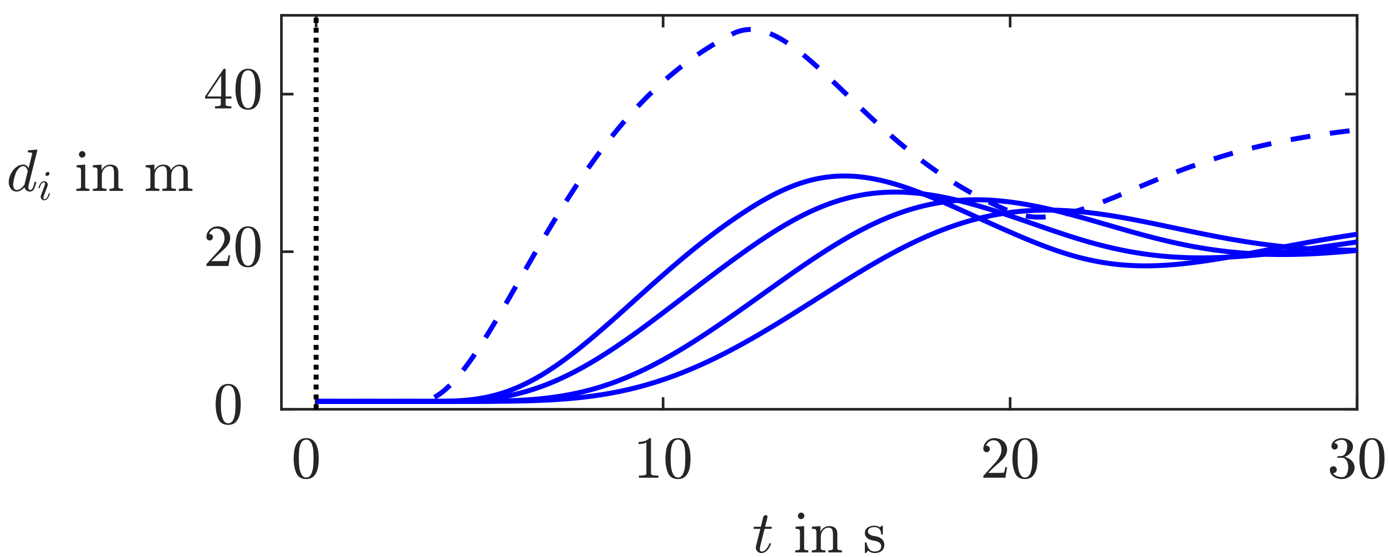

Fig. A1.63: Vehicle distances in the platoon with modified CACC

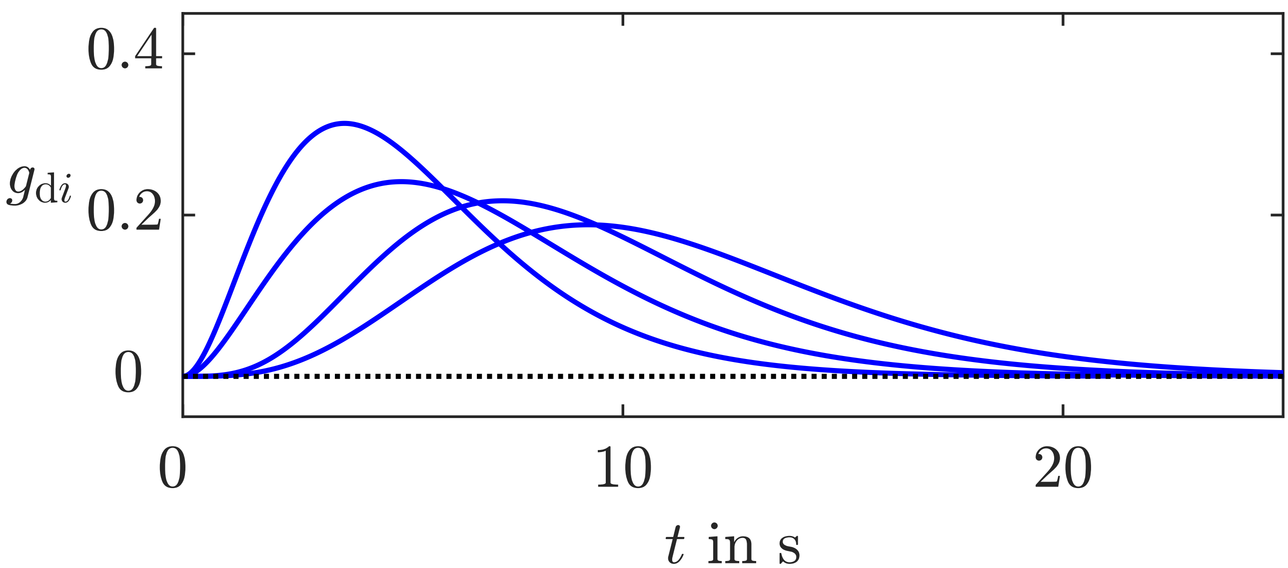

Fig. A1.64: Collision avoidance test for the modified CACC $(i = 2, ..., 5)$

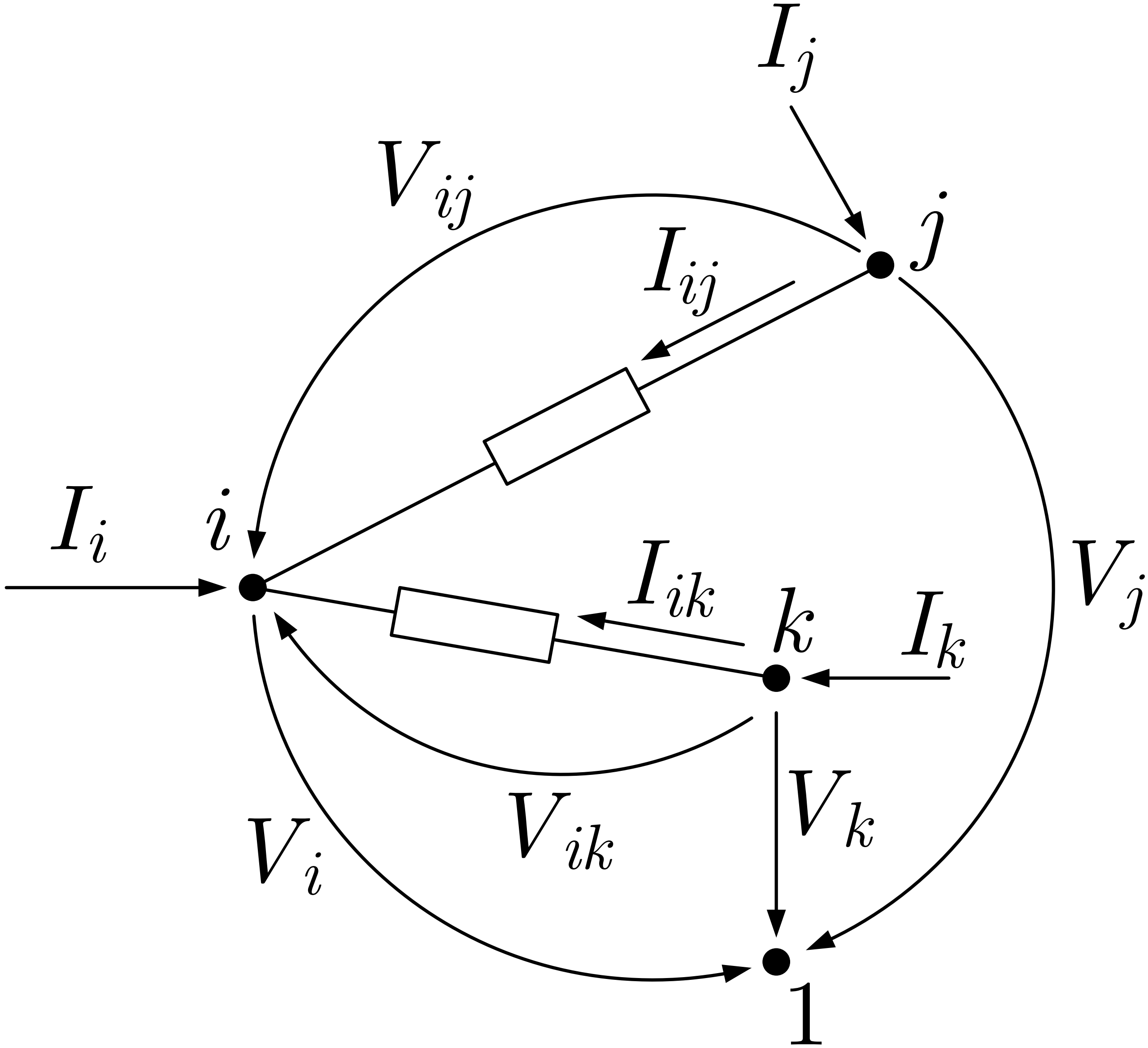

Fig. A1.65: Part of the electrical network

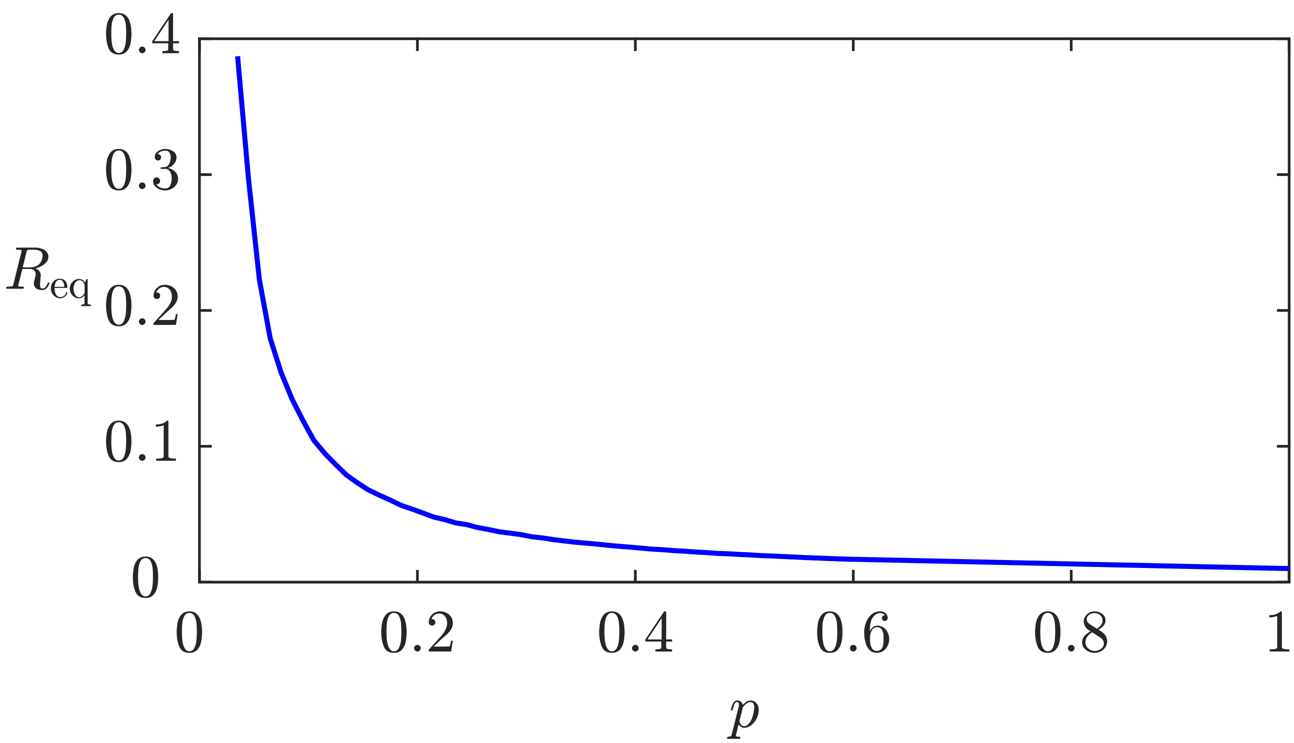

Fig. A1.66: Equivalent resistance in dependence upon the probability p

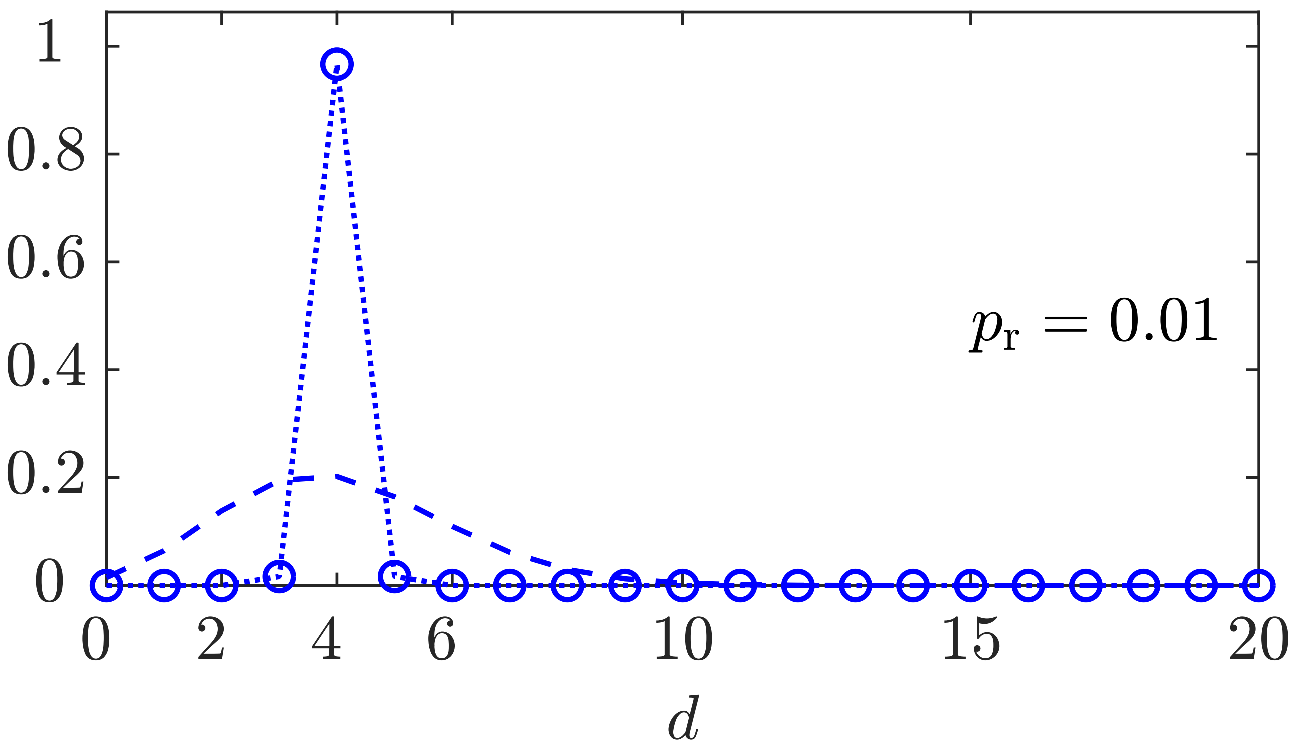

Fig. A1.67: Degree distribution of small-world networks

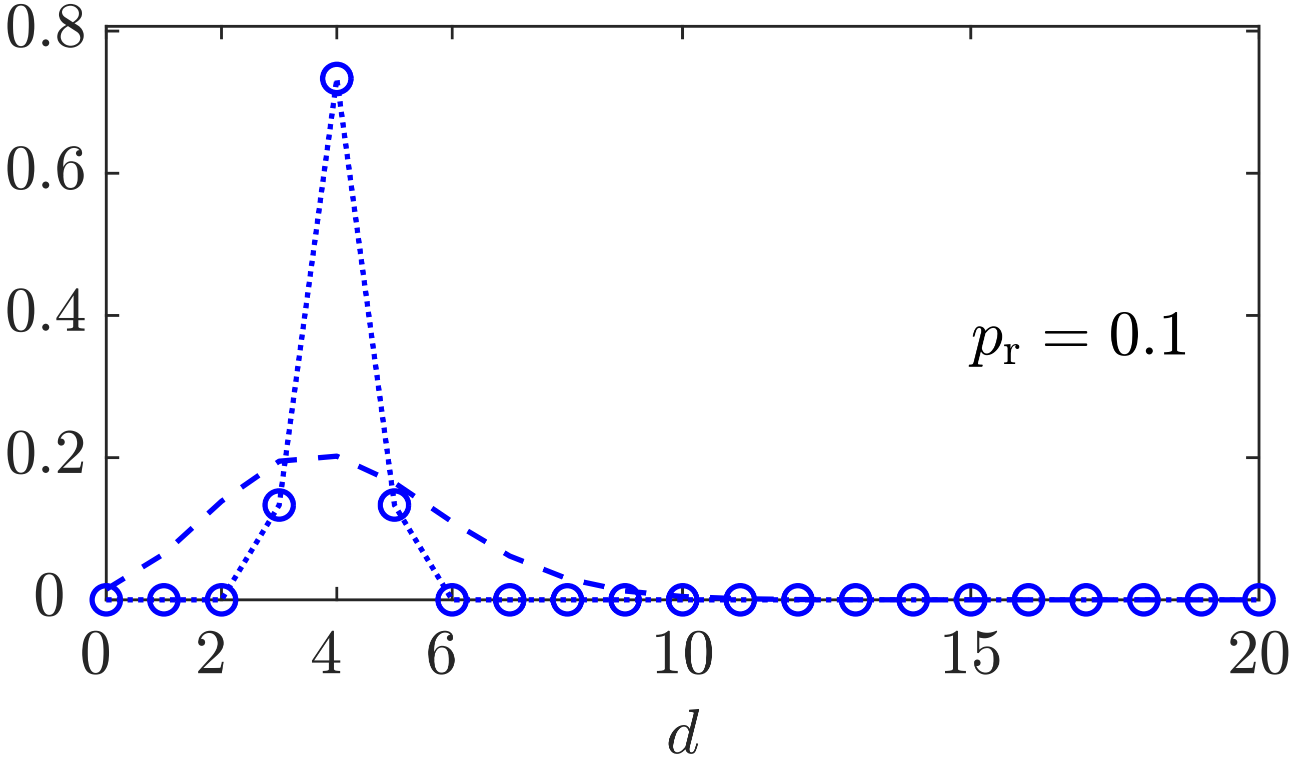

Fig. A1.67: Degree distribution of small-world networks

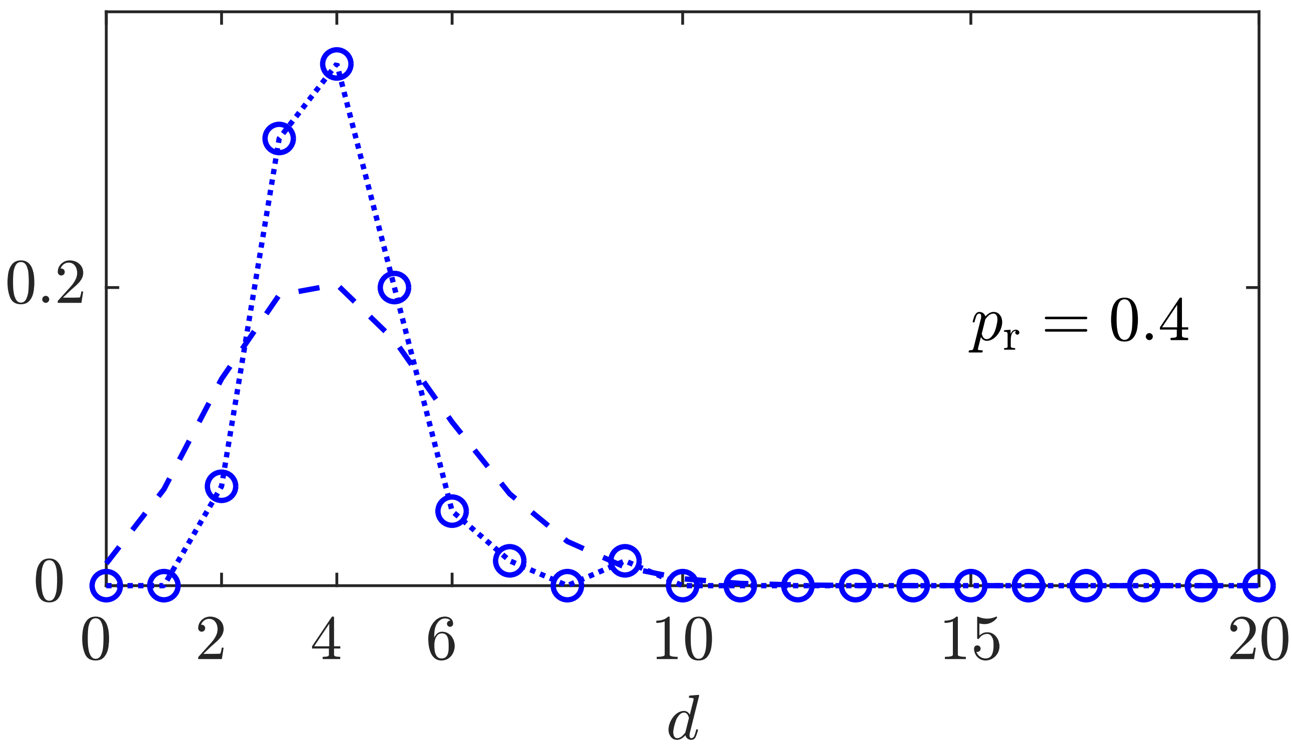

Fig. A1.67: Degree distribution of small-world networks

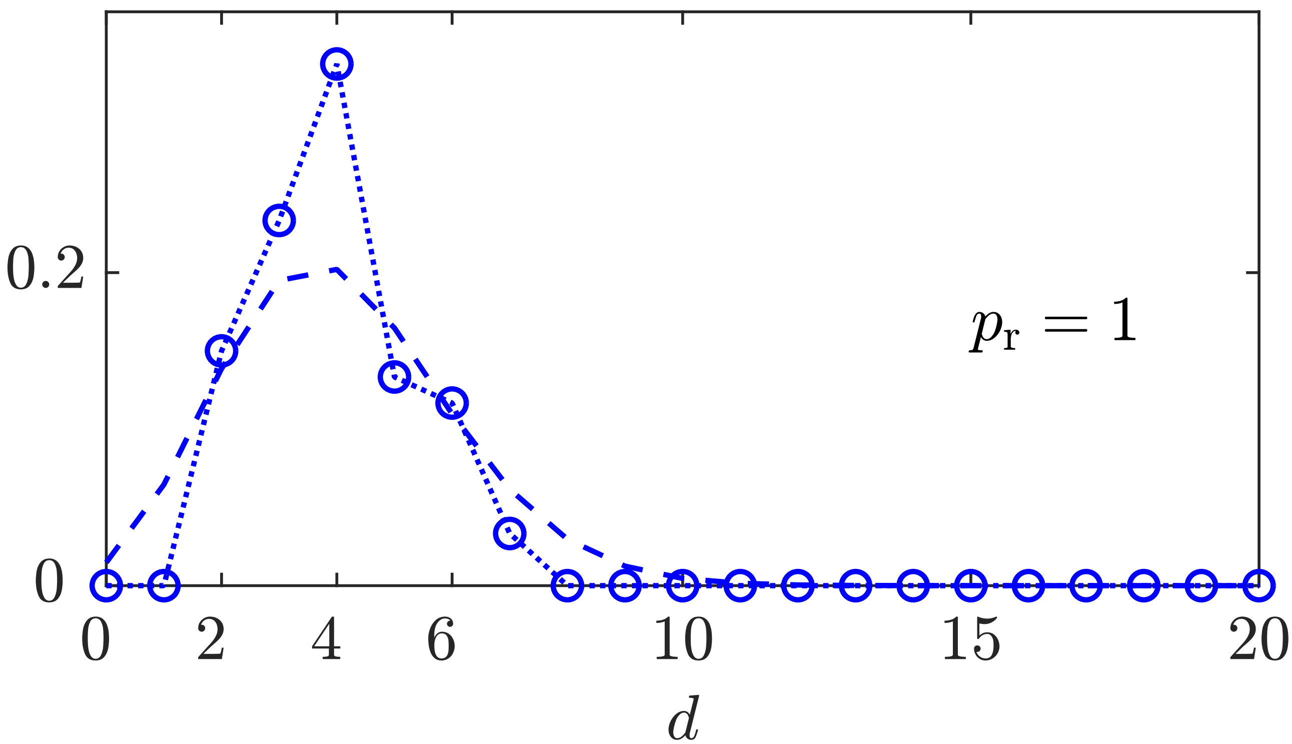

Fig. A1.67: Degree distribution of small-world networks

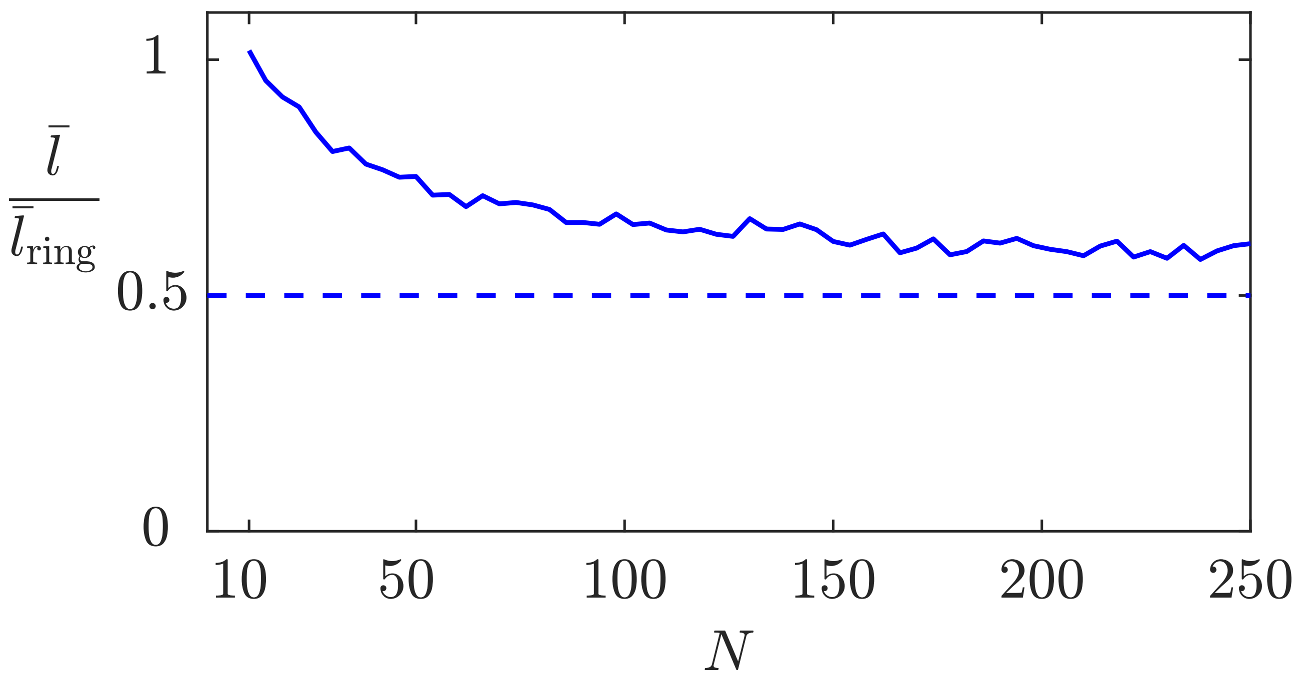

Fig. A1.68: Relative characteristic path length of a small-world network with 4 shortcuts

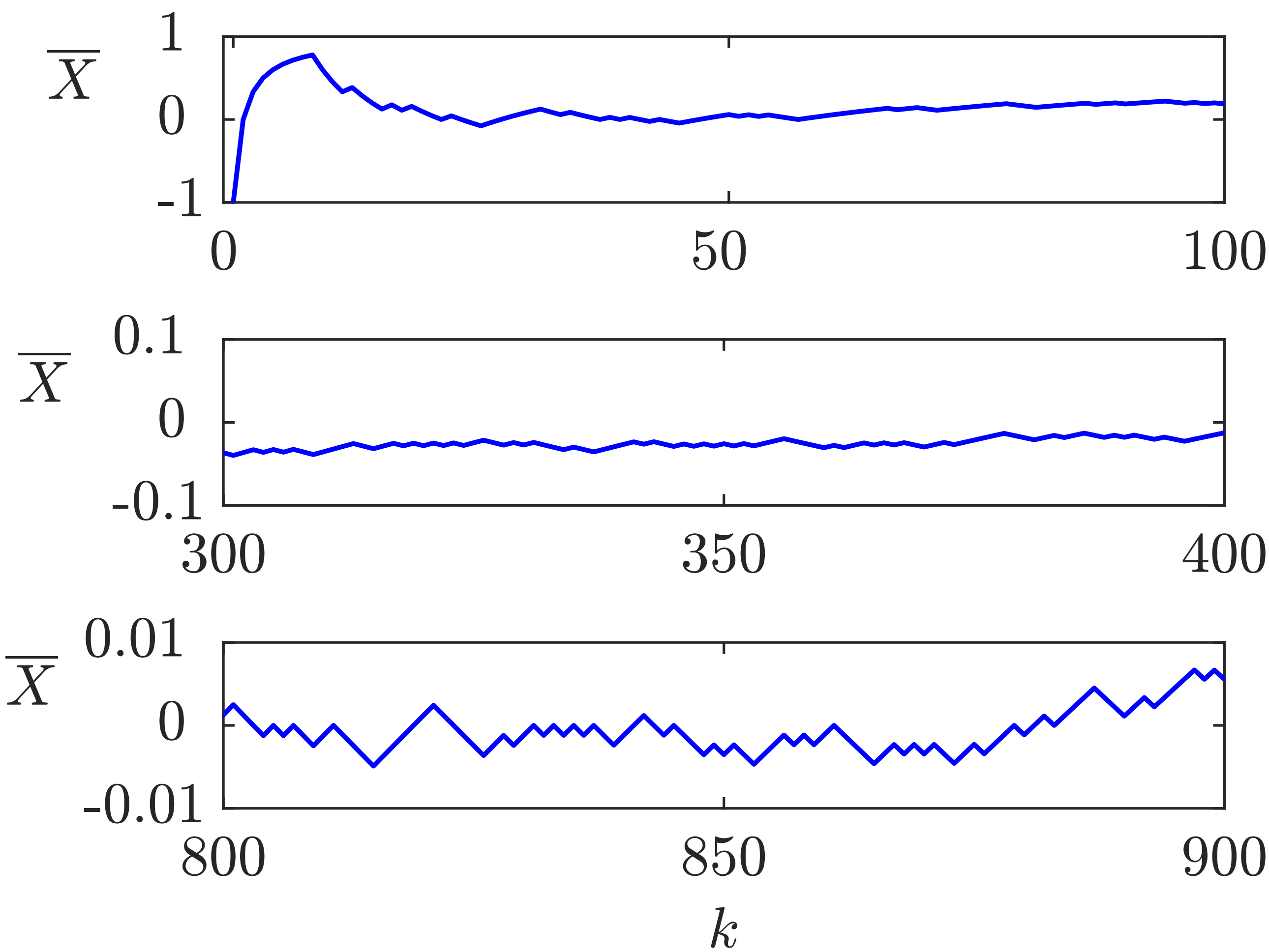

Fig. A1.69: Three parts of a convergent sequence

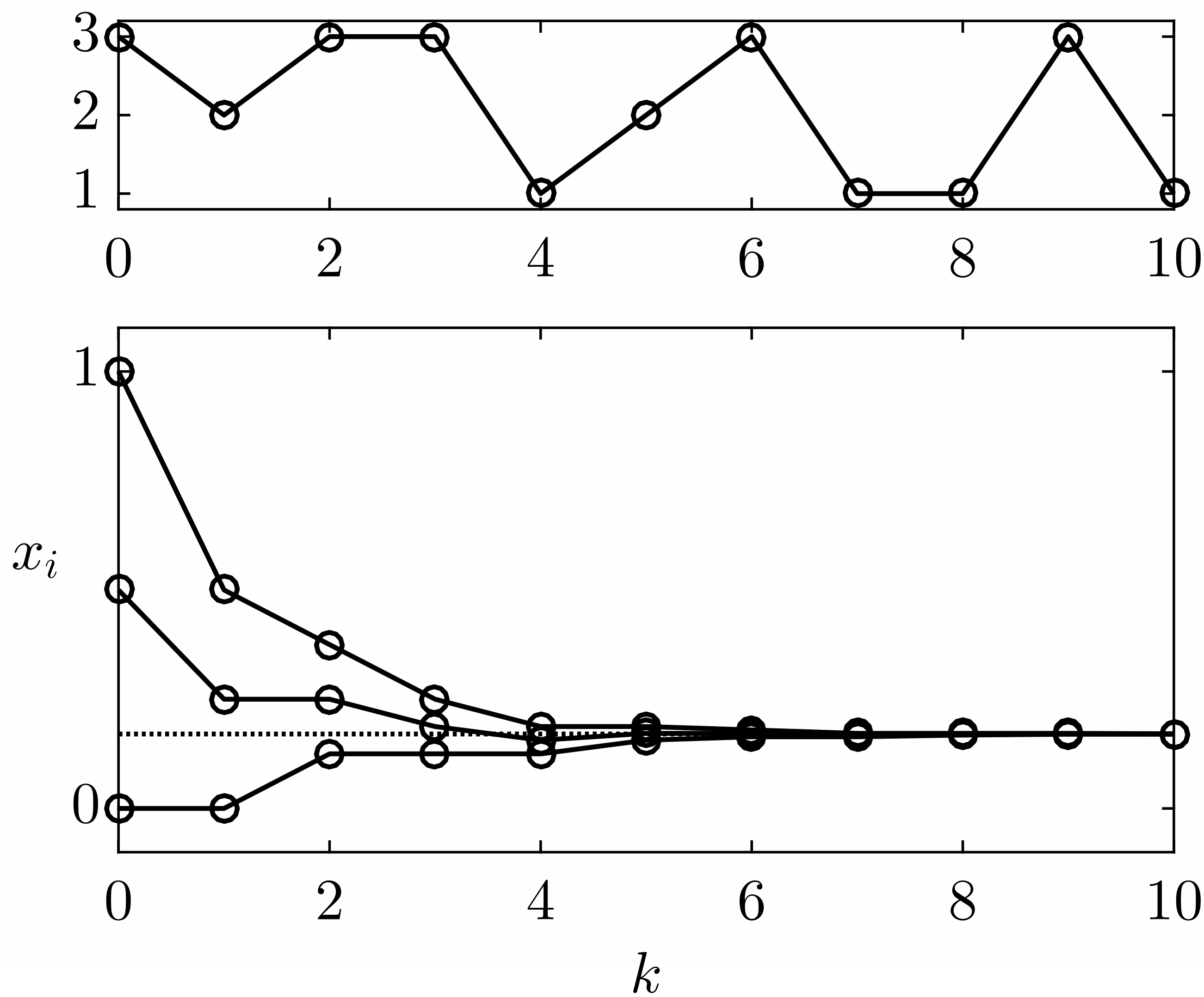

Fig. A1.70: Results of the distributed averaging algorithms for two different sequences of broadcast communications with the same initial state

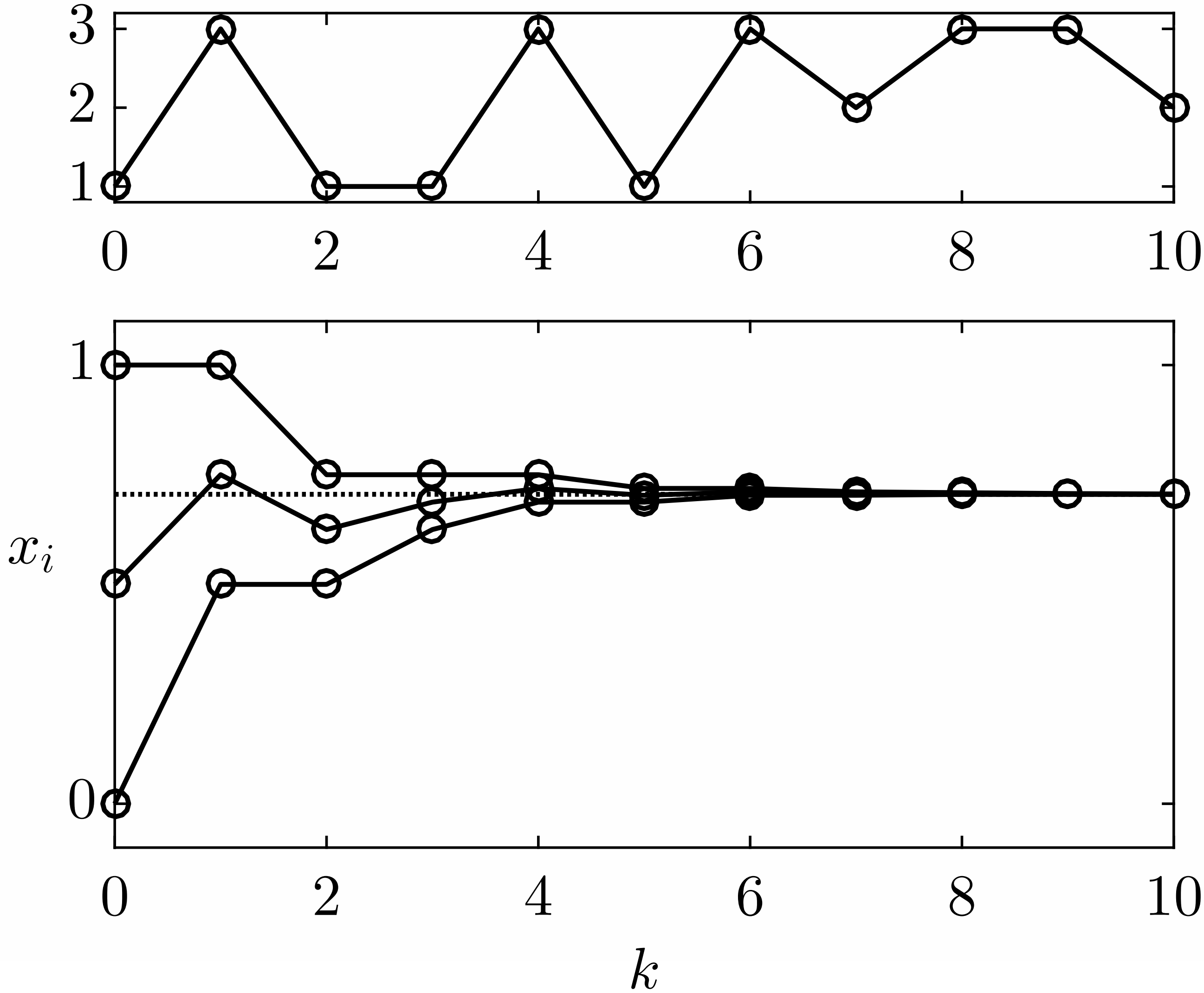

Fig. A1.70: Results of the distributed averaging algorithms for two different sequences of broadcast communications with the same initial state

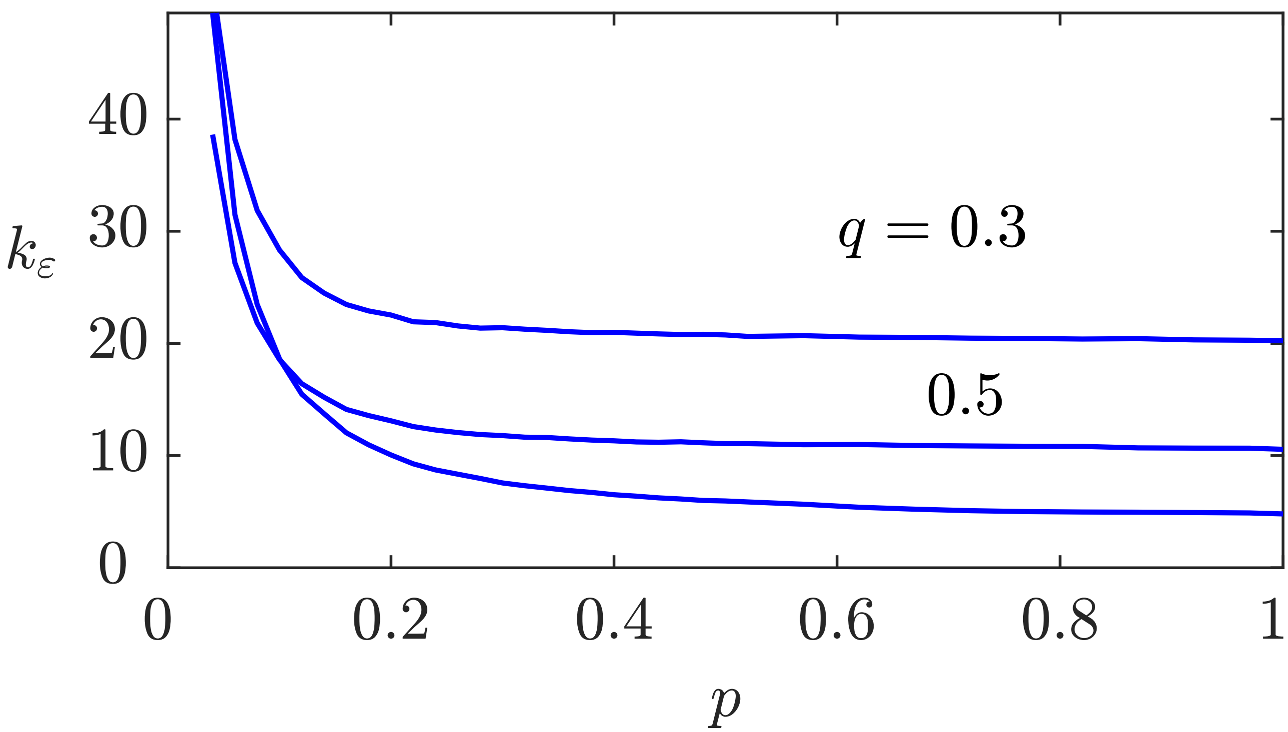

Fig. A1.71: Time-to-consensus in dependence upon the probability p of Erdös-Rényi graphs for the feedback gain $q = 0.3$, 0.5 and 0.8

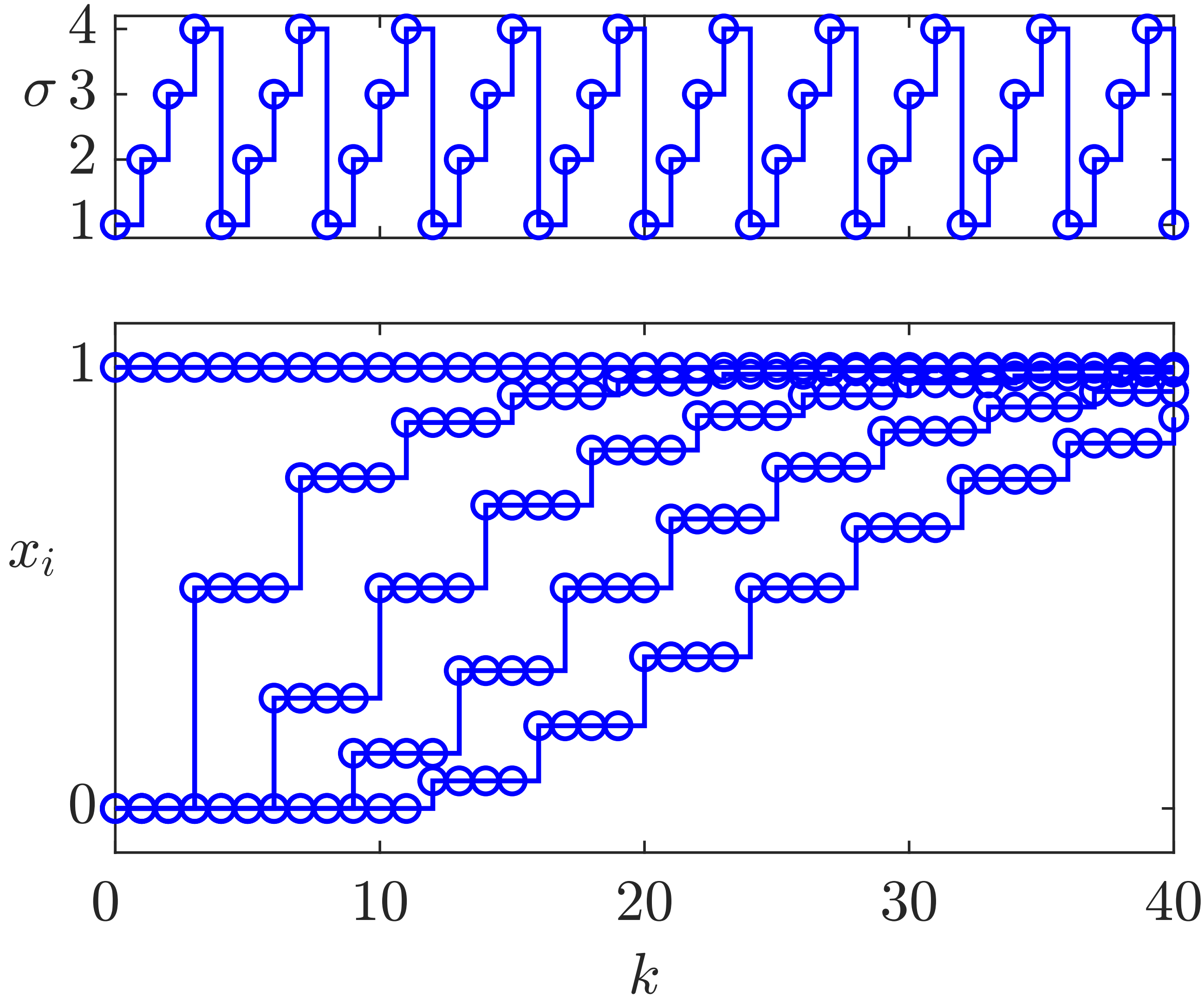

Fig. A1.72: Gossiping with deterministic communication topologies

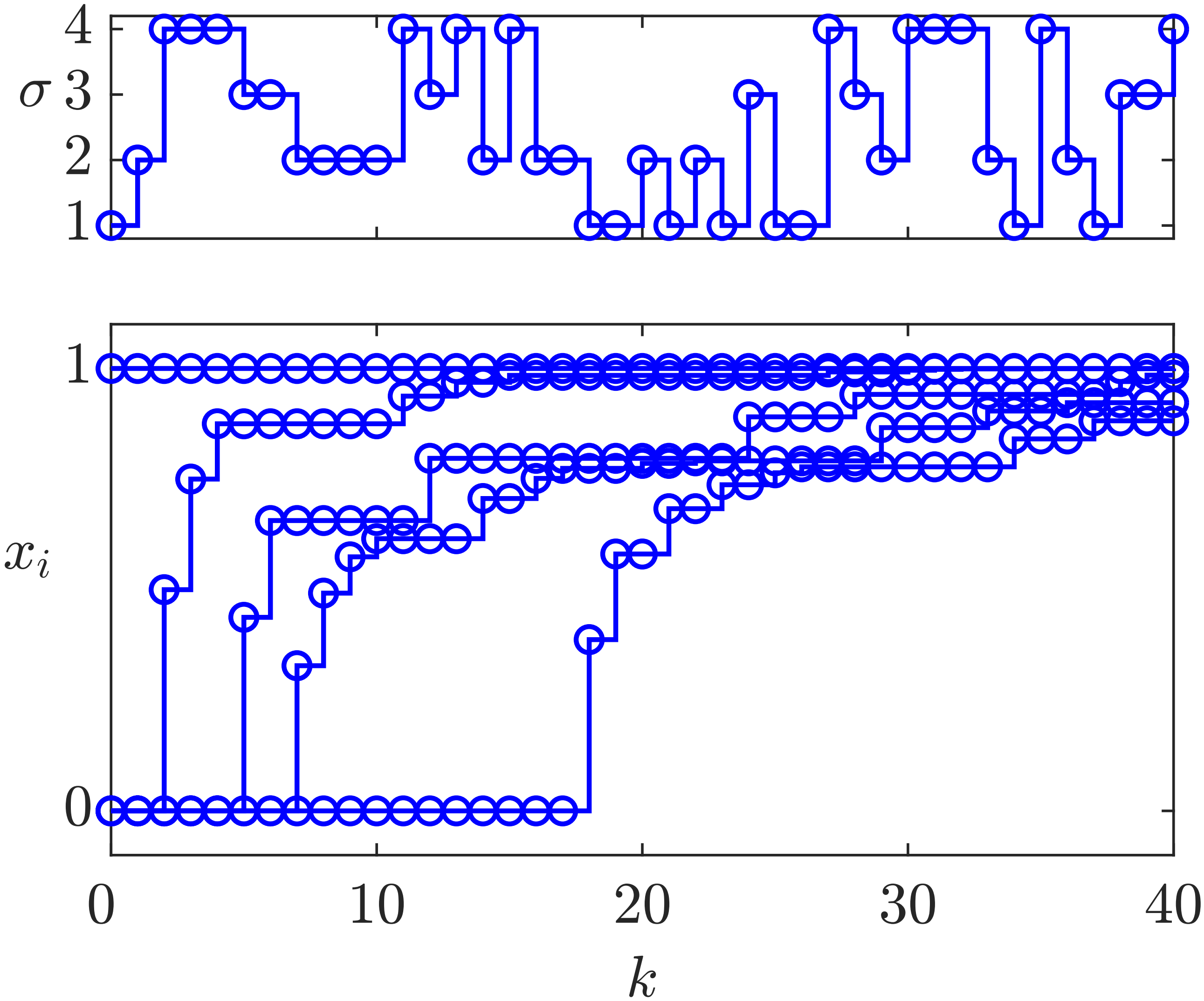

Fig. A1.73: Gossiping with random communication

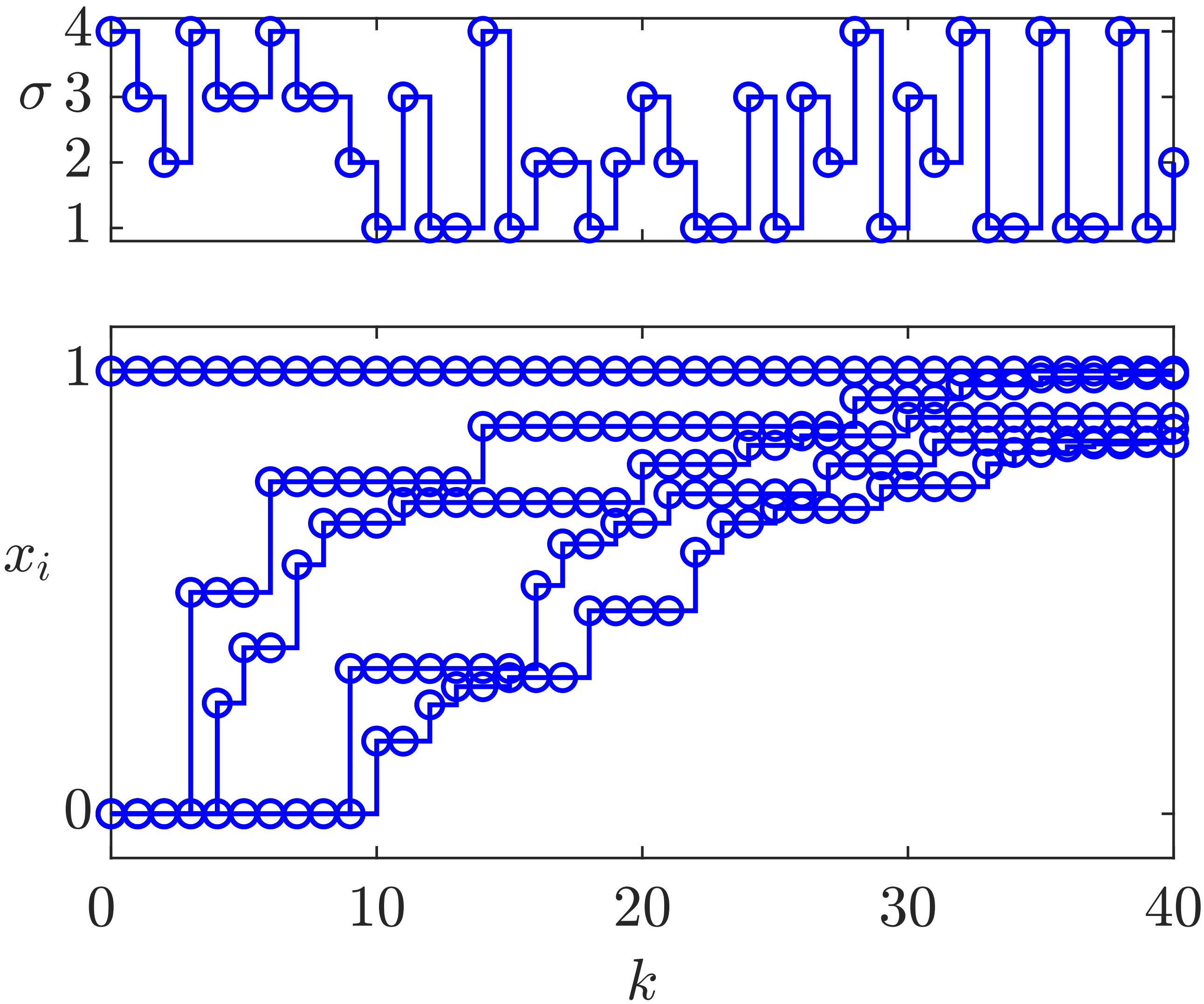

Fig. A1.73: Gossiping with random communication

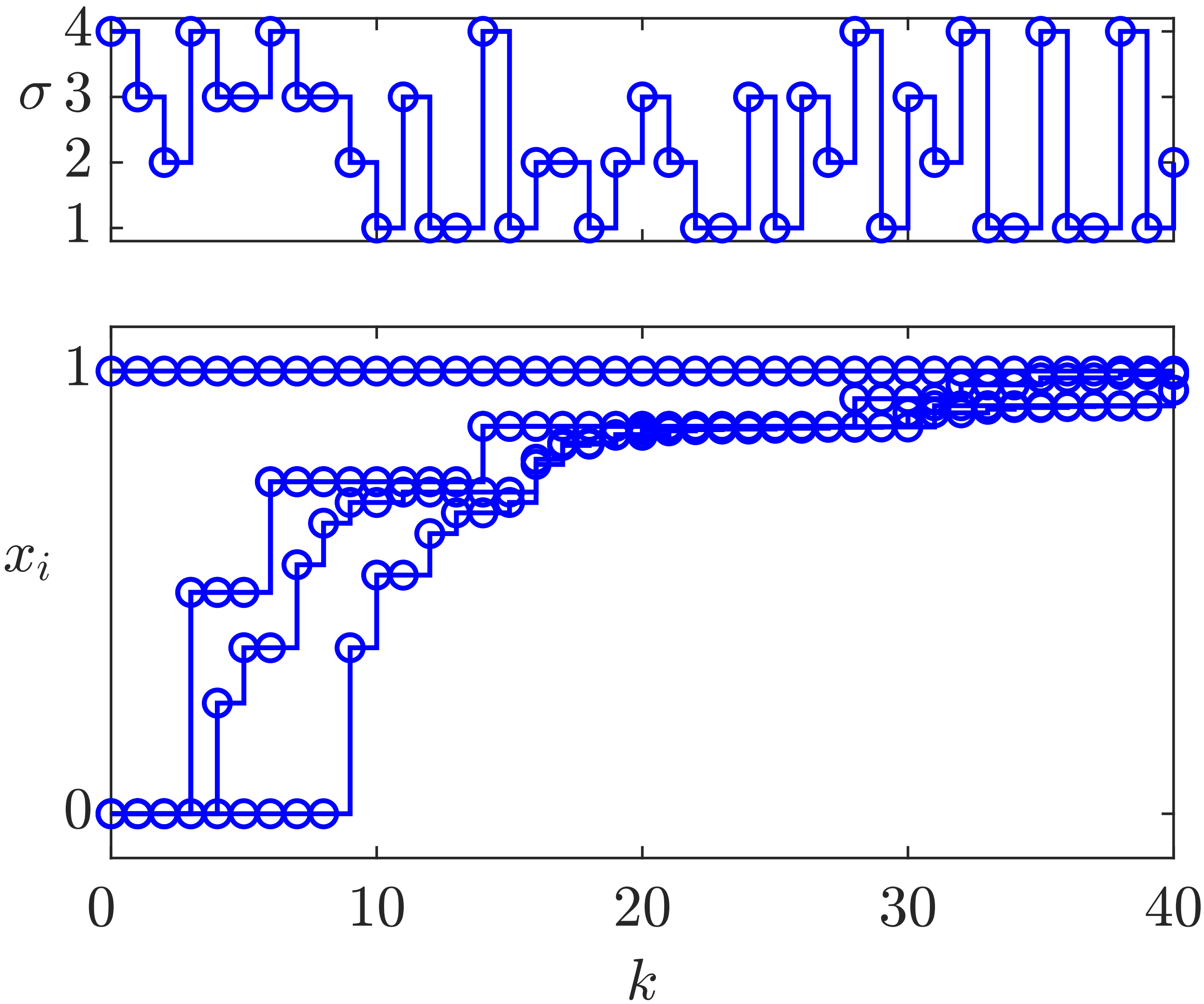

Fig. A1.74: Gossiping with the communication to the next two followers

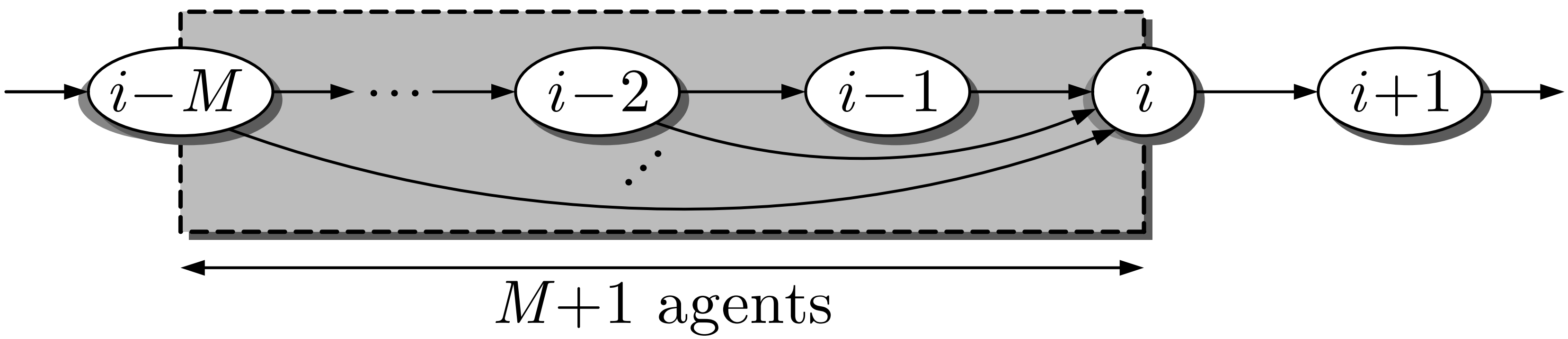

Fig. A1.75. Additional edges towards the vertex i from M predecessors

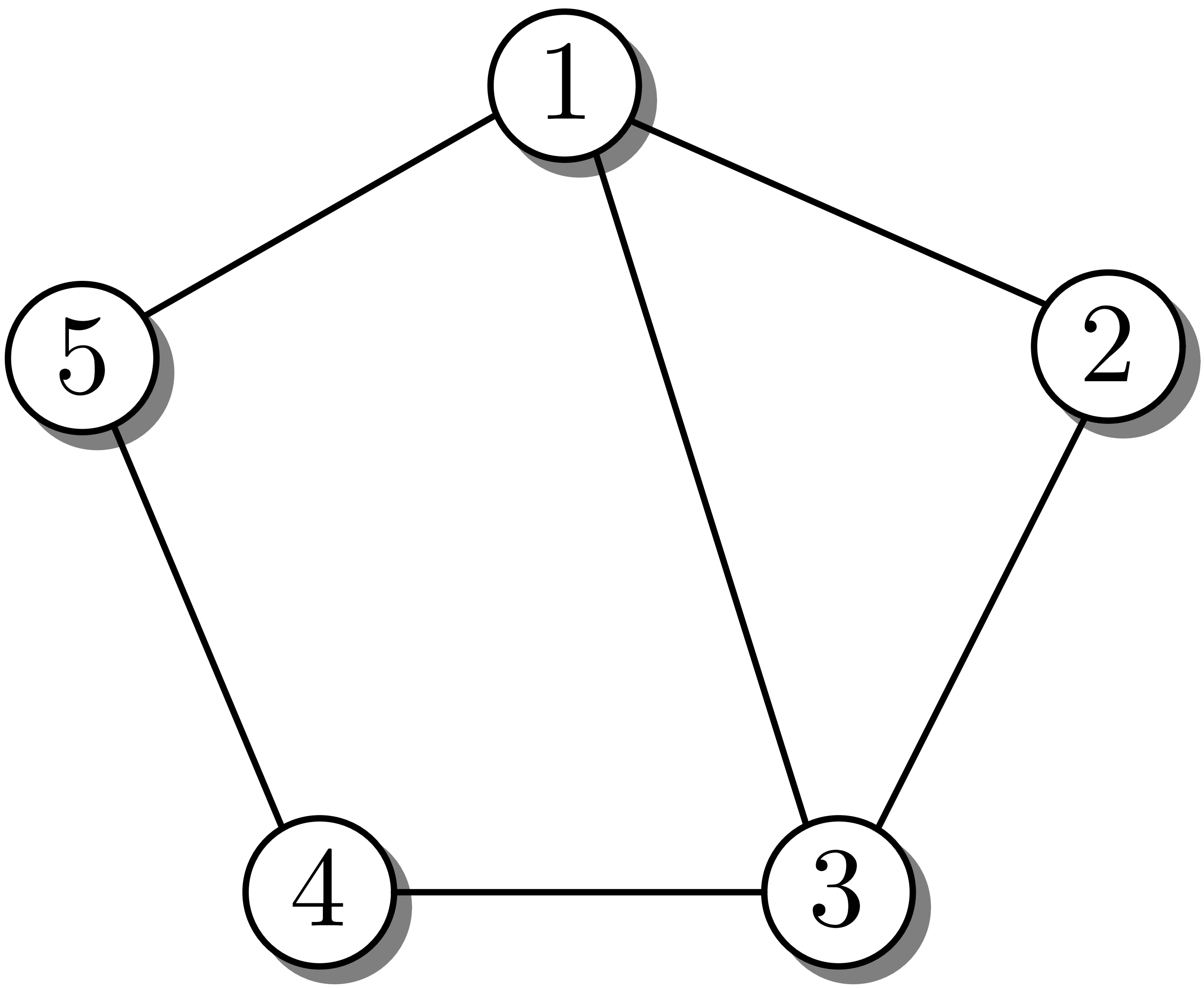

Fig. A1.76: Example for an extended bidirectional communication graph

J. Lunze: *Networked Control of Multi-Agent Systems,* Edition MoRa 2022

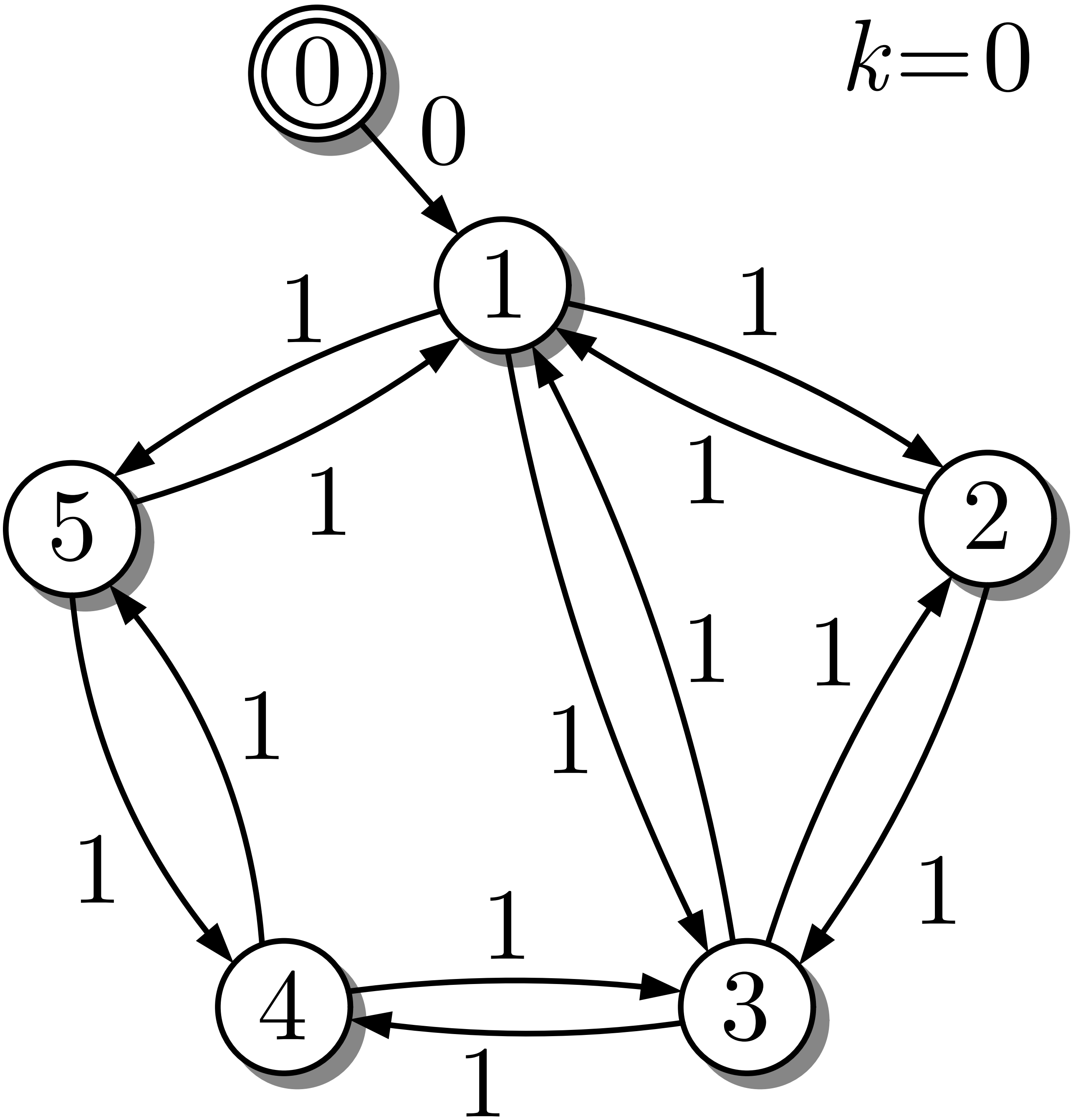

Fig. A1.77: Application of the algorithm to the network

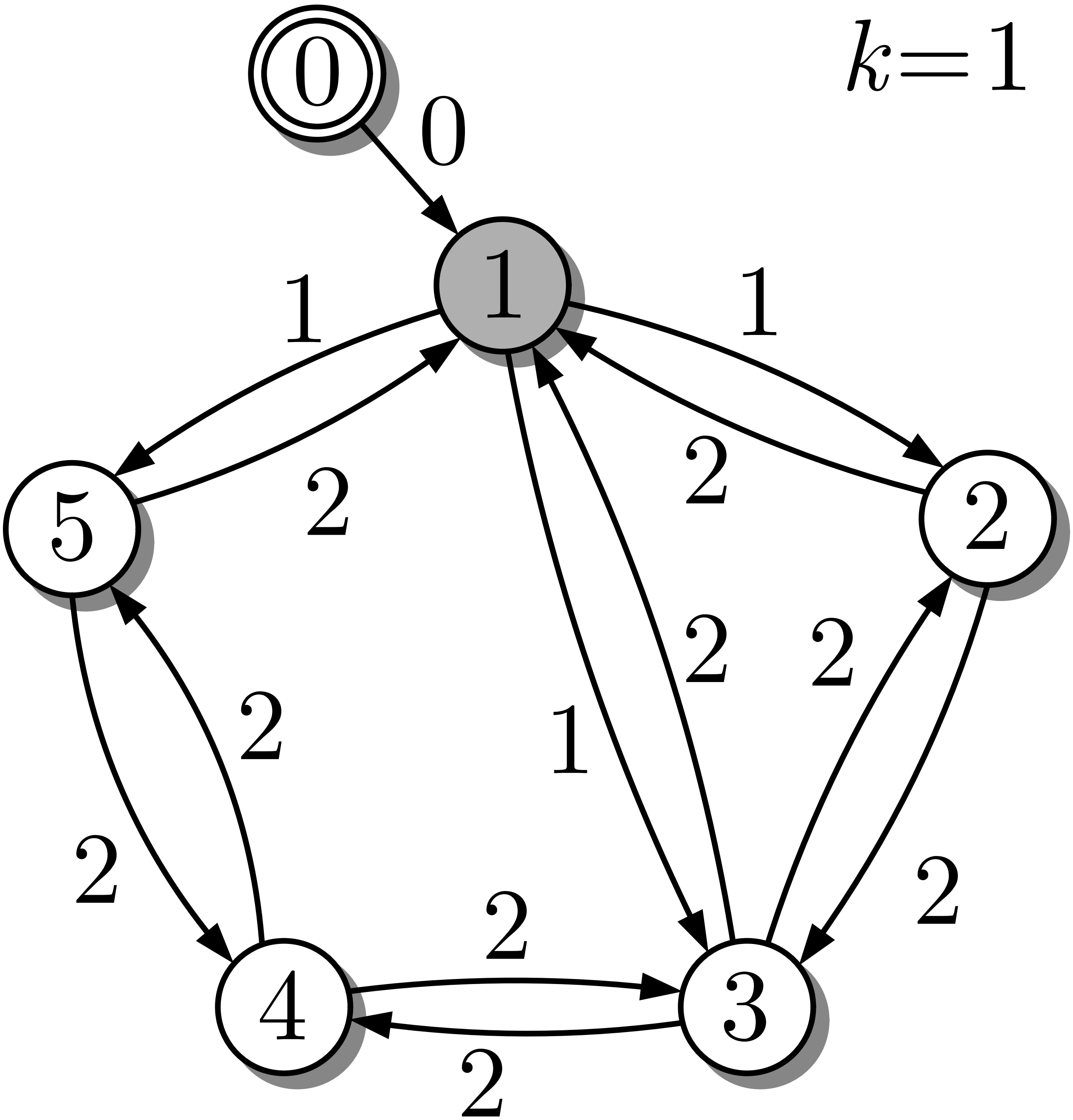

Fig. A1.77: Application of the algorithm to the network

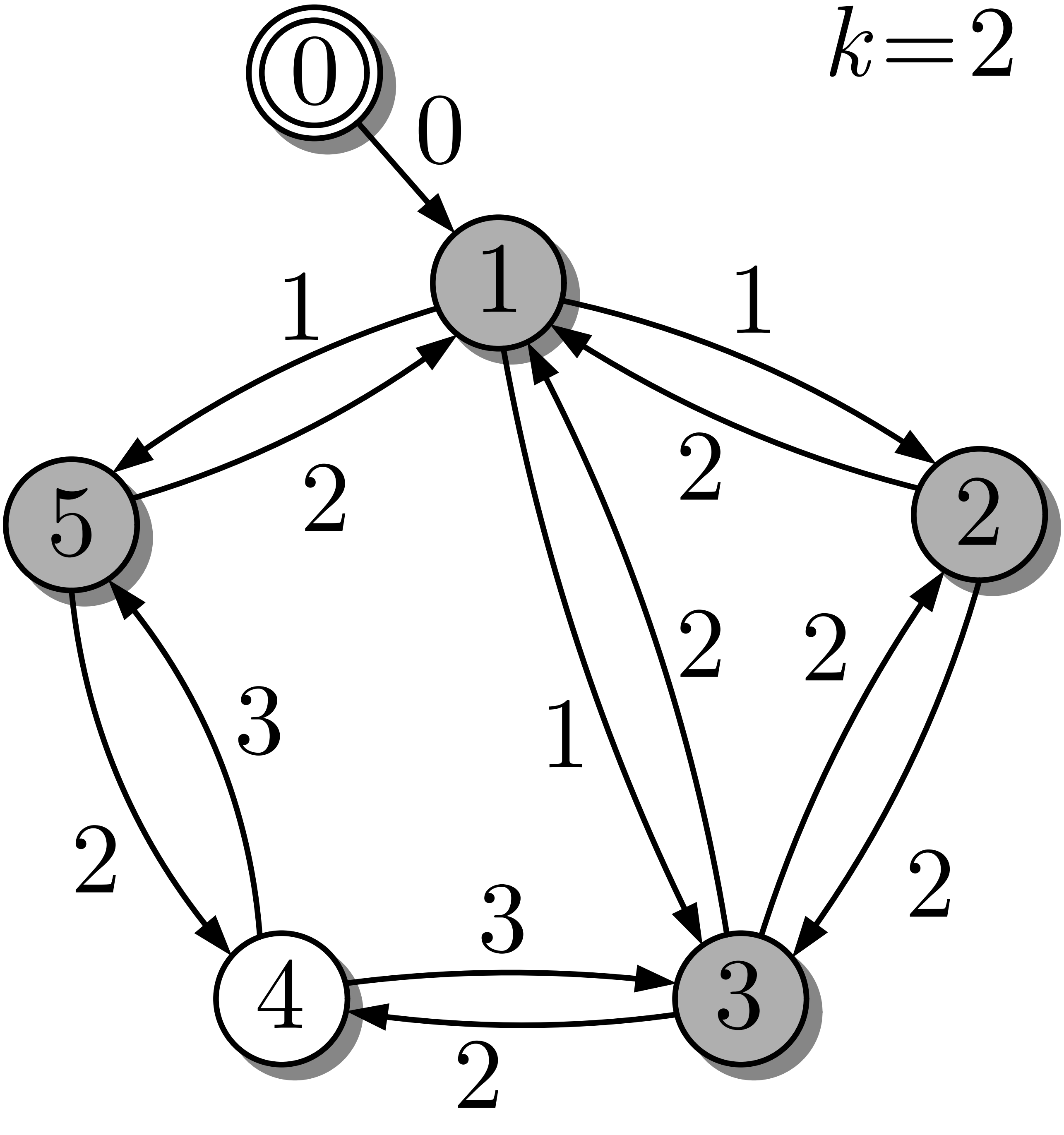

Fig. A1.77: Application of the algorithm to the network

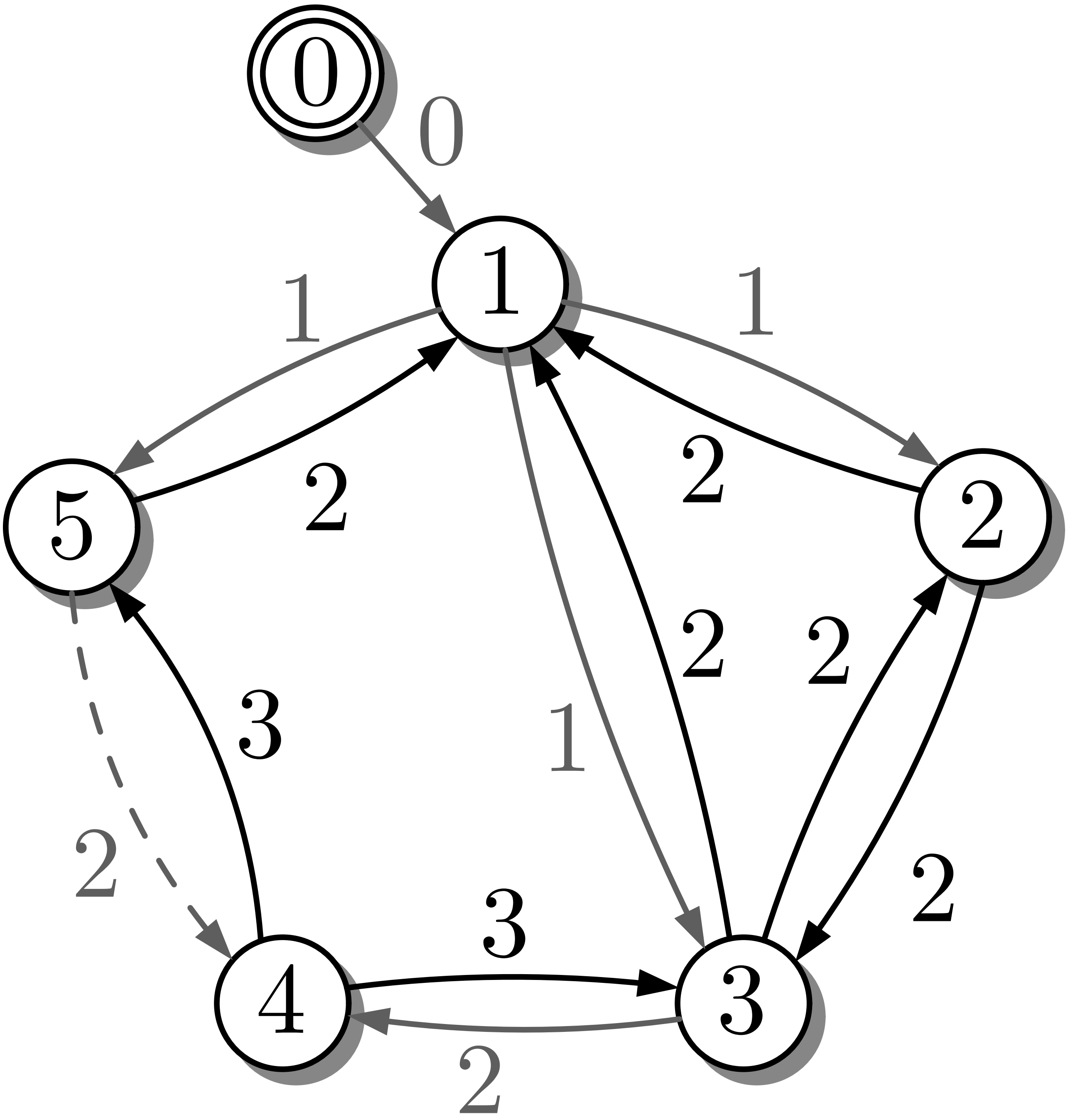

Fig. A1.78: Resulting effective communication graph and ranks of the vertices

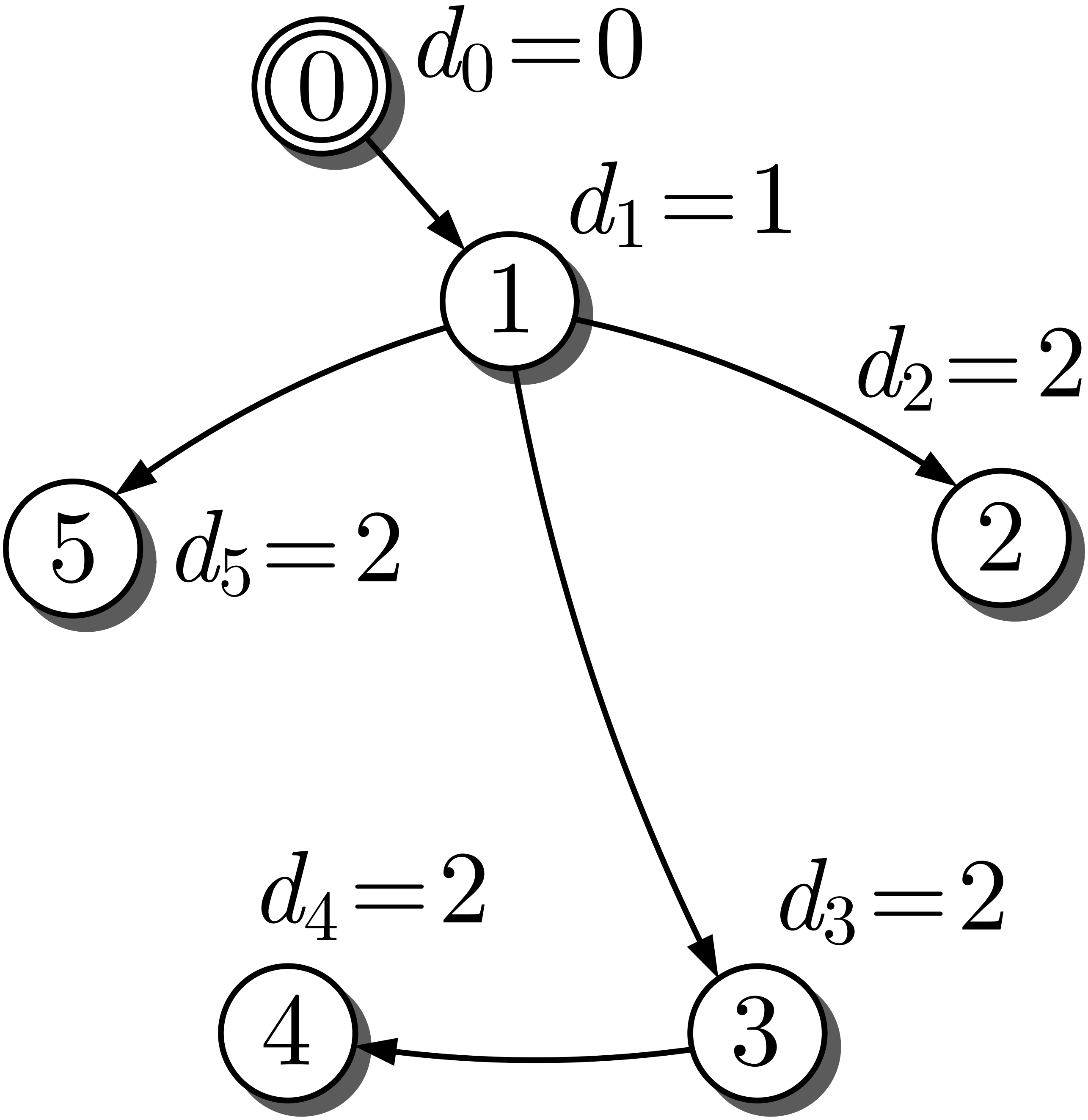

Fig. A1.78: Resulting effective communication graph and ranks of the vertices

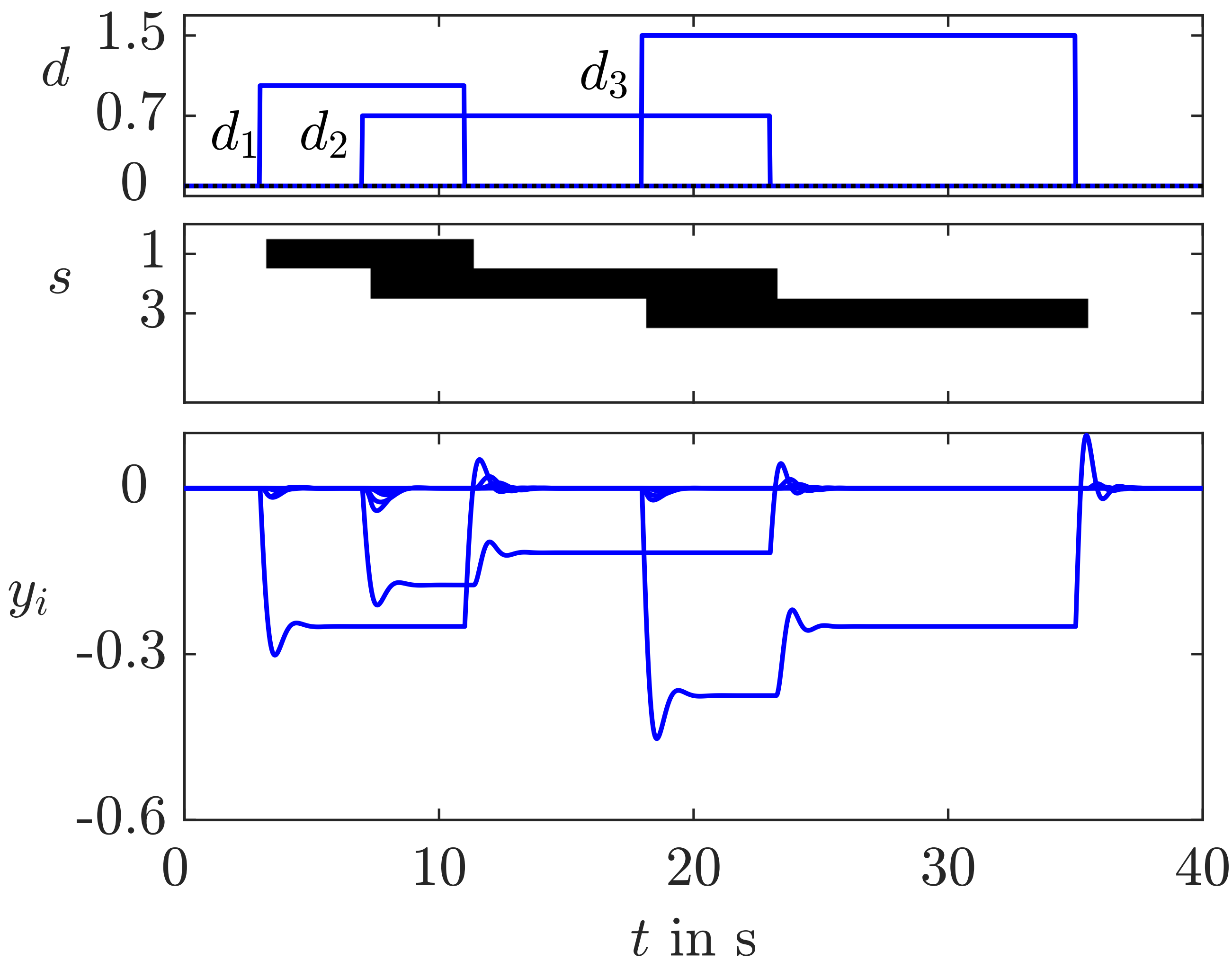

Fig. A1.79: Disturbance behaviour of the multirotor fleet with switching P controller

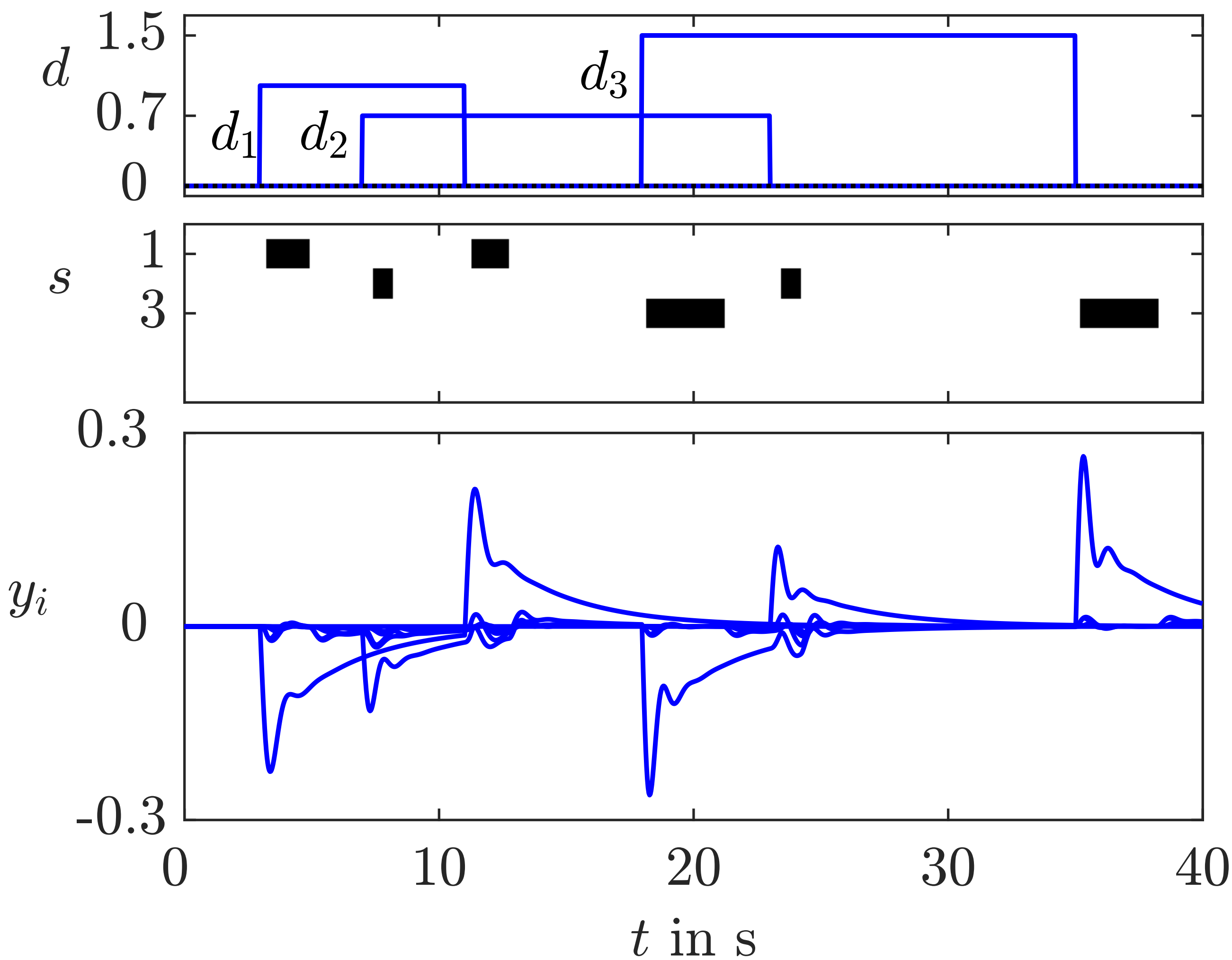

Fig. A1.79: Disturbance behaviour of the multirotor fleet with switching PI controller

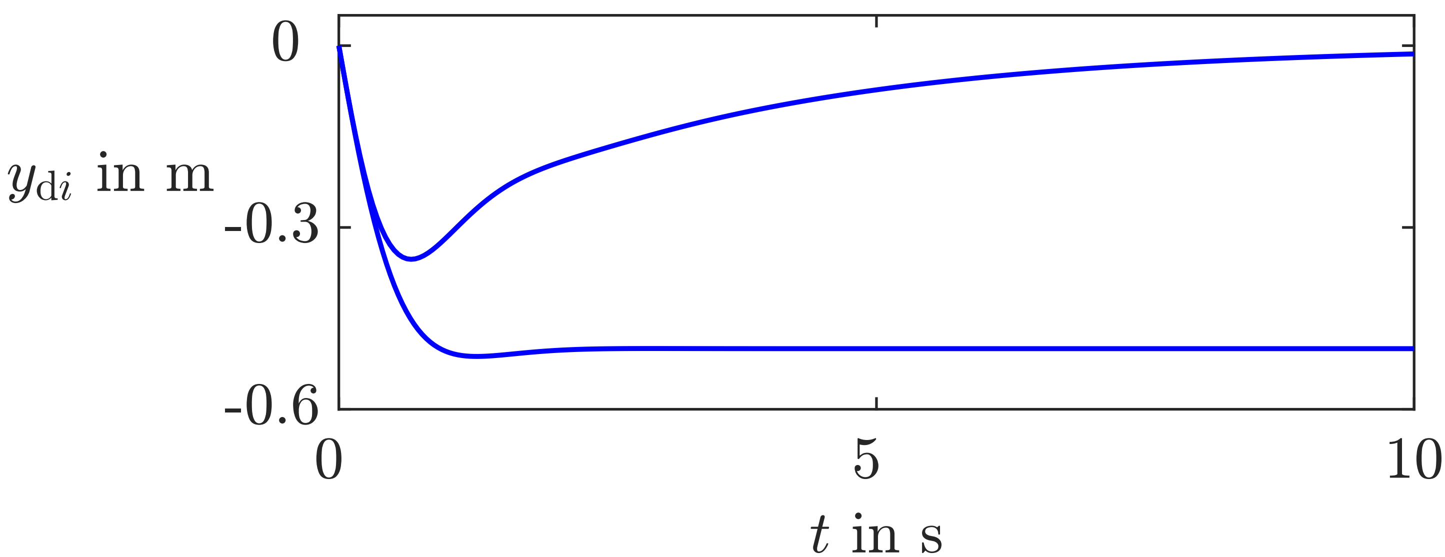

Fig. A1.80: Disturbance behaviour of the controlled multirotors

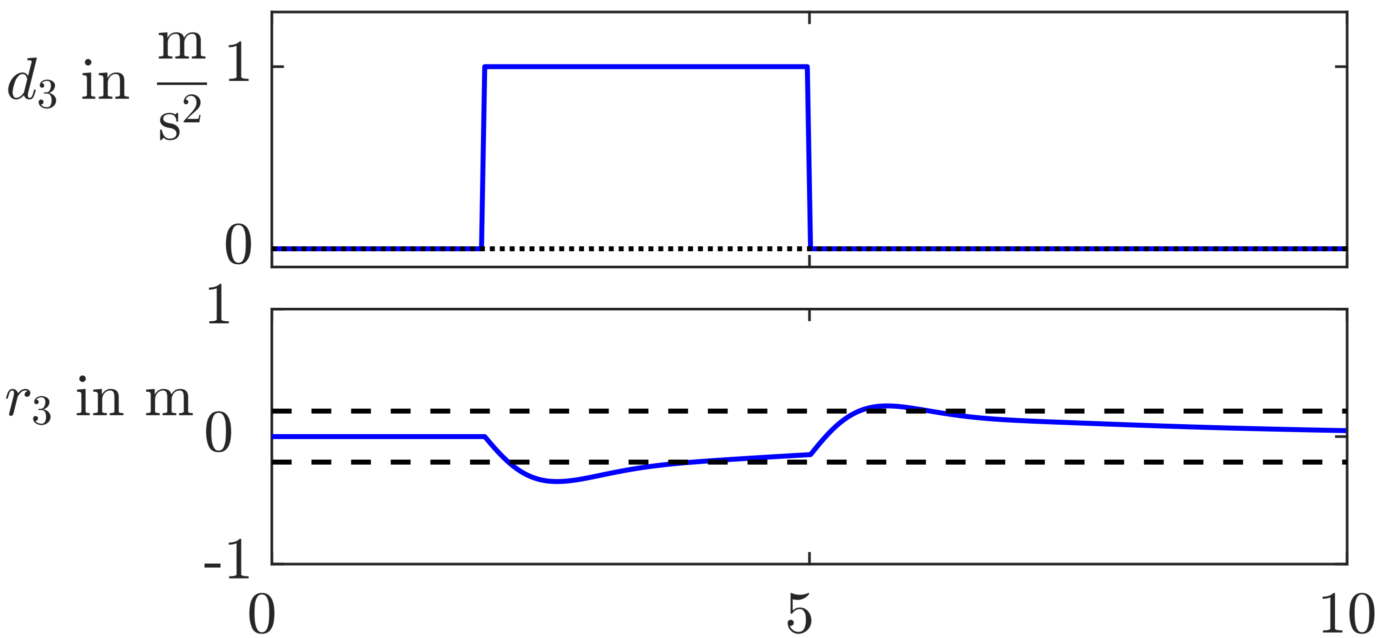

Fig. A1.81: Disturbance effect on the multirotor with PI controller

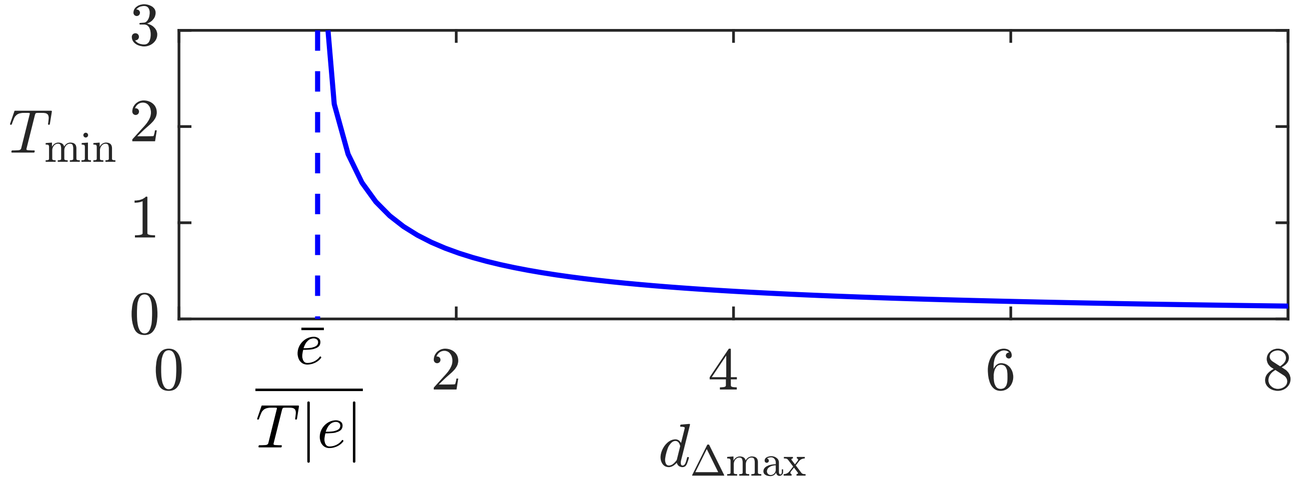

Fig. A1.82: Relation between $T_{\min}$ and $d_{\Delta\max}$

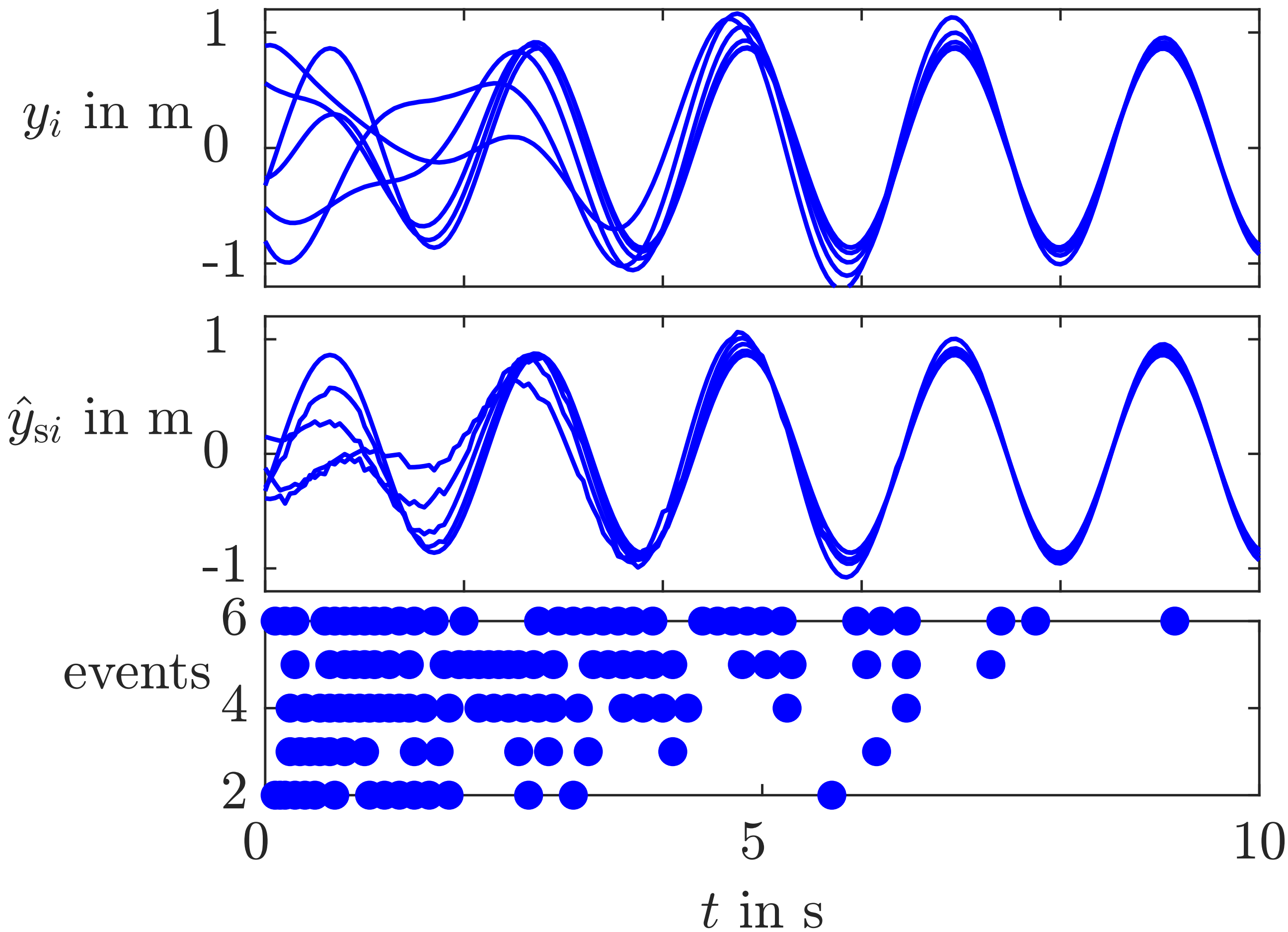

Fig. A1.83: Event-triggered synchronisation of six undamped oscillators

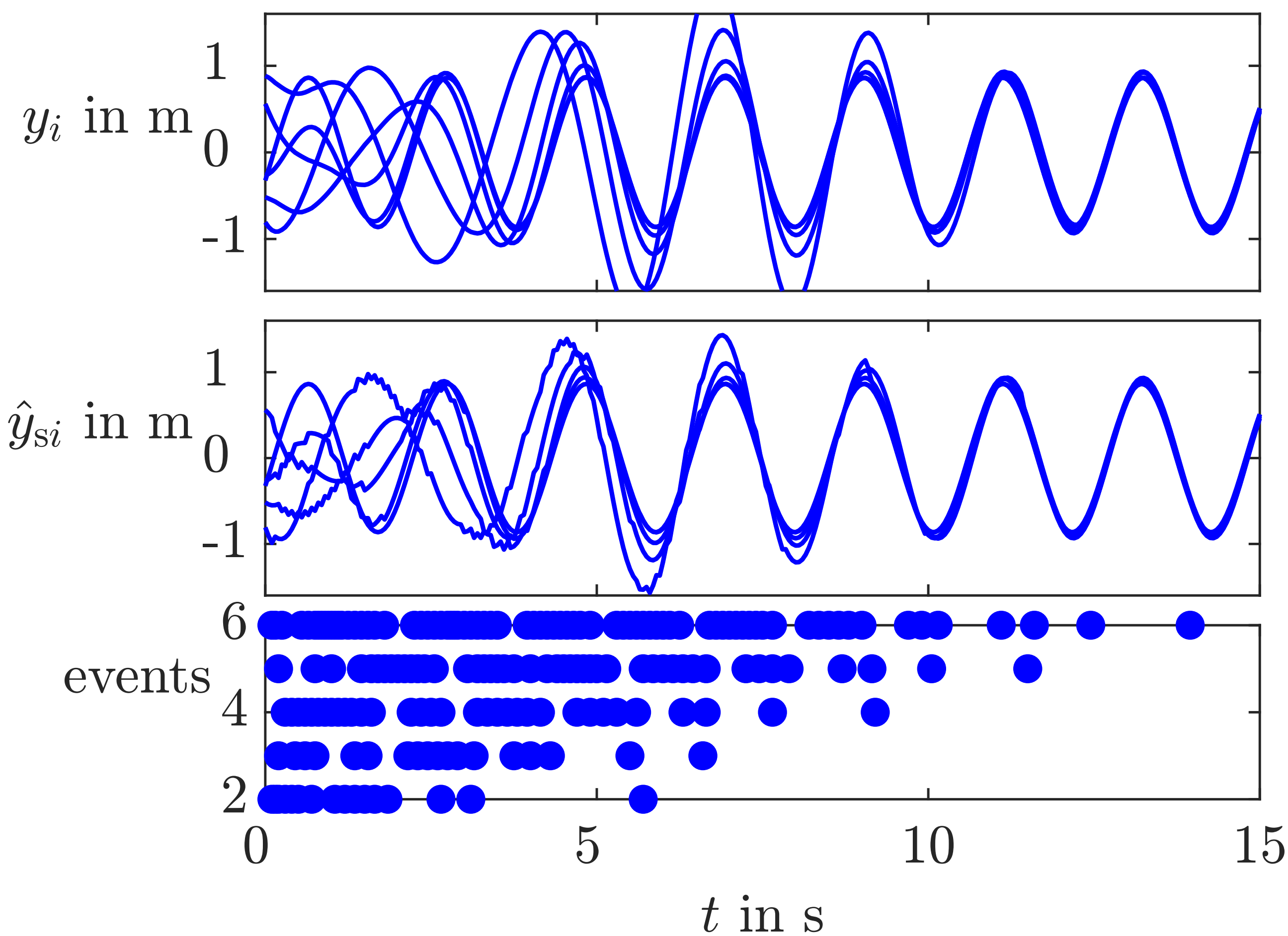

Fig. A1.84: Event-triggered synchronisation with path graph communication

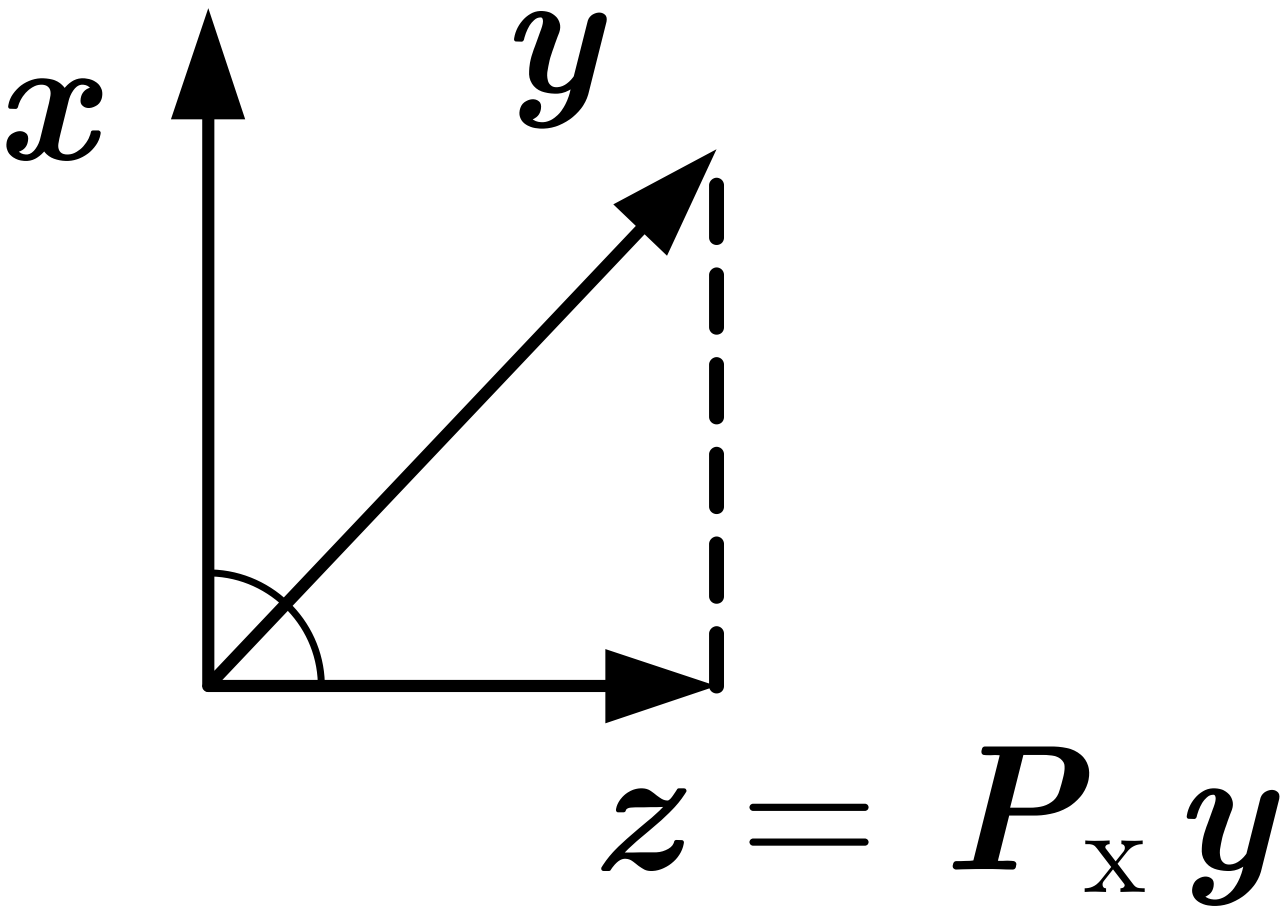

Fig. A2.1: Orthogonal projection

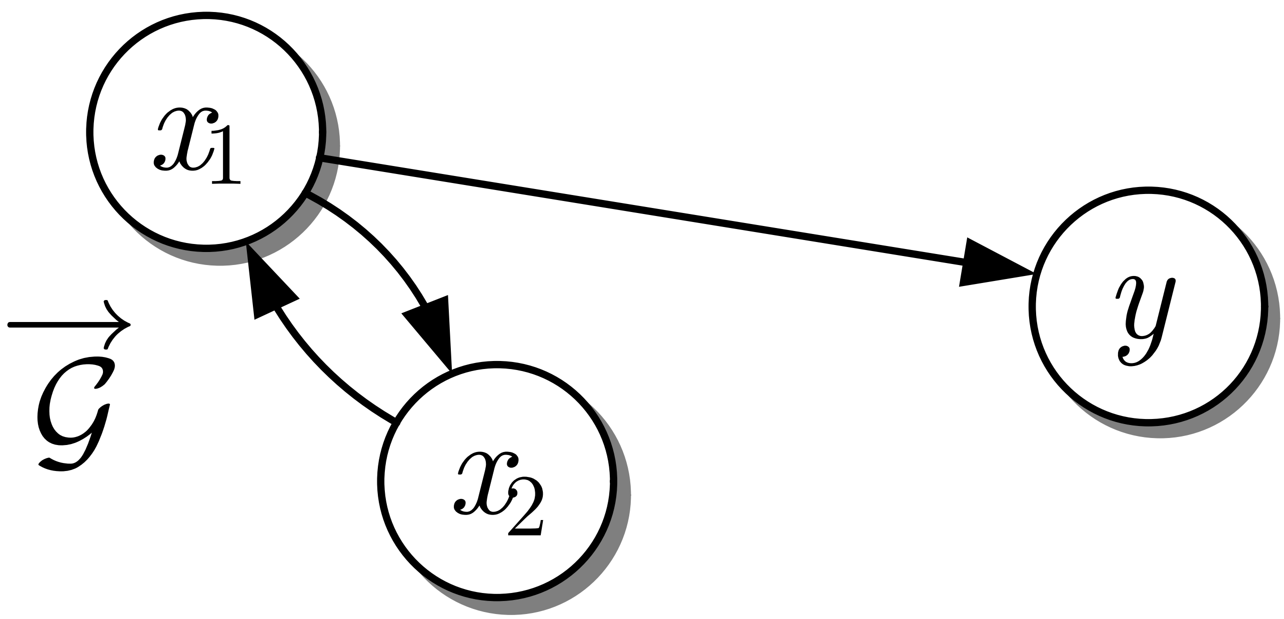

Fig. A3.1: Structure graph of an oscillator

J. Lunze: *Networked Control of Multi-Agent Systems,* Edition **MoR**a 2022

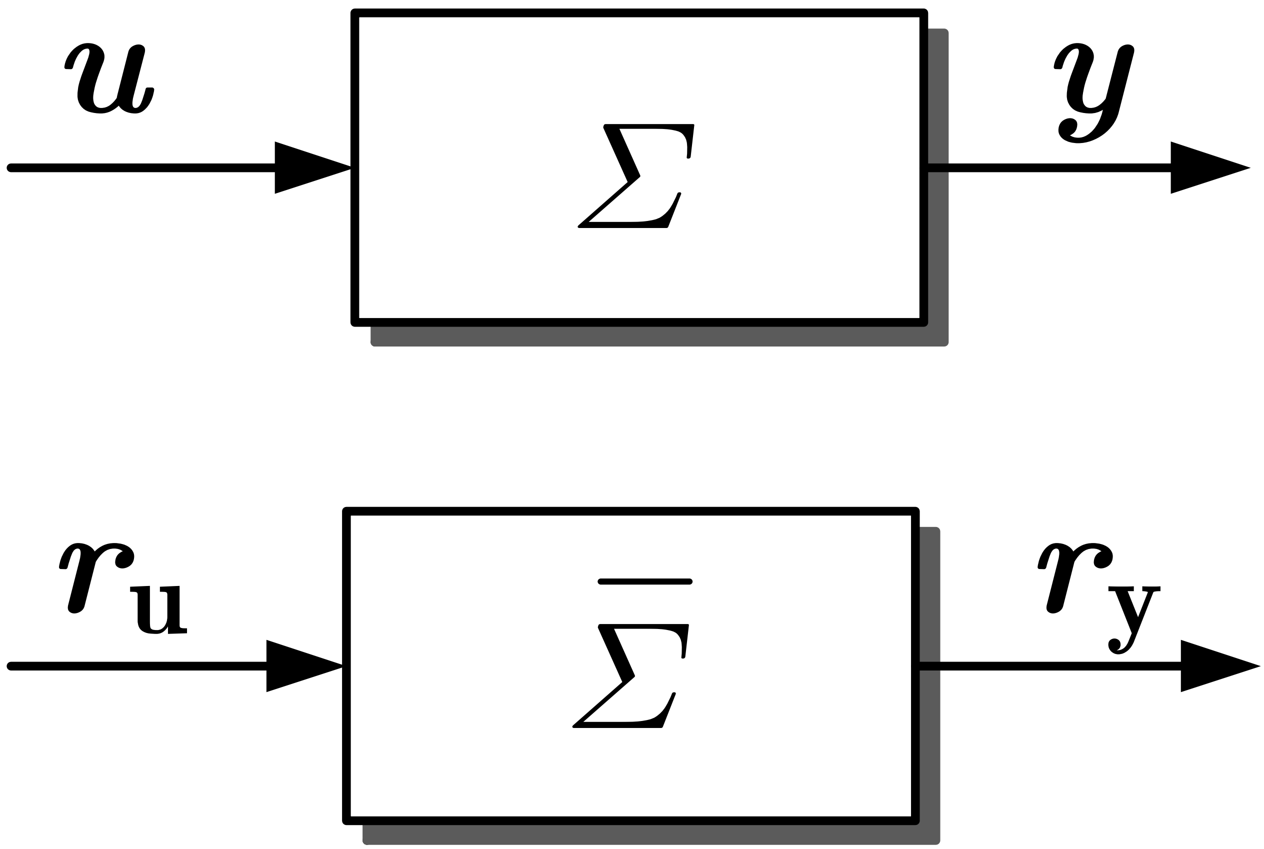

Fig. A3.2: Comparison principle

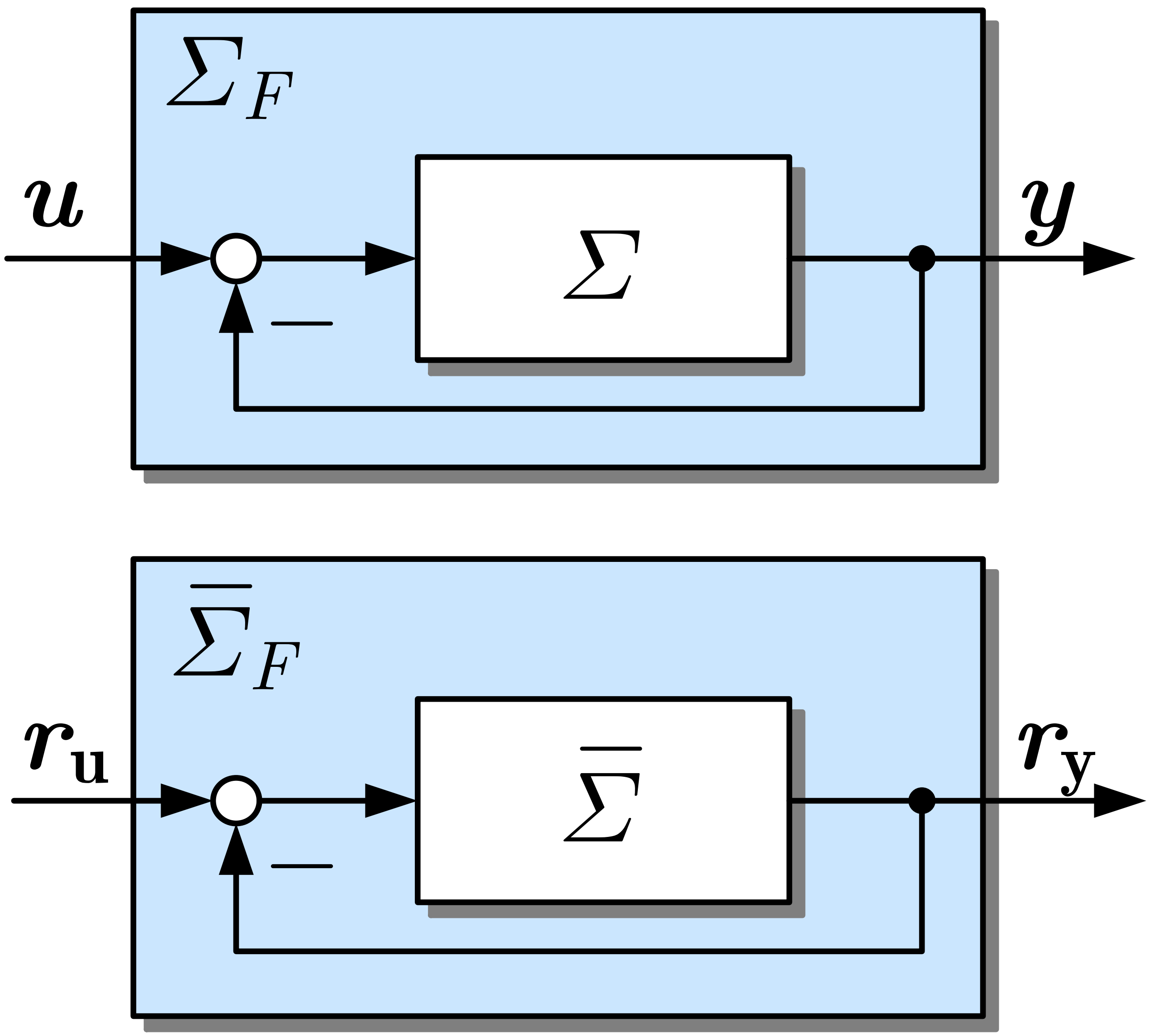

Fig. A3.3: Comparison principle applied to feedback systems

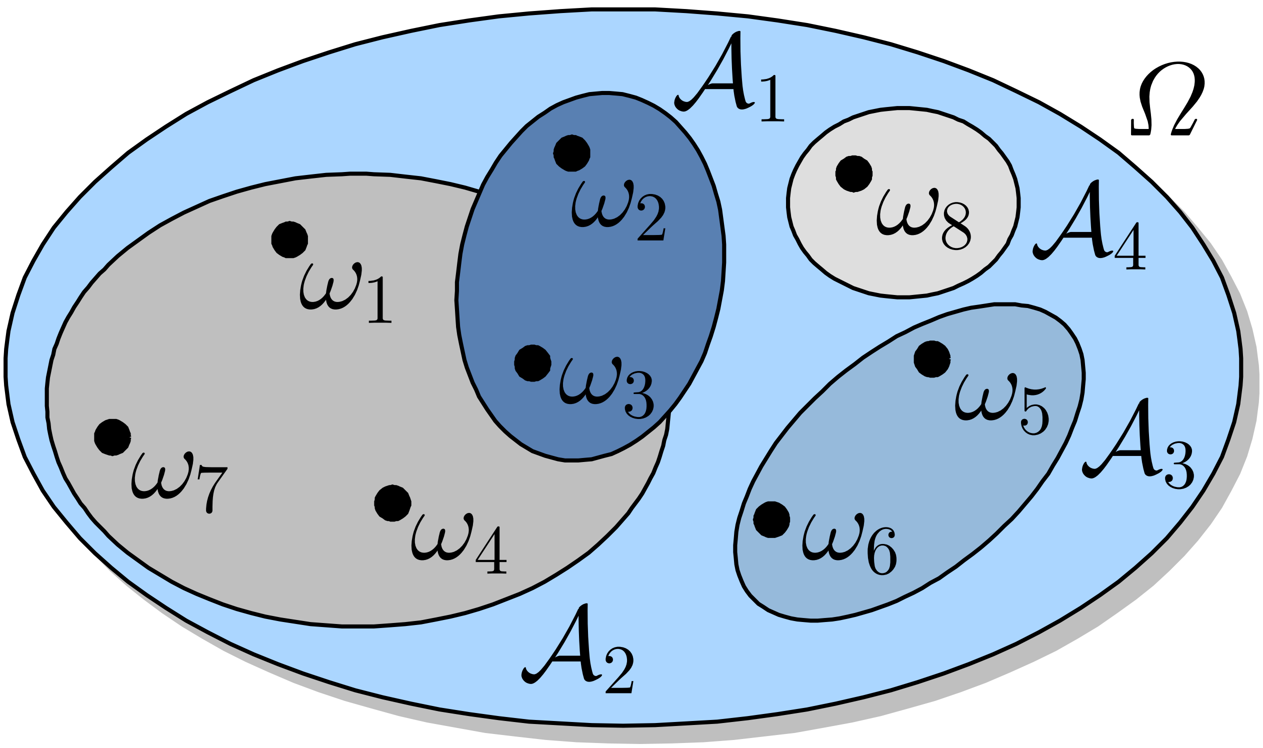

Fig. A4.1: Random events $\mathcal{A}_i$

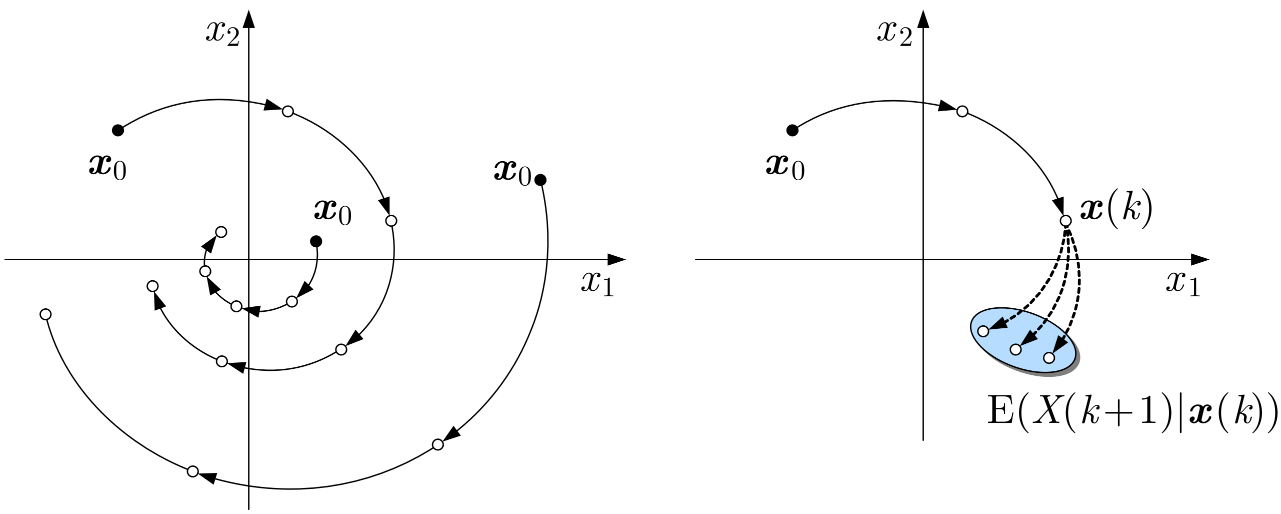

Fig. A4.2: Expected value and conditional expected value for a state sequence